METABOLIC PLASTICITY OF CANCER

EDITED BY: Tuuli Käämbre, Rafael Moreno-Sánchez and Sara Rodriguez-Enriquez
PUBLISHED IN: Frontiers in Oncology

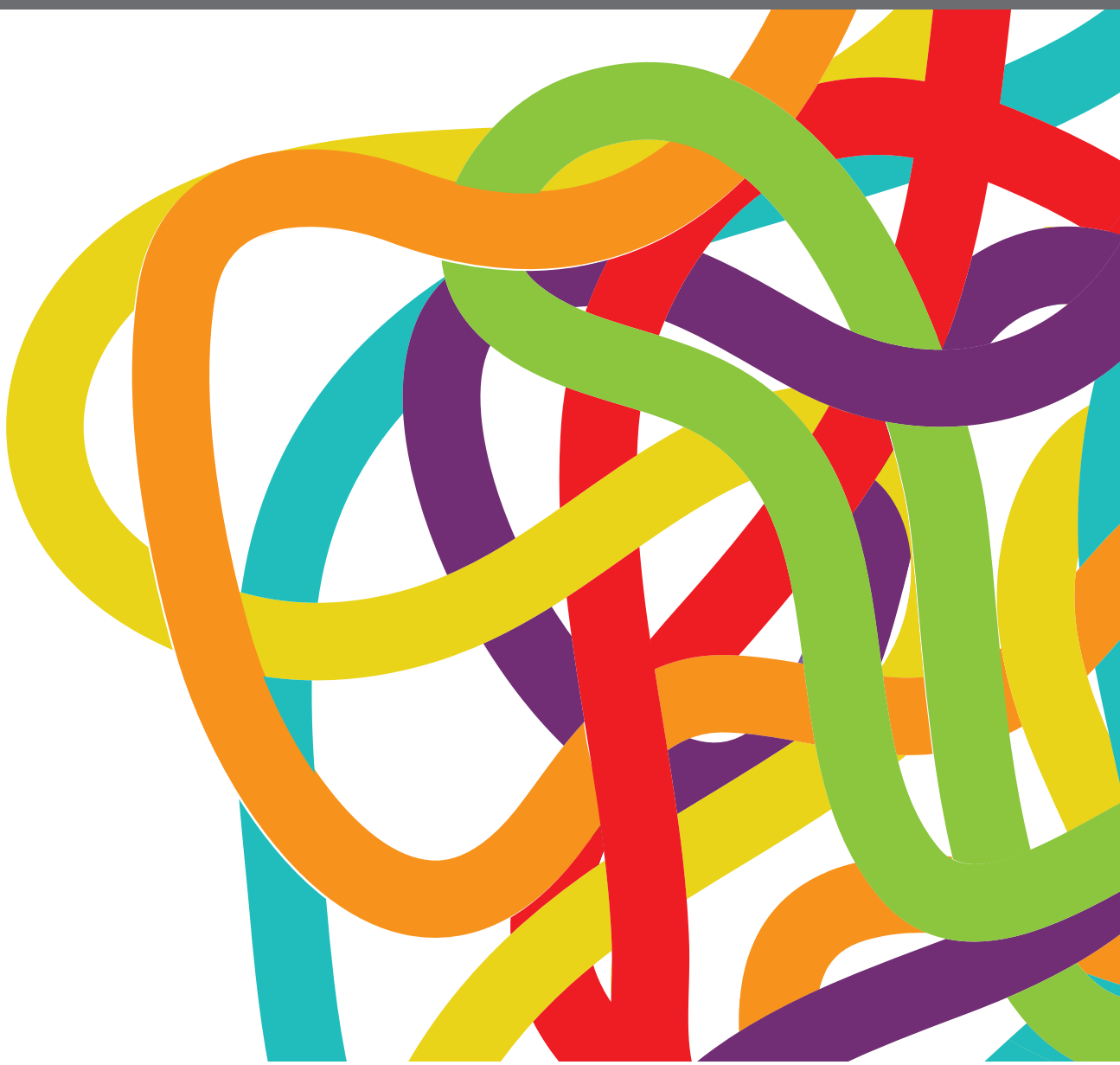

frontiers Research Topics

ISSN 1664-8714
ISBN 978-2-88966-276-0
DOI 10.3389/978-2-88966-276-0

About Frontiers

Frontiers is more than just an open-access publisher of scholarly articles: it is a pioneering approach to the world of academia, radically improving the way scholarly research is managed. The grand vision of Frontiers is a world where all people have an equal opportunity to seek, share and generate knowledge. Frontiers provides immediate and permanent online open access to all its publications, but this alone is not enough to realize our grand goals.

Frontiers Journal Series

The Frontiers Journal Series is a multi-tier and interdisciplinary set of open-access, online journals, promising a paradigm shift from the current review, selection and dissemination processes in academic publishing. All Frontiers journals are driven by researchers for researchers; therefore, they constitute a service to the scholarly community. At the same time, the Frontiers Journal Series operates on a revolutionary invention, the tiered publishing system, initially addressing specific communities of scholars, and gradually climbing up to broader public understanding, thus serving the interests of the lay society, too.

Dedication to Quality

Each Frontiers article is a landmark of the highest quality, thanks to genuinely collaborative interactions between authors and review editors, who include some of the world's best academicians. Research must be certified by peers before entering a stream of knowledge that may eventually reach the public - and shape society; therefore, Frontiers only applies the most rigorous and unbiased reviews.
Frontiers revolutionizes research publishing by freely delivering the most outstanding research, evaluated with no bias from both the academic and social point of view. By applying the most advanced information technologies, Frontiers is catapulting scholarly publishing into a new generation.

What are Frontiers Research Topics?

Frontiers Research Topics are very popular trademarks of the Frontiers Journals Series: they are collections of at least ten articles, all centered on a particular subject. With their unique mix of varied contributions from Original Research to Review Articles, Frontiers Research Topics unify the most influential researchers, the latest key findings and historical advances in a hot research area! Find out more on how to host your own Frontiers Research Topic or contribute to one as an author by contacting the Frontiers Editorial Office: researchtopics@frontiersin.org

METABOLIC PLASTICITY OF CANCER

Topic Editors:
Tuuli Käämbre, National Institute of Chemical Physics and Biophysics, Estonia
Rafael Moreno-Sánchez, Instituto Nacional de Cardiologia Ignacio Chavez, Mexico
Sara Rodriguez-Enriquez, Instituto Nacional de Cardiología, Mexico

Citation: Käämbre, T., Moreno-Sánchez, R., Rodriguez-Enriquez, S., eds. (2020). Metabolic Plasticity of Cancer. Lausanne: Frontiers Media SA.
doi: 10.3389/978-2-88966-276-0

Table of Contents

frontiers in Oncology

EDITORIAL
published: 23 October 2020
doi: 10.3389/fonc.2020.599723

Editorial: Metabolic Plasticity of Cancer

Sara Rodríguez-Enríquez[1]*, *Tuuli Kaambre*[2] *and Rafael Moreno-Sánchez*[1]

[1] Departmento de Bioquímica, Instituto Nacional de Cardiología, Ciudad de México, Mexico, [2] Chemical Biology Laboratory, National Institute of Chemical Physics and Biophysics, Tallinn, Estonia

Keywords: mitochondrial metabolism, glycolysis, cancer stem cells, drug targeting, malignant cancer

Editorial on the Research Topic

Metabolic Plasticity of Cancer

The metabolic reprogramming strategies used by cancer cells to survive and proliferate include changes in their energy metabolism status and enzyme machinery. During carcinogenesis, substantial changes in tissue oxygen, glucose (and other carbon sources) and pH occur which affect cellular energy management. Malignant cells show enhanced glycolytic capacity even in the presence of a normal oxygen concentration (Warburg hypothesis). The Warburg hypothesis also states that the mitochondrial function of cancer cells is impaired. The glycolytic part of the Warburg hypothesis has been solidly documented for the great majority of cancer types; in contrast, the mitochondrial part has been matter of intense research and controversy the last 20 years. It should be noted that in addition to OxPhos, other mitochondrial functions are (i) anaplerotic supply of intermediary metabolites for the synthesis of amino acids, fatty acids, cholesterol, glucose, and heme; (ii) ROS generation and oxidative stress management; (iii) apoptosis onset and progression; and (iv) Ca^{2+} homeostasis. These essential mitochondrial functions for cell growth and survival cannot be fulfilled by the glycolytic pathway or any other metabolic pathway.

OPEN ACCESS

Edited and reviewed by:
Maria Ida Amabile,
Sapienza University of Rome, Italy

***Correspondence:**
Sara Rodríguez-Enríquez
saren960104@hotmail.com

Specialty section:
This article was submitted to Cancer Metabolism, a section of the journal Frontiers in Oncology

Received: *27 August 2020*
Accepted: *11 September 2020*
Published: *23 October 2020*

Citation:
Rodríguez-Enríquez S, Kaambre T and Moreno-Sánchez R (2020) Editorial: Metabolic Plasticity of Cancer. Front. Oncol. 10:599723. doi: 10.3389/fonc.2020.599723

CANCER MITOCHONDRIAL METABOLISM

Recently it has been demonstrated that some typical waste metabolites produced by mammalian cells such as NH_4^+ or lactate, whose metabolic transformation requires functional mitochondria, may support cancer cell growth.

In this regard, the contribution by Prado-García et al., describe that, under a mild lactic acidosis and normoxia, A427 lung cancer cells are able to oxidize exogenous lactate favoring OxPhos and cell growth with no change in glucose consumption but diminished glycolysis, whereas A549 lung cancer cells display diminished glucose consumption, glycolysis, and OxPhos. Transcriptional response of both cancer cell lines is also different. Thus, it seems that lactic acidosis may have multiple regulatory effects on glycolysis and OxPhos. Further studies analyzing separately the effects of simple acidosis (at constant lactate), a wider range of lactate concentrations (at constant pH) and exposure times may help elucidating how energy metabolism is regulated by lactic acidosis in lung cancer cells.

Louie et al., report that MCF-7 breast cancer cells exposed to different combinations of physiological substrates (glucose, glutamine, pyruvate) activates OxPhos, displaying ATP production rates 60% greater than those shown by cells cultured with each individual substrate. This response is not observed in non-transformed C2C12 myoblasts. It would be interesting to detect and characterize this metabolic plasticity in other cancer cell types by using physiological substrate combinations including free fatty acids, lactate and ketone bodies, to establish whether this feature is unique to cancer.

Moreno-Sánchez et al., propose a novel anabolic role for mitochondrial glutamate dehydrogenase (GDH) as a NH_4^+ fixing enzyme for supporting growth of metastatic cancer cells. The kinetic constants experimentally determined in this study clearly indicate that GDH reverse reaction (from 2-oxoglutarate to glutamate and NADPH production) is favored under physiological conditions to sustain cancer growth. However, it remains to be determined why ammonium is not toxic for cancer cells and why metastatic cells are apparently better equipped to use it for cellular functions.

Koit et al. demonstrate, by using a citrate-isotope tracing method and ADP-stimulated O_2 consumption of permeabilized cells, that aggressive human breast cancer postoperational samples maintain high respiration rate and high mitochondrial citrate efflux compared to less aggressive subtypes. Citrate fluxes and O_2 consumption of two of the most used breast cancer cell lines, MCF-7 and MDA-MB231, differ from those shown by breast cancer tissue samples. This is expected because cancer cell lines are grown as bi-dimensional cultures, whereas cancer tissue is a tri-dimensional system. This tri-dimensional organization (i.e., cell-matrix interactions, variations in nutrient supply due to glucose, lactate, pH, and oxygen gradients; as well as variations in the expression of transcription factor and oncogenes), leads to changes in gene regulation, enzyme expression/ activity, and metabolic fluxes with respect to monolayer cell cultures and cell suspensions.

Lemos et al., demonstrate the importance of fatty acid β-oxidation in the development of the metastatic phenotype. By using microcalorimetry, they show that metastatic cancer cells release more heat than non-metastatic cells, correlating with an overexpressed uncoupling protein 2 (UCP-2). It should be noted that both β-oxidation and UCP-2 reaction (H^+ transport) are mitochondrial processes. The carnitine/palmitoyl-CoA transferase-1 inhibitor etomoxir decreases heat release by metastatic cells, indicating that β-oxidation is involved in thermogenesis. In addition to extent these observations to more metastatic cancer cell lines and biopsies, it would be relevant to show that metastatic cells indeed actively oxidize fatty acids by assessing O_2 consumption rates and protein levels. These observations also indicate that fatty acid β-oxidation and UCP-2 may be anti-cancer targets and that the novel biophysical approach used could be helpful for metastasis detection.

The contribution by Bouchez et al., using yeast cells as a suitable model to study the Warburg effect (where all parameters involved and their modulation can be reconstituted) demonstrates that mitochondria are not dysfunctional and importantly, that OxPhos is required to promote cell growth.

Previous work from Rodriguez-Enriquez group have also shown that OxPhos is the predominant ATP supplier (60–80% under normoxia and normoglycemia), with glycolysis having a minor role, for growth and survival of human cervix HeLa cells and microspheroids, human breast MCF-7 and MDA-MB231 cells, and rodent AS-30D ascites hepatoma cells. Glycolysis becomes the major ATP provider (55–80%) when cancer cells are subjected to severe and prolonged hypoxia (0.1% atmospheric O_2, 24–48 h) or hypoglycemia (<5 mM glucose). Recent work describes that the non-steroidal anti-inflammatory drugs celecoxib and its analog dimethyl-celecoxib, at nanomolar (3D) or micromolar (2D) concentrations, increase cisplatin, paclitaxel and doxorubicin efficacy (>60%) against human cervix cancer cell growth, OxPhos and invasiveness (>90%), without apparent effect on human HUVEC and fibroblasts (*unpublished data*).

CANCER GLYCOLYSIS

The study performed by Piga et al., in ovarian cancer xenografts shows that some glycolytic markers such as the monocarboxylate transporter MCT4 are negatively associated with survival. In turn, Vlaski-Lafarge et al., demonstrate that normal hematopoietic stem cells develop a cancer stem cell-like phenotype (by over-expressing the canonical markers CD34+ and ALDH) when they are experimentally subjected to anoxic and/or aglycemic stresses. They found that under ischemia-likeconditions, primitive hematopoietic cell mitochondria remain functional for sustaining cellular homeostasis.

Prasad-Yadav et al., review the energy metabolism of CSC derived from different cancer tissues. They conclude that CSC from breast, glioblastoma and osteosarcoma predominantly depend on glycolysis for survival while CSC from glioma, pancreas and lung depend on OxPhos (which is mainly sustained by free fatty acids and ketone bodies oxidation). Thus, the identification of the main ATP supplier may be helpful to design strategies to kill selectively cancer cells by using specific inhibitors targeting energy metabolism.

In the study by Avagliano et al., with metastatic cutaneous melanoma (CM) it is shown that both glycolysis and OxPhos are actively involved in cellular ATP formation, although the main energy supply relies on glycolysis. In addition, it is demonstrated that glycolysis activation in CM is mediated by the BRAF/MAPK signaling pathway containing a BRAF kinase mutant. Consequently, the use of BRAF/MAPK inhibitors induces in MC cells metabolic re-programming from glycolysis to OxPhos.

SIGNALING

As described in Avagliano et al. study, metabolic reprogramming in cancer cells is tightly regulated by transcriptional factors, protein kinases and/or oncogenes. Among them, the forkhead box protein C2 (FOXC2), casein kinase (CK2), and adenylate kinase (AK) have been proposed as cancer markers or even targets to deter cancer progression. Hargadon and Williams use RNA-seq dataset to detect novel tumor-promoting functions of FOXC2, including its role as a regulator of mitochondrial morphology and metabolism. Silva-Pavez and Tapia compile evidence from literature suggesting that CK2 is a switch modulator of the mitochondrial function in a PTEN-dependent mode. They conclude that PTEN, as CK2 substrate in the PI3K/Akt signaling pathway, can regulate several downstream key targets like HIF-1α and mitophagy. Therefore, the specific inhibition of CK2 in cancer cells may be a potential therapeutic strategy against cancer development.

Klepinin et al., propose AK (adenylate kinase, an ubiquitous and highly efficient enzyme involved in the adenylate nucleotide cellular homeostasis) as a novel cancer therapeutic target. They demonstrate that different AK isoforms are used by cancer cells for rewiring energy metabolism to support tumor progression and metastasis. These observations allow concluding that although cancer cells maintain a high glycolytic rate, the main ATP production derive from OxPhos. Thus, anti-mitochondrial drug therapy combined with signaling targets (FOXC2, CK2, or AK) may be an adequate adjuvant strategy to arrest proliferation of OxPhos-dependent neoplasias.

It is convenient to emphasize that most of the studies published in the present special issue of *Frontiers in Oncology*, *Cancer Metabolism section* have focused on directly assessing the metabolic function (i.e., cell growth, O_2 consumption, glucose consumption, lactate production, enzyme activities). This takes relevance because, to date, many studies published in high impact journals only rely on determining mRNA or protein levels to make inferences on the functional consequences of using for instance inhibitors or genetic manipulations. As cancer cells can only depend on both glycolysis and OxPhos for ATP supply, like non-cancer cells, the challenge appears to be in designing effective drugs that better and more specifically target cancer cells and, in particular, their mitochondria, which are now postulated as essential in all cancers.

AUTHOR CONTRIBUTIONS

All authors listed have made a substantial, direct and intellectual contribution to the work, and approved it for publication.

FUNDING

SR-E and RM-S are supported by CONACyT-Mexico Grants Nos. 283144, 239930, and 281428 (Mexico).

Conflict of Interest: The authors declare that the research was conducted in the absence of any commercial or financial relationships that could be construed as a potential conflict of interest.

frontiers in Oncology

ORIGINAL RESEARCH
published: 18 December 2019
doi: 10.3389/fonc.2019.01430

Isothermal Microcalorimetry of Tumor Cells: Enhanced Thermogenesis by Metastatic Cells

Douglas Lemos[1†], Thaís Oliveira[1†], Larissa Martins[1], Vitória Ramos de Azevedo[1], Mariana Figueiredo Rodrigues[1], Luisa Andrea Ketzer[2] and Franklin David Rumjanek[1]*

[1] *Laboratório de Bioquímica e Biologia Molecular Do Câncer, Instituto de Bioquímica Médica Leopoldo de Meis, Universidade Federal Do Rio de Janeiro, Rio de Janeiro, Brazil,* [2] *Núcleo Multidisciplinar de Pesquisa UFRJ-Xerém em Biologia (NUMPEX-Bio), Universidade Federal Do Rio de Janeiro, Duque de Caxias, Brazil*

Tumor cells exhibit rewired metabolism. We carried out comparative analyses attempting to investigate whether metabolic reprograming could be measured by isothermal microcalorimetry. Intact metastatic cell lines of tongue cell carcinoma, human and murine melanoma, lung, and breast tumors consistently released more heat than non-metastatic cells or cells displaying lower metastatic potential. In tongue squamous carcinoma cells mitochondrial enriched extract reproduced the heat release pattern of intact cells. Cytochalasin D, an actin filament inhibitor, and suppression of metastasis marker Melanoma associated gene 10 (MAGEA10) decreased heat release. Uncoupling protein 2 was highly expressed in metastatic cells, but not in non-metastatic cells. Carnitine palmitoyl transferase-1 inhibitor, Etomoxir strongly inhibited heat release by metastatic cells, thus linking lipid metabolism to thermogenesis. We propose that heat release may be a quantifiable trait of the metastatic process.

Keywords: thermogenesis, microcalorimetry, metastasis, UCP2, etomoxir, fatty acid oxidation

OPEN ACCESS

Edited by:
Tuuli Käämbre,
National Institute of Chemical Physics and Biophysics, Estonia

Reviewed by:
Cesar Cardenas,
Universidad Mayor, Chile
Sameh Saad Ali,
Children's Cancer Hospital, Egypt

***Correspondence:**
Franklin David Rumjanek
franklin@bioqmed.ufrj.br

[†]These authors have contributed equally to this work and share first authorship

Specialty section:
This article was submitted to Cancer Metabolism, a section of the journal Frontiers in Oncology

Received: *19 July 2019*
Accepted: *02 December 2019*
Published: *18 December 2019*

Citation:
Lemos D, Oliveira T, Martins L, de Azevedo VR, Rodrigues MF, Ketzer LA and Rumjanek FD (2019) Isothermal Microcalorimetry of Tumor Cells: Enhanced Thermogenesis by Metastatic Cells. Front. Oncol. 9:1430. doi: 10.3389/fonc.2019.01430

INTRODUCTION

Evidence has accumulated to show convincingly that the metabolism of tumor cells differs significantly from that of the majority of normal cells. Irrespective of the multiple alterations contributing to the so-called metabolic reprogramming, it is generally agreed that the major differences implicate the glycolytic and the tricarboxylic cycle pathways coupled to the oxidative phosphorylation (OXPHOS) system (1, 2). This is not surprising in view of the roles played by these pathways as the principal suppliers of ATP for tumor cells. In this context tumor cells are broadly classified according to the prevailing type of metabolism i.e., glycolytic or oxidative. The former derive ATP mainly from aerobic glycolysis, whereas the latter are able to recruit OXPHOS to fulfill their extra energy demands (3). However, classifying tumors as anaerobic or oxidative is not simple. The difficulties stem from the extensive and highly connected pathways, themselves being amenable to fine regulation at various levels. The precise classification of tumor cells according to the type of metabolism would require kinetic measurements of the individual key regulatory enzymes of glycolysis, pentose phosphate pathway, and OXPHOS, to name a few—plus all the relevant anaplerotic branches feeding into those cycles. To date, comprehensive biochemical models that take into consideration data from enzyme kinetics, metabolomic and fluxomic analysis and thus explain how the tumor cells apportion energy toward various processes are scarce. An explanation

should take in to consideration proliferation, intravasation into blood and lymphatic vessels and migration and colonization of distant tissues as it occurs in metastasis. For these reasons sorting tumor cells as glycolytic or oxidative is still not consensual (4). As if this were not complicated enough there is growing evidence showing that many enzymes of the glycolytic pathway have dual roles, i.e., besides exerting their canonical metabolic functions they can also act as transcription factors (5). We reasoned that one way of simplifying this scenario would be to investigate the bioenergetics of tumor and metastatic cells by focusing on a parameter intimately associated to virtually all cellular events, as thermogenesis for instance. The central question raised in the present work was: energy wise what are the general features exhibited by cells undergoing metastasis? This was dealt with by carrying out isothermal microcalorimetry assays with intact cells bearing distinct metastatic potentials. The aim was to prospect whether there were thermogenic differences between the cell lines and to correlate those with certain metabolic pathways, as well as pinpointing the organelles responsible for the adaptive thermogenesis.

MATERIALS AND METHODS

Cell Lines

Tongue squamous carcinoma cells (SCC-9, LN-1, and LN-2) were a kind gift by Dr. Michelle Agostini (6). Human melanoma cells WM983A and WM9838B and WM852 (7) were a kind gift by Dr. Michelle Botelho of Federal University of Rio de Janeiro. Murine melanoma cells 4C, 4C11–, and 4C11+ were a gift by Dr. Miriam Jaisiulionis (8). Human non-small-cell lung cancer cell lines A549 and NCI-H460 and human breast adenocarcinoma cells MCF-7 and MDA-MB-231 were acquired commercially. Metastatic potentials of the cells were determined elsewhere (6, 7) and obeyed the following hierarchy: tongue: LN-2 > LN-1 > SCC-9; murine melanoma: $4C11^{+}$ > $4C11^{-}$ > 4C; human melanoma: WM852 > WM9838B > WM983A; breast: MDA-MB-231 > MCF-7; lung: H460 > A549. Mycoplasma contamination was tested by PCR using primers described elsewhere (9).

Monolayer Cell Cultures

Unless otherwise stated cells were grown in RPMI 1640 medium (Gibco) supplemented with (10%) fetal bovine serum (FBS; Gibco BRL) and antibiotic penicillin and streptomycin (LGC Biotechnology). Tongue squamous carcinoma cells and human melanoma were cultivated in DMEM /F-12 and DMEM, respectively, pH 7.2 supplemented with (10%) fetal bovine serum (FBS; Gibco BRL), and antibiotics penicillin and streptomycin (LGC Biotechnology) at 37°C in a humidified atmosphere of 5% CO_2 in a Series 8000 WJ CO_2 incubator (Thermo Scientific). Approximately 7×10^5 cells were seeded in cell culture dish 100 × 20 mm (Sarstedt 83.3902) and grown to 90% confluence. Cells were then treated with 0.25% (W/V) trypsin (Sigma) solution containing 0.78 mM EDTA to become detached.

Microspheroid Formation

Ninety-six U shaped well plates (Corning Costar 3799) were used. 24 h before platting the wells were layered with 1% agarose to favor microspheroid formation. 3×10^4 cells/well were used for seeding. Human oral squamous carcinoma cells were incubated for 72 h under an atmosphere of 5% CO_2 at 37°C in a CO_2 incubator.

Microspheroid Dissociation

Microspheroids were gently washed twice with phosphate buffered saline pH 7.4. After centrifugation at 400 g for 5 min, cells were treated with 0.125% (W/V) trypsin (Sigma) solution containing 0.78 mM EDTA for 5 min at 37°C. After incubation, medium containing fetal bovine serum was added to inactivate trypsin and cells were then gently dissociated by repeated cycles of aspiration with a 1 mL automatic pipette until the spheroids were visually undetected. Dissociated cells were then centrifuged at 400 g for 5 min.

Cell Viability

Cell viability was assayed by the MTT method (10) and LDH release (11).

RNA Extraction and cDNA Synthesis

Total RNA was isolated from cells using TRIzol reagent (Invitrogen) according to the manufacturer's instructions. Total RNA was quantified spectrophotometrically. 1 μg RNA was treated with 1 U of RNAse-free DNAse for 30 min at 37°C. Reactions were stopped by adding 1 μL of EDTA 20 mM and heating for 10 min at 65°C. cDNA synthesis was performed using the DNAse treated RNA using the High Capacity cDNA Reverse Transcription Kit from Applied Biosystems according to the manufacturer's instructions.

Suppression of Human MAGEA10

Stable **s**pecific **s**uppression of MAGEA10 mRNA was achieved by transduction of lentiviral particles expressing oligonucleotides bearing a short hairpin structure as described elsewhere (12).

Real Time PCR

Gene expression analysis was performed using 7500 Real Time PCR (Applied Biosystems) and power SYBR-GREEN PCR master MIX (Applied Biosystems). For this test primer pairs were synthesized based on GenBank sequences of mRNA. The comparative Ct method was used to measure changes in gene expression levels (13). Actin was used as an endogenous control.

Microcalorimetry

Heat production was measured using an OMEGA Isothermal Titration Calorimeter VP-ITC from Microcal Inc. (Northampton, MA). The calorimeter sample chamber (1.8 ml) was filled with medium without FBS and the reference

Abbreviations: ATP, adenosine triphosphate; BSA, bovine serum albumin; CPT-1, carnitine palmitoyl transferase-1; DMEM, Dulbecco minimal essential medium; DTT, dithiothreitol; EDTA, ethylene diamine tetra acetate; FBS, fetal bovine serum; ITC, isothermal titration calorimetry; LDH, lactate dehydrogenase; LN, lymphonode; MAGEA10, Melanoma associated gene 10; MTT,3-[4,5-dimethylthiazole-2-yl]-2,5-diphenyltetrazolium bromide; OXPHOS, oxidative phosphorylation; PCR, polymerase chain reaction; SCC, squamous carcinoma cells; UCP2, uncoupling protein 2.

chamber was filled with Milli-Q water. After equilibration at 37°C, the reaction was started by injecting intact cells, or when indicated cell-free extracts into the sample chamber. The heat change was recorded at 5 min intervals during 35 min. The total volume of the cell suspensions injected in the sample chamber was 120 μL, and the cell count for each measurement was 1.2×10^5. The heat change measured during the initial 5 min after cell injection was discarded in order to avoid artifacts such as heat of dilution. The results were expressed by columns which represented the total heat output after 35 min incubation. Although the raw data is conventionally expressed by negative values (exothermic heat dissipation), for the sake of clarity the results were plotted as positive values. In the ITC protocol used, the results were recorded after a single injection of cells. Heat release was not recorded during longer periods in order to avoid exposing the cells to hypoxic conditions. Oxygen consumption of the cells was independently monitored using high resolution oxygraphy with Oroboros 2K equipment and oxygen was still available in the chamber after 35 min of experiment (see **Supplementary Figure 1**). The heat production protocol was adapted from de Meis et al. (14). The data were plotted using the inbuilt software Origin 5. The concentrations of inhibitors used in the microcalorimetry experiments are specified in the legends of the figures. All treatments were performed immediately before the start of each experiment.

Mitochondria Preparations

10^6 cells were homogenized with 30 passes in a Potter-Elvehjem homogenizer in ice, in a buffer containing 10 mM Tris-HCl pH 7.4, 0.25 M sucrose, 20 mM NaF and 5 mM EDTA (cell lysis buffer). The homogenates were centrifuged for 5 min at 4°C at 1,000 g. The supernatant was collected and centrifuged for 15 min at 4°C at 10,000 g. The supernatant (cytosolic fraction) was saved and the pellet (mitochondrial fraction) was suspended with the cell lysis buffer. Protein concentration was assayed using the Bradford method. For the microcalorimetry assay, DMEM/F-12 medium without serum was added to both fractions, mitochondrial and cytosolic. For the calorimetry assays of mitochondrial and cytoplasmic preparations heat exchange was normalized for protein concentration.

Western Blotting

Cell pellets were lysed in a Potter-Elvehjem homogenizer in ice during 3 min, in a buffer containing 10 mM Tris-HCl pH 7.4, 0.25 M sucrose, 20 mM NaF and 5 mM EDTA (cell lysis buffer). The homogenates were centrifuged for 5 min at 4°C at 1,000 g. The supernatant was collected and centrifuged for 15 min at 4°C at 10,000 g. The supernatant (cytosolic fraction) was saved and the pellet (mitochondrial fraction) was suspended with the cell lysis buffer. Protein concentration was assayed using the Bradford method. 40 μg of protein extracts were fractionated by standard 10% SDS-PAGE and transferred to nitrocellulose membranes by electro blotting in a buffer consisting of glycine 39 mM, Tris-base 48 mM, SDS 0.037% and methanol 20%. Proteins were detected using primary antibodies diluted in TBS, Tween 20 0.1% and BSA 5%. Mouse primary antibody against human UCP 2 was obtained from Abcam®. The secondary antibody was IRDye 800CW goat anti-mouse immunoglobulin. Bands were visualized in a Li-Cor Odyssey western blot imaging.

Statistical Analysis

Statistical analysis was performed using GraphPad Prism 6 (GraphPad Software, inc.). The results are expressed as mean ± SEM values for n independent experiments. Comparisons between groups were done by one-way ANOVA and *a posteriori* Dunnett's test. When appropriate, unpaired Student's *t*-tests or Mann-Whitney's test were employed. Differences of $p < 0.05$ were considered to be significant.

RESULTS

Metastatic Cells Release More Heat Than Non-metastatic Cells

Intact cells from murine (4C, 4C11− and 4C11+) and human melanoma (WM983A, WM983B and WM852), lung (A549 and NCI-H460), tongue (SCC-9, LN-1 and LN-2) and breast (MCF-7 and MDA-MB-231) were used for the microcalorimetry assay. The results are shown in **Figures 1A–E**. Although individually each type of tumor cell displayed different maxima for heat release, in all cases the cells with the highest metastatic potential (4C11+, WM582, H460, LN-2, and MDA-MB-231) were consistently those displaying the highest absolute values of heat release. The total heat output reflected higher rates of heat release as shown in **Supplementary Figure 2**. These results show that heat release by the different cell lines as measured at 5 min intervals was constant over time although displaying clearly distinct slopes. The cells were kept under oxygen during the experiments as shown in **Supplementary Figure 1**.

The results shown in **Figure 1** indicate that the positive correlation between the metastatic potential and heat release could be extended to several types of tumors (human or murine) with the same parental matrix or not. Whilst additional stable tumor cell lines exhibiting gradients of metastatic potential could have been added to the present list the authors believe that in this initial study a pattern can already be discerned that could be eventually generalized. For the remaining experiments described here only the human SCC tongue carcinoma cells were used. This decision was justified by the fact that with the exception of the murine melanoma cells, all other cell lines were derived from different parental matrixes (WM983B was derived from WM983A, but not WM852). Likewise for the human breast and lung cancer cells display different phylogenies. For example, MCF-7 cells are classified as luminal A, they contain estrogen and progesterone receptors and are considered as p53 wild-type. In contrast, the highly invasive MDA-MB-231 cells are classified as claudin-low (claudins are major integral membrane proteins of tight junctions), triple negative (ER^-, PR^-, and $HER2^-$) and bear mutations on p53 (15), i.e., the two cell lines constitute altogether different cell types bearing different traits. Thus, for the sake of validating the comparative analysis of parameters relating to the functional aspects associated to the transition to metastasis along the same cell line, the subsequent experiments were conducted exclusively with the tongue squamous carcinoma cells (LN-1 and LN-2) since both were derived from SCC-9

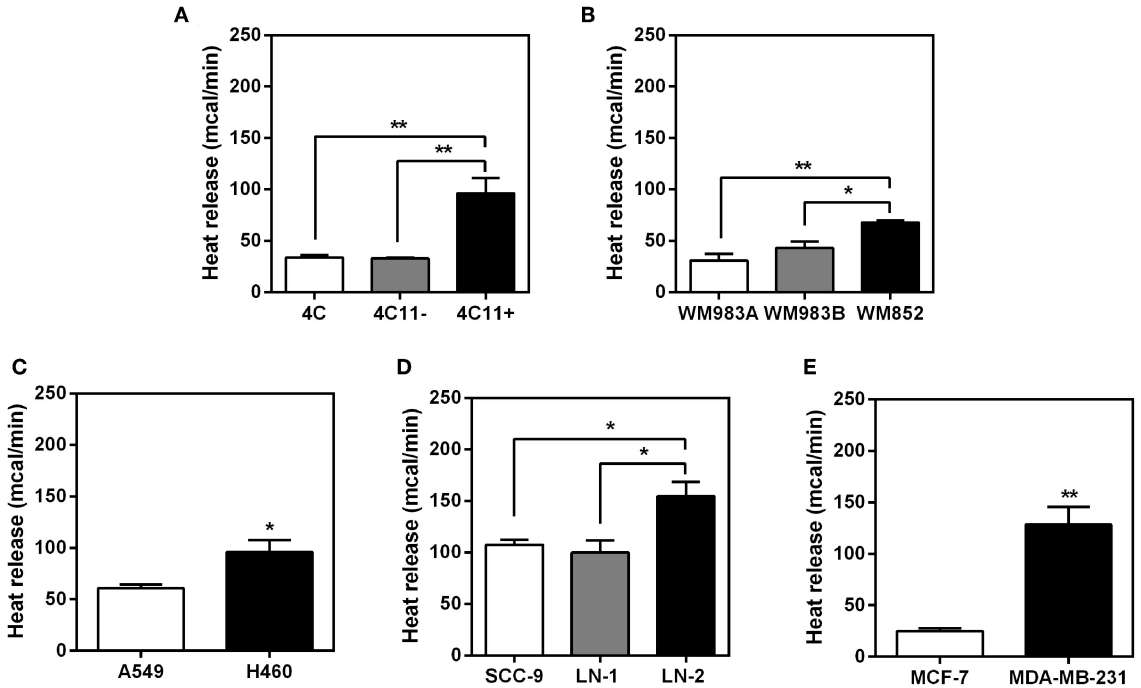

FIGURE 1 | Heat release by different types of intact tumor cells.The bars represent the release of total heat of living cells in 35 min of experiment. Bars: white—non-metastatic tumor cells; gray - cells with intermediate metastatic potential; black - cells with high metastatic potential. **(A)** Murine melanoma cells 4C, 4C11− and 4C11+; **(B)** human melanoma cells WM983A, WM983B and WM852; **(C)** human non-small-cell lung adenocarcinoma cells A549 and H460; **(D)** human oral squamous carcinoma cells SCC-9, LN-1 and LN-2; **(E)** human breast cancer cells MCF-7 and MDA-MB-231. Values were expressed as mean ± SEM. $^{*}p < 0.05$; $^{**}p < 0.01$.

cells after successive rounds of inoculation and recovery from lymph nodes (6). In attempt to mimic tumor organization *in vivo*, experiments were also conducted with 3D culture of tongue squamous carcinoma cells. **Supplementary Figure 3** shows that the pattern of higher heat release in the metastatic cells LN-2 is maintained when compared to the heat released by the non-metastatic cells SCC-9. In LN-1 there was an increase in heat release when grown in spheroid.

Suppression of MAGEA10 Reduces Heat Release by Tumor Cells

Thus, we tested next whether the thermogenic differences observed in **Figure 1** could be affected by the suppression of a protein that knowingly mediates adhesive properties of the LN cells. In a previous publication we have demonstrated that protein MAGEA10, which is highly expressed in metastatic cells, was involved in both, adhesion and motility of LN cells (12). Therefore, we carried out microcalorimetry experiments with LN cells stably suppressed for MAGEA10. The results are shown in **Figures 2A,B**. In both cell lines, LN-1 and LN-2, suppression of MAGEA10 (shMAGEA10) led to a significant reduction in heat release (**Figures 2A,B**). Although the reduction was more pronounced in LN-2 cells these were still more thermogenic than shMAGEA10 LN-1 cells (compare **Figures 2A,B**) a result which is compatible with the data shown in **Figure 1**. Also, suppression of MAGEA10 in both cell lines yields lower heat release than in untreated control SCC-9 cells. The differences in calorimetry measured between LN-1 and shMAGEA10 LN-1 and LN-2 and shMAGEA10 were ∼60 mcal and 75 mcal, respectively, measured after 35 min. It is known that the movement of cells is driven by the continuous polymerization and reorganization of actin cytoskeleton (16). Following the same reasoning, we measured the heat release of metastatic cells (LN-1 and LN-2) in the presence of cytochalasin D, an actin polymerization inhibitor. As shown in **Figure 3**, cytochalasin D reduced heat release in both cells and more markedly in LN-2 (**Figure 3B**). Together, the results shown in **Figures 2**, **3** suggest that a link exists between proteins involved in adhesion and motility and the thermogenic behavior of LN cells.

RNA and Protein Expression of UCP2 by Tumor Cells

An uncoupled protein (UCP) is a mitochondrial inner membrane protein that can dissipate energy in the form of heat during proton translocation (17). Nevertheless, to investigate this possibility we carried out experiments measuring the expression of uncoupling protein 2 (UCP2) by these cell lines. The results are shown in **Figures 4A–C**. UCP2 expression of LN-1 and LN-2 cells was much higher than SCC-9 cells (red dashed lines). Although UCP2 expression as shown by mRNA contents did not vary significantly when LN-1 and LN-2 cells were compared, the western blots shown in **Figure 4C** indicate that in LN-1 cells UCP2 protein was more abundant. A higher amount of translated protein doesn't necessarily mean higher

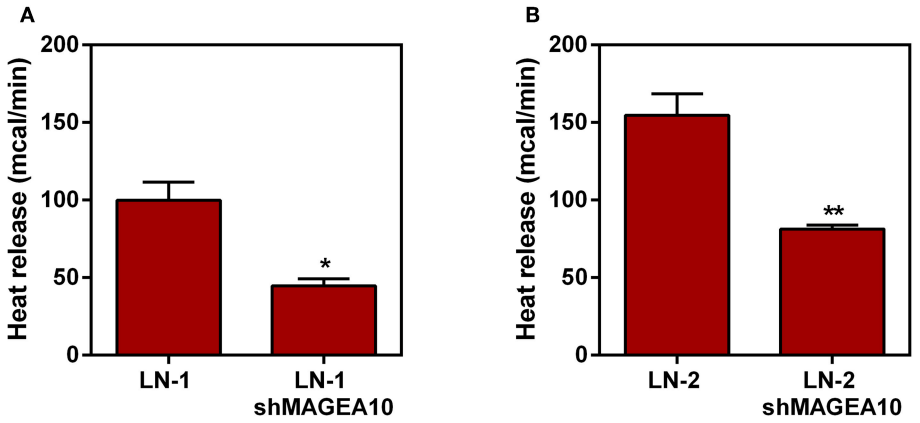

FIGURE 2 | Heat release by human oral squamous carcinoma cells LN-1 and LN-2 suppressed for MAGEA-10 expression (shMAGEA10). The bars represent the release of total heat of living cells in 35 min of experiment. **(A)** LN-1 and LN-1 shMAGEA10 cells; **(B)** LN-2 and LN-2 shMAGEA10 cells. Values were expressed as mean ± SEM. $^{*}p < 0.05$; $^{**}p < 0.01$.

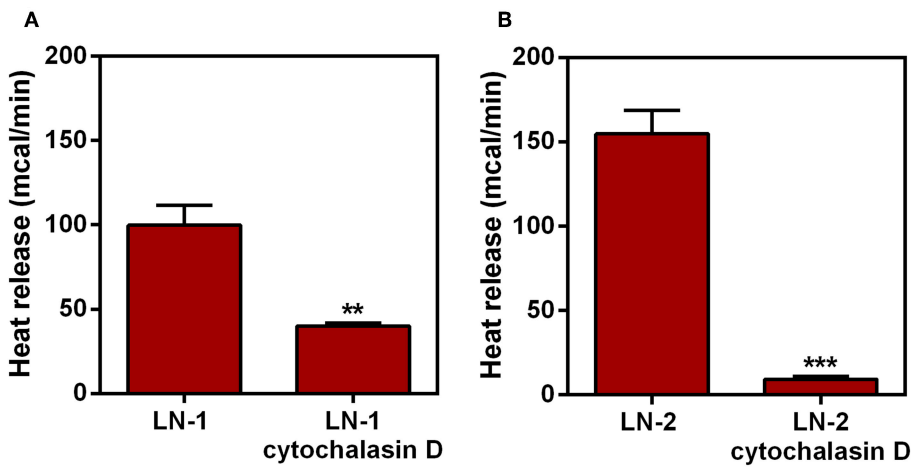

FIGURE 3 | Effect of cytochalasin D on heat release by human oral squamous carcinoma cells LN-1 and LN-2. The bars represent the release of total heat of living cells in 35 min of experiment. **(A)** Heat release by LN-1 cells untreated and treated with cytochalasin D 2 mg/mL; **(B)** heat release by LN-2 cells untreated and treated with cytochalasin D 2 mg/mL. Values were expressed as mean ± SEM. $^{**}p < 0.01$; $^{***}p < 0.001$.

activity. Additionally, **Supplementary Figure 3** shows that UCP2 expression is much higher in 3D cultures than in monolayers a result that reinforces the idea that the spatial geometry of the cultures has a considerable effect on the protein transcription. The results in **Figure 4B** show that in LN-1 shMAGEA10 cells, expression of UCP2 is significantly different from that of control pLKO cells containing a scrambled insert (red dashed line). In contrast, in LN-2 shMAGEA10 cells, there was a reduction of more than 50% in the mRNA expression of UCP2, again corroborating the results shown in **Figures 2**, **3** and reinforcing the hypothesis that adhesive/motility properties of LN-2 cells may be connected to heat dissipation.

Effect of Genipin on Heat Release by Tumor Cells

Additional evidence of the contribution of UCP2 to overall heat generation was obtained from experiments in which genipin was incubated with the intact cells followed by the microcalorimetry assay. Genipin is an aglycone that is readily incorporated by cells and acts as an inhibitor of mitochondrial enzyme uncoupling protein 2 (18, 19). The results are shown in **Figures 5A–C**. Whereas, genipin treatment did not significantly affect SCC-9 cells (**Figure 5A**), in both LN-1 and LN-2 cells, genipin promoted a clear inhibitory effect on heat release, particularly by LN-2 cells. The fact that genipin has no apparent effect on SCC-9 cells may be relevant to the result shown in **Figure 4C** which demonstrated that these cells do not synthesize UCP2. Thus, UCP2 mediated uncoupling may be a feature of metastatic cells. The differences in calorimetric measurements between treated and untreated LN-1 cells were 60 mcal (**Figure 5B**) and 90 mcal for LN-2 cells (**Figure 5C**) measured after 35 min. Taken at face value, the results in **Figure 5** indicate that UCP2 has a role in the process of thermogenesis in metastatic cells.

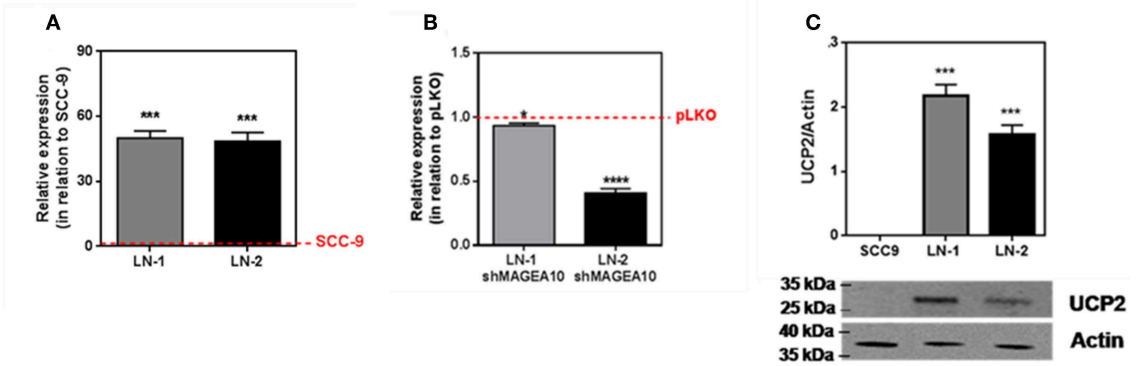

FIGURE 4 | UCP2 mRNA and protein expression in human oral squamous carcinoma cells SCC-9, LN-1 and LN-2. **(A)** UCP2 mRNA levels in LN-1 and LN-2 cells relative to SCC-9 cells; **(B)** mRNA expression levels of UCP2 in cells supressed relative to pLKO. SCC-9 and pLKO (red line), LN-1 (gray bar) and LN-2 (black bar). **(C)** Protein levels of UCP2 in cells grown as monolayers quantified from the western blot shown in the inset. The values were expressed in relation to the red dashed lines. Values were expressed as mean ± SEM. $^{*}p < 0.05$; $^{***}p < 0.001$; $^{****}p < 0.0001$.

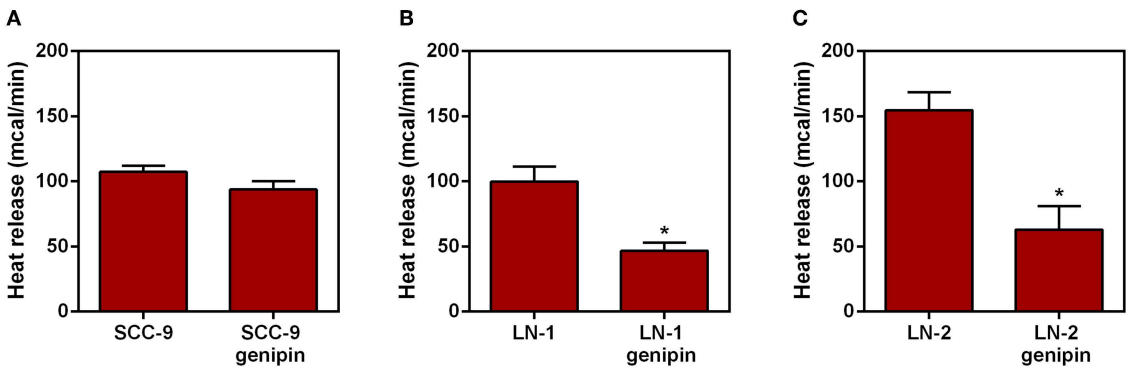

FIGURE 5 | Effect of genipin on the heat release by human oral squamous carcinoma cells SCC-9, LN-1 and LN-2 cells.The bars represent the release of total heat of living cells in 35 min of experiment. **(A)** Heat release by SCC-9 cells untreated and treated with 50 μM of genipin; **(B)** heat release by LN-1 cells untreated and treated with 50 μM of genipin; **(C)** heat release by LN-2 cells untreated and treated with 50 μM of genipin. Values were expressed as mean ± SEM. $^{*}p < 0.05$.

Effect of Oligomycin on Heat Release by Tumor Cells

The ATP synthase is a mitochondrial enzyme localized in the inner membrane that translocates protons (like UCP2). This proton translocation allows ATP synthesis from ADP (20). To verify whether the heat release observed in UCP2 modulation is related to proton translocation experiments were performed in which the intact cells were treated with oligomycin (2 μg/mL), a classical inhibitor of mitochondrial ATP synthase (21). The results are shown in **Figure 6**. LN-1 cells have a comparatively smaller inhibitory effect when compared to oligomycin treated LN-2 cells. Only LN-2 has significant reduction in heat release when treated with oligomycin (**Figure 6C**). The approximate difference between oligomycin treated samples and control were 25 mcal for SCC-9 control vs. oligomycin treatment, 40 mcal for LN-1 control vs. oligomycin treatment and 80 mcal for LN-2 control and oligomycin treatment, measured after 35 min. Oligomycin dependent reduction of thermogenesis in LN-2 cells is due to the binding of the antibiotic to the F_O portion of the mitochondrial F_O/F1 ATPase. Prevention of proton flow back into the mitochondrial matrix may have thus reduced heat release. Conversely, in untreated LN-2 cells (**Figure 6C**) gradient derived proton flow into the matrix was unimpeded and thus promoted a higher heat release.

Mitochondrial Enriched Extract From Metastatic Cells Are More Thermogenic Than Mitochondrial Extract From Non-metastatic Cells

Next we investigated which organelles were involved in the thermogenesis of LN cells. Assuming that both UCP2 and ATP synthase are mitochondrial proteins and that inhibit their inhibition could cause a significant reduction on heat release by the metastatic cells LNs (**Figures 5**, **6**) it is reasonable to assume that mitochondria may play a role in view of their central function in cell energy conversion. The next experiments were conducted with mitochondrial enriched and cytosolic extracts

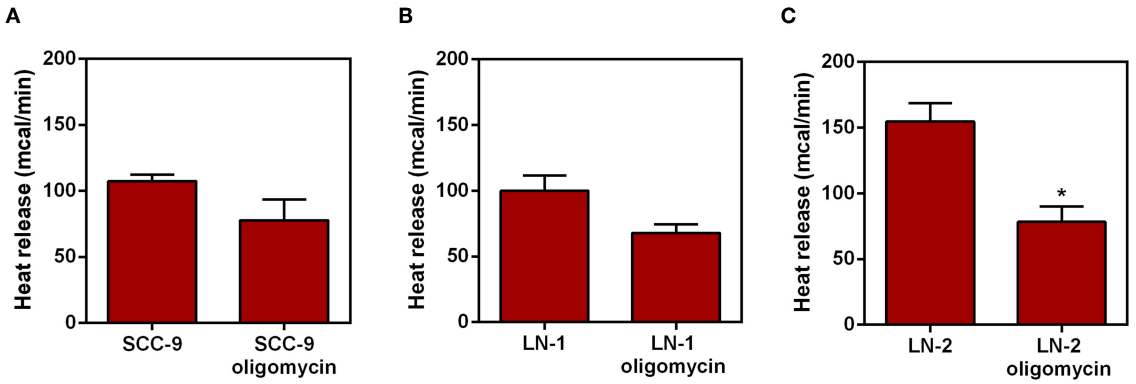

FIGURE 6 | Effect of oligomycin on heat release by human oral squamous carcinoma cells SCC-9, LN-1 and LN-2. The bars represent the release of total heat of living cells in 35 min of experiment. **(A)** Heat release by SCC-9 cells untreated and treated with oligomycin 2 μg/mL; **(B)** heat release by LN-1 cells untreated and treated with oligomycin 2 μg/mL. **(C)** Heat release by LN-2 cells untreated and treated with oligomycin 2 μg/mL. Values were expressed as mean ± SEM. $^*p < 0.05$.

obtained by differential centrifugation. The results are shown in **Figure 7**. In **Figure 7A**, it can be seen that as far as LN cells are concerned the same heat release pattern observed in **Figure 1** is reproduced, i.e., isolated mitochondria from the cells with the highest metastatic potential (LN-2) were also found to be the most thermogenic. In contrast, the results in **Figure 7B** showed that cytosolic extracts exhibited considerably less heat release than the mitochondrial extracts. Nevertheless, LN-2 cytosolic extracts were still more thermogenic than SCC-9 and LN-1 extracts. The relatively small difference observed in **Figure 7B** could be due to exothermic interactions occurring in the cytosol that are exclusive to the LN-2 cells. The LN-2 cytosolic protein network may be more complex and such interactions may reflect this high heat release. **Figures 7C,D** show that there were no differences in heat release between SCC-9 mitochondrial and cytosolic extracts, as well as between LN-1 mitochondrial and cytosolic extracts. The highest difference was observed when LN-2 mitochondrial and cytosolic extracts were compared (**Figure 7E**). The results in **Figure 7** indicate that mitochondria could have been partially responsible for the thermogenic behavior of LN-2 cells.

Effect of Etomoxir on Heat Release by Tumor Cells

A link between UCP2 and fatty acid catabolism and transport has already been suggested (19). Prompted by this we then tested whether etomoxir, an inhibitor of the enzyme carnitine palmitoyl transferase-1 (CPT1), had any effect on the heat release by SCC-9 and LN-2 cells. The results are shown in **Figure 8**. Whereas, 300 μM etomoxir discreetly affected heat release by SCC-9 and LN-1cells (**Figures 8A,B**), the effect of the inhibitor on LN-2 cells was quite pronounced (**Figure 8C**). Etomoxir produced a reduction of ∼110 mcal, a result which not only confirms that mitochondria are accessory to the thermogenic profile of metastatic cells, but also that this involves the participation of fatty acid oxidation on the energy metabolism of LN-2 cells. Reduced thermogenesis caused by 300 μM etomoxir could not be attributed to harmful effects on the cells, since neither LDH release nor the MTT viability assays (**Supplementary Figures 4A,B**) indicated cytotoxicity.

DISCUSSION

Isothermal titration calorimetry is a powerful and versatile technique that has been used extensively in chemistry and biology to measure thermodynamic parameters such as enthalpy, Gibbs free energy and binding affinities in chemical reactions and enzyme kinetics. Albeit not so numerous, the applications of ITC have gone beyond binary ligand reactions and also included the study of whole living cells. Thus, microcalorimetry studies have been applied to microorganisms (22–24) and to cells and tissues slices (25). When studying the interactions of biomolecules in solution the titration relies mainly on multiple injections of the samples, whereas with whole cells, single injections may be the method of choice (26). This was the approach utilized here.

Our results (**Figure 1**) showed that in several types of cancer a direct correlation existed between malignancy and total heat released. This observation supports the proposal that tumor cells do indeed display a reprogrammed metabolism and that metastasis might resort to metabolic pathways that supply extra energy to enable processes such as increased motility and invasiveness. The results described here obtained with cell suspensions are in agreement with the pioneering work of Kallerhoff et al. (27) who measured heat release of tissue samples from the human urogenital tracts, including prostate, bladder, kidney and testicular tissue. Kallerhoff et al. showed that it was possible to differentiate normal from tumor cells, although they could only speculate that the difference found may have been attributable to a higher metabolic activity.

As we observed this increase in heat release exclusively in metastatic cell lines among the different tissues used (**Figure 1**), we decided to investigate what would be the interference, an

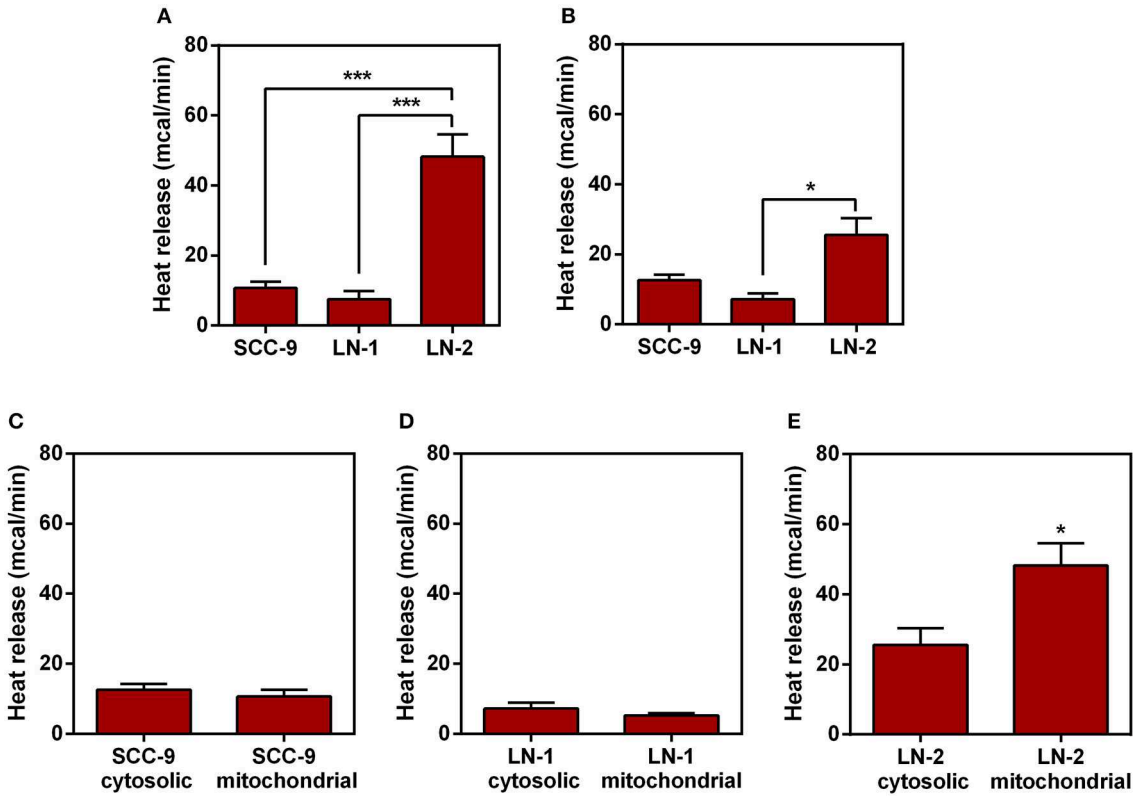

FIGURE 7 | Comparison of heat release by protein extracts enriched with mitochondrial or cytoplasmic fractions.The protein extracts were obtained from human oral squamous carcinoma cells SCC-9, LN-1 and LN-2. The bars represent the release of total heat of protein extracts in 35 min of experiment. **(A)** Protein extracts enriched with mitochondrial fraction of SCC-9, LN-1 and LN-2; **(B)** protein extracts enriched with cytoplasmic fraction of SCC-9, LN-1 and LN-2; **(C)** protein extracts enriched with mitochondrial and cytoplasmic fractions of SCC-9 cells; **(D)** protein extracts enriched with mitochondrial and cytoplasmic fractions of LN-1 cells; **(E)** protein extracts enriched with mitochondrial and cytoplasmic fractions of LN-2 cells. Values were expressed as mean ± SEM. $^{*}p < 0.05$; $^{***}p < 0.001$.

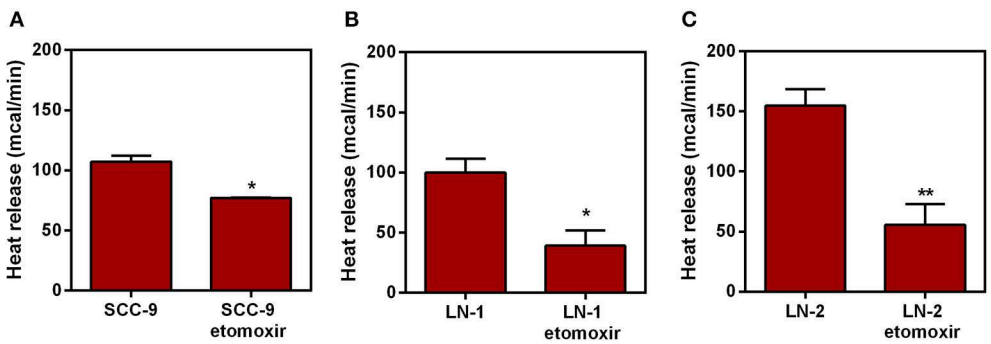

FIGURE 8 | Effect of etomoxir on the heat release by human oral squamous carcinoma cells SCC-9, LN-1 and LN-2 cells. The bars represent the release of total heat of living cells in 35 min of experiment. **(A)** Heat release by SCC-9 cells untreated and treated with 300 μM of etomoxir; **(B)** Heat release by LN-1 cells untreated and treated with 300 μM of etomoxir. **(C)** Heat release by LN-2 cells untreated and treated with 300 μM of etomoxir. Values were expressed as mean ± SEM. $^{*}p < 0.05$; $^{**}p < 0.01$.

increase of enthalpy, modulating MAGEA10, a protein closely related to the metastatic characteristics of tongue squamous carcinoma cells as shown in a paper by our group (12). Silencing this protein promotes a significant reduction in heat release (**Figure 2**), particularly in LN-2 cells. In addition to adhesion/motility, a contribution from MAGEA10 proteins and other members of the MAGE family could be selected. For example, MAGE proteins are known to be assembled with E3 RING ubiquitin alloys to form MAGE-RING alloys (MRLs) that function in many cell lines, including tumor cell proliferation (28) and total heat production. As shown in a previous paper (12), by silencing MAGEA10 in LN-1 and LN-2 cells, we observed

a reduction as measured by migration and invasion. Indeed, by inhibiting the polymerization of the actin with cytochalasin D, we observed a smaller heat release, especially in the more aggressive cell line (**Figure 3**). It has been previously shown that cytochalasin D effect, on cell migration, can be an antitumor mechanism (29). From this, we can infer that the low heat release observed in the LN-2 cell line, both in MAGEA10 silencing and cytochalasin D treatment, may be linked to the loss of metastatic characteristics such as migration and invasion (12, 30, 31).

In an attempt to investigate the heat source, we analyzed the expression of uncoupling proteins in tongue squamous cancer cell lines. The family of UCPs, mainly UCP2 and UCP3, is known to have a direct relationship with thermogenic signals from recurrent biochemical reactions within mitochondria, such as fatty acid oxidation (32, 33). Thus, in addition to the fact that UCP2 has a different expression in different tissues, it has been implicated as an enhancer of endothelial cell resistance to oxidative stress (34). As well as having a role in metabolic reprogramming in skin epidermal cells (35). Taken together, these results reinforce the correlation between UCP2 and metastasis (36). Our data shown that LN-1 and LN-2 cells have high UCP2 expression when compared to SCC-9 (**Figures 4A–C**). Furthermore, the silencing of MAGEA10 led to a significant reduction in UCP2 expression in the most metastatic line (**Figure 4B**). In **Figures 1**, **2**, we observe that the increase in heat release is accompanied by a high expression of UCP2 in LN-2. Additionally, the reduction in thermogenesis, when LN-2 is silenced to MAGEA10, is accompanied by a low expression in the UCP2 gene in this cell line. These results suggest that this uncoupling protein plays an important role in the thermogenic levels of metastatic cells of tongue squamous carcinoma. This interpretation was consistent with the results shown in **Figure 5**, which show that UCP2 inhibitor genipin significantly reduced the heat released by LN-1 and LN-2 cells, but not by SCC-9 cells. Notwithstanding this observation, it should be mentioned that genipin is known to have other effects than UCP2 inhibition. This includes anti-proliferative actions on tumor cells (37). Genipin has also been shown to be a water soluble crosslinking agent (38). Given the last one property of genipin, it would not be surprising to observe a reduction in heat release promoted by the inhibitor, since interactions between polymers are generally exothermic. Since no genipin effect was observed in SCC-9, a cell line that not expressing UCP2 (**Figure 4C**). It is plausible that the reduction in heat release observed in LN-1 and LN-2 does not occur due to the possible non-specific effects of genipin.

Considering the possible interference of UCP2 in thetermogenic mechanism of metastatic cells, we directed our investigation in order to find the major source of this heat released. As UCP2 is a mitochondrial uncoupling protein, we evaluated the heat released by this organelle. The results shown in **Figure 7** confirmed that preparations cell-free extracts enriched in mitochondria were more thermogenic than cytosolic extracts and that mitochondria obtained from the more aggressive LN-2 cells were also more thermogenic than mitochondria from LN-1 and SCC-9 cells. Whilst those results substantiated the idea that mitochondria may be responsible, at least partially, for the heat output of the metastatic cells, it must be mentioned that the heat released by the isolated organelles may differ from that measured in intact cells. Ideally the comparison should be conducted by measuring the absolute thermal contribution of mitochondria within the cellular milieu. Thus, our data point to a possible mitochondrial contribution in metastatic cell thermogenesis. Although there is little information, thus contributing to cell migration, about mitochondrial regulation

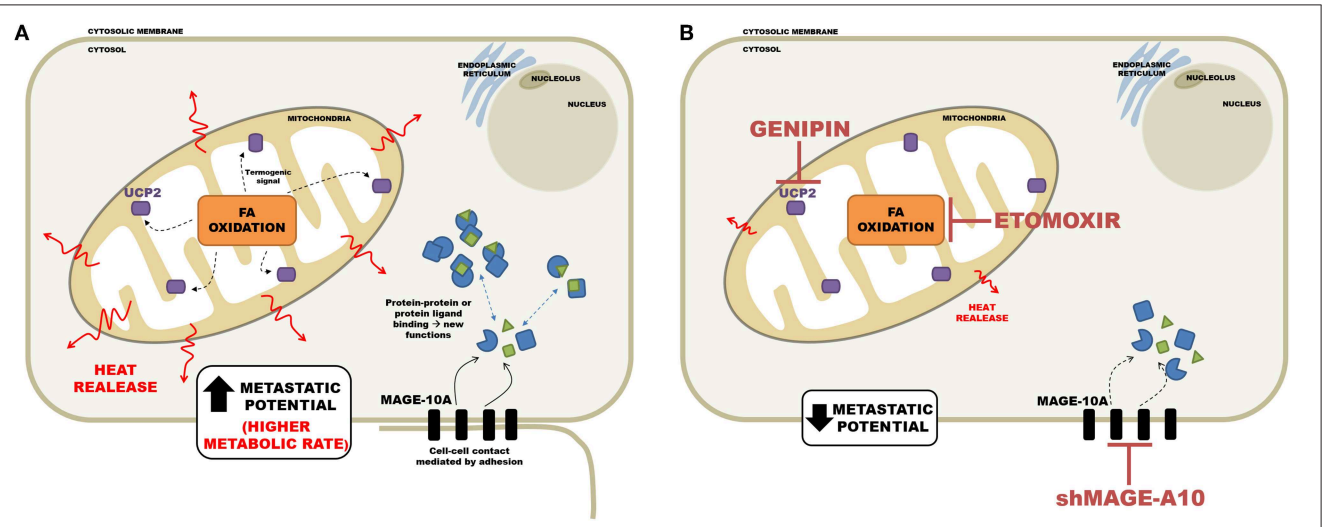

FIGURE 9 | Schematic representation of the relationship between metastatic potential and heat release in the tumor cell. **(A)** Cell with high metastatic potential has important proteins for regulating functioning cell-cell interaction and migration, such as MAGEA10; as well as an active mitochondria, the communication between β-oxidation and high levels of UCP2, resulting in a high thermogenesis. **(B)** Silencing of MAGEA10 and/or pharmacological inhibition of UCP2 and CPT1-A, results in less heat release. This suggests an important participation of these proteins in thermogenesis.

of migration, it is known that this organelle can interact closely with the endoplasmic reticulum to perform Ca^{2+} signaling, aiding in the mechanism of metastatic cell migration (39, 40). It has been reported that the AMPK pathway may participate in the mechanical transduction of motility events in breast cancer cells such as MDA-MB-231 (41). Thus, we can suggest that the high release of heat energy by mitochondria may help the migratory/invasive potential of the most aggressive cell lines.

Therefore, aware of the high heat release in mitochondrial extracts, and the high regulation of UCP2 through more or less intense thermogenic signals from fatty acid oxidation in mitochondria (32, 33), we analyzed the interference of β-oxidation inhibition on the global heat release of cell lines. Our data showed that when treated with etomoxir, the cell lines were less thermogenic (**Figure 8**), with the most dramatic reduction in LN-2. By further investigating the metabolism of tongue squamous carcinoma cells, the results presented here extend our previous work (42) and reinforce the idea that metastatic cells extract the excess energy from mitochondrial pathways, particularly by channeling ATP from fatty acid oxidation. Similar results were obtained by our group using melanoma (43) and human breast cancer cells (44). It is conceivable that the role of lipid metabolism in metastasis involves not only energy production but also that of a building block supplier for membrane biogenesis. Metabolic pathways involving fatty acid can also generate signaling lipids (45, 46). Our own results, using high-resolution oxygen, confirmed the implication of lipid metabolism in metastasis. A comparative analysis of mouse melanoma cells exhibiting different degrees of metastatic potential showed that fatty acid oxidation was significantly increased in the more aggressive cell lines (43). In addition, metabolomic analysis of LN-2 cells showed that they were able to accumulate among other metabolites, malonate, methyl malonic acid, n-acetyl, and unsaturated fatty acids (CH_2) n (42). Reprograming of lipid metabolism of tumor cells may promote cell migration (47, 48), suggesting that mitochondrial fatty acid metabolism could serve as the energy base for regulating migration processes that are important for metastasis.

In conclusion the diagram in **Figure 9** summarizes the main findings of this work and shows the main regulatory events in metastasis. The isothermal titration microcalorimetry approach used in the present work afforded a non-invasive, real-time, sensitive way to assess the net energy output of living tumor cells. We argue that the data presented here reflected mainly the summation of enthalpies related to metabolic rates and that mitochondrial metabolism may occupy a central role in sustaining the malignant phenotype.

DATA AVAILABILITY STATEMENT

The datasets generated for this study are available on request to the corresponding author.

AUTHOR CONTRIBUTIONS

DL, TO, LM, and VA performed the experiments. MR contributed to cell culture. LK supervised the microcalorimetry experiments. FR conceived the experiments, coordinated the project, and wrote the manuscript.

FUNDING

This work was supported by CNPq (304106/2014-3), FAPERJ [E-26/201.251/2014 (204500)], CAPES and Fundação do Câncer (Project: The bioenergetics of the metastatic process—Edital de pesquisa Programa de Oncobiologia 2017).

ACKNOWLEDGMENTS

The authors are grateful to Bruna dos Santos Mendonça for the kind gift of LN cells containing the MAGEA10 mRNA short hairpin lentiviral particles constructs and Jéssica Mari Kawashima for the assistance in some experiments. The authors also wish to acknowledge Dr. Elizabeth A. Blackburn (University of Edinburgh) and Dr. Theo Luiz Ferraz de Souza (Federal University of Rio de Janeiro) for their critical opinions and expert advice during the preparation of the manuscript. The authors are indebted to Prof. Vivian Rumjanek for the help in revising the manuscript and suggestions regarding interpretation of the results and discussion.

SUPPLEMENTARY MATERIAL

The Supplementary Material for this article can be found online at: https://www.frontiersin.org/articles/10.3389/fonc.2019.01430/full#supplementary-material

REFERENCES

1. Porporato PE, Payen VL, Perez-Escuredo J, De Saedeleer CJ, Danhier P, Copetti T, et al. A mitochondrial switch promotes tumor metastasis. *Cell Rep.* (2014) 8:754–66. doi: 10.1016/j.celrep.2014.06.043
2. Maiuri MG, Kroemer G. Essential role for oxidative phosphorylation in cancer progression. *Cell Metab.* (2015) 21:11–2. doi: 10.1016/j.cmet.2014.12.013
3. Moreno-Sanchez R, Hernández-Marin A, Saavedra E, Pardo JP, Ralph SJ, Rodriguez-Enriquez S. Who controls the ATP supply in cancer cells? Biochemistry lessons to understand cancer energy metabolism. *Int J BiochemCellBio.* (2014) l50:10–23. doi: 10.1016/j.biocel.2014.01.025
4. Moreno-Sanchez R, Saavedra E, Gallardo-Perez J, Rumjanek FD, Rodriguez-Enriquez S. Understanding the cancer cell phenotype beyond the limitations of current omics analyses. *FEBS J.* (2016) 283:54–73. doi: 10.1111/febs.13535
5. Lincet H, Icard P. How do glycolytic enzymes favour cancer cell proliferation by nonmetabolic functions? *Oncogene.* (2015) 29:3751–9. doi: 10.1038/onc.2014.320
6. Agostini M, Almeida LY, Bastos DC, Ortega RM, Moreira FS, Seguin F, et al. The fatty acid synthase inhibitor orlistat reduces the growth and metastasis of orthotopic tongue oral squamous cell carcinoma. *Mol Cancer Therap.* (2014) 13:585–95. doi: 10.1158/1535-7163.MCT-12-1136
7. Trika M, Timar J, Lundy SK, Szekeres K, Caim Porter YAT, Hohnn KV. The high affinity αIIβ3 integrin is involved in invasion of human melanoma cells. *Cancer Res.* (1997) 57:2522–8.

8. Oba-Shinjo SM, Correa M, Ricca TI, Molognoni F, Pinhal MA, Neves IA, et al. Melanocyte transformation associated with substrate adhesion impediment. *Neoplasia*. (2006) 8:231–41. doi: 10.1593/neo.05781
9. Freshney RI. *Culture of Animal Cells: A Manual of Basic Techniques and Specialized Applications 7th ed*. Glasgow: Wiley (2016).
10. Mosmann T. Rapid colorimetric assay for cellular growth and survival: application to proliferation and cytotoxicity assays. *J Immunol Methods*. (1983) 65:55–63. doi: 10.1016/0022-1759(83)90303-4
11. Korzeniewski C, Callewaert DM. An enzyme-release assay for natural cytotoxicity. *J Immunol Methods*. (1983) 64:313–20. doi: 10.1016/0022-1759(83)90438-6
12. Mendonça BDS, Agostini M, Aquino IG, Dias WB, Bastos DC, Rumjanek FD. Suppression of MAGE A-10 alters the metastatic phenotype of tongue squamous cell carcinoma cells. *BiochemBiophys Rep*. (2017) 10:267–73. doi: 10.1016/j.bbrep.2017.04.009
13. Livak K J, Schmittgen TD. Analysis of relative gene expression data using real-time quantitative PCR and the 2(-Delta DeltaC(T)) method. *Methods*. (2001) 25:402–8. doi: 10.1006/meth.2001.1262
14. de Meis L, Ketzer LA,Costa RM, Andrade IR, Benchimol M. Fusion of the endoplasmic reticulum and mitochondrial outer membrane in rats brown adipose tissue: activation of thermogenesis by Ca^{2+}. *PLoS ONE*. (2010) 5:e9439. doi: 10.1371/journal.pone.0009439
15. Holliday DL, Speirs V. Choosing the right cell line for breast cancer research. *Breast Cancer Res*. (2011) 13:215. doi: 10.1186/bcr2889
16. Blanchoin L, Boujemaa-Paterski R, Sykes C, Plastino J. Actin dynamics, architecture, and mechanics in cell motility. *Physiol Rev*. (2014) 94:235–63. doi: 10.1152/physrev.00018.2013
17. Bouillaud F, Alves-Guerra MC, Ricquier D. UCPs, at the interface between bioenergetics and metabolism. *BiochimBiophys Acta*. (2016) 1863:2443–56. doi: 10.1016/j.bbamcr.2016.04.013
18. Pitt MA. Overexpression of uncoupling protein-2 in cancer: metabolic and heat changes, inhibition and the effects on drug resistance. *Immunopharmacology*. (2015) 23:365–9. doi: 10.1007/s10787-015-0250-3
19. Chaudhuri L, Srivastava RK, Kos F, Shrikant PA. Uncoupling protein 2 regulates metabolic reprogramming and fate of antigen-stimulated CD8+ T cells. *Cancer Immunol Immunother*. (2016) 65:869–74. doi: 10.1007/s00262-016-1851-4
20. García-Aguilar A, Cuezva JM. A review of the inhibition of mitochondrial ATP synthase by IF1 *in vivo*: reprogramming energy metabolism and inducing mitohormesis. *Front Physiol*. (2018) 9:1322. doi: 10.3389/fphys.2018.01322
21. Lardy HA. Antibioticinhibitors of mitochondrial energy transfer. *Pharmacol Ther*. (1980) 11:649–60. doi: 10.1016/0163-7258(80)90044-3
22. Vine GJ, Bishop AH. The analysis of microorganisms by microcalorimetry in the pharmaceutical industry. *Curr Pharm Biotechnol*. (2005) 6:223–38. doi: 10.2174/1389201054022878
23. Zaharia DC, Muntean AA, Popa MG, Steriade AT, Balint O, Micut R, et al. Comparative analysis of Staphylococcus aureus and Escherichia coli microcalorimetric growth. *BMC Microbiol*. (2013) 13:171. doi: 10.1186/1471-2180-13-171
24. Solokhina A, Brückner D, Bonkat G, Braissant O. Metabolic activity of mature biofilms of Mycobacterium tuberculosis and other non-tuberculous mycobacteria. *Sci Rep*. (2017) 7:9225. doi: 10.1038/s41598-017-10019-4
25. Nässberger L. *In vitro* measurements of heat production rate of rat kidney. A microcalorimetric study. *Res Exp Med*. (1990) 190:193–201. doi: 10.1007/PL00020022
26. Silva-Alves JM, Mares-Guia TR, Oliveira JS, Costa-Silva SS, Bretz PCR, Araújo SS, et al. Glucose-induced heat production, insulin secretion and lactate production in isolated Wistar rat pancreatic islets. *Thermochimica Acta*. (2008) 474:67–71. doi: 10.1016/j.tca.2008.04.010
27. Kallerhoff M, Karnebogen M, Singer D, Dettenbach A, Gralher U, Ringert RH. Microcalorimetric measurements carried out on isolated tumorous and nontumorous tissue samples from organs in the urogenital tract in comparison to histological and impulse-cytophotometric investigation. *Urol Res*. (1996) 24:83–91. doi: 10.1007/BF00431084
28. Lee AK, Potts PR. A comprehensive guide to the MAGE family of ubiquitin ligases. *J Mol Biol*. (2017) 429:1114–2. doi: 10.1016/j.jmb.2017.03.005
29. Huang J-L, Dai H-F, Wang H, Yu L, Mei W-L. Cytotoxic active metabolites from endophytic fungus S15 From Hainan Plum-Yew (*Cephalotaxus hainanensis*). *J Microbiol*. (2010) 30:10–14.
30. Cooper JA. Effects of cytochalasin and phalloidin on actin. *J Cell Biol*. (1987) 105:1473–8. doi: 10.1083/jcb.105.4.1473
31. Kustermans G, Piette J, Legrand-Poels S. Actin-targeting natural compounds as tools to study the role of actin cytoskeleton in signal transduction. *Biochem Pharmacol*. (2008) 76:1310–22. doi: 10.1016/j.bcp.2008.05.028
32. Li LX, Skorpen F, Egeberg K, Jörgensen IH, Grill V. Induction of uncoupling protein 2 mRNA in beta-cells is stimulated by oxidation of fatty acids but not by nutrient oversupply. *Endocrinology*. (2002) 143:1371–7. doi: 10.1210/endo.143.4.8717
33. Brand MD, Esteves TC. Physiological functions of the mithocondrial uncoupling proteins UCP2 and UCP3. *Cell Metabolism*. (2005) 2:85–93. doi: 10.1016/j.cmet.2005.06.002
34. Koziel A, Sobieraj L, Jarmuszkiewicz W. Increased activity of mitochondrial uncoupling protein 2 improves stress resistance in cultured endothelial cells exposed in vitro to high glucose levels. *Am J Physiol Heart CircPhysiol*. (2015) 309:H147–56. doi: 10.1152/ajpheart.00759.2014
35. Sreedhar A, Cassell T, Smith P, Lu D, Nam HW, Lane AN, et al. UCP2 overexpression redirects glucose into anabolic metabolic pathways. *Proteomics*. (2018) 19:e1800353. doi: 10.1002/pmic.201800353
36. Jaburek M, Miyamoto S, Mascio P, Garlid KD, Jezek P. Hydroperoxy fatty acid cycling mediated by mitochondrial uncoupling protein UCP2. *J Biol Chem*. (2004) 279:53097–102. doi: 10.1074/jbc.M405339200
37. Shanmugan MK, Shen H, Tang FR, Arfuso F, Rajesh M, Wang L, et al. Potential role of genipin in cancer therapy. *Pharmacol Res*. (2018) 133:195–200. doi: 10.1016/j.phrs.2018.05.007
38. Manickam B, Sreedharan R, Elumalai M. 'Genipin'- the natural watersoluble cross-linking agent and its importance in the modified drug delivery systems: an overview. *Curr Drug Deliv*. (2014) 11:139–45. doi: 10.2174/15672018113106660059
39. Tsai FC, Seki A, Yang HW, Hayer A, Carrasco S, Malmersjö S, et al. A polarized Ca2+, diacylglycerol and STIM1 signalling system regulates directed cell migration. *Nat Cell Biol*. (2014) 16:133–44. doi: 10.1038/ncb2906
40. Romero-Garcia S, Prado-Garcia H. Mitochondrial calcium: transport and modulation of cellular processes in homeostasis and cancer (Review). *Int J Oncol*. (2019) 54:1155–67. doi: 10.3892/ijo.2019.4696
41. Steele HE, Guo Y, Li BY, Na S. Mechanotransduction of mitochondrial AMPK and its distinct role in flow-induced breast cancer cell migration. *Biochem Biophys Res Commun*. (2019) 514:524–9. doi: 10.1016/j.bbrc.2019.04.191
42. Sant'Anna Silva CB, Santos GC, Campos SPC, Oliveira Gomes AM, Perez-Valencia JA, Rumjanek FD. Metabolic profiles of oral squamous carcinoma cell lines relies on a higher demand of lipid metabolism in metastatic cells. *Front. Oncol*. (2018) 8:13. doi: 10.3389/fonc.2018.00013
43. Rodrigues MF, Obre E, de Melo FH, Santos GC Jr, Jaisiulionis MG, Rossignol R, et al. Enhanced OXPHOS, glutaminolysis and β- oxidation constitute the metastatic phenotype of melanoma cells. *Biochem J*. (2016) 473:703–15. doi: 10.1042/BJ20150645
44. Rodrigues MF, Carvalho É, Pezzuto P, Rumjanek FD, Amoêdo ND. Reciprocal modulation of histone deacetylase inhibitors sodium butyrate and trichostatin A on the energy metabolism of breast cancer cells. *J Cell Biochem*. (2015) 116:797–808. doi: 10.1002/jcb.25036
45. Luo X, Zhao X, Cheng C, Li N, Liu Y, Cao Y. The implication of signalling lipids in cancer metastasis. *Exp Mol Med*. (2018) 50:127. doi: 10.1038/s12276-018-0150-x
46. Kus K, Kij A, Zakrzewska A, Jasztal A, Stojak M, Walczak M, et al. Alterations in arginine and energy metabolism, structural and signalling lipids in metastatic breast cancer in mice detected in plasma by

targeted metabolomics and lipidomics. *Breast Cancer Res.* (2018) 20:148. doi: 10.1186/s13058-018-1075-y

47. Zhang ZG, Zhang HS, Sun HL, Liu HY, Liu MY, Zhou, Z. KDM5B promotes breast cancer cell proliferation and migration via AMPK-mediated lipid metabolism reprogramming. *Exp Cell Res.* (2019) 379:182–90. doi: 10.1016/j.yexcr.2019.04.006
48. Serna-Marquez N, Villegas-Comonfort S, Galindo-Hernandez, O. Role of LOXs and COX-2 on FAK activation and cell migration induced by linoleic acid in MDA-MB-231 breast cancer cells. *Cell Oncol.* (2013) 36:65–77. doi: 10.1007/s13402-012-0114-4

Conflict of Interest: The authors declare that the research was conducted in the absence of any commercial or financial relationships that could be construed as a potential conflict of interest.

frontiers in Oncology

CORRECTION
published: 24 March 2020
doi: 10.3389/fonc.2020.00367

Corrigendum: Isothermal Microcalorimetry of Tumor Cells: Enhanced Thermogenesis by Metastatic Cells

Douglas Lemos[1†], *Thaís Oliveira*[1†], *Larissa Martins*[1], *Vitória Ramos de Azevedo*[1], *Mariana Figueiredo Rodrigues*[1], *Luisa Andrea Ketzer*[2] *and Franklin David Rumjanek*[1*]

[1] *Laboratório de Bioquímica e Biologia Molecular Do Câncer, Instituto de Bioquímica Médica Leopoldo de Meis, Universidade Federal Do Rio de Janeiro, Rio de Janeiro, Brazil,* [2] *Núcleo Multidisciplinar de Pesquisa UFRJ-Xerém em Biologia (NUMPEX-Bio), Universidade Federal Do Rio de Janeiro, Duque de Caxias, Brazil*

Keywords: thermogenesis, microcalorimetry, metastasis, UCP2, etomoxir, fatty acid oxidation

OPEN ACCESS

Edited and reviewed by:
Tuuli Käämbre,
National Institute of Chemical Physics and Biophysics, Estonia

***Correspondence:**
Franklin David Rumjanek
franklin@bioqmed.ufrj.br

†These authors have contributed equally to this work and share first authorship

Specialty section:
This article was submitted to Cancer Metabolism, a section of the journal Frontiers in Oncology

Received: *23 January 2020*
Accepted: *02 March 2020*
Published: *24 March 2020*

Citation:
Lemos D, Oliveira T, Martins L, de Azevedo VR, Rodrigues MF, Ketzer LA and Rumjanek FD (2020) Corrigendum: Isothermal Microcalorimetry of Tumor Cells: Enhanced Thermogenesis by Metastatic Cells. Front. Oncol. 10:367. doi: 10.3389/fonc.2020.00367

A Corrigendum on

Isothermal Microcalorimetry of Tumor Cells: Enhanced Thermogenesis by Metastatic Cells
by Lemos, D., Oliveira, T., Martins, L., de Azevedo, V. R., Rodrigues, M. F., Ketzer, L. A., et al. (2019). Front. Oncol. 9:1430. doi: 10.3389/fonc.2019.01430

In the original article, there was a mistake in **Figure 8** as published. Figure 5 and 8 were erroneously duplicated. Both figures correspond to the effect of genipin on heat release. **Figure 8** should correspond to the effect of etomoxir. The corrected **Figure 8** appears below.

The authors apologize for this error and state that this does not change the scientific conclusions of the article in any way. The original article has been updated.

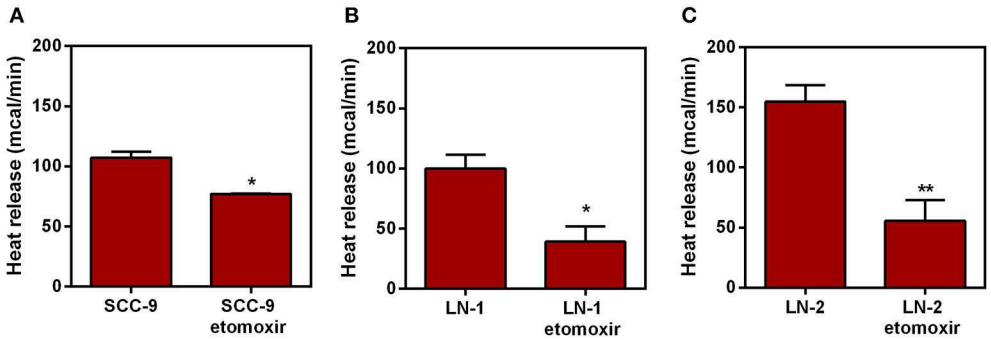

FIGURE 8 | Effect of etomoxir on the heat release by human oral squamous carcinoma cells SCC-9, LN-1 and LN-2 cells. The bars represent the release of total heat of living cells in 35 min of experiment. **(A)** Heat release by SCC-9 cells untreated and treated with 300 μM of etomoxir; **(B)** Heat release by LN-1 cells untreated and treated with 300 μM of etomoxir. **(C)** Heat release by LN-2 cells untreated and treated with 300 μM of etomoxir. Values were expressed as mean ± SEM. $^{*}p < 0.05$; $^{**}p < 0.01$.

frontiers in Oncology

DATA REPORT
published: 27 February 2020
doi: 10.3389/fonc.2020.00267

RNA-seq Analysis of Wild-Type vs. FOXC2-Deficient Melanoma Cells Reveals a Role for the FOXC2 Transcription Factor in the Regulation of Multiple Oncogenic Pathways

Kristian M. Hargadon and Corey J. Williams*

Hargadon Laboratory, Department of Biology, Hampden-Sydney College, Hampden-Sydney, VA, United States

Keywords: RNA-seq, melanoma, FOXC2, gene regulation, oncogene, differential expression

OPEN ACCESS

Edited by:
Tuuli Käämbre, National Institute of Chemical Physics and Biophysics, Estonia

Reviewed by:
Daria Capece, Imperial College London, United Kingdom
Joe Harvey Taube, Baylor University, United States

****Correspondence:***
Kristian M. Hargadon
khargadon@hsc.edu

Specialty section:
This article was submitted to Cancer Metabolism, a section of the journal Frontiers in Oncology

Received: *04 December 2019*
Accepted: *17 February 2020*
Published: *27 February 2020*

Citation:
Hargadon KM and Williams CJ (2020) RNA-seq Analysis of Wild-Type vs. FOXC2-Deficient Melanoma Cells Reveals a Role for the FOXC2 Transcription Factor in the Regulation of Multiple Oncogenic Pathways. Front. Oncol. 10:267. doi: 10.3389/fonc.2020.00267

INTRODUCTION

The forkhead box protein C2 (FOXC2) transcription factor has recently emerged as a key regulator of tumor progression in many cancer types. First implicated as a potential oncogenic transcription factor due to its overexpression/nuclear localization in invasive breast carcinomas, particularly those of the aggressive basal-like subtype (1), FOXC2 has since been linked to the progression of a number of epithelial-derived malignancies. Indeed, FOXC2 overexpression and nuclear localization are poor prognostic indicators of survival in patients with prostate cancer (2), hepatocellular carcinoma (3), NSCLC (4), colorectal cancer (5), glioma (6), gastric cancer (7), and esophageal as well as oral tongue squamous cell carcinomas (8, 9). Studies employing murine and human tumor cell lines have confirmed the oncogenic potential of the FOXC2 transcription factor, highlighting its ability to promote several hallmarks of cancer progression, including proliferation (5, 9), epithelial-mesenchymal transition (EMT) (10), invasion and metastasis (11), glycolytic metabolism (12), stemness (13), and drug resistance (14, 15). Based on these diverse tumor-promoting functions and the breadth of tumor types in which FOXC2 is dysregulated, it is important to improve our understanding of this transcription factor's regulation of oncogenic pathways in cancer cells.

While previous studies have focused on FOXC2 in the context of cancers originating from epithelial tissues, we recently demonstrated that FOXC2 is also a key contributor to the progression of melanoma (16). Using CRISPR-Cas9 gene editing technology, we engineered a variant of the B16-F1 murine melanoma cell line that carries a bi-allelic disruption in the *Foxc2* gene and that does not express FOXC2 protein, and we reported that this B16-F1ΔFOXC2 variant grows out with slower kinetics as a subcutaneous tumor than its parental counterpart. We also reported select data from RNA-sequencing (RNA-seq) and pathway-focused qRT-PCR array-based differential gene expression studies in the B16-F1 vs. B16-F1ΔFOXC2 melanomas that highlighted a role for FOXC2 in: (1) the positive regulation of genes associated with the cellular response to xenobiotics and oxidative stress and (2) the negative regulation of genes associated with interferon (IFN) responsiveness. These findings were particularly intriguing in light of our analysis of data from The Cancer Genome Atlas (TCGA), which revealed that *FOXC2* expression levels correlate negatively with survival of melanoma patients treated with either dacarbazine chemotherapy or ipilimumab immunotherapy. In this Data Report, we now provide a more thorough description of our RNA-seq data obtained from the B16-F1 and B16-F1ΔFOXC2 melanoma cell lines. Importantly, these data reveal a role for FOXC2 in the regulation of multiple pathways with oncogenic potential in

melanoma, and they offer mechanistic insights into FOXC2-associated tumor progression that may be applicable to other cancer types as well.

METHODS

Cell Lines

B16-F1 murine melanoma cells were purchased from the American Type Culture Collection (Manassas, VA, USA) and grown in RPMI-1640 medium supplemented with 2 mM L-glutamine, 2 g/l glucose, and 2 g/l sodium bicarbonate (Thermo Fisher Scientific, Waltham, MA, USA), as well as 10% fetal bovine serum (Premium Select, Atlanta Biologicals, Norcross, GA, USA). B16-F1ΔFOXC2 cells were generated as described (16) and maintained in the same growth medium as the parental cell line. All cultures were grown at 37°C in a 5% CO_2 incubator and passaged at 80–90% confluence.

RNA Isolation

B16-F1 or B16-F1ΔFOXC2 melanoma cells ($1e^6$) were plated onto 60 × 15 mm cell culture dishes and grown for 24 h to ∼90% confluence before isolating RNA with an RNeasy Mini Kit (Qiagen, Germantown, MD, USA) according to the manufacturer's recommendations. On-column DNase-digestion with Qiagen's RNase-free DNase Set was performed during extraction. RNA integrity and genomic DNA contamination were examined by standard denaturing agarose gel electrophoresis, and all samples (five independent replicates per group) passed quality control assessment. RNA was quantified with an Epoch Spectrophotometer (BioTek, Winooski, VT, USA), and A260/280 and A260/230 ratios were both ≥2.0 for all samples.

Preparation of Libraries for RNA-seq

RNA samples were shipped overnight on dry ice to Arraystar, Inc. (Rockville, MD, USA) for analysis using the company's Illumina Hi-seq 6G RNA-sequencing service. mRNA was isolated from total RNA (1–2 μg per sample) with oligo (dT) magnetic beads using the NEBNext® Poly(A) mRNA Magnetic Isolation Module (New England BioLabs, Ipswich, MA). RNA was fragmented to sizes between 400 and 600 bp and reverse transcribed into 1st strand cDNA using random hexamer primers according to manufacturer recommendations in the KAPA Stranded RNA-Seq Library Prep Kit (Illumina, San Diego, CA). Using this kit, 2nd strand synthesis was performed to incorporate dUTP into strand-specific libraries, and the double-stranded cDNA was end-repaired, A-tailed, adaptor ligated, and PCR amplified. Completed libraries were qualified with an Agilent 2100 Bioanalyzer using the Agilent DNA 1000 Kit (Agilent, Santa Clara, CA) and quantified by absolute quantification qPCR. Barcoded libraries were mixed in equal amounts, denatured to single stranded DNA with 0.1 M NaOH, loaded onto channels of the flow cell at 8 pM concentration, and amplified *in situ* using a TruSeq SR Cluster Kit v3-cBot-HS (Illumina). Sequencing was carried out by running 150 cycles for both ends on an Illumina HiSeq 4000 instrument.

RNA-seq Data Processing and Analysis

Image analysis and base calling were performed using Solexa pipeline v1.8 (Off-Line Base Caller software, v1.8). Sequence quality was examined using FastQC software (v0.11.7), and raw sequencing data that passed Illumina chastity filtering were analyzed. Fragments were 5′, 3′-adaptor trimmed and filtered ≤20 bp reads with cutadapt software (v1.17). The trimmed reads were mapped to reference genome GRCm38 using Hisat 2 software (v2.1.0). Transcript abundances for each sample were estimated with StringTie (v1.3.3), and the normalized expression level (FPKM value) of known genes was calculated with the R package ballgown (v2.10.0). An FPKM mean of ≥0.5 in a given biological group was used to calculate the number of identified genes per group. Using these identified genes, differential gene expression analysis was performed with ballgown and the following cutoffs to filter differentially expressed genes: fold change ≥ 1.5, $p \leq 0.05$, and mean FPKM ≥ 0.5 in at least one group. Gene ontology (GO) enrichment analysis of differentially expressed genes was performed using standard GO Terms from the Gene Ontology Resource (http://www.geneontology.org) and a Fisher's exact test to estimate statistical significance of the enrichment of terms between the B16-F1 and B16-F1ΔFOXC2 cell lines. Similarly, pathway analysis of differentially expressed genes was performed using the Kyoto Encyclopedia of Genes and Genomes (KEGG) database, and a Fisher's exact test was used to estimate the statistical significance of pathways enriched with differentially expressed mRNAs between the two cell lines.

Data Deposition

RNA-seq data discussed in this publication have been deposited in NCBI's Gene Expression Omnibus (17) under Dataset Name "RNA-seq Analysis of Differential Gene Expression in Wild-type Versus FOXC2-deficient B16-F1 Melanomas" and are freely accessible through GEO Series accession number GSE134296, available at https://www.ncbi.nlm.nih.gov/geo/query/acc.cgi?acc=GSE134296 (18). This dataset includes both raw data in .fastq format as well as a matrix table of processed data (.xlsx format) with the normalized FPKM expression values for known genes from each sample.

OVERVIEW AND REUSE OF DATA

We recently reported that expression of the *FOXC2* gene in melanoma biopsies is an unfavorable prognostic indicator of patient survival following treatment with either chemotherapy or immunotherapy (16). In that study, we also described a novel CRISPR-Cas9 gene-edited variant of the murine B16-F1 melanoma that we engineered to lack the FOXC2 transcription factor (B16-F1ΔFOXC2). Using this model, we demonstrated a role for FOXC2 in promoting melanoma progression, and we highlighted select data from an RNA-seq analysis of the B16-F1 and B16-F1ΔFOXC2 melanomas that we now describe here in more detail. With 5 replicate RNA samples isolated from each tumor cell line, a Quality score of Q30 >82% for each sample (Q30 = 99.9% base calling accuracy), and a high level of correlation between samples within each biological group (Pearson R2 correlation > 0.993 between replicates, **Figure 1A**),

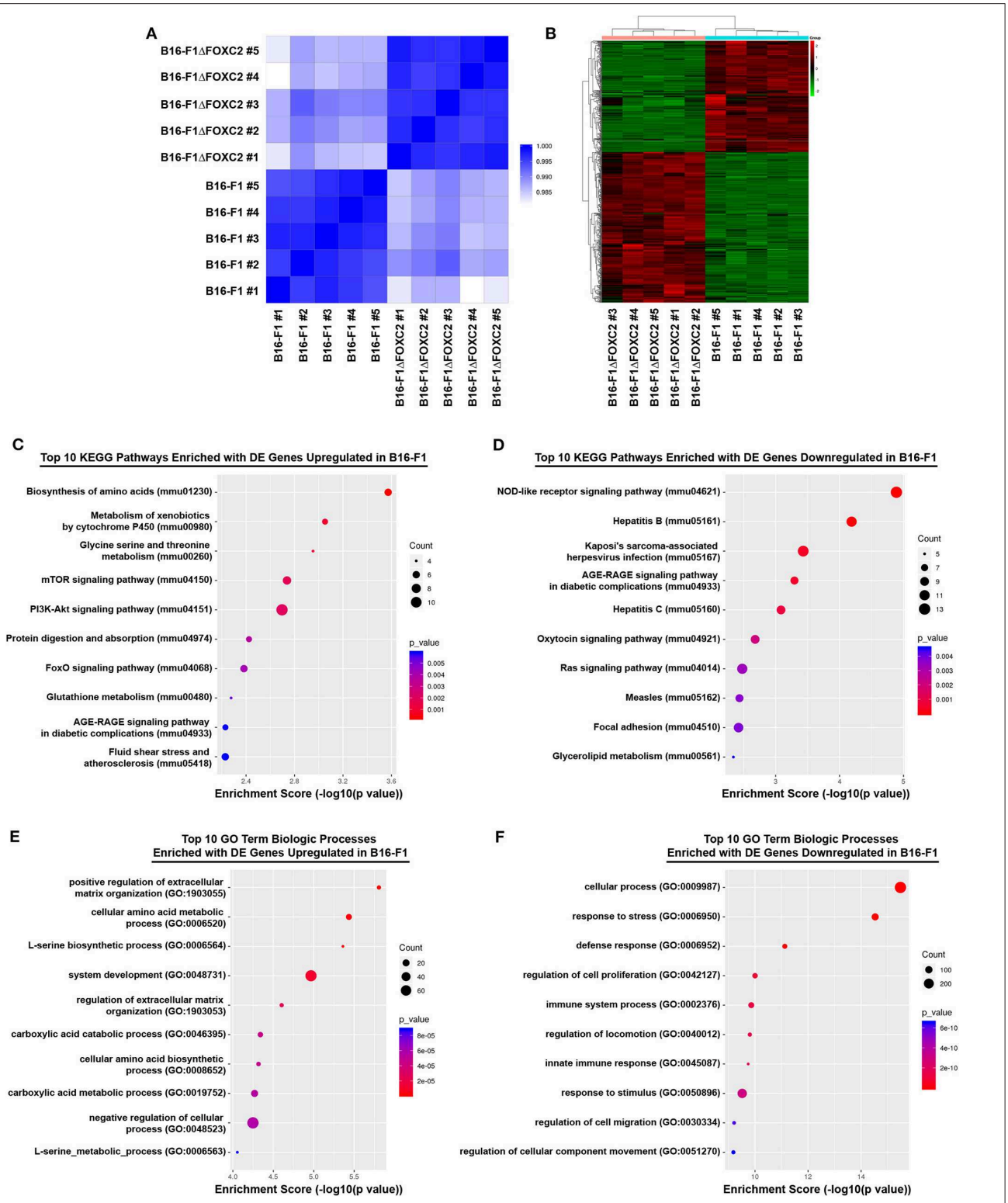

FIGURE 1 | RNA-seq correlation and differential gene expression analyses of B16-F1 and B16-F1ΔFOXC2 murine melanomas. RNA-seq analysis was performed on RNA isolated from five replicate samples for each biological group. The Pearson R2 correlation heat map of gene expression levels between all samples is shown in **(A)**. The hierarchical clustering heat map of differentially expressed genes between B16-F1 and B16-F1ΔFOXC2 is shown in **(B)**. KEGG Pathway and Gene Ontology analyses were performed to identify pathways and biological processes significantly enriched with differentially upregulated and downregulated genes in B16-F1. Enrichment score dot plots showing gene counts and statistical significance as determined by a Fisher's exact test are presented for the top 10 KEGG pathways enriched in differentially expressed (DE) genes in **(C,D)** and for the top 10 Biologic Process-related GO Terms enriched in DE genes in **(E,F)**.

TABLE 1 | Summary of RNA-seq differential gene expression in B16-F1 vs. B16-F1ΔFOXC2 melanoma.

Top 30 DE genes upregulated in B16-F1 vs. B16-F1ΔFOXC2							
Gene	**Fold change**	***p*-value**	***q*-value**	**Gene**	**Fold change**	***p*-value**	***q*-value**
Fscn1	20.17	1.04E-07	1.19E-05	*Iqgap*	3.65	9.60E-09	2.88E-06
Cbr3	9.24	3.04E-10	2.76E-07	*Ece1*	3.60	5.30E-12	6.14E-08
Mbp	8.53	1.71E-09	9.88E-07	*Cntln*	3.60	1.28E-11	6.14E-08
Pdpn	7.51	2.26E-10	2.39E-07	*Trim25*	3.59	6.35E-09	2.28E-06
Foxr2	7.27	1.52E-10	1.91E-07	*Zfp521*	3.54	6.63E-11	1.05E-07
Mcoln3	5.77	3.10E-11	7.27E-08	*Cort*	3.51	1.72E-05	0.00031
Lmo1	5.53	1.85E-08	4.52E-06	*Epha3*	3.45	6.81E-07	3.81E-05
Dcdc2a	5.10	6.71E-10	5.01E-07	*Tmlhe*	3.42	2.11E-11	6.70E-08
Plp2	4.88	3.24E-08	6.03E-06	*Cyp26b1*	3.39	3.12E-06	9.21E-05
Nqo1	4.77	3.03E-10	2.76E-07	*Pafah1b3*	3.33	6.56E-11	1.05E-07
Taf9b	4.67	1.58E-07	1.49E-05	*Prrg4*	3.27	1.43E-07	1.37E-05
Nostrin	4.64	4.77E-09	2.13E-06	*Hoxd13*	3.26	4.86E-09	2.13E-06
Col4a1	4.52	4.54E-08	6.95E-06	*Rnf113a2*	3.22	2.08E-07	1.77E-05
Vgll3	4.37	1.18E-07	1.24E-05	*Armcx1*	3.20	3.75E-08	6.45E-06
Tor4a	3.65	6.21E-08	8.57E-06	*Pmp22*	3.16	2.91E-08	5.68E-06
Top 30 DE genes downregulated in B16-F1 vs. B16-F1ΔFOXC2							
Lgals3	−7.73	2.22E-09	1.22E-06	*Pla2g2e*	−2.70	3.27E-05	0.00049
Oas1a	−6.41	9.54E-09	2.88E-06	*Ksr1*	−2.66	3.64E-09	1.78E-06
Mgll	−5.87	1.99E-05	0.00034	*Itgb3*	−2.66	2.85E-08	5.68E-06
Isg15	−4.22	3.24E-07	2.41E-05	*Pet2*	−2.63	1.45E-11	6.14E-08
Tagln2	−4.21	3.28E-08	6.03E-06	*Sphk1*	−2.63	2.45E-05	0.00040
Oas1g	−3.82	5.70E-08	8.04E-06	*Stat1*	−2.61	2.08E-07	1.77E-05
Lcp1	−3.59	1.76E-06	6.49E-05	*St6gal1*	−2.61	8.63E-05	0.00095
Hsd11b1	−3.36	1.13E-07	1.24E-05	*Met*	−2.58	0.0014	0.0074
Mogat1	−3.35	8.77E-07	4.51E-05	*Arfgef3*	−2.58	4.20E-06	0.00011
Ifi27	−3.11	1.92E-07	1.70E-05	*Tinagl1*	−2.54	5.38E-06	0.00014
Trpm1	−2.88	1.37E-05	0.00026	*Adam23*	−2.54	8.24E-10	5.81E-07
Ifitm3	−2.83	3.62E-06	0.00010	*Fam129a*	−2.54	1.50E-06	6.03E-05
Ddx58	−2.81	1.52E-06	6.03E-05	*Mapre3*	−2.54	7.81E-07	4.11E-05
Xaf1	−2.77	1.13E-05	0.00023	*Egr1*	−2.54	8.19E-05	0.00091
Fam178b	−2.74	6.35E-08	8.68E-06	*Ecm1*	−2.53	1.44E-05	0.00027

List of the top 30 upregulated and downregulated genes in B16-F1 vs. B16-F1ΔFOXC2 melanoma cells as determined by RNA-seq analysis. q value = false discovery rate (FDR)-adjusted p-value.

this dataset provides a high-quality profile of the FOXC2-associated transcriptome in melanoma cells, and it will serve as a useful tool to investigators interested in studying FOXC2 function in the context of cancer.

In the differential gene expression analysis of our RNA-seq data, we defined B16-F1ΔFOXC2 as the reference sample so that genes upregulated in the wild-type B16-F1 cell line could be interpreted as those positively regulated (directly or indirectly) by FOXC2, whereas genes downregulated in B16-F1 would represent those negatively regulated by FOXC2. We identified 598 genes differentially expressed (fold-change $\geq$ 1.5, $p \leq 0.05$, and mean FPKM $\geq$ 0.5 in at least one group) by these cell lines: of these, 254 genes were upregulated in B16-F1, implicating a role for FOXC2 in their induction, and 344 genes were downregulated in B16-F1, reflecting FOXC2-associated repression of these genes (**Figure 1B**). We performed KEGG Pathway analysis and GO Biologic Process analysis of this cohort of genes and report here the top 10 pathways and GO Terms enriched with these differentially expressed genes (**Figures 1C–F**). The 30 most highly up- and downregulated of all of these genes are also shown in **Table 1**.

Our recent study highlighted several differentially expressed genes upregulated in B16-F1 that are associated with GO Terms related to the cellular response to xenobiotics and oxidative stress. We also noted in that study the downregulation in B16-F1 of several genes associated with GO Terms related to IFN responsiveness (16). Our current KEGG Pathway analysis supports these findings, with significant enrichment of B16-F1

upregulated genes in pathways related to xenobiotic metabolism and glutathione metabolism as well as significant enrichment of B16-F1 downregulated genes in pathways related to viruses and Nod-like receptor signaling, all of which include several genes involved in cellular responses to IFN. Indeed, many of the most significantly up- and downregulated genes listed in **Table 1** have functions related to these particular pathways and were validated by qRT-PCR in our previous study.

Our data supports previously reported functions of FOXC2 in other cancer types and provides potential molecular insights into the oncogenic activity of this transcription factor. With regard to FOXC2's well-established role in promoting chemotherapy resistance in tumor cells (14, 15, 19, 20), our data suggests potential mechanisms by which this chemoresistance may be achieved, including induction of genes associated with drug metabolism such as the carbonyl reductase gene *Cbr3*, the oxidoreductase gene *Nqo1*, the cytochrome P450 family member *Cyp26b1*, and several members belonging to the glutathione S-transferase gene family (which fall outside of the top 30 upregulated genes shown in **Table 1**). Our findings are also consistent with work in other tumor and non-tumor models demonstrating a role for FOXC2 in the activation of PI3K-Akt-mTOR signaling (5, 20, 21), as we found that several genes associated with the PI3K-Akt signaling pathway (mmu04151) and the mTOR signaling pathway (mmu04150) were upregulated in B16-F1 as compared to its FOXC2-deficient counterpart. These genes include the *Pik3r2* gene, which encodes the p85β regulatory subunit of PI3K known to induce oncogenic transformation and cellular proliferation (22, 23), and the *Insr* gene, whose protein product drives various oncogenic activities through PI3K signaling (24). FOXC2 is also well-known for its ability to promote EMT and tumor cell migration/invasion (10, 25), and our findings suggest potential mechanisms by which these hallmarks of cancer progression might be regulated by FOXC2 as well. In this regard, some of the most highly upregulated genes in B16-F1 include *Fscn1* (20.17-fold upregulation) and *Pdpn* (7.51-fold upregulation). The fascin protein encoded by *Fscn1* organizes F-actin into bundles needed to form cellular protrusions that enhance tumor cell migration (26), and the actin-rich podoplanin protein encoded by *Pdpn* enhances tumor cell invasion, most likely by stabilizing invadopodia that trigger extracellular matrix (ECM) degradation (27, 28). Additionally, FOXC2-associated downregulation of genes belonging to the Focal adhesion pathway (mmu04510), such as the fibronectin-encoding *Fn1* gene and the integrin-encoding *Itgb3* gene, the latter of which is a known direct target of FOXC2 (29), may contribute to ECM remodeling and the altered adhesion of tumor cells to ECM components that occurs during the invasion process.

In addition to offering molecular insight into the previously described oncogenic activities of FOXC2, the RNA-seq dataset described herein highlights potentially novel tumor-promoting functions for this transcription factor as well. Of note, although previous work has demonstrated FOXC2-associated regulation of glycolysis (12), fatty acid oxidation (30), and mitochondrial metabolism (31), a role for FOXC2 in other metabolic pathways has not been reported to date. Interestingly, our differential gene expression analyses suggest the likelihood that FOXC2 also contributes to amino acid metabolism, as several GO Terms and Kegg Pathways related to amino acid biosynthesis and metabolism were significantly enriched with genes upregulated in the FOXC2-expressing B16-F1 cell line. Many of these genes, including *Phgdh*, *Psat1*, and *Psph*, play important roles in serine biosynthesis, a process that has been shown to accelerate melanoma progression and confer resistance of *BRAF* V600E mutant melanoma to the targeted inhibitor vemurafenib (32, 33). To date, only one other group has demonstrated a role for FOXC2 as a regulator of amino acid metabolism. In a recent study by Ramirez-Peña et al., FOXC2 was found to negatively regulate glutamine utilization in breast cancer cells undergoing EMT by downregulating expression of the GLS2 glutaminase (31). Our data now highlight the potential for FOXC2 to modify additional metabolic pathways in cancer cells, suggesting that this transcription factor may contribute to a variety of metabolic adaptations over the course of tumor progression.

Another previously unappreciated function of FOXC2 revealed by our data is its negative regulation of genes associated with IFN signaling, a finding that is particularly intriguing in light of recent studies demonstrating that both type I IFN and IFNγ signaling pathways within tumor cells are critical to the efficacy of cancer immunotherapies (34–37). Indeed, our recent analysis of melanoma patient TCGA data showed that *FOXC2* expression correlates negatively with progression-free survival (PFS) of patients treated with the CTLA-4 immune checkpoint inhibitor ipilimumab (16). Though the mechanism by which FOXC2 might promote resistance to checkpoint blockade therapy remains to be elucidated, it is interesting that in our murine model FOXC2 negatively regulated the expression of several IFN signaling pathway components, including the *Ddx58* gene encoding RIG-I and the *Stat1*/*Stat2*/*Stat3* and *Irf7*/*Irf9* transcription factor genes. FOXC2 expression was also associated with downregulation of various IFN-stimulated genes, including *Oas1a*, *Oas1g*, *Isg15*, *Ifi27*, *Ifi35*, *Ifitm3*, *Ifit1*, and *Ifit3*, among others. In keeping with our observation of FOXC2-associated downregulation of *Ddx58* expression and the aforementioned link between *FOXC2* expression and poor PFS of melanoma patients on ipilimumab, it is worth noting that Heidegger et al. recently demonstrated the importance of tumor cell-intrinsic activation of RIG-I in the success of checkpoint blockade therapy (38). Interestingly, RIG-I deficiency in cancer cells was also recently linked to the induction of tolerogenic dendritic cells (39), a cell type that could impact the efficacy of several immune-based therapies and one that is of particular interest to our laboratory (40, 41). We are therefore eager to explore in our model how FOXC2's negative regulation of RIG-I and other IFN pathway genes might contribute to tumor immune evasion and various forms of resistance to clinically relevant cancer immunotherapies.

It is worth noting that one potential limitation of our current study is its utilization of a murine, rather than human, melanoma cell line. Going forward, it will indeed be worth validating our findings with a similar approach in frequently studied human melanoma cell lines, such as A375 and SK-MEL-3. In order to gain additional insights into FOXC2

activity in human melanoma, we are also in the process of evaluating by immunohistochemistry how FOXC2 expression levels in melanoma patient biopsies correlate with expression of proteins of interest that have emerged from this study. Together with analyses evaluating how FOXC2 expression and subcellular localization correlate with clinicopathological features and patient outcome, these findings are likely to yield important questions related to the basic biology of FOXC2 function in melanoma that can be easily addressed in our B16-F1/B16-F1ΔFOXC2 model. Additionally, though B16-F1 is a subclone of B16 melanoma and therefore lacks the genetic diversity of a naturally arising heterogeneous tumor, it nevertheless recapitulates many features of highly aggressive human melanomas, and it has become a useful model system for investigating several hallmarks of tumor progression both *in vitro* and *in vivo* (42). Ongoing work in this model, which does not carry mutations in the *BRAF* and *PTEN* genes frequently associated with melanoma (43, 44), may be particularly relevant to understanding the progression of the still large percentage of melanomas not driven by mutations in these two genes. In this regard, that our B16-F1ΔFOXC2 model represents to our knowledge the first complete FOXC2 knockout cell line underscores the potential utility of this system for gaining important mechanistic insights into a potentially alternate driver of melanoma progression. Moreover, with evidence continuing to emerge that FOXC2 can function as an oncogenic driver of various other cancer types, comparative studies between our wild-type and complete FOXC2 knockout melanoma cell lines are likely to reveal important functions for this transcription factor that are of broad relevance to other forms of cancer as well.

In conclusion, this Data Report describes a high-quality RNA-seq dataset that we believe will serve as an important resource for investigators interested in studying the oncogenic activity of FOXC2. Importantly, our differential gene expression analyses not only offer potential molecular explanations for well-established FOXC2-driven hallmarks of cancer progression but also suggest novel tumor-promoting functions for this transcription factor. Going forward, we hope these data will invite new questions about the oncogenic functions of FOXC2 and ultimately drive future studies that aim to: (1) improve our understanding of FOXC2 activity in cancer cells and (2) inform therapeutic strategies designed to interfere with FOXC2-associated cancer progression.

DATA AVAILABILITY STATEMENT

The RNA-seq data discussed in this article have been made publicly available in NCBI's Gene Expression Omnibus under Dataset Name "RNA-seq Analysis of Differential Gene Expression in Wild-type Versus FOXC2-deficient B16-F1 Melanomas" (GEO Series accession number GSE134296).

AUTHOR CONTRIBUTIONS

KH was responsible for all aspects of the experimental work and writing of this article. CW contributed to the generation of the B16-F1ΔFOXC2 cell line and assisted with analysis of the RNA-seq data described herein. Both authors approved the submitted version of this manuscript.

FUNDING

This research was supported by funding from Virginia's Commonwealth Health Research Board (Grant #375-01-14), a Jeffress Trust Awards Program in Interdisciplinary Research Grant from the Thomas F. and Kate Miller Jeffress Memorial Trust (Bank of America, N.A., Trustee), and a Hampden-Sydney College Research Grant from the Arthur Vining Davis endowment (to KH). This work was also supported by a VFIC Undergraduate Science Research Fellowship CW.

ACKNOWLEDGMENTS

We also thank Mr. Michael Hargadon and Mrs. Patricia Hargadon for generous donations to support the involvement of Hampden-Sydney College undergraduate students in this research.

REFERENCES

1. Mani SA, Yang J, Brooks M, Schwaninger G, Zhou A, Miura N, et al. Mesenchyme Forkhead 1 (FOXC2) plays a key role in metastasis and is associated with aggressive basal-like breast cancers. *Proc Natl Acad Sci USA*. (2007) 104:10069–74. doi: 10.1073/pnas.0703900104
2. Børretzen A, Gravdal K, Haukaas SA, Beisland C, Akslen LA, Halvorsen OJ. FOXC2 expression and epithelial–mesenchymal phenotypes are associated with castration resistance, metastasis and survival in prostate cancer. *J Pathol Clin Res*. (2019) 5:272–86. doi: 10.1002/cjp2.142
3. Shimoda Y, Ubukata Y, Handa T, Yokobori T, Watanabe T, Gantumur D, et al. High expression of forkhead box protein C2 is associated with aggressive phenotypes and poor prognosis in clinical hepatocellular carcinoma. *BMC Cancer*. (2018) 18:597. doi: 10.1186/s12885-018-4503-6
4. Jiang W, Fan H, Qian C, Ding J, Wang Q, Pang X. Prognostic value of high FoxC2 expression in resectable non-small cell lung cancer, alone or in combination with E-cadherin expression. *BMC Cancer*. (2016) 16:16. doi: 10.1186/s12885-016-2056-0
5. Cui YM, Jiang D, Zhang SH, Wu P, Ye YP, Chen CM, et al. FOXC2 promotes colorectal cancer proliferation through inhibition of FOXO3a and activation of MAPK and AKT signaling pathways. *Cancer Lett*. (2014) 353:87–94. doi: 10.1016/j.canlet.2014.07.008
6. Wang YW, Yin CL, Zhang HY, Hao J, Yang YY, Liao H, et al. High expression of forkhead box protein C2 is related to poor prognosis in human gliomas. *Asian Pac J Cancer Prev*. (2014) 15:10621–5. doi: 10.7314/APJCP.2014.15.24.10621
7. Zhu JL, Song YX, Wang ZN, Gao P, Wang MX, Dong YL, et al. The clinical significance of mesenchyme forkhead 1 (FoxC2) in gastric carcinoma. *Histopathology*. (2013) 62:1038–48. doi: 10.1111/his.12132
8. Nishida N, Mimori K, Yokobori T, Sudo T, Tanaka F, Shibata K, et al. FOXC2 is a novel prognostic factor in human esophageal squamous cell carcinoma. *Ann Surg Oncol*. (2011) 18:535–42. doi: 10.1245/s10434-010-1274-y
9. Imayama N, Yamada S, Yanamoto S, Naruse T, Matsushita Y, Takahashi H, et al. FOXC2 expression is associated with tumor proliferation and invasion potential in oral tongue squamous cell carcinoma. *Pathol Oncol Res*. (2015) 21:783–91. doi: 10.1007/s12253-014-9891-6

10. Li C, Ding H, Tian J, Wu L, Wang Y, Xing Y, et al. Forkhead box protein C2 promotes epithelial-mesenchymal transition, migration and invasion in cisplatin-resistant human ovarian cancer cell line (SKOV3/CDDP). *Cell Physiol Biochem*. (2016) 39:1098–110. doi: 10.1159/000447818
11. Cui YM, Jiao HL, Ye YP, Chen CM, Wang JX, Tang N, et al. FOXC2 promotes colorectal cancer metastasis by directly targeting MET. *Oncogene*. (2015) 34:4379–90. doi: 10.1038/onc.2014.368
12. Song L, Tang H, Liao W, Luo X, Li Y, Chen T, et al. FOXC2 positively regulates YAP signaling and promotes the glycolysis of nasopharyngeal carcinoma. *Exp Cell Res*. (2017) 357:17–24. doi: 10.1016/j.yexcr.2017.04.019
13. Hollier BG, Tinnirello AA, Werden SJ, Evans KW, Taube JH, Sarkar TR, et al. FOXC2 expression links epithelial-mesenchymal transition and stem cell properties in breast cancer. *Cancer Res*. (2013) 73:1981–92. doi: 10.1158/0008-5472.CAN-12-2962
14. Li C, Ding H, Tian J, Wu L, Wang Y, Xing Y, et al. Forkhead box protein C2 (FOXC2) promotes the resistance of human ovarian cancer cells to cisplatin in vitro and *in vivo*. *Cell Physiol Biochem*. (2016) 39:242–52. doi: 10.1159/000445620
15. He Y, Xie H, Yu P, Jiang S, Wei L. FOXC2 promotes epithelial–mesenchymal transition and cisplatin resistance of non-small cell lung cancer cells. *Cancer Chemother Pharmacol*. (2018) 82:1049–59. doi: 10.1007/s00280-018-3697-2
16. Hargadon KM, Györffy B, Strong EW, Tarnai BD, Thompson JC, Bushhouse DZ, et al. The FOXC2 transcription factor promotes melanoma outgrowth and regulates expression of genes associated with drug resistance and interferon responsiveness. *Cancer Genomics Proteomics*. (2019) 16:491–503. doi: 10.21873/cgp.20152
17. Edgar R, Domrachev M, Lash AE. Gene expression omnibus: NCBI gene expression and hybridization array data repository. *Nucleic Acids Res*. (2002) 30:207–10. doi: 10.1093/nar/30.1.207
18. Hargadon KM, Williams CJ. RNA-seq analysis of differential gene expression in wild-type versus FOXC2-deficient B16-F1 melanomas. *Cancer Genomics Proteomics*. (2019) 16:491–503.
19. Paranjape AN, Soundararajan R, Werden SJ, Joseph R, Taube JH, Liu H, et al. Inhibition of FOXC2 restores epithelial phenotype and drug sensitivity in prostate cancer cells with stem-cell properties. *Oncogene*. (2016) 35:5963–76. doi: 10.1038/onc.2015.498
20. Yang C, Cui X, Dai X, Liao W. Downregulation of Foxc2 enhances apoptosis induced by 5-fluorouracil through activation of MAPK and AKT pathways in colorectal cancer. *Oncol Lett*. (2016) 11:1549–54. doi: 10.3892/ol.2016.4097
21. Gan L, Liu Z, Jin W, Zhou Z, Sun C. Foxc2 enhances proliferation and inhibits apoptosis through activating Akt/mTORC1 signaling pathway in mouse preadipocytes. *J Lipid Res*. (2015) 56:1471–80. doi: 10.1194/jlr.M057679
22. Ito Y, Hart JR, Ueno L, Vogt PK. Oncogenic activity of the regulatory subunit p85β of phosphatidylinositol 3-kinase (PI3K). *Proc Natl Acad Sci USA*. (2014) 111:16826–29. doi: 10.1073/pnas.1420281111
23. Ito Y, Vogt PK, Hart JR. Domain analysis reveals striking functional differences between the regulatory subunits of phosphatidylinositol 3-kinase (PI3K), p85α and p85β. *Oncotarget*. (2017) 8:55863–76. doi: 10.18632/oncotarget.19866
24. Malaguarnera R, Belfiore A. The insulin receptor: a new target for cancer therapy. *Front Endocrinol*. (2011) 2:93. doi: 10.3389/fendo.2011.00093
25. Pham TND, Perez White BE, Zhao H, Mortazavi F, Tonetti DA. Protein kinase C α enhances migration of breast cancer cells through FOXC2-mediated repression of p120-catenin. *BMC Cancer*. (2017) 17:832. doi: 10.1186/s12885-017-3827-y
26. Li J, Zhang S, Pei M, Wu L, Liu Y, Li H, et al. FSCN1 promotes epithelial-mesenchymal transition through increasing Snail1 in ovarian cancer cells. *Cell Physiol Biochem*. (2018) 49:1766–77. doi: 10.1159/000493622
27. Wicki A, Lehembre F, Wick N, Hantusch B, Kerjaschki D, Christofori G. Tumor invasion in the absence of epithelial-mesenchymal transition: podoplanin-mediated remodeling of the actin cytoskeleton. *Cancer Cell*. (2006) 9:261–72. doi: 10.1016/j.ccr.2006.03.010
28. Martín-Villar E, Borda-d'Agua B, Carrasco-Ramirez P, Renart J, Parsons M, Quintanilla M, et al. Podoplanin mediates ECM degradation by squamous carcinoma cells through control of invadopodia stability. *Oncogene*. (2015) 34:4531–44. doi: 10.1038/onc.2014.388
29. Hayashi H, Sano H, Seo S, Kume T. The Foxc2 transcription factor regulates angiogenesis via induction of integrin beta3 expression. *J Biol Chem*. (2008) 283:23791–800. doi: 10.1074/jbc.M800190200
30. Gan L, Liu Z, Chen Y, Dan Luo, Feng F, Liu G, et al. α-MSH and Foxc2 promote fatty acid oxidation through C/EBPβ negative transcription in mice adipose tissue. *Sci Rep*. (2016) 6:36661. doi: 10.1038/srep36661
31. Ramirez-Peña E, Arnold J, Shivakumar V, Joseph R, Vidhya Vijay G, et al. The epithelial to mesenchymal transition promotes glutamine independence by suppressing GLS2 expression. *Cancers*. (2019) 11:E1610. doi: 10.3390/cancers11101610
32. Sullivan MR, Mattaini KR, Dennstedt EA, Nguyen AA, Sivanand S, Reilly MF, et al. Increased serine synthesis provides an advantage for tumors arising in tissues where serine levels are limiting. *Cell Metab*. (2019) 29:1410–21.e4. doi: 10.1016/j.cmet.2019.02.015
33. Ross KC, Andrews AJ, Marion CD, Yen TJ, Bhattacharjee V. Identification of the serine biosynthesis pathway as a critical component of BRAF inhibitor resistance of melanoma, pancreatic, and non–small cell lung cancer cells. *Mol Cancer Ther*. (2017) 16:1596–609. doi: 10.1158/1535-7163.MCT-16-0798
34. Wang X, Schoenhals JE, Li A, Valdecanas DR, Ye H, Zang F, et al. Suppression of type I IFN signaling in tumors mediates resistance to anti-PD-1 treatment that can be overcome by radiotherapy. *Cancer Res*. (2017) 77:839–50. doi: 10.1158/0008-5472.CAN-15-3142
35. Zaretsky JM, Garcia-Diaz A, Shin DS, Escuin-Ordinas H, Hugo W, Hu-Lieskovan S, et al. Mutations associated with acquired resistance to PD-1 blockade in melanoma. *N Engl J Med*. (2016) 375:819–29. doi: 10.1056/NEJMoa1604958
36. Gao J, Shi LZ, Zhao H, Chen J, Xiong L, He Q, et al. Loss of IFN-γ pathway genes in tumor cells as a mechanism of resistance to anti-CTLA-4 therapy. *Cell*. (2016) 167:397–404. doi: 10.1016/j.cell.2016.08.069
37. Shin DS, Zaretsky JM, Escuin-Ordinas H, Garcia-Diaz A, Hu-Lieskovan S, Kalbasi A, et al. Primary resistance to PD-1 blockade mediated by *JAK1/2* mutations. *Cancer Discov*. (2017) 7:188–201. doi: 10.1158/2159-8290.CD-16-1223
38. Heidegger S, Wintges A, Stritzke F, Bek S, Steiger K, Koenig PA, et al. RIG-I activation is critical for responsiveness to checkpoint blockade. *Sci Immunol*. (2019) 4:eaau8943. doi: 10.1126/sciimmunol.aau8943
39. Zhong M, Zhong C, Cui W, Wang G, Zheng G, Li L, et al. Induction of tolerogenic dendritic cells by activated TGF-β/Akt/Smad2 signaling in RIG-I-deficient stemness-high human liver cancer cells. *BMC Cancer*. (2019) 19:439. doi: 10.1186/s12885-019-5670-9
40. Hargadon KM, Bishop JD, Brandt JP, Hand ZC, Ararso YT, Forrest OA. Melanoma-derived factors alter the maturation and activation of differentiated tissue-resident dendritic cells. *Immunol Cell Biol*. (2016) 94:24–38. doi: 10.1038/icb.2015.58
41. Hargadon KM. Strategies to improve the efficacy of dendritic cell-based immunotherapy for melanoma. *Front Immunol*. (2017) 8:1594. doi: 10.3389/fimmu.2017.01594
42. Kuzu OF, Nguyen FD, Noory MA, Sharma A. Current state of animal (mouse) modeling in melanoma research. *Cancer Growth Metastasis*. (2015) 8 (Suppl. 1):81–94. doi: 10.4137/CGM.S21214
43. Fang X-Y, Song R, Chen W, Yang Y-Y, Gu Y-H, Shu Y-Q et al. PRL-3 promotes the malignant progression of melanoma via triggering dephosphorylation and cytoplasmic localization of NHERF1. *J Invest Dermatol*. (2015) 135:2273–82. doi: 10.1038/jid.2015.154
44. Hooijkas AI, Gadiot J, van der Valk M, Mooi WJ, Blank CU. Targeting BRAFV600E in an inducible murine model of melanoma. *Am J Pathol*. (2012) 181:785–94. doi: 10.1016/j.ajpath.2012.06.002

Conflict of Interest: The authors declare that the research was conducted in the absence of any commercial or financial relationships that could be construed as a potential conflict of interest.

frontiers in Oncology

ORIGINAL RESEARCH
published: 09 April 2020
doi: 10.3389/fonc.2020.00429

Physiological Role of Glutamate Dehydrogenase in Cancer Cells

Rafael Moreno-Sánchez, Álvaro Marín-Hernández*, Juan C. Gallardo-Pérez, Silvia C. Pacheco-Velázquez, Diana X. Robledo-Cadena, Joaquín Alberto Padilla-Flores, Emma Saavedra and Sara Rodríguez-Enríquez*

Departamento de Bioquímica, Instituto Nacional de Cardiología, Ciudad de México, Mexico

NH_4^+ increased growth rates and final densities of several human metastatic cancer cells. To assess whether glutamate dehydrogenase (GDH) in cancer cells may catalyze the reverse reaction of NH_4^+ fixation, its covalent regulation and kinetic parameters were determined under near-physiological conditions. Increased total protein and phosphorylation were attained in NH_4^+-supplemented metastatic cells, but total cell GDH activity was unchanged. Higher V_{max} values for the GDH reverse reaction vs. forward reaction in both isolated hepatoma (HepM) and liver mitochondria [rat liver mitochondria (RLM)] favored an NH_4^+-fixing role. GDH sigmoidal kinetics with NH_4^+, ADP, and leucine fitted to Hill equation showed n_H values of 2 to 3. However, the $K_{0.5}$ values for NH_4^+ were over 20 mM, questioning the physiological relevance of the GDH reverse reaction, because intracellular NH_4^+ in tumors is 1 to 5 mM. In contrast, data fitting to the Monod–Wyman–Changeux (MWC) model revealed lower K_m values for NH_4^+, of 6 to 12 mM. *In silico* analysis made with MWC equation, and using physiological concentrations of substrates and modulators, predicted GDH N-fixing activity in cancer cells. Therefore, together with its thermodynamic feasibility, GDH may reach rates for its reverse, NH_4^+-fixing reaction that are compatible with an anabolic role for supporting growth of cancer cells.

Keywords: ammonium, metastatic cancer cells, GDH kinetics, cooperativity, monod–wyman–changeux model

OPEN ACCESS

Edited by:
Antonio Giuseppe Naccarato, University of Pisa, Italy

Reviewed by:
Andrea Mozzarelli, University of Parma, Italy
Yuanping Xiong, The First Affiliated Hospital of Nanchang University, China

****Correspondence:***
Rafael Moreno-Sánchez
rafael.moreno@cardiologia.org.mx
Álvaro Marín-Hernández
marinhernndez@yahoo.com.mx

Specialty section:
This article was submitted to Cancer Metabolism, a section of the journal Frontiers in Oncology

Received: *13 January 2020*
Accepted: *10 March 2020*
Published: *09 April 2020*

Citation:
Moreno-Sánchez R, Marín-Hernández Á, Gallardo-Pérez JC, Pacheco-Velázquez SC, Robledo-Cadena DX, Padilla-Flores JA, Saavedra E and Rodríguez-Enríquez S (2020) Physiological Role of Glutamate Dehydrogenase in Cancer Cells. Front. Oncol. 10:429. doi: 10.3389/fonc.2020.00429

INTRODUCTION

It has been proposed that the primary metabolic function of glutamate dehydrogenase [GDH; Glu + $NAD(P)^+$ + H_2O <-> 2-OG + NH_3 (or NH_4^+) + NAD(P)H + H^+; EC: 1.4.1.3] is to produce ammonia, or the toxic ion ammonium (NH_4^+), either for urea synthesis in liver, or for direct clearance in kidney (1–5), or to produce 2-oxoglutarate (2-OG) for export to neurons from astrocytes (6). In the forward, oxidative deaminating reaction, GDH provides reducing equivalents as NADPH for oxidative stress management in the mitochondrial matrix and 2-OG for Krebs cycle and oxidative phosphorylation. This canonical role of GDH is a consequence of the efficient transference by transaminases of the α-amino group of several amino acids to 2-OG forming glutamate (Glu). However, it has been shown that the predominant source of ammonium in liver derives from glutamine, not from glutamate (6), and the GDH reaction seems positioned near its thermodynamic equilibrium (3). Moreover, significant GDH activity is also present in mitochondria of nonureogenic organs, such as heart, skeletal muscle, and brain, and the gene encoding GDH1 in humans is expressed in all tissues, whereas the GDH2 gene expression is specific for nerve tissues and testis (4, 5), although the kinetic properties of both GDH isoenzymes are

not significantly different (4). Hence, an ammonium-producing role for GDH can be contested. It appears that the mammalian homohexameric GDH may also have other functions different from that of ammonium supplier, for instance, that of nitrogen assimilation, as well as accessory roles, such as its binding to chromosome X-linked inhibitor of apoptosis protein (XIAP) preventing XIAP inhibition on caspases and thereby promoting cell death (7) and its histone H3-specific tail proteolytic activity in the nucleus (8).

A nitrogen-storing (aminating) role for liver GDH was early proposed by McGivan and Chappell (9) based on their analysis of the rates of the enzyme and surrounding pathways and GDH reaction equilibrium constant. Furthermore, the equilibrium constant ($K_{EQ} = [2\text{-OG}] \times [NADPH] \times [H^+] \times [NH_4^+]/[Glu] \times [NADP^+]$) of the GDH reaction, of $\sim 1 \times 10^{-15}$ M^2 (10) that becomes $\sim 1 \times 10^{-8}$ M at pH 7.0, indicates that the reverse reaction (i.e., glutamate formation from 2-OG) is thermodynamically favorable under physiological conditions, when at least low micromolar ammonium concentrations are present. On this issue, it is worth recalling that the directionality of a given reaction is dictated only by its K_{EQ} value and the actual mass action ratio of [products]/[substrates], even within pathways working in steady state, in which the reaction is kept away from equilibrium because the coupling, adjacent reactions do not allow the products to accumulate. What the kinetic properties of a given enzyme govern, either whether it is down-regulated, overexpressed, or mutated, is the rate at which the reaction proceeds in the forward or reverse direction.

In addition to lactate, ammonium can also be found in the solid tumor microenvironment at levels significantly greater (0.14–5 mM) than those (0.027–0.05 mM) of the healthy organ microenvironments and plasma (5, 11–14). This is caused by the tumor accelerated glutamine metabolism (15–17), as well as by ammonium simple diffusion across the plasma membrane and tumor defective vasculature. High ammonium concentrations are extremely toxic for normal cells and organs, being particularly critical under metabolic acidosis. In the brain, ammonium primarily affects neurons, because it competes with K^+ for inward transport via Na^+/K^+ ATPase and Na^+K^+ Cl^- cotransporter (18), and hence ion homeostasis, electric resting and action potentials, and nerve transmission are compromised. In contrast, high ammonium seems innocuous for human cancer cells and rather promotes partial restoration of proliferation of glutamine-depleted cancer cells (19–21) and increased rates of proliferation and tumor growth of glutamine-supplemented cancer cells (5, 21).

Increased transcription of the GDH genes is found in many cancer types (5, 22–24). Although transcription of glutamine synthetase (another enzyme involved in ammonium assimilation) is also increased in some cancer cells (5, 25), it was recently shown by metabolic tracing analysis with [^{15}N]amide-glutamine or [^{15}N]-NH_4Cl in breast and prostate cancer cells and tumor xenografts in mice that ammonium was primarily assimilated to glutamate through the GDH reverse reaction and then to proline, glutathione, and direct products of the glutamate-dependent transaminase reactions (5, 26); no urea cycle intermediates were labeled, discarding a role for carbamoyl phosphate synthetase I (the mitochondrial matrix isoform) in cancer ammonium assimilation. Furthermore, kinetic modeling of the mitochondrial NADPH/GSH/ROS pathway predicted that, at physiological values of the NADPH/$NADP^+$ (of 0.5–2) and 2OG/Glut (of 0.01–0.1) ratios, GDH behaved as an NADPH consumer catalyzing its reverse reaction, which becomes thermodynamically favored by the presence of micromolar concentrations of ammonium (27). Theoretical modeling of central carbon and nitrogen metabolism also predicted that, when cells take up external ammonium, GDH reverse reaction is required for supporting cell proliferation (28). Indeed, addition of millimolar ammonium to the culture medium significantly increases the growth of human breast MCF-7 and T47D cancer cells (5, 21).

However, a direct and essential role of GDH in ammonium assimilation of cancer cells appears controversial because the GDH activities (V_{max}) are lower in cancer mitochondria, and GDH shows very low affinity for ammonium, with apparent Michaelis–Menten constants (K_m or $K_{0.5}$) of 8 to 80 mM (27, 29–35). It is noted that these kinetic parameters have been calculated from experimental data fitted to the Hill equation for sigmoidal kinetic behavior and under variable and non-saturating ADP concentrations, an allosteric activator; in addition, the assay pH values used have not been within the physiological range.

A systematic analysis of the GDH activity in cancer mitochondria has not been yet undertaken. Therefore, in the present study, the GDH kinetics was also examined in both liver and hepatoma mitochondria. The simple Hill equation and the more complex Monod–Wyman–Changeux (MWC) equation for exclusive binding (36) were tested as models to fully describe the sigmoidal and cooperative kinetic behavior of GDH. The latter model was able to determine GDH V_{max} values, K_s or K_m for substrates, catalytic efficiencies (V_{max}/K_m), activation constants (K_a) for ADP and leucine, inhibition constant (K_i) for GTP, and other relevant parameters related to its cooperative behavior. These GDH kinetic properties, together with the determination of the GDH reaction metabolites in the cell, provided the required information to envision the mechanisms by which GDH may play a key role, as an inorganic nitrogen-fixation device in cancer cells, for amino acids and nucleotides syntheses and cell growth.

RESULTS

Ammonium Stimulates Growth of Human Metastatic Cancer Cells

Addition of NH_4Cl (0.1–10 mM) to bidimensional (2-D) human HeLa, MDA-MB-231, PC3, HTC116, and Colo205 metastatic cancer cell cultures clearly decreased their duplication times, stimulated their proliferation rates, and allowed to reach higher final cell densities at the stationary phase (**Figure 1**; **Table 1**). In contrast, growth rates and final cell densities of 2-D human breast cancer MCF-7, cervix SiHa, prostate DU145, and lung A549 cancer cells, which have low metastatic potential, were not affected by ammonium supplementation of 0.5 to 10 mM NH_4Cl, except for a significant stimulatory effect on μ, the

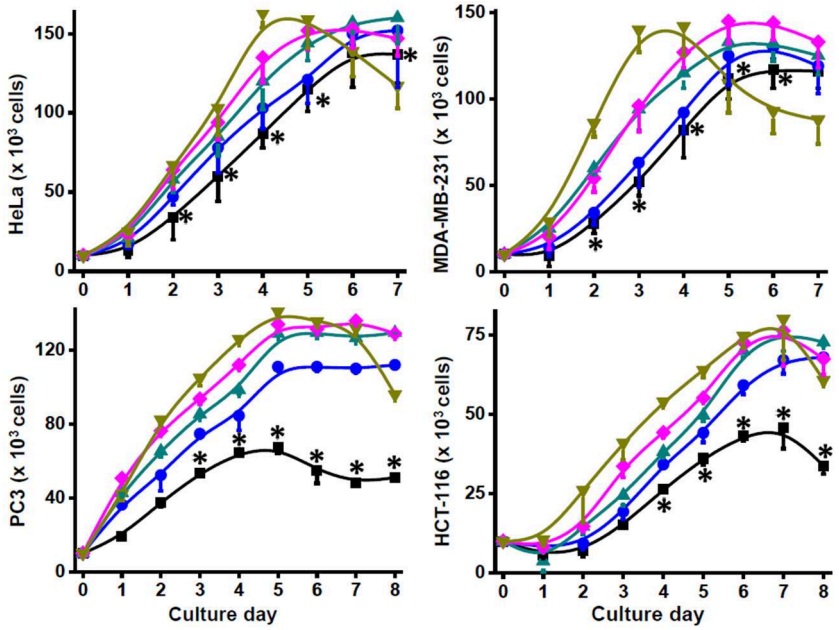

FIGURE 1 | Growth of human metastatic cancer cells with ammonium. Cancer HeLa, MDA-MB-231, PC3, and HCT116 cells (20×10^3 cells/well) were grown in 96-well plates in the presence of 0 (■), 0.5 (•), 1 (▲), 5 (♦), and 10 (▼) mM NH_4Cl. Cell growth was monitored by counting cellular density every 24 h. Viability was >90% in all culture conditions. Data shown represent the mean ± SD of at least three different preparations. Statistical analysis was performed using one-way ANOVA with Scheffé comparison test. *$P < 0.01$ vs. 1, 5, or 10 mM NH_4Cl.

specific cell growth rate, and maximal density at 10 mM in MCF-7 cells (**Table 1**), and increased proliferation rates at 0.1 and 0.5 mM NH_4Cl in DU145 cells (data not shown) but significantly decreased cell densities at ammonium concentrations higher than 1 mM (**Table 1**).

Ammonium toxicity was not apparent (cell morphology was preserved, and viability was higher than 90%), except for a moderate decrease in cell density at 10 mM in the stationary phase of 2-D cultures of HeLa, MDA-MB-231, PC3, and HTC116 cells (**Figure 1**). In contrast, ammonium severely decreased growth of non-cancer mouse 3T3 fibroblasts and human HFF-1 fibroblasts with IC_{50} values around 1 mM (data not shown); higher ammonium concentrations significantly affected duplication times, specific growth rates, and maximal cell densities of mouse and human fibroblasts (**Table 1**). Glutamine removal from the culture medium induced an acute decrease in the growth rates of HeLa and MDA-MB-231 cells; NH_4Cl (1–10 mM) addition did not rescue their growth (data not shown). In this last regard, it is noted that cell culture in glutamine-lacking medium is not a physiologically realistic condition. In addition, transcription of genes involved in proliferation and other processes in cancer cells may be regulated by glutamine (5, 19, 37). Therefore, ammonium supplementation experiments in glutamine-depleted media were not further pursued.

Ammonium supplementation to the tridimensional multicellular tumor spheroids of HeLa cells did not stimulate growth, but in fact 5 and 10 mM ammonium inhibited it (**Figure 2A**). For MDA-MB-231 multicellular tumor spheroid (MCTS), which were significantly smaller than those of HeLa MCTS, ammonium in the 0.5–5 mM range promoted enhanced growth rates, whereas it was clearly toxic at 10 mM (**Figure 2B**).

Effect of Ammonium Supplementation on GDH Protein Level and Activity

Ammonium supplementation induced either a small (HeLa, DU145) or large (MDA-MB-231) increase, or no change (Colo 205), in the total GDH (GDH1 + GDH2) protein content in metastatic cancer cells, and no change in non-metastatic (MCF-7) cells (**Figure 3A**).

The total GDH reverse reaction activity (GDH1 + GDH2) with NADPH as cosubstrate in HeLa and MCF-7 cells was detectable and significant (35–70 mU/mg protein), and also similar to that determined in AS-30D hepatoma cells. However, these GDH activities did not allow for reliable measurements at variable ammonium for determining K_m values; significant interference of cell suspensions due to turbidity, despite the addition of triton x-100, occurred on the determination of GDH activity. Addition of 5 mM NH_4Cl to the culture medium and growth for 5 days did not alter the total GDH activity or induced a slight (∼20%) decrease (data not shown) in HeLa and MCF-7 cells.

Covalent GDH Regulation

Glutamate dehydrogenase may undergo a variety of posttranslational modifications, which apparently may also affect activity (38–40). Indeed, immunoprecipitation assays revealed that GDH in HeLa and MDA-MB-231 cells showed significant phosphorylation and acetylation, which were further

TABLE 1 | Effect of ammonium supplementation on cancer cell proliferation.

	Duplication time (h)			μ (h^{-1})			Maximal cellular densities ($\times 10^3$)		
	Control	NH_4Cl (mM)		Control	NH_4Cl (mM)		Control	NH_4Cl (mM)	
		+5	+10		+5	+10		+5	+10
Metastatic cells									
MDA-MB-231	32 ± 1	26 ± 3 *	25 ± 1*	0.47 ± 0.05	0.61 ± 0.06*	0.9 ± 0.07*	82 ± 16	145 ± 13*	142 + 17*
HeLa	31 ± 3	25.5 ± 2*	24 ± 2*	0.63 ± 0.04	0.77 ± 0.03*	0.8 ± 0.05*	87 ± 9	153 ± 13*	163 ± 9*
PC3	36 ± 2	28 + 2*	26 ± 1*	0.57 ± 0.06	1.01 ± 0.04*	1.05 ± 0.03*	68 ± 3.5	136 ± 2*	141 ± 1.4*
HCT116	69 ± 3	45 ± 1*	39 ± 2*	0.36 ± 0.05	0.49 ± 0.03*	0.51 ± 0.02*	45 ± 7	76 ± 11*	80 ± 13*
Colo 205	80 ± 5	48 ± 2*	44 ± 4*	0.53 ± 0.02	0.62 ± 0.05*	0.63 ± 0.04*	45 ± 7	68 ± 6*	66 ± 6*
Low metastatic cells									
MCF-7	34 ± 1	37 ± 2	45 ± 6	0.34 ± 0.05	0.38 ± 0.02	0.69 ± 0.03*	44 ± 7	72 ± 6*	76 ± 5*
SiHa	48 ± 3	51 ± 4	55 ± 5	0.60 ± 0.04	0.58 ± 0.05	0.55 ± 0.07	90 ± 6	86 ± 7	82 ± 5
DU145	26 ± 2	32 ± 2*	35 ± 3*	1.0 ± 0.06	0.47 ± 0.07*	0.55 ± 0.04*	106 ± 8	92 ± 6	85 ± 4*
A549	25 ± 3	20 ± 2	17 ± 3*	0.78 ± 0.05	0.82 ± 0.04	0.85 ± 0.06*	41 ± 5	49 ± 4	56 ± 2*
Non-cancer cells									
3T3	26 ± 0.5	46 ± 2*	60 ± 1*	0.7 ± 0.02	0.43 ± 0.1*	0.32 ± 0.003*	131 ± 5	45 ± 3*	36 ± 2*
HFF-1	32 ± 7	38 ± 12	55 ± 2*	0.75 ± 0.1	0.65 ± 0.08	0.4 ± 0.1*	93 ± 5	60 ± 10*	46 ± 3*

*The number of independent cell cultures assayed (n) was 3. Statistical analysis was performed using one-way ANOVA with Scheffé comparison test. *P ≤ 0.05 or 0.01 vs. control; the cell viability in all conditions was >90%. The maximal cellular densities were reached for HeLa and MDA-MB-231 cells at day 4; for PC3, 3T3, HFF-1, and DU145 cells at day 5; for Colo-205, MCF-7, A549, and SiHa cells at day 6; and for HCT 116 cells at day 7.*

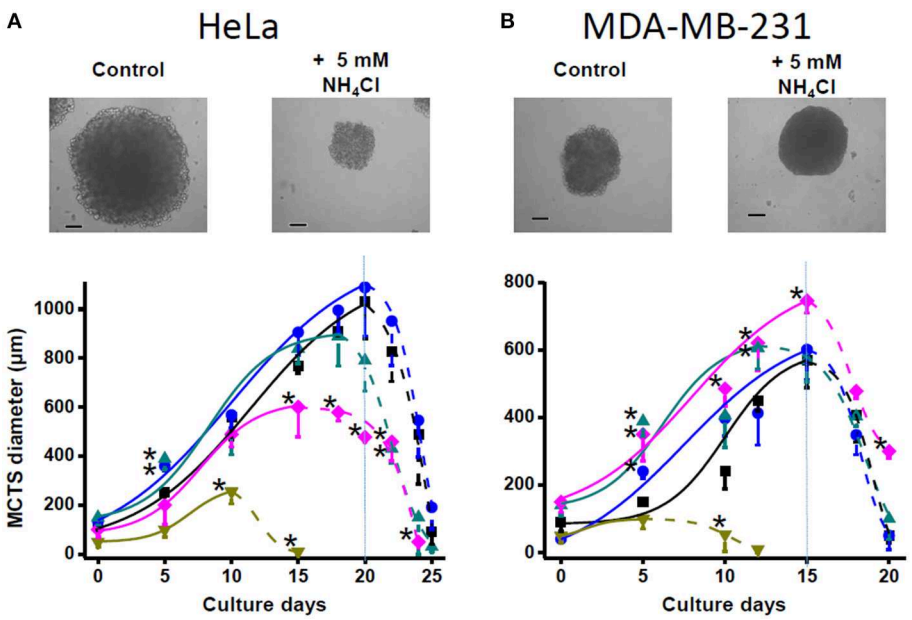

FIGURE 2 | Effect of ammonium supplementation on MCTS growth. **(A)** HeLa and **(B)** MDA-MB-231 cells (2×10^4 cells/mL) were seeded in 2% (wt/vol) agarose-coated culture dishes in DMEM with 0 (■), 0.5 (•), 1 (▲), 5 (♦), and 10 (▼) mM NH_4Cl. Spheroid micrographs were taken at day 20 (HeLa) or day 15 (MDA-MB-231); bars represent 200 µm. Fresh DMEM medium was replaced every 3 days. The spheroid growth was determined at the indicated times by measuring MCTS diameter. Data shown represent the mean ± SD of at least 30 MCTS (10 MCTS from each preparation), $n = 3$ different preparations. Statistical analysis was performed using one-way ANOVA with Scheffé comparison test. *$P < 0.01$ vs. non-treated MCTS.

increased by 5 day growth in the presence of ammonium (**Figures 3B,C**).

As a direct control and to discard the participation of the nuclear GDH2 isoform, mitochondria isolated from AS-30D hepatoma ascites cells and rat liver were also used to assess mitochondrial matrix GDH1 covalent modifications. The GDH1 content in AS-30D hepatoma mitochondria (HepM) was slightly lower than that of RLM. Furthermore, phosphorylation of Ser

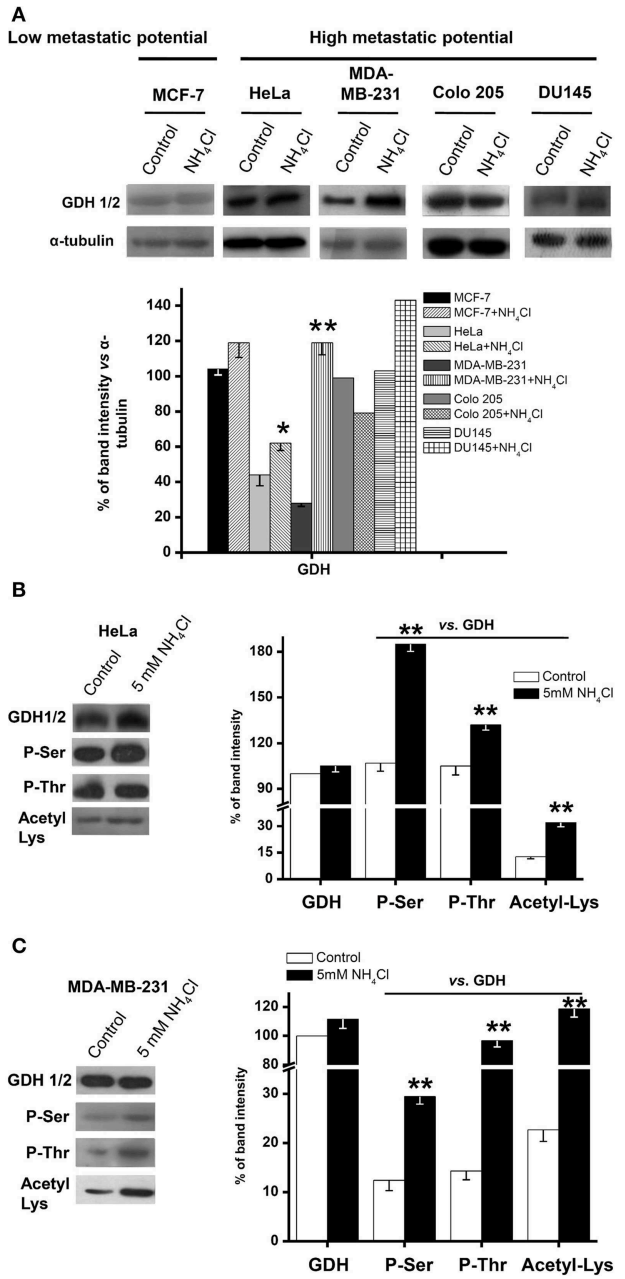

FIGURE 3 | Glutamate dehydrogenase covalent modifications in human metastatic cancer cells. Total GDH protein content by Western blotting **(A)** and GDH phosphorylation and acetylation status by immunoprecipitation **(B,C)** were determined, as described in *Materials and Methods*, in MCF-7, HeLa, MDA-MB-231, Colo 205, and DU145 cells exposed to 5 mM NH_4Cl (except for DU145, which was exposed to 1 mM) for 5 days in 2-D cultures. Representative results are shown. α-Tubulin was used as loading control and for data normalization in the Western blot experiments **(A)**; the control GDH protein signal of each individual experiment (no NH_4^+ added) was used for initial normalization of the GDH signal with NH_4^+ in the immunoprecipitation assays **(B,C)**, followed by comparison of the phosphorylation and acetylation signals against their respective total immunoprecipitated GDH (control or 5 mM NH_4Cl) signal. Densitometric analysis represents the mean ± SD of three independent cell cultures (except for Colo 205 and DU145, $n = 2$). Statistical analysis was performed using one-way ANOVA with Scheffé comparison test. $^*P < 0.05$, $^{**}P < 0.01$ vs. control.

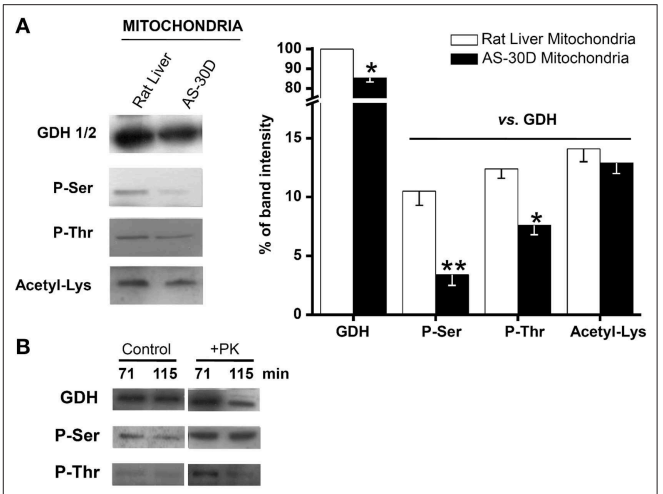

FIGURE 4 | Phosphorylation and acetylation status of GDH in isolated mitochondria. Representative Western blots and relative protein contents are shown. Data represent the mean ± SD of three different preparations. **(A)** The RLM GDH protein signal was used for initial normalization of the HepM GDH signal, followed by comparison of the phosphorylation and acetylation signals against their respective GDH (control or 5 mM NH_4Cl) signal. **(B)** Phosphorylation of HepM GDH by commercial phosphorylase kinase. HepM fractions (10 mg protein/mL) were incubated at 30°C for the indicated times with 41 mM α-glycerophosphate, 20 mM Tris pH 7.4, 1 mM $CaCl_2$, 5 mM ATP, 7 mM $MgCl_2$, 300 mM trehalose, and 40 U rabbit muscle phosphorylase kinase (PK). Controls were also carried out under the same conditions, but PK was omitted from the mix reaction. Statistical analysis was performed using one-way ANOVA with Scheffé comparison test.$^*P < 0.05$, $^{**}P < 0.01$ vs. RLM.

and Thr residues was also significantly lower in HepM GDH1, whereas Lys acetylation was similar to that of RLM GDH1 (**Figure 4A**). Ser phosphorylation was the covalent modification that better correlated with GDH1 activity, because it was approximately three times lower in HepM vs. RLM (**Figure 4A**), which was similar to the difference in activity (see below). HepM GDH1 phosphorylation (**Figure 4B**), by a commercial rabbit muscle phosphorylase kinase, produced a moderate but significant increase in activity of 45% ± 39% ($n = 4$).

GDH Reverse (Aminating) Activity in Hepatoma Mitochondria

The apparent affinity of GDH1 for ammonium is low (the reported $K_{0.5}$ values for ammonium are in the 15–60 mM range), which raises doubts on the physiological significance of the presumed GDH1 N-fixing role because ammonium physiological concentrations are much lower. To solidly establish whether GDH1 is able to catalyze its reverse reaction under physiological conditions in cancer cells, a systematic analysis of its kinetic properties is required, in which the affinity constant for ammonium is adequately determined.

The most common GDH1 assay reaction medium usually contains EDTA, a divalent metal cation chelating agent, because it is known that Mg^{2+} may inhibit its activity. However, in the 0- to 0.4-mM range of added $MgCl_2$, GDH1 activity was not affected; at 1 mM Mg^{2+}, <10% inhibition was attained,

and at 2 mM Mg^{2+}, ∼20% inhibition was achieved. Null Mg^{2+} effects on GDH1 activity have also been previously reported (31). These observations suggested that the regulatory roles of ADP and GTP on GDH are independent on whether the nucleotides are bound to the enzyme as Mg complexes or free forms. Spermidine has been also claimed to inhibit GDH, but in our hands, this polyamine in the 0–5 mM range was innocuous and at 20 mM indeed inhibited GDH activity by 20% (data not shown). GDH1 exhibited a marked hysteresis after several minutes of reaction, depending on the incubation conditions; however, this behavior was not further explored. Moreover, for an appropriate kinetic analysis, initial rate determinations were used because only these can be reliably associated to the added substrate concentrations (before they start changing), and products have not been accumulated to significant levels that may affect enzyme rate.

The sigmoidal behavior regarding NH_4^+ and ADP and the hyperbolic behavior regarding 2-OG and NADPH of the HepM GDH1 activity (**Figure 5**) were highly similar to that displayed by RLM GDH (data not shown). The sigmoidal patterns were fitted to the Hill equation that yields $K_{0.5}$ values for the variable substrate, and which are approximated but not proper K_m or K_s (k_{-1}/k_1, rapid equilibrium constants) values. The kinetic analysis was carried out at the indicated pH values to encompass the mitochondrial matrix physiological pH range of 7.2 to 8.2 (41, 42); more alkaline pH values are reached only in the absence of Pi, which is not a physiological condition. The only marked effect of higher pH was an increased K_m for NADPH and lower $K_{0.5}$ for ADP in both mitochondrial types (**Table 2**). Indeed, the pH profile of the GDH1 reverse activity in both mitochondrial types showed maximal rates in the 7.0–7.5 range, sharply decreasing at lower and higher pH values (data not shown). A similar pH profile was reported for the ox liver GDH forward reaction (43), as well as the human GDH1 reverse reaction (34).

The V_{max} and catalytic efficiency (V_{max}/K_m) values were markedly (4- to 8-fold) lower in HepM (**Table 2**). However, the ligand binding parameters were similar between HepM and RLM, except for a slightly higher IC_{50} value for GTP at pH 7.5 in HepM GDH1. The Hill coefficient values lower than 3 suggested that GDH has a moderate cooperativity among its six subunits. Similar Hill coefficient values have been previously reported (32, 35).

The $K_{0.5}$ and Hill coefficient values determined were within the range of values ($K_{0.5NH4+}$ = 6.5–80 mM, K_{m2OG} = 0.47–4.5 mM, K_{mNADPH} = 0.02–0.12 mM, and n_H= 1.6–2.4) reported for recombinant human GDH isoforms (GDH1 and GDH2), bovine liver GDH, Ox brain GDH, dogfish liver GDH, rat brain GDH, and bovine brain GDH isoforms, at the pH range of 7.4–8.7 (29, 33–35, 44, 45). It should be noted that the lower $K_{0.5}$ values for ammonium were attained at alkaline pH values (33–35, 44).

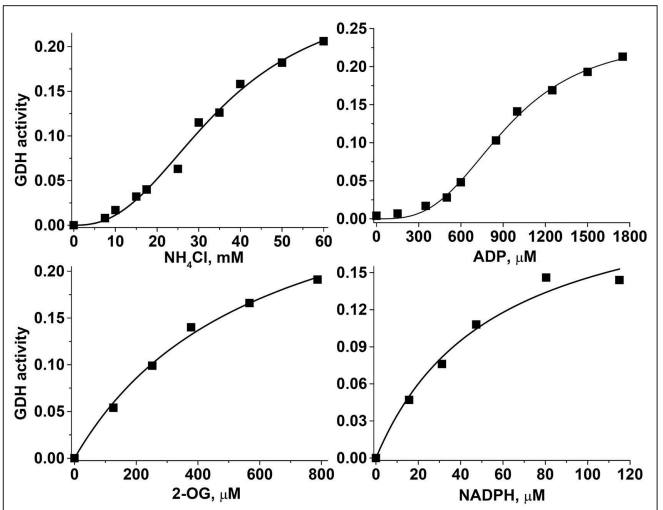

FIGURE 5 | Kinetics of the hepatoma mitochondria reverse GDH reaction. For these representative experiments, 219 μg protein of HepM was incubated in KME buffer at pH 7.20 and 37°C. The saturation curves with variables NH_4Cl and ADP were fitted to the Hill equation, whereas the saturation curves with variables 2-OG and NADPH were fitted to the Michaelis–Menten equation. The units of the GDH activity were Δabsorbance at 340 nm min^{-1}.

GDH1 Reverse (Aminating) Activity Can Be Fitted to the MWC Model

The sigmoidal kinetic behavior of GDH1 regarding the substrate NH_4^+ and the activators ADP and leucine has been commonly fitted to the Hill equation, $v = \frac{Vmax[S]^{n_H}}{K'+[S]^{n_H}}$. In this equation, cooperativity is assessed by the Hill coefficient n_H value, whereas K' does not represent directly a measurement of affinity, although some researchers have interpreted as such. The Hill equation does not allow for estimation of affinities for allosteric activators and inhibitors either. Therefore, an effort was made to fit the experimental GDH1 data to the MWC equation for ligand exclusive binding (36). Thus, Equation 1 (see below) does allow the experimental determination of actual ligand affinity values. Initial attempts yielded poor fitting because the number of interacting subunits (n) was fixed to 6, and V_{max} was considered to be unique. However, analysis of **Figure 5** and other similar results indicated that ADP was an essential allosteric activator because no significant activity was displayed in its absence, and the apparent V_{max} clearly changed, depending on the ADP concentration added. Then, when it was assumed that V_{max} changes with the ADP concentration ($V_{max,ADP}$), and n was allowed to freely vary, the data fitted MWC Equation 1 exceptionally well (**Figure 6**).

MWC equation:

$$v = \frac{Vmax_{ADP}\frac{[NH_4^+]}{Km_{NH4+}}\left(1+\frac{[NH_4^+]}{Km_{NH4+}}\right)^{n-1}}{L'+\left(1+\frac{[NH_4^+]}{Km_{NH4+}}\right)^{n}} \quad (1)$$

Modification of L by allosteric inhibitor:

$$L' = L\left(1+\frac{[GTP]}{Ki_{GTP}}\right)^{n}$$

TABLE 2 | Kinetic parameters of mitochondrial GDH for the reverse reaction derived from the Hill equation.

GDH kinetic parameters	pH 7.2		pH 7.5	
	HepM	RLM	HepM	RLM
V_{max}, mU/mg protein	202 ± 63 (9)*	818 ± 168 (10)	168 ± 39 (6)*	725 ± 179 (5)
$K_{0.5}$ NH_4^+, mM	25.2 ± 8 (9)	23.9 ± 3.7 (9)	26.8 ± 7.2 (6)	18.2 ± 5.9 (5)
n_H	2.12 ± 0.7 (9)	1.97 ± 0.8 (9)	1.5 ± 0.7 (6)	1.4 ± 0.4 (5)
$V_{max}/K_{0.5}$ NH_4^+, min^{-1} mg^{-1} mL^{-1}	0.008	0.034	0.006	0.039
$K_{0.5}$ ADP, μM	564 ± 167 (4)	567 ± 125 (3)	281 ± 134 (4)	285 (2)
n_H	2.77 ± 0.7 (4)	2.4 ± 0.3 (3)	2.6 ± 0.4 (4)	2.34 (2)
$K_{0.5}$ Leu, mM	2.6 (2)	3.9 (2)	ND	ND
n_H	2.8 (2)	2.75 (2)		
K_m 2-OG, μM	442 ± 160 (5)	371 ± 232 (6)	733 ± 325 (4)	396 ± 75 (3)
V_{max}/K_m 2-OG, min^{-1} mg^{-1} mL^{-1}	0.45	2.20	0.22	1.83
K_m NADPH, μM	46 ± 14 (6)	56.6 ± 26 (3)	109 ± 4 (3)	133 ± 28 (3)
IC_{50} GTP, μM	114 ± 29 (4)	139 ± 21 (4)	147 ± 32 (3)	244 (2)

*N.D., not determined; Leu, leucine. Statistical analysis was performed using Student t-test. *P < 0.01 vs. RLM. The number of independent preparations assayed is indicated between parentheses.*

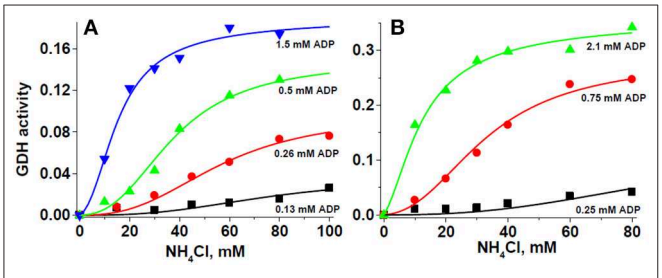

FIGURE 6 | Glutamate dehydrogenase kinetics obeys the ligand exclusive binding MWC model. For these representative experiments, 280 μg protein of HepM **(A)**, and 90 μg protein of RLM **(B)** were incubated in KME + HEPES buffer at pH 7.50 and 37°C. The solid lines represent the simultaneous global fitting of all experimental points to the exclusive ligand binding MWC Equation 1. The χ2 values of the non-linear regression analyses were 0.00003 and 0.00013 for HepM GDH and RLM GDH, respectively. The V_{max} values in ΔAbs/min at each ADP concentration were 0.037 ± 0.009 (0.13 mM ADP), 0.099 ± 0.010 (0.26 mM ADP), 0.153 ± 0.008 (0.5 mM ADP), and 0.193 ± 0.011 (1.5 mM ADP) for HepM GDH; and 0.131 ± 0.113 (0.25 mM ADP), 0.295 ± 0.022 (0.75 mM ADP), and 0.367 ± 0.024 (2.1 mM ADP) for RLM GDH.

Modification of L by allosteric activator

$$L' = \frac{L}{\left(1 + \frac{[ADP]}{Ka_{ADP}}\right)^n}$$

Surprisingly, the K_m values for ammonium were significantly lower, at approximately 9 mM at pH 7.5 (**Table 3**), than the $K_{0.5}$ values derived from the Hill equation (**Table 2**). The K_a values for ADP were in the submillimolar range, well within the ADP physiological concentrations. It is noted that this is the first time that affinity ($1/K_m$; $1/K_a$) values are produced for the cooperativity ligands of GDH1. Furthermore, n was not near 6, the actual number of GDH1 subunits, but rather it was near 3 (**Table 3**). Linearization of the MWC equation for exclusive ligand binding by using the Horn–Bornig equation (36) rendered n values also close to 3 (data not shown). In turn, the large L values indicate that GDH1, in the absence of its essential activator ADP, is preferentially stabilized as an inactive form. Ammonium at saturating concentrations (>50 mM) was unable to trigger cooperativity and activity in the absence of ADP; in other words, catalysis was negligible with no ADP. With ADP, the T inactive conformation transforms into an active R state. The exclusive binding MWC model with variable (ADP-dependent) V_{maxADP} (Equation 1) also simulated that the V_{max} and catalytic efficiency (V_{max}/K_m) values (estimated at saturating ADP concentrations) of GDH1 in HepM were significantly (2.5- to 4.5-fold) lower than those of GDH1 in RLM (**Table 3**).

Data of the GTP inhibition on GDH1 activity also fitted well to the MWC Equation 1 (**Figure 7**). These experiments were carried out in the presence of saturating ADP. This was the reason why L values were now too low (**Table 4**); that is, ADP transformed most of the inactive T enzyme forms into active R forms. Nevertheless, GTP was still able to exert a potent inhibitory effect on the reverse GDH1 activity, with K_i values in the low micromolar range. It is noted that the K_m values for ammonium derived from the GTP allosteric inhibition (**Table 4**) were highly similar to those derived from the ADP allosteric activation (**Table 3**), which provided further validation to the MWC Equation 1 that it can accurately reproduce the GDH1 kinetic behavior.

Assessment of the GDH Reverse Reaction Activity *in vivo*

For estimation of the GDH1 activity under physiological conditions, Equation 2 was applied. This equation represents the concerted transition model of MWC for exclusive ligand

TABLE 3 | Kinetic parameters of GDH with ADP derived from the MWC equation.

GDH kinetic parameters	pH 7.2		pH 7.5	
	HepM	RLM	HepM	RLM
V_{max}, mU/mg protein	203 ± 65* (3)	878 ± 86 (5)	182 ± 51* (5)	750 ± 151 (4)
K_m NH_4^+, mM	11.2 ± 3.5 (3)	18.0 ± 11 (5)	9.3 ± 7.2 (4)	8.8 ± 4.1 (4)
V_{max}/K_m NH_4^+, min^{-1} mg^{-1} mL^{-1}	0.018	0.048	0.019	0.085
n	2.6 ± 0.3 (3)	3.8 ± 1.0 (5)	2.9 ± 0.7 (4)	2.7 ± 0.3 (4)
L_0	3,387 ± 4,165 (3)	5,120 ± 9,017 (5)	4,705 ± 3,876 (4)	207,232 ± 378,128 (4)
K_a ADP, mM	0.42 ± 0.26 (3)	0.51 ± 0.14 (5)	0.44 ± 0.37 (3)	0.11 ± 0.14 (4)

*Statistical analysis was performed using Student t-test. *P < 0.001 vs. RLM. The number of independent preparations assayed is indicated between parentheses.*

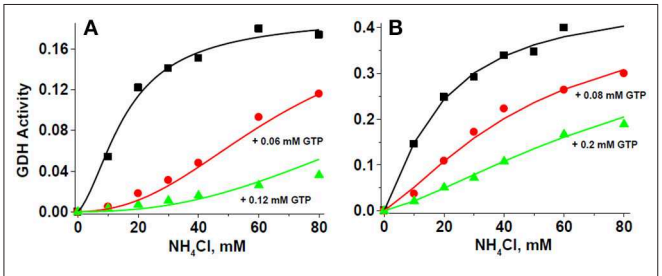

FIGURE 7 | GTP inhibition of GDH activity fits the MWC equation. For these representative experiments, 279 μg protein of HepM **(A)** and 86 μg protein of RLM **(B)** were incubated in KME + HEPES buffer at pH 7.50 and 37°C. The solid lines represent the simultaneous global fitting of all experimental points to the exclusive ligand binding MWC Equation 1. The χ^2 values of the non-linear regression analyses were 0.00005 and 0.00013 for HepM GDH and RLM GDH, respectively. The V_{max} values in ΔAbs/min at saturating ADP concentration were 0.199 ± 0.013 (1.5 mM ADP) for HepM GDH; and 0.471 ± 0.041 (2.1 mM ADP) for RLM GDH.

binding including GTP inhibition and ADP activation (Equation 1), together with ordered Bi-Bi Michaelis–Menten terms for 2-OG and NADPH. L is the allosteric transition constant; K_{aADP} is the activation constant for ADP, and K_{iGTP} is the inhibition constant for GTP.

$$v = \mathrm{V\,max}\left(\frac{\frac{[\mathrm{NADPH}]}{Km_{\mathrm{NADPH}}}\frac{[2\mathrm{OG}]}{Km_{2\mathrm{OG}}}}{1+\frac{[\mathrm{NADPH}]}{Km_{\mathrm{NADPH}}}+\frac{[\mathrm{NADPH}]}{Km_{\mathrm{NADPH}}}\frac{[2\mathrm{OG}]}{Km_{2\mathrm{OG}}}}\right)\times \left(\frac{\frac{[\mathrm{NH_4^+}]}{Km_{\mathrm{NH4+}}}\left(1+\frac{[\mathrm{NH_4^+}]}{Km_{\mathrm{NH4+}}}\right)^{n-1}}{\frac{L\left(1+\frac{[\mathrm{GTP}]}{Ki_{\mathrm{GTP}}}\right)^{n}}{\left(1+\frac{[\mathrm{ADP}]}{Ka_{\mathrm{ADP}}}\right)^{n}}+\left(1+\frac{[\mathrm{NH_4^+}]}{Km_{\mathrm{NH4+}}}\right)^{n}}\right) \quad (2)$$

The metabolite concentrations either determined in the present study or reported (**Table 5**) as well as the kinetic parameters here determined (**Tables 2–4**), together with Equation 2, were used to predict the GDH1 activity under *in vivo* conditions. It should be noted that the ATP content determined in HepM and RLM (**Table 5**) was attained in mitochondria incubated in the absence of external nucleotides, which is not a physiological condition. The NH_4^+, ATP, glutamate, and ADP contents in RLM were similar to other previously reported (46–48).

Of greater significance for the present study, the ADP content was lower in HepM than in RLM (**Table 5**). Then, at 0.6–1.6 mM NH_4^+ and in presence of 0.6 mM ADP, the mitochondrial GDH activity in the aminating reverse reaction would be of 0.11 to 0.34 nmol/min * mg protein, whereas in presence of 2 mM ADP the activity would range from 1.1 to 3.3 nmol/min * mg protein in HepM (**Figure 8**).

DISCUSSION

Ammonium Promotes Metastatic Cancer Cell Proliferation

Ammonium supplementation to glutamine-containing culture media was able to stimulate growth of the highly malignant HeLa, MDA-MB-231, PC3, HCT116, and Colo205 cancer cells in 2-D cultures. These human cancer cell lines are metastatic and hence have heightened abilities for migration, invasion, and colonization in glutamine-containing media (51–56). They also show enhanced drug resistance due to overexpression of plasma membrane multidrug pumping ATPases, including P-glycoprotein and multidrug resistance protein-1 (57). Interestingly, MCF-7 cells, a human breast cancer cell line with an attenuated metastatic potential (51), as well as SiHa and A549 cells, showed no significant growth stimulation by ammonium addition to glutamine-containing media. In a previous study, it was also reported that ammonium (2–5 mM) only slightly stimulated MCF-7 cell proliferation (21).

A less clear effect of ammonium on 3-D cancer cell growth was probably due to the development of hypoxic and hypoglycemic areas within MCTS (58); greater hypoxic areas develop in greater MCTS such as those formed by HeLa cells. Prolonged hypoxia of cancer cells induces severe suppression of mitochondrial functions (59). Because ammonium assimilation is primarily a mitochondrial function, and GDH1 and a glutamine synthetase isoform (another enzyme able to incorporate ammonium) are localized in the mitochondrial matrix, the putative ammonium assimilation in cancer cells could be impaired when the mitochondrial function is compromised.

Metastatic cancer cells were best equipped for ammonium assimilation than non-metastatic cancer cells in glutamine-containing culture media. This interesting observation was not further examined in the present study, but it might reflect an essential requirement during migration, invasion, and/or colonization. Indeed, GDH and glutamine synthetase have been proposed as sensitive markers of metastasis in colorectal and

TABLE 4 | Kinetic parameters of the GDH inhibition by GTP derived from the MWC equation.

GDH kinetic parameters	pH 7.2		pH 7.5	
	HepM	RLM	HepM	RLM
V_{max}, mU/mg protein	163 ± 78* (3)	848 ± 119 (3)	178 ± 56 (3)	714 (2)
K_m NH_4^+, mM	12.0 ± 2.6 (3)	8.5 ± 4.5 (3)	10.3 ± 2.6 (3)	5.6 ± 3.6 (3)
n	1.99 ± 0.65 (3)	2.17 ± 0.25 (3)	3.3 ± 1.3 (3)	1.6 ± 0.2 (3)
L'	8.8 ± 11 (3)	20 ± 28 (3)	31 ± 34 (3)	14 ± 20 (3)
K_i GTP, μM	28 ± 27 (3)	60 ± 10 (3)	64 ± 59 (3)	31.7 ± 7 (3)

$P < 0.001$ vs. RLM. The number of independent preparations assayed is indicated between parentheses.

TABLE 5 | Contents of intramitochondrial metabolites.

Metabolites (mM)		HepM		RLM	
		+ Gln + Pyr-Mal	+ Pyr-Mal	+ Gln + Pyr-Mal	+ Pyr-Mal
2-Oxoglutarate		2.1 (2)	0.5 (1)	N.M. 0.4–1 [6,a]	N.M. 0.11 [1,d]
NH_4^+ in		1.1 ± 0.5 (3)	<0.1 mM (3)	2.4 ± 2.3 (3) 5 [4,a]	0.9 ± 1 (3)
NH_4^+ out		3.6 ± 1.1 (3)	0.1 ± 0.2 (3)	0.9 ± 0.7 (3) 0.4 [4,a]	0.1 ± 0.1 (3)
ATP		0.6 ± 0.1 (4)	0.7 ± 0.01 (3)	2.3 ± 0.2 (3) 10 [5,b] 7.7–9 [6,a]	1.5 ± 0.4 (3) 6.3 [3,c]
ADP	Without external ADP	0.6 ± 02 (4)	0.6 (1)	0.7 (2)	N.M.
	With external ADP	0.7 (2)	N.M.	1.7 (2) 5.3 [5,b] 7.3–8.9 [6,a]	N.M.
GTP		0.14 (2)	N.M	N.M.	N.M. 0.15–0.2 [3,c]
Glutamate		9.5 (2)	2.6 (2)	1.9 (1) 10–11 [6,a]	1.6 (1)
NAPDH		N.M.	N.M.	N.M. 1.2 [2.a] 4.8–4.9 [6,a]	N.M.
$NADP^+$		N.M.	N.M.	N.M. 0.5 [2,a] 0.1–0.35 [6,a]	N.M.

Mitochondria were incubated for 10 min as described in Materials and Methods with either 4 mM glutamine, 1 mM pyruvate, and 2 mM malate (Gln+Pyr-Mal) or 1 mM pyruvate and 2 mM malate (+Pyr-Mal). When mitochondria were exposed to external ADP, 5 mM ADP was added after 10 min incubation; 2 min later, the reaction was stopped, and intramitochondrial ADP was determined. See Materials and Methods for a detailed description of the procedure used for the preparation of mitochondrial extracts and determination of metabolites. N.M., not measured. The number of independent preparations assayed is indicated between parentheses. Values taken from [1]Moreno-Sánchez et al. (27), [2]Liu and Kehrer (49), [3]Smith et al. (50), [4]Wanders et al. (47), [5]Akerboom et al. (48), [6]Wanders et al. (46). Amino acids used in the published data were [a]glutamate (2–20 mM) or [b]alanine (10 mM) plus malate (2 mM). In the absence of amino acids, the substrates were [c]2-OG (1 mM) plus malate (1 mM) or [d]pyruvate (1 mM) plus malate (2 mM).

ovarian cancers, respectively (23, 25). This issue clearly deserves further experimental analysis.

GDH Covalent Modification–Activity Relationship

It was previously demonstrated by using short hairpin RNA technology and performing metabolomic tracing analysis of [^{15}N]amide-glutamine metabolism that GDH was the primary step of ammonium assimilation in human breast cancer MCF-7 and T47D cells (5). Increased tumor spheroid growth prompted by ammonium was suppressed by GDH down-regulation; the alternative ammonium assimilation routes catalyzed by carbamoyl phosphate synthetase I and glutamine synthetase were unable to rescue the increased spheroid growth with ammonium.

It has been reported that gene expression of GDH1 and glutaminase is increased by ammonium in the culture medium of metastatic Hep3B (human hepatoma) cells under normoxia (20). Moreover, the levels of GDH mRNA and protein are significantly higher in metastatic cancers vs. low metastatic cancers (19, 23, 26). GDH gene transcription was not assessed here. Likewise,

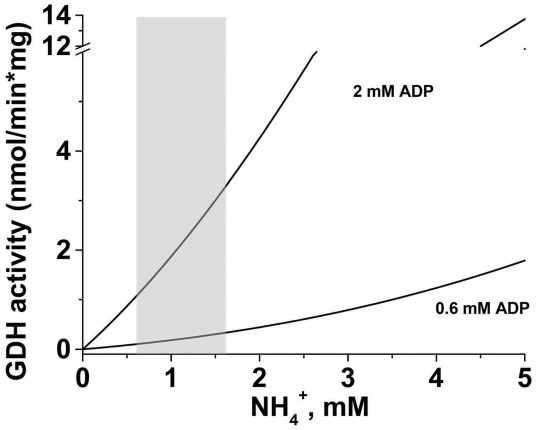

FIGURE 8 | Simulation of GDH activity in the presence of modulators. For estimation of the GDH activity under physiological conditions, Equation 2 was used. The kinetic parameters at pH 7.5 were taken from **Tables 2**, **3**, and concentrations of substrates and modulators were taken from **Table 4**. The gray-shaded area represents the range of NH_4^+ concentrations that can be found in cancer mitochondria when glutamine is oxidized (**Table 4**). *In silico* analysis was performed in the OriginPro 8 software with the following concentration values: 2.1 mM 2-oxoglutarate, 0.6 or 2 mM ADP, 0.14 mM GTP, and 1.2 mM NADPH.

ammonium supplementation significantly increased the GDH protein levels in the metastatic cancer HeLa, DU145, and MDA-MB-231cells, whereas it did not change in the low metastatic MCF-7 and metastatic Colo 205 cells. In addition, the degree of GDH (Ser/Thr) phosphorylation and (Lys) acetylation did markedly increase in HeLa and MDA-MB-231cells. All these changes in metastatic cells enhance GDH activity.

Phosphorylation of GDH1 seems to confer greater catalytic efficiency (V_{max}/K_m, increased V_{max} and lower K_m for $NADP^+$) and structural stability (38). However, in this last study, protein phosphorylation was not directly assessed, but it was rather assumed, and the changes determined in V_{max} and K_m were marginal. Ammonium supplementation certainly induced increased GDH covalent modification in 2-D HeLa and MDA-MB-231 cells. In addition, Ser phosphorylation was the covalent modification that better correlated with GDH activity, because it was approximately three times lower in HepM vs. RLM (**Figure 4**), which was similar to the difference in activity (**Tables 2**–**4**). Furthermore, direct GDH phosphorylation did slightly affect V_{max}, indicating that covalent modifications might regulate GDH activity. Perhaps, phosphorylation and acetylation of GDH might also regulate its stability or subcellular localization, but this issue clearly requires further experimental analysis.

Kinetic Properties of Tumor Mitochondria GDH1

To have an accurate estimate of the level of active enzyme under *in vivo* conditions, with the physiological covalent modifications included, V_{max} must be determined in intact cells and mitochondria rather than in isolated enzymes to revealing the actual content of active enzyme expressed. AS-30D hepatoma cells are a cancer cell model that allows for preparing functional, tightly coupled mitochondria with high yields; this cannot be achieved with human cancer cell cultures using the available commercial kits for preparing mitochondria. Thus, mitochondrial matrix enzymes from cancer cells can be readily and reliably analyzed. A systematic kinetic analysis of GDH1 activity in hepatoma mitochondria was undertaken to elucidate its kinetic parameters, including K_m values for NH_4^+, 2-OG, and NADPH; catalytic efficiencies (V_{max}/K_m); K_a values for ADP and leucine; K_i value for GTP; Hill coefficient n; and allosteric transition constant L. For comparison, liver mitochondria GDH1 was also characterized.

The V_{max} values for the reverse reaction were near one order of magnitude greater than those determined for the forward reaction with $NADP^+$ (27). Higher V_{max} values for the GDH1 reverse reaction than for the forward reaction have been also previously described by others (4, 9). Thus, at least from a kinetic standpoint, GDH can readily be able to catalyze the assimilatory reaction with ammonium under near-physiological conditions.

Many mutations described for kidney GDH lead to a diminished ability of GTP to affect activity (3). However, HepM GDH1 was equally sensitive to GTP inhibition than RLM GDH1 indicating that both enzymes showed similar GTP K_i values. Moreover, other ligand binding constants (K_m, $K_{0.5}$, K_a) were also similar between both enzymes. The high similarity of the GDH binding parameters between HepM and RLM clearly indicated that the GDH1 isoform expressed in hepatoma cells has no mutations, or if mutations occurred, they were silent as no functional consequences were apparent. The only difference was the lower content of GDH1 active protein in HepM; that is, its V_{max} and catalytic efficiency (V_{max}/K_m) values were clearly lower, which derived from both covalent modifications and lower protein content.

In several studies where GDH activity has been determined, ADP has been used at 1 mM. However, it should be noted that such ADP concentration is not saturating for GDH at pH of 7–7.5, and hence greater concentrations are required (>2 mM) to take the enzyme to its fully active R form. On the other hand, the pH profile of the GDH1 reverse activity suggested the involvement of histidine and cysteine residues in GDH catalysis. From previous studies (60–63), it has been indicated that indeed His and Cys, as well as Lys residues, are involved in GDH catalysis (deamination/amination) and 2OG/Glu binding. However, in these last studies, ADP was used at non-saturating concentrations when assessing activity, and hence, full display of kinetic properties was not achieved. Further inactivation analysis, pH profile, and site-directed mutagenesis studies should help in clarifying the nature of the actual residues involved in both catalysis and ligand binding.

The purified bovine GDH has six subunits, each with binding sites for substrates, and pyridine and purine nucleotides. Subunit cooperative interaction is promoted by ADP and inhibited by GTP. The Hill coefficient (n_H) values, determined to be 2.3–2.8 when varying ADP (**Table 2**), suggested that GDH has a moderate cooperativity among its six subunits (32, 35). In turn, the GDH kinetics fitted to the concerted MWC exclusive binding Equation 1 yielded n values near 3 when varying NH_4^+ and

ADP (**Table 3**). Then, according to the MWC model, in the absence of essential activators, the six enzyme subunits were in the inactive, tense (T) state, whereas, in the presence of ADP, the enzyme progressively transforms up to three subunits into the active, relaxed R state. Therefore, as GDH is structured as an association of two trimers, an explanation of the kinetic data might be that the enzyme behaved as a dimer of two independent or semi-independent trimers.

GDH Reverse Reaction Under Physiological Conditions

NAD^+ and $NADP^+$ have similar standard redox potentials, but NAD^+ predominantly serves for catabolism and ATP generation, whereas NADPH is the main reducing agent for biosynthetic pathways (64). The mammalian liver and brain GDHs show similar affinities for NAD^+ (K_m = 0.17–0.83 mM) and $NADP^+$ (K_m = 0.16–1.22 mM), as well as for NADH (K_m = 0.028–0.12 mM) and NADPH (K_m = 0.022–0.12 mM) (32, 33, 44, 45, 65, 66). In consequence, both NADH and NADPH are possible products of the forward GDH reaction, as well as substrates of the reverse reaction. The high activity and high affinity for NADH of the respiratory chain (67) do not allow the mitochondrial matrix NADH content to build up, and this is the reason why the NADH/NAD^+ ratios are low (0.05–0.18) in functional mitochondria (31, 46, 49, 68). In turn, NADH cannot be used by the enzymes involved in the GSH/oxidative stress metabolism, whereas NADPH is not a respiratory chain substrate. Then, the GDH reverse reaction with NADH as cosubstrate is unfavorable. In contrast, the intramitochondrial NADPH/$NADP^+$ ratios are usually around one or even higher (46, 49). Thus, the GDH reverse reaction with NADPH is more likely to occur than with NADH under physiological conditions. Under prolonged hypoxia, oxidative phosphorylation is depressed, and NADH and ADP accumulate, further favoring the GDH reverse reaction.

There are also reports (22, 69–71) stating that GDH preferentially catalyzes the forward, oxidative deamination reaction than the reverse, reductive amination reaction in cancer cells. However, the actual K_{EQ} value of the GDH reaction indicates that the reverse reaction is thermodynamically favored when at least micromolar ammonium concentrations are present. Therefore, with millimolar ammonium concentrations within cancer cells (Ehrlich ascites mouse cells, 0.4–2.3 mM) (72) and in the surrounding microenvironment (0.8–3 mM) (5), the only possible GDH reaction, regardless of the GDH isoform and subcellular localization, is that of N assimilation.

The data of the present study reveal that the kinetic properties of GDH1 make feasible the reverse reaction under physiological conditions. For instance, the GDH reverse reaction is favored by its higher V_{max} value (vs. forward reaction V_{max}); that is, GDH1 has a higher catalytic capacity for its reverse reaction. The reverse GDH reaction is also thermodynamically favored in the presence of micromolar ammonium concentrations and physiological mitochondrial matrix Glu/2-OG (1–10) and NADPH/$NADP^+$ (∼1) ratios, despite its high K_m values for ammonium, which were above the physiological range of concentrations. In this last regard, it was here determined that cancer mitochondria actively produce ammonium from glutamine, in a reaction catalyzed by glutaminase, leading to higher mitochondrial matrix and extramitochondrial ammonium concentrations, which in turn are sufficient to drive the GDH reverse reaction. An alternative and supplementary source of ammonium might be AMP deamination in the cytosol, which is also enhanced in cancer cells (73). Thus, the emerging scenario for glutamate/glutamine metabolism in cancer mitochondria seems to privilege the conservation and further formation of glutamate as an N-carrier/donor, in which both glutamine and 2-OG are transformed into glutamate.

Interestingly, treatment with the so-called ammonia-scavenging drugs (phenylacetate and phenylbutyrate, which in fact conjugate with glutamine to form phenylacetylglutamine and phenylbutyrylglutamine, which are excreted) arrests growth of prostate cancer, renal cancer, and leukemia cell lines (74, 75). Phenylbutyrate also decreases by 35 to 45% the size of tumors in rodents (76). However, phenylacetate has shown a negligible antitumor activity in clinical trials (77).

Total GDH activity in intact cancer cells was approximately one-third of the GDH1 activity determined in isolated hepatoma mitochondria. Likewise, it has also been estimated that the mitochondrial volume within a cell amounts up to ∼30% of total cellular volume. In consequence, the GDH activity determined in cells seemed to mostly correspond to that of the mitochondrial GDH1 isoform.

The *in silico* simulation of GDH1 activity with physiological concentrations of substrates and modulators, and using the MWC equation for exclusive binding, predicted an activity in the range of 1.1 to 3.3 nmol/min × mg (with 2 mM ADP) in isolated mitochondria. By considering that the mitochondrial fraction corresponds to 30% of cellular protein, the GDH activity scaled up to intact cells might oscillate between 0.33 and 0.99 nmol/min * mg cell protein. This GDH activity range for the reverse reaction is well within the range of fluxes determined for biosynthesis of protein (2.5–8.8 nmol/min * mg protein), glycogen (0.25–0.55 nmol/min * mg protein), urea (2.4–28 nmol/min * mg protein), and fatty acids (0.09–10.7 nmol/min * mg protein), or it is even above those of cholesterol (0.014–0.025 nmol/min * mg protein) and nucleotides (0.1 nmol/min * mg protein), in normal and tumor cells (78–83). Then, it seems thermodynamically and kinetically feasible that GDH may contribute to accelerate cancer cell proliferation by providing glutamate, through its reverse NH_4^+ fixing reaction.

Ammonium, at millimolar concentrations, induced increased growth rates of metastatic cancer cells, but not of non-cancer cells in which it was toxic. The kinetic properties of GDH, as well as the thermodynamically favorable GDH reverse reaction, when at least micromolar ammonium concentrations are present, support that the physiological GDH role in cancer cells is to catalyze the NH_4^+ fixation to promote proliferation. The MWC equation predicted, at physiological concentrations of substrates and modulators, a rate of ammonium assimilation catalyzed by tumor GDH completely compatible with the anabolic rates required for active cell proliferation.

MATERIALS AND METHODS

Chemicals

Ammonium chloride, ADP, DTT, EDTA, GTP, glutamate, glutamine, 2-OG, 3-phosphoglycerate, L-leucine, NAD^+, $NADP^+$, NADPH, NADH, Triton X-100, MgCl2, MOPS, HEPES, Tris, imidazole, acrylamide, GDH (no. G2626), rabbit muscle phosphorylase kinase (no. P2014), and agarose were from Sigma Chem. Co. (St. Louis, MO, USA). Anti-GDH1/2 (no. sc-160383); anti-α-tubulin (no. sc-5286); antiacetylated lysine (no. ab190479); anti-P-Ser (Q5phospho-ser; Qiagen no.37430); and anti-P-Thr (Q7phospho-Thr; Qiagen no.37420) were purchased from Santa Cruz (sc) Biotechnology (Santa Cruz, CA, USA), Abcam (ab) (Cambridge, MA, USA), or Qiagen (Venlo, the Netherlands). Glyceraldehyde-3-phosphate dehydrogenase (GAPDH, no. 105686) and HK (no. 11426362001) were from Roche (Mannheim, Germany). Recombinant phosphoglycerate kinase (PGK) was from *Entamoeba histolytica* (84).

Cell Growth and Culture

Propagation and isolation of AS-30D ascites hepatoma cells and culture of human cervix cancer HeLa and SiHa cells, human breast cancer MDA-MB-231 and MCF-7 cells, human prostate cancer PC3 and DU145, human lung A549, human colorectal HCT116 and Colo 205 cells, human HFF-1 fibroblasts, and mouse 3T3 fibroblasts were carried out in Dulbecco modified eagle medium (DMEM) plus 25 mM glucose as previously described (51, 55, 59, 85–87). All cancer and non-cancer cell lines used were purchased from ATCC and cultured in DMEM (Sigma-Aldrich) supplemented with 10% fetal bovine serum (Biowest, Nuaillé, France) and 10,000 U penicillin/streptomycin (Sigma-Aldrich) and placed under a humidified atmosphere of 5% CO_2/95% air at 37°C. Genotyping (INMEGEN, Tlalpan, Mexico city, Mexico) of the cancer cell lines showed >90% of the canonic allelic markers displayed in the ATCC original clones.

For 2-D cultures, 20×10^3 cells/well were grown in 96-well plates in the presence or absence of different ammonium chloride concentrations; the addition of NH_4Cl pH 7.0 did not change the pH of the culture medium (DMEM + 25 mM glucose). Cell growth was followed by counting cellular density every 24 h during 7 to 8 days. Viability was determined by the trypan blue assay, which revealed <10% cellular death (54). The duplication time was determined by using the following equation: $n = \frac{1}{\frac{[3.32(\log N_F - \log N_I)]}{(t_F - t_I)}}$, where N_F represents the number of cultured cells at the end of the exponential growth phase; N_I represents the number of cells at the beginning of the growth curve; t_F is the final time at which cells were harvested, and t_I is the initial culture time. The specific growth rate μ was calculated from the slope of a semilogarithmic plot of cell densities in the exponential growth phase vs. time (88).

For tridimensional (3-D) cultures, HeLa and MDA-MB-231 cells (2×10^4 cells/mL) were seeded in 2% (wt/vol) agarose-coated culture dishes in 5 mL DMEM (+ 25 mM glucose) with the indicated ammonium chloride concentrations. After 5 days, the culture medium was refreshed, and the MCTSs formed were placed under slow orbital shaking (20–50 rpm) at 37°C and 95% air/5% CO_2. Fresh culture medium with 25 mM glucose ± NH_4Cl was replaced every 3 days, which helped to discard incompletely formed spheroids. The spheroid growth was determined at the indicated times by measuring MCTS diameter with a calibrated reticule (1/10 mm) in an inverted phase contrast microscope (Zeiss, Thornwood, NY, USA) (86).

Isolation of Mitochondria

Tightly coupled mitochondria were isolated from fed-rat liver (RLM) and AS-30D cells (HepM) as described elsewhere (89, 90). Both mitochondrial preparations were subjected to further dilution in SHE buffer (250 mM sucrose, 10 mM HEPES, 1 mM EGTA, pH 7.3) and centrifugation (12,857 × g for 10 min at 4°C); these steps were repeated thrice to minimize the presence of contaminating cytosolic proteins. The resulting mitochondrial fractions were resuspended at 30 to 80 mg protein/mL in SHE buffer with 1 mM PMSF, 1 mM EDTA, 5 mM DTT, and 10% glycerol, and stored at −70°C until use for determination of enzyme activity and Western blotting. Animal manipulation was carried out in accordance with the recommendations stated by the Mexican Official Standard NOM-062-ZOO-1999 norm.

GDH Activity

The GDH activity assay for the reverse reaction was determined at 37°C in KME (120 mM KCl, 20 mM K-Mops, 1 mM K-EGTA) buffer at pH 7.2, or in KME buffer + 10 mM HEPES at pH 7.5, and in the presence of 0.8 mM $MgCl_2$, 0.02% Triton X-100, 0 to 2.4 mM ADP, 0–0.75 mM 2-OG, 0.15–0.2 mM NADPH, and 0.07–0.1 mg protein for RLM or 0.2–0.3 mg protein for HepM; for the saturation curves with NADPH, 25 to 30% lower protein contents were used. The specific GDH reaction was started by adding 5–100 mM NH_4Cl. Negligible spurious consumption of NADPH was attained under the described conditions; presence of significant levels of GDH ligands derived from the mitochondrial matrix can be discarded because of the large dilution of the mitochondrial preparation in the reaction assay (at least 40 times and usually 100 times or more). The decrease in the absorbance at 340 nm was followed for several minutes (∼10 min) to allow for full development of the pronounced enzyme hysteretic behavior, although the initial signal decrease (1–3 min) was taken to calculate the GDH rates. The protein concentration ranges used for each mitochondrial type were well within the linearity range of enzyme activity. To calculate the kinetic parameters, the experimental data were fitted by non-linear regression analysis to the Hill or MWC equation, using the Microcal Origin 5.0 software (OriginLab, Northampton, MA, USA).

Western Blotting and Immunoprecipitation Assays

Mitochondria were solubilized in RIPA lysis buffer [phosphate-buffered saline 1× pH 7.2, 1% IGEPAL NP40, 0.1% sodium dodecyl sulfate (SDS), and 0.05% sodium deoxycholate] plus 1 mM of PMSF (phenyl methanesulfonyl fluoride) and one tablet of complete protease inhibitors cocktail (Roche) and subjected to SDS–polyacrylamide gel electrophoresis in 12.5% polyacrylamide gels. The proteins were immobilized

on polyvinylidene fluoride membranes and immunoblotted with human anti-GDH (1:1000 dilution); specific proteins were revealed with peroxide-conjugated secondary antibodies (anti-goat, no. sc-2768; anti-rabbit, no. sc-2317; anti-mouse, no. sc-2005), followed by chemiluminescence detection as previously described (91). Covalent GDH modification was assessed by initially immunoprecipitating with the specific anti-GDH antibody followed by detection with antibodies anti–phospho-Ser, anti–phospho-Thr, and anti-acetylLys as previously described (27).

Determination of Metabolites

Freshly prepared mitochondria (10 mg protein/mL) were incubated in KME buffer + 2 mM K-phosphate at 37°C under smooth orbital shaking with either 1 mM pyruvate + 2 mM malate or 4 mM glutamine + 1 mM pyruvate + 2 mM malate. After 10 min, aliquots were withdrawn, mixed with ice-cold KME buffer, and centrifuged at 17,000 × g for 1 min at 4°C. The supernatant was mixed with ice-cold 3% (vol/vol) perchloric acid (PCA) in 1 mM EDTA and kept in ice. The mitochondrial pellet was resuspended in cold KME buffer and centrifuged at 17,000 × g for 1 min at 4°C. This procedure was repeated once. The final mitochondrial pellet was mixed with ice cold 3% PCA/1 mM EDTA. The two fractions were neutralized with 3 M KOH/0.1 mM Tris and stored at −72°C until use for determination of ammonium, 2OG, Glu, ADP, and ATP by standard enzymatic methods (92, 93).

The intramitochondrial GTP content was estimated from the difference between the content of ATP + GTP determined by assay with *Eh*PGK (which can take either GTP or ATP as substrate, with 0-fold higher affinity for the first) and ATP content determined by assay with HK. It was assumed that HK does not use GTP as substrate. The stock solutions of GTP, ADP, 2-OG, NH_4^+, and Glu were also routinely calibrated by standard enzymatic methods (92, 93). The GTP stock was prepared in presence of 1 mM EDTA, making it stable for several weeks. GTP in the stock solution was determined in a coupled enzymatic assay with *Eh*PGK (2 U) and GAPDH (2 U) in presence of 5 mM MgCl2, 1 mM EDTA, 2 mM DTT, 0.15 mM NADH, and 2 mM 3-phosphoglycerate.

Statistical Data Analysis

The data represent the mean ± standard deviation (SD) of at least three independent cell preparations (n). For statistics between two experimental groups, Student *t*-test analysis was used (94). For statistics between three or more experimental groups, one-way analysis of variance (ANOVA)/*post hoc* Scheffé analysis was used (94, 95). For both, $P < 0.05$ was used as statistical significance criterion.

DATA AVAILABILITY STATEMENT

All datasets generated for this study are included in the article.

AUTHOR CONTRIBUTIONS

RM-S and ÁM-H: conceptualization. RM-S, ÁM-H, JG-P, SP-V, DR-C, and JP-F: investigation. RM-S and ÁM-H writing—original draft preparation. RM-S, ÁM-H, ES, and SR-E: writing—review and editing.

FUNDING

This present work was partially supported by CONACyT-Mexico grants Nos. 239930 and 281428 (RM-S), A1-S-40481 (ÁM-H), 283144 (SR-E), and 282663 (ES).

REFERENCES

1. Schoolwerth AC, Nazar BL, LaNoue KF. Glutamate dehydrogenase activation and ammonia formation by rat kidney mitochondria. *J Biol Chem*. (1978) 253:6177–83.
2. Nelson DL, Cox MM. *Lehninger Principles of Biochemistry*, 7th ed. New York, NY: Freeman WH (2017).
3. Treberg JR, Brosnan ME, Watford M, Brosnan JT. On the reversibility of glutamate dehydrogenase and the source of hyperammonemia in the hyperinsulinism/hyperammonemia syndrome. *Adv Enzyme Reg*. (2010) 50:34–43. doi: 10.1016/j.advenzreg.2009.10.029
4. Bunik V, Artiukhov A, Aleshin V, Mkrtchyan G. Multiple forms of glutamate dehydrogenase in animals: structural determinants and physiological implications. *Biology*. (2016) 5:53. doi: 10.3390/biology5040053
5. Spinelli JB, Yoon H, Ringel AE, Jeanfavre S, Clish CB, Haigis MC. Metabolic recycling of ammonia via glutamate dehydrogenase supports breast cancer biomass. *Science*. (2017) 358:941–6. doi: 10.1126/science.aam9305
6. Nissim I. Newer aspects of glutamine/glutamate metabolism: the role of acute pH changes. *Am J Physiol*. (1999) 277:F493. doi: 10.1152/ajprenal.1999.277.4.F493
7. Verhagen AM, Kratina TK, Hawkins CJ, Silke J, Ekert PG, Vaux DL. Identification of mammalian mitochondrial proteins that interact with IAPs via N-terminal IAP binding motifs. *Cell Death Diff*. (2007) 14:348–57. doi: 10.1038/sj.cdd.4402001
8. Mandal P, Chauhan S, Tomar RS. H3 clipping activity of glutamate dehydrogenase is regulated by stefin B and chromatin structure. *FEBS J*. (2014) 281:5292–308. doi: 10.1111/febs.13069
9. McGivan JD, Chappell JB. On the metabolic function of glutamate dehydrogenase in rat liver. *FEBS Lett*. (1975) 52:1–7. doi: 10.1016/0014-5793(75)80624-7
10. Engel PC, Dalziel K. The equilibrium constants of the glutamate dehydrogenase systems. *Biochem J*. (1967) 105:691–5. doi: 10.1042/bj1050691
11. Chance WT, Cao L, Nelson JL, Foley-Nelson T, Fischer JE. Hyperammonemia in anorectic tumor-bearing rats. *Life Sci*. (1988) 43:67–74. doi: 10.1016/0024-3205(88)90238-X
12. Chance WT, Cao L, Foley-Nelson T, Nelson JL, Fischer JE. Possible role of ammonia in experimental cancer anorexia. *Brain Res*. (1989) 486:316–24. doi: 10.1016/0006-8993(89)90518-0
13. Gamcsik MP, Constantinidis I, Glickson JD. *In vivo* 14N nuclear magnetic resonance spectroscopy of tumors: detection of ammonium and trimethylamine metabolites in the murine radiation induced fibrosarcoma 1. *Cancer Res*. (1991) 51:3378–83.
14. Eng CH, Yu K, Lucas J, White E, Abraham RT. Ammonia derived from glutaminolysis is a diffusible regulator of autophagy. *Sci Signal*. (2010) 3:ra31. doi: 10.1126/scisignal.2000911
15. Reitzer LJ, Wice BM, Kennell D. Evidence that glutamine, not sugar, is the major energy source for cultured HeLa cells. *J Biol Chem*. (1979) 254:2669–76.
16. Segura JA, Medina MA, Alonso FJ, Sanchez-Jimenez F, Núñez de Castro I. Glycolysis and glutaminolysis in perifused Ehrlich ascites tumour cells. *Cell Biochem Funct*. (1989) 7:7–10. doi: 10.1002/cbf.290070103

17. Cluntun AA, Lukey MJ, Cerione RA, Locasale JW. Glutamine Metabolism in Cancer: Understanding the Heterogeneity. *Trends Cancer*. (2017) 3:169–80. doi: 10.1016/j.trecan.2017.01.005
18. Kelly T, Rose CR. Ammonium influx pathways into astrocytes and neurones of hippocampal slices. *J Neurochem*. (2010) 115:1123–36. doi: 10.1111/j.1471-4159.2010.07009.x
19. Lie S, Wang T, Forbes B, Proud CG, Petersen J. The ability to utilise ammonia as nitrogen source is cell type specific and intricately linked to GDH, AMPK and mTORC1. *Sci Rep*. (2019) 9:1461. doi: 10.1038/s41598-018-37509-3
20. Meng M, Chen S, Lao T, Liang D, Sang N. Nitrogen anabolism underlies the importance of glutaminolysis in proliferating cells. *Cell Cycle*. (2010) 9:3921–32. doi: 10.4161/cc.9.19.13139
21. Merhi A, Delrée P, Marini AM. The metabolic waste ammonium regulates mTORC2 and mTORC1 signaling. *Sci Rep*. (2017) 7:44602. doi: 10.1038/srep44602
22. Jin L, Li D, Alesi GN, Fan J, Kang HB, Lu Z, et al. Glutamate dehydrogenase 1 signals through antioxidant glutathione peroxidase 1 to regulate redox homeostasis and tumor growth. *Cancer Cell*. (2015) 27:257–70. doi: 10.1016/j.ccell.2014.12.006
23. Liu G, Zhu J, Yu M, Cai C, Zhou Y, Yu M, et al. Glutamate dehydrogenase is a novel prognostic marker and predicts metastases in colorectal cancer patients. *J Transl Med*. (2015) 13:144. doi: 10.1186/s12967-015-0500-6
24. Zhang J, Wang G, Mao Q, Li S, Xiong W, Lin Y, et al. Glutamate dehydrogenase (GDH) regulates bioenergetics and redox homeostasis in human glioma. *Oncotarget*. (2016) 5:1–12. doi: 10.18632/oncotarget.7657
25. Fan S, Wang Y, Zhang Z, Lu J, Wu Z, Shan Q, et al. High expression of glutamate-ammonia ligase is associated with unfavorable prognosis in patients with ovarian cancer. *J Cell Biochem*. (2018) 119:6008–15. doi: 10.1002/jcb.26797
26. Takeuchi Y, Nakayama Y, Fukusaki E, Irino Y. Glutamate production from ammonia via glutamate dehydrogenase 2 activity supports cancer cell proliferation under glutamine depletion. *Biochem Biophys Res Commun*. (2018) 495:761–7. doi: 10.1016/j.bbrc.2017.11.088
27. Moreno-Sánchez R, Marín-Hernández Á, Gallardo-Pérez JC, Vázquez C, Rodríguez-Enríquez S, Saavedra E. Control of the NADPH supply and GSH recycling for oxidative stress management in hepatoma and liver mitochondria. *Biochim Biophys Acta Bioenerg*. (2018) 1859:1138–50. doi: 10.1016/j.bbabio.2018.07.008
28. Mazat JP, Ransac S. The Fate of Glutamine in Human Metabolism. The interplay with glucose in proliferating cells. *Metabolites*. (2019) 9:81. doi: 10.3390/metabo9050081
29. Corman L, Prescott LM, Kaplan NO. Purification and kinetic characteristics of dogfish liver glutamate dehydrogenase. *J Biol Chem*. (1967) 242:1383–90.
30. Di Prisco G, Banay-Schwartz M, Strecker HJ. Glutamate dehydrogenase in nuclear and mitochondrial fractions of rat liver. *Biochem Biophys Res Commun*. (1968) 33:606–12. doi: 10.1016/0006-291X(68)90339-2
31. Bailey J, Bell ET, Bell JE. Regulation of bovine glutamate dehydrogenase. The effects of pH ADP. *J Biol Chem*. (1982) 257:5579–83.
32. Colon AD, Plaitakis A, Perakis A, Berl S, Clarke DD. Purification and characterization of a soluble and a particulate glutamate dehydrogenase from rat brain. *J Neurochem*. (1986) 46:1811–9. doi: 10.1111/j.1471-4159.1986.tb08500.x
33. Cho SW, Lee J, Choi SY. Two soluble forms of glutamate dehydrogenase isoproteins from bovine brain. *Eur J Biochem*. (1995) 233:340–6. doi: 10.1080/12265071.1998.9647411
34. Kanavouras K, Mastorodemos V, Borompokas N, Spanaki C, Plaitakis A. Properties and molecular evolution of human GLUD2 (neural and testicular tissue-specific) glutamate dehydrogenase. *J Neurosci Res*. (2007) 85:3398–406. doi: 10.1111/j.1432-1033.1995.340_1.x
35. Zaganas I, Pajecka K, Wendel Nielsen C, Schousboe A, Waagepetersen HS, Plaitakis A. The effect of pH and ADP on ammonia affinity for human glutamate dehydrogenases. *Metab Brain Dis*. (2013) 28:127–31. doi: 10.1007/s11011-013-9382-6
36. Segel IH. *Enzyme Kinetics: Behavior and Analysis of Rapid Equilibrium and Steady State Enzyme Systems*. New York, NY: Wiley (1975).
37. Cacace A, Sboarina M, Vazeille T, Sonveaux P. Glutamine activates STAT3 to control cancer cell proliferation independently of glutamine metabolism. *Oncogene*. (2017) 36:2074–84. doi: 10.1038/onc.2016.364
38. Bell RA, Storey KB. Regulation of liver glutamate dehydrogenase by reversible phosphorylation in a hibernating mammal. *Comp Biochem Physiol B Biochem Mol Biol*. (2010) 157:310–6. doi: 10.1016/j.cbpb.2010.07.005
39. Herrero-Yraola A, Bakhit SM, Franke P, Weise C, Schweiger M, Jorcke D, et al. Regulation of glutamate dehydrogenase by reversible ADP-ribosylation in mitochondria. *EMBO J*. (2001) 20:2404–12. doi: 10.1093/emboj/20.10.2404
40. Schlicker C, Gertz M, Papatheodorou P, Kachholz B, Becker CF, Steegborn C. Substrates and regulation mechanisms for the human mitochondrial sirtuins Sirt3 and Sirt5. *J Mol Biol*. (2008) 382:790–801. doi: 10.1016/j.jmb.2008.07.048
41. Poburko D, Santo-Domingo J, Demaurex N. Dynamic regulation of the mitochondrial proton gradient during cytosolic calcium elevations. *J Biol Chem*. (2011) 286:11672–84. doi: 10.1074/jbc.M110.159962
42. Santo-Domingo J, Demaurex N. Perspectives on: SGP symposium on mitochondrial physiology and medicine: the renaissance of mitochondrial pH. *J Gen Physiol*. (2012) 139:415–23. doi: 10.1085/jgp.201110767
43. Di Prisco G. Effect of pH and ionic strength on the catalytic and allosteric properties of native and chemically modified ox liver mitochondrial glutamate dehydrogenase. *Arch Biochem Biophys*. (1975) 171:604–12. doi: 10.1016/0003-9861(75)90070-3
44. Rife JE, Cleland WW. Kinetic mechanism of glutamate dehydrogenase. *Biochemistry*. (1980) 19:2321–8. doi: 10.1021/bi00552a007
45. McCarthy AD, Tipton KF. Ox glutamate dehydrogenase. Comparison of the kinetic properties of native and proteolysed preparations. *Biochem J*. (1985) 230:95–9. doi: 10.1042/bj2300095
46. Wanders RJ, Meijer AJ, Groen AK, Tager JM. Bicarbonate and the pathway of glutamate oxidation in isolated rat-liver mitochondria. *Eur J Biochem*. (1983) 133:245–54. doi: 10.1111/j.1432-1033.1983.tb07455.x
47. Wanders RJ, Hoek JB, Tager JM. Origin of the ammonia found in protein-free extracts of rat-liver mitochondria and rat hepatocytes. *Eur J Biochem*. (1980) 110:197–202. doi: 10.1111/j.1432-1033.1980.tb04855.x
48. Akerboom TP, Bookelman H, Zuurendonk PF, van der Meer R, Tager JM. Intramitochondrial and extramitochondrial concentrations of adenine nucleotides and inorganic phosphate in isolated hepatocytes from fasted rats. *Eur J Biochem*. (1978) 84:413–20. doi: 10.1111/j.1432-1033.1978.tb12182.x
49. Liu H, Kehrer JP. The reduction of glutathione disulfide produced by t-butyl hydroperoxide in respiring mitochondria. *Free Radic Biol Med*. (1996) 20:433–42. doi: 10.1016/0891-5849(95)02093-4
50. Smith CM, Bryla J, Williamson JR. Regulation of mitochondrial alpha-ketoglutarate metabolism by product inhibition at alpha-ketoglutarate dehydrogenase. *J Biol Chem*. (1974) 249:1497–505.
51. Gallardo-Pérez JC, Rivero-Segura NA, Marín-Hernández A, Moreno-Sánchez R, Rodríguez-Enríquez S. GPI/AMF inhibition blocks the development of the metastatic phenotype of mature multi-cellular tumor spheroids. *Biochim Biophys Acta- Mol Cell Res*. (2014) 1843:1043–53. doi: 10.1016/j.bbamcr.2014.01.013
52. Liu W, Zhang X, Zhao J, Li J, Cui Z, Mao X. Inhibition of cervical cancer cell metastasis by benzothiazole through up-regulation of E-cadherin expression. *Microb Pathog*. (2017) 111:182–6. doi: 10.1016/j.micpath.2017.08.050
53. Oono K, Takahashi K, Sukehara S, Kurosawa H, Matsumura T, Taniguchi S, et al. Inhibition of PC3 human prostate cancer cell proliferation, invasion and migration by eicosapentaenoic acid and docosahexaenoic acid. *Mol Clin Oncol*. (2017) 7:217–20. doi: 10.3892/mco.2017.1287
54. Wasilewski A, Krajewska U, Owczarek K, Lewandowska U, Fichna J. Fatty acid amide hydrolase (FAAH) inhibitor PF-3845 reduces viability, migration and invasiveness of human colon adenocarcinoma Colo-205 cell line: an in vitro study. *Acta Biochim Pol*. (2017) 64:519–25. doi: 10.18388/abp.2017_1520
55. Pacheco-Velázquez SC, Robledo-Cadena DX, Hernández-Reséndiz I, Gallardo-Pérez JC, Moreno-Sánchez R, Rodríguez-Enríquez S. Energy metabolism drugs block triple negative breast metastatic cancer cell phenotype. *Mol Pharm*. (2018) 15:2151–64. doi: 10.1021/acs.molpharmaceut.8b00015
56. Piao SS, Shang B. Pizotifen inhibits the proliferation and migration of colon cancer HCT116 cells by down-regulating WNT signaling pathway. *Ann Clin Lab Sci*. (2019) 49:183–8.
57. Hu T, Li Z, Gao CY, Cho CH. Mechanisms of drug resistance in colon cancer and its therapeutic strategies. *World J Gastroenterol*. (2016) 22:6876–89. doi: 10.3748/wjg.v22.i30.6876

58. Walenta S, Doetsch J, Mueller-Klieser W, Kunz-Schughart LA. Metabolic imaging in multicellular spheroids of oncogene-transfected fibroblasts. *J Histochem Cytochem*. (2000) 48:509–22. doi: 10.1177/002215540004800409
59. Rodríguez-Enríquez S, Carreño-Fuentes L, Gallardo-Pérez JC, Saavedra E, Quezada H, Vega A, et al. Oxidative phosphorylation is impaired by prolonged hypoxia in breast and possibly in cervix carcinoma. *Int J Biochem Cell Biol*. (2010) 42:1744–51. doi: 10.1016/j.biocel.2010.07.010
60. Tudball N, Bailey-wood R, Thomas, P. The role of histidine residues in glutamate dehydrogenase. *Biochem J*. (1972) 129:419–25. doi: 10.1042/bj1290419
61. Pandey A, Sheikh S, Katiyar S. Identification of cysteine and lysine residues present at the active site of beef liver glutamate dehydrogenase by o-phthalaldehyde. *BBA- Prot Struct Mol Enzym*. (1996) 1293:122–8. doi: 10.1016/0167-4838(95)00235-9
62. Yoon HY, Cho EH, Yang SJ, Lee HY, Huh JW, Choi MM, et al. Reactive amino acid residues involved in glutamate-binding of human glutamate dehydrogenase isozymes. *Biochimie*. (2004) 86:261–7. doi: 10.1016/j.biochi.2004.04.005
63. Yang SJ, Cho EH, Choi MM, Lee HJ, Huh JW, Choi SY, et al. Critical role of the cysteine 323 residue in the catalytic activity of human glutamate dehydrogenase isozymes. *Mol Cells*. (2005) 19:97–103.
64. Engel PC. Glutamate dehydrogenases: the why and how of coenzyme specificity. *Neurochem Res*. (2014) 39:426–32. doi: 10.1007/s11064-013-1089-x
65. Ottolina G, Carrea G, Riva S, Bückmann AF. Coenzymatic properties of low molecular-weight and macromolecular N6-derivatives of NAD+ and NADP+ with dehydrogenases of interest for organic synthesis. *Enzyme Microb Technol*. (1990) 12:596–602. doi: 10.1016/0141-0229(90)90133-B
66. Lee WK, Shin S, Cho SS, Park JS. Purification and characterization of glutamate dehydrogenase as another isoprotein binding to the membrane of rough endoplasmic reticulum. *J Cell Biochem*. (1999) 76:244–53.
67. Grivennikova VG, Kapustin AN, Vinogradov AD. Catalytic activity of NADH-ubiquinone oxidoreductase (complex I) in intact mitochondria. *evidence for the slow active/inactive transition. J Biol Chem*. (2001) 276:9038–44. doi: 10.1074/jbc.M009661200
68. Veech RL, Guynn R, Veloso D. The time-course of the effects of ethanol on the redox and phosphorylation states of rat liver. *Biochem J*. (1972) 127:387–97. doi: 10.1042/bj1270387
69. McDaniel HG, Jenkins R, Yeh M, Razzaque A. Glutamic dehydrogenase from rat heart mitochondria. *II. Kinetic characteristics. J Mol Cell Cardiol*. (1984) 16:303–9. doi: 10.1016/S0022-2828(84)80601-X
70. Csibi A, Fendt SM, Li C, Poulogiannis G, Choo AY, Chapski DJ, et al. The mTORC1 pathway stimulates glutamine metabolism and cell proliferation by repressing SIRT4. *Cell*. (2013) 153:840–54. doi: 10.1016/j.cell.2013.04.023
71. Jin L, Chun J, Pan C, Kumar A, Zhang G, Ha Y, et al. The PLAG1-GDH1 axis promotes anoikis resistance and tumor metastasis through CamKK2-AMPK signaling in LKB1-deficient lung cancer. *Mol Cell*. (2018) 69:87–99.e7. doi: 10.1016/j.molcel.2017.11.025
72. Carrascosa JM, Martínez P, Núñez de Castro I. Nitrogen movement between host and tumor in mice inoculated with Ehrlich ascitic tumor cells. *Cancer Res*. (1984) 44:3831–5.
73. Vannoni D, Bernini A, Carlucci F, Civitelli S, Di Pietro MC, Leoncini R, et al. Enzyme activities controlling adenosine levels in normal and neoplastic tissues. *Med Oncol*. (2004) 21:187–95. doi: 10.1385/MO:21:2:187
74. Samid D, Shack S, Sherman LT. Phenylacetate: a novel nontoxic inducer of tumor cell differentiation. *Cancer Res*. (1992) 52:1988–92.
75. Franco OE, Onishi T, Umeda Y, Soga N, Wakita T, Arima K, et al. Phenylacetate inhibits growth and modulates cell cycle gene expression in renal cancer cell lines. *Anticancer Res*. (2003) 23:1637–42.
76. Carducci MA, Nelson JB, Chan-Tack KM, Ayyagari SR, Sweatt WH, Campbell PA, et al. Phenylbutyrate induces apoptosis in human prostate cancer and is more potent than phenylacetate. *Clin Cancer Res*. (1996) 2:379–87.
77. Chang SM, Kuhn JG, Robins HI, Schold SC, Spence AM, Berger MS, et al. Phase II study of phenylacetate in patients with recurrent malignant glioma: a North American Brain Tumor Consortium report. *J Clin Oncol*. (1999) 17:984–90.
78. Petcu LG, Plaut GW. NADP-specific isocitrate dehydrogenase in regulation of urea synthesis in rat hepatocytes. *Biochem J*. (1980) 190:581–92. doi: 10.1042/bj1900581
79. Crawford JM, Blum JJ. Quantitative analysis of flux along the gluconeogenic, glycolytic and pentose phosphate pathways under reducing conditions in hepatocytes isolated from fed rats. *Biochem J*. (1983) 212:585–98. doi: 10.1042/bj2120585
80. Gibbons GF, Pullinger CR. Diurnal variations in the effects of an unsaturated-fat-containing diet on fatty acid and cholesterol synthesis in rat hepatocytes. *Biochem J*. (1986) 239:617–23. doi: 10.1042/bj2390617
81. Portais JC, Schuster R, Merle M, Canioni P. Metabolic flux determination in C6 glioma cells using carbon-13 distribution upon [1-13C]glucose incubation. *Eur J Biochem*. (1993) 217:457–68. doi: 10.1111/j.1432-1033.1993.tb18265.x
82. Metallo CM, Walther JL, Stephanopoulos G. Evaluation of 13C isotopic tracers for metabolic flux analysis in mammalian cells. *J Biotechnol*. (2009) 144:167–74. doi: 10.1016/j.jbiotec.2009.07.010
83. Antoniewicz MR. A guide to (13)C metabolic flux analysis for the cancer biologist. *Exp Mol Med*. (2018) 50:19. doi: 10.1038/s12276-018-0060-y
84. Saavedra E, Encalada R, Pineda E, Jasso-Chávez R, Moreno-Sánchez R. Glycolysis in Entamoeba histolytica. *Biochemical characterization of recombinant glycolytic enzymes and flux control analysis. FEBS J*. (2005) 272:1767–83. doi: 10.1111/j.1742-4658.2005.04610.x
85. Moreno-Sánchez R, Gallardo-Pérez JC, Rodríguez-Enríquez S, Saavedra E, Marín-Hernández Á. Control of the NADPH supply for oxidative stress handling in cancer cells. *Free Radic Biol Med*. (2017) 112:149–61. doi: 10.1016/j.freeradbiomed.2017.07.018
86. Rodríguez-Enríquez S, Pacheco-Velázquez SC, Marín-Hernández Á, Gallardo-Pérez JC, Robledo-Cadena DX, Hernández-Reséndiz I, et al. Resveratrol inhibits cancer cell proliferation by impairing oxidative phosphorylation and inducing oxidative stress. *Toxicol Appl Pharmacol*. (2019) 370:65–77. doi: 10.1016/j.taap.2019.03.008
87. González-Chávez Z, Vázquez C, Mejia-Tlachi M, Márquez-Dueñas C, Manning-Cela R, Encalada R, et al. Gamma-glutamylcysteine synthetase and tryparedoxin 1 exert high control on the antioxidant system in *Trypanosoma cruzi* contributing to drug resistance and infectivity. *Redox Biol*. (2019) 26:101231. doi: 10.1016/j.redox.2019.101231
88. McAtter JA, Davis JM. Basic cell culture technique and the maintenance of cell lines. In: Davis JM, editors. *Basic Cell Culture. A Practical Approach*. New York, NY: IRL Press at Oxford University Press (1994). pp. 93–147.
89. López-Gómez FJ, Torres-Márquez ME, Moreno-Sánchez R. Control of oxidative phosphorylation in AS-30D hepatoma mitochondria. *Int J Biochem*. (1993) 25:373–7. doi: 10.1016/0020-711X(93)90627-Q
90. Moreno-Sánchez R. Regulation of oxidative phosphorylation in mitochondria by external free Ca2+ concentrations. *J Biol Chem*. (1985) 260:4028–4034.
91. Gallardo-Pérez JC, Adán-Ladrón de Guevara A, Marín-Hernández A, Moreno-Sánchez R, Rodríguez-Enríquez S. HPI/AMF inhibition halts the development of the aggressive phenotype of breast cancer stem cells. *BBA-Mol Cell Res*. (2017) 1864:1679–90. doi: 10.1016/j.bbamcr.2017.06.015
92. Bergmeyer HU. *Methods of Enzymatic Analysis*. Weinheim: Verlag Chemie (1974).
93. Humphries BA, Melnychuk M, Donegan EJ, Snee RD. Automated enzymatic assay for plasma ammonia. *Clin Chem*. (1979) 25:26–30. doi: 10.1093/clinchem/34.9.1866
94. Krzywinski M, Altman N. Points of significance: comparing samples—part I. *Nat Methods*. (2014) 11:215–6. doi: 10.1038/nmeth.2858
95. Klockars AJ, Hancock GR. Scheffé's more powerful protected post hoc procedure. *J Educ Behav Stat*. (2000) 25:13–19. doi: 10.3102/10769986025001013

Conflict of Interest: The authors declare that the research was conducted in the absence of any commercial or financial relationships that could be construed as a potential conflict of interest.

frontiers in Oncology

ORIGINAL RESEARCH
published: 12 May 2020
doi: 10.3389/fonc.2020.00713

Normal Hematopoetic Stem and Progenitor Cells Can Exhibit Metabolic Flexibility Similar to Cancer Cells

Marija Vlaski-Lafarge[1,2]*, *Veronique Labat*[1,2], *Alexandra Brandy*[1,2], *Alice Refeyton*[1,2], *Pascale Duchez*[1,2], *Laura Rodriguez*[1,2], *Nyere Gibson*[1], *Philippe Brunet de la Grange*[1,2] *and Zoran Ivanovic*[1,2]

[1] *R&D Department, Etablissement Français du Sang Nouvelle Aquitaine, Bordeaux, France,* [2] *Inserm/U1035, University of Bordeaux, Bordeaux, France*

It is known that cancer stem cells (CSCs) with the largest proliferative capacity survive the anoxic and/or ischemic conditions present inside tumorous tissue. In this study we test whether normal stem cells can survive under the same conditions due to cancer cell-like metabolic adaptations. We cultivated a $CD34^+$ population with a majority of hematopoietic progenitors, and a $CD34^+CD38^{low}CD133^+CD90^+CD45RA^-$ population, highly enriched in hematopoietic stem cells (HSCs), under anoxic, anoxic/aglycemic ("ischemia-like"), or physiological conditions (3% O_2). Results showed, despite a reduction in total cell fold expansion proportionate to the decrease in O_2 concentration; $CD34^+$ cells, aldehyde dehydrogenase-expressing primitive cells, and committed progenitors expanded, even in anoxia. Interestingly, under ischemia-like conditions, stem and $CD34^+$ cell populations are maintained at day-0 level. Cell-cycle analysis further revealed an accumulation of cells in the G0/G1 phase in anoxia or anoxia/aglycemia, with a fraction of cells (~40%) actively cycling (SG2M phases). Also stem cell analysis showed that in these conditions a long-term Scid Repopulating activity was equal to that found with 3% O_2. In addition stem cells with the highest proliferative capacity were maintained in anoxia/aglycemia and in anoxia. The estimated ATP profile, active mitochondrial content, and succinate accumulation are indicative of anaerobic mitochondrial respiration in both HSCs and $CD34^+$ progenitors under ischemia-like conditions. We demonstrate here that primitive hematopoietic cells show similar metabolic flexibility to CSCs, allowing them to survive a lack of O_2 and O_2/glucose. Our study reveals that this feature is not the consequence of malignant transformation, but an attribute of stemness.

Keywords: cancer stem cells, hematopoietic stem cells, metabolism, bioenergetics, mitochondrial respiration

OPEN ACCESS

Edited by:
Tuuli Käämbre, National Institute of Chemical Physics and Biophysics, Estonia

Reviewed by:
Stephen John Ralph, Griffith University, Australia
Amilcare Barca, University of Salento, Italy

***Correspondence:**
Marija Vlaski-Lafarge
marija.vlaski@efs.sante.fr

Specialty section:
This article was submitted to Cancer Metabolism, a section of the journal Frontiers in Oncology

Received: *29 February 2020*
Accepted: *15 April 2020*
Published: *12 May 2020*

Citation:
Vlaski-Lafarge M, Labat V, Brandy A, Refeyton A, Duchez P, Rodriguez L, Gibson N, Brunet de la Grange P and Ivanovic Z (2020) Normal Hematopoetic Stem and Progenitor Cells Can Exhibit Metabolic Flexibility Similar to Cancer Cells. Front. Oncol. 10:713. doi: 10.3389/fonc.2020.00713

INTRODUCTION

The concept of cancer stem cells (CSCs) is well-established (1). CSCs display functions similar to normal stem cells, including self-renewal, differentiation potential, migration, a high proportion of cells in G0 phase, and drug resistance. Also, as normal stem cells, CSCs represent the small fraction of tumor cell population capable of self-regeneration as well as of propagation of the malignant cell

population giving rise to new tumors in tissues other than those from which the cancer originates (2).

In addition, functional, normal, and CSCs share several metabolic traits. Cancer cells show flexible, metabolic reprograming phenotypes which use an array of energetic fuels to enable survival, and proliferation under various conditions (3, 4). Proliferating tumor cells tend toward a glycolytic metabolism, even under aerobic conditions, in order to acquire the precursors necessary for increased biosynthesis (5). This high demand for glycolysis occurs without loss of mitochondrial activity (TCA cycle/respiration) (6). It should be stressed that, contrary to common assumption, the Warburg effect is not in fact specific to malignancy (2). A glycolytic metabolic profile has been shown to be an intrinsic property of hematopoietic stem cells (HSCs), related to stemness, enabling the cells to reside in areas with extremely low O_2 (hematopoietic niche). But this metabolic profile is also maintained when HSCs are outside of the physiological niche (2). Indeed, HSCs from bone marrow or mobilized in peripheral blood exhibit a glycolytic metabolic profile even when cultured under non-physiologically high atmospheric air O_2 concentrations (7, 8).

However, both HSCs and cancer cells possess active mitochondria that contribute to their maintenance, and retain the ability for oxidative phosphorylation (6, 9). Besides their role in energy production, mitochondria also play a role in recycling NAD^+ and maintaining the glycolytic flow, generating intermediates for anabolic pathways, epigenetic control, and protection against oxidative stress. They also have the ability to change swiftly to OXPHOS in order to meet the high energy demands linked to differentiation toward mature somatic cells (10).

In cancer cells, targeted depletion of mitochondrial DNA reduces the tumorigenic potential of cancer cells *in vitro* and *in vivo* (11, 12). Also, quiescent and circulating cancer cells rely highly on mitochondrial respiration (11, 13). The tumorous cells' metabolic flexibility between a predominantly biosynthetic or bioenergetic purpose is a result of this apparent dichotomy (glycolysis/mitochondrial respiration). Recent data show that the cancer cells with the greatest stem cell potential are responsible for the durability of the disease and can survive under severe conditions, such as anoxia and/or ischemia, created inside the tumor tissue. This ability to survive also depends on the metabolic consequences of anaerobic mitochondrial respiration. The mechanism described includes the use of fumarate as the final electron acceptor (fumarate respiration or "disproportionation of malate") (14).

We thus want to test the hypothesis that HSCs, unlike mature cells, can survive under extreme conditions (anoxia and ischemia-like) due to metabolic adaptation, including anaerobic mitochondrial activity.

Our study, based on functional and metabolic analysis of HSCs, points to flexible energetic nature and high metabolic adaptability as being features common to stem cells, rather than specific to CSCs.

Abbreviations: AA, anoxia/aglycemia; ALDH, aldehyde dehydrogenase; Ann/PI, annexin/propidum iodide; ATP, adenosine triphosphate; CB, cord blood; CFC, colony forming cell; CSCs, cancer stem cells; IL-3, interleukin-3; HPCs, hematopoietic progenitor cells; HSCs, hematopoetic stem cells; MFI, Mean fluorescence intensity; MTG, Mitotracker green; NAD, nicotinamide adenine dinucleotide; SCF, stem cell factor; TCA, cycle-tricarboxylic acid cycle; TPO, thrombopoietin.

MATERIALS AND METHODS

Cell Sorting and Culture

$CD34^+$ Cell Isolation

Cord blood (CB) samples delivered (with the mother's approval) to the Cell Therapy Unit of the French Blood Institute, Bordeaux, that had been rejected for banking, were used for the experiments (In compliance with national French regulation, declared to the Ministry of Research: DC-2019-3720). CB $CD34^+$ cells were isolated using an immunomagnetic technique (Miltenyi Biotec, Paris, France) and stored at −80°C (15).

$CD34^+CD38^{low}CD133^+CD90^+CD45RA^-$ Cell Sorting

$CD34^+$ cells were thawed in 4% human serum albumin (Vialebex, LFB-biomedicament, Courtabeuf, France) and labeled with anti-CD34-BV421 (BD Biosciences, San Diego, CA, USA), anti-CD38-PC7, anti-CD133-PE (EXBIO, Vestec, Czech Republic), anti-CD90-APC, and anti-CD45RA-FITC antibodies (Pharmigen, San Diego, CA, USA). The desired cell population was selected using a FACS Aria III cytometer (BD Biosciences, San Diego, CA, USA) (16).

Cell Culture

$CD34^+$ or $CD34^+CD38^{low}CD133^+CD90^+CD45RA^-$ cells were plated in Stem-alpha A medium without glucose (Stem Alpha SA, Saint-Genis-l'Argentiere, France), supplemented with penicillin/streptomycin (PS) (100 ng/L), and cytokines: SCF 100 ng/mL, IL-3 0.5 ng/mL, TPO 10 ng/mL. Cells were incubated under physiological conditions (3% O_2, with glucose 1 g/L), anoxia (0% O_2, with glucose 1 g/L), or anoxia/aglycemia (AA, 0% O_2, without glucose) for 5–7 days at 37°C. The conditions with 3% O_2 were obtained in an O_2 and CO_2 controller-culture chamber (PRO-OX and PRO-CO_2, Biospherix, NY) (15). Anoxia was achieved using a hermetically sealed modular incubator chamber (Billups-Rothenberg, CA) in which ambient air was replaced with a mixture of 95% nitrogen and 5% CO_2 (Air Liquide, Paris, France). At the end of the incubation period, cell expansion was estimated by cell counting.

Apoptosis Assay

Apoptosis was detected with an Annexin V-FITC kit (Beckman Coulter, Carlsbad, CA, USA) according to the manufacturer's protocol. Briefly, 10^5 cells from each of the experimental conditions were stained with Annexin V-FITC solution (AnnV) and propidium iodide (PI, 250 μg/mL) for 15 min at 4°C in the dark, washed in phosphate buffer saline (PBS), and analyzed with a flow cytometer (BD Bioscience, FACS Canto II) (17). This technique allow to detect: unlabelled viable cell subpopulation ($AnnV^-$/ PI^-); early apoptotic cell subpopulation that have

bound only AnnV (Ann^+/PI^-); necrotic cell subpopulation (representing the cells in post-apoptosis necrosis or late apoptosis) that have both bound AnnV and have been labeled with PI (Ann^+/PI^+).

Cell Cycle Analysis

For cell cycle analysis, 10^5 cells were washed with PBS, centrifuged at 43 g for 5 min at 4°C, and the pellets were resuspended in 100 µl of PBS. Cells were then fixed with 900 µl of 70% cold ethanol (added dropwise), and incubated for 1 h at 4°C. Cells were washed and resuspended in PBS with 0.2 mg/mL of bovine RNase A and incubated for 1 h at 37°C in the dark. PI (10 µg/mL) was added, and the analysis was performed using flow cytometry (Bioscience, FACS Canto II) (17). The percentage of cells in each of the different cell cycle phases (G0/G1, S, and G2/M) was calculated from the linear graph on which cell counts were plotted relative to cell DNA content. The reagents were provided by Sigma Aldrich.

CFC Assay

The committed hematopoietic progenitors', colony-forming cell (CFC), including colony-forming unit granulocyte, monocyte (CFU-GM), burst-forming unit erythroid (BFU-E), colony-forming unit granulocyte, erythrocyte, monocyte, megakaryocyte (CFU-GEMM) were assayed as described previously (18). Cells (250 cells/mL) were seeded in cytokine-supplemented methylcellulose in a 24-well-plate (MethoCult H4034 Optimum, Stem Cell Technologies, Canada). After 15 days of incubation, CFCs were counted using an inverted microscope.

Aldehyde Dehydrogenase (ALDH) Activity

ALDH labeling was undertaken using an Aldefluor reagent (ALDF) (Stem Cell Technologies, Canada) according to the manufacturer's instructions. Activated ALDF substrate was rapidly added to a suspension of 10^5 cells in 100 µL of ALDF assay buffer and incubated for 30 min at 37°C in the dark. As a negative control, an aliquot of ALDF-stained cells was incubated with the ALDH inhibitor diethylaminobenzaldehyde. Cells were washed, resuspended in 200 µL of assay buffer, and analyzed with a flow cytometer (BD Bioscience, FACS Canto II) (15).

Proliferative, Clonogenic, and Differentiation Potential Evaluation by the Single-Cell Culture Method

The method was performed as it was previously published (16, 19).

Proliferative Capacity

Single cells selected from each of the experimental conditions were assayed into individual wells of 96-well-plates. Each well-contained 200 µl of the Stem alpha A medium, supplemented with glucose (1 g/l) and cytokines (see above). Plates were incubated at 20% O_2 and 5% CO_2 for 14 days at 37°C. The entire cell content produced in the primary culture from one individual cell was reseeded into 24-well-plates under the same culture conditions. Secondary culture cell content was re-evaluated at Day-28. Clone categories were established according to the number of cells produced: (C1 = 0; C2 = 1,000–4,000; C3 = 5,000–10,000; C4 = 13,500–14,000; C5 = 15,000–15,500 cells).

Clonogenic Capacity

Methylcellulose colony formation was assessed by sorting single cells from the different experimental conditions into individual wells of a 96-well-plate, containing 100 µl of methylcellulose (MethoCult H4034). The plates were incubated at 20% O_2 and 5% CO_2 for 15 days at 37°C. The colonies from the committed progenitors were then counted. Each colony was harvested, and replated into an individual well of a 24-well-plate containing methylcellulose (250 µl). The plates were incubated for 14 days at 37°C secondary colony formation was then assessed.

Differentiation Potential

For *in vitro* differentiation assays, cells from each of the experimental conditions were incubated for 14 days in the same manner as described for the proliferative capacity analysis. 24-well-plates had been seeded with murine stromal cells (MS5) in a αMEM medium (Gibco, Thermo Fisher, Langenselbold, Germany) with 10% fetal calf serum and PS (100 ng/L). At the end of the incubation period in liquid culture, hematopoietic cells were co-cultivated on MS5 for 30 days with a complete RPMI medium (Thermo Fisher, Langenselbold, Germany, with SCF 100 ng/mL, IL-3 0.5 ng/mL, G-CSF 100 ng/mL, TPO 10 ng/mL, 10% fetal calf serum, and PS) at 37°C. At the end of the incubation period, hematopoietic cells from each well were harvested and labeled at 4°C for 20 min in the dark with anti-CD19-PE, anti-CD33-APC (BD, Biosciences, San Diego, CA, USA), and anti-CD45-FITC antibodies (IOTest, Beckman Coulter, Carlsbad, CA, USA), and analyzed with a flow cytometer.

Scid Repopulating Cells (SRC) Assay

All experiments involving animals were performed in compliance with French regulation (License No: 3306002). From each of the experimental conditions, the equivalent of 300 Day-0 $CD34^+CD38^{low}CD133^+CD90^+CD45RA^-$ cells at Day-7 were injected into the retro-orbital vein of 6–10-week-old NOD-Shi-Scid/IL-2Rgnull (NOG) mice (animal-keeping facility, University of Bordeaux, France). The mice had been prepared using an intraperitoneal injection of Busulfan 25 mg/kg (Busilvex, Pierre Fabre, Boulogne, France) (20). Positive control mice (injected with 300 Day-0 CD34+CD38lowCD133+CD90+CD45RA- cells) and negative control mice (non-injected) were included. After 12 weeks, animals were euthanized and their femora were extracted. The femoral bone marrow was flushed with 1 ml of RPMI medium (Gibco, Thermo Fisher, Langenselbold, Germany) supplemented with 4% human serum albumin. The cells contained in 100 µl of this cell suspension were stained with anti-human antibodies: CD45-FITC, CD19-PE, and CD33-APC, for 20 min at 4°C in the dark, washed with PBS and analyzed on a FACS Canto II (21). The positivity threshold for human CD45, CD33, CD19 chimerism was >0.1% of analyzed cells.

ATP Content

ATP levels were quantified using the ATP Bioluminescence Assay Kit HS II kit (Roche, Switzerland) in accordance with the

manufacturer's recommendations, as it was previously published (15). A total of 10^3 cells per well were used in a 96-well-plate. Luminescence, directly proportional to the concentration of ATP, was detected using a luminometer at $\alpha = 562$ nm (Promega GloMax). In order to determine the total cellular and mitochondrial ATP production, cells were incubated for 10 min in the absence of or in the presence of inhibitors of the mitochondrial complexes I and III, rotenone, and antimycin (1 μM), respectively. These inhibitors were added simultaneously in order to curb electron flow through the mitochondrial electron transport chain, and so prevent generation of the proton motive force enabling ATP production by ATP synthase. The proportion of cellular ATP produced by mitochondria was calculated using the decrease in total ATP detected in the presence of these inhibitors.

Mitochondrial Content

Mitochondria were detected using mitochondrial-selective fluorescent labeling with MitoTracker Green, according to the manufacturer's instructions (Molecular Probes). A total of 10^4 cells were treated with Mitotracker green (100 nM) for 20 min at 37°C in the dark, then washed in PBS and analyzed using flow cytometry as previously published (17).

Succinate Content

The succinate that had accumulated during cell culture was detected in the culture supernatant at the end of the incubation period according to the manufacturer's instructions (Succinate assay kit, Abcam, UK). Cell suspensions were harvested, washed and resuspended in 100 μl of ice-cold succinate assay buffer. The suspensions were centrifuged, and the collected supernatants were filtered using a 10 kDa spin filter. Fifty microliter of each sample or standard dilution were mixed with the same volume of the reaction mix or background control mix and incubated for 30 min at 37°C. The absorbance intensity was measured at 450 nm using a microplate reader (Evolis, Biorad). Each value was adjusted with the background control, in order to eliminate any non-specific absorbance that may have resulted from the possible presence of reduced nicotinamide adenine dinucleotide (NADH). Succinate concentration was then determined based on the standard curve.

Statistical Analysis

The Wilcoxon-Mann–Whitney paired comparison test was used to examine the significance of the difference between the various experimental conditions ($p < 0.05$, $p < 0.01$, and $p < 0.001$ were considered to be statistically significant).

RESULTS

Hematopoietic Stem and Progenitor Cell Survival in the Anoxia and AA

In order to test our hypothesis that primitive hematopoietic cells can survive under conditions commonly found in tumor tissue, we assayed both a total $CD34^+$ population ($CD34^+$) with a majority of hematopoietic progenitors (HPCs) and a rare minority of stem cells and a selected $CD34^+CD38^{low}CD133^+CD90^+CD45RA^-$ population highly enriched in hematopoietic stem cells (HSCs, "stem") under anoxic, anoxic/aglycemic (ischemia like, "AA"), or physiological conditions (3% O_2) for seven days.

Based on the difference in cell numbers between Day-0 and post-incubation, the results showed that the entire cell population survived under AA conditions, in both the stem and $CD34^+$ total population, with slight expansion in anoxia (**Figure 1A**). We decided to investigate whether this property was associated with the functional characteristics of hematopoietic cells within the heterogeneous $CD34^+$ population. Primitive hematopoietic cells expressing ALDH, as well as committed progenitors incubated in anoxia, yielded a significant level of amplification compared to Day-0. The maintenance in number of both cell populations under AA conditions is indicative of metabolic adaptation to glucose and O_2 shortage (**Figure 1B**). As expected, these conditions yielded a significantly lower number of cells than physiological conditions (3% O_2), which allow optimal cell expansion (**Figures 1A,B**). Cellular viability was estimated using Annexin V/Propidium iodide labeling (Ann/PI). Similar percentage of apoptotic cells (including the subpopulation expressing Ann^+/PI^-) or necrotic cells (subpopulation expressing Ann^+/PI^+). was detected in both stem and $CD34^+$ cells, under all conditions (**Figure 1C**). We further analyzed the cell cycle phase distribution with PI staining (**Figure 1D**). When incubated under restricted conditions, there was a significant accumulation of cells in the non-dividing G0/G1 phase of the cell cycle, compared to physiological conditions. However, a fraction (∼40%) of the cell population was still actively proliferating (S and G2/M phases) in AA and anoxia (**Figure 1D**). This distribution could be responsible for the cultures' maintenance and/or slight expansion in the absence of O_2 with/without glucose, allowing for a ∼20% apoptosis rate. The observed survival of primitive hematopoietic cells, irrespective of the conditions (anoxia, AA) indicates their flexible metabolic nature.

Stem Cell Functions Are Maintained *in vitro* in Anoxia and AA

The population enriched in stem cells was analyzed by single cell assay in order to detect stem cell traits—self-renewal, proliferation, and multipotency—*in vitro* at an individual cell level.

In order to estimate the cell's proliferative capacity, we counted the number of cells produced in a secondary culture, having replated the cells descending from a single cell (seeded in a primary liquid culture) (**Figure 2A**). This secondary culture allowed us to detect both the total number of cells per well—total progeny of the initial single cell—and the proportion of clones produced by $CD34^+$ cells in the primary culture. They were then sorted into five categories (see above, Material and methods). The more primitive the cell, the greater its progeny in the secondary culture, due to a higher proliferative potential. Our results showed that the cells producing the most proliferative clones (categories 4 and 5) were present only under AA conditions (**Figure 2A**). Using an approach based on

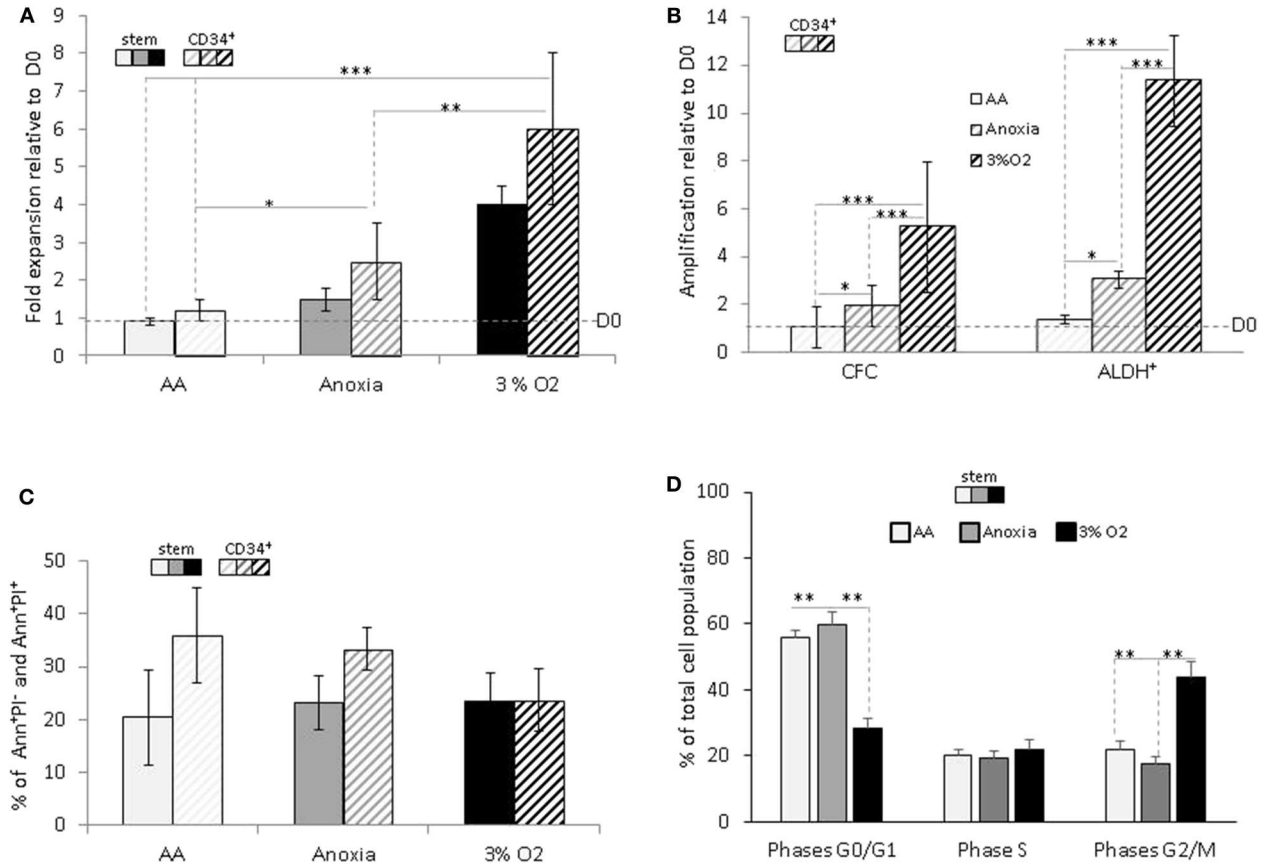

FIGURE 1 | Hematopoietic stem and progenitor cell amplification, survival and cycling upon O_2 and glucose shortage. The total $CD34^+$ population ($CD34^+$) and selected $CD34^+CD38^{low}CD133^+CD90^+CD45RA^-$ highly enriched in hematopoietic stem cells ("stem") population were analyzed after seven days of culture under anoxic/aglycemic (AA), anoxic, or physiological oxygen-level conditions (3% O_2). **(A)** Evaluation of cell expansion. The bars represent mean fold expansion relative to Day-0 (D0). **(B)** Hematopoietic progenitor amplification. The average fold expansion of committed progenitors (CFC) or aldehyde dehydrogenase ($ALDH^+$)-expressing primitive progenitors within the total $CD34^+$ population relative to D0 is represented with bars. **(C)** Apoptosis assessment with Ann/PI labeling. The average percentage of apoptotic (Ann^+/PI^-) or necrotic cells (Ann^+/PI^+, i.e., cells in post-apoptosis necrosis or late apoptosis) detected amongst stem and $CD34^+$ cells, is represented with bars. **(D)** Cell cycle analysis. Distribution of the cultivated "stem" cells in G0/G1, S, and G2/M phases of the cell cycle are represented by the average percentage shown with bars. The data are presented using a mean ±SD format over at least six experiments. Asterisks indicate a statistically significant difference between experimental conditions at $^*p < 0.05$, $^{**}p < 0.01$, or $^{***}p<0.001$, Wilcoxon-Mann–Whitney test. Ann, Annexin; PI, Propidium iodide.

methylcellulose culture, we found that the number of individual cells giving primary colonies (plating efficiency) was the highest under AA conditions (**Figure 2B**, Primary colonies). All cells from the individual cell-derived colonies (each primary culture well) were harvested, dissociated, and plated in individual wells in the secondary methylcellulose culture in order to assess replating efficiency (*in vitro* surrogate for "self-renewal"). Secondary colonies only grew from those primary colonies which contained self-renewed primitive progenitors. Replating efficiency was observed under all conditions, but the highest proportion of initially seeded single cells able to produce colonies in secondary culture was detected under AA conditions (**Figure 2B**, Secondary colonies). We then tested if these primary colonies could undergo myeloid or lymphoid lineage differentiation on a mesenchymal stroma layer, proving their multipotency. For this, we ascertained the percentage of human $CD45^+$ cells (a pan-hematopoietic cell marker) expressing markers of the myeloid ($CD33^+$) or lymphoid ($CD19^+$) lineage differentiation. The proportions detected were equal under all culture conditions (**Supplementary Figure 1**). The results indicate that the basic stem cell functions of self-renewal and multipotency are not comprised by incubation in anoxia or AA.

Long-Term *in vivo* Hematopoietic Reconstitution Upon Transplantation of the Cells Cultivated in Anoxia and AA

When assaying stem cells, the most effective method is to track their ability to reconstitute haematopoiesis in immunosuppressed mice 12–16 weeks after transplantation (22, 23). We analyzed the presence of the human cell marker CD45 12 weeks after xeno-transplantation of NOG mice. We found significant human cell engraftment in the mice's bone marrow (**Figure 3**, upper panel). Graft efficiency was defined as the number of mice testing positive for human $CD45^+$ cells relative to the total number of mice injected.

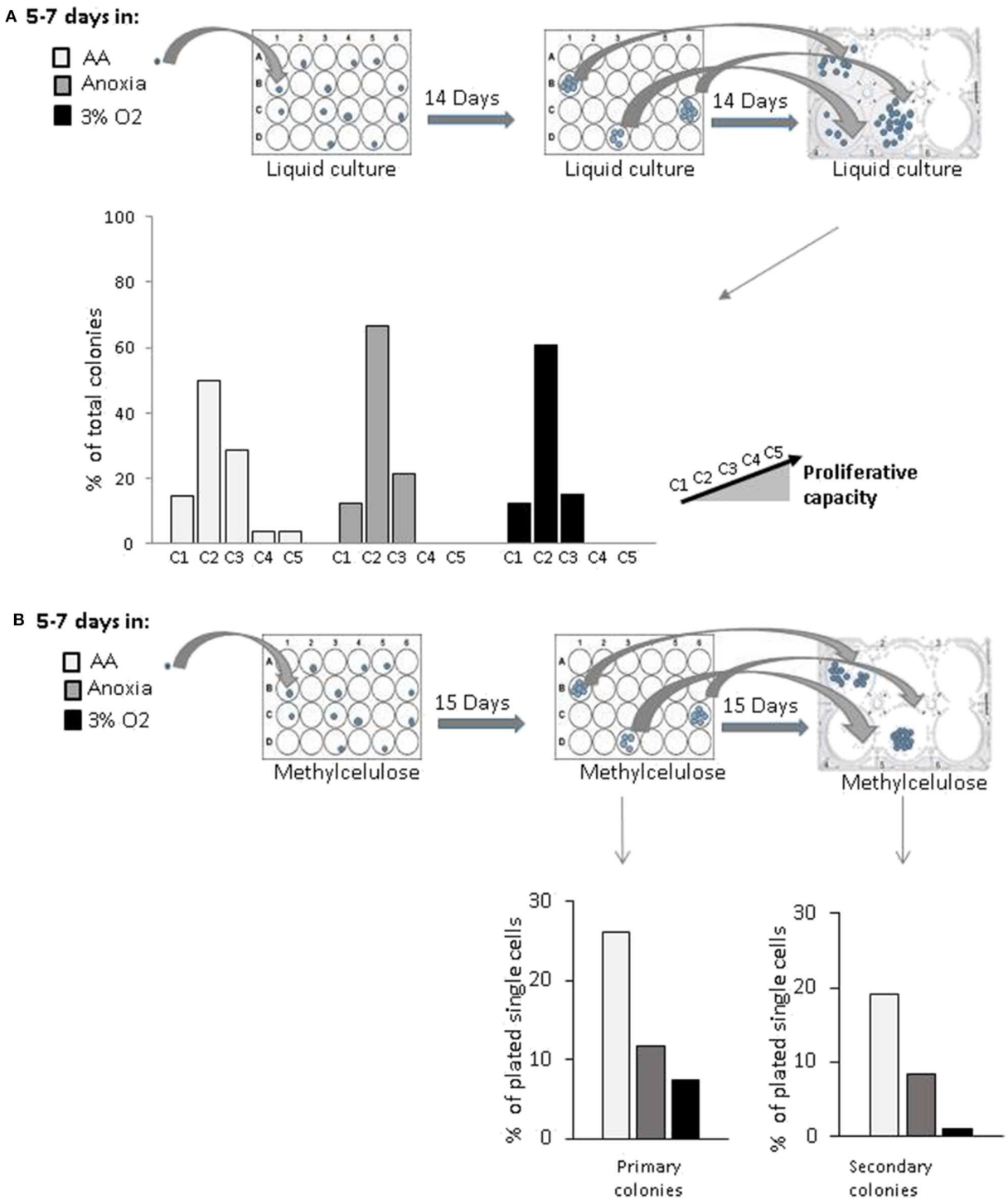

FIGURE 2 | *in vitro* evaluation of proliferative and clonogenic potential of individual $CD34^+CD38^{low}CD133^+CD90^+CD45RA^-$ cells in single-cell culture. $CD34^+CD38^{low}CD133^+CD90^+CD45RA^-$ cells were incubated under anoxic/aglycemic (AA), anoxic, or physiological oxygen conditions (3% O_2) for 5–7 days at 37°C and then analyzed. **(A)** Proliferation potential was assayed by selecting single cells from each experimental condition and placing these into individual wells. The cell progeny produced in primary culture from one individual cell were reseeded and secondary culture cell production was assessed. Clone categories were established according to the number of cells produced: (C1 = 0; C2 = 1,000–4,000; C3 = 5,000–10,000; C4 = 13,500–14,000; C5 = 15,000–15,500 cells). The data are shown with bars representing the percentage of total identified individual cell clones according to size **(B)** Clonogenic potential. Methylcellulose colony formation was assayed by sorting single cells from the various experimental conditions into individual wells. Primary colonies were then enumerated, replated individually in methylcellulose-containing wells and the secondary colonies scored. The results are displayed with bars representing the percentage of total identified individual cell cultures giving rise to primary colonies or secondary colonies.

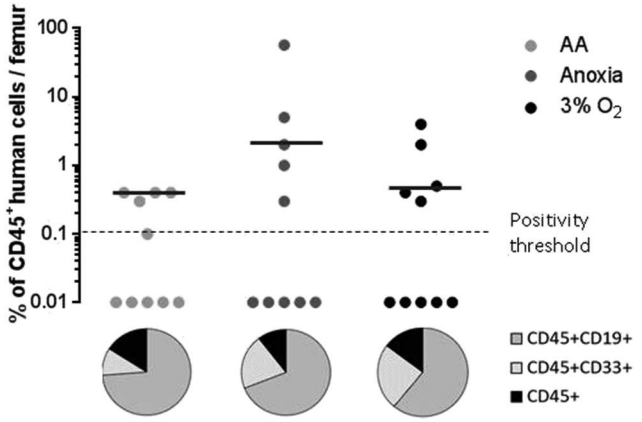

FIGURE 3 | Long-term hematopoietic reconstitution capacity of the $CD34^+CD38^{low}CD133^+CD90^+CD45RA^-$ cultured in the absence of O_2 and with/without glucose. Scid repopulating activity of $CD34^+CD38^{low}CD133^+CD90^+CD45RA^-$ cells cultivated in AA, anoxia or 3% O_2 was evaluated based on human $CD45^+$ chimerism in the bone marrow of NOG mice, 12 weeks after injected cultures with the Day-7 equivalent of 300 Day-0 cells. Femoral bone marrow cells were labeled with human CD45 antibodies and the level of human CD45 chimerism was assimilated to the amount of $CD45^+$ cells in the mouse bone marrow. The data are displayed using circles, with each mouse being represented by one circle. Median values of CD45 chimerism are indicated by dashed lines (upper panel). Human myeloid and lymphoid cell differentiation was estimated with the level of expression of human $CD45^+CD33^+$ and $CD45^+CD19^+$ markers, respectively, in mouse bone marrow. The average percentage of human CD19 and CD33 expression in the human $CD45^+$ population are presented in the pie chart (lower panel).

This ratio was equal for all experimental conditions (**Figure 3**, upper panel). The mean percentage of $CD45^+$ cells—level of CD45 chimerism—was consistent in AA and anoxia as well as under physiological conditions. These results indicate a long-term ability maintained by the stem cell population, throughout incubation, for hematopoietic reconstruction, a trait attributable to the most primitive HSCs. $CD45^+CD33^+$ and $CD45^+CD19^+$ markers were then used to detect human myeloid or lymphoid differentiation, respectively (**Figure 3**, pie chart). This property was again detected under all conditions. The ratio of $CD45^+CD33^+$ to $CD45^+CD19^+$ cell subpopulations indicated that cells incubated in AA tend toward lymphoid lineage more than in anoxia and 3% O_2 (**Figure 3**, pie chart).

ATP Production, Active Mitochondrial, and Succinate Content in Hematopoietic Stem and Progenitor Cells in Anoxia and AA

In order to reveal the specific bioenergetic profile enabling hematopoietic cell survival without O_2 or glucose, we analyzed the cellular ATP content (**Figure 4A**). Firstly, this showed a significant decrease in the total level of ATP in anoxia and AA compared to 3% O_2, indicating a decrease in cellular ATP production. After simultaneous introduction of inhibitors of mitochondrial complexes I and III (rotenone and antimycin, respectively), the decrease in total ATP indicated the fraction of ATP produced by mitochondria. We found that most of the ATP in AA is produced by mitochondria; apart from the observation that anaerobic mitochondrial ATP production is active in AA, the simultaneous addition of inhibitors prevented us from distinguishing the specific effect of either complex (**Figure 4A**). This phenomenon was observed in both the stem and total $CD34^+$ cell populations. To see whether these changes were associated with a difference in mitochondrial mass content, we labeled the cells with Mitotracker green at the end of the incubation period. This is a compound which binds to active polarized mitochondria, indicating cellular mitochondrial mass (24). We found a similar quantity of active mitochondria per cell under all conditions, amongst stem cells as well as the total $CD34^+$ population (**Figure 4B**). This would suggest that mitochondrial content was not affected by the absence of O_2 or glucose. Furthermore, compared to HSCs, the mitochondrial content in $CD34^+$ cells was significantly higher under all conditions, indicating that in terms of bioenergetics, progenitor cells are more dependent on mitochondrial respiration than stem cells (**Figure 4B**).

In a recent publication, Tomitsuka et al. described how cancer cells can survive in ischemia where anaerobic mitochondrial fumarate respiration is activated (25). Using this fumarate as the final electron acceptor, then it is reduced into succinate that accumulates during culture. To test if, under our AA conditions, anaerobic mitochondrial respiration works in the same manner as in cancer cells, we measured the level of succinate in culture supernatants. The results show that the succinate content in AA supernatant is significantly higher compared to 3% O_2 and anoxia (**Figure 4C**). These results point clearly to succinate accumulation under ischemia-like conditions and suggest the activation of fumarate respiration as an energetic pathway in HSCs/HPCs under these circumstances. Interestingly, this was detected in stem and $CD34^+$ cells, indicating that HSCs as well HPCs can exhibit metabolic adaptions to survive in ischemia-like conditions and activate anaerobic mitochondrial respiration.

DISCUSSION

Our study demonstrates that HSCs/HPCs are capable of maintaining their functional traits, high proliferative capacity, and multipotency in the absence of O_2 and/or glucose. Although cell numbers were significantly reduced in comparison with physiological conditions, a significant fraction of surviving cells was actively cycling independent of O_2 and/or glucose omission (**Figure 1**). Moreover, primitive CB progenitors and stem cells ($ALDH^+$), as well as committed progenitors, were even seen to multiply despite the absence of O_2, indicating an oxygen-independent mechanism, which is arrested by glucose shortage. This is consistent with data showing a link between glucose import and cell proliferation in normal as well as cancer cells, in order to provide the carbon intermediates for biosynthesis (4, 26).

Using our method, the greatest capacity to adapt was detected in the stem cell population, wherein SRC (Scid repopulating cell) activity was equivalent to that which was detected under

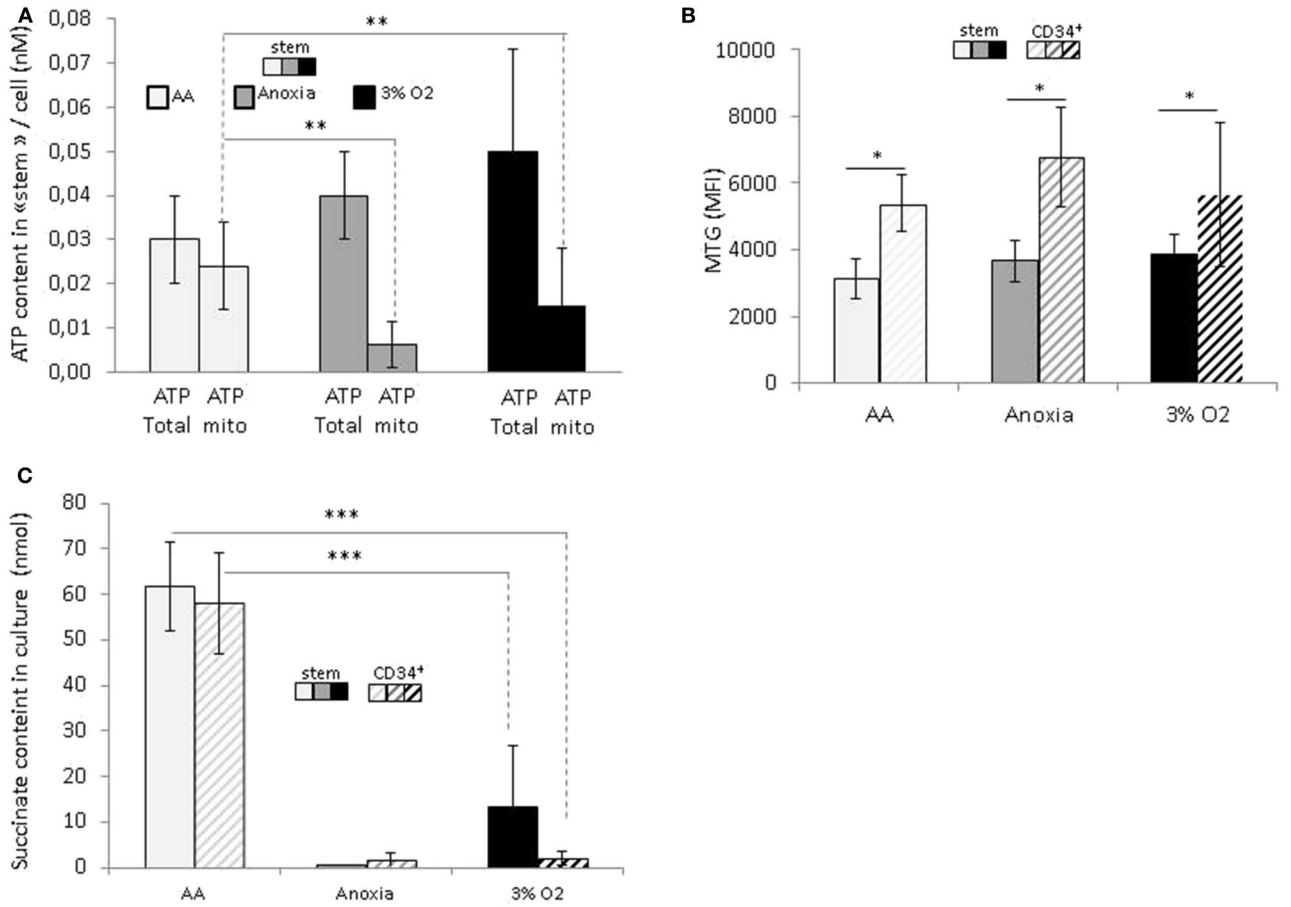

FIGURE 4 | Energetic profile of hematopoietic stem and progenitor cells and succinate accumulation in culture upon O_2 or O_2 and glucose shortage. At the end of the 7-day incubation period, total $CD34^+$ cells and stem cells ($CD34^+CD38^{low}CD133^+CD90^+CD45RA^-$) were analyzed **(A)** ATP level assessment. The bars represent the mean cellular total or mitochondrial ATP level. The data are presented as a mean ± SD from five experiments **(B)** Mitochondrial mass is determined by MTG staining and the results are presented as the MTG mean fluorescence intensity (MFI). The data are displayed as the mean ± SD of four independent experiments. **(C)** Succinate content determination in the culture supernatant. Data are presented as the mean ± SD of three independent measurements. Asterisks indicate a significant difference between the different experimental conditions at $*p < 0.05$, $**p < 0.01$, or $***p < 0.001$, Wilcoxon-Mann–Whitney test.

optimal physiological conditions (**Figure 3**). Notably, under ischemia-like conditions, we identified the cell subpopulation with the highest proliferative capacity, indicating an association between high metabolic robustness and the most primitive of cells.

Various articles describe how O_2 is a functional regulator of HSCs/HPCs. Our results are consistent with and could indeed extend, those showing that although low O_2 concentration, close to that found in bone marrow stem cell niches (0.1%), induced the return of half of the CB $CD34^+$ cells or murine hematopoietic progenitor non-leukemic factor-depending cell Paternsen (FDCP) mix-cell line to G0 phase, it also selected the small proportion of self-renewing cells in the proliferating phase of cycle, without impairing their functional capacity, SRC activity, or clonogenicity (27, 28). Further, a 1% O_2 concentration enables HSC enrichment as well as primitive erythroid progenitors within CB $CD34^+$ cell population (29–31). In addition, our study confirmed that well-adapted physiologically-relevant low O_2 concentration (3%) allows simultaneous HSC maintenance and committed progenitor expansion (18).

These data reflect the behavior of HSCs/HPCs in a physiological environment. Adult or neonatal primitive hematopoietic cells reside in low oxygen areas and develop within a 1–4% gradient of O_2 (32, 33). Furthermore, as has been shown, most primitive HSCs reside in areas with very low blood perfusion, implying a limited supply not only of O_2 but also of blood-born nutrients (34), i.e., an ischemia-like environment is common to HSCs. In the niche, HSCs are in a quiescent phase, and are occasionally recruited into the cell cycle (35, 36). They must also remain capacity for rapid proliferation in response to extrinsic cues, indicating great metabolic plasticity which enables energetic reprogramming on the basis of various functional demands (2).

These properties are in common to cancer cells. While cell growth is markedly reduced under conditions of very low O_2 levels, cancer cells (leukemic cell culture) are capable of expanding significantly compared to Day-0 (37). These

hypoxia-resistant cells shown to be highly immature progenitors (37). Also, severe hypoxia selects *ex vivo* a cell subset with stem cell potential in a population of myelodysplastic syndrome bone marrow cells (38). The cells that survive under these conditions have been shown to be the leukemic stem cells which are potentially responsible for the disease relapsing (39). We have demonstrated here for CB HSCs/HPCs, as has been shown for cancer cells, that expansion is possible at a low oxygen level until glucose is no longer available in the culture medium. In summary, these data indicate that primitive hematopoietic cells, as well as cancer progenitor and stem cells, adapt to survive anoxia and ischemia, conditions often found in cancerous tissue.

Furthermore, our results show that under ischemia-like conditions, primitive hematopoietic cell mitochondria remain functional, and use anaerobic ATP synthesis in order to sustain cellular homeostasis (**Figure 4**). Recently, evidence has shown fumarate respiration to be an anaerobic energetic pathway utilized by cancer cells in ischemic tumor tissue. In this instance, fumarate is utilized as the final electron acceptor, and fumarate reduction is coupled with an anaerobically-functioning electron transport chain in which electrons are transferred from NADH to fumarate via the complex I, ubiquinone, and a reverse reaction of the complex II (fumarate reductase), resulting in succinate formation. Only complex I functions as a proton pump, generating a proton gradient that drives ATP synthesis (25).

The accumulation of succinate we detected suggests that primitive hematopoietic cells activate fumarate respiration under ischemia-like conditions (**Figure 4**), meaning that HSCs/HPCs could in fact adapt by using the same metabolic energetic solvating pathway as cancer cells. By introducing a fumarate reductase-specific inhibitor, and assessing HSC/HPC population maintenance, we were able to identify activation of the NADH fumarate reductase system. We observed that introducing pyrvinium pamoate (which inhibits NADH fumarate reductase), prevents mesenchymal stem cells surviving under ischemia-like conditions, and triggers energetic failure (unpublished data, article in preparation). Based on these findings and the results presented in this article, we propose that this system could be activated under ischemia-like conditions in HSCs/HPCs.

It should be noted that when analyzing the metabolic pathway in anaerobic respiration, such analysis should include fatty acid β-oxidation (a known alternative energetic fuel in the face of a glucose shortage) as fatty acid β-oxidation yields reducing equivalents of nicotinamide adenine dinucleotide (NADH) (40). These could deliver electrons to the electron transport chain (complex I), thereby sustaining anaerobic mitochondrial ATP generation via fumarate respiration in an anoxic and aglycemic environment.

Our study provides evidence that primitive hematopoietic cells exhibit metabolic and energetic flexibility, notably the ability to shift between aerobic, or anaerobic energetic modes in order to adapt to various environmental conditions. These features, especially "fumarate respiration," were thus far considered to be specific to cancer cells, which is clearly not the case. We propose that since they are common to both, normal and cancer stem cells, these primitive metabolic features should be considered as markers of stemness.

Our work provides findings that could be important in the development of cell therapy procedures.

DATA AVAILABILITY STATEMENT

All datasets generated for this study are included in the article/**Supplementary Material**.

AUTHOR CONTRIBUTIONS

VL, AB, AR, PD, and LR performed the experiments. PB provided intellectual input and helped with data analysis. NG edited the text and corrected the translation. ZI provided the original idea for the project. MV-L and ZI conceived the study and wrote the manuscript. MV-L supervised the experimental work and did the data analysis.

FUNDING

This study was supported by the Etablissement Français du Sang Nouvelle Aquitaine Bordeaux, regional research and development budget.

ACKNOWLEDGMENTS

Our thanks go to Mrs. Elisabeth Doutreloux-Volkmann (EFS Nouvelle Aquitaine, Bordeaux) and Ms. NG for language corrections.

SUPPLEMENTARY MATERIAL

The Supplementary Material for this article can be found online at: https://www.frontiersin.org/articles/10.3389/fonc.2020.00713/full#supplementary-material

Supplementary Figure 1 | *in vitro* evaluation of the differentiation potential of individual $CD34^+CD38^{low}CD133^+CD90^+CD45RA^-$ cells in single-cell culture. Single cells were selected from the various experimental conditions (AA, anoxia, or 3% O_2), and plated into individual wells. Clones produced in primary culture from one individual cell were co-cultivated on a mesenchymal stromal layer for 30 days. Cells were then collected and assayed for myeloid ($CD45^+CD33^+$) or lymphoid differentiation ($CD45^+CD19^+$). Results are shown with bars representing the mean percentage of $CD45^+CD33^+$ or $CD45^+CD19^+$-expressing cells obtained per colony developed from one individual cell.

REFERENCES

1. Lapidot T, Sirard C, Vormoor J, Murdoch B, Hoang T, Caceres-Cortes J, et al. A cell initiating human acute myeloid leukaemia after transplantation into SCID mice. *Nature.* (1994) 367:645–8. doi: 10.1038/367645a0
2. Ivanovic Z, Vlaski-Lafarge M. (2015). *Anaerobiosis and Stemnes An Evolutionary Paradigm.* Elsvier: Academic Press.
3. Deberardinis RJ, Chandel NS. Fundamentals of cancer metabolism. *Sci Adv.* (2016) 2:e1600200. doi: 10.1126/sciadv.1600200
4. Pavlova NN, Thompson CB. The emerging hallmarks of cancer metabolism. *Cell Metab.* (2016) 23:27–47. doi: 10.1016/j.cmet.2015.12.006
5. Warburg O, Wind F, Negelein E. The metabolism of tumors in the body. *J Gen Physiol.* (1927) 8:519–30. doi: 10.1085/jgp.8.6.519

6. Obre E, Rossignol R. Emerging concepts in bioenergetics and cancer research: metabolic flexibility, coupling, symbiosis, switch, oxidative tumors, metabolic remodeling, signaling and bioenergetic therapy. *Int J Biochem Cell Biol.* (2015) 59:167–81. doi: 10.1016/j.biocel.2014.12.008
7. Takubo K, Nagamatsu G, Kobayashi CI, Nakamura-Ishizu A, Kobayashi H, Ikeda E, et al. Regulation of glycolysis by Pdk functions as a metabolic checkpoint for cell cycle quiescence in hematopoietic stem cells. *Cell Stem Cell.* (2013) 12:49–61. doi: 10.1016/j.stem.2012.10.011
8. Kocabas F, Xie L, Xie J, Yu Z, Deberardinis RJ, Kimura W, et al. Hypoxic metabolism in human hematopoietic stem cells. *Cell Biosci.* (2015) 5:39. doi: 10.1186/s13578-015-0020-3
9. Ito K, Carracedo A, Weiss D, Arai F, Ala U, Avigan DE, et al. A PML-PPAR-delta pathway for fatty acid oxidation regulates hematopoietic stem cell maintenance. *Nat Med.* (2012) 18:1350–8. doi: 10.1038/nm.2882
10. Ito K, Suda T. Metabolic requirements for the maintenance of self-renewing stem cells. *Nat Rev Mol Cell Biol.* (2014) 15:243–56. doi: 10.1038/nrm3772
11. Cavalli LR, Varella-Garcia M, Liang BC. Diminished tumorigenic phenotype after depletion of mitochondrial DNA. *Cell Growth Differ.* (1997) 8:1189–98.
12. Tan AS, Baty JW, Dong LF, Bezawork-Geleta A, Endaya B, Goodwin J, et al. Mitochondrial genome acquisition restores respiratory function and tumorigenic potential of cancer cells without mitochondrial DNA. *Cell Metab.* (2015) 21:81–94. doi: 10.1016/j.cmet.2014.12.003
13. Lebleu VS, O'connell JT, Gonzalez Herrera KN, Wikman H, Pantel K, Haigis MC, et al. PGC-1alpha mediates mitochondrial biogenesis and oxidative phosphorylation in cancer cells to promote metastasis. *Nat Cell Biol.* (2014) 992–1003:1001–15. doi: 10.1038/ncb3039
14. Tomitsuka E, Kita K, Esumi H. An anticancer agent, pyrvinium pamoate inhibits the NADH-fumarate reductase system–a unique mitochondrial energy metabolism in tumour microenvironments. *J Biochem.* (2012) 152:171–83. doi: 10.1093/jb/mvs041
15. Vlaski M, Negroni L, Kovacevic-Filipovic M, Guibert C, Brunet De La Grange P, Rossignol R, et al. Hypoxia/hypercapnia-induced adaptation maintains functional capacity of cord blood stem and progenitor cells at 4 degrees C. *J Cell Physiol.* (2014) 229:2153–65. doi: 10.1002/jcp.24678
16. Majeti R, Park CY, Weissman IL. Identification of a hierarchy of multipotent hematopoietic progenitors in human cord blood. *Cell Stem Cell.* (2007) 1:635–45. doi: 10.1016/j.stem.2007.10.001
17. Vlaski-Lafarge M, Loncaric D, Perez L, Labat V, Debeissat C, Brunet De La Grange P, et al. Bioenergetic changes underline plasticity of murine embryonic stem cells. *Stem Cells.* (2019) 37:463–75. doi: 10.1002/stem.2965
18. Ivanovic Z, Hermitte F, Brunet De La Grange P, Dazey B, Belloc F, Lacombe F, et al. Simultaneous maintenance of human cord blood SCID-repopulating cells and expansion of committed progenitors at low O2 concentration (3%). *Stem Cells.* (2004) 22:716–24. doi: 10.1634/stemcells.22-5-716
19. Loncaric D, Labat V, Debeissat C, Brunet De La Grange P, Rodriguez L, Vlaski-Lafarge M, et al. The majority of cells in so-called "mesenchymal stem cell" population are neither stem cells nor progenitors. *Transfus Clin Biol.* (2019) 26:316–23. doi: 10.1016/j.tracli.2018.08.157
20. Chevaleyre J, Duchez P, Rodriguez L, Vlaski M, Villacreces A, Conrad-Lapostolle V, et al. Busulfan administration flexibility increases the applicability of scid repopulating cell assay in NSG mouse model. *PLoS ONE.* (2013) 8:e74361. doi: 10.1371/journal.pone.0074361
21. Lapostolle V, Chevaleyre J, Duchez P, Rodriguez L, Vlaski-Lafarge M, Sandvig I, et al. Repopulating hematopoietic stem cells from steady-state blood before and after *ex vivo* culture are enriched in the CD34(+)CD133(+)CXCR4(low) fraction. *Haematologica.* (2018) 103:1604–15. doi: 10.3324/haematol.2017.183962
22. Dick JE, Bhatia M, Gan O, Kapp U, Wang JC. Assay of human stem cells by repopulation of NOD/SCID mice. *Stem Cells.* (1997) 15(Suppl. 1):199–203. doi: 10.1002/stem.5530150826
23. Hammoud M, Vlaski M, Duchez P, Chevaleyre J, Lafarge X, Boiron JM, et al. Combination of low O(2) concentration and mesenchymal stromal cells during culture of cord blood CD34(+) cells improves the maintenance and proliferative capacity of hematopoietic stem cells. *J Cell Physiol.* (2012) 227:2750–8. doi: 10.1002/jcp.23019
24. Mantel C, Messina-Graham S, Broxmeyer HE. Upregulation of nascent mitochondrial biogenesis in mouse hematopoietic stem cells parallels upregulation of CD34 and loss of pluripotency: a potential strategy for reducing oxidative risk in stem cells. *Cell Cycle.* (2010) 9:2008–17. doi: 10.4161/cc.9.10.11733
25. Tomitsuka E, Kita K, Esumi H. The NADH-fumarate reductase system, a novel mitochondrial energy metabolism, is a new target for anticancer therapy in tumor microenvironments. *Ann N Y Acad Sci.* (2010) 1201:44–9. doi: 10.1111/j.1749-6632.2010.05620.x
26. Vander Heiden MG, Deberardinis RJ. Understanding the Intersections between Metabolism and Cancer Biology. *Cell.* (2017) 168:657–69. doi: 10.1016/j.cell.2016.12.039
27. Hermitte F, Brunet De La Grange P, Belloc F, Praloran V, Ivanovic Z. Very low O2 concentration (0.1%) favors G0 return of dividing CD34+ cells. *Stem Cells.* (2006) 24:65–73. doi: 10.1634/stemcells.2004-0351
28. Guitart AV, Debeissat C, Hermitte F, Villacreces A, Ivanovic Z, Boeuf H, et al. Very low oxygen concentration (0.1%) reveals two FDCP-Mix cell subpopulations that differ by their cell cycling, differentiation and p27KIP1 expression. *Cell Death Differ.* (2011) 18:174–82. doi: 10.1038/cdd.2010.85
29. Cipolleschi MG, Dello Sbarba P, Olivotto M. The role of hypoxia in the maintenance of hematopoietic stem cells. *Blood.* (1993) 82:2031–7. doi: 10.1182/blood.V82.7.2031.2031
30. Cipolleschi MG, D'ippolito G, Bernabei PA, Caporale R, Nannini R, Mariani M, et al. Severe hypoxia enhances the formation of erythroid bursts from human cord blood cells and the maintenance of BFU-E *in vitro*. *Exp Hematol.* (1997) 25:1187–94.
31. Ivanovic Z, Dello Sbarba P, Trimoreau F, Faucher JL, Praloran V. Primitive human HPCs are better maintained and expanded *in vitro* at 1 percent oxygen than at 20 percent. *Transfusion.* (2000) 40:1482–8. doi: 10.1046/j.1537-2995.2000.40121482.x
32. Parmar K, Mauch P, Vergilio JA, Sackstein R, Down JD. Distribution of hematopoietic stem cells in the bone marrow according to regional hypoxia. *Proc Natl Acad Sci USA.* (2007) 104:5431–6. doi: 10.1073/pnas.0701152104
33. Ivanovic Z. Hypoxia or in situ normoxia: The stem cell paradigm. *J Cell Physiol.* (2009) 219:271–5. doi: 10.1002/jcp.21690
34. Levesque JP, Winkler IG. Hierarchy of immature hematopoietic cells related to blood flow and niche. *Curr Opin Hematol.* (2011) 18:220–5. doi: 10.1097/MOH.0b013e3283475fe7
35. Bradford GB, Williams B, Rossi R, Bertoncello I. Quiescence, cycling, and turnover in the primitive hematopoietic stem cell compartment. *Exp Hematol.* (1997) 25:445–53.
36. Yamazaki S, Ema H, Karlsson G, Yamaguchi T, Miyoshi H, Shioda S, et al. Nonmyelinating Schwann cells maintain hematopoietic stem cell hibernation in the bone marrow niche. *Cell.* (2011) 147:1146–58. doi: 10.1016/j.cell.2011.09.053
37. Giuntoli S, Rovida E, Gozzini A, Barbetti V, Cipolleschi MG, Olivotto M, et al. Severe hypoxia defines heterogeneity and selects highly immature progenitors within clonal erythroleukemia cells. *Stem Cells.* (2007) 25:1119–25. doi: 10.1634/stemcells.2006-0637
38. Masala E, Valencia-Martinez A, Pillozzi S, Rondelli T, Brogi A, Sanna A, et al. Severe hypoxia selects hematopoietic progenitors with stem cell potential from primary Myelodysplastic syndrome bone marrow cell cultures. *Oncotarget.* (2018) 9:10561–71. doi: 10.18632/oncotarget.24302
39. Rovida E, Marzi I, Cipolleschi MG, Dello Sbarba P. One more stem cell niche: how the sensitivity of chronic myeloid leukemia cells to imatinib mesylate is modulated within a "hypoxic" environment. *Hypoxia.* (2014) 2:1–10. doi: 10.2147/HP.S51812
40. Houten SM, Wanders RJ. A general introduction to the biochemistry of mitochondrial fatty acid beta-oxidation. *J Inherit Metab Dis.* (2010) 33:469–77. doi: 10.1007/s10545-010-9061-2

Conflict of Interest: The authors declare that the research was conducted in the absence of any commercial or financial relationships that could be construed as a potential conflict of interest.

frontiers in Oncology

MINI REVIEW
published: 19 May 2020
doi: 10.3389/fonc.2020.00660

Adenylate Kinase and Metabolic Signaling in Cancer Cells

Aleksandr Klepinin[1], Song Zhang[2], Ljudmila Klepinina[1], Egle Rebane-Klemm[1], Andre Terzic[2], Tuuli Kaambre[1] and Petras Dzeja[2]**

[1] *Laboratory of Chemical Biology, National Institute of Chemical Physics and Biophysics, Tallinn, Estonia,* [2] *Department of Cardiovascular Medicine, Mayo Clinic, Rochester, MN, United States*

A hallmark of cancer cells is the ability to rewire their bioenergetics and metabolic signaling circuits to fuel their uncontrolled proliferation and metastasis. Adenylate kinase (AK) is the critical enzyme in the metabolic monitoring of cellular adenine nucleotide homeostasis. It also directs AK→ AMP→ AMPK signaling controlling cell cycle and proliferation, and ATP energy transfer from mitochondria to distribute energy among cellular processes. The significance of AK isoform network in the regulation of a variety of cellular processes, which include cell differentiation and motility, is rapidly growing. Adenylate kinase 2 (AK2) isoform, localized in intermembrane and intra-cristae space, is vital for mitochondria nucleotide exchange and ATP export. AK2 deficiency disrupts cell energetics, causes severe human diseases, and is embryonically lethal in mice, signifying the importance of catalyzed phosphotransfer in cellular energetics. Suppression of AK phosphotransfer and AMP generation in cancer cells and consequently signaling through AMPK could be an important factor in the initiation of cancerous transformation, unleashing uncontrolled cell cycle and growth. Evidence also builds up that shift in AK isoforms is used later by cancer cells for rewiring energy metabolism to support their high proliferation activity and tumor progression. As cell motility is an energy-consuming process, positioning of AK isoforms to increased energy consumption sites could be an essential factor to incline cancer cells to metastases. In this review, we summarize recent advances in studies of the significance of AK isoforms involved in cancer cell metabolism, metabolic signaling, metastatic potential, and a therapeutic target.

Keywords: adenylate kinase, energy metabolism, phosphotransfer, mitochondria, cancer

OPEN ACCESS

Edited by:
Stefano Falone,
University of L'Aquila, Italy

Reviewed by:
Daria Capece,
Imperial College London,
United Kingdom
Paul Dent,
Virginia Commonwealth University,
United States
Elisabetta Benedetti,
University of L'Aquila, Italy

****Correspondence:***
Aleksandr Klepinin
aleksandr.klepinin@kbfi.ee
Petras Dzeja
dzeja.petras@mayo.edu

Specialty section:
This article was submitted to Cancer Metabolism, a section of the journal Frontiers in Oncology

Received: *15 February 2020*
Accepted: *08 April 2020*
Published: *19 May 2020*

Citation:
Klepinin A, Zhang S, Klepinina L, Rebane-Klemm E, Terzic A, Kaambre T and Dzeja P (2020) Adenylate Kinase and Metabolic Signaling in Cancer Cells. Front. Oncol. 10:660. doi: 10.3389/fonc.2020.00660

INTRODUCTION

The significance of metabolism and metabolic signaling in human diseases is rapidly growing. New features and molecular players that are vital for cell homeostasis and function are being uncovered. Well-organized high-energy phosphoryl transfer systems are required to mediate intracellular communication between ATP-consuming and ATP-producing cellular compartments and thus to maintain normal growth and development of the cell (1–5). The main components of the cellular phosphotransfer system are AK, creatine kinase (CK), and glycolytic networks (1, 2). The significance of organized phosphotransfer was demonstrated by genetic manipulations in animal models, cellular systems, and alterations or mutations in separate phosphotransfer enzymes, which are associated with human diseases (6–16). Studies on *Drosophila* and mice model demonstrate that deletion of adenylate kinase 2 (AK2) is embryonically lethal, signifying

the importance of AK phosphotransfer network in cell homeostasis (13, 17–19). In humans, mutations in the mitochondrial AK2 gene are associated with reticular dysgenesis characterized by immunodeficiency and sensorineural deafness, where processes of nucleotide signaling, cell differentiation, and motility are affected (15, 16, 20). So far, nine isoforms of adenylate kinase (AK1–AK9) and several subforms have been found and well characterized in mammalian cells (21). AK, which catalyzes reaction 2ADP↔AMP+ATP, is a recognized facilitator of AMP metabolic signaling, optimizing intracellular energetic communication, and local ATP supply (5, 22). Historically, the function of AK has been ascribed to *de novo* adenine nucleotide synthesis and cell energy economy through regulation of nucleotide ratios in different intracellular compartments and AMP-sensitive metabolic enzymes (14, 23, 24). The unique properties of AK lie on its ability to deliver γ- and β-phosphoryl groups of ATP, thereby doubling the ATP energetic potential. Moreover, the AK network provides an efficient mechanism for high-energy phosphoryl transport from mitochondria to ATP utilization sites (2). Evolutionary AK isoforms have been positioned to different subcellular compartments (21, 25). AK1, AK7, and AK8 are solely found in the cytosol; AK2, AK3, and AK4 are located in the mitochondria; and AK5 and AK9 can be found in either the cytosol or nucleus. Only AK1 and AK6 are known to be expressed in all tissues, whereas AK5 is expressed only in the brain (21). In the cytosol, the main isoform is AK1, which is predominantly expressed in high energy demand tissues such as the brain, heart, and skeletal muscles. AK2 is strategically located in the mitochondrial intermembrane and cristae space to facilitate high-energy phosphoryl exchange between mitochondria and cytosol (22). Two other AK isoforms, AK3 and AK4, are located in the mitochondrial matrix and are involved in the regulation of mitochondrial Krebs cycle and oxidative phosphorylation (OXPHOS), whereas AK5 and AK6 isoforms that are localized in the nucleus could serve to fulfill the energy needs of nuclear processes. In general, distinct intracellular localization and kinetic properties of AK isoforms favor energy support of specific cellular processes ranging from muscle contraction, electrical activity, cell motility, unfolded protein response, and mitochondrial/nuclear energetics (22). Importantly, reprogramming of energy metabolism has been proposed as one of the hallmarks of cancer (26), which is required to drive biosynthesis pathways necessary for rapid cell replication and proliferation. Cancer cells are believed to have a greater reliance on glycolytic phosphotransfer (27, 28). However, during the last decade, it was found that some tumors contain numerous mitochondria producing ATP predominantly *via* OXPHOS (29–31). The observed shift in hexokinase (HK) isoforms, upregulation of HK2 in cancer cells (32), indicates a closer integration of mitochondria with glycolytic phosphotransfer (see **Figure 1**). The association of HK2 with mitochondria and expression of pyruvate kinase PKM2 could promote effective yet uncontrolled energy distribution in cancer cells (27, 33, 34). Phosphotransfer enzymes such as CK and AK have been implicated in cancer cell proliferation (35, 36). However, it is not clear whether the redistribution of phosphotransfer enzymes, especially those which are localized in mitochondria, occurs during cancer formation. In this review, we focus on the significance of AK isoforms in the rewiring of cancer cell energy metabolism and AMP signaling. Specifically, we will overview how AK isoforms, localized in mitochondria (AK2 and AK4), and their main communication partners cytosolic AK (AK1 and AK6) are involved in cancer formation and metastasis.

Abbreviations: AK, adenylate kinase; CK, creatine kinase; CKmit, mitochondrial creatine kinase; CKB, brain-type creatine kinase; MOM, mitochondrial outer membrane; ANT, adenine nucleotide translocase; AMPK, AMP-activated protein kinase; CSCs, cancer stem cells; NB, neuroblastoma; VDAC, voltage-dependent anion channel; ABC, ATP-binding cassette; FADD, Fas-associated protein with death domain; HIF, hypoxia-inducible factor; hCINAP, human coilin-interacting nuclear ATPase protein; DUSP26, dual-specificity phosphatase 26; OXPHOS, oxidative phosphorylation; AMPD, AMP-deaminase; 5′-NT, 5′-nucleotidase; LDHA, lactate dehydrogenase A; HK, hexokinase.

ADENYLATE KINASE 2 AND MITOCHONDRIAL CREATINE KINASE INTERPLAY IN MALIGNANT TRANSFORMATION

AK2 and mitochondrial CK (CKmit) are major phosphotransfer enzymes located in the intermembrane/cristae space in mitochondria (3, 14, 22). AK2 and CKmit provide nucleotide exchange and metabolic signaling capacity, allowing mitochondria to export ATP and reception of cytosolic feedback signals such as ADP, AMP, and creatine (22, 23, 37). Phosphotransfer enzymes CK and AK have been implicated in cancer cell proliferation (35, 36). In general, CK is involved in cancerous transformation, as CKB (brain-type CK) is upregulated in a variety of cancers to support growing energy needs (38). The elevation of creatine metabolites was noted in drug-resistant cancer cells (39). However, in other cancer types, the downregulation of CKB and rewiring of metabolism may play an important role in colon cancer progression (40). Moreover, several studies have demonstrated that in colorectal cancer (41), breast cancer (42), neuroblastoma (35), prostate cancer (43), and sarcoma (36, 44), the CKmit was downregulated. The reduction of CKmit in cancer cells was associated with the upregulation of adenylate kinase AK2 isoform in intermembrane space (36, 41, 42, 45, 46) (see **Table 1**). There is evidence that the expression of AK2 on the cell surface could facilitate nucleotide signaling and metastatic potential (60). It was found that Ak2 gene expression is upregulated in the metastatic pancreatic endocrine neoplasms (60), indicating the significance of nucleotide metabolic signaling in cancer invasion (61). Moreover, increased expression of the Ak2 on the surface of the metastatic F9DR murine terato-carcinoma cells compared with the nonmetastatic F9B9 cell line has been demonstrated (53). Furthermore, a recent study showed that AK2 has prognostic and therapeutic potential in lung adenocarcinoma (55). The knockdown of AK2 suppressed proliferation, migration, and invasion, as well as induced apoptosis and autophagy in human lung adenocarcinoma cells. In this regard, the AK2-FADD (Fas-associated protein with death domain) mediated apoptosis pathway was found to be defective in some tumor cells,

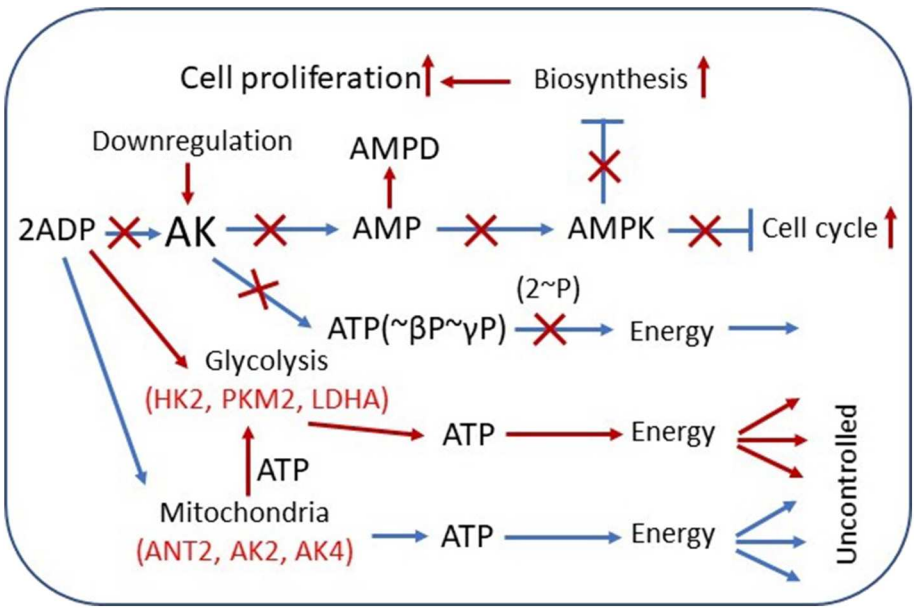

FIGURE 1 | Overview of adenylate kinase (AK) isoform involvement in the rewiring of cancer cell metabolic signaling and energetic circuits. Increased competition for cytosolic ADP downregulates AK-mediated AMP signaling, reducing control over cell cycle and proliferation. AK expression is downregulated in several tumors. AMP can be consumed by AMPD and by 5′-NT, also overexpressed in some cancer cells. Augmented glycolytic metabolism, owing to higher affinity, scavenges cytosolic ADP, and uses mitochondrial ATP to drive glucose conversion to lactate. Overexpression of glycolytic HK2, PKM2, and LDHA and mitochondrial ANT2, AK2, AK4, and other genes in cancer cells promotes rewiring of energetic circuits resulting in unrestrained energy distribution. The result of these metabolic transformations is deficient AMP signaling and AMPK-mediated control of cellular katabolic and anabolic processes. Red color indicates the augmented pathways and gene expression in cancer cells. AMPD, AMP-deaminase; HK2, hexokinase 2; LDHA, lactate dehydrogenase A; ANT2, adenine nucleotide translocase 2; AMPK, AMP-activated protein kinase.

which may contribute to tumor development by preventing apoptosis (62). A recent study indicates that AK2 and FADD are crucial for caspase-10 activation upon metabolic stress, and this activation is independent of death receptors and extrinsic pathway of apoptosis (63). Moreover, the deletion of the Ak2 gene or exit AK2 from mitochondria during apoptosis disrupts nucleotide exchange between mitochondria and cytosol, causing hyperpolarization of mitochondria and reactive oxygen species (ROS) production (20). It was found that the presence of AK2 in mitochondrial cristae nanochannels is critical for ATP export (2, 22). There are evidence that the AK2 upregulation could be used by cancer cells to support energy supply to biosynthetic processes and cellular growth (18, 64). These results, as well as studies on CK and AK knockout mice, demonstrate remarkable plasticity of cellular energetics and phosphotransfer systems, which could be used in cancer cells to promote uncontrolled cell growth (9, 17, 22, 65).

ADENYLATE KINASE MODULATE TUMOR CELL RESPONSE TO SURVIVE UNDER OXIDATIVE STRESS

The ability to conduct metabolic signaling and rewire metabolism is critical for cell survival. The AK4 isoform increased expression has been associated with a poor clinical outcome marker for lung cancer (56) as well as for glioma patients (57) (see **Table 1**). It was found that AK4 expression is under tight control of noncoding RNA. The AK4 is negatively regulated by microRNA miR-556-3p and positively by circular RNA of ATP-binding cassette (ABC) subfamily B member 10, circ-ABCB10 (66). In same study was demonstrated that downregulation of AK4 restrained lung cancer progression and sensitized lung cancer cells to cisplatin (66). Moreover, new data indicate that AK4 was shown to be involved in the radioresistance of esophageal cancer cells (67) and in chemoresistance of other cancers (68, 69). Previously, it was suggested that overexpression of AK4 could protect cells against oxidative stress (70). Other studies on HeLa (68) and HEK293 cells (71) demonstrated that tumor cells respond to a hypoxic condition by upregulating the AK4. However, in HepG2 cells (71), it was found that under oxidative stress, AK4 oppositely was downregulated. Although AK4 might be downregulated, it can still regulate OXPHOS because it retains the nucleotide-binding capability, and it can interact with the mitochondrial adenine nucleotide translocase (ANT) (70). It was found that knockout of AK4 increased cellular ATP through raised OXPHOS activity as well as mitochondrial number (68). Fujisawa and colleagues in 2016 have proposed that there are two mechanisms how AK4 regulates mitochondrial respiration in cancer cells (68). First, in cancer cells, AK4 interacts with ANT, which forms with voltage-dependent anion channel (VDAC) and HK transmembrane complex AK4-ANT-VADC-HK (see **Figure 1**). Under the hypoxic conditions, the

TABLE 1 | Adenylate kinase isoforms in cancer.

Enzyme	Type of cancer	Status in tumor	Localization	Function/therapeutic target	Experimental model	References
AK	Lung cancer	↓	-	Negative regulator of cancer	Tissue samples	(47)
AK	Hepatomas	↓	-	Decreased during de-differentiation of cancer cells	Rat liver and hepatomas	(48)
AK	Colon cancer	↑	-	Metabolic regulator. Energy distribution shifts from CK toward AK	Tissue samples	(41, 49)
AK1	Transformed embryonic fibroblasts	↓	Cytosol	Negative regulator of tumor malignant	ras^{V12}/E1A-transformed primary mouse embryonic fibroblasts	(50)
AK2	Breast cancer	↑	Mitochondria intermembrane space	Prognostic and therapeutic target	Estrogen receptor-negative breast cancer tissue samples	(51)
AK2	Breast cancer	↑	Mitochondria intermembrane space	Oncotarget of the breast CSC	Breast CSC	(52)
AK2	Breast cancer and neuroblastoma	↑	Mitochondria intermembrane space	Oncotarget of the poorly differentiated cancer cells	Tissue samples and cancer cell lines	(46)
AK2	Embryonic carcinoma	↑	Mitochondria intermembrane space	Metabolic regulator. Energy distribution shifts from CK toward AK	Cell lines	(36)
AK2	Teratocarcinoma	↑	Plasma membrane	Overexpressed on the plasma membrane in metastatic cells	Cell lines	(53)
AK2	Breast cancer	↓	Nuclear	Negative regulator of tumor cell growth via DUSP26/FADD signaling	Breast cancer cell lines and tissue samples	(54)
AK2	Lung cancer	↑	Mitochondria intermembrane space	Associated with poor survival of patients. Prognostic and therapeutic potential	Tissue samples	(55)
AK4	Lung cancer	↑	Mitochondrial matrix	Associated with poor survival of patients. Prognostic and therapeutic potential	Tissue samples and various cell lines	(56)
AK4	Glioma	↑	Mitochondrial matrix	A key regulator of intracellular ATP level. Prognostic and therapeutic potential	Tissue samples and cancer cell lines	(57)
AK6	Breast cancer Colon cancer	↑	Nuclear	Promote cancer cell growth. Prognostic and therapeutic potential	Colon adenocarcinoma and breast cancer tissues	(58)
AK6	Colon cancer	↑	Cytosol	Glycolysis regulator via phosphorylation LDHA. Modulator of CSC invasion and metastasis activity	CSC from tissues	(59)

complex supports the high glycolytic activity of cancer cells. It allows efficient ADP recycling between mitochondrial ATP synthesis and glucose phosphorylation by HK, which interacts with the mitochondrial outer membrane (MOM) (68, 72). In addition, in hepatoma cells (73), it was found that up to 50% of ATP is provided by intramembrane space located AK2 through VDAC binding to HK. Thus, AK2 may also be a member of the metabolic circuit channeling ADP–ATP in and out of mitochondria. The second mechanism is related to the fact that AK4 and AK3 have highly homologous sequences; therefore, they compete with each other for their substrates (68). According to this mechanism, AK4 interferes with AK3 action in supplying of the GDP required for the conversion of succinyl-CoA to succinate. That is why overexpression of AK4 in HeLa cells induces a decrease in Krebs cycle metabolites such as succinate, fumarate, and malate while glutamine and glutamate are increased. In several tumors, it was shown that the predominate substrate for mitochondria is glutamine (74). However, further studies are needed to confirm the role of AK4 in mitochondria and Krebs cycle substrate metabolism.

ADENYLATE KINASE NETWORK ROLE IN CANCER STEM CELLS

Traditional therapies against cancer, such as chemotherapy and radiotherapy, have many limitations. The limitation is due to systematic and local toxicity as well as drug resistance of small populations of tumor cells that have self-renewal properties. This small population of cells is called cancer stem cells (CSCs) (75). Previously, studies on CSC have shown that the cancer resistance for chemotherapy is related to increased OXPHOS in CSC. That is why a new generation of cancer

chemotherapy could be targeted against pathways that interact with OXPHOS, such as the phosphotransfer system. Lamb and colleagues have shown on the breast cancer model that mitochondrial mass is a new biomarker of CSC, which have increased AK2 expression level (see **Table 1**) (52). In our previous study on neuroblastoma (NB) (46), which contains numerous CSC (76), and embryonal carcinoma cells (36), we also found that those cells have a high activity of AK2 (see **Table 1**). Moreover, another feature of CSC is that mitochondria are localized around the cell nucleus (77). There is evidence that AK2 can play an important role in communication between mitochondria and the nucleus (78). In another study using proteomic analysis of mouse teratocarcinoma cells (53), it was demonstrated that metastatic cancer cells have increased AK2 levels than have nonmetastatic cancer cells (see **Table 1**). As metastasis is related to cell motility, positioning of phosphotransfer enzymes to sites of increased energy consumption could be an important factor of tumor formation (59). The AK4 has been identified as a biomarker of metastasis in lung cancer (56, 79, 80). Overexpression of AK4 promoted lung cancer metastasis by enhancing hypoxia-inducible factor HIF-1 stability and epithelial-to-mesenchymal transition under hypoxia (79). Moreover, it was found that aferin-A could suppress AK4-HIF-1a signaling and may serve as a novel anti-metastatic agent in lung cancer (79). The AK4 was also implicated in breast and bladder cancers, where it promoted cell proliferation and invasion (81, 82). Furthermore, it was demonstrated that another AK isoform AK6 could affect colorectal cancer migration and invasion (59). Although significant progress has been made, at this time, the complete role of the AK system in cancer metastasis is still unclear. Moreover, the other reason why CSCs are drug resistant relates to the increased expression of ABC transporters in those cells (83, 84). The model for ABC transporters was proposed (85), which is based on ^{31}P solid-state NMR spectroscopy, suggesting that intrinsic ATPase is coupled with AK activity where AK participates in ATP exchange. It is known that cytosolic and membrane-associated AK can regulate the activity of another ABC protein—K-ATP channel (86, 87). Nevertheless, the exact role of AK in supporting adenylate charge and function of ABC transporters in CSC remains unknown yet. In this respect, the ABC transporters are not unique proteins that possess both ATPase and AK activities; there are other proteins like AK6 (58), also known as transcription factor TAF9, human coilin interacting nuclear ATPase protein (hCINAP), and highly conserved DNA repair complex Rad50 (88).

PARADOXES REGARDING THE ROLE OF ADENYLATE KINASE IN TUMOR FORMATION

Cancer is a very complex and diverse phenomenon, including tissue specificity and different phases. Enzymatic changes can be different in the initial and advanced stages of tumor growth (89, 90). There are some contradictory studies where it was found that in lung cancer and hepatoma, AK was downregulated compared with that in normal tissue (47, 48) (see **Table 1**), whereas a recent study has shown that high expression of AK2 correlates with a worse prognosis for lung cancer patients (55) (see **Table 1**). In mouse embryonic fibroblasts, it was demonstrated that during their transformation into tumor cells, a significant reduction of AK1 expression occurs (50). More recently, the existence of AK1 additional gene product AK1β has been reported, and it is known that the AK1β expression level is regulated by p53 (91). In some cancers, p53 is mutated or suppressed. In this context, experiments on mouse embryonic fibroblast (50) have shown that during their transformation into tumor cells, augmentation of AK1 might be related to the downregulation of AK1β (see **Table 1**). Also, Kim et al. have postulated that AK2 is a negative regulator of tumor growth (54) (see **Table 1**). They demonstrated that in some cells, the AK2 localized not only in mitochondria but also in the nucleus, where it interacted with dual-specificity phosphatase 26 (DUSP26). This protein complex can dephosphorylate FADD leading to suppressed cell growth. They also suggested that AK2 downregulation was associated with breast cancer formation. In contrast, Speers and colleagues have found that AK2 is overexpressed in ER-negative breast cancer (51) (see **Table 1**). They proposed that AK2 should be a novel target for the treatment of ER-negative breast cancer. Indeed, a diterpene lactone neoandrographolide from extracts of the traditional medicinal herb *Andrographis paniculata* has been suggested to inhibit AK2 and have strong anticancer properties (92). Nevertheless, studies on human breast cancer and colorectal cancer demonstrated another AK isoform AK6 was overexpressed during cancer formation (58) (see **Table 1**). These data correlate with our previous studies on colorectal and breast cancers (41, 46) (see **Table 1**). It was also shown, that in both colon and breast tissues, AK6 is located not only in nuclear but also in the cytosol. However, only in cytosolic compartmentalized AK6 did expression level increase during tumorogenesis of breast and colorectal cancer cells (58) (see **Table 1**). They have found that AK6's main function is to regulate ribosome assembly and, consequently, protein expression and cancer cell growth. Recently, it was demonstrated that hCINAP or AK6 is a potent modulator of metabolic reprogramming by phosphorylating LDHA, a key player in cancer glycolysis (59) (see **Table 1**). Thus, AK isoform role can be different depending on cancer cell type and development stage.

ADENYLATE KINASE-MEDIATED AMP METABOLIC SIGNALING IN CANCER CELLS

In recent years, AK-mediated AMP signaling is emerging as one of the most versatile systems in the regulation of diverse cellular processes (5, 22, 93). Particularly, AMP signaling to AMP-activated protein kinase (AMPK) plays a critical role in adjusting ATP-producing and ATP-consuming processes (90, 94) (**Figure 1**). In several cancers, it has been demonstrated

that AMPK, a master regulator of cellular energy homeostasis, possesses tumor suppressor function (95–97). In cells, AMPK activation/suppression is regulated via changes in cellular AMP levels. The principal activator of AMPK is the AK-catalyzed pathway, where it monitors cellular ATP–ADP balance and signals to AMPK by increased AMP cellular level. A recent study indicates that AK and AMPK cooperate to maintain cellular ATP levels (98). On the other end, AMP-deaminase (AMPD) and 5′-nucleotidase (5′-NT) suppress AMPK via decreasing AMP cellular levels (22, 99, 100). Moreover, the product of AMPD and 5'-NT reactions is adenosine, an immunosuppressive metabolite. At a high level in tumors, adenosine can promote cell growth, invasion, metastasis of cancer cells, and tumor immune evasion (101). Our previous work has demonstrated that in NB and heart adenocarcinoma cells HL-1, their mitochondrial permeability for AMP was increased than in healthy cells (46). It is known that AK2, which has unique localization in mitochondrial space, has a high affinity for AMP among AMP metabolizing enzymes. Therefore, it has been proposed that the AK2's primary function is to regulate intracellular AMP levels and to guard the cellular adenine nucleotide pool (22). Our study also suggested that cancer cells have a high level of AK2 (46) (**Figure 1**). Altogether, in cancer cells, most cellular AMP transport occurs via MOM where it is converted immediately to ADP and channeled into, maintaining a low cytosolic AMP concentration. Recent direct measurements of AK-mediated metabolic flux indicate that cancer cells have suppressed ATP β-phosphoryl energetics and AMP signaling, as indicated from ^{18}O-labeling experiments demonstrating that highly aggressive breast cancer cells MDAMB231 have lower β-ATP[^{18}O] turnover (AMP phosphorylation) than have the control MCF10A cells (Klepinin et al., in preparation). This could be due to the rewiring of energy metabolism and glycolytic takeover. Activated glycolysis usually suppresses AK metabolic flux apparently by scavenging ADP (102) (**Figure 1**). Suppression of AK phosphotransfer, AMP generation, and consequent signaling through AMPK could be the biggest culprit of a cancerous transformation of a cell (**Figure 1**). There is also evidence that other AMP removal pathway enzymes like AMPD2 as well as 5′-NT are upregulated in colorectal cancer (103, 104). In this regard, the 5′-NT expression in breast cancer depends on tumor estrogen receptor status, suggesting a coordinated network (105). Our previous work has shown that in several tumors, MOM permeability has also increased for ADP, which may be related with keeping an intracellular ADP level low (41, 42, 49, 106) (see **Figure 1**). It was found that not only AMP but also ADP can regulate the activity of AMPK (107). Further studies are needed to elucidate detailed mechanisms: (1) how increased MOM permeability for ADP and AMP and (2) raised expression of AMP metabolizing enzymes can regulate intracellular nucleotide levels and the activity of AMPK and (3) what the significance is of AMP metabolic signaling in cancer progression.

CONCLUSIONS

The present review is a snapshot from recent AK studies that focused on the significance of AK network in energetics and metabolic signaling in cancer cells. Of the nine AK isoforms (AK1–AK9), four of them (AK1, AK2, AK4, and AK6) are involved in the progression of malignant transformation. Studies indicate that AK isoforms (AK1, AK2, AK4, and AK6) have an important role in the regulation of cancer cell metabolism, metabolic signaling, and cell migration and invasion. Moreover, at the initial stage, suppression of AK phosphotransfer and AMP generation and consequently signaling through AMPK by a variety of factors could be the biggest culprit of the cancerous transformation of a cell. Downregulation of AK→ AMP→ AMPK signaling can lead to the loss of control of cell cycle, growth, and proliferation. In the later stages, as emerging data suggest, cancer cells may use the shift in AK isoforms and other phosphotransfer enzymes to rewire their energy supply circuits to support proliferation and metastasis. Knockdown of overexpressed AK2 in human lung adenocarcinoma cells suppressed proliferation, migration, and invasion as well as induced apoptosis and autophagy. In this regard, a diterpene lactone neoandrographolide from extracts of the traditional medicinal herb *Andrographis paniculata* has been suggested to inhibit AK2 and has strong anticancer properties. Further studies that involve all AK isoforms have the potential to bring new understanding and novel therapeutic strategies targeting the AK isoform network to suppress growth and metastasis of cancer cells.

AUTHOR CONTRIBUTIONS

AK and SZ performed the study design, development of methodology, data analysis and interpretation, drafting of the manuscript, and critical revision. LK and ER-K analyzed and interpreted data and performed manuscript review. AT, TK, and PD performed the study conception, design, writing, and reviewing of the manuscript.

FUNDING

This work was supported by the National Institutes of Health/National Heart, Lung, and Blood Institute (HL 85744-09) and U24DK100469 (Mayo Clinic Metabolomics Resource Core); Marriott Foundation and Department of Cardiovascular Medicine, Mayo Clinic, Rochester, MN, USA; Institutional Research Funding IUT23-1 of the Estonian Ministry of Education and Research; and Estonia national scholarship program Kristjan Jaak, which is funded and managed by Archimedes Foundation in collaboration with the Estonian Ministry of Education and Research.

REFERENCES

1. Dzeja P, Chung S, Terzic A. Integration of adenylate kinase, glycolytic and glycogenolytic circuits in cellular energetics. In: Saks V, editor. *Molecular System Bioenergetics: Energy for Life*. Weinheim: Wiley-VCH. (2007). p. 265–301. doi: 10.1002/9783527621095.ch8
2. Dzeja PP, Terzic A. Phosphotransfer networks and cellular energetics. *J Exp Biol.* (2003) 206:2039–47. doi: 10.1242/jeb.00426
3. Saks V, Dzeja P, Schlattner U, Vendelin M, Terzic A, Wallimann T. Cardiac system bioenergetics: metabolic basis of the Frank-Starling law. *J Physiol.* (2006) 571:253–73. doi: 10.1113/jphysiol.2005.101444
4. Saks V, Monge C, Anmann T, Dzeja P. Integrated and organized cellular energetic systems: theories of cell energetics, compartmentation and metabolic channeling. In: Saks V, editor. *Molecular System Bioenergetics: Energy for Life*. Weinheim: Wiley-VCH. (2007). p. 59–109. doi: 10.1002/9783527621095.ch3
5. Zhang S, Nemutlu E, Terzic A, Dzeja P. Adenylate kinase isoform network: a major hub in cell energetics and metabolic signaling. system biology of metabolic and signaling networks. *Springer Ser Biophys.* (2014) 16:145–62. doi: 10.1007/978-3-642-38505-6_6
6. Dzeja PP, Bast P, Pucar D, Wieringa B, Terzic A. Defective metabolic signaling in adenylate kinase AK1 gene knock-out hearts compromises post-ischemic coronary reflow. *J Biol Chem.* (2007) 282:31366–72. doi: 10.1074/jbc.M705268200
7. Dzeja PP, Terzic A, Wieringa B. Phosphotransfer dynamics in skeletal muscle from creatine kinase gene-deleted mice. *Mol Cell Biochem.* (2004) 256-257:13–27. doi: 10.1023/B:MCBI.0000009856.23646.38
8. Janssen E, de Groof A, Wijers M, Fransen J, Dzeja PP, Terzic A, et al. Adenylate kinase 1 deficiency induces molecular and structural adaptations to support muscle energy metabolism. *J Biol Chem.* (2003) 278:12937–45. doi: 10.1074/jbc.M211465200
9. Janssen E, Terzic A, Wieringa B, Dzeja PP. Impaired intracellular energetic communication in muscles from creatine kinase and adenylate kinase (M-CK/AK1) double knock-out mice. *J Biol Chem.* (2003) 278:30441–9. doi: 10.1074/jbc.M303150200
10. Steeghs K, Benders A, Oerlemans F, de Haan A, Heerschap A, Ruitenbeek W, et al. Altered Ca2+ responses in muscles with combined mitochondrial and cytosolic creatine kinase deficiencies. *Cell.* (1997) 89:93–103. doi: 10.1016/S0092-8674(00)80186-5
11. van Deursen J, Heerschap A, Oerlemans F, Ruitenbeek W, Jap P, ter Laak H, et al. Skeletal muscles of mice deficient in muscle creatine kinase lack burst activity. *Cell.* (1993) 74:621–31. doi: 10.1016/0092-8674(93)90510-W
12. van Horssen R, Janssen E, Peters W, van de Pasch L, Lindert MM, van Dommelen MM, et al. Modulation of cell motility by spatial repositioning of enzymatic ATP/ADP exchange capacity. *J Biol Chem.* (2009) 284:1620–7. doi: 10.1074/jbc.M806974200
13. Horiguchi T, Fuka M, Fujisawa K, Tanimura A, Miyoshi K, Murakami R, et al. Adenylate kinase 2 deficiency limits survival and regulates various genes during larval stages of Drosophila melanogaster. *J Med Invest.* (2014) 61:137–50. doi: 10.2152/jmi.61.137
14. Noma T. Dynamics of nucleotide metabolism as a supporter of life phenomena. *J Med Invest.* (2005) 52:127–36. doi: 10.2152/jmi.52.127
15. Lagresle-Peyrou C, Six EM, Picard C, Rieux-Laucat F, Michel V, Ditadi A, et al. Human adenylate kinase 2 deficiency causes a profound hematopoietic defect associated with sensorineural deafness. *Nat Genet.* (2009) 41:106–11. doi: 10.1038/ng.278
16. Pannicke U, Honig M, Hess I, Friesen C, Holzmann K, Rump EM, et al. Reticular dysgenesis (aleukocytosis) is caused by mutations in the gene encoding mitochondrial adenylate kinase 2. *Nat Genet.* (2009) 41:101–5. doi: 10.1038/ng.265
17. Dzeja PP, Chung S, Faustino RS, Behfar A, Terzic A. Developmental enhancement of adenylate kinase-AMPK metabolic signaling axis supports stem cell cardiac differentiation. *PLoS ONE.* (2011) 6:e19300. doi: 10.1371/journal.pone.0019300
18. Fujisawa K, Murakami R, Horiguchi T, Noma T. Adenylate kinase isozyme 2 is essential for growth and development of Drosophila melanogaster. *Comp Biochem Physiol.* (2009) 153:29–38. doi: 10.1016/j.cbpb.2009.01.006
19. Zhang S, Nemutlu E, Dzeja P. Metabolomic profiling of adenylate kinase AK1-/- and AK2+/- transgenic mice: effect of physical stress. *Circulation.* (2010) 122:A20435.
20. Ghaloul-Gonzalez L, Mohsen AW, Karunanidhi A, Seminotti B, Chong H, Madan-Khetarpal S, et al. Reticular dysgenesis and mitochondriopathy induced by adenylate kinase 2 deficiency with atypical presentation. *Sci Rep.* (2019) 9:15739. doi: 10.1038/s41598-019-51922-2
21. Panayiotou C, Solaroli N, Karlsson A. The many isoforms of human adenylate kinases. *Int J Biochem Cell Biol.* (2014) 49:75–83. doi: 10.1016/j.biocel.2014.01.014
22. Dzeja P, Terzic A. Adenylate kinase and AMP signaling networks: metabolic monitoring, signal communication and body energy sensing. *Int J Mol Sci.* (2009) 10:1729–72. doi: 10.3390/ijms10041729
23. Dzeja PP, Zeleznikar RJ, Goldberg ND. Adenylate kinase: kinetic behavior in intact cells indicates it is integral to multiple cellular processes. *Int J Mol Sci.* (1998) 184:169–82. doi: 10.1007/978-1-4615-5653-4_13
24. Noda L. Adenylate kinase. In: Boyer P, editor. *The Enzymes, 3rd edition*. New York, NY: Academic Press. (1973). p. 279-305. doi: 10.1016/S1874-6047(08)60068-2
25. Van Rompay AR, Johansson M, Karlsson A. Phosphorylation of nucleosides and nucleoside analogs by mammalian nucleoside monophosphate kinases. *Pharmacol Ther.* (2000) 87:189–98. doi: 10.1016/S0163-7258(00)00048-6
26. Hanahan D, Weinberg RA. Hallmarks of cancer: the next generation. *Cell.* (2011) 144:646–74. doi: 10.1016/j.cell.2011.02.013
27. Chung S, Arrell DK, Faustino RS, Terzic A, Dzeja PP. Glycolytic network restructuring integral to the energetics of embryonic stem cell cardiac differentiation. *J Mol Cell Cardiol.* (2010) 48:725–34. doi: 10.1016/j.yjmcc.2009.12.014
28. Fantin VR, St-Pierre J, Leder P. Attenuation of LDH-A expression uncovers a link between glycolysis, mitochondrial physiology, and tumor maintenance. *Cancer cell.* (2006) 9:425–34. doi: 10.1016/j.ccr.2006.04.023
29. Jose C, Bellance N, Rossignol R. Choosing between glycolysis and oxidative phosphorylation: a tumor's dilemma? *Biochim Biophys Acta.* (2011) 1807:552–61. doi: 10.1016/j.bbabio.2010.10.012
30. Moreno-Sanchez R, Rodriguez-Enriquez S, Marin-Hernandez A, Saavedra E. Energy metabolism in tumor cells. *FEBS J.* (2007) 274:1393–418. doi: 10.1111/j.1742-4658.2007.05686.x
31. Moreno-Sanchez R, Rodriguez-Enriquez S, Saavedra E, Marin-Hernandez A, Gallardo-Perez JC. The bioenergetics of cancer: is glycolysis the main ATP supplier in all tumor cells? *Biofactors.* (2009) 35:209–25. doi: 10.1002/biof.31
32. Han CY, Patten DA, Lee SG, Parks RJ, Chan DW, Harper ME, et al. p53 Promotes chemoresponsiveness by regulating hexokinase II gene transcription and metabolic reprogramming in epithelial ovarian cancer. *Mol Carcinog.* (2019) 58:2161–74. doi: 10.1002/mc.23106
33. Masters C. Cellular differentiation and the microcompartmentation of glycolysis. *Mech Ag Dev.* (1991) 61:11–22. doi: 10.1016/0047-6374(91)90003-I
34. Zahra K, Dey T, Ashish, Mishra SP, Pandey U. Pyruvate Kinase M2 and Cancer: The Role of PKM2 in Promoting Tumorigenesis. *Front Oncol.* (2020) 10:159. doi: 10.3389/fonc.2020.00159
35. Klepinin A, Chekulayev V, Timohhina N, Shevchuk I, Tepp K, Kaldma A, et al. Comparative analysis of some aspects of mitochondrial metabolism in differentiated and undifferentiated neuroblastoma cells. *J Bioenerg Biomembr.* (2014) 46:17–31. doi: 10.1007/s10863-013-9529-5
36. Ounpuu L, Klepinin A, Pook M, Teino I, Peet N, Paju K, et al. 2102Ep embryonal carcinoma cells have compromised respiration and shifted bioenergetic profile distinct from H9 human embryonic stem cells. *Biochim Biophys Acta Gen Subj.* (2017) 1861:2146–54. doi: 10.1016/j.bbagen.2017.05.020
37. Gellerich FN, Gizatullina Z, Trumbeckaite S, Nguyen HP, Pallas T, Arandarcikaite O, et al. The regulation of OXPHOS by extramitochondrial calcium. *Biochim Biophys Acta.* (2010) 1797:1018–27. doi: 10.1016/j.bbabio.2010.02.005
38. Li XH, Chen XJ, Ou WB, Zhang Q, Lv ZR, Zhan Y, et al. Knockdown of creatine kinase B inhibits ovarian cancer progression by decreasing glycolysis. *Int J Biochem Cell Biol.* (2013) 45:979–86. doi: 10.1016/j.biocel.2013.02.003

39. Dewar BJ, Keshari K, Jeffries R, Dzeja P, Graves LM, Macdonald JM. Metabolic assessment of a novel chronic myelogenous leukemic cell line and an imatinib resistant subline by H NMR spectroscopy. *Metabolomics.* (2010) 6:439–50. doi: 10.1007/s11306-010-0204-0
40. Mooney SM, Rajagopalan K, Williams BH, Zeng Y, Christudass CS, Li Y, et al. Creatine kinase brain overexpression protects colorectal cells from various metabolic and non-metabolic stresses. *J Cell Biochem.* (2011) 112:1066–75. doi: 10.1002/jcb.23020
41. Kaldma A, Klepinin A, Chekulayev V, Mado K, Shevchuk I, Timohhina N, et al. An in situ study of bioenergetic properties of human colorectal cancer: the regulation of mitochondrial respiration and distribution of flux control among the components of ATP synthasome. *Int J Biochem Cell Biol.* (2014) 55:171–86. doi: 10.1016/j.biocel.2014.09.004
42. Kaambre T, Chekulayev V, Shevchuk I, Karu-Varikmaa M, Timohhina N, Tepp K, et al. Metabolic control analysis of cellular respiration in situ in intraoperational samples of human breast cancer. *J Bioenerg Biomembr.* (2012) 44:539–58. doi: 10.1007/s10863-012-9457-9
43. Amamoto R, Uchiumi T, Yagi M, Monji K, Song Y, Oda Y, et al. The expression of ubiquitous mitochondrial creatine kinase is downregulated as prostate cancer progression. *J Cancer.* (2016) 7:50–9. doi: 10.7150/jca.13207
44. Patra S, Bera S, SinhaRoy S, Ghoshal S, Ray S, Basu A, et al. Progressive decrease of phosphocreatine, creatine and creatine kinase in skeletal muscle upon transformation to sarcoma. *Febs Journal.* (2008) 275:3236–47. doi: 10.1111/j.1742-4658.2008.06475.x
45. Lam YW, Yuan Y, Isaac J, Babu CV, Meller J, Ho SM. Comprehensive identification and modified-site mapping of S-nitrosylated targets in prostate epithelial cells. *PLoS ONE.* (2010) 5:e9075. doi: 10.1371/journal.pone.0009075
46. Klepinin A, Ounpuu L, Guzun R, Chekulayev V, Timohhina N, Tepp K, et al. Simple oxygraphic analysis for the presence of adenylate kinase 1 and 2 in normal and tumor cells. *J Bioenerg Biomembr.* (2016) 48:531–48. doi: 10.1007/s10863-016-9687-3
47. Balinsky D, Greengard O, Cayanis E, Head JF. Enzyme activities and isozyme patterns in human lung tumors. *Cancer Res.* (1984) 44:1058–62.
48. Criss WE, Litwack G, Morris HP, Weinhouse S. Adenosine triphosphate: adenosine monophosphate phosphotransferase isozymes in rat liver and hepatomas. *Cancer Res.* (1970) 30:370–5.
49. Chekulayev V, Mado K, Shevchuk I, Koit A, Kaldma A, Klepinin A, et al. Metabolic remodeling in human colorectal cancer and surrounding tissues: alterations in regulation of mitochondrial respiration and metabolic fluxes. *Biochem Biophys Rep.* (2015) 4:111–25. doi: 10.1016/j.bbrep.2015.08.020
50. Vasseur S, Malicet C, Calvo EL, Dagorn JC, Iovanna JL. Gene expression profiling of tumours derived from ras(V12)/EIA-transformed mouse embryonic fibroblasts to identify genes required for tumour development. *Mol Cancer.* (2005) 4:4. doi: 10.1186/1476-4598-4-4
51. Speers C, Tsimelzon A, Sexton K, Herrick AM, Gutierrez C, Culhane A, et al. Identification of novel kinase targets for the treatment of estrogen receptor-negative breast cancer. *Clin Cancer Res.* (2009) 15:6327–40. doi: 10.1158/1078-0432.CCR-09-1107
52. Lamb R, Bonuccelli G, Ozsvari B, Peiris-Pages M, Fiorillo M, Smith DL, et al. Mitochondrial mass, a new metabolic biomarker for stem-like cancer cells: Understanding WNT/FGF-driven anabolic signaling. *Oncotarget.* (2015) 6:30453–71. doi: 10.18632/oncotarget.5852
53. Roesli C, Borgia B, Schhemann C, Gunthert M, Wunderli-Allenspach H, Giavazzi R, et al. Comparative analysis of the membrane proteome of closely related metastatic and nonmetastatic tumor cells. *Cancer Res.* (2009) 69:5406–14. doi: 10.1158/0008-5472.CAN-08-0999
54. Kim H, Lee HJ, Oh Y, Choi SG, Hong SH, Kim HJ, et al. The DUSP26 phosphatase activator adenylate kinase 2 regulates FADD phosphorylation and cell growth. *Nat Commun.* (2014) 5:4351. doi: 10.1038/ncomms4351
55. Liu H, Pu Y, Amina Q, Wang Q, Zhang M, Song J, et al. Prognostic and therapeutic potential of Adenylate kinase 2 in lung adenocarcinoma. *Sci Rep.* (2019) 9:17757. doi: 10.1038/s41598-019-53594-4
56. Jan YH, Tsai HY, Yang CJ, Huang MS, Yang YF, Lai TC, et al. Adenylate kinase-4 is a marker of poor clinical outcomes that promotes metastasis of lung cancer by downregulating the transcription factor ATF3. *Cancer Res.* (2012) 72:5119–29. doi: 10.1158/0008-5472.CAN-12-1842
57. Lanning NJ, Looyenga BD, Kauffman AL, Niemi NM, Sudderth J, DeBerardinis RJ, et al. A mitochondrial RNAi screen defines cellular bioenergetic determinants and identifies an adenylate kinase as a key regulator of ATP levels. *Cell Rep.* (2014) 7:907–17. doi: 10.1016/j.celrep.2014.03.065
58. Bai DM, Zhang JF, Li TT, Hang RL, Liu Y, Tian YL, et al. The ATPase hCINAP regulates 18S rRNA processing and is essential for embryogenesis and tumour growth. *Nat Commun.* (2016) 7:12310. doi: 10.1038/ncomms12310
59. Ji Y, Yang C, Tang Z, Yang Y, Tian Y, Yao H, et al. Adenylate kinase hCINAP determines self-renewal of colorectal cancer stem cells by facilitating LDHA phosphorylation. *Nat Commun.* (2017) 8:15308. doi: 10.1038/ncomms15308
60. Hansel DE, Rahman A, House M, Ashfaq R, Berg K, Yeo CJ, et al. Met proto-oncogene and insulin-like growth factor binding protein 3 overexpression correlates with metastatic ability in well-differentiated pancreatic endocrine neoplasms. *Clin Cancer Res.* (2004) 10(18 Pt 1):6152–8. doi: 10.1158/1078-0432.CCR-04-0285
61. Karhemo PR, Hyvonen M, Laakkonen P. Metastasis-associated cell surface oncoproteomics. *Front Pharmacol.* (2012) 3:192. doi: 10.3389/fphar.2012.00192
62. Lee HJ, Pyo JO, Oh Y, Kim HJ, Hong SH, Jeon YJ, et al. AK2 activates a novel apoptotic pathway through formation of a complex with FADD and caspase-10. *Nat Cell Biol.* (2007) 9:1303–10. doi: 10.1038/ncb1650
63. Kumari R, Deshmukh RS, Das S. Caspase-10 inhibits ATP-citrate lyase-mediated metabolic and epigenetic reprogramming to suppress tumorigenesis. *Nat Commun.* (2019) 10:4255. doi: 10.1038/s41467-019-12194-6
64. Oshima K, Saiki N, Tanaka M, Imamura H, Niwa A, Tanimura A, et al. Human AK2 links intracellular bioenergetic redistribution to the fate of hematopoietic progenitors. *Biochem Biophys Res Commun.* (2018) 497:719–25. doi: 10.1016/j.bbrc.2018.02.139
65. Dzeja PP, Hoyer K, Tian R, Zhang S, Nemutlu E, Spindler M, et al. Rearrangement of energetic and substrate utilization networks compensate for chronic myocardial creatine kinase deficiency. *J Physiol.* (2011) 589:5193–211. doi: 10.1113/jphysiol.2011.212829
66. Wu Z, Gong Q, Yu Y, Zhu J, Li W. Knockdown of circ-ABCB10 promotes sensitivity of lung cancer cells to cisplatin via miR-556-3p/AK4 axis. *BMC Pulm Med.* (2020) 20:10. doi: 10.1186/s12890-019-1035-z
67. Zang C, Zhao F, Hua L, Pu Y. The miR-199a-3p regulates the radioresistance of esophageal cancer cells via targeting the AK4 gene. *Cancer Cell Int.* (2018) 18:186. doi: 10.1186/s12935-018-0689-6
68. Fujisawa K, Terai S, Takami T, Yamamoto N, Yamasaki T, Matsumoto T, et al. Modulation of anti-cancer drug sensitivity through the regulation of mitochondrial activity by adenylate kinase 4. *J Exp Clin Cancer Res.* (2016) 35:48. doi: 10.1186/s13046-016-0322-2
69. Lei W, Yan C, Ya J, Yong D, Yujun B, Kai L. MiR-199a-3p affects the multi-chemoresistance of osteosarcoma through targeting AK4. *BMC Cancer.* (2018) 18:631. doi: 10.1186/s12885-018-4460-0
70. Liu RJ, Strom AL, Zhai JJ, Gal J, Bao SL, Gong WM, et al. Enzymatically inactive adenylate kinase 4 interacts with mitochondrial ADP/ATP translocase. *Int J Biochem Cell B.* (2009) 41:1371–80. doi: 10.1016/j.biocel.2008.12.002
71. Kong F, Binas B, Moon JH, Kang SS, Kim HJ. Differential expression of adenylate kinase 4 in the context of disparate stress response strategies of HEK293 and HepG2 cells. *Arch Biochem Biophys.* (2013) 533:11–7. doi: 10.1016/j.abb.2013.02.014
72. Pedersen PL. Warburg, me and Hexokinase 2: Multiple discoveries of key molecular events underlying one of cancers' most common phenotypes, the "Warburg Effect", i.e., elevated glycolysis in the presence of oxygen. *J Bioenerg Biomembr.* (2007) 39:211–22. doi: 10.1007/s10863-007-9094-x
73. Nelson BD, Kabir F. Adenylate Kinase Is a Source of Atp for Tumor Mitochondrial Hexokinase. *Biochimica Et Biophysica Acta.* (1985) 841:195–200. doi: 10.1016/0304-4165(85)90021-2
74. Choi YK, Park KG. Targeting Glutamine Metabolism for Cancer Treatment. *Biomol Ther (Seoul).* (2018) 26:19–28. doi: 10.4062/biomolther.2017.178
75. Deshmukh A, Deshpande K, Arfuso F, Newsholme P, Dharmarajan A. Cancer stem cell metabolism: a potential target for cancer therapy. *Mol Cancer.* (2016) 15:555. doi: 10.1186/s12943-016-0555-x

76. Ross RA, Spengler BA. Human neuroblastoma stem cells. *Semin Cancer Biol.* (2007) 17:241–7. doi: 10.1016/j.semcancer.2006.04.006
77. Song IS, Jeong JY, Jeong SH, Kim HK, Ko KS, Rhee BD, et al. Mitochondria as therapeutic targets for cancer stem cells. *World J Stem Cells.* (2015) 7:418–27. doi: 10.4252/wjsc.v7.i2.418
78. Dzeja PP, Bortolon R, Perez-Terzic C, Holmuhamedov EL, Terzic A. Energetic communication between mitochondria and nucleus directed by catalyzed phosphotransfer. *Proc Natl Acad Sci USA.* (2002) 99:10156–61. doi: 10.1073/pnas.152259999
79. Jan YH, Lai TC, Yang CJ, Lin YF, Huang MS, Hsiao M. Adenylate kinase 4 modulates oxidative stress and stabilizes HIF-1alpha to drive lung adenocarcinoma metastasis. *J Hematol Oncol.* (2019) 12:12. doi: 10.1186/s13045-019-0698-5
80. Jan YH, Lai TC, Yang CJ, Huang MS, Hsiao M. A co-expressed gene status of adenylate kinase 1/4 reveals prognostic gene signature associated with prognosis and sensitivity to EGFR targeted therapy in lung adenocarcinoma. *Sci Rep.* (2019) 9:12329. doi: 10.1038/s41598-019-48243-9
81. Xin F, Yao DW, Fan L, Liu JH, Liu XD. Adenylate kinase 4 promotes bladder cancer cell proliferation and invasion. *Clin Exp Med.* (2019) 19:525–34. doi: 10.1007/s10238-019-00576-5
82. Zhang J, Yin YT, Wu CH, Qiu RL, Jiang WJ, Deng XG, et al. AK4 promotes the progression of HER2-positive breast cancer by facilitating cell proliferation and invasion. *Dis Markers.* (2019) 2019:8186091. doi: 10.1155/2019/8186091
83. Schatton T, Murphy GF, Frank NY, Yamaura K, Waaga-Gasser AM, Gasser M, et al. Identification of cells initiating human melanomas. *Nature.* (2008) 451:345–U11. doi: 10.1038/nature06489
84. Adams JM, Strasser A. Is tumor growth sustained by rare cancer stem cells or dominant clones? *Cancer Res.* (2008) 68:4018–21. doi: 10.1158/0008-5472.CAN-07-6334
85. Kaur H, Lakatos-Karoly A, Vogel R, Noll A, Tampe R, Glaubitz C. Coupled ATPase-adenylate kinase activity in ABC transporters. *Nat Commun.* (2016) 7:13864. doi: 10.1038/ncomms13864
86. Dzeja PP, Terzic A. Phosphotransfer reactions in the regulation of ATP-sensitive K+ channels. *Faseb J.* (1998) 12:523–9. doi: 10.1096/fasebj.12.7.523
87. Carrasco AJ, Dzeja PP, Alekseev AE, Pucar D, Zingman LV, Abraham MR, et al. Adenylate kinase phosphotransfer communicates cellular energetic signals to ATP-sensitive potassium channels. *Proc Natl Acad Sci USA.* (2001) 98:7623–8. doi: 10.1073/pnas.121038198
88. Bhaskara V, Dupre A, Lengsfeld B, Hopkins BB, Chan A, Lee JH, et al. Rad50 adenylate kinase activity regulates DNA tethering by Mre11/Rad50 complexes. *Mol Cell.* (2007) 25:647–61. doi: 10.1016/j.molcel.2007.01.028
89. Boissan M, Schlattner U, Lacombe ML. The NDPK/NME superfamily: state of the art. *Lab Invest.* (2018) 98:164–74. doi: 10.1038/labinvest.2017.137
90. Gonzalez A, Hall MN, Lin SC, Hardie DG. AMPK and TOR: the yin and yang of cellular nutrient sensing and growth control. *Cell Metab.* (2020) 31:472–92. doi: 10.1016/j.cmet.2020.01.015
91. Collavin L, Lazarevic D, Utrera R, Marzinotto S, Monte M, Schneider C. wt p53 dependent expression of a membrane-associated isoform of adenylate kinase. *Oncogene.* (1999) 18:5879–88. doi: 10.1038/sj.onc.1202970
92. Sholihah MM, Indarto D, Pramana TY. The inhibitory effect ofAndrographis paniculataextract on proliferation of breast cancer cell line. *Mat Sci Eng.* (2019) 546:062029. doi: 10.1088/1757-899X/546/6/062029
93. Hardie DG. AMP-activated protein kinase: a cellular energy sensor with a key role in metabolic disorders and in cancer. *Biochem Soc Trans.* (2011) 39:1–13. doi: 10.1042/BST0390001
94. Hardie DG. AMP-activated/SNF1 protein kinases: conserved guardians of cellular energy. *Nat Rev.* (2007) 8:774–85. doi: 10.1038/nrm2249
95. Dasgupta B, Chhipa RR. Evolving Lessons on the Complex Role of AMPK in Normal Physiology and Cancer. *Trends Pharmacol Sci.* (2016) 37:192–206. doi: 10.1016/j.tips.2015.11.007
96. Hardie DG, Alessi DR. LKB1 and AMPK and the cancer-metabolism link - ten years after. *BMC Biol.* (2013) 11:36. doi: 10.1186/1741-7007-11-36
97. Shackelford DB, Shaw RJ. The LKB1-AMPK pathway: metabolism and growth control in tumour suppression. *Nat Rev Cancer.* (2009) 9:563–75. doi: 10.1038/nrc2676
98. Takaine M, Imamura H, Yoshida S. AMP-activated protein kinase and adenylate kinase prevent the ATP catastrophe and cytotoxic protein aggregation. *bioRxiv.* (2019) 801738. doi: 10.1101/801738
99. Plaideau C, Liu JM, Hartleib-Geschwindner J, Bastin-Coyette L, Bontemps F, Oscarsson J, et al. Overexpression of AMP-metabolizing enzymes controls adenine nucleotide levels and AMPK activation in HEK293T cells. *Faseb Journal.* (2012) 26:2685–94. doi: 10.1096/fj.11-198168
100. Plaideau C, Lai YC, Kviklyte S, Zanou N, Lofgren L, Andersen H, et al. Effects of pharmacological amp deaminase inhibition and ampd1 deletion on nucleotide levels and AMPK activation in contracting skeletal muscle. *Chem Biol.* (2014) 21:1497–510. doi: 10.1016/j.chembiol.2014.09.013
101. Leone RD, Emens LA. Targeting adenosine for cancer immunotherapy. *J Immunother Cancer.* (2018) 6:57. doi: 10.1186/s40425-018-0360-8
102. Olson LK, Schroeder W, Robertson RP, Goldberg ND, Walseth TF. Suppression of adenylate kinase catalyzed phosphotransfer precedes and is associated with glucose-induced insulin secretion in intact HIT-T15 cells. *J Biol Chem.* (1996) 271:16544–52. doi: 10.1074/jbc.271.28.16544
103. Wang F, Liu Y, Jiang J, Qin Y, Ge X, Li J, et al. High expression of AMPD2 and obesity are associated with poor prognosis in colorectal cancer. *Int J Clin Exp Pathol.* (2018) 11:216–23.
104. Parr C, Jiang WG. Quantitative analysis of lymphangiogenic markers in human colorectal cancer. *Int J Oncol.* (2003) 23:533–9. doi: 10.3892/ijo.23.2.533
105. Spychala J, Lazarowski E, Ostapkowicz A, Ayscue LH, Jin A, Mitchell BS. Role of estrogen receptor in the regulation of ecto-5'-nucleotidase and adenosine in breast cancer. *Clin Cancer Res.* (2004) 10:708–17. doi: 10.1158/1078-0432.CCR-0811-03
106. Klepinin A, Ounpuu L, Mado K, Truu L, Chekulayev V, Puurand M, et al. The complexity of mitochondrial outer membrane permeability and VDAC regulation by associated proteins. *J Bioenerg Biomembr.* (2018) 50:339–54. doi: 10.1007/s10863-018-9765-9
107. Xiao B, Sanders MJ, Underwood E, Heath R, Mayer FV, Carmena D, et al. Structure of mammalian AMPK and its regulation by ADP. *Nature.* (2011) 472:230–3. doi: 10.1038/nature09932

Conflict of Interest: The authors declare that the research was conducted in the absence of any commercial or financial relationships that could be construed as a potential conflict of interest.

frontiers in Oncology

REVIEW
published: 22 May 2020
doi: 10.3389/fonc.2020.00722

Metabolic Plasticity of Melanoma Cells and Their Crosstalk With Tumor Microenvironment

Angelica Avagliano[1], Giuseppe Fiume[2], Alessandra Pelagalli[3,4], Gennaro Sanità[5], Maria Rosaria Ruocco[5], Stefania Montagnani[1] and Alessandro Arcucci[1]**

[1] Department of Public Health, University of Naples Federico II, Naples, Italy, [2] Department of Experimental and Clinical Medicine, University "Magna Graecia" of Catanzaro, Catanzaro, Italy, [3] Department of Advanced Biomedical Sciences, University of Naples Federico II, Naples, Italy, [4] Institute of Biostructures and Bioimages, National Research Council, Naples, Italy, [5] Department of Molecular Medicine and Medical Biotechnology, University of Naples Federico II, Naples, Italy

Cutaneous melanoma (CM) is a highly aggressive and drug resistant solid tumor, showing an impressive metabolic plasticity modulated by oncogenic activation. In particular, melanoma cells can generate adenosine triphosphate (ATP) during cancer progression by both cytosolic and mitochondrial compartments, although CM energetic request mostly relies on glycolysis. The upregulation of glycolysis is associated with constitutive activation of BRAF/MAPK signaling sustained by $BRAF^{V600E}$ kinase mutant. In this scenario, the growth and progression of CM are strongly affected by melanoma metabolic changes and interplay with tumor microenvironment (TME) that sustain tumor development and immune escape. Furthermore, CM metabolic plasticity can induce a metabolic adaptive response to BRAF/MEK inhibitors (BRAFi/MEKi), associated with the shift from glycolysis toward oxidative phosphorylation (OXPHOS). Therefore, in this review article we survey the metabolic alterations and plasticity of CM, its crosstalk with TME that regulates melanoma progression, drug resistance and immunosurveillance. Finally, we describe hallmarks of melanoma therapeutic strategies targeting the shift from glycolysis toward OXPHOS.

Keywords: cutaneous melanoma, tumor microenvironment, metabolic alterations, OXPHOS, therapeutic strategies

OPEN ACCESS

Edited by:
Sara Rodriguez-Enriquez, Instituto Nacional de Cardiología, Mexico

Reviewed by:
Philippe Marchetti, INSERM U1172 Center de Recherche Jean Pierre Aubert, France
Helen Rizos, Macquarie University, Australia

****Correspondence:***
Angelica Avagliano
angelica.avagliano@unina.it
Alessandro Arcucci
alessandro.arcucci2@unina.it

Specialty section:
This article was submitted to Cancer Metabolism, a section of the journal Frontiers in Oncology

Received: *03 February 2020*
Accepted: *16 April 2020*
Published: *22 May 2020*

Citation:
Avagliano A, Fiume G, Pelagalli A, Sanità G, Ruocco MR, Montagnani S and Arcucci A (2020) Metabolic Plasticity of Melanoma Cells and Their Crosstalk With Tumor Microenvironment. Front. Oncol. 10:722. doi: 10.3389/fonc.2020.00722

INTRODUCTION

Cutaneous melanoma (CM) is highly aggressive tumor characterized by an increasing worldwide incidence more distributed in the Eastern than in Western European countries (1). Among the three different CM clinically and histomorphologically steps, Vertical Growth Phase (VGP) represents the tumorigenic and /or mitogenic stage of CM (2). In VGP step, CM can metastasize to lymph nodes, brain, lung, bone, and liver albeit the size of primary tumor is still small (2). The dramatic invasive behavior of melanoma cells depends on neural crest origin of melanocytes (3). Melanoma cells derive from the malignant transformation of melanocytes affected by the constitutive activation of oncogenic signaling and cancer metabolic reprogramming, which are processes interacting each other (4–7). Oncogenic signaling pathways in malignant melanocytes can be activated by mutations in BRAF, NRAS, and neurofibromatosis type 1 (NF1) gene. Based on the genetic mutations, CM is grouped into 4 genomic subtypes represented by BRAF mutants, NRAS mutants, neurofibromatosis type 1 (NF1) mutants, and triple-wild-type tumors (8).

BRAF mutations, target of therapeutic strategies, dramatically affect CM metabolism, depending mainly on glycolytic metabolism. Glycolysis leads to production of adenosine triphosphate (ATP) and building block intermediates useful for cancer progression (2, 6, 8). It is important to note that in normoxic microenvironment, melanoma cells metabolize up to 80% of glucose into lactate, and that hypoxia augments this metabolic process (6, 9, 10). This elevated rate of glucose transformation into lactate, even in normoxic microenvironment, has been showed by Otto Warburg and it is termed Warburg effect (11, 12). However, it is noteworthy that also in hypoxic melanoma microenvironment the mitochondria of cancer cells work and thus can sustain melanoma dissemination (13).

Cancer cells successfully are able to adapt to the nutritional changes and restrictions of the tumor microenvironment (TME), through dynamic modulations of both cytosolic and mitochondrial metabolic pathways in order to produce ATP during cancer progression (2). Most relevant molecular drivers that participate to melanoma metabolic plasticity include AKT, BRAF, p14ARF, MYC, NRAS, phosphatidylinositol-4,5-bisphosphate 3 kinase catalytic subunit α (PIK3CA) and phosphatase and tensin homolog (PTEN) (14–20). Anyway, the remarkable metabolic flexibility and reprogramming of melanoma cells account for the impressive aggressiveness of CM and can also sustain resistance response to BRAF/MEK inhibitors (BRAFi/MEKi) and immunotherapy (2, 6). In this scenario the metabolic crosstalk between cancer cells and TME dramatically affects the metabolic choice, the growth and therapeutic resistance of CM (2). Therefore, in this article we discussed the metabolic plasticity of CM and the metabolic interactions of melanoma cells with TME, leading to tumor development, therapeutic resistance and immune escape. Finally, we highlighted the therapeutic strategies targeting the shift from glycolysis toward oxidative phosphorylation (OXPHOS).

GLYCOLYSIS AND LACTIC FERMENTATION

Rapidly proliferating melanoma cells produce ATP and carbon precursors for cell growth and proliferation mainly through glycolysis and lactic fermentation, independently by oxygen levels. This process is named "Warburg effect" or aerobic glycolysis (21).

Hypoxia-inducible factor 1 (HIF-1), that is a master regulator of numerous hypoxia-inducible genes and of glycolysis in melanoma, is usually inhibited during normoxia due to the rapid degradation of its subunit HIF-1α. However, many experimental evidence showed that HIF-1α and several of its target genes are strongly upregulated in melanoma cells not only during hypoxia, but also in normoxic conditions (22, 23). Additionally, under normoxia, melanoma cells can regulate and stabilize HIF-1α at the translational level, through mTOR and melanoma antigen-11 (MAGE11) (22), that is involved in the inhibition of prolyl hydroxylase domain protein 2 (PHD2), a HIF-1α negative regulator (24). Consequently, the upregulation and the protein stabilization of HIF-1α lead to the glycolysis induction in melanoma cells and to melanoma development and progression both in the presence and in the absence of oxygen (22, 25). Furthermore, it has been reported that the aberrant and constitutively activation of oncogenic signaling pathways, such as MAPK/ERK, phosphatidylinositol 3-kinase (PI3K)/AKT, mutated microphthalmia-associated transcription factor (MITF), endothelin dependent signaling, and ROS/NFkB pathways, are involved in the enhanced expression of HIF-1α in melanoma cells, independently by oxygen levels (22, 26–29). Interestingly, since MITF pathway activation and BRAF mutations, leading to MAPK signaling activation, occur, respectively, in about 10–20% (30) and 50% (31) of melanomas, it is possible to assume that the constitutive expression of HIF-1α is not a rare event in melanoma (32) and strictly correlates with melanoma aggressiveness and malignancy (23). In more detail, it has been reported that $BRAF^{V600E}$ mutation, leading to the constitutive activation of ERK1/2 and MAPK pathway, sustains aerobic glycolysis through the activation of transcriptional factors, including HIF-1α and c-myc (22) (**Figure 1**). HIF-1α by interacting with HIF-1β, that generally is constitutively expressed (34), promotes the transcriptional activation of lactate dehydrogenase (LDH), aldolase, and enolase 1 (ENO1) (35) and consequently leads to an increase of glycolytic fluxes. In addition, HIF-1α turns on pyruvate dehydrogenase kinase (PDK), which prevents the entry of pyruvate in tricarboxylic acid (TCA) cycle by inhibiting pyruvate dehydrogenase (PDH) (33). More specifically, PDH converts pyruvate into acetyl-CoA in the mitochondria and the PDK-mediated inhibition of PDH leads to a lower consumption of pyruvate in the mitochondrion, and consequently, making a higher amount of pyruvate available in the cytosol. The increase of cytosolic pyruvate promotes a sustained lactic fermentation, consequently increasing lactate production (33). Persistent and sustained ERK1/2 activation, induced by mutant BRAF or KRAS, leads to mitochondrial translocation of phosphoglycerate kinase 1 (PGK1) and phosphorylation of PDK1, which in turn inactivates PDH, contributing to aerobic glycolytic switch in cancer (36). Further, glycolytic flux and glucose uptake are also stimulated by MYC, which transcriptionally activates LDH, glucose transporter 1 (GLUT-1), and hexokinase 2 (HK2) (37, 38).

Surprisingly, additional mechanisms promoting glycolysis in melanoma involve both the activation and the inhibition of the transcriptional factor and OXPHOS inducer MITF. As briefly stated before, the activation of MITF can promote the induction of HIF-1α, that is the master regulator of glycolysis (28). Interestingly, also MITF inhibition, via MAPK pathway, leads to glycolysis in melanoma cells. In particular, the constitutive activation of BRAF/MAPK pathway leads to the suppression of MITF, that thereby cannot activate the peroxisome proliferator-activated receptor γ 1-α (PGC1-α), an important driver of mitochondrial biogenesis and respiration. This leads to the metabolic switch toward glycolysis in melanoma cells (39). Even if these findings seem to be contradictory, they greatly highlight the complexity of melanoma pathogenesis: in fact the mutational status of melanoma cells and the microenvironmental signals can activate or inhibit

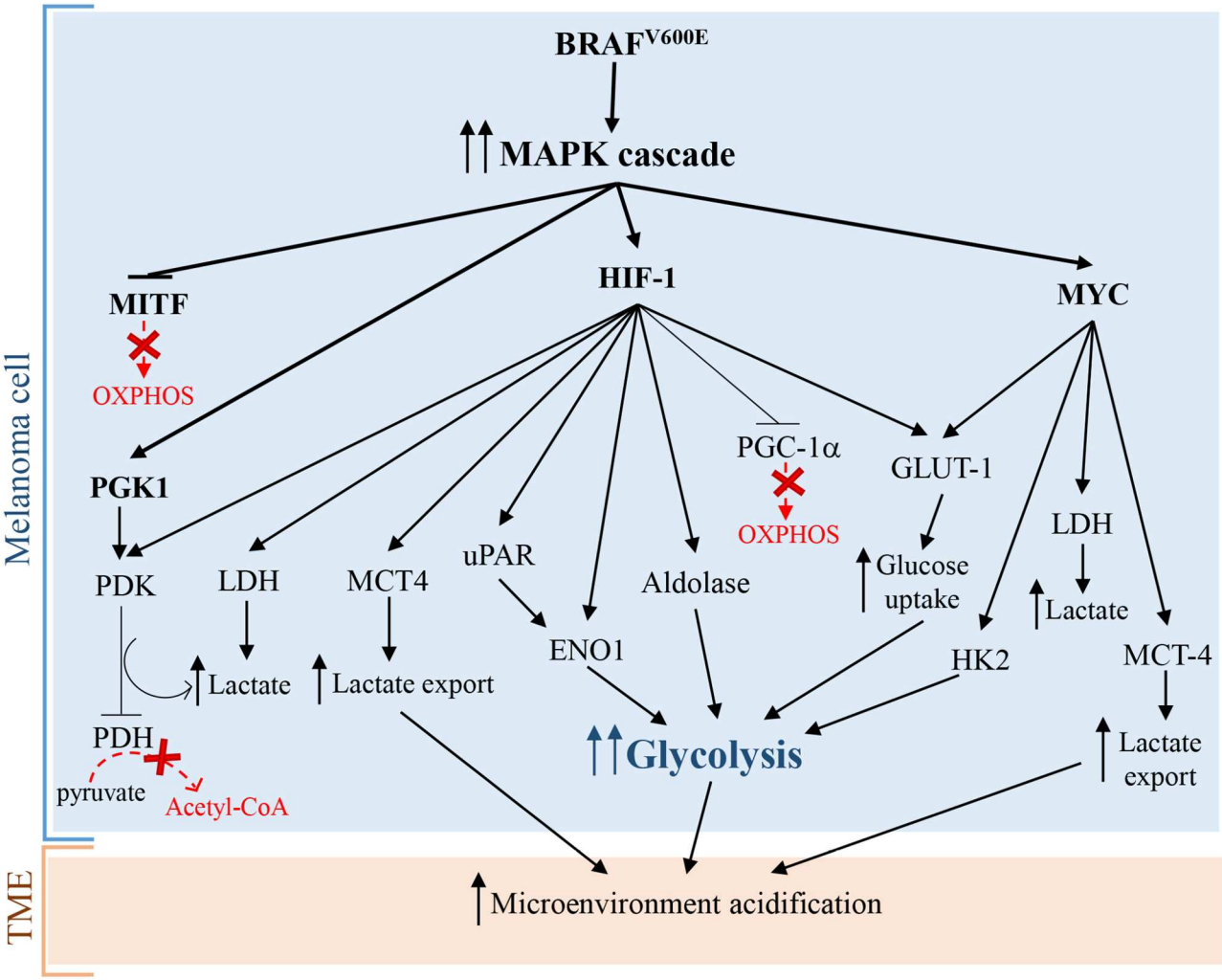

FIGURE 1 | Warburg effect in melanoma cells caused by BRAF^{V600E} mutation leading to constitutive activation of MAPK pathway. Arrows indicate activation and T-bars show inhibition. Dotted red arrows, also indicated by a "red X," symbolize inactive pathways, while solid T-bars and arrows indicate active signaling during Warburg effect.

specific molecular pathways in order to promote the "Warburg phenotype" in melanoma cells.

Furthermore, a sustained PI3K/AKT/mTOR signaling pathway positively acts on HIF-1α transcription and activity, triggering glycolysis through the synthesis of glycolytic enzymes (40, 41). Several mechanisms can activate PI3K/AKT/mTOR signaling in melanoma, including the loss of tumor suppressor PTEN functions, mutations in AKT and PIK3CA, and compensatory signaling through growth factor receptors (19, 42, 43). Interestingly, PTEN loss in melanoma cells increases extracellular acidification rate (ECAR), likely due to an increased production of lactate (44). Pyruvate kinase (PK) is the glycolytic enzyme converting phosphoenolpyruvate (PEP) to pyruvate in the last reaction of glycolysis. PKM2 is the most representative isoenzyme of the glycolytic enzyme PK. In cancer cells the isoform PKM2 is highly expressed (45) but is endowed with a low activity (46). More specifically, tyrosine kinases including FGFR1, BCR-ABL, and Jak2 phosphorylate glycolytic enzymes, such as PKM2. Tyrosine phosphorylation of glycolytic enzymes induces on one hand the activation of most glycolytic enzymes, thus increasing glycolytic rate, while on the other hand reduces the activity of PKM2, promoting paradoxically Warburg Effect (47). Rather than favoring the glycolytic fluxes with ATP production, the low PKM2 activity leads to an increased amount of glycolytic intermediates upstream PK reaction, providing precursors of several biological macromolecules, including nucleotides from glucose-6-phosphate (G6P), amino sugars, glycolipids and glycoproteins from fructose-6-phosphate (F6P), lipids from dihydrogenacetone-phosphate, serine from 3-phosphoglycerate, amino acids, and pyrimidines from PEP (45). Therefore, low PKM2 activity is a pivotal feature of cancer cells needing continuously precursors of biological

macromolecules for their sustained and persistently elevated replicative rate (48). Interestingly, the phosphorylation of PKM2 by ERK rapidly transforms active tetrameric PKM2 into inactive monomers. The inactive monomeric form of PKM2 is able to translocate into the nucleus and induces the expression of many glycolytic enzyme genes, through epigenetic modifications of their promoters, by the phosphorylation of histone H3 (49).

The stimulation of aerobic glycolysis is highly depending on glucose uptake. Specifically, the transcription of the glucose transporter GLUT-1 is strictly regulated by HIF-1α (50, 51). The up-regulation of GLUT-1 is a common feature of the metabolic reprogramming in many tumors and can be associated with a high tumor grade (52–54). In particular, in CM compared to melanocytic nevi, it has been reported a higher GLUT-1 protein expression, which is positively associated with mitotic activity, melanoma progression, and metastasis (55, 56). Interestingly, the evaluation of GLUT-1 cellular localization, by immunohistochemistry, in 225 malignant melanomas and 175 benign nevi showed that GLUT-1 is frequently localized at cell membrane in melanoma, while in nevi this localization is infrequent (57). In other studies, GLUT-1 expression inversely correlated with overall survival (OS) or disease free survival (DFS) hence representing a tumor prognostic marker (58).

Lactic fermentation is a fundamental process, which converts pyruvate into lactate, reconstituting all the NAD+ that had been transformed into NADH during glycolysis. Consequently, to remove excess acid and to sustain glycolysis, lactate is secreted into the microenvironment, through monocarboxylate transporters (MCTs) (59). Interestingly, many cancers cells, including melanoma cells, take up lactate through MCT-1 and metabolize it, supplying the TCA cycle. Some evidences show that an increased transport of lactate correlates with worse outcomes (60). Therefore, lactate consumption could represent an useful biomarker of cancer progression. MCT-1 and MCT-4 represent the main bidirectional and ATP-independent transporters of lactate and related monocarboxylates through cell membrane, even though the directionality of transport is dependent on lactate and proton concentration gradients (61, 62). Pinheiro et al. demonstrated that in melanoma, the hyperexpression of GLUT-1 and MCT-4 correlated significantly with progression from primary to metastatic tumors. These data indicated that the glycolytic phenotype and lactate secretion synergistically act in promoting melanoma metastasis (63). In glycolytic tumor cells, HIF-1α and MYC upregulate MCT-4 to promote the secretion of lactate into the TME (64, 65). Recently, Tasdogan et al. showed that metabolic differences among melanoma cells confer a different ability to form metastases, depending on the function of the MCT-1 transporter (66). Specifically, by experiments of metabolites tracing, using ^{13}C-labeled nutrients, they identified efficient and inefficient melanoma metastasizers. Efficient melanoma metastasizers were characterized by high ability to uptake lactate, depending on MCT-1 expression. In addition, lactate uptake was strictly associated with a high enrichment in metabolites related to the TCA cycle (citrate, glutamate, and malate), suggesting that carbon atoms were transferred from lactate to TCA. Conversely, MCT-1 inhibition led to reduction of lactate uptake but was barely effective on primary tumors growth (66). Furthermore, inhibition of MCT-1 was linked to reduction of circulating melanoma cells and decreased CM metastatic capability in patient-derived xenografts and in mouse melanomas. Consistently with previous works, they found that inhibition of MCT-1 or MCT-4 in melanoma cells induces oxidative stress, through the inhibition of lactate export, and a reduced glycolysis (66). Additionally, clinical evidences further support the concept that melanoma mostly relies on glycolysis. For example, the positron emission tomography (PET) with an analog of glucose, i.e., the 2-deoxy-2-[fluorine-18]fluoro-D-glucose (^{18}F-FDG), is an excellent imaging tool that exploits the glucose avidity of melanoma cells for the detection of widespread metastasis, for staging and restaging and for the evaluation of therapy response (67). Even if ^{18}F-FDG PET has no role in early cutaneous melanoma (68), it can be considered a sensitive method superior to routine and conventional methods (i.e., ultrasound, radiography, histology or clinical examination, and follow-up, etc.) for the detection of distant metastases from malignant melanomas (69). Indeed, ^{18}FDG-PET scanning shows 100% of sensitivity and 100% of accuracy for detecting visceral and abdominal nodal metastases, and superficial lymph node metastases, respectively (67). Furthermore, glycolytic melanoma cells produce high levels of LDH-5 that is the more effective isoenzyme in the catalysis of pyruvate to lactate, in order to produce ATP (70, 71). LDH-5, that reflects the Warburg phenotype in cancer cells, can be used as an accurate predictor of prognosis and response to treatments in melanoma patients. In fact, it has been reported that LDH-5 expression is easily detected both in histologic melanoma sections and in the serum of melanoma patients, and strongly correlates with prognosis. Particularly, translational studies reported that high LDH blood levels allow the identification of melanoma patients with worse prognosis (72) and that may not benefit from immunotherapy (2).

PENTOSE PHOSPHATE PATHWAY

The pentose phosphate pathway (PPP) sustains survival and growth of cancer cells through the generation of pentose phosphate sugars, which will be utilized for nucleic acid synthesis and will provide nicotinamide-adenine dinucleotide phosphate (NADPH). On its turn, NADPH will be essential for fatty acid (FA) synthesis and will sustain cell survival (73). The PPP is mainly regulated at glucose-6-phosphate dehydrogenase (G6PD) level, which acts as a "gatekeeper" of this pathway. G6PD catalyses the irreversible reaction of transformation of G6P into 6-phosphogluconolactone in a rate-determining step, generating NADPH (74). Subsequently, G6PD activity determines both the metabolic fate among glycolysis and PPP, and the oxidative PPP flux (75). The hyper-expression of G6PD is frequent in cancer cells and could be considered a biomarker of poor prognosis, indicating that G6PD has a fundamental role in tumorigenesis (76). Another important enzyme in the PPP, playing a pivotal role in melanoma proliferation and progression, is the transketolase (TKT). TKT converts excess of ribose-5-phosphate (R5P) into glyceradehyde-3-phosphate (G3P) and F6P through a number

of reactions. Furthermore, G3P is metabolized also in glycolysis, and F6P can be converted into G6P that re-enters the oxidative PPP to produce further NADPH (77). Elevated TKT expression levels were reported in melanoma as well in lung, breast and prostate cancer cells. More specifically, exposure to UVA augments the proliferation of melanoma cells, by increasing the expression levels of TKT in melanoma (78).

OXIDATIVE PHOSPHORYLATION AND KREBS CYCLE

To generate ATP, melanoma cells adopt mainly glycolysis. In some cases, to cope energetic and metabolites demand, melanoma cells can also perform a massive OXPHOS. This metabolism is mainly driven by PGC1-α, which contributes to transcriptional induction of several mitochondrial genes (39, 79, 80) involved in specific mitochondrial processes including DNA replication, transcription, fission and fusion. In addition, hyper-expression of PGC1-α correlates with a decreased OS in patients with stage III melanoma (81) and with resistance to MAPK pathway inhibitors (MAPKi) (79, 80). Furthermore, PGC1-α-high expressing melanoma cells show a reduced sensitivity to reactive oxygen species (ROS), conferring an increased metastatic potential (81). Conversely, PGC1-α knockdown leads to the inhibition of ROS-scavenging gene expression, associated with an increased cell sensitivity to ROS (81) and the inhibition of metastatic spread of B16–F10 melanoma cells (82). MITF is a positive regulator of PGC1-α expression and other OXPHOS genes, including ATP5B, ATP5D (encoding for components of ATP synthase complex), CYC1 (encoding for cytochrome c1), NDUFA8, NDUFA9, NDUFB10, NDUFC2, NDUFS3 (encoding for components of NADH dehydrogenase complex), SDHB (encoding for succinate dehydrogenase subunit B) (39, 79, 83), while HIF-1α reduces PGC1-α expression levels by preventing the transcription of MITF (84, 85). AMP-activated protein kinase (AMPK) is an additional regulator of PGC1-α expression (86). In presence of a high cytoplasmic ratio of AMP/ATP, the kinase LKB1 phosphorylates and activates AMPK, which in its turn suppresses mTORC1 and inhibits anabolic reactions. Moreover, the activation of AMPK promotes mitochondrial gene expression *via* PGC1-α (86, 87). In glycolytic tumors, phosphorylation of ERK (pERK) prevents the activation of LKB1 and, consequently, reduces PGC1-α expression levels, inhibiting the typical response to energy deficiency (88).

The TCA cycle represents another mitochondrial pathway playing a pivotal role in tumor formation and progression. The TCA cycle occurs in the mitochondrial matrix and is an amphibolic pathway, in which multiple catabolic and anabolic pathways converge. In the last decade, it has been showed that several intermediates of Krebs cycle, including succinate, α-ketoglutarate, itaconate, fumarate, 2-hydroxyglutarate, are characterized by "non-metabolic" functions. These metabolites are involved in epigenetic modifications or post-translational protein modifications, that affect the immune response and contribute to pathological conditions, such as initiation and progression of carcinogenesis (89). α-ketoglutarate and succinate levels can regulate the activity of HIF-1α via prolyl hydroxylases (PHDs), promoting a metabolic switch from OXPHOS to glycolysis (90). Specifically, PHD uses molecular oxygen to hydroxylate HIF-1α, at specific residues of proline. Hydroxylation recruits on HIF-1α the protein Von Hippel-Lindau (VHL) E3 ubiquitin ligase, which ubiquitinates and subsequently promotes the proteasome-dependent degradation of HIF-1α (91). Interestingly, a recent work (92) shows that MITF, through the transcriptional regulation of SDHB, contributes to prolong hypoxia response. Specifically, under hypoxia, by the action of BHLHE40/DEC1, the levels of MITF expression and activity decrease (85). Consequently, because SDHB converts succinate in fumarate, the levels of succinate increase. On its turn, succinate inhibits PHD, preventing HIF-1α degradation (90). In addition, increased amount of succinate can affect the regulation of multiple enzymes through the process of succinylation (93). It has been shown that cytoplasmic aspartate levels can promote tumor progression in melanoma, through the suppression of arginosuccinate synthetase 1 (ASS1), which, in the urea cycle, converts aspartate into arginosuccinate. The increase of intracellular levels of aspartate activates the carbamoyl phosphate synthetase II (CAD), which, consequently, leads to an increased synthesis of nucleotides and promotes melanoma cell proliferation (94).

Glutamine represents the main metabolite able to replenish the TCA cycle of precursors, required for the synthesis of fats, nucleic acids and amino acids (95). Furthermore, glutamine metabolism provides energy and is pivotal for cellular redox homeostasis (96). Differently from melanoma, other glycolytic tumors replenish the TCA cycle of precursors through the action of enzyme pyruvate carboxylase which produces oxaloacetate from pyruvate (97). Interestingly, in melanoma the contribution of pyruvate carboxylase to the TCA cycle is very low (21, 98, 99). After entering the cell through the glutamine receptor SLC1A5, glutamine is deaminated to glutamate by the action of cytosolic glutaminase (6). Consequently, glutamate is converted into α-ketoglutarate, through reactions catalyzed by either glutamate dehydrogenase 1 (GDH1) or mitochondrial alanine and aspartate aminotransferase (GOT2 and GPT2) and enters the TCA cycle. Interestingly, through a reductive carboxylation of α-ketoglutarate, tumor cells are able to reverse Krebs cycle, thereby increasing the amount of citrate to be used for FA synthesis. Of note, under low presence of oxygen, α-ketoglutarate, which derives from deamination of glutamate, provides over one-third of total citrate necessary for FA synthesis (21). The main enzymes required for the production of citrate through the carboxylation of α-ketoglutarate are cytosolic and mitochondrial isocitrate dehydrogenases, respectively IDH1 and IDH2. Some works reported that mutations in these genes sporadically arise in melanoma (83, 84) and cause a growth advantage to melanoma cell lines bearing BRAF mutations (85).

FATTY ACID OXIDATION

In the last years, fatty acid oxidation (FAO) in cancer has been extensively studied and growing evidences show

its contribution in melanoma progression. Comparative analyses between melanoma cells and benign nevi show that carnitine palmitoyltransferase 2 (CPT) 2, an enzyme critical for translocation of long-chain Fas, is one of the most upregulated gene in melanoma (100). Interestingly, melanoma cells treated with MAPKi showed an increase of CD36 levels and fatty acid oxidation (FAO) levels in a manner dependent by peroxisome proliferator-activated receptor (PPAR-α) and CPT1A (101). Of note, the sustained FAO is essential for survival of $BRAF^{V600E}$-mutant melanoma cells, under the MAPKi-induced metabolic stress prior to acquiring drug resistance (101). Being the metastasis formation a process that require a huge amount of nutrients, FAs can provide an ATP boost for the dissemination of tumor cells. In addition, FAs can provide acetyl-CoA, which, in the TCA cycle, is essential for citrate formation and, consequently, for NADPH production *via* IDH1, participating to the redox balance in tumor cells (102). Interestingly, some proteins that bind and process lipids, including phospholipase D3 (PLD3), inositol triphosphate protein kinase B (ITPKB), inositol triphosphate receptor 3 (ITPR3), fatty acid binding protein 3 (FABP3), have been found strongly upregulated in melanoma (100). In addition, a recent comparative analysis of proteome of melanoma cells revealed a higher OXPHOS and lipid metabolism in melanoma cells "responder" to immunotherapy (103). More in detail, Harel et al. showed that a higher OXPHOS and lipid metabolism augment the antigen presentation of melanoma cells, through the increase of MHC proteins expression (HLA-A, HLA-C, and B2M which consist MHCI, and CD74, a chaperone of MHCII), of several factors involved in the antigen processing and presentation machinery (including TAP1 and TAP2 which are peptide antigen transporters, TAPBP which acts as a bridge between the MHC and the peptide transporters), and PSME1, a component of proteasome. Consequently, the higher expression of MHC molecules promotes a better response upon immunotherapy by T cells (103).

MELANOMA MICROENVIRONMENT ACIDIFICATION AND ITS INFLUENCE ON MELANOMA GROWTH AND THERAPEUTIC RESISTANCE

The acidification of microenvironment is a hallmark of CM (2) (**Figure 2**). In fact, pH gradient of melanoma cells is totally different respect to that of normal cells (104). Cancer cells display an intracellular pH (pHi) > 7.4 and extracellular pH (pHe) ranging from 6.7 to 7.1. Conversely, normal cells display pHi of about 7.2 and pHe of about 7.4 (104). The extracellular acidosis is linked to metabolic changes of melanoma cells and angiogenesis (2). The alterations in cancer cell metabolism are represented mainly by upregulation of glycolysis leading to protons and LDHA-dependent lactate generation (10). Both protons and lactate are transported out of cancer cells by MCT-4, proton exchangers and transporters, in order to elude intracellular acidosis (10, 105). It is noteworthy that stromal cells can take extracellular lactate to produce pyruvate, successively secreted to furnish melanoma cells (106). Furthermore, also PPP and glutaminolysis sustain microenvironment acidification through secretion of carbon dioxide (CO_2) (2).

Angiogenesis process generates new blood vessels from already formed vessels (107). In particular, the vasculature affects dramatically the metabolism of solid tumors because the distance of cancer cells from new vessels influences metabolic option between glycolysis and OXPHOS (108). Furthermore, angiogenesis and vascular network, characterized by both hypervascularisation and hypovascularisation, influence the tumorigenic, mitogenic and metastasizing VGP step of CM (2, 3, 109, 110). Both hypervascularisation and hypovascularisation depend on the loss of homeostasis between pro-angiogenic and anti-angiogenic factors (111). This pathological condition leads to migration and proliferation of endothelial cells, whose excess sustains the development of disorganized and hyperpermeable blood vessels (111). Additionally, blood vessels of TME are also compressed by cancer cells. These structural alterations of tumor blood vessels lead to an increase of resistance to blood flow associated with a reduction of blood supply (111). Furthermore, in highly aggressive melanomas, cancer cells can acquire an endothelial phenotype which enables their participation in angiogenesis (112). It is noteworthy that hyperpermeability of cancer vessels generates the lack of pressure gradient modulating the circulation of both fluid and macromolecules and sustains hypoxia by hindering the transport of oxygen. The hypoxia, generated also by high oxygen consumption of cancer and endothelial cells (111), sustains acidosis through up-regulation of glycolytic pathway mostly linked to the stabilization of HIF-1α, the principal inductor of aerobic glycolysis in cancer (113, 114). Therefore, HIF triggers up-regulation of plasma membrane transporters, exchangers, pumps and enzymes, all of which keep pHi of cancer cells around neutral values or even lightly alkaline (114, 115). However, the acidification of melanoma microenvironment can be transient or chronic and is associated with alterations of cancer cells and, as discussed below, of immune cells (**Figure 2**). Furthermore, a recent work of Acker's group indicates that metabolic alterations of melanoma cells, hypoxia, HIF-1 and microenvironment acidosis are regulated by a common positive feedback (116). HIF-1α not only regulates both anaerobic and aerobic glycolysis in melanoma cells, but also enhances the expression of genes involved in both tumor invasion and glycolysis. In particular, under hypoxia (117, 118) and normoxia (119), HIF-1α can increase the expression of urokinase plasminogen activator receptor (uPAR), which in turn leads to a glycolytic and invasive phenotype in melanoma cells in a EGFR-dependent manner with involvement of the PI3K/mTOR/HIF-1α pathway (117–119). The binding of the urokinase plasminogen activator (uPA) to its receptor uPAR, expressed in one-third of melanomas (120), sustains the expression of the extracellular matrix metalloproteinases inducer (EMPPRIN) and of ENO1, which both connect lactate homeostasis and glycolysis with the invasive phenotype of melanoma cells (119). Therefore, uPA/uPAR system in melanoma cells could be a molecular connection between invasion capability and glycolytic metabolism (119).

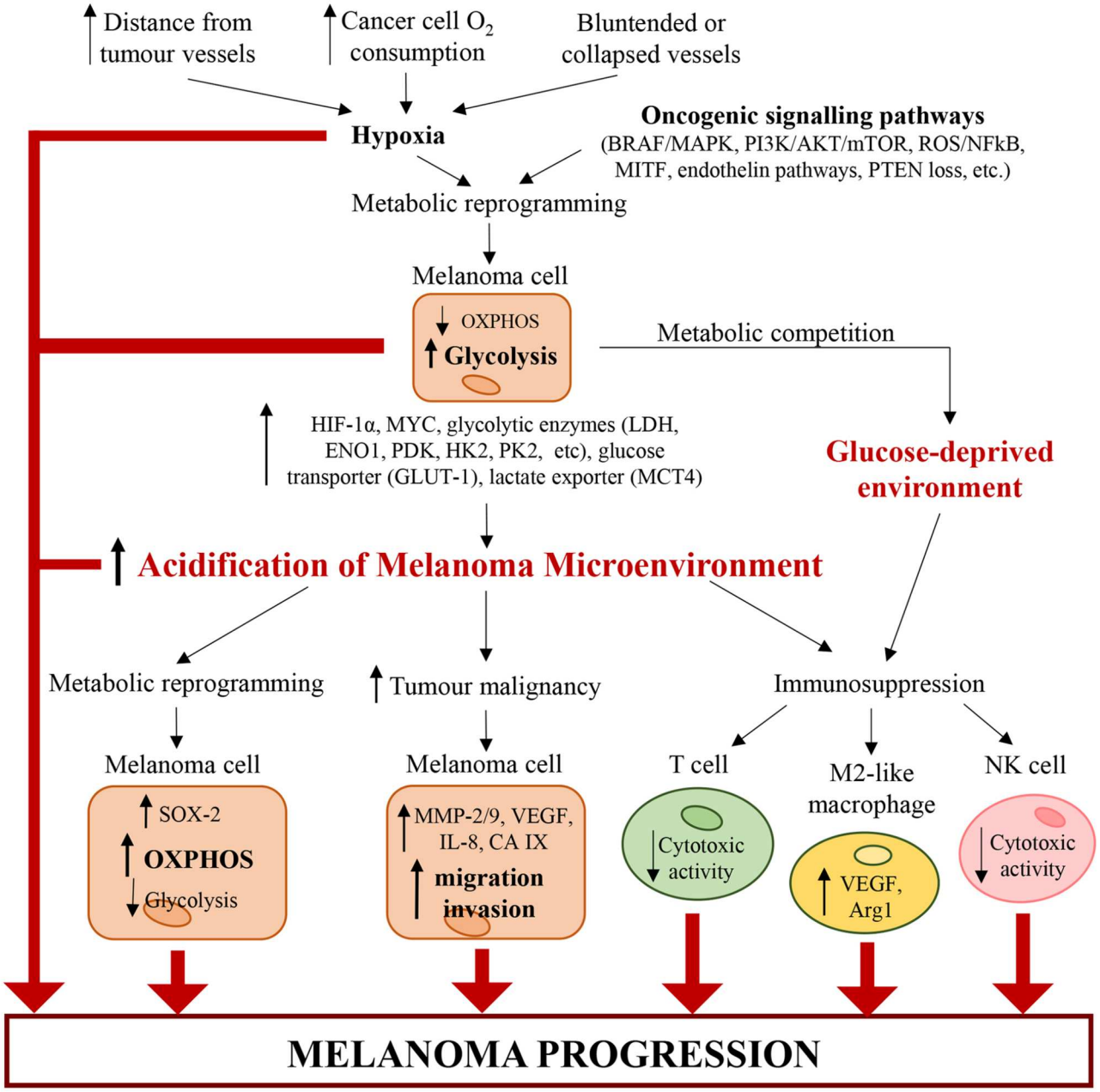

FIGURE 2 | Alterations of cancer and immune cells associated with melanoma microenvironment acidification. Hypoxia (caused by increasing distance from tumor vessels, structural abnormalities of tumor vasculature and high cancer cell O_2 consumption) and genetic mutations (such as $BRAF^{V600E}$, loss of PTEN, etc.) trigger a metabolic reprogramming in melanoma cells, which increase glycolysis. Glycolytic melanoma cells promote an abnormal extracellular accumulation of lactate and protons and thus induce the acidification of TME. In turn, the acidic TME triggers a metabolic reprogramming in melanoma cells, which increase OXPHOS and decrease glycolysis. Additionally, tumor acidity increases melanoma malignancy by enhancing the migratory and invasive capability of melanoma cells and their capability to produce proteases (such as MMP-2/9, cathepsin, etc.) and pro-angiogenic factors (such as VEGF-A, IL-8, etc.). Acidity generates an immunosuppressive milieu, where T cells and NK cells lose their cytotoxic activity, and macrophages acquire the protumorigenic M2-like phenotype. Also glycolytic melanoma cells contribute to the generation of this immunosuppressive environment. In fact, by mediating glucose restriction, melanoma cells alter T cell metabolism and reduce their cytotoxic activity. Therefore, the pH and oxygen gradients in the tumor mass lead to molecular and metabolic changes in cancer and immune cells, which work together and cooperate to sustain melanoma progression.

Furthermore, Laurenzana et al. showed that there is a strong connection between uPAR levels in BRAF mutant melanoma cells and response to BRAF inhibition (121). In fact, melanoma cells, expressing different levels of uPAR, show variable responsiveness to Vemurafenib. These experimental evidences suggest that uPAR levels could predict outcome of

targeted therapy in patients affected by BRAF mutant melanoma (121). CM microenvironment acidification can confer a growth advantage to cancer cells by selecting cells resistant to acidic conditions (122), even if cancer cells can respond to acidic microenvironment in different ways. In particular, Peppicelli et al. demonstrated that acidic microenvironment may trigger in melanoma cells a metabolic shift toward OXPHOS and mesenchymal phenotype, associated with high invasiveness and pro-metastatic property (13).

Biguanide metformin, that is a molecule used in the treatment of type 2 diabetes, specifically inhibits the mitochondrial respiratory chain (MRC) complex 1. It leads to NADH oxidation decrease and to reduction of both proton gradient across the inner mitochondrial membrane and oxygen consumption rate (123). Metformin treatment inhibits both epithelial-mesenchymal transition (EMT) markers and OXPHOS at concentration of 10 mM, which is non-toxic for cancer cells grown in a standard pH medium. Furthermore, this treatment inhibits remarkably proliferation and colony formation of acidic melanoma cells, grown in acidic microenvironment. Therefore, the capacity of metformin to hinder EMT and OXPHOS supports the supplement of metformin to therapy of advanced melanoma (13, 124).

Transient treatment of A375-M6 melanoma cells with acidic medium increases expression of SOX2 with respect to control cancer cells grown in standard medium (125). Extracellular acidosis induces a metabolic switch toward OXPHOS and a concurrent slowdown of acidic cancer cells to a more glycolytic metabolism (126). The silencing of SOX2 gene shifts the metabolism of acidic melanoma cells toward glycolysis, thus making cancer cells less vulnerable to metformin treatment (125, 126). SOX2 is a transcription factor regulating, under acidic condition, the metabolic shift toward OXPHOS and downregulates HIF-1α by binding to its promoter (125, 126). Recent studies highlighted that the extracellular acidity of melanoma TME may provide an environment sustaining dormancy of melanoma cells, which exhibit low replication rate, high resistance to apoptosis and autophagy (127). Tumor dormancy is an important process implicated in tumor immune escape and drug resistance (128, 129). Jia et al. showed that low levels of SOX2 expression are linked to cycle arrest, melanoma cell stemness and tumor dormancy leading long-term tumor survival, and relapse (130).

Other studies showed that acidosis induces apoptosis and autophagic pathway (131–133). Böhme et al. showed that chronic acidosis triggers in melanoma cells a senescence-like phenotype with $MITF^{low}/AXL^{high}$ signature and cellular translation reprogramming. This phenotype, induced by extracellular acidosis, is associated with therapeutic outcome in CM (134).

Transient or chronic extracellular acidification increases carbonic anhydrase IX (CAIX) expression (135). CAIX is a transmembrane enzyme that is an important regulator of cancer cells pHi (136, 137). CAIX enzymatic activity affects viability of acidic cancer cells in CM, and its inhibition could represent a new therapeutic strategy (135). In particular, Chafe et al. analyzed the expression of CAIX in a cohort of 449 patients affected by CM. They showed that CAIX levels are linked to worse OS (138). CAIX inhibition, through SLC-0011 treatment, reduces extracellular acidosis and improves the response to anti–programmed cell death protein 1 (PD-1) and anti–cytotoxic T-lymphocyte-associated protein-4 (CTLA-4) blockade. These effects are associated with reduction of melanoma growth (138).

Lipid rafts are plasma membrane subdomains containing high concentrations of cholesterol and glycosphingolipids (139). V-type H^+-ATPases enzymes are proton pumps, present in lipid rafts, and whose plasma membrane overexpression is correlated with cancer metastasis (140–142). The enzymatic activity of these H^+ pumps supports extracellular acidosis that sustains the activity of proteolytic enzymes, such as metalloproteinases (MMPs) and cathepsins, and promotes drug resistance and metastasis (104). Inhibition of V-ATPases in melanoma cells, by using the plant-derived monoterpene Myrtenal, hampers the electrochemical H+ gradient across the cell membranes, triggers cell death and decreases tumor cell migration and invasion *in vitro* (143). Moreover, V-ATPases inhibition reduces metastasis *in vivo* (143). Acidic microenvironment induces cancer cells to synthesize and secrete proteases such as MMP9 and 2, cathepsin B and L, all of which can degrade extracellular matrix (ECM) proteins (122). Furthermore, melanoma cells increase the secretion of the proangiogenic factors VEGF-A and IL-8 (144). All these experimental evidences strongly support a relation between extracellular acidosis and malignant progression, higher invasion, and metastasis of melanoma cells. In particular, the dissemination of CM strongly depends on the spreading and propagation of cancer cells to lymphatic vessels and regional lymph nodes, respectively (145). The lymph nodes are the prevalent site of CM metastasis. Both in A375P melanoma cell line and in melanoma cells derived from a human metastatic lesion, extracellular acidosis induces the expression of VEGF-C. This growth factor, that is secreted by both melanoma cells and tumor associated macrophages (TAMs), induces dramatically lymphoangiogenesis (146).

Exosomes could have a significant role in solid tumor progression because they have an unlimited access to the lymphatic system and blood vessels (147–149). Boussadia et al. showed that acidic microenvironment sustains exosome secretion of melanoma cells (150). Consequently, extracellular acidosis trough a massive release and intra-tumoral uptake of exosomes, triggers a more malignant and metastatic phenotype in melanoma cells. In fact, pH naïve melanoma cells, exposed to exosomes generated in an acidic medium, develop migratory and invasive capability probably associated with transfer of metastatic exosomal proteins, sustaining cell motility and angiogenesis (150). Furthermore, exosomes from melanoma cells could contribute to extracellular acidification, by interacting with normal stromal fibroblasts located in distant sites from primary tumors (151). In particular, exposure of human adult dermal fibroblasts to human melanoma-derived exosomes leads to fibroblast metabolic reprogramming associated with increase of aerobic glycolysis, decrease of OXPHOS and extracellular acidification induction (151). In particular, the activity of exosomal miR-155 and miR-210 regulates upregulation of aerobic glycolysis in fibroblasts. Therefore, cancer cell exosomes could influence stromal cell metabolism, thus contributing to

the generation of a pre-metastatic niche that sustains metastatic process (151).

It is known that melanoma microenvironment acidification hinders immunotherapy response (2). Additionally, LDH serum level is a well-known prognostic factor of survival in CM (2, 152). In fact, LDH levels significantly affect response, progression-free survival (PFS) and OS of CM patients treated with antibodies targeting CTLA-4 (ipilimumab) or PD-1 (nivolumab, pembrolizumab), or with ipilimumab plus nivolumab combined therapy (152). Lactate can contribute to tumor escape from immune response by impairing cytotoxic T lymphocytes (CTLs) metabolism and function (153). High levels of lactate are linked to a significant decrease of CD8+ T and NK cell number and activity, both in *vitro* and in *vivo* (154). Furthermore, Collegio et al. showed in murine experimental model that lactate induces in macrophages a pro-tumoral M2-like phenotype, characterized by the induction of VEGF and arginase 1 (Arg1) expression (155). Therefore, the efficacy of immunotherapy could be improved by counteracting microenvironment acidification and lactate extracellular accumulation. As stated before, CAIX inhibition though SLC-0011 treatment decreases the acidification of melanoma microenvironment. SLC-0011 treatment combined with immune-checkpoint inhibitors enhances anti–PD-1 and anti–CTLA-4 blockade effectiveness (138). Another possibility to ameliorate immunotherapy outcome could be represented by LDH inhibitors, which however cannot be used in melanoma therapy, because preclinical analyses of anticancer activity have demonstrated their low therapeutic effectiveness associated with harmful side effects (156).

Diclofenac and lumiracoxib are non-steroidal anti-inflammatory drugs (NSAIDs), approved for clinical use, that display structural similitude (157). In particular, diclofenac induces apoptosis, associated with mitochondrial dysfunction, and restrains both glucose metabolism and MYC expression in melanoma (158, 159). It is noteworthy that both NSAIDs could be utilized to counteract lactate extracellular accumulation (157).

METABOLIC CROSSTALK BETWEEN MELANOMA CELLS AND TME

The TME of solid tumors such as CM is extremely complex. In fact, it includes ECM molecules, represented by laminin and collagen, growth factors, including VEGF, nutrients, such as glucose, blood and lymphatic tumor vessels, various concentrations of oxygen, cancer and stromal cells, that influence each other to sustain tumor growth, progression and metastasis (9, 160, 161). Non-cancer stromal cells are represented by endothelial cells, pericytes, immune cells, fibroblasts, fibroblast aggregates, myofibroblasts, cancer associated fibroblasts (CAFs), activated adipocytes, and mesenchymal stem cells (MSCs) (9, 162–165). In the complex, melanoma microenvironment represents a niche produced and regulated by the bidirectional interactions of melanoma cells with surrounding cells, tumor vessels and ECM (166). This crosstalk dramatically influences the development of disease and therapeutic resistance (2). In solid tumor cancer cells trigger a constitutive wound healing response that provokes an unregulated inflammation and a constitutive stroma activation (167). In particular, during melanoma growth and development, cancer tissue recruits and activates host tissue cells which sustain the development and progression of tumor, by supporting the metabolism of cancer cells (167). Therefore, the several activated stromal cells can differentiate into macrophages, mast cells, adipocytes and CAFs, which in turn begin to secrete cytokines, induce a turnover of ECM thus playing an important role in tumor growth (167).

Metabolic Crosstalk Between Fibroblasts and Melanoma Cells

Fibroblasts, fibroblast aggregates, myofibroblasts and CAFs represent important constituents of melanoma stromal microenvironment (163, 165, 168). It is known that normal dermal fibroblasts, before CAF differentiation, hamper melanoma formation at its early stage (169). Conversely, senescent fibroblasts support melanoma growth (170). During melanoma development fibroblast aggregates are formed in dermis and their interaction with melanoma cells leads to fibroblast reprogramming linked to CAF differentiation (163). Anyway during melanoma development and progression, skin fibroblasts, through direct contact with malignant melanocytes, and/or the stimulation by humoral mediators and ROS, undergo a metabolic transformation which leads to fibroblast constitutive activation and thus CAF differentiation (9).

Direct contact between melanoma cells and fibroblasts are modulated by cadherins and connexins (171). In CM cancer cells proliferate, penetrate basement membrane and infiltrate into corium. Furthermore, a change from E-cadherin to N-cadherin expression, during melanoma development, not only frees cancer cells from epidermal keratinocytes, but also provides new adhesive characteristics (171). Via N-cadherin and gap junctions regulated by connexins, melanoma cells interact with N-cadherin-positive fibroblasts (171). In particular, connexins-mediated gap junctions regulate TME interactions between melanoma cells among each other and with the stromal cells (172). Connexins belong to a family of transmembrane proteins building gap junctions. These proteins are essential for gap junctional intercellular communication (GJIC) by exchange small molecules such as ions, signaling molecules (cAMP, ATP) and amino acids (172). Furthermore, GJIC mediates also miRNA transfer (173). The expression of connexin-43 (Cx43), over the last few years, has been associated with cancer recurrence, metastatic spread and poor survival (174). Furthermore, it is conceivable that Cx43 mediated connection could couple metabolic profile of melanoma tissue with regulation of cancer growth. In fact, Cx43 hemi channel regulates proliferation by regulating intracellular ATP and Ca^{2+} levels (175). Notably, inhibition of Cx43 channel activity sustains melanoma cell proliferation, while overexpression of Cx43 increases gap junction GJ coupling and reduces cell growth. Furthermore, Cx43 overexpression in FMS human melanoma cell lines increases apoptosis and is linked to a decrease of melanoma growth and metastatic capability (176).

Paracrine interaction, leading to CAF differentiation, is affected by tumor cell-derived growth factors and cytokines such as transforming growth factor β (TGF-β), epidermal growth factor (EGF), platelet-derived growth factor α/β (PDGFα/β), basic fibroblast growth factor (bFGF, also known as FGF2), interleukin 6 (IL-6), and interleukin 1β (IL-1β) (7). In particular, TGF-β influences significantly CAF differentiation, because it sustains the increase of fibroblast ROS that modulate α-SMA expression which is a marker of CAFs (7). Expression of Nodal, one of the member of the TGF superfamily, is positively correlated with melanoma (177). Nodal induces, together with Snail and TGF-β signaling pathway activation, the differentiation of normal fibroblasts into CAFs which sustain melanoma growth both *in vitro* and *in vivo* (177).

It is known that ROS are important modulators of the interplay between fibroblasts and cancer cells. ROS homeostasis is affected by the balance between ROS generation and both enzymatic and non-enzymatic antioxidant systems: the destroying of this equilibrium drives oxidative stress, which participates in tumor development (9). In particular, ROS production can be the result of melanocytes metabolism, melanin metabolism and UV radiation, altered metabolism of transformed cells (178). Melanoma cells derive from epidermal melanocytes in skin, which is a moderately hypoxic tissue (179). Melanocytes produce ROS through mitochondria, melanosomes, NADPH oxidase (NOX) family enzymes, different arachidonic acid oxygenase activities, and nitric oxide synthase (NOS) activity/uncoupling (179). Furthermore, melanocytes are highly exposed to oxidative stress because of the pro-oxidant state linked to melanin production, and the intrinsic antioxidant defenses weakened by pathologic conditions (179). In particular, it is noteworthy that melanin protects melanocytes by adsorbing UV radiation, but its synthesis is linked to higher levels of intracellular ROS that may sustain carcinogenesis (180). Furthermore, even if melanocytes are protected by endogenous melanin which absorbs ROS generated by UV radiation, melanin can be oxidized by exposure at higher UV doses, thus leading to ROS generation (180). However, both acute and chronic UV radiations trigger the skin to produce ROS, whose impact is exacerbated by the relative deficiency of melanocytes in the repair of oxidative DNA lesions (180). It is remarkable that hydrogen peroxide (H_2O_2) is a ROS regulating tyrosinase, the key enzyme for melanin synthesis in normal melanocytes and melanoma cells (181). Tumor hypoxia can contribute to ROS production by triggering the mitochondrial production of superoxide anion that is transformed to H_2O_2 by SOD2 activity. In particular, H_2O_2 is a very stable and permeable ROS, that can pass through both mitochondrial and cell membranes. It is the principal ROS in the regulation of signaling transduction pathways and modulates significantly the behavior of non-cancer and cancer cells (9, 182, 183). In solid tumors microenvironment, cancer cells generate high levels of ROS associated with mitochondrial dysfunction, upregulation of NOX-1 and NOX-4, and modifications of antioxidant enzymes (7). The mitochondrial dysfunction leads to the shift toward aerobic glycolysis, named as stated before "Warburg effect," which is an early step of carcinogenesis, and can also arise before the development of hypoxia. In cancer cells both "Warburg effect" and mitochondrial malfunctioning augment lactate and ROS levels and reduce antioxidant molecules (9). There are many works that showed the high level of oxidative stress in melanoma cells *in vitro* (184–188). However, even if it is possible to suppose that CM is a reactive oxygen driver tumor, the association between oxidative stress and human CM development and progression is still less studied (179). Anyway, the contribution of NOX-4 to transformed phenotype of melanoma cells by modulating G2-M cell cycle progression, suggests that specific signals of NOX family enzymes affect CM development (189). Furthermore, Ribeiro-Pereira et al. showed that ROS produced by the NOX, most likely NOX4, can sustain melanoma cells through the focal adhesion kinase (FAK) pathway, and thus maintain adhesion contacts and cell viability (190). ROS can trigger a cascade of intra- and intercellular signals driving metabolic reprogramming of both cancer cells and fibroblasts, and CAF differentiation. In particular, H_2O_2 from cancer cells triggers in CAFs an oxidative stress, connected with decrease of mitochondrial function and increase of both glucose uptake and ROS levels. Therefore, ROS produce a reactive microenvironment, where the energy needed for cancer cell proliferation is sustained by constitutively activated CAFs (9). Compared with normal fibroblasts, CAFs are characterized by slower proliferation rate, increased migratory capability, and resistance to apoptotic stimuli (2, 7, 163).

It is noteworthy that solid tumors like melanoma represent a heterogeneous metabolic environment, where the interaction between cancer cells and cancer microenvironment leads to a form of "parasitic" cancer metabolism (191). This metabolic model has been called by Lisanti's group "two-compartment tumor metabolism" or the "autophagic tumor stroma model of cancer" (192). The "autophagic tumor stroma model of cancer" is associated with clinical outcome in many tumors such as melanoma. In fact, in lymph node metastases of malignant melanoma loss of stromal caveolin 1 (Cav-1) expression, that is a marker of autophagy, glycolysis, and oxidative stress, strongly predicts clinical outcome (7, 193). Furthermore, the involvement of CAFs in melanoma dissemination is confirmed by study analyzing the clinical importance of Cav-1 expression in CM. In particular, loss of Cav-1 in CAFs could sustain metastatic process by producing a glycolytic microenvironment (193). Catabolic CAFs satisfy high-energy demands of cancer cells and sustain anabolic cancer growth, through secretion of considerable quantity of energy-rich fuels, like L-lactate, ketone bodies, glutamine, and free FAs (7, 191). Particularly, CAFs from human melanomas and colon cancers, characterized by high levels of glycolytic activity, glucose uptake, lactate production, glycolytic enzyme expression and decrease of oxygen consumption, support the CAF catabolic model (194). IDH3α, a key enzyme in the TCA cycle, regulates metabolic switch toward aerobic glycolysis in CAFs from melanomas and colon cancers. IDH3α downregulation in CAFs increases HIF-1α levels (194).

The horizontal transfer of mitochondria is another important mechanism that connects stromal and tumor cells (195, 196). *In vivo* studies performed by using melanoma cells without mitochondrial DNA ($B16\rho^0$ cells) showed that mouse stromal cells can transfer whole and intact mitochondria in $B16\rho^0$

cells, which consequently re-acquire respiratory function and the capability to form tumors efficiently. It is important to note that tumor cells without mitochondrial DNA form tumors with a very long delay with respect to their parental cells. Therefore, altogether these data suggest that even if many tumor cells rely mostly on the glycolytic metabolism, they also need mitochondrial respiration for promoting tumor formation and progression successfully and efficiently (196).

Adipocytes in the Metabolic Crosstalk With Melanoma Cells

Metastatic melanomas often grow in subcutaneous tissues and can be associated with a poor prognosis (197). The subcutaneous tissues contain mainly adipocytes which can promote tumor progression (197–199). Zhang et al. showed a mechanism associated with the capability of adipocytes to sustain melanoma progression and demonstrated a new therapeutic target of melanoma microenvironment (197). In particular, they showed that adipocytes induce *in vitro* proliferation and invasion of adjacent melanoma cells by transferring lipids to cancer cells and thus modifying the metabolism of melanoma cells (197). The lipids, used by melanoma cells in the β-oxidation pathway, decrease the dependence on *de novo* lipogenesis. Furthermore, the transfer of lipids from adipocytes to cancer cells is regulated by FATP/SLC27A family of lipid transporters, which localize on cancer cell surface. Melanoma cells overexpress FATP1/SLC27A1 that, in transgenic zebrafish experimental model, work together with $BRAF^{V600E}$ in sustaining CM development. Inhibition of Fatty Acid Transporter Proteins (FATPs), through the small-molecule inhibitor Lipofermata, decreases melanoma lipid uptake, invasion, and growth (197). Adipocytes secrete large amounts of exosomes, which are then taken up by melanoma cells, thus supporting migratory and invasive capability (200). These exosomes contain protein regulating and inducing FAO in melanoma cells. Furthermore, in obese humans, both the number of adipocytes-secreted exosomes and their influence on FAO-dependent cell migration are dramatically increased. These experimental evidences might in part offer an explanation for poorer prognosis of obese melanoma patients (200).

Metabolic Interplay Between Immune and Melanoma Cells

It is known that in TME the crosstalk between melanoma and immune cells affects immune response (201). In particular, high metabolic plasticity of melanoma cells and changes in melanoma microenvironment can lead to the activation of immune escape mechanisms and formation of an immunosuppressive niche, hindering immunotherapy effectiveness (2, 202–204). The upregulation of glycolysis associated with remarkable secretion of lactate and extracellular acidosis results in dramatic changes of stromal immune cells. In this scenario T cells (205) and their metabolic crosstalk with cancer cells influence significantly the immune homeostasis of melanoma microenvironment and response to immunotherapy (2). The upregulation of glycolysis in melanoma cells produces a microenvironment lacking glucose, where tumor cells and tumor-infiltrating lymphocytes (TILs) are competitor for glucose uptake. In fact, intra-tumoral CD4 T cells display indicators of glucose deprivation and decreased anti-tumor effector functions, indicating that a glucose-poor TME might participate in TIL exhaustion (206). In particular, TILs exhibit an increased expression of several "anergy" signature genes, and a decreased rate of glycolysis linked to a reduction of the glycolytic metabolite PEP. In particular, PEP reduction leads to defects in both Ca^{2+}- nuclear factor of activated T cells (NFAT) signaling and T cell activation by increasing sarco/ER Ca2+-ATPase (SERCA)-mediated Ca2+ re-uptake, thereby suppressing CD4+ T cell-mediated immune surveillance (206). Notably, metabolic reprogramming of TILs, by overexpression of phosphoenolpyruvate carboxykinase 1 (PCK1), that converts oxaloacetate (OAA) into PEP, increases their anti-tumor activities in the glucose-deprived TME (206). It is noteworthy that in murine melanoma experimental model, CD8+ TILs, which interact with a hypoglycemic and hypoxic TME, maintain their anti-tumor immune surveillance by shifting their metabolism toward OXPHOS, through the PPAR-α signaling activation and increasing FA catabolism (207). OXPHOS induction in TILs improves efficacy of PD-1 blockade therapy in murine experimental models (208). Additionally, the increase of FA catabolism in TILs might improve cancer immunotherapy in patients affected by tumors with low glucose content (207). Glycolysis satisfies the high energetic demand of activated T cells for their proliferation and cytokine synthesis, and the efficient secretion of lactate through MCT-1 allows to continue glycolysis in T cells. However, during melanoma progression, the high levels of lactate in TME hinder lactate export through MCT-1 from human CTLs. The lactate accumulated in CTLs inhibits their proliferation, cytokine production and decreases their cytotoxic activity. In particular, lactate decreases IL-2 and interferon γ (IFNγ) levels in CTLs (153). Furthermore, it is conceivable that the consequence of lactate accumulation on the immune system is dependent on the acidification rather than on the lactate itself (153, 209–211).

Arginine metabolism contributes to tumor progression and immunoescape. Arginine can be synthesized in two steps through the action of two tightly coupled enzymes, argininosuccinate synthetase (ASS) and argininosuccinate lyase (ASL). In particular, ASS catalyses the conversion of citrulline and aspartic acid to argininosuccinate, which is subsequently transformed into arginine and fumaric acid by ASL (212). Several tumors such as malignant melanoma, are arginine auxotrophic. Downregulation of the enzyme ASS, a well-known rate-limiting step in arginine synthesis, induces an intrinsic dependence on extracellular arginine caused by incapacity to synthesize arginine for growth (213). Therefore, high microenvironmental arginine uptake by cancer cells leaves little for T cells and drives reduction of their proliferation and survival (202). Furthermore, arginine is a precursor of nitric oxide (NO) whose level is a prognostic marker of cancer outcome for melanoma patients (214). NO can promote melanoma development through its immunosuppression activity, inhibition of apoptosis, stimulation of protumorigenic cytokines, activation of TAMs and alteration of angiogenic processes (214). Furthermore, NO can react with superoxide anions to yield peroxynitrite, which induces

apoptosis in T cells (202). It is remarkable that arginine metabolism significantly contributes to inflammatory tumor environment (215). In fact, NO activates cyclooxygenase-2 (COX-2) and other inflammatory factors and thus generates a pro-oxidant microenvironment sustaining cancer cell growth and suppressing anti-tumor immunity (215). Additionally, NO has an anti-apoptotic influence in human melanoma cells, and the expression of inducible nitric oxide synthase (iNOS), that produces NO, is linked to worse survival in patients with Stage III melanoma (216).

HALLMARKS OF THERAPIES TARGETING THE SHIFT OF MELANOMA FROM GLYCOLYSIS TOWARD OXPHOS

BRAF mutations induce melanoma cell proliferation, mitochondrial alterations (39) and fragmentation (217), and consequently the metabolic switch from OXPHOS toward glycolysis (218). Despite their glycolytic phenotype, melanoma cells harboring $BRAF^{V600E}$ mutation exhibit high metabolic flexibility, which thus can represent a promising and successful target in melanoma therapy. After an initial cancer regression in BRAFi/MEKi-treated patients, a subset of melanoma cells can acquire a metabolic drug-resistant phenotype, characterized by the enhancement of mitochondrial biogenesis, mitochondrial activity and mitochondrial content (2, 219, 220). The metabolic reprogramming from glycolysis toward OXPHOS is an adaptive response, which allows melanoma cells to provide ATP levels and avoid cell death process despite the inhibition of glycolysis induced by BRAFi/MEKi treatment (220). Additionally, a large subset of melanomas is characterized by high levels of PGC1-α and increased OXPHOS metabolism independently of BRAF mutational status (81). Therefore, mitochondria and OXPHOS represent metabolic vulnerabilities to exploit for the design of new and more effective therapeutic strategies targeting both PGC1-α-positive melanomas and BRAF mutant melanomas (31). In BRAF-mutant melanomas, the use of drugs targeting mitochondrial biogenesis and mitochondrial metabolism in combination with BRAFi/MEKi may enhance and delay BRAFi/MEKi-induced cell death and resistance in melanoma, respectively (2). Furthermore, since mitochondrial addiction caused by MAPKi treatment makes melanoma cells more sensitive to mitochondria inhibition, the combination therapy with both oncogenic kinase inhibitors and mitochondrial inhibitors not only can increase MAPKi efficacy and delay resistance, but also can decrease doses of mitochondrial inhibitors and thus reduce toxicity to normal tissues (221). The co-treatment of melanoma cells with BRAFi and antidiabetic drugs phenformin and metformin, which strongly inhibit the complex I of the MRC, results in a synergistic inhibition of melanoma cell viability (**Table 1**) (222). Additionally, Yuan et al. also reported that phenformin can delay the appearance of BRAFi-resistant melanoma cells (222). Another potent and selective inhibitor of the complex I of MRC is represented by BAY 87-2243. This compound reduces the total cellular ATP levels, increases ROS production, and thereby leads to oxidative damage and subsequent cell death *in vitro*. BAY 87-2243 exerts a potent anti-tumor effect by reducing melanoma growth also in various mouse models *in vivo*. Interestingly, the inhibition of complex I caused by the use of BAY 87-2243 in association with vemurafenib (BRAFi) significantly reduces melanoma tumor growth *in vivo* when compared with their use as single agents (**Table 1**) (223). The efficacy of mitochondrial complex I inhibitors in melanoma treatment was also supported by Carpenter et al. who demonstrated that deguelin strongly suppresses the proliferation of vemurafenib-resistant melanoma cells by blocking the mitochondrial complex I. Of note, deguelin induces selectively toxicity only in cancer cells, without affecting the viability of normal human melanocytes *in vitro* (**Table 1**) (224).

Furthermore, it is known that NSAIDs, commonly used in clinical practice as cyclooxygenase inhibitors, induce cytotoxicity in various cancer cell lines, including melanoma cells (158). Additionally, Brummer et al. reported that two NSAIDs, diclofenac and lumiracoxib, reduce melanoma cell proliferation by targeting both respiration and glycolytic activity. In particular, diclofenac and lumiracoxib restrict energy metabolism by decreasing significantly both lactate release and OXPHOS via MITF down-regulation. Interestingly the combination of vemurafenib with either anti-metabolic NSAIDs is synergistic and results in a more pronounced decrease of proliferation and induction of cell death in human melanoma cells (**Table 1**) (157).

In vitro and *in vivo* studies revealed that SR4 and niclosamide, two small molecules mitochondria uncouplers, can be used successfully in the treatment of naïve wild type, $BRAF^{V600E}$ and NRAS mutants, vemurafenib-resistant melanomas and melanomas with greater OXPHOS phenotype (**Table 1**). In fact, both SR4 and niclosamide, independently of BRAF or NRAS mutational status, promote energetic stress in melanoma cells by uncoupling mitochondrial OXPHOS, reducing intracellular ATP levels and consequently promoting the activation of the metabolic tumor suppressor AMP-activated kinase (AMPK) and the inhibition of mTOR pathway. As a result of this acute energetic stress, both the uncouplers promote cell cycle arrest and mitochondrial-dependent apoptosis in melanoma cells (219). Other studies supported the use of pharmacological direct AMPK activators, such as 5-aminoimidazole-4-carboxamide ribonucleoside (AICAR) (225, 226) and GSK621 (227), in the treatment of human melanomas. BAM15 is a second-generation mitochondrial uncoupling agent, which specifically inhibits OXPHOS with minimal off-target effects and consequences on cell viability. BAM15 causes cell death and alters proliferation when used in combination with low concentrations of PLX4032 or GSK1120212, which are BRAFi and MEKi respectively (**Table 1**) (228).

As discussed above, mitochondrial biogenesis is a drug resistance mechanism, activated by melanoma cells upon long-term exposure to MAPKi, and represents a promising therapeutic target in melanoma. PGC1-α, a key regulator of mitochondrial biogenesis and metabolism, is highly expressed in melanomas with OXPHOS phenotype and it is also upregulated in BRAFi/MEKi-resistant melanomas. However, the depletion of PGC1-α should be avoided in melanoma treatment because

TABLE 1 | List of molecules targeting mitochondrial metabolism in CM.

Agents	Mechanism	Metabolic target	References
Phenformin/metformin	• Inhibition of complex I of MRC.	OXPHOS	(222)
BAY 87-2243	• Inhibition of complex I of MRC.	OXPHOS	(223)
Deguelin	• Inhibition of complex I of MRC.	OXPHOS	(224)
NSAIDs (diclofenac/lumiracoxib)	• Reduction of lactate release and MITF downregulation.	Glycolysis and OXPHOS	(157, 158)
SR4/ niclosamide	• Activation of AMPK, inhibition of mTOR and consequently induction of acute energetic stress.	OXPHOS	(219)
BAM15	• Inhibition of OXPHOS.	OXPHOS	(228)
Inhibitors of ERR	• Inhibition of ERRα.	OXPHOS and mitochondrial biogenesis	(229)
Inhibitors of TRAP1/TFAM	• Inhibitors of mitochondrial protein folding/mitochondrial genome replication and transcription.	Mitochondrial biogenesis	(232)
G-TPP	• Inhibition of TRAP1, involved in mitochondrial protein folding.	Mitochondrial biogenesis	(233)
PEITC	• Inhibition of glutathione S-transferase and complex I of MRC.	Glutathione metabolism	(234)
Sulfasalazine	• Inhibition of xCT.	Glutathione biosynthesis	(235)
Vorinostat	• Inhibition of histone deacetilase and suppression of SLC7A11 gene, which encodes xCT.	Glutathione biosynthesis	(239)
BPTES	• Inhibition of glutaminolysis.	Glutamine metabolism	(241)
BenSer	• Inhibition of the glutamine transporter ASCT2.	Glutamine metabolism	(242)
NAMPT inhibitors	• Reduction of NAD and ATP levels, depolarization of the inner mitochondrial membrane with loss of mitochondrial membrane potential and ROS release.	NAD biosynthetic pathway	(243)

PGC1-α has a dual role in CM: it favors tumor growth and survival through the induction of oxidative metabolism and suppresses melanoma cell invasion and metastatic dissemination (229). Therefore, the depletion of PGC1-α in melanomas not only results in acute energy deficit caused by reduction of mitochondria metabolism (230), but also makes non-metastatic melanoma cells highly invasive (231). To overcome the dichotomy of PGC1-α, several studies were performed to identify components of PGC1-α protein complexes involved only in the metabolic regulation of mitochondria and not in the control of cell migration. Through these studies, the estrogen-related orphan nuclear receptors α (ERRα) was identified as a PGC1-α-dependent component, which promotes expression of genes involved only in OXPHOS, and not in the regulation of cell migration. Furthermore, *in vitro* and *in vivo* studies revealed that ERRα inhibition, as well as PGC1-α silencing, decreases mitochondrial respiration and cell proliferation in PGC1-α-positive melanoma cell lines. On the contrary, the inhibition of ERRα does not promote, unlike PGC1-α depletion, melanoma cell invasion. Taken together all these data suggest that ERRα may represent a promising metabolic target in the treatment of PGC1-α-positive melanomas (**Table 1**) (229). In addition to PGC1-α, other important regulators of mitochondrial biogenesis are represented by tumor necrosis factor receptor-associated protein 1 (TRAP1) and mitochondrial transcription factor A (TFAM). In particular, TRAP1 and TFAM are involved in mitochondrial protein folding and mitochondrial genome replication and transcription, respectively. However, Wu et al. reported that the inhibition of mitochondrial biogenesis through the depletion of TRAP1 or TFAM, but not of PGC1-α, increases the efficacy of MAPKi (**Table 1**) (232). Of note, gamitrinib, a small molecule inhibitor of TRAP1, synergizes with MAPKi and induces apoptotic cell death, mitochondrial dysfunction and suppression of tumor growth both *in vitro* and *in vivo* (**Table 1**) (80, 232). Furthermore, gamitrinib-triphenylphosphonium (G-TPP) was acquired through the attachment of a triphenylphosphonium (TPP^+) group, which gives to gamitrinib a preferential tropism to mitochondria. Georg Karpel-Massler et al. demonstrated that G-TPP synergizes with inhibitors of anti-apoptotic Bcl-2 family proteins (BH3-mimetics) and together they increase intrinsic apoptotic cell death and reduce the tumor growth rate in orthotopic melanoma model. Interestingly, in BRAFi-resistant melanoma models, this combination therapeutic strategy safely and significantly prolongs host survival (233).

In MAPKi-resistant melanoma cells, the metabolic reprogramming toward mitochondrial respiration, leads to increased level of oxidative stress and ROS production. Consequently, in order to resist ROS generation and therefore to survive under oxidative stress, resistant melanoma cells enhance the metabolism of the antioxidant glutathione. Hence, glutathione metabolism can represent another promising metabolic target in melanoma treatment. BRAFi-resistant melanoma cells are resensitized to vemurafenib when treated with phenethyl isothiocyanate (PEITC), an inhibitor of glutathione S-transferase (234, 235), which is involved in cellular detoxification through the conjugation of glutathione to a wide range of substrates (236). Furthermore, PEITC could increase the cytotoxicity of BRAFi by a rapid depletion of glutathione and by inhibiting the mitochondrial electron transport complex

I (**Table 1**) (235, 237). Additionally, to inhibit glutathione metabolism and thereby increase BRAFi therapy, melanoma cells can be treated with inhibitors of the cystine/glutamate antiporter (xCT), which mediates the uptake of cystine, a precursor for glutathione biosynthesis (**Table 1**) (238). Khamari et al. reported that sulfasalazine, an inhibitor of xCT, approved for the treatment of inflammatory bowel disease, is also able to delay the growth of BRAFi-resistant melanoma *in vitro* (**Table 1**) (235). Vorinostat, an histone deacetylase inhibitor (HDACi), enhances the levels of ROS in both MAPKi-sensitive and resistant melanoma cells by suppressing the expression of the Solute Carrier Family 7 Member 11 (SLC7A11) gene, encoding xCT (**Table 1**) (239). However, this leads to apoptotic cell death only in drug-resistant melanoma cells. In fact, in patients with melanoma resistant to BRAFi/MEKi therapy, vorinostat induces cell death only in drug-resistant melanoma cells. These data provide important clinical evidence for the use of vorinostat to eliminate new drug-resistant cells. Taken together all this evidence leads Wang et al. to assume that the pulsatile treatment with vorinostat, followed by a switch back to BRAFi/MEKi treatment, can get longer PFS benefit for melanoma patients with respect to the intermittent MAPKi only regimen (239). Furthermore, melanoma intracellular ROS over-production, caused by MAPKi treatment, can represent another important metabolic vulnerability in melanoma. In fact, it is possible to exploit ROS over-production in melanoma cells by using ROS activated pro-drugs in combination with MAPKi (**Table 1**). In particular, Yuan et al. demonstrated that A100 that is a ROS activated amine-containing compound, in combination with dabrafenib significantly suppresses *in vitro* melanoma cell proliferation and three-dimensional (3D) matrigel growth. Furthermore, they showed that A100 is able to restore sensitivity to BRAFi in BRAFi-resistant melanoma cells. Therefore, these results suggested that the combination therapy with a ROS activated pro-drug, such as A100, and a MAPKi, such as dabrafenib, could represent a potential strategy to treat BRAF-mutant melanoma patients and to overcome drug resistance (**Table 1**) (240).

MAPKi-resistant melanoma cells switch from glucose to mitochondrial glutamine metabolism and acquire the glutamine-addicted phenotype that represents a promising anti-tumor target. In fact, the use of the glutaminolysis inhibitor Bis-2-(5-phenylacetamido-1,2,4-thiadiazol-2-yl)ethyl sulfide (BPTES), in combination with BRAFi, enhances significantly the anti-tumor activity of BRAFi (**Table 1**) (241). Furthermore, glutamine transporter ASCT2 represents a potential therapeutic target for both BRAF wild type and $BRAF^{V600E}$ melanoma. In fact, the knockdown of ASCT2 or its pharmacological inhibition by Benzylserine (BenSer) suppresses melanoma cell growth and proliferation (**Table 1**) (242).

Audrito et al. showed that when melanoma cells acquire BRAFi-resistance, NAD levels increase and the NAD biosynthetic pathway, relying predominantly on the rate-limiting enzyme nicotinamide phosphoribosyltransferase (NAMPT) becomes the dominant one. NAMPT that is involved in the conversion of nicotinamide to NAD, has been found upregulated in tissue biopsies from melanoma patients after the development of BRAFi resistance (242). Additionally, melanoma cell lines overexpressing NAMPT develop soon BRAFi resistance and grow rapidly. This makes NAMPT an actionable target for melanoma treatment. In fact, *in vitro* studies revealed that melanoma treatment with NAMPT inhibitors (NAMPTi) reduces NAD and ATP, depolarizes the inner mitochondrial membrane with loss of mitochondrial membrane potential, triggers ROS release, halts cells in the G2/M phase and induces apoptosis. Furthermore, NAMPTi reduce tumor growth and enhance survival in mouse xenograft models (**Table 1**) (243).

List of molecules, described in the text, and whose use in combination with MAPKi may overcome drug resistance and/or improve the effectiveness of current therapeutic strategies targeting melanoma, is showed in **Table 1**.

CONCLUSIONS

CM tissue represents a very heterogeneous metabolic network influenced by metabolic reprogramming and plasticity of cancer cells whose interaction with TME leads to tumor progression and dissemination. The metabolic reprogramming of CM can be driven principally by $BRAF^{V600E}$ mutant kinase, that induces upregulation of glycolysis also in normoxic conditions. $BRAF^{V600E}$ mutation, glycolysis upregulation, structure and physiology of tumor vessels contribute dramatically to microenvironment acidification, which selects cancer cells with growth and proliferation advantages compared with non-transformed cells (2).

The capability of melanoma cells to shift their metabolic status between cytosolic glycolysis and mitochondrial respiration, in order to generate ATP and building block intermediates for cell growth, proliferation and dissemination, enables CM to modify dramatically its energetic pathways, in response to both microenvironmental changes and therapeutic strategies. In particular, the acidosis as well as BRAFi/MEKi treatment may switch the glycolytic metabolism of melanoma cells toward OXPHOS. The upregulation of mitochondrial metabolism correlates with increase in ROS levels and antioxidant systems and allows melanoma cells to offset glycolysis inhibition triggered by BRAFi/MEKi treatment. This process makes melanoma cells more dependent on mitochondria metabolism for proliferation and represents a weak point of cells resistant to MAPK inhibition. The integrated therapy with BRAFi/MEKi and molecules directed specifically toward cancer cell mitochondrial biogenesis and metabolism, and/or cellular antioxidant activity, is a promising strategy to counteract melanoma progression. In this complicated scenario, the microenvironment acidification, the interactions and the consequent metabolic crosstalk between melanoma and stromal cells sustain melanoma growth, and, by generating an immunosuppressive TME, can hinder immune response.

Therefore, a better elucidation of the melanoma metabolic alterations and crosstalk between cancer cells and TME may highlight further metabolic weakness and improve the efficacy of currently used therapies.

AUTHOR CONTRIBUTIONS

AAv and AAr planned the manuscript. AAv, AAr, GF, and AP wrote the manuscript. GS screened international scientific literature. MR and SM revised the manuscript and all of the authors accepted the final version.

FUNDING

This study was funded by the Italian Ministry of Education, Universities and Research through the grants: Integrated mechanobiology approaches for a precise medicine in cancer treatment (award number: PRIN-20177TTP3S), and by the Regione Campania SATIN grant 2018–2020.

REFERENCES

1. Siegel RL, Miller KD, Jemal A. Cancer statistics (2015). *CA Cancer J Clin*. (2015) 65:5–29. doi: 10.3322/caac.21254
2. Ruocco MR, Avagliano A, Granato G, Vigliar E, Masone S, Montagnani S, et al. Metabolic flexibility in melanoma: a potential therapeutic target. *Semin Cancer Biol.* (2019) 59:187–207. doi: 10.1016/j.semcancer.2019.07.016
3. Arozarena I, Wellbrock C. Targeting invasive properties of melanoma cells. *FEBS J*. (2017) 284:2148–62. doi: 10.1111/febs.14040
4. Gandhi SA, Kampp J. Skin cancer epidemiology, detection, and management. *Med Clin North Am*. (2015) 99:1323–35. doi: 10.1016/j.mcna.2015.06.002
5. Spagnolo F, Queirolo P. Upcoming strategies for the treatment of metastatic melanoma. *Arch Dermatol Res*. (2012) 304:177–84. doi: 10.1007/s00403-012-1223-7
6. Ratnikov BI, Scott DA, Osterman AL, Smith JW, Ronai ZA. Metabolic rewiring in melanoma. *Oncogene*. (2017) 36:147–57. doi: 10.1038/onc.2016.198
7. Avagliano A, Granato G, Ruocco MR, Romano V, Belviso I, Carfora A, et al. Metabolic reprogramming of cancer associated fibroblasts: the slavery of stromal fibroblasts. *Biomed Res Int*. (2018) 2018:6075403. doi: 10.1155/2018/6075403
8. Davis EJ, Johnson DB, Sosman JA, Chandra S. Melanoma: what do all the mutations mean? *Cancer*. (2018) 124:3490–9. doi: 10.1002/cncr.31345
9. Arcucci A, Ruocco MR, Granato G, Sacco AM, Montagnani S. Cancer: an oxidative crosstalk between solid tumor cells and cancer associated fibroblasts. *Biomed Res Int*. (2016) 2016:4502846. doi: 10.1155/2016/4502846
10. Denko NC. Hypoxia, HIF1 and glucose metabolism in the solid tumour. *Nat Rev Cancer*. (2008) 8:705–13. doi: 10.1038/nrc2468
11. Fischer GM, Vashisht Gopal YN, McQuade JL, Peng W, DeBerardinis RJ, Davies MA. Metabolic strategies of melanoma cells: mechanisms, interactions with the tumor microenvironment, and therapeutic implications. *Pigment Cell Melanoma Res*. (2018) 31:11–30. doi: 10.1111/pcmr.12661
12. Warburg O. On the origin of cancer cells. *Science*. (1956) 123:309–14. doi: 10.1126/science.123.3191.309
13. Peppicelli S, Toti A, Giannoni E, Bianchini F, Margheri F, Del Rosso M, et al. Metformin is also effective on lactic acidosis-exposed melanoma cells switched to oxidative phosphorylation. *Cell Cycle*. (2016) 15:1908–18. doi: 10.1080/15384101.2016.1191706
14. Davies MA. The role of the PI3K-AKT pathway in melanoma. *Cancer J*. (2012) 18:142–7. doi: 10.1097/PPO.0b013e31824d448c
15. Davies H, Bignell GR, Cox C, Stephens P, Edkins S, Clegg S, et al. Mutations of the BRAF gene in human cancer. *Nature*. (2002) 417:949–54. doi: 10.1038/nature00766
16. Rizos H, Darmanian AP, Holland EA, Mann GJ, Kefford RF. Mutations in the INK4a/ARF melanoma susceptibility locus functionally impair p14ARF. *J Biol Chem*. (2001) 276:41424–34. doi: 10.1074/jbc.M105299200
17. Kraehn GM, Utikal J, Udart M, Greulich KM, Bezold G, Kaskel P, et al. Extra c-myc oncogene copies in high risk cutaneous malignant melanoma and melanoma metastases. *Br J Cancer*. (2001) 84:72–9. doi: 10.1054/bjoc.2000.1535
18. Jakob JA, Bassett RL, Ng CS, Curry JL, Joseph RW, Alvarado GC, et al. NRAS mutation status is an independent prognostic factor in metastatic melanoma. *Cancer*. (2012) 118:4014–23. doi: 10.1002/cncr.26724
19. Omholt K, Kröckel D, Ringborg U, Hansson J. Mutations of PIK3CA are rare in cutaneous melanoma. *Melanoma Res*. (2006) 16:197–200. doi: 10.1097/01.cmr.0000200488.77970.e3
20. Stahl JM, Cheung M, Sharma A, Trivedi NR, Shanmugam S, Robertson GP. Loss of PTEN promotes tumor development in malignant melanoma. *Cancer Res*. (2003) 63:2881–90.
21. Scott DA, Richardson AD, Filipp FV, Knutzen CA, Chiang GG, Ronai ZA, et al. Comparative metabolic flux profiling of melanoma cell lines: beyond the warburg effect. *J Biol Chem*. (2011) 286:42626–34. doi: 10.1074/jbc.M111.282046
22. Kuphal S, Winklmeier A, Warnecke C, Bosserhoff AK. Constitutive HIF-1 activity in malignant melanoma. *Eur J Cancer*. (2010) 46:1159–69. doi: 10.1016/j.ejca.2010.01.031
23. Mills CN, Joshi SS, Niles RM. Expression and function of hypoxia inducible factor-1 alpha in human melanoma under non-hypoxic conditions. *Mol Cancer*. (2009) 8:104. doi: 10.1186/1476-4598-8-104
24. Aprelikova O, Pandolfi S, Tackett S, Ferreira M, Salnikow K, Ward Y, et al. Melanoma antigen-11 inhibits the hypoxia-inducible factor prolyl hydroxylase 2 and activates hypoxic response. *Cancer Res*. (2009) 69:616–24. doi: 10.1158/0008-5472.CAN-08-0811
25. Kumar SM, Yu H, Edwards R, Chen L, Kazianis S, Brafford P, et al. Mutant V600E BRAF increases hypoxia inducible factor-1α expression in melanoma. *Cancer Res*. (2007) 67:3177–84. doi: 10.1158/0008-5472.CAN-06-3312
26. Fukuda R, Hirota K, Fan F, Jung Y Do, Ellis LM, Semenza GL. Insulin-like growth factor 1 induces hypoxia-inducible factor 1-mediated vascular endothelial growth factor expression, which is dependent on MAP kinase and phosphatidylinositol 3-kinase signaling in colon cancer cells. *J Biol Chem*. (2002) 277:38205–11. doi: 10.1074/jbc.M203781200
27. Bertolotto C, Lesueur F, Giuliano S, Strub T, De Lichy M, Bille K, et al. A SUMOylation-defective MITF germline mutation predisposes to melanoma and renal carcinoma. *Nature*. (2011) 480:94–8. doi: 10.1038/nature10539
28. Buscà R, Berra E, Gaggioli C, Khaled M, Bille K, Marchetti B, et al. Hypoxia-inducible factor 1α is a new target of microphthalmia- associated transcription factor (MITF) in melanoma cells. *J Cell Biol*. (2005) 170:49–59. doi: 10.1083/jcb.200501067
29. Spinella F, Rosanò L, Di Castro V, Decandia S, Nicotra MR, Natali PG, et al. Endothelin-1 and endothelin-3 promote invasive behavior via hypoxia-inducible factor-1α in human melanoma cells. *Cancer Res*. (2007) 67:1725–34. doi: 10.1158/0008-5472.CAN-06-2606
30. Cronin JC, Wunderlich J, Loftus SK, Prickett TD, Wei X, Ridd K, et al. Frequent mutations in the MITF pathway in melanoma. *Pigment Cell Melanoma Res*. (2009) 22:435–44. doi: 10.1111/j.1755-148X.2009.00578.x
31. Ashton TM, Gillies McKenna W, Kunz-Schughart LA, Higgins GS. Oxidative phosphorylation as an emerging target in cancer therapy. *Clin Cancer Res*. (2018) 24:2482–90. doi: 10.1158/1078-0432.CCR-17-3070
32. Han ZB, Ren H, Zhao H, Chi Y, Chen K, Zhou B, et al. Hypoxia-inducible factor (HIF)-1α directly enhances the transcriptional activity of stem cell factor (SCF) in response to hypoxia and epidermal growth factor (EGF). *Carcinogenesis*. (2008) 29:1853–61. doi: 10.1093/carcin/bgn066
33. Kim JW, Tchernyshyov I, Semenza GL, Dang C V. HIF-1-mediated expression of pyruvate dehydrogenase kinase: a metabolic switch required for cellular adaptation to hypoxia. *Cell Metab*. (2006) 3:177–85. doi: 10.1016/j.cmet.2006.02.002
34. Semenza GL. Targeting HIF-1 for cancer therapy. *Nat Rev Cancer*. (2003) 3:721–32. doi: 10.1038/nrc1187
35. Semenza GL, Jiang BH, Leung SW, Passantino R, Concordat JP, Maire P, et al. Hypoxia response elements in the aldolase A, enolase 1,

and lactate dehydrogenase a gene promoters contain essential binding sites for hypoxia-inducible factor 1. *J Biol Chem*. (1996) 271:32529–37. doi: 10.1074/jbc.271.51.32529
36. Li X, Jiang Y, Meisenhelder J, Yang W, Hawke DH, Zheng Y, et al. Mitochondria-translocated PGK1 functions as a protein kinase to coordinate glycolysis and the TCA cycle in tumorigenesis. *Mol Cell*. (2016) 61:705–19. doi: 10.1016/j.molcel.2016.02.009
37. Stine ZE, Walton ZE, Altman BJ, Hsieh AL, Dang CV. MYC, metabolism, and cancer. *Cancer Discov*. (2015) 5:1024–39. doi: 10.1158/2159-8290.CD-15-0507
38. Zeller KI, Jegga AG, Aronow BJ, O'Donnell KA, Dang CV. An integrated database of genes responsive to the Myc oncogenic transcription factor: identification of direct genomic targets. *Genome Biol*. (2003) 4:R69. doi: 10.1186/gb-2003-4-10-r69
39. Haq R, Shoag J, Andreu-Perez P, Yokoyama S, Edelman H, Rowe GC, et al. Oncogenic BRAF regulates oxidative metabolism via PGC1α and MITF. *Cancer Cell*. (2013) 23:302–15. doi: 10.1016/j.ccr.2013.02.003
40. Hudson CC, Liu M, Chiang GG, Otterness DM, Loomis DC, Kaper F, et al. Regulation of hypoxia-inducible factor 1 expression and function by the mammalian target of rapamycin. *Mol Cell Biol*. (2002) 22:7004–14. doi: 10.1128/MCB.22.20.7004-7014.2002
41. Land SC, Tee AR. Hypoxia-inducible factor 1α is regulated by the mammalian target of rapamycin (mTOR) via an mTOR signaling motif. *J Biol Chem*. (2007) 282:20534–43. doi: 10.1074/jbc.M611782200
42. Davies MA, Stemke-Hale K, Tellez C, Calderone TL, Deng W, Prieto VG, et al. A novel AKT3 mutation in melanoma tumours and cell lines. *Br J Cancer*. (2008) 99:1265–8. doi: 10.1038/sj.bjc.6604637
43. Kwong LN, Davies MA. Navigating the therapeutic complexity of PI3K pathway inhibition in melanoma. *Clin Cancer Res*. (2013) 19:5310–9. doi: 10.1158/1078-0432.CCR-13-0142
44. Cascone T, McKenzie JA, Mbofung RM, Punt S, Wang Z, Xu C, et al. Increased tumor glycolysis characterizes immune resistance to adoptive T cell therapy. *Cell Metab*. (2018) 27:977–87.e4. doi: 10.1016/j.cmet.2018.02.024
45. Israelsen WJ, Vander Heiden MG. Pyruvate kinase: function, regulation and role in cancer. *Semin Cell Dev Biol*. (2015) 43:43–51. doi: 10.1016/j.semcdb.2015.08.004
46. Christofk HR, Vander Heiden MG, Wu N, Asara JM, Cantley LC. Pyruvate kinase M2 is a phosphotyrosine-binding protein. *Nature*. (2008) 452:181–6. doi: 10.1038/nature06667
47. Wiese EK, Hitosugi T. Tyrosine kinase signaling in cancer metabolism: PKM2 paradox in the warburg effect. *Front Cell Dev Biol*. (2018) 6:79. doi: 10.3389/fcell.2018.00079
48. Gao X, Wang H, Yang JJ, Liu X, Liu ZR. Pyruvate kinase M2 regulates gene transcription by acting as a protein kinase. *Mol Cell*. (2012) 45:598–609. doi: 10.1016/j.molcel.2012.01.001
49. Yang W, Zheng Y, Xia Y, Ji H, Chen X, Guo F, et al. ERK1/2-dependent phosphorylation and nuclear translocation of PKM2 promotes the warburg effect. *Nat Cell Biol*. (2012) 14:1295–304. doi: 10.1038/ncb2629
50. Pouysségur J, Dayan F, Mazure NM. Hypoxia signalling in cancer and approaches to enforce tumour regression. *Nature*. (2006) 441:437–43. doi: 10.1038/nature04871
51. Shaw RJ. Glucose metabolism and cancer. *Curr Opin Cell Biol*. (2006) 18:598–608. doi: 10.1016/j.ceb.2006.10.005
52. Iwasaki K, Yabushita H, Ueno T, Wakatsuki A. Role of hypoxia-inducible factor-1α, carbonic anhydrase-IX, glucose transporter-1 and vascular endothelial growth factor associated with lymph node metastasis and recurrence in patients with locally advanced cervical cancer. *Oncol Lett*. (2015) 10:1970–8. doi: 10.3892/ol.2015.3524
53. Nemejcová K, Rosmusová J, Bártu M, Dura M, Tichá I, Dundr P. Expression of glut-1 in normal endometrium and endometrial lesions: analysis of 336 cases. *Int J Surg Pathol*. (2017) 25:389–96. doi: 10.1177/1066896916683510
54. Ma X, Hui Y, Lin L, Wu Y, Zhang X, Liu P. Clinical significance of COX-2, GLUT-1 and VEGF expressions in endometrial cancer tissues. *Pakistan J Med Sci*. (2015) 31:280–4. doi: 10.12669/pjms.312.6604
55. Slominski A, Kim TK, Brozyna AA, Janjetovic Z, Brooks DLP, Schwab LP, et al. The role of melanogenesis in regulation of melanoma behavior: melanogenesis leads to stimulation of HIF-1α expression and HIF-dependent attendant pathways. *Arch Biochem Biophys*. (2014) 563:79–93. doi: 10.1016/j.abb.2014.06.030
56. Koch A, Lang SA, Wild PJ, Gantner S, Mahli A, Spanier G, et al. Glucose transporter isoform 1 expression enhances metastasis of malignant melanoma cells. *Oncotarget*. (2015) 6:32748–60. doi: 10.18632/oncotarget.4977
57. Dura M, Němejcová K, Jakša R, Bártu M, Kodet O, Tichá I, et al. Expression of glut-1 in malignant melanoma and melanocytic nevi: an immunohistochemical study of 400 cases. *Pathol Oncol Res*. (2019) 25:361–8. doi: 10.1007/s12253-017-0363-7
58. Mihic-Probst D, Ikenberg K, Tinguely M, Schraml P, Behnke S, Seifert B, et al. Tumor cell plasticity and angiogenesis in human melanomas. *PLoS ONE*. (2012) 7:e33571. doi: 10.1371/journal.pone.0033571
59. Dimmer KS, Friedrich B, Lang F, Deitmer JW, Broer S. The low-affinity monocarboxylate transporter MCT4 is adapted to the export of lactate in highly glycolytic cells. *Biochem J*. (2000) 350:219–27. doi: 10.1042/bj3500219
60. Faubert B, Li KY, Cai L, Hensley CT, Kim J, Zacharias LG, et al. Lactate metabolism in human lung tumors. *Cell*. (2017) 171:358–71.e9. doi: 10.1016/j.cell.2017.09.019
61. Halestrap AP. Monocarboxylic acid transport. *Compr Physiol*. (2013) 3:1611–43. doi: 10.1002/cphy.c130008
62. Hong CS, Graham NA, Gu W, Espindola Camacho C, Mah V, Maresh EL, et al. MCT1 modulates cancer cell pyruvate export and growth of tumors that co-express MCT1 and MCT4. *Cell Rep*. (2016) 14:1590–601. doi: 10.1016/j.celrep.2016.01.057
63. Pinheiro C, Miranda-Gonçalves V, Longatto-Filho A, Vicente ALSA, Berardinelli GN, Scapulatempo-Neto C, et al. The metabolic microenvironment of melanomas: prognostic value of MCT1 and MCT4. *Cell Cycle*. (2016) 15:1462–70. doi: 10.1080/15384101.2016.1175258
64. Payen VL, Porporato PE, Baselet B, Sonveaux P. Metabolic changes associated with tumor metastasis, part 1: tumor pH, glycolysis and the pentose phosphate pathway. *Cell Mol Life Sci*. (2016) 73:1333–48. doi: 10.1007/s00018-015-2098-5
65. Ullah MS, Davies AJ, Halestrap AP. The plasma membrane lactate transporter MCT4, but not MCT1, is up-regulated by hypoxia through a HIF-1α-dependent mechanism. *J Biol Chem*. (2006) 281:9030–7. doi: 10.1074/jbc.M511397200
66. Tasdogan A, Faubert B, Ramesh V, Ubellacker JM, Shen B, Solmonson A, et al. Metabolic heterogeneity confers differences in melanoma metastatic potential. *Nature*. (2019) 577:115–120. doi: 10.1038/s41586-019-1847-2
67. Almuhaideb A, Papathanasiou N, Bomanji J. 18F-FDG PET/CT imaging in oncology. *Ann Saudi Med*. (2011) 31:3–13. doi: 10.5144/0256-4947.2011.3
68. Wagner JD, Schauwecker D, Davidson D, Logan T, Coleman JJ, Hutchins G, et al. Inefficacy of F-18 fluorodeoxy-D-glucose-positron emission tomography scans for initial evaluation in early-stage cutaneous melanoma. *Cancer*. (2005) 104:570–9. doi: 10.1002/cncr.21189
69. Eigtved A, Andersson AP, Dahlstrøm K, Rabøl A, Jensen M, Holm S, et al. Use of fluorine-18 fluorodeoxyglucose positron emission tomography in the detection of silent metastases from malignant melanoma. *Eur J Nucl Med*. (2000) 27:70–5. doi: 10.1007/PL00006666
70. Zhuang L, Scolyer RA, Murali R, McCarthy SW, Zhang XD, Thompson JF, et al. Lactate dehydrogenase 5 expression in melanoma increases with disease progression and is associated with expression of Bcl-XL and Mcl-1, but not Bcl-2 proteins. *Mod Pathol*. (2010) 23:45–53. doi: 10.1038/modpathol.2009.129
71. Koukourakis MI, Giatromanolaki A, Sivridis E. Lactate dehydrogenase isoenzymes 1 and 5: differential expression by neoplastic and stromal cells in non-small cell lung cancer and other epithelial malignant tumors. *Tumor Biol*. (2003) 24:199–202. doi: 10.1159/000074430
72. Hersey P, Watts RN, Xu DZ, Hackett J. Metabolic approaches to treatment of melanoma. *Clin Cancer Res*. (2009) 15:6490–4. doi: 10.1158/1078-0432.CCR-09-0251
73. Patra KC, Hay N. The pentose phosphate pathway and cancer. *Trends Biochem Sci*. (2014) 39:347–54. doi: 10.1016/j.tibs.2014.06.005
74. Hilf R, Ickowicz R, Bartley JC, Abraham S. Multiple molecular forms of glucose-6-phosphate dehydrogenase in normal, preneoplastic, and neoplastic mammary tissues of mice. *Cancer Res*. (1975) 35:2109–16.

75. Kathagen-Buhmann A, Schulte A, Weller J, Holz M, Herold-Mende C, Glass R, et al. Glycolysis and the pentose phosphate pathway are differentially associated with the dichotomous regulation of glioblastoma cell migration versus proliferation. *Neuro Oncol*. (2016) 18:1219–29. doi: 10.1093/neuonc/now024
76. Ju HQ, Lu YX, Wu QN, Liu J, Zeng ZL, Mo HY, et al. Disrupting G6PD-mediated redox homeostasis enhances chemosensitivity in colorectal cancer. *Oncogene*. (2017) 36:6282–92. doi: 10.1038/onc.2017.227
77. Benito A, Polat IH, Noé V, Ciudad CJ, Marin S, Cascante M. Glucose-6-phosphate dehydrogenase and transketolase modulate breast cancer cell metabolic reprogramming and correlate with poor patient outcome. *Oncotarget*. (2017) 8:106693–706. doi: 10.18632/oncotarget.21601
78. Rünger TM. Mechanisms of melanoma promotion by ultraviolet radiation. *J Invest Dermatol*. (2016) 136:1751–2. doi: 10.1016/j.jid.2016.04.001
79. Gopal YNV, Rizos H, Chen G, Deng W, Frederick DT, Cooper ZA, et al. Inhibition of mTORC1/2 overcomes resistance to MAPK pathway inhibitors mediated by PGC1α and oxidative phosphorylation in melanoma. *Cancer Res*. (2014) 74:7037–47. doi: 10.1158/0008-5472.CAN-14-1392
80. Zhang G, Frederick DT, Wu L, Wei Z, Krepler C, Srinivasan S, et al. Targeting mitochondrial biogenesis to overcome drug resistance to MAPK inhibitors. *J Clin Invest*. (2016) 126:1834–56. doi: 10.1172/JCI82661
81. Vazquez F, Lim JH, Chim H, Bhalla K, Girnun G, Pierce K, et al. PGC1α expression defines a subset of human melanoma tumors with increased mitochondrial capacity and resistance to oxidative stress. *Cancer Cell*. (2013) 23:287–301. doi: 10.1016/j.ccr.2012.11.020
82. Lebleu VS, O'Connell JT, Gonzalez Herrera KN, Wikman H, Pantel K, Haigis MC, et al. PGC-1α mediates mitochondrial biogenesis and oxidative phosphorylation in cancer cells to promote metastasis. *Nat Cell Biol*. (2014) 16:992–1003. doi: 10.1038/ncb3039
83. McQuade JL, Vashisht Gopal Y. Counteracting oxidative phosphorylation-mediated resistance of melanomas to MAPK pathway inhibition. *Mol Cell Oncol*. (2015) 2:e991610. doi: 10.4161/23723556.2014.991610
84. Abildgaard C, Guldberg P. Molecular drivers of cellular metabolic reprogramming in melanoma. *Trends Mol Med*. (2015) 21:164–71. doi: 10.1016/j.molmed.2014.12.007
85. Feige E, Yokoyama S, Levy C, Khaled M, Igras V, Lin RJ, et al. Hypoxia-induced transcriptional repression of the melanoma-associated oncogene MITF. *Proc Natl Acad Sci USA*. (2011) 108:E924–33. doi: 10.1073/pnas.1106351108
86. Shackelford DB, Shaw RJ. The LKB1-AMPK pathway: metabolism and growth control in tumour suppression. *Nat Rev Cancer*. (2009) 9:563–75. doi: 10.1038/nrc2676
87. Cantó C, Gerhart-Hines Z, Feige JN, Lagouge M, Noriega L, Milne JC, et al. AMPK regulates energy expenditure by modulating NAD+ metabolism and SIRT1 activity. *Nature*. (2009) 458:1056–60. doi: 10.1038/nature 07813
88. Zheng B, Jeong JH, Asara JM, Yuan YY, Granter SR, Chin L, et al. Oncogenic B-RAF negatively regulates the tumor suppressor LKB1 to promote melanoma cell proliferation. *Mol Cell*. (2009) 33:237–47. doi: 10.1016/j.molcel.2008.12.026
89. Ryan DG, Murphy MP, Frezza C, Prag HA, Chouchani ET, O'Neill LA, et al. Coupling krebs cycle metabolites to signalling in immunity and cancer. *Nat Metab*. (2019) 1:16–33. doi: 10.1038/s42255-018-0014-7
90. Epstein ACR, Gleadle JM, McNeill LA, Hewitson KS, O'Rourke J, Mole DR, et al. *C. elegans* EGL-9 and mammalian homologs define a family of dioxygenases that regulate HIF by prolyl hydroxylation. *Cell*. (2001) 107:43–54. doi: 10.1016/S0092-8674(01)00507-4
91. Groulx I, Lee S. Oxygen-dependent ubiquitination and degradation of hypoxia-inducible factor requires nuclear-cytoplasmic trafficking of the von Hippel-Lindau tumor suppressor protein. *Mol Cell Biol*. (2002) 22:5319–36. doi: 10.1128/MCB.22.15.5319-5336.2002
92. Louphrasitthiphol P, Ledaki I, Chauhan J, Falletta P, Siddaway R, Buffa FM, et al. MITF controls the TCA cycle to modulate the melanoma hypoxia response. *Pigment Cell Melanoma Res*. (2019) 32:792–808. doi: 10.1111/pcmr.12802
93. Park J, Chen Y, Tishkoff DX, Peng C, Tan M, Dai L, et al. SIRT5-mediated lysine desuccinylation impacts diverse metabolic pathways. *Mol Cell*. (2013) 50:919–30. doi: 10.1016/j.molcel.2013.06.001
94. Rabinovich S, Adler L, Yizhak K, Sarver A, Silberman A, Agron S, et al. Diversion of aspartate in ASS1-deficient tumours fosters de novo pyrimidine synthesis. *Nature*. (2015) 527:379–83. doi: 10.1038/nature15529
95. Deberardinis RJ, Cheng T. Q's next: the diverse functions of glutamine in metabolism, cell biology and cancer. *Oncogene*. (2010) 29:313–24. doi: 10.1038/onc.2009.358
96. Choi YK, Park KG. Targeting glutamine metabolism for cancer treatment. *Biomol Ther*. (2018) 26:19–28. doi: 10.4062/biomolther.2017.178
97. Gray LR, Tompkins SC, Taylor EB. Regulation of pyruvate metabolism and human disease. *Cell Mol Life Sci*. (2014) 71:2577–604. doi: 10.1007/s00018-013-1539-2
98. Phannasil P, Thuwajit C, Warnnissorn M, Wallace JC, MacDonald MJ, Jitrapakdee S. Pyruvate carboxylase is up-regulated in breast cancer and essential to support growth and invasion of MDA-MB-231 cells. *PLoS One*. (2015) 10. doi: 10.1371/journal.pone.0129848
99. Sellers K, Fox MP, Ii MB, Slone SP, Higashi RM, Miller DM, et al. Pyruvate carboxylase is critical for non-small-cell lung cancer proliferation. *J Clin Invest*. (2015) 125:687–98. doi: 10.1172/JCI72873
100. Sumantran VN, Mishra P, Sudhakar N. Microarray analysis of differentially expressed genes regulating lipid metabolism during melanoma progression. *Indian J Biochem Biophys*. (2015) 52:125–31.
101. Aloia A, Müllhaupt D, Chabbert CD, Eberhart T, Flückiger-Mangual S, Vukolic A, et al. A fatty acid oxidation-dependent metabolic shift regulates the adaptation of BRAF-mutated melanoma to MAPK inhibitors. *Clin Cancer Res*. (2019) 25:6852–67. doi: 10.1158/1078-0432.CCR-19-0253
102. Carracedo A, Cantley LC, Pandolfi PP. Cancer metabolism: fatty acid oxidation in the limelight. *Nat Rev Cancer*. (2013) 13:227–32. doi: 10.1038/nrc3483
103. Harel M, Ortenberg R, Varanasi SK, Mangalhara KC, Mardamshina M, Markovits E, et al. Proteomics of melanoma response to immunotherapy reveals mitochondrial dependence. *Cell*. (2019) 179:236–50.e18. doi: 10.1016/j.cell.2019.08.012
104. Webb BA, Chimenti M, Jacobson MP, Barber DL. Dysregulated pH: a perfect storm for cancer progression. *Nat Rev Cancer*. (2011) 11:671–7. doi: 10.1038/nrc3110
105. Spugnini EP, Sonveaux P, Stock C, Perez-Sayans M, De Milito A, Avnet S, et al. Proton channels and exchangers in cancer. *Biochim Biophys Acta - Biomembr*. (2015) 1848:2715–26. doi: 10.1016/j.bbamem.2014.10.015
106. Koukourakis MI, Giatromanolaki A, Harris AL, Sivridis E. Comparison of metabolic pathways between cancer cells and stromal cells in colorectal carcinomas: a metabolic survival role for tumor-associated stroma. *Cancer Res*. (2006) 66:632–7. doi: 10.1158/0008-5472.CAN-05-3260
107. Carmeliet P, Jain RK. Angiogenesis in cancer and other diseases. *Nature*. (2000) 407:249–57. doi: 10.1038/35025220
108. Martinez-Outschoorn UE, Peiris-Pagés M, Pestell RG, Sotgia F, Lisanti MP. Cancer metabolism: a therapeutic perspective. *Nat Rev Clin Oncol*. (2017) 14:11–31. doi: 10.1038/nrclinonc.2016.60
109. Bandarchi B, Ma L, Navab R, Seth A, Rasty G. From melanocyte to metastatic malignant melanoma. *Dermatol Res Pract*. (2010) 2010:583748. doi: 10.1155/2010/583748
110. Shain AH, Bastian BC. From melanocytes to melanomas. *Nat Rev Cancer*. (2016) 16:345–58. doi: 10.1038/nrc.2016.37
111. Jain RK. Normalizing tumor vasculature with anti-angiogenic therapy: a new paradigm for combination therapy. *Nat Med*. (2001) 7:987–9. doi: 10.1038/nm0901-987
112. Marzagalli M, Raimondi M, Fontana F, Montagnani Marelli M, Moretti RM, Limonta P. Cellular and molecular biology of cancer stem cells in melanoma: possible therapeutic implications. *Semin Cancer Biol*. (2019) 59:221–35. doi: 10.1016/j.semcancer.2019.06.019
113. Dang CV, Kim JW, Gao P, Yustein J. The interplay between MYC and HIF in cancer. *Nat Rev Cancer*. (2008) 8:51–6. doi: 10.1038/nrc2274
114. Chiche J, Brahimi-Horn MC, Pouysségur J. Tumour hypoxia induces a metabolic shift causing acidosis: a common feature in cancer. *J Cell Mol Med*. (2010) 14:771–94. doi: 10.1111/j.1582-4934.2009.00994.x
115. Weljie AM, Jirik FR. Hypoxia-induced metabolic shifts in cancer cells: moving beyond the warburg effect. *Int J Biochem Cell Biol*. (2011) 43:981–9. doi: 10.1016/j.biocel.2010.08.009

116. Filatova A, Seidel S, Bögürcü N, Gräf S, Garvalov BK, Acker T. Acidosis acts through HSP90 in a PHD/ VHL-independent manner to promote HIF function and stem cell maintenance in glioma. *Cancer Res*. (2016) 76:5845–56. doi: 10.1158/0008-5472.CAN-15-2630
117. Rofstad EK, Mathiesen B, Galappathi K. Increased metastatic dissemination in human melanoma xenografts after subcurative radiation treatment: radiation-induced increase in fraction of hypoxic cells and hypoxia-induced up-regulation of urokinase-type plasminogen activator receptor. *Cancer Res*. (2004) 64:13–8. doi: 10.1158/0008-5472.CAN-03-2658
118. Graham CH, Fitzpatrick TE, McCrae KR. Hypoxia stimulates urokinase receptor expression through a heme protein-dependent pathway. *Blood*. (1998) 91:3300–7. doi: 10.1182/blood.V91.9.3300
119. Laurenzana A, Chillà A, Luciani C, Peppicelli S, Biagioni A, Bianchini F, et al. uPA/uPAR system activation drives a glycolytic phenotype in melanoma cells. *Int J Cancer*. (2017) 141:1190–200. doi: 10.1002/ijc.30817
120. Mahmood N, Mihalcioiu C, Rabbani SA. Multifaceted role of the urokinase-type plasminogen activator (uPA) and its receptor (uPAR): diagnostic, prognostic, and therapeutic applications. *Front Oncol*. (2018) 8:24. doi: 10.3389/fonc.2018.00024
121. Laurenzana A, Margheri F, Biagioni A, Chillà A, Pimpinelli N, Ruzzolini J, et al. EGFR/uPAR interaction as druggable target to overcome vemurafenib acquired resistance in melanoma cells. *EBioMedicine*. (2019) 39:194–206. doi: 10.1016/j.ebiom.2018.12.024
122. Böhme I, Bosserhoff AK. Acidic tumor microenvironment in human melanoma. *Pigment Cell Melanoma Res*. (2016) 29:508–23. doi: 10.1111/pcmr.12495
123. Vial G, Detaille D, Guigas B. Role of mitochondria in the mechanism(s) of action of metformin. *Front Endocrinol*. (2019) 10:294. doi: 10.3389/fendo.2019.00294
124. Jaune E, Rocchi S. Metformin: focus on melanoma. *Front Endocrinol*. (2018) 9:472. doi: 10.3389/fendo.2018.00472
125. Andreucci E, Pietrobono S, Peppicelli S, Ruzzolini J, Bianchini F, Biagioni A, et al. SOX2 as a novel contributor of oxidative metabolism in melanoma cells. *Cell Commun Signal*. (2018) 16:87. doi: 10.1186/s12964-018-0297-z
126. Pelicano H, Martin DS, Xu RH, Huang P. Glycolysis inhibition for anticancer treatment. *Oncogene*. (2006) 25:4633–46. doi: 10.1038/sj.onc.1209597
127. Peppicelli S, Andreucci E, Ruzzolini J, Laurenzana A, Margheri F, Fibbi G, et al. The acidic microenvironment as a possible niche of dormant tumor cells. *Cell Mol Life Sci*. (2017) 74:2761–71. doi: 10.1007/s00018-017-2496-y
128. Sosa MS, Bragado P, Aguirre-Ghiso JA. Mechanisms of disseminated cancer cell dormancy: an awakening field. *Nat Rev Cancer*. (2014) 14:611–22. doi: 10.1038/nrc3793
129. Goss PE, Chambers AF. Does tumour dormancy offer a therapeutic target? *Nat Rev Cancer*. (2010) 10:871–7. doi: 10.1038/nrc2933
130. Jia Q, Yang F, Huang W, Zhang Y, Bao B, Li K, et al. Low levels of sox2 are required for melanoma tumor-repopulating cell dormancy. *Theranostics*. (2019) 9:424–35. doi: 10.7150/thno.29698
131. Famulski KS, Macdonald D, Paterson MC, Sikora E. Activation of a low pH-dependent nuclease by apoptotic agents. *Cell Death Differ*. (1999) 6:281–9. doi: 10.1038/sj.cdd.4400495
132. Marino ML, Pellegrini P, Di Lernia G, Djavaheri-Mergny M, Brnjic S, Zhang X, et al. Autophagy is a protective mechanism for human melanoma cells under acidic stress. *J Biol Chem*. (2012) 287:30664–76. doi: 10.1074/jbc.M112.339127
133. Wojtkowiak JW, Rothberg JM, Kumar V, Schramm KJ, Haller E, Proemsey JB, et al. Chronic autophagy is a cellular adaptation to tumor acidic pH microenvironments. *Cancer Res*. (2012) 72:3938–47. doi: 10.1158/0008-5472.CAN-11-3881
134. Böhme I, Bosserhoff A. Extracellular acidosis triggers a senescence-like phenotype in human melanoma cells. *Pigment Cell Melanoma Res*. (2020) 33:41–51. doi: 10.1111/pcmr.12811
135. Andreucci E, Peppicelli S, Carta F, Brisotto G, Biscontin E, Ruzzolini J, et al. Carbonic anhydrase IX inhibition affects viability of cancer cells adapted to extracellular acidosis. *J Mol Med*. (2017) 95:1341–53. doi: 10.1007/s00109-017-1590-9
136. Robertson N, Potter C, Harris AL. Role of carbonic anhydrase IX in human tumor cell growth, survival, and invasion. *Cancer Res*. (2004) 64:6160–5. doi: 10.1158/0008-5472.CAN-03-2224
137. Neri D, Supuran CT. Interfering with pH regulation in tumours as a therapeutic strategy. *Nat Rev Drug Discov*. (2011) 10:767–77. doi: 10.1038/nrd3554
138. Chafe SC, McDonald PC, Saberi S, Nemirovsky O, Venkateswaran G, Burugu S, et al. Targeting hypoxia-induced carbonic anhydrase IX enhances immune-checkpoint blockade locally and systemically. *Cancer Immunol Res*. (2019) 7:1064–78. doi: 10.1158/2326-6066.CIR-18-0657
139. Pike LJ. Lipid rafts: bringing order to chaos. *J Lipid Res*. (2003) 44:655–67. doi: 10.1194/jlr.R200021-JLR200
140. Martínez-Zaguilán R, Raghunand N, Lynch RM, Bellamy W, Martinez GM, Rojas B, et al. pH and drug resistance. I. functional expression of plasmalemmal V-type H+-ATPase in drug-resistant human breast carcinoma cell lines. *Biochem Pharmacol*. (1999) 57:1037–46. doi: 10.1016/S0006-2952(99)00022-2
141. Yoshinaka K, Kumanogoh H, Nakamura S, Maekawa S. Identification of V-ATPase as a major component in the raft fraction prepared from the synaptic plasma membrane and the synaptic vesicle of rat brain. *Neurosci Lett*. (2004) 363:168–72. doi: 10.1016/j.neulet.2004.04.002
142. Hendrix A, Sormunen R, Westbroek W, Lambein K, Denys H, Sys G, et al. Vacuolar H+ ATPase expression and activity is required for Rab27B-dependent invasive growth and metastasis of breast cancer. *Int J Cancer*. (2013) 133:843–54. doi: 10.1002/ijc.28079
143. Martins BX, Arruda RF, Costa GA, Jerdy H, de Souza SB, Santos JM, et al. Myrtenal-induced V-ATPase inhibition - A toxicity mechanism behind tumor cell death and suppressed migration and invasion in melanoma. *Biochim Biophys Acta*. (2019) 1863:1–12. doi: 10.1016/j.bbagen.2018.09.006
144. Rofstad EK, Mathiesen B, Kindem K, Galappathi K. Acidic extracellular pH promotes experimental metastasis of human melanoma cells in athymic nude mice. *Cancer Res*. (2006) 66:6699–707. doi: 10.1158/0008-5472.CAN-06-0983
145. Jour G, Ivan D, Aung PP. Angiogenesis in melanoma: an update with a focus on current targeted therapies. *J Clin Pathol*. (2016) 69:472–83. doi: 10.1136/jclinpath-2015-203482
146. Peppicelli S, Bianchini F, Contena C, Tombaccini D, Calorini L. Acidic pH via NF-κB favours VEGF-C expression in human melanoma cells. *Clin Exp Metastasis*. (2013) 30:957–67. doi: 10.1007/s10585-013-9595-4
147. De Toro J, Herschlik L, Waldner C, Mongini C. Emerging roles of exosomes in normal and pathological conditions: new insights for diagnosis and therapeutic applications. *Front Immunol*. (2015) 6:203. doi: 10.3389/fimmu.2015.00203
148. Qin X, Xu H, Gong W, Deng W. The tumor cytosol miRNAs, fluid miRNAs and exosome miRNAs in lung cancer. *Front Oncol*. (2014) 4:357. doi: 10.3389/fonc.2014.00357
149. Kahlert C. Exosomes in tumor microenvironment influence cancer progression and metastasis. *J Mol Med*. (2014) 91:431–7. doi: 10.1007/s00109-013-1020-6
150. Boussadia Z, Lamberti J, Mattei F, Pizzi E, Puglisi R, Zanetti C, et al. Acidic microenvironment plays a key role in human melanoma progression through a sustained exosome mediated transfer of clinically relevant metastatic molecules. *J Exp Clin Cancer Res*. (2018) 37:245. doi: 10.1186/s13046-018-0915-z
151. La Shu S, Yang Y, Allen CL, Maguire O, Minderman H, Sen A, et al. Metabolic reprogramming of stromal fibroblasts by melanoma exosome microRNA favours a pre-metastatic microenvironment. *Sci Rep*. (2018) 12:12905. doi: 10.1038/s41598-018-31323-7
152. Feichtinger RG, Lang R. Targeting L-Lactate metabolism to overcome resistance to immune therapy of melanoma and other tumor entities. *J Oncol*. (2019) 2019:2084195. doi: 10.1155/2019/2084195
153. Fischer K, Hoffmann P, Voelkl S, Meidenbauer N, Ammer J, Edinger M, et al. Inhibitory effect of tumor cell-derived lactic acid on human T cells. *Blood*. (2007) 109:3812–9. doi: 10.1182/blood-2006-07-035972
154. Brand A, Singer K, Koehl GE, Kolitzus M, Schoenhammer G, Thiel A, et al. LDHA-associated lactic acid production blunts tumor immunosurveillance by T and NK cells. *Cell Metab*. (2016) 24:657–71. doi: 10.1016/j.cmet.2016.08.011
155. Colegio OR, Chu NQ, Szabo AL, Chu T, Rhebergen AM, Jairam V, et al. Functional polarization of tumour-associated macrophages by tumour-derived lactic acid. *Nature*. (2014) 513:559–63. doi: 10.1038/nature13490

156. Doherty JR, Cleveland JL. Targeting lactate metabolism for cancer therapeutics. *J Clin Invest*. (2013) 123:3685–92. doi: 10.1172/JCI69741
157. Brummer C, Faerber S, Bruss C, Blank C, Lacroix R, Haferkamp S, et al. Metabolic targeting synergizes with MAPK inhibition and delays drug resistance in melanoma. *Cancer Lett*. (2019) 442:453–63. doi: 10.1016/j.canlet.2018.11.018
158. Albano F, Arcucci A, Granato G, Romano S, Montagnani S, De Vendittis E, et al. Markers of mitochondrial dysfunction during the diclofenac-induced apoptosis in melanoma cell lines. *Biochimie*. (2013) 95:934–45. doi: 10.1016/j.biochi.2012.12.012
159. Gottfried E, Lang SA, Renner K, Bosserhoff A, Gronwald W, Rehli M, et al. New aspects of an old drug - diclofenac targets MYC and glucose metabolism in tumor cells. *PLoS ONE*. (2013) 8:e6698. doi: 10.1371/journal.pone.0066987
160. Postovit LM, Seftor EA, Seftor REB, Hendrix MJC. Influence of the microenvironment on melanoma cell fate determination and phenotype. *Cancer Res*. (2006) 66:7833–6. doi: 10.1158/0008-5472.CAN-06-0731
161. Ruiter D, Bogenrieder T, Elder D, Herlyn M. Melanoma-stroma interactions: structural and functional aspects. *Lancet Oncol*. (2002) 3:35–43. doi: 10.1016/S1470-2045(01)00620-9
162. Shiga K, Hara M, Nagasaki T, Sato T, Takahashi H, Takeyama H. Cancer-associated fibroblasts: Their characteristics and their roles in tumor growth. *Cancers*. (2015) 7:2443–58. doi: 10.3390/cancers7040902
163. Dror S, Sander L, Schwartz H, Sheinboim D, Barzilai A, Dishon Y, et al. Melanoma miRNA trafficking controls tumour primary niche formation. *Nat Cell Biol*. (2016) 18:1006–17. doi: 10.1038/ncb3399
164. Alkasalias T, Moyano-Galceran L, Arsenian-Henriksson M, Lehti K. Fibroblasts in the tumor microenvironment: shield or spear? *Int J Mol Sci*. (2018) 19:1532. doi: 10.3390/ijms19051532
165. Avagliano A, Ruocco MR, Nasso R, Aliotta F, Sanità G, Iaccarino A, et al. Development of a stromal microenvironment experimental model containing proto-myofibroblast like cells and analysis of its crosstalk with melanoma cells: a new tool to potentiate and stabilize tumor suppressor phenotype of dermal myofibroblasts. *Cells*. (2019) 8:1435. doi: 10.3390/cells8111435
166. Andrlová H, Mastroianni J, Madl J, Kern JS, Melchinger W, Dierbach H, et al. Biglycan expression in the melanoma microenvironment promotes invasiveness via increased tissue stiffness inducing integrin-β1 expression. *Oncotarget*. (2017) 8:42901–16. doi: 10.18632/oncotarget.17160
167. Hutchenreuther J, Leask A. *Why Target the Tumor Stroma in Melanoma?* Netherlands: Springer (2018).
168. Zhou L, Yang K, Andl T, Wickett RR, Zhang Y, Randall Wickett R, et al. Perspective of targeting cancer-associated fibroblasts in melanoma. *J Cancer*. (2015) 6:717–26. doi: 10.7150/jca.10865
169. Zhou L, Yang K, Randall Wickett R, Zhang Y. Dermal fibroblasts induce cell cycle arrest and block epithelial–mesenchymal transition to inhibit the early stage melanoma development. *Cancer Med*. (2016) 5:1566–79. doi: 10.1002/cam4.707
170. Guan X, LaPak KM, Hennessey RC, Yu CY, Shakya R, Zhang J, et al. Stromal senescence by prolonged CDK4/6 inhibition potentiates tumor growth. *Mol Cancer Res*. (2017) 15:237–49. doi: 10.1158/1541-7786.MCR-16-0319
171. Li G, Satyamoorthy K, Meier F, Berking C, Bogenrieder T, Herlyn M. Function and regulation of melanoma-stromal fibroblast interactions: when seeds meet soil. *Oncogene*. (2003) 22:3162–71. doi: 10.1038/sj.onc.1206455
172. Brandner JM, Haass NK. Melanoma's connections to the tumour microenvironment. *Pathology*. (2013) 45:443–52. doi: 10.1097/PAT.0b013e328363b3bd
173. Aasen T, Mesnil M, Naus CC, Lampe PD, Laird DW. Gap junctions and cancer: communicating for 50 years. *Nat Rev Cancer*. (2016) 16:775–88. doi: 10.1038/nrc.2016.105
174. Bonacquisti EE, Nguyen J. Connexin 43 (Cx43) in cancer: implications for therapeutic approaches via gap junctions. *Cancer Lett*. (2019) 442:439–44. doi: 10.1016/j.canlet.2018.10.043
175. Song D, Liu X, Liu R, Yang L, Zuo J, Liu W. Connexin 43 hemichannel regulates H9c2 cell proliferation by modulating intracellular ATP and [Ca2+]. *Acta Biochim Biophys Sin*. (2010) 42:472–82. doi: 10.1093/abbs/gmq047
176. Tittarelli A, Guerrero I, Tempio F, Gleisner MA, Avalos I, Sabanegh S, et al. Overexpression of connexin 43 reduces melanoma proliferative and metastatic capacity. *Br J Cancer*. (2015) 113:259–67. doi: 10.1038/bjc.2015.162
177. Li Z, Zhang J, Zhou J, Lu L, Wang H, Zhang G, et al. Nodal facilitates differentiation of fibroblasts to cancer-associated fibroblasts that support tumor growth in melanoma and colorectal cancer. *Cells*. (2019) 8:538. doi: 10.3390/cells8060538
178. Wittgen HGM, Van Kempen LCLT. Reactive oxygen species in melanoma and its therapeutic implications. *Melanoma Res*. (2007) 17:400–9. doi: 10.1097/CMR.0b013e3282f1d312
179. Obrador E, Liu-Smith F, Dellinger RW, Salvador R, Meyskens FL, Estrela JM. Oxidative stress and antioxidants in the pathophysiology of malignant melanoma. *Biol Chem*. (2019) 400:589–612. doi: 10.1515/hsz-2018-0327
180. Jenkins NC, Grossman D. Role of melanin in melanocyte dysregulation of reactive oxygen species. *Biomed Res Int*. (2013) 2013:908797. doi: 10.1155/2013/908797
181. Karg E, Odh G, Wittbjer A, Rosengren E, Rorsman H. Hydrogen peroxide as an inducer of elevated tyrosinase level in melanoma cells. *J Invest Dermatol*. (1993) 100(2 Suppl.):209S−13S. doi: 10.1111/1523-1747.ep12465218
182. Arcucci A, Ruocco MR, Albano F, Granato G, Romano V, Corso G, et al. Analysis of extracellular superoxide dismutase and Akt in ascending aortic aneurysm with tricuspid or bicuspid aortic valve. *Eur J Histochem*. (2014) 58:200–6. doi: 10.4081/ejh.2014.2383
183. Arcucci A, Ruocco MR, Amatruda N, Riccio A, Tarantino G, Albano F, et al. Analysis of extracellular superoxide dismutase in fibroblasts from patients with systemic sclerosis. *J Biol Regul Homeost Agents*. (2014) 25:647–54.
184. Yamanishi DT, Buckmeier JA, Meyskens FL. Expression of c-jun, jun-B, and c-fos proto-oncogenes in human primary melanocytes and metastatic melanomas. *J Invest Dermatol*. (1991) 97:349–53. doi: 10.1111/1523-1747.ep12480698
185. Meyskens FL, McNulty SE, Buckmeier JA, Tohidian NB, Spillane TJ, Kahlon RS, et al. Aberrant redox regulation in human metastatic melanoma cells compared to normal melanocytes. *Free Radic Biol Med*. (2001) 31:799–808. doi: 10.1016/S0891-5849(01)00650-5
186. Sander CS, Chang H, Hamm F, Elsner P, Thiele JJ. Role of oxidative stress and the antioxidant network in cutaneous carcinogenesis. *Int J Dermatol*. (2004) 43:326–35. doi: 10.1111/j.1365-4632.2004.02222.x
187. Liu F, Gomez Garcia AM, Meyskens FL. NADPH oxidase 1 overexpression enhances invasion via matrix metalloproteinase-2 and epithelial-mesenchymal transition in melanoma cells. *J Invest Dermatol*. (2012) 132:2033–41. doi: 10.1038/jid.2012.119
188. Denat L, Kadekaro AL, Marrot L, Leachman SA, Abdel-Malek ZA. Melanocytes as instigators and victims of oxidative stress. *J Invest Dermatol*. (2014) 134:1512–8. doi: 10.1038/jid.2014.65
189. Yamaura M, Mitsushita J, Furuta S, Kiniwa Y, Ashida A, Goto Y, et al. NADPH oxidase 4 contributes to transformation phenotype of melanoma cells by regulating G 2 -M cell cycle progression. *Cancer Res*. (2009) 69:2647–54. doi: 10.1158/0008-5472.CAN-08-3745
190. Ribeiro-Pereira C, Moraes JA, De Jesus Souza M, Laurindo FR, Arruda MA, Barja-Fidalgo C. Redox modulation of FAK controls melanoma survival - Role of NOX4. *PLoS ONE*. (2014) 9:e99481. doi: 10.1371/journal.pone.0099481
191. Capparelli C, Guido C, Whitaker-Menezes D, Bonuccelli G, Balliet R, Pestell TG, et al. Autophagy and senescence in cancer-associated fibroblasts metabolically supports tumor growth and metastasis, via glycolysis and ketone production. *Cell Cycle*. (2012) 11:2285–302. doi: 10.4161/cc.20718
192. Salem AF, Whitaker-Menezes D, Lin Z, Martinez-Outschoorn UE, Tanowitz HB, Al-Zoubi MS, et al. Two-compartment tumor metabolism: autophagy in the tumor microenvironment, and oxidative mitochondrial metabolism (OXPHOS) in cancer cells. *Cell Cycle*. (2012) 11:2545–56. doi: 10.4161/cc.20920
193. Wu KN, Queenan M, Brody JR, Potoczek M, Sotgia F, Lisanti MP, et al. Loss of stromal caveolin-1 expression in malignant melanoma metastases predicts poor survival. *Cell Cycle*. (2011) 10:4250–5. doi: 10.4161/cc.10.24.18551
194. Zhang D, Wang Y, Shi Z, Liu J, Sun P, Hou X, et al. Metabolic reprogramming of cancer-associated fibroblasts by IDH3α downregulation. *Cell Rep*. (2015) 10:1335–48. doi: 10.1016/j.celrep.2015.02.006

195. Tan AS, Baty JW, Dong LF, Bezawork-Geleta A, Endaya B, Goodwin J, et al. Mitochondrial genome acquisition restores respiratory function and tumorigenic potential of cancer cells without mitochondrial DNA. *Cell Metab*. (2015) 21:81–94. doi: 10.1016/j.cmet.2014.12.003
196. Dong LF, Kovarova J, Bajzikova M, Bezawork-Geleta A, Svec D, Endaya B, et al. Horizontal transfer of whole mitochondria restores tumorigenic potential in mitochondrial DNA-deficient cancer cells. *Elife*. (2017) 6:e22187. doi: 10.7554/eLife.22187
197. Zhang M, Di Martino JS, Bowman RL, Campbell NR, Baksh SC, Simon-Vermot T, et al. Adipocyte-derived lipids mediate melanoma progression via FATP proteins. *Cancer Discov*. (2018) 8:1006–25. doi: 10.1158/2159-8290.CD-17-1371
198. Dirat B, Bochet L, Dabek M, Daviaud D, Dauvillier S, Majed B, et al. Cancer-associated adipocytes exhibit an activated phenotype and contribute to breast cancer invasion. *Cancer Res*. (2011) 71:2455–65. doi: 10.1158/0008-5472.CAN-10-3323
199. Muller C, Nieto L, Valet P. Unraveling the local influence of tumor-surrounding adipose tissue on tumor progression: cellular and molecular actors involved. In: Kolonin M, editor. *Adipose Tissue and Cancer*. New York, NY: Springer (2013) p. 121–46. doi: 10.1007/978-1-4614-7660-3_7
200. Lazar I, Clement E, Dauvillier S, Milhas D, Ducoux-Petit M, LeGonidec S, et al. Adipocyte exosomes promote melanoma aggressiveness through fatty acid oxidation: a novel mechanism linking obesity and cancer. *Cancer Res*. (2016) 76:4051–7. doi: 10.1158/0008-5472.CAN-16-0651
201. Lim S, Phillips JB, Da Silva LM, Zhou M, Fodstad O, Owen LB, et al. Interplay between immune checkpoint proteins and cellular metabolism. *Cancer Res*. (2017) 77:1245–9. doi: 10.1158/0008-5472.CAN-16-1647
202. Marzagalli M, Ebelt ND, Manuel ER. Unraveling the crosstalk between melanoma and immune cells in the tumor microenvironment. *Semin Cancer Biol*. (2019) 59:236–50. doi: 10.1016/j.semcancer.2019.08.002
203. Lacroix R, Rozeman EA, Kreutz M, Renner K, Blank CU. Targeting tumor-associated acidity in cancer immunotherapy. *Cancer Immunol Immunother*. (2018) 67:1331–48. doi: 10.1007/s00262-018-2195-z
204. Peske JD, Woods AB, Engelhard VH. Control of CD8 T-cell infiltration into tumors by vasculature and microenvironment. *Adv Cancer Res*. 128:263–307. doi: 10.1016/bs.acr.2015.05.001
205. Albano F, Vecchio E, Renna M, Iaccino E, Mimmi S, Caiazza C, et al. Insights into thymus development and viral thymic infections. *Viruses*. (2019) 11:836. doi: 10.3390/v11090836
206. Ho PC, Bihuniak JD, MacIntyre AN, Staron M, Liu X, Amezquita R, et al. Phosphoenolpyruvate is a metabolic checkpoint of anti-tumor T cell responses. *Cell*. (2015) 162:1217–28. doi: 10.1016/j.cell.2015.08.012
207. Zhang Y, Kurupati R, Liu L, Zhou XY, Zhang G, Hudaihed A, et al. Enhancing CD8+ T cell fatty acid catabolism within a metabolically challenging tumor microenvironment increases the efficacy of melanoma immunotherapy. *Cancer Cell*. (2017) 32:377–91.e9. doi: 10.1016/j.ccell.2017.08.004
208. Chamoto K, Chowdhury PS, Kumar A, Sonomura K, Matsuda F, Fagarasan S, et al. Mitochondrial activation chemicals synergize with surface receptor PD-1 blockade for T cell-dependent antitumor activity. *Proc Natl Acad Sci USA*. (2017) 114:E761–70. doi: 10.1073/pnas.1620433114
209. Mendler AN, Hu B, Prinz PU, Kreutz M, Gottfried E, Noessner E. Tumor lactic acidosis suppresses CTL function by inhibition of p38 and JNK/c-Jun activation. *Int J Cancer*. (2012) 131:633–40. doi: 10.1002/ijc.26410
210. Nakagawa Y, Negishi Y, Shimizu M, Takahashi M, Ichikawa M, Takahashi H. Effects of extracellular pH and hypoxia on the function and development of antigen-specific cytotoxic T lymphocytes. *Immunol Lett*. (2015) 167:72–86. doi: 10.1016/j.imlet.2015.07.003
211. Pilon-Thomas S, Kodumudi KN, El-Kenawi AE, Russell S, Weber AM, Luddy K, et al. Neutralization of tumor acidity improves antitumor responses to immunotherapy. *Cancer Res*. (2016) 76:1381–90. doi: 10.1158/0008-5472.CAN-15-1743
212. Yoon JK, Frankel AE, Feun LG, Ekmekcioglu S, Kim KB. Arginine deprivation therapy for malignant melanoma. *Clin Pharmacol Adv Appl*. (2012) 5:11–9. doi: 10.2147/CPAA.S37350
213. Delage B, Fennell DA, Nicholson L, McNeish I, Lemoine NR, Crook T, et al. Arginine deprivation and argininosuccinate synthetase expression in the treatment of cancer. *Int J Cancer*. (2010) 126:2762–72. doi: 10.1002/ijc.25202
214. Yarlagadda K, Hassani J, Foote IP, Markowitz J. The role of nitric oxide in melanoma. *Biochim Biophys Acta Rev Cancer*. (2017) 1868:500–9. doi: 10.1016/j.bbcan.2017.09.005
215. Kim SH, Roszik J, Grimm EA, Ekmekcioglu S. Impact of l-arginine metabolism on immune response and anticancer immunotherapy. *Front Oncol*. (2018) 8:67. doi: 10.3389/fonc.2018.00067
216. Ekmekcioglu S, Ellerhorst JA, Prieto VG, Johnson MM, Broemeling LD, Grimm EA. Tumor iNOS predicts poor survival for stage III melanoma patients. *Int J Cancer*. (2006) 119:861–6. doi: 10.1002/ijc.21767
217. Serasinghe MN, Wieder SY, Renault TT, Elkholi R, Asciolla JJ, Yao JL, et al. Mitochondrial division is requisite to RAS-induced transformation and targeted by oncogenic MAPK pathway inhibitors. *Mol Cell*. (2015) 57:521–36. doi: 10.1016/j.molcel.2015.01.003
218. Smith LK, Rao AD, McArthur GA. Targeting metabolic reprogramming as a potential therapeutic strategy in melanoma. *Pharmacol Res*. (2016) 107:42–7. doi: 10.1016/j.phrs.2016.02.009
219. Figarola JL, Singhal J, Singhal S, Kusari J, Riggs A. Bioenergetic modulation with the mitochondria uncouplers SR4 and niclosamide prevents proliferation and growth of treatment-naïve and vemurafenib-resistant melanomas. *Oncotarget*. (2018) 9:36945–65. doi: 10.18632/oncotarget.26421
220. Audrito V, Managò A, Gaudino F, Deaglio S. Targeting metabolic reprogramming in metastatic melanoma: the key role of nicotinamide phosphoribosyltransferase (NAMPT). *Semin Cell Dev Biol*. (2019) 98:192–201. doi: 10.1016/j.semcdb.2019.05.001
221. Corazao-Rozas P, Guerreschi P, André F, Gabert PE, Lancel S, Dekiouk S, et al. Mitochondrial oxidative phosphorylation controls cancer cell's life and death decisions upon exposure to MAPK inhibitors. *Oncotarget*. (2016) 7:39473–85. doi: 10.18632/oncotarget.7790
222. Yuan P, Ito K, Perez-Lorenzo R, Del Guzzo C, Lee JH, Shen CH, et al. Phenformin enhances the therapeutic benefit of BRAFV600E inhibition in melanoma. *Proc Natl Acad Sci USA*. (2013) 110:18226–31. doi: 10.1073/pnas.1317577110
223. Schöckel L, Glasauer A, Basit F, Bitschar K, Truong H, Erdmann G, et al. Targeting mitochondrial complex I using BAY 87-2243 reduces melanoma tumor growth. *Cancer Metab*. (2015) 3:11. doi: 10.1186/s40170-015-0138-0
224. Carpenter EL, Chagani S, Nelson D, Cassidy PB, Laws M, Ganguli-Indra G, et al. Mitochondrial complex I inhibitor deguelin induces metabolic reprogramming and sensitizes vemurafenib-resistant BRAFV600E mutation bearing metastatic melanoma cells. *Mol Carcinog*. (2019) 58:1680–90. doi: 10.1002/mc.23068
225. Petti C, Vegetti C, Molla A, Bersani I, Cleris L, Mustard KJ, et al. AMPK activators inhibit the proliferation of human melanomas bearing the activated MAPK pathway. *Melanoma Res*. (2012) 22:341–50. doi: 10.1097/CMR.0b013e3283544929
226. Woodard J, Platanias LC. AMP-activated kinase (AMPK)-generated signals in malignant melanoma cell growth and survival. *Biochem Biophys Res Commun*. (2010) 398:135–9. doi: 10.1016/j.bbrc.2010.06.052
227. Chen L, Chen Q, Deng G, Kuang S, Lian J, Wang M, et al. AMPK activation by GSK621 inhibits human melanoma cells *in vitro* and *in vivo*. *Biochem Biophys Res Commun*. (2016) 480:515–21. doi: 10.1016/j.bbrc.2016.10.040
228. Serasinghe MN, Gelles JD, Li K, Zhao L, Abbate F, Syku M, et al. Dual suppression of inner and outer mitochondrial membrane functions augments apoptotic responses to oncogenic MAPK inhibition. *Cell Death Dis*. (2018) 9:29. doi: 10.1038/s41419-017-0044-1
229. Luo C, Balsa E, Thomas A, Hatting M, Jedrychowski M, Gygi SP, et al. ERRα maintains mitochondrial oxidative metabolism and constitutes an actionable target in PGC1α-elevated melanomas. *Mol Cancer Res*. (2017) 15:1366–75. doi: 10.1158/1541-7786.MCR-17-0143
230. Lim JH, Luo C, Vazquez F, Puigserver P. Targeting mitochondrial oxidative metabolism in melanoma causes metabolic compensation through glucose and glutamine utilization. *Cancer Res*. (2014) 74:3535–45. doi: 10.1158/0008-5472.CAN-13-2893-T
231. Luo C, Lim JH, Lee Y, Granter SR, Thomas A, Vazquez F, et al. A PGC1α-mediated transcriptional axis suppresses melanoma metastasis. *Nature*. (2016) 537:422–6. doi: 10.1038/nature19347
232. Wu LW, Zhang G, Herlyn M. Mitochondrial biogenesis meets chemoresistance in BRAF-mutant melanoma. *Mol Cell Oncol*. (2016) 3:e1179381. doi: 10.1080/23723556.2016.1179381

233. Karpel-Massler G, Ishida CT, Bianchetti E, Shu C, Perez-Lorenzo R, Horst B, et al. Inhibition of mitochondrial matrix chaperones and antiapoptotic Bcl-2 family proteins empower antitumor therapeutic responses. *Cancer Res*. (2017) 77:3513–26. doi: 10.1158/0008-5472.CAN-16-3424
234. Kumari V, Dyba MA, Holland RJ, Liang YH, Singh SV, Ji X. Irreversible inhibition of glutathione S-transferase by phenethyl isothiocyanate (PEITC), a dietary cancer chemopreventive phytochemical. *PLoS ONE*. (2016) 11:e0163821. doi: 10.1371/journal.pone.0163821
235. Khamari R, Trinh A, Gabert PE, Corazao-Rozas P, Riveros-Cruz S, Balayssac S, et al. Glucose metabolism and NRF2 coordinate the antioxidant response in melanoma resistant to MAPK inhibitors. *Cell Death Dis*. (2018) 9:325. doi: 10.1038/s41419-018-0340-4
236. Ketterer B, Coles B, Meyer DJ. The role of glutathione in detoxication. *Environ Health Perspect*. (1983) 49:59. doi: 10.1289/ehp.834959
237. Chen G, Chen Z, Hu Y, Huang P. Inhibition of mitochondrial respiration and rapid depletion of mitochondrial glutathione by β-phenethyl isothiocyanate: mechanisms for anti-leukemia activity. *Antioxidants Redox Signal*. (2011) 15:2911–21. doi: 10.1089/ars.2011.4170
238. Lim JKM, Delaidelli A, Minaker SW, Zhang HF, Colovic M, Yang H, et al. Cystine/glutamate antiporter xCT (SLC7A11) facilitates oncogenic RAS transformation by preserving intracellular redox balance. *Proc Natl Acad Sci USA*. (2019) 116:9433–42. doi: 10.1073/pnas.1821323116
239. Wang L, Leite de Oliveira R, Huijberts S, Bosdriesz E, Pencheva N, Brunen D, et al. An acquired vulnerability of drug-resistant melanoma with therapeutic potential. *Cell*. (2018) 173:1413–25.e14. doi: 10.1016/j.cell.2018.04.012
240. Yuan L, Mishra R, Patel H, Abdulsalam S, Greis KD, Kadekaro AL, et al. Utilization of reactive oxygen species targeted therapy to prolong the efficacy of braf inhibitors in melanoma. *J Cancer*. (2018) 9:4665–76. doi: 10.7150/jca.27295
241. Baenke F, Chaneton B, Smith M, Van Den Broek N, Hogan K, Tang H, et al. Resistance to BRAF inhibitors induces glutamine dependency in melanoma cells. *Mol Oncol*. (2016) 10:73–84. doi: 10.1016/j.molonc.2015.08.003
242. Wang Q, Beaumont KA, Otte NJ, Font J, Bailey CG, Van Geldermalsen M, et al. Targeting glutamine transport to suppress melanoma cell growth. *Int J Cancer*. (2014) 135:1060–71. doi: 10.1002/ijc.28749
243. Audrito V, Managò A, La Vecchia S, Zamporlini F, Vitale N, Baroni G, et al. Nicotinamide phosphoribosyltransferase (NAMPT) as a therapeutic target in BRAF-mutated metastatic melanoma. *J Natl Cancer Inst*. (2018) 110. doi: 10.1093/jnci/djx198

Conflict of Interest: The authors declare that the research was conducted in the absence of any commercial or financial relationships that could be construed as a potential conflict of interest.

frontiers in Oncology

ORIGINAL RESEARCH
published: 12 June 2020
doi: 10.3389/fonc.2020.00807

Lactic Acidosis in the Presence of Glucose Diminishes Warburg Effect in Lung Adenocarcinoma Cells

Heriberto Prado-Garcia†, Andrea Campa-Higareda and Susana Romero-Garcia†*

Department of Chronic-Degenerative Diseases, National Institute of Respiratory Diseases "Ismael Cosío Villegas", Mexico City, Mexico

Lactic acidosis (3 to 40 mM, pH < 6.9) is a condition found in solid tumors because tumor cells have a high rate of glucose consumption and lactate production even in the presence of oxygen; nevertheless, the microenvironment might still provide a sufficient glucose supply. Lactic acidosis has been proposed to shift metabolism from aerobic glycolysis toward oxidative phosphorylation (OXPHOS). We tested if lung tumor cells cultured under lactic acidosis shift their metabolism from glycolysis to OXPHOS by consuming extracellular lactate, increasing growth rate. We analyzed lung adenocarcinoma (A-549, A-427) cell lines and non-transformed fibroblast cells (MRC-5), which were cultured using RPMI-1640 medium initially containing lactate (2 mM) and glucose (10 mM), at pH 7.2 or 6.2 and oxygen tension 21% O_2 (normoxia) or 2% O_2 (hypoxia). We obtained growth curves, as well as glucose consumption and lactate production rates (measured during exponential growth) for each cell line. HIF-1α (Hypoxia-inducible factor 1 α), CS (citrate synthase) and AMPK (AMP-activated protein kinase) transcript levels were analyzed using RT-qPCR. By flow cytometry, we determined: (a) expression of glucose transporters (GLUT)1 and 4; (b) lactate transporters (MCT)1 and 4; (c) cell cycle profile, and (d) protein levels of HIF-1α, total and phosphorylated AMPK (pAMPK). Mitochondrial functionality was evaluated by measuring O_2 consumption in tumor cells using polarography and a Clark-type electrode. Tumor and non-transformed cells used both aerobic glycolysis and OXPHOS for obtaining energy. As of 48 h of culture, lactate levels ranged from (4.5–14 mM), thus forming a lactic environment. Lactic acidosis diminished GLUT1/GLUT4 expression and glucose consumption in A-549, but not in A-427 cells, and induced differential expression of HIF-1α, AMPK, and CS transcripts. A-427 cells increased pAMPK and HIF-1α levels and shifted their metabolism increasing OXPHOS; thus supporting cell growth. Conversely, A-549 cells increased HIF-1α protein levels, but did not activate AMPK and diminished OXPHOS. A-549 cells survived by arresting cells in G1-phase. Our findings show that lactic acidosis diminishes Warburg effect in tumor cells, but this change does not necessarily promote a shift to OXPHOS. Hence, lung adenocarcinomas show a differential metabolic response even when they are under the same microenvironmental conditions.

Keywords: tumor metabolic shift, tumor metabolic symbiosis, mitochondrial function, aerobic glycolysis, oxidative metabolism

OPEN ACCESS

Edited by:
Tuuli Käämbre, National Institute of Chemical Physics and Biophysics, Estonia

Reviewed by:
Jianrong Lu, University of Florida, United States
Maria Letizia Taddei, University of Florence, Italy

****Correspondence:***
Susana Romero-Garcia
sugar_cia@yahoo.com

†ORCID:
Heriberto Prado-Garcia
orcid.org/0000-0002-4932-3244
Susana Romero-Garcia
orcid.org/0000-0003-4539-0578

Specialty section:
This article was submitted to Cancer Metabolism, a section of the journal Frontiers in Oncology

Received: *31 January 2020*
Accepted: *24 April 2020*
Published: *12 June 2020*

Citation:
Prado-Garcia H, Campa-Higareda A and Romero-Garcia S (2020) Lactic Acidosis in the Presence of Glucose Diminishes Warburg Effect in Lung Adenocarcinoma Cells. Front. Oncol. 10:807. doi: 10.3389/fonc.2020.00807

INTRODUCTION

In solid tumors, lactate concentrations range from 3 to 40 mM and, intratumoral pH can be as low as 6.0 (1). Also, intratumoral glucose levels are estimated in a proportion of 1:40 with respect to plasma levels; thus, lactic acidosis along with glucose availability is a condition that can be found in the tumor microenvironment (2). This condition is the result of metabolic reprogramming, where tumor cells increase glycolysis and produce lactate from pyruvate even under oxygen availability (Warburg effect). Lactate can be also produced from the metabolism of glutamine through glutaminolysis (3). Lactate can be exported out of the cell using the monocarboxylate-4 transporter (MCT4), while MCT1 can facilitate both its import and export depending on the pH gradient (4, 5).

It has been reported that lactic acidosis has a key role in malignant development through different mechanisms (6–8). One of such mechanisms is through supporting the metabolic shift; for instance, breast tumor cells (4T1 cells) under lactic acidosis diminish aerobic glycolysis and show a non-glycolytic phenotype, characterized by a high oxygen consumption rate. In contrast, in the absence of lactic acidosis, 4T1 tumor cells exhibit a high glycolytic rate (Warburg effect) (6). Another report indicates that different tumor cell lines are able to revert from Warburg effect into OXPHOS when they are exposed to lactic acidosis (20 mM and pH 6.7) (7). In this report, the metabolic shift was proved by determining the quantity of ATP produced by tumor cells using both pathways: glycolysis and OXPHOS. While under lactic acidosis, glycolysis and OXPHOS provide 13.4–5.7% and 86.6–94.3 of total ATP, respectively; without lactic acidosis, glycolysis and OXPHOS generate 52.2–23.7% and 47.8–76.3%, respectively (7). But some questions remain such as which is the carbon source that tumor cells use under lactic acidosis in the presence of glucose? And how does this shift affect tumor growth?

Interestingly, this metabolic shift from aerobic glycolysis to OXPHOS in the presence of lactic acidosis should be supporting tumor metabolic symbiosis. In this phenomenon, tumor cells localized in the vicinity of blood vessels shift their metabolism toward a more oxidative metabolism and use lactate for feeding Krebs cycle in spite of the presence of glucose. This behavior allows tumor cells localized away from blood vessels to have access to glucose and produce lactate (9). When tumor metabolic symbiosis was described in breast cancer, it was shown that normoxic cells expressed MCT1 to import lactate and perform OXPHOS, and the amount of glucose uptake was lower in MCT1-positive cells than in hypoxic MCT4-positive cells that consumed more glucose and produced lactate (10). In this context, the expression of glucose and lactate transporters in tumor cells under lactic acidosis becomes crucial in the tumor metabolic symbiosis. It has been reported that glucose transporter (GLUT1) expression is upregulated in tumor cells under hypoxia but lactic acidosis suppresses the hypoxic induction of the transporter (11). GLUT4 can be expressed in insulin-sensitive tissues, fat and muscle, GLUT4 can also be found in 6.6% of lung carcinomas, whereas GLUT1 is expressed in 74% of lung-carcinomas samples (12). Nonetheless, there are no reports that show how expression levels of GLUT4 are regulated in tumor cells cultured under lactic acidosis. Regarding lactate transporters, tumors that exhibit graded metabolic heterogeneity contain cells expressing both MCT1 and MCT4 transports. In contrast, tumors expressing high levels of MCT4 do not favor metabolic symbiosis (10). However, the relation of the MCT1 and MCT4 expression on tumor cells and lactic acidosis in the microenvironment remains unclear.

Adenosine monophosphate-activated protein kinase (AMPK) regulates energy metabolism, but its participation in tumor metabolism remains uncertain. Yan et al. showed that loss of tumor suppressor folliculin (FLCN) induces the constitutive activation of AMPK, which results in peroxisome proliferator-activated receptor gamma coactivator 1-alpha (PGC-1α)-mediated mitochondrial biogenesis and increased ROS production. ROS induces hypoxia-inducible factor (HIF) transcriptional activity, driving the Warburg metabolic reprogramming. Thus, HIF can be indirectly activated by AMPK (13). Additionally, AMPK enhances glycolysis and glycolytic rate by directly phosphorylating 6-phosphofructo-2-kinase (PFK2) in H1299 tumor cells grown under glucose-limiting conditions (14). Conversely, inactivation of AMPK has been shown to increase HIF-1α expression, which in turn increases aerobic glycolysis and cellular biosynthesis in tumor cells. Thus, AMPK may be a negative regulator of the Warburg effect and suppresses tumor growth *in vivo* (15). Besides of hypoxia or AMPK inactivation, an acidic extracellular space also leads to the formation of a pseudo-hypoxic condition by increasing HIF function. Acidosis acts through HSP90, in a PHD/VHL-independent manner, to promote HIF function and maintenance of tumor stem cells in glioma (16, 17).

We hypothesized that if lung adenocarcinoma cells are in the presence of lactic acidosis with glucose availability, then tumor cells will perform the metabolic shift from aerobic glycolysis to OXPHOS, supported by AMPK activation.

MATERIALS AND METHODS

Cell Lines

Three human tumor cell lines were used in this study. We included A-549 and A-427 cell lines, because they belong to the histological type of lung adenocarcinoma, which is the most prevalent subtype of lung carcinomas. MCF-7 cell line is a breast cancer cell line, it was included because it has been shown that can consume lactate in the absence of glucose (18). MRC-5 fibroblasts were included as control because they are proliferative non-transformed cells. All cell lines and fibroblast cells were obtained from the American Type Culture Collection (Manassas, VA, USA).

Growth Curves

We used complete RPMI-1640 medium (Sigma-Aldrich, St. Louis, MO, USA) that contained 2 mM lactate and 10 mM glucose, it was supplemented with 10% heat-inactivated FCS (fetal calf serum, Hyclone, Logan, Utah, USA), 100 U/mL of penicillin and 100 μg/mL of streptomycin. Two 24-well plates were seeded equivalently. One plate was used for normoxic

conditions, while the other was used for hypoxic conditions. A-427, A-549 and MCF-7 cells were seeded at a density of 1×10^5 cells/mL, and 5×10^4 cells/mL were seeded for MRC-5 cells.

Six wells of each plate were seeded with 1 mL of cellular suspension prepared in RPMI-1640 adjusted at pH 7.2. Other six wells of each plate were seeded with 1 mL of a cellular suspension prepared in RPMI-1640 adjusted at pH 6.2 using HCl (37% v/v). Normoxic cells were incubated in a humidified chamber at 37°C with filtered atmospheric air (21% oxygen) and 5% CO_2. Hypoxic cells were incubated at 37°C, in a humidified Billups-Rothenberg chamber (Del Mar, CA, USA) with a gas atmosphere of 2% oxygen, 93% nitrogen, and 5% of CO_2.

Every 8, 12, or 24 h, depending on the cell line and until completing 96 h, cell viability and cellular count were determined with trypan blue dye exclusion using a TC20 Automated Cell Counter (Bio-Rad Laboratories, Inc., USA). All cultures were repeated by triplicate. The specific growth rate (μ) was determined during exponential growth, as previously reported (19).

Annexin V/7-AAD Assay

To determine viability, early apoptosis and necrosis of tumor cells and fibroblast cells, the method of apoptosis determination by Annexin V and 7-AAD was used. After 48 h of incubation, cells were harvested, washed with PBS and resuspended in 100 µL of Annexin V (0.5 µg/mL) (BioLegend, San Diego, CA, USA) in HEPES buffer. After incubation during 15 min, 7-aminoactinomycin D (7-AAD, BioLegend, 0.1 µg/mL) in HEPES buffer was added. Flow cytometry was performed using a Becton Dickinson FACSCanto II flow cytometer. The analysis was done using FlowJo V10 Software (Beckton Dickinson, Ashland, Or, USA).

Cell Cycle Analysis

For cell cycle analysis, 1×10^5 cells/mL of MRC-5, A-549, A-427, and MCF-7 cells were seeded per well in 24-well tissue culture plates. Cells were cultured during 48 h under the different conditions described above. Cells were harvested by trypsinization, washed with PBS, fixed using ethanol 70% v/v and permeabilized using Triton X-100 0.5 % v/v. Then, samples were stained with 7-AAD in the dark at room temperature for 20 min. A total of 25,000 events from 7-AAD-area versus 7-AAD-wide gate were acquired. Cultures and staining were independently performed at least two times.

Determination of Glucose and Lactate

The supernatant from one well of the 24-well plates was removed every 8, 12, or 24 h, depending on the cell line and until completing 96 h. After measuring the volume, cell-free supernatants were stored at −20°C for subsequent analysis. A sample of the initial culture media was stored at −20°C and it was considered the time zero in the metabolites' analysis.

Using membranes that contain immobilized specific enzymes (d-glucose oxidase and l-lactate oxidase; YSI, Ohio, USA) and a YSI 2900 biochemistry analyzer (Yellow Springs Instruments, Ohio, USA), we determined the concentration of glucose and l-lactate in supernatants, as reported in (19). The evaporated volume was used to correct the quantity of each metabolite. Glucose consumption rate ($q_{SGlucose}$) and lactate production rate ($q_{PLactate}$) were calculated in the exponential phase of growth using the following formulas:

$q_{SGlucose} = \mu\ (h^{-1})$ * consumed glucose (µM) /cell number obtained during exponential phase * 1×10^6

$q_{PLactate} = \mu\ (h^{-1})$ * produced lactate (µM) / cell number obtained during exponential phase * 1×10^6

Determination of GLUT1, GLUT4, MCT1 and MCT4 Expression on Cell Membrane

We used flow cytometry for determination of the expression of GLUT1, GLUT4, MCT1, and MCT4 on cancer and fibroblast cells. Cultures were initially seeded with 1×10^5 cells/mL for A-549, A-427, and MCF-7 cell lines, 2×10^5 cells/mL for A-427 and 1.5×10^5 cells/mL for MRC-5 in 24-well plates. After 48 h of incubation, cells were harvested using EDTA-MOPS. Dead cells were excluded by using the Zombie NIR fixable viability kit (BioLegend, San Diego, CA, USA), as previously reported (19). After washing with PBS supplemented with albumin (1% w/v) and sodium azide (0.1% w/v), cells were immunostained with antibodies against GLUT1 (GLUT1-PE, clone 202915) from R&D Systems (Abingdon, UK), GLUT4 (GLUT4-Alexa 647) from Novus Biological (Abingdon, UK), MCT1 (MCT1-Alexa 647), and MCT4 (MCT4-Alexa 488) both from Bioss (Massachusetts, USA) incubating at room temperature for 30 min. Then cells were washed and fixed with paraformaldehyde (1% w/v) for further analysis using a FACS Canto II flow cytometer. At least 10,000 events were acquired from the region of viable cells. The results were analyzed with FlowJo V10 software. The median fluorescence intensity (MFI) values for GLUT1-PE, GLUT4-Alexa 647, MCT1-Alexa 647 and MCT4-Alexa 488 were determined. MFI values for the expression of GLUT1, GLUT4, MCT1 and MCT4 were normalized with respect to the condition of pH 7.2 and normoxia. The results are reported as relative MFI values (rMFI).

Analysis of Mitochondrial Function

Mitochondrial function was evaluated measuring oxygen consumption using a Clark type electrode and the biological oxygen monitor system YSI 5300A (YSI incorporated, Yellow Springs, Ohio, USA). The reaction took place in a chamber with constant temperature of 37°C and constant stirring. The oxygen monitor system was calibrated according manufacturer's instructions.

After 48 h of incubation under the four tested conditions, lung adenocarcinoma cells (A-549 and A-427) were harvested by trypsinization. After a wash with PBS, cells were resuspended to obtain a cellular concentration of 1×10^6 cells in 300 µL of respiration buffer. Respiration buffer contained KCl 120 mM, MgCl•6H2O 10 mM, EDTA 1 mM, $KHPO_4$•$7H_2O$ 8.1 mM, K_2HPO_4 1.46 mM, pH = 7.4 adjusted with KOH 10M. Cellular suspension (300 µL) was placed in the reaction chamber that already had 700 µL of oxygen-saturated respiration buffer at 37°C, in order to have 1×10^6 cells/mL in the reaction chamber. The chamber was sealed and the oxygen concentration was registered each second using Hterm Software

v. 0.8.1. In this way, basal respiration rate of tumor cells was obtained before digitonin addition (7.5 μg/mL) allowing cell permeabilization during 5 min. Then substrates and inhibitors of the respiratory chain where added to the reaction chamber in the following order and final concentrations: glutamate 10 mM, malate 5 mM, ADP/$MgCl_2$ 1 mM, rotenone 10 μM, succinate 10 mM, antimycinA 10 μM as previously reported (20). The oxygen concentration in the reaction chamber was calibrated considering the oxygen-maximum saturation of the respiration buffer at atmospheric pressure of 585 mmHg at Mexico City at 37°C, which is 400 nM O_2/mL. We obtained the oxygen consumption (nM O_2/mL*1 × 10^6 cells) versus time (min) plots. All the analyses of the mitochondrial function were made by tetraplicate.

RNA Extraction

After 48 h of incubation under the conditions above mentioned, total RNA was isolated from tumor cells (A-549, A-427, MCF-7) and fibroblasts (MRC-5) using ZR-Duet DNA/RNA Miniprep according to manufacturer's instructions (Zymo Research, Irvine, CA, USA). Total RNA was treated with RNAse free DNAse I (Thermo Scientific, Waltham, MA, USA) according to the manufacturer's protocol. Quality and quantity of RNA were evaluated by A_{260} and A_{280} using NanoDrop 2000 (Thermo Scientific, Waltham, MA, USA). Total RNA was reverse-transcribed using the kit Maxima First Strand cDNA Synthesis Kit for RT-qPCR (Thermo Scientific, Waltham, MA, USA). The cDNA obtained was stored at−20°C for further analysis.

Transcriptional Analysis of HIF-1α, AMPK and CS Using RT-qPCR

We used RT-qPCR to determine the transcript levels of HIF-1α, AMPK and CS. qPCR was performed in a semi-quantitative form using an ABI Prism 7500 Sequence Detector (Applied Biosystems, Foster City, CA). qPCR reaction contained SYBR Select Master Mix (Thermo Scientific, Waltham, MA, USA), cDNA as template and a pair of specific primers (HIF1α-F: 5′-CAG TCG ACA CAG CCT GGA T-3′ and HIF1α-R: 5′-TGG CAA GCA TCC TGT ACT GT-3′; AMPK-F: 5′-CAG GCC ATA CCC TTG ATG AAT-3′ and AMPK-R: 5′-TTC TTC CTT CGT ACA CGC AAA T-3′; CS-F: 5′- ACC TGT CAG CGA GAG TTT GC-3′ and CS-R: 5′- CCC AAA CAG GAC CGT GTA GT-3′. Validation curves were run using 18S rRNA, which was selected as endogenous control for all analyzed genes (18S-F: 5′-TAC CGC AGC TAG GAA TAA TGG-3′ and 18S-R: 5′- CGT CTT CGA ACC TCC GAC TT-3′).

PCR reactions were performed in 96-well reaction plates using the recommended parameters (10 min at 95°C, 40 cycles of 95°C for 15 s, and 60°C for 1 min.). Each PCR reaction was performed by triplicate and two non-template controls were included. Data were analyzed with Sequence Detection Software v 1.3.1 (Thermo Scientific, Waltham, MA, USA) to establish the PCR cycle at which the fluorescence exceeded a set of cycle threshold (Ct) for each sample. Comparative $2^{-\Delta\Delta Ct}$ method was used for target gene expression analysis (21). After normalization using the 18S rRNA housekeeping gene, normalized data of AMPK, HIF-1α, and CS expression from tumor and fibroblast cells were compared with the average of normalized data from same genes, expressed in tumor and fibroblast cells cultured in neutral pH media under normoxia. This condition was set as the value of 1 and was used as calibrator to compare data from the acidic conditions under normoxia or hypoxia.

Analysis of HIF-1α, AMPK and pAMPK Protein Levels

HIF-1α, AMPK and pAMPK protein levels were determined in A-549, A-427, and MCF-7 tumor cell lines and MRC-5 fibroblast cells by flow cytometry. After 48 h of incubation under the tested conditions described above, HIF-1α and total AMPK were examined as previously reported (19). Briefly, cells were harvested by trypsinization, they were washed with PBS and stained with Zombie NIR. Then, cells were fixed and permeabilized with Transcription Factor Staining Buffer Set (Invitrogen) according to manufacturer's instructions. After permeabilization, cells were resuspended in 100 μL of PE mouse anti-HIF-1α monoclonal antibody (clone 546-16, BioLegend) or rabbit anti-AMPK alpha-1 polyclonal antibody (dilution 1:1000, cat. no. bs-10344R, Bioss Antibodies) for 45 min. In the case of AMPK staining, cells were further washed and incubated with Alexa 488 mouse anti-rabbit monoclonal antibody (Molecular Probes, Eugene Oregon) for 30 min. Finally, cells were washed and fixed using paraformaldehyde (1% w/v).

To evaluate the protein levels of phosphorylated form of AMPK, after incubation, cells were treated with Phosflow Fix Buffer I/Phosflow Perm Buffer III (BD Phosphoflow) according to manufacturer's protocol. Briefly, cells were detached and incubated with Phosflow Fix Buffer I at 37°C for 10 min. Then, cells were washed and incubated with Phosflow Perm Buffer III on ice for 30 min. After permeabilization, cells were washed with PBS/BSA and resuspended in 100 μL of rabbit anti-AMPK alpha-1/2 (Thr183/Thr172) polyclonal antibody (dilution 1:1000, cat. no. bs-4002R, Bioss Antibodies).

After 45 min of incubation with the primary antibody, cells were washed and incubated with Alexa 488 mouse anti-rabbit monoclonal antibody for 30 min. Cells were washed and resuspended in paraformaldehyde (1% w/v) to proceed with the flow cytometric analysis.

At least 10,000 events were acquired from the region of viable cells. The results were analyzed with FlowJo V10 software. The MFI values for HIF-1α, AMPK, and pAMPK were determined. Then the relative MFI (rMFI) was obtained using the formula rMFI= MFI treatment/MFI control. The control condition was pH7 and normoxia.

Statistical Analysis

All values are expressed as the mean ± standard error. We used GraphPad Prism 7 software to test changes between groups. We usually established as the control group, the condition with the medium with lactate/glucose, pH7 and normoxia, and the differences between the control group and condition-tested groups were analyzed using unpaired Student's *T*-test. Significant differences between groups were considered at $p < 0.05$.

RESULTS

Lactic Acidosis Differentially Affected Growth Rate of Tumor Cells

The initial concentrations of lactate and glucose in all cultures were 2 mM and 10 mM, respectively. All tumor cells consumed glucose and produced lactate during the exponential and stationary phases. As of 48 h of cell culture, lactate was accumulated in the extracellular medium reaching quantities up to 20 mM; thus, tumor and non-transformed cells created a lactic environment. Lactic acidosis (pH = 6.2) with the presence of glucose significantly increased the growth rate of A-427 tumor cells in comparison with neutral lactosis. Conversely, this same condition diminished the growth rate of A-549, MCF-7, and MRC-5 cells, significant differences were found under the normoxic condition (**Figure 1**, **Table 1**). Under hypoxia, only A-549 cells significantly diminished their growth rate when they were cultured under lactic acidosis in comparison with neutral lactosis (**Table 1**). As expected MRC-5 cells grew slower than tumor cells in all conditions tested in this study (**Figure 1**, **Table 1**). Remarkably, none of the tumor cell lines increased their growth rate under hypoxia in comparison with normoxia (**Table 1**).

After finding that lactic acidosis differentially affected tumor growth rate, we wanted to know how this condition affected cell viability and cell cycle progression in tumor and fibroblast cells. We found that, whereas the viability of MRC-5 and A-427 cells did not change, the viability of A-549 cells increased and the viability of MCF-7 cells diminished when these cells were cultured under lactic acidosis in comparison with neutral lactosis, either under normoxia or hypoxia (**Figure 2A**). Interestingly, the analysis of the cell cycle profile of MRC-5 cells showed that lactic acidosis significantly increased subG1 cell percentages and diminished G1 and S cell percentages in comparison with neutral lactosis (**Figure 2B**). In A-549 cell line, lactic acidosis significantly increased percentages of cells in G1-phase with a concomitant reduction in the percentages of cells in S-phase cell, in comparison with A-549 cells cultured under neutral lactosis (**Figure 2B**). A-549 and MCF-7 cells increased subG1 cell percentages under lactic acidosis irrespective of oxygen availability. Conversely, A-427 cells cultured under lactic acidosis did not modify the cell cycle profile in comparison with cells cultured under neutral lactosis (**Figure 2B**).

Lactic Acidosis Diminished the Specific Rate of Lactate Production in Tumor Cells During the Exponential Growth Phase, but Only A-549 Cells Diminished the Specific Rate of Glucose Consumption

As above indicated, all cell lines consumed glucose and produced high amounts of lactate. At the end of the culture, we found that A-427 cell line consumed more glucose and produced more lactate than A-549, MCF-7 and MRC-5 cells under the four tested conditions (**Figure 3A**). None of the cell lines (tumor cells and non-transformed cells) consumed lactate under lactic acidosis

TABLE 1 | Specific growth rate of tumor cell lines and fibroblast cells.

Cell line	Normoxia		Hypoxia	
	pH 7.2 ($x10^{-2}$ h^{-1})	pH 6.2 ($x10^{-2}$ h^{-1})	pH 7.2 ($x10^{-2}$ h^{-1})	pH 6.2 ($x10^{-2}$ h^{-1})
MRC-5	1.1(0.3)	−0.4(0.3)*	0.8(0.4)	0.5(0.4)
A-549	2.3(0.2)	1.8(0.1)*	1.8(0.2)	1.5(0.1)*
A-427	1.9(0.2)	2.4(0.1)*	1.5(0.3)	1.4(0.2)
MCF-7	2.1(0.7)	1.6(0.6)	1.9(0.5)	1.8(0.5)

*Specific rate of growth was determined on exponential phase. All cultures were made by triplicate in tissue-culture plate using RPMI-1640 with glucose (10 mM) and lactate (2 mM) and pH 7.2 or pH 6.2 under normoxia or hypoxia. Values are expressed as mean (std error). *p < 0.05 difference with respect to normoxia pH 7.2 condition.*

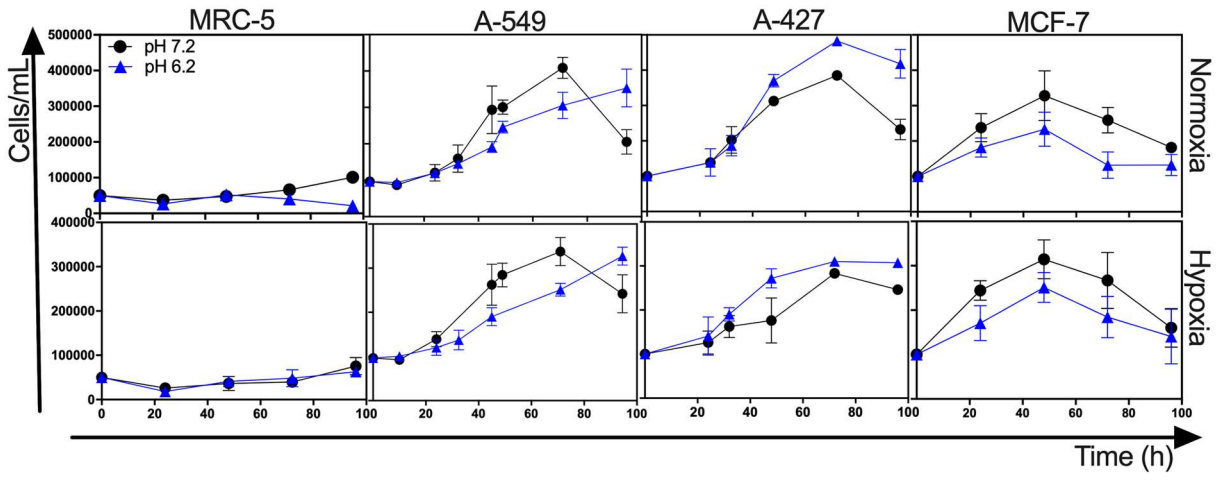

FIGURE 1 | Growth curves of MRC-5 fibroblast cells and A-549, A-427, and MCF-7 tumor cells followed through 96 h, using RPMI-1640 glucose (10 mM) and lactate (2 mM) adjusted at pH 7.2 or pH 6.2 under normoxia (21% O_2) or hypoxia (2% O_2).

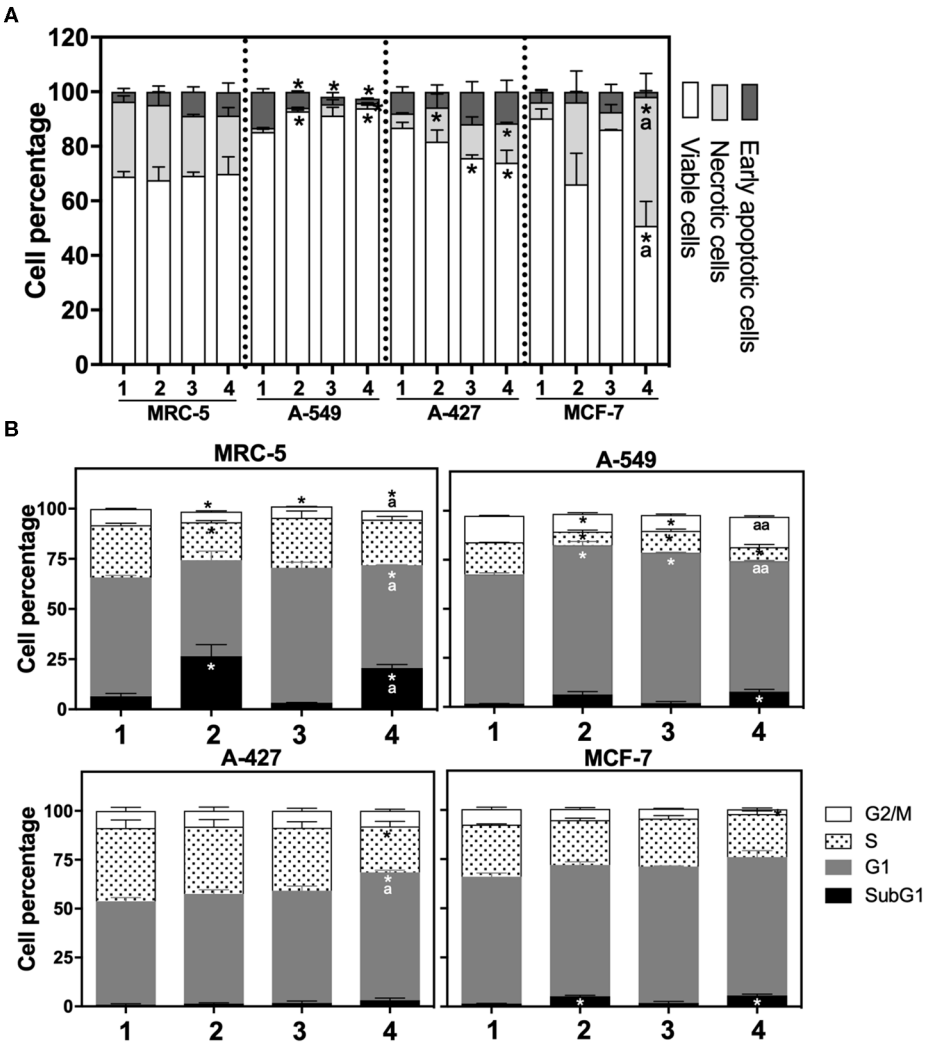

FIGURE 2 | (A) Percentage of viability, necrosis and early apoptosis in lung cancer and fibroblast cells determined by AnnexinV/7-AAD assay. **(B)** Cell cycle profile of MRC-5 fibroblast cells, A-549, A-427, and MCF-7 tumor cells. (1) Normoxia, pH 7.2; (2) Normoxia, pH 6.2; (3) Hypoxia, pH 7.2 and (4) Hypoxia, pH 6.2. Bars represent mean+SEM. *p<0.05 difference with respect to normoxia & pH7.2. $^{a}p < 0.05$, $^{aa}p < 0.01$ difference with respect to hypoxia and pH7.2.

independently of the oxygen concentration; instead, all cell lines consumed glucose (**Figure 3A**). But at the end of 96 h of cell culture, when glucose levels were very low, A-549, A-427, and MCF-7 cells consumed lactate; as opposed to MCR-5 fibroblast cells, which did not consume lactate throughout the culture (**Figure 3A**).

During exponential phase, the specific rate of lactate production ($q_{PLactate}$) of tumor and fibroblast cells tended to diminish when cells were cultured under lactic acidosis in comparison with neutral conditions under normoxia or hypoxia (**Figure 3B**). As it was expected, under hypoxia all tumor and fibroblast cells tended to increase $q_{PLactate}$ in comparison with normoxia regardless of the pH (**Figure 3B**).

When tumor cells were cultured under acidosis compared with neutral conditions, the specific rate of glucose consumption ($q_{SGlucose}$) of A-427 and MCF-7 tumor cells and MCR-5 cells did not change during exponential phase (**Figure 3C**); in contrast, the $q_{SGlucose}$ of A-549 cells significantly diminished (**Figure 3C**). As expected, under hypoxia all tumor and fibroblast cells increased their specific rate of glucose consumption ($q_{PGlucose}$) in comparison with normoxia (**Figure 3C**).

Lactic Acidosis Diminished GLUT1 and GLUT4 Expression in A-549 Cells, but Not in A-427 Cells

To know the effect of acidosis on glucose transporters expression, we evaluated GLUT1 and GLUT4 expression on tumor cells after 48 h of incubation. Representative flow cytometric analyses for GLUT1 and GLUT4 of A-427, MRC-5, A-549, and MCF-7 cells are shown in (**Figure 4A** and **Supplementary Figure 1**).

Lactic acidosis increased GLUT1 levels in A-427 cells in comparison with neutral lactosis under normoxia. In contrast, lactic acidosis significantly diminished GLUT1

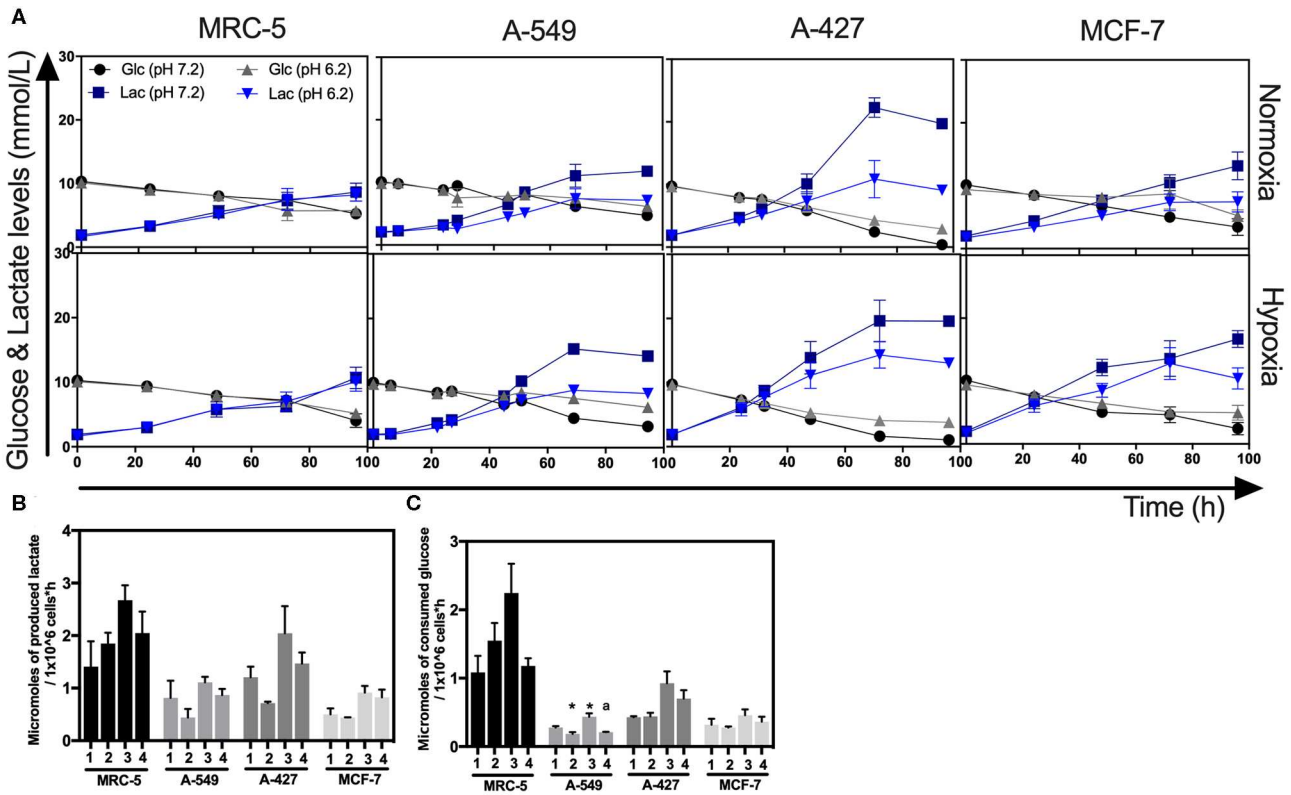

FIGURE 3 | Glucose and lactate metabolism in tumor and fibroblast cells. **(A)** Kinetics of glucose and lactate levels from cultures of MRC-5, A-549, A-427, and MCF-7 followed through 96 h, using RPMI-1640 at pH 7.2 or pH 6.2 under normoxia (21% O_2) or hypoxia (2% O_2). **(B)** Specific rate of lactate production obtained during exponential phase of growth of tumor and fibroblast cells. **(C)** Specific rate of glucose consumption obtained during exponential phase of growth of tumor and fibroblast cells. Bars represent mean + SEM. $^{*}p < 0.05$ difference with respect to normoxia and pH7.2. $^{a}p < 0.05$ difference with respect to hypoxia and pH7.2.

expression levels in A-549, MCF-7, and MRC-5 cells in comparison with neutral conditions under both normoxia and hypoxia (**Figure 4B**). Contrary to A-549 cells, lactic acidosis increased GLUT4 expression levels in A-427 cells, compared with neutral conditions under normoxia or hypoxia. Interestingly, hypoxia increased GLUT4 expression levels in A-427 and MCR-5 cells in comparison with normoxia (**Figure 4C**).

Additionally, it has been reported that hypoxia can increase glucose consumption (11, 12). Accordingly, we found that hypoxia tended to increase GLUT1 and GLUT4 expressions in A-549, A-427 and MCF-7 tumor cells and MCR-5 fibroblast cells; but only A-427 cells presented significant differences, and MCF-7 did not increase GLUT4 under hypoxia (**Figures 4B,C**).

Lactic Acidosis Diminished the Expression of Both Monocarboxylate Transporters MCT1 and MCT4 in Lung Adenocarcinoma Cells

Regarding lactate metabolism, none of cell lines consumed lactate during the exponential phase of the growth curve, lactate concentrations were always increasing in the media up to 72 h of culture (**Figure 3A**). To corroborate this finding, we evaluated MCT1 and MCT4 expression on tumor cells after 48 h of incubation. Representative flow cytometric analyses for MCT1 and MCT4 of A-427 MRC-5, A-549 and MCF-7 cells are shown in (**Figure 4D** and **Supplementary Figure 1**). We found that under lactic acidosis, A-427 and A-549 tumor cells and MRC-5 cells diminished MCT1 levels with respect to neutral conditions independently of the oxygen tension, although only A-549 cells presented significant differences. In contrast, MCF-7 cells significantly increased MCT1 expression only when these cells were cultured under normoxia (**Figure 4E**).

When we analyzed MCT4 expression, we found that lactic acidosis also diminished MCT4 expression in A-427 and A-549 tumors cells and MRC-5 fibroblast cells (**Figure 4F**); these data corroborate our previous result where lactic acidosis tended to diminish $q_{PLactate}$ of tumor cell lines in comparison with neutral conditions (**Figure 3B**). In contrast, MCF-7 cells tended to increase MCT4 expression under lactic acidosis and normoxia (**Figure 4F**). Interestingly, under neutral lactosis and hypoxia, A-549 and A-427 lung cancer cells increased MCT4 expression in comparison with normoxia (**Figure 4F**), which correlates with an increased $q_{PLactate}$ in hypoxia with respect to normoxia (**Figure 3B**).

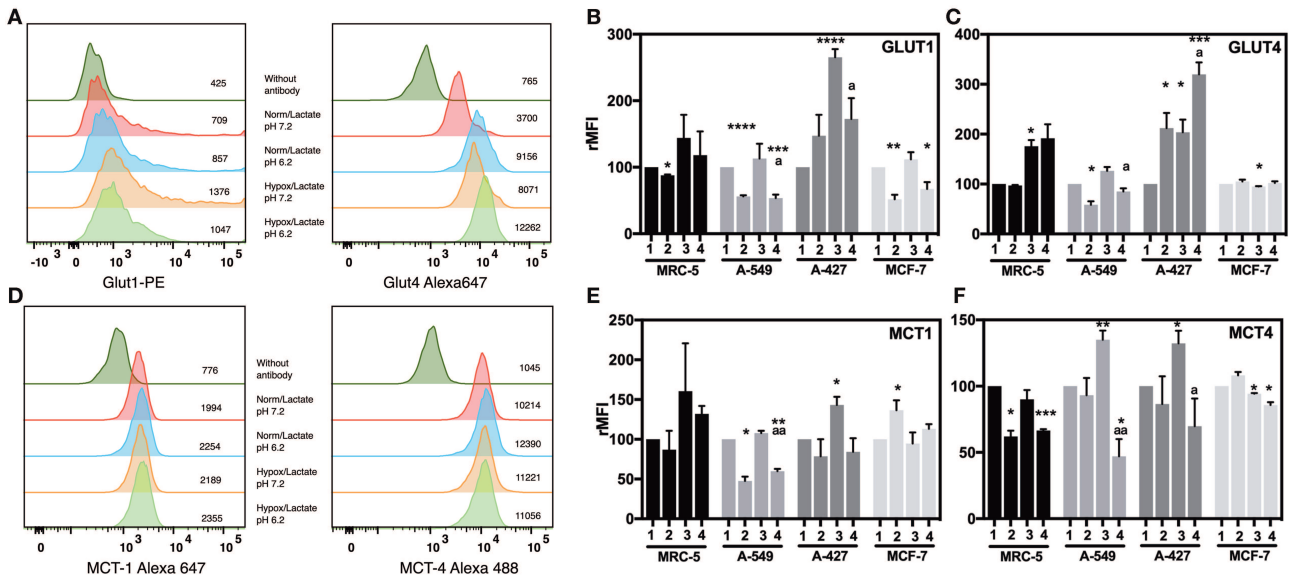

FIGURE 4 | Analysis of the expression of glucose and monocarboxylate transporters on tumor and fibroblast cells. **(A)** Histograms of a representative experiment of GLUT1 and 4 and **(D)** MCT1 and 4 expression analysis on A-427 tumor cell line. Analysis was performed on Zombie-NIR low (viable) cells and MFI values for each treatment are shown. Relative media fluorescence intensity (rMFI) of **(B)** GLUT1 and **(C)** GLUT4 on tumor and fibroblast cells. Relative media fluorescence intensity (rMFI) of **(E)** MCT1 and **(F)** MCT4 on tumor and fibroblast cells. Bars represent data of at least two independent culture experiments expressed in mean + SEM. $^{*}p < 0.05$, $^{**}p < 0.01$, $^{***}p < 0.001$, $^{****}p < 0.0001$ difference with respect to normoxia and pH7.2. $^{a}p < 0.05$, $^{aa}p < 0.01$ difference with respect to hypoxia and pH7.2.

Under Lactic Acidosis, Mitochondrial Respiration of A-427 Cells Was Increased but Mitochondrial Respiration of A-549 Cells Was Diminished

After finding that lactic acidosis diminished lactate production by tumor cells, we evaluated the effect of acidosis on mitochondrial functionality in lung tumor cells; thus, we determined the oxygen consumption in A-549 and A-427 cells using a Clark-type electrode.

We found that A-549 cells consumed more oxygen per minute than A-427 cells under both conditions: lactic acidosis and neutral lactosis (see Basal respiration in **Table 2**). However, in A-549 cells cultured under lactic acidosis, the oxygen consumption per minute significantly diminished in comparison with A-549 cells cultured under neutral conditions. In contrast, the basal respiration rate of A-427 cells cultured under lactic acidosis increased in comparison with A-427 cells that were cultured under neutral lactosis (**Table 2**). Interestingly, the respiratory state III or maximal respiration state, obtained after adding glutamate, malate and ADP, was higher in A-427 cells cultured under lactic acidosis than cells cultured under neutral lactosis (**Table 2**).

When we added succinate, the substrate for the complex III of OXPHOS, the oxygen consumption rate was significantly higher in tumor cells cultured under lactic acidosis (**Table 2**). Thus, the complex III of both tumor cell lines was more active when these cell lines were cultured under lactic acidosis.

TABLE 2 | Evaluation of mitochondrial respiration of A-549 and A-427 tumor cells using different substrates and inhibitors of the respiratory chain.

Cell line	A-549		A-427	
Media	**pH 7.2**	**pH 6.2**	**pH 7.2**	**pH 6.2**
Basal respiration	1.8 (0.8)	0.72 (0.13)*	0.3(0.15)	0.5(0.005)*
Glutamate/Malate/ADP	0.6 (0.3)	0.6(0.3)	0.13(0.002)	0.5(0.12)*
Rotenone	−0.13(0.01)	−1.5(0.3)	−0.3(0.01)	−0.3(0.01)
Succinate	0.38(0.15)	0.7(0.1)*	0.17(0.05)	0.5(0.3)*
AntimycinA	−0.24(0.01)	−0.4(0.05)*	−0.06(0.01)	−0.21(0.1)*

Oxygen consumption rate (nM consumed oxygen/min × 10^6 cells) was determined on tumor cells after 48 h of incubation under normoxia. Experiments were made by tetraplicate. Values are expressed as mean (std dev).
$^{*}p < 0.05$ difference with respect to normoxia pH 7.2 condition.

The Differential Expression of HIF-1α, AMPK and CS Transcript Levels Correlated With the Energetic Metabolism of Tumor Cells Under Lactic Acidosis

To figure out how the metabolism of tumor and fibroblast cells was regulated under lactic acidosis, we evaluated AMPK, HIF-1α, and CS transcript levels on these cells after 48 h of incubation under the four culture conditions.

When we compared the transcript levels of tumor cells grown under lactic acidosis in comparison with neutral lactosis, we found that A-549 and MCF-7 tumor cells and MRC-5 fibroblast cells significantly diminished AMPK transcript levels under

normoxia (**Figure 5A**). These cells also presented a significant increase of HIF-1α transcript levels and a significant decrease of CS expression under normoxia (**Figures 5B,C**). These data suggest that mitochondrial activity is diminished in A-549 and MCF-7 tumor cells and MRC-5 fibroblast cells cultured under lactic acidosis and normoxia. Interestingly, we found a strong inhibition of CS expression in MRC-5, but not in tumor cells, cultured under hypoxia independent of pH (**Figure 5C**). In contrast, when we compared the transcript levels of A-427 tumor cells grown under lactic acidosis in comparison with neutral lactosis, we found that A-427 cells did not change the AMPK transcript levels under normoxia (**Figure 5A**). This phenomenon was accompanied by a significant reduction of HIF-1α transcript levels and an increase of CS expression (**Figures 5B,C**). Taken together our data indicate that mitochondrial activity is increased in A-427 cells cultured under lactic acidosis and normoxia.

Additionally, hypoxia significantly increased HIF-1α transcript levels in MRC-5 fibroblast cells and A-427 tumor cells (**Figure 5B**). This result correlated with the increase of GLUT1 expression in MRC-5 and A-427 cells under hypoxia compared with normoxia (**Figure 4B**).

Protein Analysis of HIF-1α, AMPK and pAMPK Correlated With the Energetic Metabolism of Adenocarcinoma Cells Cultured Under Lactic Acidosis

To corroborate the transcriptional analysis, we evaluated the protein levels of total and phosphorylated AMPK (pAMPK), as well as HIF-1α in tumor and fibroblast cells cultured under the analyzed conditions after 48 h incubation. Representative flow cytometric analyses for AMPK, pAMPK, and HIF-1alpha are shown in (**Figures 6A–C**). For the determination of the phosphorylated form of AMPK, we included as control serum-starved cells (FCS-free RPMI-1640 medium), because this condition lowers basal phosphorylation levels. We found that in MCR-5 cells, MFI values for pAMPK were the lowest and consequently presented the less phosphorylated state, followed by MCF-7 cells and A-549 cells, being rMFI values 0.39, 0.87, and 0.90, respectively. Interestingly, A-427 cells presented the highest levels of pAMPK (rMFI = 1.77). A similar phenomenon has been reported in L6 myotubes, which respond to insulin and, under serum starvation, increase the levels of pAMPK and GLUT4, leading to increase of glucose uptake (22). Interestingly A-427 was the only cell line where GLUT4 expression levels responded to changes in the microenvironment (see **Figure 4C**).

We also found that under lactic acidosis, MRC-5 cells diminished total AMPK and HIF-1α levels independent of oxygen tension (**Figures 6D,F**). Lactic acidosis diminished pAMPK levels only when cells were cultured under normoxia (**Figure 6E**). These results correlated with the transcript levels in MRC-5 cells for AMPK but not with HIF-1α (**Figures 5A,B**).

A-549 cells cultured under lactic acidosis or hypoxia increased HIF-1α protein levels, but pAMPK levels did not change in comparison with neutral lactosis and normoxia (**Figures 6E,F**).

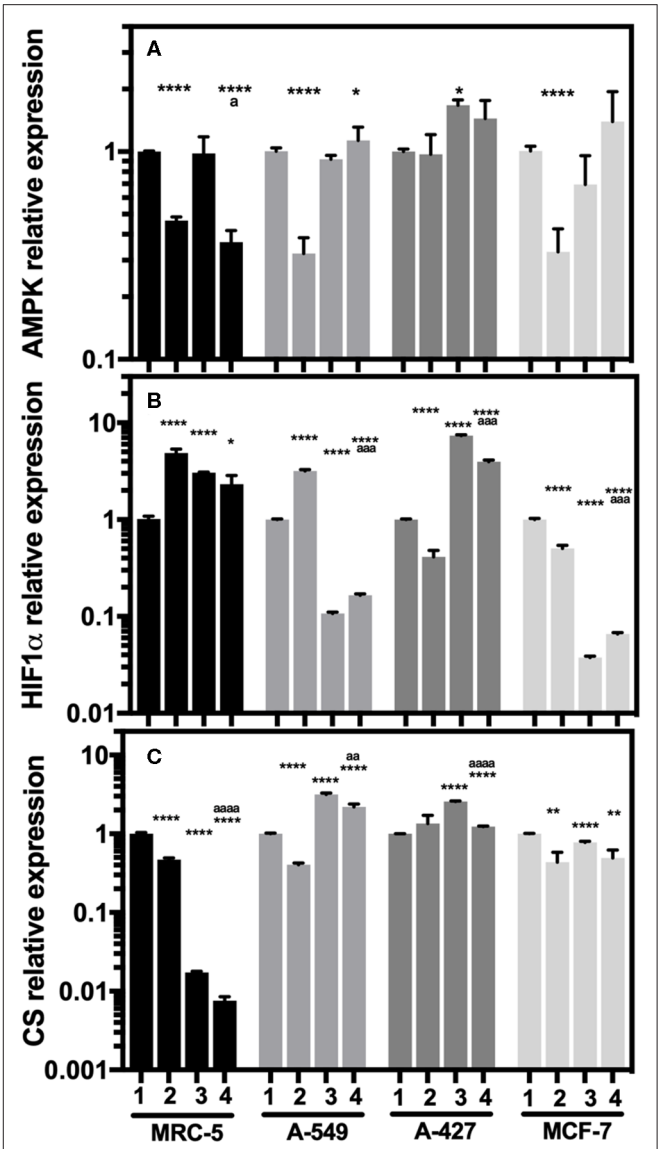

FIGURE 5 | Relative quantification of AMPK, HIF-1α, and CS transcript levels in cancer cell lines and fibroblasts cultured for 48 h. **(A)** AMPK, **(B)** HIF-1α, and **(C)** CS relative expression in the tumor cells and fibroblast cultured under lactic acidosis with respect to neutral lactosis under normoxia, this condition was set as the value of 1. (1) Normoxia, pH 7.2; (2) Normoxia, pH 6.2; (3) Hypoxia, pH 7.2 and (4) Hypoxia, pH 6.2. Bars represent transcriptional data of two independent culture experiments expressed in mean+SEM. $^{*}p < 0.05$, $^{**}p < 0.01$, $^{****}p < 0.0001$ difference with respect to normoxia and pH7.2. $^{a}p < 0.05$, $^{aaa}p < 0.001$, $^{aaaa}p < 0.0001$ difference with respect to hypoxia and pH 7.2.

A-427 cells cultured under lactic acidosis or hypoxia increased total and pAMPK levels, as well as HIF-1α protein levels in comparison with neutral lactosis and normoxia (**Figure 6**). These results correlated with the transcript analysis of A-427 cells cultured under hypoxia, where AMPK and HIF-1α mRNA levels increased (**Figures 5A,B**).

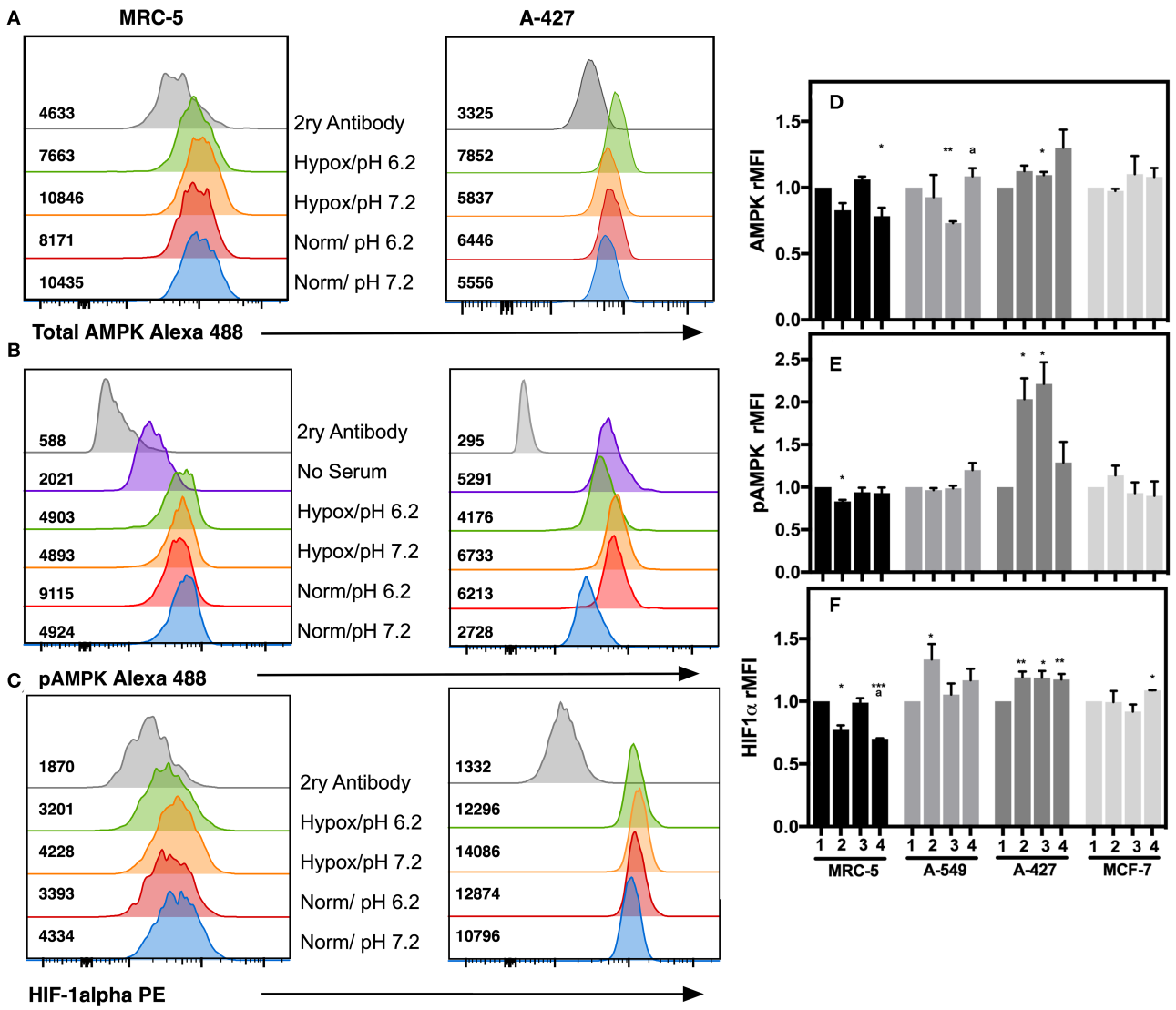

FIGURE 6 | Determination of intracellular protein levels of total and phosphorylated AMPK, and HIF-1α in cancer cell lines and fibroblasts cultured for 48h. Histograms of a representative experiment for the determination of **(A)** AMPK, **(B)** pAMPK, and **(C)** HIF-1α proteins on MCR-5 fibroblast cells and A-427 adenocarcinoma cells, MFI values for each treatment are shown. rMFI of **(D)** AMPK, **(E)** pAMPK, and **(F)** HIF-1α intracellular protein levels in fibroblast and tumor cells cultured during 48 h under (1) Normoxia, pH 7.2; (2) Normoxia, pH 6.2; (3) Hypoxia, pH 7.2 and (4) Hypoxia, pH 6.2. Bars represent data of two independent experiments expressed in mean + SEM. $^{*}p < 0.05$, $^{**}p < 0.01$, $^{***}p < 0.001$ difference with respect to normoxia and pH7.2. $^{a}p < 0.05$, difference with respect to hypoxia and pH 7.2.

MCF-7 cells cultured under lactic acidosis or hypoxia did not change total and phosphorylated AMPK, nor HIF-1α protein levels in comparison with neutral lactosis and normoxia (**Figure 6**). These results correlated with the transcript analysis of MCF-7 cells cultured under lactic acidosis and hypoxia, where the AMPK and HIF-1α mRNA levels did not change (**Figures 5A,B**).

DISCUSSION

Because lactic acidosis with glucose availability is a frequent condition found in solid tumors, we wanted to investigate if tumor cells fulfilled the metabolic shift under lactic acidosis and normoxic or hypoxic conditions. Lactic acidosis under normoxia or hypoxia affected differentially the growth, glucose and lactate transporters expression, glucose consumption and lactate production, as well as mitochondrial functionality of both lung tumor cell lines (A-549 and A-427), in spite of both being adenocarcinomas.

Our data support that there is a tumor-metabolic heterogeneity, because cell lines like A-549 and MCF-7 cultured under control conditions exhibited a more oxidative metabolism, evidenced by a higher O_2 consumption, while A-427 cells presented a more glycolytic metabolism because they consumed less oxygen per minute. Nonetheless,

A-427 tumor cells were more adaptable to an acidic microenvironment, because they could shift to a more oxidative metabolism.

These results correlated with the heterogeneous metabolic phenotypes found in solid lung tumors *in vivo* (23). A-427 cells cultured under lactic acidosis and normoxia increased their growth rate, possibly supported by the increased expression of both the ubiquitously and the insulin-responsive glucose transporters (GLUT1 and GLUT4).

To our knowledge this is the first report that shows that lactic acidosis can induce GLUT4 expression in some tumor cells under normoxia or hypoxia.

AMPK activation may indirectly increase the expression of the glucose transporters. Although A-427 cultured under lactic acidosis and normoxia maintained the same AMPK transcript levels, total AMPK protein levels were slightly augmented, while AMPK activation was increased, as evidenced by higher levels of phosphorylation. In this regard, it has been reported that AMPK activation upregulates energy-producing catabolic processes, including glycolysis through GLUT1, GLUT4, HK, and PFK2 upregulation, as well as fatty acid oxidation induced by downregulating acetyl-coA carboxylase 2 (24). Also, Ching et al. previously showed that activation of AMPK under serum starvation conditions is required for glucose transport mediated by GLUT4 (22). Thus our data suggest that some lung tumor cells might exhibit a response to lactic acidosis similar to that presented by myotubes under serum starvation. The diminished mRNA levels of HIF-1α correlated with an increased expression of citrate synthase, alongside with the increase of mitochondrial respiration rate in A-427 cells cultured under lactic acidosis and normoxia; nonetheless, HIF-1α protein levels presented a slight increase. This apparent inconsistency could be caused by the stress-induced chaperone protein HSP390, which has been reported to interact with HIF-1α, protecting it from proteasomal degradation (16).

Tumor cells cultured under lactic acidosis exhibit an energetic metabolic shift for obtaining energy, first by aerobic glycolysis and then by OXPHOS (7). Remarkably, we now report that this phenomenon is mediated by an increase in the activity of the OXPHOS complexes I and III in A-427 cells. Taken together, these results indicate that lactic acidosis promoted the metabolic shift from aerobic glycolysis to oxidative metabolism in A-427 lung adenocarcinoma cells. This change might be advantageous because these tumor cells increased the growth rate under lactic acidosis, whereas MRC-5 non-transformed cells increased the percentage of dead cells under this same condition.

On the other hand, the growth rate of A-549 cells diminished when these cells were cultured under lactic acidosis regardless of oxygen tension. This result correlated with the decreased expression of both glucose transporters. Although under lactic acidosis and normoxia AMPK transcript levels were reduced, neither the protein nor activated AMPK levels changed. This possibly allowed the increase of HIF-1α at transcript and protein levels, as it has been observed that AMPKα deletion promotes elevated HIF-1α protein levels in two different tumor cell lines under normoxia (15). Our results suggest that the increased expression of HIF-1α promoted the decrease in citrate synthase expression, which correlated with the reduced respiration rate.

It has been reported that hypoxia-mediated HIF-1α upregulation increases the levels of GLUT1 (25); however, A-549 cells cultured under lactic acidosis downregulated the levels of both glucose transporters. These results agree with those previously reported by Giatromanolaki et al. who indicated that acidosis can eliminate the hypoxia-induced expression of glucose transporters (11); moreover, it has been reported that inhibition of AMPK and CaMKK (calcium/calmodulin-dependent protein kinase) inhibits GLUT4 translocation (26).

Taken together, our results indicate that in A-549 cells, lactic acidosis diminished Warburg effect, because lactate levels and lactate production rate were lower than in cells cultured under neutral lactosis. Importantly, although A-549 cells diminished Warburg effect, they did not shifted their metabolism, because respiration rate did not increase. Interestingly, even when A-549 cells were cultured under lactic acidosis and with glucose availability, these cells diminished their growth, but they did not die. Instead, A-549 cells maintained viability by promoting an arrest in G1-phase. A similar phenomenon has been observed in breast tumor cells (4T1), which induce G1 arrest, autophagy and inhibit apoptosis as survival mechanisms to protect cells from glucose deprivation-induced death when they are cultured under lactic acidosis (27).

We found that the non-transformed MRC-5 cells cultured under neutral lactosis and normoxia produced up to 10 mM of lactate, they also presented higher CS transcript levels under normoxia in comparison with hypoxia. Thus, MRC-5 fibroblast cells cultured under neutral lactosis and normoxia used both OXPHOS and aerobic glycolysis for obtaining energy. MRC-5 cells cultured under lactic acidosis and normoxia or hypoxia diminished their growth rate, the expression of GLUT1, MCT1 and MCT4, the transcript levels of AMPK and CS, as well as the protein levels of AMPK and HIF-1α in comparison with neutral lactosis, though only under normoxia the differences were significant. Under lactic acidosis and normoxic conditions the reduced expression of GLUT1 and monocarboxylate transporters was possibly promoted by the reduction of both HIF-1α and AMPK protein levels. Additionally, lactic acidosis inhibited cell cycle progression in MRC-5 fibroblast by reducing the transition of cells from G1-phase to S-phase, which correlated with the reduction of cell growth rate, and the increase in cell death. Thus, lactic acidosis might be a deleterious condition for proliferative non-transformed cells.

Wu et al. reported that lactic acidosis promoted a metabolic shift from aerobic glycolysis to OXPHOS, because the protons of intracellular acidosis inhibit the activity of some glycolytic enzymes (7). Our results partially support the findings of Wu et al., as we found that lactic acidosis diminished Warburg effect in lung adenocarcinoma cells, because they diminished lactate production rate, lactate levels and MCT1 and MCT4 expression under this condition. However, we did not find that reduction of aerobic glycolysis necessarily shifts the metabolism into OXPHOS; in view that although A-549 cells diminished aerobic glycolysis, they did not increase OXPHOS. In fact,

A-549 cells cultured under lactic acidosis diminished their basal respiration rate.

Tumor cells that in the presence of glucose and normoxia opt to consume lactate rather than glucose might support tumor development by two mechanisms: tumor metabolic symbiosis (10, 28) and reverse Warburg effect (29).

A recent report suggests that non-glucose nutrients have potential contributions in well-perfused tumor areas *in vivo,* but some human lung tumor may use lactate as a carbon source (30). We found that none of the tumor cells consumed lactate during the exponential phase under the tested conditions. On the contrary, under lactic acidosis and regardless of oxygen tension, adenocarcinoma cells and fibroblast cells diminished MCT1 expression after 48 h of culture. However, when the three tumor cells reached the end of the culture (96 h) and levels of glucose were about 4 mM, they consumed small quantities of lactate, a phenomenon that did not occur in non-transformed cells.

Thus, our results suggest that tumor cells might participate in the metabolic symbiosis phenomenon when they are not in the exponential phase of cell growth. Although lactic acidosis may diminish glucose transporter expression in some adenocarcinoma cells, if they have glucose availability, they will continue consuming glucose during the exponential phase. Additionally, some adenocarcinoma cells cultured under lactic acidosis shifted their metabolism from Warburg effect to OXPHOS, because they increased their basal respiration rate which may be supported by the strong activation of AMPK.

DATA AVAILABILITY STATEMENT

The datasets generated for this study are available upon reasonable request from the corresponding author.

AUTHOR CONTRIBUTIONS

SR-G designed the study. SR-G, AC-H, and HP-G performed the experiments. HP-G and SR-G wrote and critically reviewed the manuscript. All authors contributed to manuscript revision, read and approved the submitted version.

FUNDING

This work was supported by the Consejo Nacional de Ciencia y Tecnología (CONACyT) grant: CB-2011-167623.

ACKNOWLEDGMENTS

We thank Daniela Alejandra Castro-Flores for her invaluable technical support.

SUPPLEMENTARY MATERIAL

The Supplementary Material for this article can be found online at: https://www.frontiersin.org/articles/10.3389/fonc.2020.00807/full#supplementary-material

REFERENCES

1. Dai C, Sun F, Zhu C, Hu X. Tumor environmental factors glucose deprivation and lactic acidosis induce mitotic chromosomal instability–an implication in aneuploid human tumors. *PLoS One.* (2013) 8:e63054. doi: 10.1371/journal.pone.0063054
2. Walenta S, Mueller-Klieser WF. Lactate: mirror and motor of tumor malignancy. *Semin Radiat Oncol.* (2004) 14:267–74. doi: 10.1016/j.semradonc.2004.04.004
3. Romero-Garcia S, Lopez-Gonzalez JS, Baez-Viveros JL, Aguilar-Cazares D, Prado-Garcia H. Tumor cell metabolism: an integral view. *Cancer Biol Ther.* (2011) 12:939–48. doi: 10.4161/cbt.12.11.18140
4. Eilertsen M, Andersen S, Al-Saad S, Kiselev Y, Donnem T, Stenvold H, et al. Monocarboxylate transporters 1-4 in NSCLC: MCT1 is an independent prognostic marker for survival. *PLoS One.* (2014) 9:e105038. doi: 10.1371/journal.pone.0105038
5. Halestrap AP, Price NT. The proton-linked monocarboxylate transporter (MCT) family: structure, function and regulation. *Biochem J.* (1999) 343 Pt 2:281–99.
6. Xie J, Wu H, Dai C, Pan Q, Ding Z, Hu D, et al. Beyond Warburg effect–dual metabolic nature of cancer cells. *Sci Rep.* (2014) 4:4927. doi: 10.1038/srep04927
7. Wu H, Ying M, Hu X. Lactic acidosis switches cancer cells from aerobic glycolysis back to dominant oxidative phosphorylation. *Oncotarget.* (2016) 7:40621–9. doi: 10.18632/oncotarget.9746
8. Raghunand N, Gatenby RA, Gillies RJ. Microenvironmental and cellular consequences of altered blood flow in tumours. *Br J Radiol.* (2003) 76 Spec No 1:S11–22. doi: 10.1259/bjr/12913493
9. Pisarsky L, Bill R, Fagiani E, Dimeloe S, Goosen RW, Hagmann J, et al. Targeting metabolic symbiosis to overcome resistance to anti-angiogenic therapy. *Cell Rep.* (2016) 15:1161–74. doi: 10.1016/j.celrep.2016.04.028
10. Sonveaux P, Vegran F, Schroeder T, Wergin MC, Verrax J, Rabbani ZN, et al. Targeting lactate-fueled respiration selectively kills hypoxic tumor cells in mice. *J Clin Invest.* (2008) 118:3930–42. doi: 10.1172/jci36843
11. Giatromanolaki A, Liousia M, Arelaki S, Kalamida D, Pouliliou S, Mitrakas A, et al. Differential effect of hypoxia and acidity on lung cancer cell and fibroblast metabolism. *Biochem Cell Biol.* (2017) 95:428–36. doi: 10.1139/bcb-2016-0197
12. Ito T, Noguchi Y, Satoh S, Hayashi H, Inayama Y, Kitamura H. Expression of facilitative glucose transporter isoforms in lung carcinomas: its relation to histologic type, differentiation grade, and tumor stage. *Mod Pathol.* (1998) 11:437–43.
13. Yan M, Gingras MC, Dunlop EA, Nouet Y, Dupuy F, Jalali Z, et al. The tumor suppressor folliculin regulates AMPK-dependent metabolic transformation. *J Clin Invest.* (2014) 124:2640–50. doi: 10.1172/jci71749
14. Chaube B, Malvi P, Singh SV, Mohammad N, Viollet B, Bhat MK. AMPK maintains energy homeostasis and survival in cancer cells via regulating p38/PGC-1α-mediated mitochondrial biogenesis. *Cell Death Discov.* (2015) 1:15063. doi: 10.1038/cddiscovery.2015.63
15. Faubert B, Boily G, Izreig S, Griss T, Samborska B, Dong Z, et al. AMPK is a negative regulator of the Warburg effect and suppresses tumor growth *in vivo*. *Cell Metab.* (2013) 17:113–24. doi: 10.1016/j.cmet.2012.12.001
16. Filatova A, Seidel S, Bogurcu N, Graf S, Garvalov BK, Acker T. Acidosis Acts through HSP90 in a PHD/VHL-Independent Manner to Promote HIF Function and Stem Cell Maintenance in Glioma. *Cancer Res.* (2016) 76:5845–56. doi: 10.1158/0008-5472.can-15-2630
17. Pertega-Gomes N, Vizcaino JR, Attig J, Jurmeister S, Lopes C, Baltazar F. A lactate shuttle system between tumour and stromal cells is associated with poor prognosis in prostate cancer. *BMC Cancer.* (2014) 14:352. doi: 10.1186/1471-2407-14-352

18. Kennedy KM, Scarbrough PM, Ribeiro A, Richardson R, Yuan H, Sonveaux P, et al. Catabolism of exogenous lactate reveals it as a legitimate metabolic substrate in breast cancer. *PLoS ONE.* (2013) 8:e75154. doi: 10.1371/journal.pone.0075154
19. Romero-Garcia S, Prado-Garcia H, Valencia-Camargo AD, Alvarez-Pulido A. Lactic acidosis promotes mitochondrial biogenesis in lung adenocarcinoma cells, supporting proliferation under normoxia or survival under hypoxia. *Front Oncol.* (2019) 9:1053. doi: 10.3389/fonc.2019.01053
20. Kuznetsov AV, Veksler V, Gellerich FN, Saks V, Margreiter R, Kunz WS. Analysis of mitochondrial function in situ in permeabilized muscle fibers, tissues and cells. *Nat Protoc.* (2008) 3:965–76. doi: 10.1038/nprot.2008.61
21. Romero-Garcia S, Prado-Garcia H, Lopez-Gonzalez JS. Transcriptional analysis of hnRNPA0, A1, A2, B1, and A3 in lung cancer cell lines in response to acidosis, hypoxia, and serum deprivation conditions. *Exp Lung Res.* (2014) 40:12–21. doi: 10.3109/01902148.2013.856049
22. Ching JK, Rajguru P, Marupudi N, Banerjee S, Fisher JS. A role for AMPK in increased insulin action after serum starvation. *Am J Physiol Cell Physiol.* (2010) 299:C1171–9. doi: 10.1152/ajpcell.00514.2009
23. Chen PH, Cai L, Huffman K, Yang C, Kim J, Faubert B, et al. Metabolic diversity in human non-small cell lung cancer cells. *Mol Cell.* (2019) 76:838–51 e5. doi: 10.1016/j.molcel.2019.08.028
24. Mulukutla BC, Khan S, Lange A, Hu WS. Glucose metabolism in mammalian cell culture: new insights for tweaking vintage pathways. *Trends Biotechnol.* (2010) 28:476–84. doi: 10.1016/j.tibtech.2010.06.005
25. Cao X, Fang L, Gibbs S, Huang Y, Dai Z, Wen P, et al. Glucose uptake inhibitor sensitizes cancer cells to daunorubicin and overcomes drug resistance in hypoxia. *Cancer Chemother Pharmacol.* (2007) 59:495–505. doi: 10.1007/s00280-006-0291-9
26. Kim N, Lee JO, Lee HJ, Lee YW, Kim HI, Kim SJ, et al. AMPK, a metabolic sensor, is involved in isoeugenol-induced glucose uptake in muscle cells. *J Endocrinol.* (2016) 228:105–14. doi: 10.1530/joe-15-0302
27. Wu H, Ding Z, Hu D, Sun F, Dai C, Xie J, et al. Central role of lactic acidosis in cancer cell resistance to glucose deprivation-induced cell death. *J Pathol.* (2012) 227:189–99. doi: 10.1002/path.3978
28. Phipps C, Molavian H, Kohandel M. A microscale mathematical model for metabolic symbiosis: investigating the effects of metabolic inhibition on ATP turnover in tumors. *J Theor Biol.* (2015) 366:103–14. doi: 10.1016/j.jtbi.2014.11.016
29. Martinez-Outschoorn UE, Balliet RM, Rivadeneira DB, Chiavarina B, Pavlides S, Wang C, et al. Oxidative stress in cancer associated fibroblasts drives tumor-stroma co-evolution: A new paradigm for understanding tumor metabolism, the field effect and genomic instability in cancer cells. *Cell Cycle.* (2010) 9:3256–76. doi: 10.4161/cc.9.16.12553
30. Hensley CT, Faubert B, Yuan Q, Lev-Cohain N, Jin E, Kim J, et al. Metabolic heterogeneity in human lung tumors. *Cell.* (2016) 164:681–94. doi: 10.1016/j.cell.2015.12.034

Conflict of Interest: The authors declare that the research was conducted in the absence of any commercial or financial relationships that could be construed as a potential conflict of interest.

frontiers in Oncology

MINI REVIEW
published: 18 June 2020
doi: 10.3389/fonc.2020.00893

Protein Kinase CK2 in Cancer Energetics

Eduardo Silva-Pavez† *and Julio C. Tapia**

Programa de Biología Celular y Molecular, Instituto de Ciencias Biomédicas, Facultad de Medicina, Universidad de Chile, Santiago, Chile

Protein kinase CK2 (formerly known as casein kinase 2) is abnormally elevated in many cancers. This may increase tumor aggressiveness through CK2-dependent phosphorylation of key proteins in several signaling pathways. In this work, we have compiled evidence from the literature to suggest that CK2 also modulates a metabolic switch characteristic of cancer cells that enhances resistance to death, due to either drugs or to a microenvironment deficient in oxygen or nutrients. Concurrently, CK2 may help to preserve mitochondrial activity in a PTEN-dependent manner. PTEN, widely recognized as a tumor suppressor, is another CK2 substrate in the PI3K/Akt signaling pathway that promotes cancer viability and aerobic glycolysis. Given that CK2 can regulate Akt as well as two of its main effectors, namely mTORC1 and β-catenin, we comprehensively describe how CK2 may modulate cancer energetics by regulating expression of key targets and downstream processes, such as HIF-1 and autophagy, respectively. Thus, the specific inhibition of CK2 may lead to a catastrophic death of cancer cells, which could become a feasible therapeutic strategy to beat this devastating disease. In fact, ATP-competitive inhibitors, synthetic peptides and antisense oligonucleotides have been designed as CK2 inhibitors, some of them used in preclinical models of cancer, of which TBB and silmitasertib are widely known. We will finish by discussing a hypothetical scenario in which cancer cells are "addicted" to CK2; i.e., in which many proteins that regulate signaling pathways and metabolism-linked processes are highly dependent on this kinase.

Keywords: casein kinase CK2, warburg effect, metabolic switch, aerobic glycolysis, mitochondrial function, hypoxia, autophagy

OPEN ACCESS

Edited by:
Sara Rodriguez-Enriquez, Instituto Nacional de Cardiología, Mexico

Reviewed by:
Parames C. Sil, Bose Institute, India
Elisabetta Benedetti, University of L'Aquila, Italy

***Correspondence:**
Julio C. Tapia
jtapiapineda@uchile.cl

†***Present address:***
Eduardo Silva-Pavez, Center for Integrative Biology, Faculty of Sciences, Universidad Mayor, Santiago, Chile

Specialty section:
This article was submitted to Cancer Metabolism, a section of the journal Frontiers in Oncology

Received: *30 January 2020*
Accepted: *06 May 2020*
Published: *18 June 2020*

Citation:
Silva-Pavez E and Tapia JC (2020) Protein Kinase CK2 in Cancer Energetics. Front. Oncol. 10:893. doi: 10.3389/fonc.2020.00893

HIGHLIGHTS

- Modulation of the Warburg effect and mitochondrial activity.
- Involvement in an Akt and β-catenin-associated metabolic switch.
- Modulation of cancer energetics through autophagy.
- Functional interaction with β-catenin and HIF-1α.

INTRODUCTION

Protein kinase CK2 (formerly known as casein kinase 2) is a constitutively-active kinase that is expressed ubiquitously in eukaryotes (1–3). This butterfly-shaped enzyme is formed by catalytic (α or α') and regulatory (β) subunits and phosphorylates serine o threonine residues within an acidic context (S/TXXD/E/pS/pT/pY), as found in hundreds of proteins in various subcellular

compartments, signaling pathways, survival and metabolism-linked processes. CK2 has been shown to be critical in embryonic development, differentiation, immunity, cell survival, epithelial homeostasis and circadian rhythms (4–7). CK2 is also involved in the etiology of many diseases such as multiple sclerosis, cystic fibrosis, chronic intestinal inflammation, cardiac hypertrophy, atherosclerosis, thrombosis, diabetes mellitus, neurological and psychiatric disorders (7–11). In cancer, although CK2 by itself is not an oncogene, some studies have confirmed the tumorigenic potential of this kinase by regulating cellular processes that are characteristic of malignant transformation such as cell cycle progression, tumor growth and death resistance (12). CK2 has been implicated in the regulation of proteins and survival pathways that support chemoresistance, for example, by acquisition of a multi-drug resistance (MDR) phenotype, favoring drug efflux and DNA repair mechanisms (13). Recently, CK2 has been also shown to regulate expression of stemness genes, surface markers and ATP-dependent pumps, accounting for promotion of a stem-like phenotype in colorectal cancer cells (14).

CK2 mRNA levels have been shown to be increased in cancer cells, suggesting that transcriptional mechanisms may play a role in the increase in their protein levels (15). However, post-transcriptional and post-translational mechanisms may also be involved (15–18). Elevated levels of CK2 can be taken as an aggressiveness biomarker, especially the catalytic α subunit, which has been associated to poor prognosis in hepatocellular carcinoma, also correlating with metastatic risk in breast cancer (19, 20). In addition, nuclear localization of CK2α correlates with poor prognosis in renal, prostate and colorectal cancer (21–23), while nuclear localization of CK2β is a marker for predicting outcome of patients with gastric carcinoma (24). In line with this, CK2 has been raised as an attractive therapeutic target for treatment of solid tumors and hematologic malignancies with different kinase inhibitors, including ATP-competitive inhibitors, synthetic peptides and antisense oligonucleotides in preclinical models (25). Moreover, different CK2 inhibitors targeting the catalytic site have been designed, such as 4,5,6,7-tetrabromobenzotriazole (TBB) and silmitasertib (formerly CX-4945) (26). Silmitasertib and CIGB-300, a cell-permeable peptide inhibitor of CK2 (25, 27), have been used in several clinical trials for the treatment of different human cancers (www.clinicaltrials.gov). Nevertheless, CK2 catalyzes the phosphorylation of more than 300 substrates, defining it as the second most pleiotropic member of the human kinome (26, 28), and it also modulates several signal transduction pathways (29). Thus, this apparent pleiotropy must be taken into account before CK2 inhibitors are used to treat cancer or other diseases. Pharmacological inhibition of CK2 may cause unexpected effects, for instance, widespread alterations in alternative splicing of a wide number of genes or inhibition of Cdc2-like kinases, as indeed has been reported elsewhere (28, 30, 31).

More light on the latter could be shed by microRNA studies. Several miRNAs have been reported to downregulate CK2 expression. For example, co-overexpression of miR-760, miR-186, miR-337-3p, and miR-216b decreases CK2α protein levels in IMR-90 human lung fibroblast cells (16). These miRNAs are capable of binding to the 3'-UTR of CK2α mRNA and, consequently, to inhibit its protein expression (16). On the other hand, inhibition of CK2 by quinalizarin in 3T3-L1 pre-adipocyte cells increased miR-27a and miR-27b levels, which target the mRNA of PPARγ, a protein involved in regulation of fatty acid storage and glucose metabolism (32, 33). Also, miR-125b levels have been shown to be significantly decreased in breast cancer (18). This miRNA binds to the 3'-UTR of CK2α mRNA, leading to its decreased expression (18). Furthermore, inhibition of CK2 activity with TBB decreases cell viability and proliferation in MCF-7 breast cancer cells, which correlates with changes in different miRNAs (34). Likewise, CK2β knockdown leads to downregulation of different miRNAs related to cellular processes such as EMT and invasion in MCF10A breast epithelial cells (35). Nevertheless, whether the CK2-related miRNAs are successful in modulating metabolism and bioenergetics in cancer cells remains unknown.

Finally, a growing tumor has a high demand for energy and metabolites necessary for macromolecule biosynthesis. Cancer cells obtain energy mainly from aerobic glycolysis but generate lactate as the final product. This metabolic switch, known as the Warburg effect, is a widely accepted hallmark of cancer (36); however, recent studies indicate that cancer cells may also fully oxidize glucose, which suggests that mitochondrial function is crucial for oncogenesis and progression (37). In any case, either the Warburg effect or mitochondrial function is modulated by the activity of signaling proteins, providing adaptive advantages against a continuously-changing microenvironment. In this review, we compile evidence from the literature suggesting a plausible role for CK2 in modulating several processes related to the energetic changes occurring in a cancer cell, which may ultimately drive a metabolic switch that enhances malignant progression.

MODULATION OF MITOCHONDRIAL FUNCTION

CK2 has been proposed to modulate the Warburg effect in colorectal, esophageal and bladder cancer cells (**Table 1**). The presence of CK2 increases lactate dehydrogenase A (LDHA) expression and activity as well as proliferation in some of these cells (38–40). This CK2-dependent metabolic switch also promotes *in vitro* invasiveness, partly due to the regulated differential expression of two pyruvate kinase isoforms, PKM1 and PKM2 (39). The constitutively-active PKM1 isoform is down-regulated in cells overexpressing CK2, while the PKM2 isoform is imported into the nucleus (39). PKM2 is a cofactor of hypoxia-inducible factor-1 (HIF-1), whose transcriptional targets are LDHA, glucose transporter 1 (GLUT1), and pyruvate dehydrogenase kinase 1 (PDK1) (64). Of note, both pharmacological inhibition and siRNA-mediated silencing of CK2 lead to inhibition of the Warburg effect observed in bladder cancer cells (40).

Mitochondrial function is essential to the metabolic switch that is characteristic of cancer (**Table 1**). Qaiser et al. showed that CK2 may help to preserve mitochondrial activity in

TABLE 1 | Effect of CK2 activity alterations on both mitochondrial- and energetics-related components in several cancers.

CK2 alterations	Effects	Cancers	References
Overexpression	Increment of LDHA expression and activity, down-regulation of PKM1 isoform and nuclear import of PKM2 isoform.	Colorectal, esophagus, bladder	(38–40)
Overexpression	Increased glucose consumption and extracellular lactate levels, which is blocked by inhibition of LDHA.	Colorectal	(38, 39)
siRNA silencing	Inhibition of the Warburg effect.	Bladder	(40)
Inhibition (TBB)	Mitochondrial membrane depolarization.	Prostate	(41)
NE	β-catenin-dependent increased expression of MCT-1 and PDK1.	Colorectal	(42, 43)
Overexpression	β-catenin-dependent increased expression of survivin.	Colorectal	(44–46)
NE	Survivin increases the Warburg effect through mitochondrial complex II stability.	Colorectal	(47)
NE	β-catenin-dependent increased expression of c-Myc, ASCT2, and glutaminase.	Colorectal, breast	(48)
NE[a]	p27, p62, and probably ULK-1, are substrates of CK2.	Colorectal	(49–51)
Inhibition (TBB, quinalizarin)	ATF4-regulated expression of proteins at autophagy, amino acid biosynthesis and transport, lipid and glucose metabolisms.	Colorectal	(52–57)
Inhibition (silmitasertib)	Reduction of mTORC1 activity.	Colorectal, squamous, lung	(51, 58, 59)
Inhibition (TBB, siRNA)	HIF1α-regulated expression of aldolase and p53.	Hepatocellular, cervical	(60–63)

NE, not experimentally demonstrated for this cancer.
[a]*only suggested for ULK1.*

prostate cancer cells. They found CK2 enriched in mitochondria from several prostate cancer cell lines, somehow supporting membrane polarity, which is also essential for the electron transport chain. Thus, pharmacological inhibition of CK2 may generate rapid membrane depolarization just before the onset of apoptosis (41). This effect may be dependent on the tumor suppressor phosphatase and tensin homolog (PTEN), which is also phosphorylated by CK2, promoting its stability and cytoplasmic enrichment (65).

Indeed, phospho-PTEN mimics the tumorigenic effects observed upon deletion or mutant inactivation of its coding gene (66). Expression of a long PTEN isoform (PTENα) has been observed in prostate cancer cells with loss of PTEN function. This isoform is generated by alternative translation at a non-canonical CUG initiation site in the 5'UTR. PTENα is mainly located in the mitochondria and interacts with normal PTEN. Together, these isoforms stabilize PTEN-induced kinase 1 (PINK1), a serine/threonine kinase associated with degradation of dysfunctional mitochondria (67). Interestingly, ectopic PTENα expression in PTEN-null cell lines leads to increased mitochondrial function accompanied by elevated ATP production and cytochrome c oxidase activity (68). In this alternative translation of PTEN, recognition of the start codon is strongly regulated by the stoichiometry of various eukaryotic initiation factors (eIF) that form the pre-initiation complex (PIC) along with other proteins. CK2 and the mammalian target of rapamycin complex 1 (mTORC1) coordinate PIC assembly, promoting proliferation upon stimulation with growth factors and nutrients (69). Here, the two kinases activate the translation process by phosphorylation of eIF2β. Of note, CK2-mediated phosphorylation of eIF5 has been deemed important for cell cycle progression (70); however, recognition of CUG at the PTENα 5'UTR is mediated by eIF2α (68). Therefore, whether eIF2α is a target of CK2 or has a role in the PTENα/PTEN complex in supporting PINK1 stabilization at the mitochondrial membrane remains entirely unknown.

PI3K/AKT AND β-CATENIN-RELATED METABOLIC SWITCH

PTEN is a widely-known tumor suppressor in the PI3K/Akt signaling pathway (**Table 1**), which plays a key role in cancer due to its relationship with cellular processes involved in proliferation, apoptosis, and invasiveness, as well as energetics (71). Akt activation is achieved by phosphorylation at Thr-308 by the phosphoinositide-dependent kinase 1 (PDK-1) and at Ser-473 by mTORC2 (mTOR complex 2). CK2 phosphorylates Akt at Ser-129, a residue located in a linking region between the PH and catalytic domains, which stabilizes and increases β-catenin activity (44), suggesting an important role for CK2 in regulating cancer energetics and malignant progression of several cancers. Once fully activated, Akt dissociates from the membrane and phosphorylates various proteins, including tuberous sclerosis complex 1/2 (TSC1/2) in the PI3K/Akt/mTORC1 signaling pathway (72).

Akt also phosphorylates β-catenin at Ser-552 (73), an essential component of the canonical Wnt signaling pathway (**Table 1**). Thus, Akt may be sufficient to promote both the metabolic switch and proliferation of several types of cancer cells (71). The canonical Wnt signaling pathway is involved in cell proliferation, migration, and other events traditionally considered to be hallmarks of cancer. In unstimulated cells, β-catenin is down-regulated by a multiproteic complex formed by Axin, GSK-3β, and the tumor suppressor APC. Axin facilitates the phosphorylation of β-catenin by GSK-3β at specific serine and threonine residues at its N-terminal end, driving β-catenin to its ubiquitination and degradation by the proteasome (74, 75). Conversely, aberrant activation of the canonical Wnt pathway in cancer leads to β-catenin stabilization, nuclear translocation, and interaction with the TCF/LEF family of transcription factors (76). Nuclear β-catenin thus drives expression of proteins such as c-Myc, cyclin-D1, cyclooxygenase-2 (COX-2), and survivin (45, 74, 77), which are primarily related to proliferation,

apoptosis resistance, and metastasis, as well as other proteins such as monocarboxylate transporter-1 (MCT-1) and pyruvate dehydrogenase kinase-1 (PDK1), which are associated to cancer energetics (42, 43). Interestingly, the β-catenin antagonist Chibby is related to inhibition of the metabolic switch observed in nasopharyngeal carcinoma (78).

Canonical Wnt pathway activity is increased when β-catenin is phosphorylated at Ser-552 by the Akt kinase (73). Moreover, Akt is phosphorylated by CK2 at Ser-129, which stabilizes and increases β-catenin activity (44), strongly suggesting an important role for CK2 in regulating cancer energetics and malignant progression of several cancers. In addition to Akt, CK2 can also directly up-regulate β-catenin activity by phosphorylating it at Thr-393, which should impede its binding to Axin and APC. Disruption of this binding would block proteasomal degradation, increase stability, and boost nuclear activity of β-catenin (79–82). Several findings have demonstrated that the catalytic CK2α subunit indeed activates the canonical Wnt pathway. This subunit increases β-catenin, COX-2, and survivin expression at the transcriptional level, promoting proliferation and apoptosis resistance in colorectal cancer cells (44, 46, 83). Of note, survivin increases the Warburg effect in PC3 prostate cancer cells by increasing mitochondrial complex II stability (47). Likewise, increased survivin levels correlate with enhanced aerobic glycolysis attributable to mitochondrial function regulation in neuroblastoma cells (84).

Another target of CK2 and β-catenin, oncogenic c-Myc, also has a role in the Warburg effect by inducing the expression of genes related to glucose-derived energetics and glutamine-dependent metabolism, such as the glutamine transporter (ASCT2) and the enzyme glutaminase (48). Interestingly, in colorectal and breast cancer cells, the canonical Wnt pathway may contribute to the maintenance of stemness by regulating the metabolic switch in cancer stem cells (48). Catalytic CK2α subunit overexpression may also increase glucose consumption and extracellular lactate levels in colorectal cancer cells (39). Besides, glucose (but not glutamine) is necessary for the maintenance of CK2α-dependent viability, migration, and invasion in these cells, while those properties are blocked upon inhibition of LDHA (38). This strongly suggests that reduction of migration and invasion via LDHA inhibition could be used as a potential therapy for CK2α-dependent tumors.

Upon silencing of β-catenin expression in breast cancer cells, levels of proteins involved in glucose metabolism and the tricarboxylic acid (TCA) cycle are decreased, while levels of proteins associated with lipid metabolism are increased (85). Additionally, β-catenin silencing promotes the use of acetate while decreasing use of glucose for fatty acid synthesis (85). Finally, β-catenin silencing in breast cancer cells decreases mRNA levels of the peroxisome proliferator-activated receptor gamma coactivator 1-α (PGC-1α), mitochondrial transcription factor A (TFAM), nuclear respiratory factor-1 (Nrf1), and GLUT-1, thus increasing levels of acetyl-CoA carboxylase (ACC), fatty acid synthase (FASN), and sterol regulatory element-binding protein 1 (Srebp1) (85). Interestingly, activation of EGFR induces translocation of the PKM2 enzyme to the nucleus, where it interacts with β-catenin and thereby increases c-Myc expression (86).

MODULATION OF CANCER ENERGETICS BY AUTOPHAGY

A key component of the PI3K/Akt/mTORC1 signaling pathway is the mTOR subunit (**Table 1**), a Ser/Thr protein kinase frequently deregulated in cancer (87, 88). As with the C1 complex, mTOR regulates processes involved in growth-associated metabolism such as protein synthesis through phosphorylation of the effector S6 kinase 1 (S6K1), which promotes ribosomal translation by phosphorylating the ribosomal protein S6 (88). MTORC1 also stimulates translation of the mitochondrial fission process 1 (MTFP1) protein, which controls mitochondrial fission and apoptosis (89). Mitochondrial function is also modulated by mTORC1 through regulation of TFAM levels, promoting mitochondrial DNA replication, transcription, and mitochondrial biogenesis (90). In addition, mTORC1 is crucial in autophagy, a catabolic process of cellular response to low levels of nutrients and growth factors, in which lysosomal enzymes degrade intracellular components and molecules to maintain energetic homeostasis and viability (88).

Despite the above, the role of autophagy as an oncogenic factor or tumor suppressor is controversial and may depend on the origin and progression of the tumor (91). The molecular mechanism for regulating autophagy involves various proteins, including mTORC1, which is down-regulated by the TSC1/2 complex but up-regulated by the Akt kinase, which phosphorylates and inactivates TSC1/2 (71). Consequently, TSC1/2 inactivation favors activation of Rheb, a small GTPase that induces autophagy through both p27/Kip1- and mTORC1-dependent mechanisms. The cell-cycle inhibitor p27/Kip1 has been shown to have a key role in the cellular effect of Rheb in response to serum deprivation in colorectal cancer cells (92). Rheb interacts with and activates mTORC1, which then phosphorylates ULK-1, a kinase responsible for triggering autophagic flux, which is characterized by decreased p62 levels (87, 88, 93). Interestingly, both p27 (49) and p62 (50), and probably also ULK-1 (51), are proteins phosphorylated by CK2.

Genetic and epigenetic alterations in some components of the PI3K/Akt/mTORC1 pathway have been described, such as activating mutations in oncogenes PI3KCA (94) and mTOR (95), loss of function of tumor suppressor PTEN (96), and overexpression of oncogene Akt (97). All of these alterations contribute to an aberrant activation of the pathway, leading to increased tumor growth and ultimately a metastatic phenotype (98). CK2 phosphorylates Akt at Ser-129, and the mutation of this residue to alanine causes a marked decrease in Akt activity. Furthermore, pharmacological inhibition of CK2 or siRNA-mediated reduction of CK2α diminish Akt activity, which is independent of its phosphorylation at Thr-308 and Ser-473 (99). In addition, phosphorylation at Ser-129 has been suggested to play a key role in promoting proliferation of colorectal cancer cells in a β-catenin-dependent way (44), but also in glioblastoma and lung cancer cells through mTORC1 activation (58, 100).

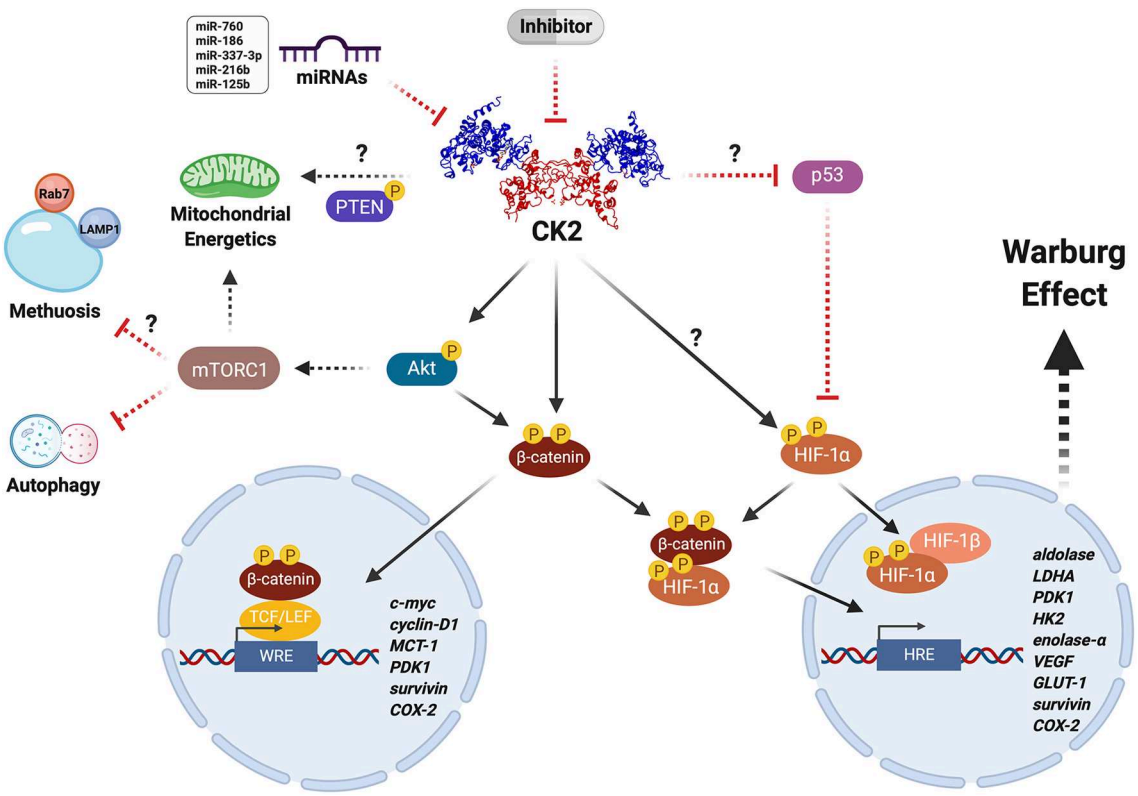

FIGURE 1 | CK2 modulates the Warburg effect in cancer cells under unfavorable conditions. CK2 (PDB: 1JWH) may have a central role in regulating the activity and stability of various proteins including Akt, PTEN, β-catenin, and HIF-1α, under physiological and pathological conditions. CK2-dependent activation of the Wnt/β-catenin, PI3K/Akt/mTORC1, and p53/HIF-1α signaling pathways in cancer cells leads to a metabolic switch that supports proliferation and resistance to death due to either neoplastic drugs or an oxygen- and nutrient-deficient microenvironment, as a result of increased expression of genes that collectively enhance mitochondrial function and glucose metabolism. Altogether, this may be heavily altered upon inhibition with very specific compounds like the CK2 inhibitor, silmitasertib, or alternatively some miRNAs (more details in text). However, whether the latter are able to modulate metabolism and bioenergetics in cancer cells remains yet unknown.

Evidence in the literature suggests that CK2 modulates mTORC1 activity, and decreasing CK2α expression leads to increased autophagy-dependent cell death (ADCD) in glioblastoma cells, which correlates with decreased phosphorylation of S6K1 and Akt (100). Interestingly, expression of proteins that participate in autophagy, amino acid biosynthesis and transport, lipid and glucose metabolism are regulated by Activating Transcription Factor 4 (ATF4) (52, 53). Indeed, CK2 neutralizes the function of ATF4 by phosphorylation; however, under CK2 inhibition, protein levels and transcriptional activity of ATF4 increase (54–56). Moreover, ATF4 promotes the expression of the transcriptional C/EBP Homologous Protein (CHOP) factor, which induces apoptosis via ER stress signaling in colon cancer cells (55, 57). Of note, ATF4 participates, together with the protein kinase RNA-like endoplasmic reticulum kinase (PERK) and eIF2α, in the formation of respiratory chain supercomplexes by increasing levels of SR-related CTD-associated factor 1 (SCAF1), consequently enhancing mitochondrial respiration (101).

In addition, CK2 inhibition with silmitasertib induces autophagy-triggered apoptosis when used alone in rat and human chondrocytes (102). Silmitasertib treatment correlates with decreased mTORC1 activity and massive formation of large acidic LC3-negative cytoplasmic vacuoles in colorectal cancer cells (**Figure 1**). However, while there has been no significant evidence of enhanced autophagy in the presence of silmitasertib, studies have shown elevated levels of a macropinocytosis-linked cell death known as methuosis after silmitasertib treatment (51). In this context, modest levels of autophagy and macropinocytosis should coexist to promote survival in adverse energetic conditions (i.e., unfavorable levels of nutrients, oxygen, etc.); however, CK2 inhibition may cause a shift toward aberrant macropinosome formation, ultimately leading to increased cell death. On the other hand, silmitasertib combined with the EGFR inhibitor erlotinib produces a complete inhibition of the

PI3K/Akt/mTORC1 pathway, inducing apoptosis in squamous carcinoma and lung cancer cells (58). Moreover, a combination of silmitasertib and another EGFR inhibitor, gefitinib, decreases proliferation and induces apoptosis in lung cancer cells (59).

A HARMFUL LINKAGE WITH β-CATENIN AND HIF-1α

Tumors progress in a hypoxic or low-oxygen microenvironment. In this cellular context, the protein HIF-1 plays an essential role in the metabolic switch that promotes the survival of cancer cells (103, 104). HIF-1 is a transcription factor formed by two subunits, HIF-1α, whose expression is inducible, and HIF-1β, also known as aryl hydrocarbon receptor nuclear translocator (ARNT), whose expression is constitutive. In the presence of oxygen, the HIF-1α subunit is cytosolically hydroxylated at prolines, allowing for recruitment of a ubiquitin-ligase complex that contains the Von Hippel-Lindau (VHL) tumor suppressor protein, promoting HIF-1α degradation. Under hypoxia, enhanced HIF-1 stability and activity help tumor cells to survive (105). Stable HIF-1α translocates to the nucleus and interacts with HIF-1β for binding to hypoxic response elements (HRE) at promoter sequences, inducing expression of genes linked to the metabolic switch and other hallmarks of cancer, such as aldolase, LDHA, PDK1, hexokinase 2 (HK2), enolase-α, VEGF, GLUT-1, survivin, and COX-2 (104, 106). Consequently, VHL inactivation also increases the stability of HIF-1α, its nuclear translocation, and expression of target genes (107). For example, over 90% of renal cell carcinomas (RCC) harbor a biallelic inactivation of the VHL gene, becoming highly dependent on aerobic glycolysis for ATP production. Thus, pharmacological impairment of glucose transport results in specific death of RCCs (107, 108).

CK2 activity and levels are elevated in hepatocellular and cervical cancer cells grown under hypoxia, concomitant with increased nuclear localization (60, 61). Interestingly, CK2 inhibition with TBB, 5,6-dichloro-1-β-D-ribofuranosylbenzimidazole (DRB), or apigenin, as well as overexpression of a dominant negative form of CK2α or siRNA-mediated silencing, are all capable of decreasing the transcriptional activity of HIF-1 without altering its protein levels or HRE-binding capacity (60). However, other CK2 inhibitors, such as E9 and silmitasertib, induce a significant decrease in HIF-1α levels in the same cells (62). In addition, CK2 decreases the stability of the tumor suppressor VHL in embryonic kidney cells, while its inhibition with TBB leads to its stabilization, triggering HIF-1 degradation and thereby diminished HRE-associated transcriptional activity (109). These findings strongly suggest an important role for CK2 in regulating HIF-1 stability and activity (**Figure 1**).

Low levels of oxygen inhibit the canonical Wnt pathway in colorectal cancer cells, thereby decreasing expression of its target genes. Here, HIF-1α may be able to interact with β-catenin, preventing its interaction with Tcf-4 (105). Likewise, the HIF-1α/β-catenin complex may bind to the HRE of target genes. Moreover, β-catenin silencing significantly decreases the viability of colorectal cancer cells, likely through inhibition of HIF-1-dependent transcriptional activity (105). On the other hand, COX-2 expression is increased under hypoxia in colorectal cancer cells. The binding of HIF-1α to the HRE of the COX-2 promoter has been observed under these conditions, increasing prostaglandin E2 (PGE2) synthesis and favoring cell proliferation (110). Similar β-catenin-dependent regulated COX-2 expression and PGE2 synthesis have been observed in colorectal and breast cancer cells, as well as in embryonic kidney cells growing under normal oxygen levels, where CK2 expression was either up- or down-regulated (83). While expression of HRE target genes associated with the metabolic switch was not assessed in this study, a role for the HIF-1α/β-catenin complex cannot be ruled out (**Figure 1**). In fact, an *in silico* analysis showed that HIF-1α contains five putative phosphorylation sites for CK2, namely Ser-551, Ser-581, Ser-786, Thr-700, and Thr-796 (60). Moreover, pharmacological inhibition of CK2 with DRB and apigenin decreases aldolase mRNA levels and VEGF secretion in hepatocellular cancer cells exposed to hypoxia (60). Likewise, CK2 inhibition in cervical and hepatocellular cancer cells grown under hypoxia drives an increase in the tumor suppressor p53, its interaction with HIF-1α, and blockage of interaction with HIF-1β, thereby inhibiting HRE-dependent transcriptional activity (63).

CONCLUDING REMARKS/PERSPECTIVES

CK2 catalyzes the phosphorylation of more than 300 substrates, thereby constituting the second most pleiotropic member of the human kinome (26, 28). Some CK2 protein substrates are crucial in various signaling pathways linked to hallmarks of cancer. Thus, it is easy to understand how this kinase may modulate cancer malignancy. In this respect, CK2 is thought of as a non-oncogene target to which some cancers may become "addicted," as proposed early on by Ruzzene and Pinna (29). We have here compiled evidence from the literature suggesting an important role for CK2 in the capacity of some cancer cells to undergo a metabolic switch that confers resistance to death by therapeutic drugs or in response to an unfavorable microenvironment. It is possible that CK2 inhibition may be catastrophic for cancer cells addicted to CK2, leading to massive cell death directly or indirectly perhaps by modulating the function of key targets responsible for the Warburg effect, such as β-catenin or HIF-1, or even by regulating mitochondrial activity via PTEN or autophagy via mTORC1 (**Figure 1**). Something like this seems to happen in colorectal cancer cells treated with the CK2 inhibitor silmitasertib. These cells fall into an irreversible process of self-destruction known as methuosis, a massive entry of extracellular material by macropinocytosis (51).

In a scenario in which cells are addicted to CK2, many proteins that modulate signaling pathways might be highly dependent upon this kinase, along with other key factors modulating glucose metabolism. This fact highlights a putative role of CK2 as an aggressiveness biomarker. Indeed, the catalytic α subunit may serve as a poor prognosis factor in liver and breast cancer (19, 20), while nuclear localization of both

catalytic α and regulatory β subunits may be independently used for predicting the outcome of patients with gastric, renal, prostate or colorectal cancer (21–23). Consequently, specific CK2 inhibition may lead to a loss of viability and metabolic catastrophe in cancer cells. The ubiquitous expression of CK2 and its role in many physiological processes raise some doubts concerning its feasibility as a therapeutic target. However, inhibition of CK2 with silmitasertib, when combined with other drugs such as cisplatin, paclitaxel, temozolomide, gemcitabine or gefitinib, among others, has shown synergistic effects in preclinical models of cancer by decreasing tumor growth (13). Moreover, addiction to CK2 would seem to make cancer cells very susceptible to highly specific inhibitors. In fact, several preclinical studies of newly specific CK2 inhibitors have yielded very promising results. Thus, inhibition of CK2 in CK2-addicted tumors, i.e., cells with markedly elevated CK2 expression and activity, may offer a real therapeutic opportunity in the future.

AUTHOR CONTRIBUTIONS

ES-P and JT designed and outlined the structure, contents of the review, contributed to the literature review, discussion, and writing of the manuscript. All authors contributed to manuscript revision and approved the version to be published.

FUNDING

This study was sponsored by Líneas de apoyo a la investigación financiadas por el ICBM (2020) and Fondo Nacional de Desarrollo Científico y Tecnológico-Chile (FONDECYT 1160889).

ACKNOWLEDGMENTS

Authors wish to thank Dr. Verónica A. Burzio (Universidad Andrés Bello and Fundación Ciencia & Vida) for her valuable critical reading of this work.

REFERENCES

1. Pinna LA, Meggio F. Protein kinase CK2 ("casein kinase-2") and its implication in cell division and proliferation. *Prog Cell Cycle Res.* (1997) 3:77–97. doi: 10.1007/978-1-4615-5371-7_7
2. Allende JE, Allende CC. Protein kinase CK2: an enzyme with multiple substrates and a puzzling regulation. *FASEB J.* (1995) 9:313–23. doi: 10.1096/fasebj.9.5.7896000
3. Litchfield DW. Protein kinase CK2: structure, regulation and role in cellular decisions of life and death. *Biochem J.* (2003) 369:1–15. doi: 10.1042/bj20021469
4. Wilhelm N, Kostelnik K, Montenarh M. Protein kinase CK2 is implicated in early steps of the differentiation of pre-adipocytes into adipocytes. *Mol Cell Biochem.* (2012) 365:37–45. doi: 10.1007/s11010-012-1241-y
5. Jang SW, Hwang SS, Kim HS, Lee KO, Kim MK, Lee W, et al. Casein kinase 2 is a critical determinant of the balance of Th17 and Treg cell differentiation. *Exp Mol Med.* (2017) 49:e375. doi: 10.1038/emm.2017.132
6. Götz C, Montenarh M. Protein kinase CK2 in development and differentiation. *Biomed Rep.* (2017) 127–33. doi: 10.3892/br.2016.829
7. Gibson SA, Benveniste EN. Protein kinase CK2 : an emerging regulator of immunity. *Trends Immunol.* (2018) 39:82–5. doi: 10.1016/j.it.2017.12.002
8. Castello J, Ragnauth A, Friedman E, Rebholz H. CK2 — an emerging target for neurological and psychiatric disorders. *Pharmaceuticals.* (2017) 10:7. doi: 10.3390/ph10010007
9. Cozza G, Pinna LA, Moro S. Kinase CK2 inhibition: an update. *Curr Med Chem.* (2013) 20:671–93. doi: 10.2174/092986713804999312
10. Koch S, Capaldo CT, Hilgarth RS, Fournier B, Parkos CA, Nusrat A. Protein kinase CK2 is a critical regulator of epithelial homeostasis in chronic intestinal inflammation. *Mucosal Immunol.* (2013) 6:2–11. doi: 10.1038/mi.2012.57
11. Ampofo E, Nalbach L, Menger MD, Montenarh M, Götz C. Protein kinase CK2 — a putative target for the therapy of diabetes mellitus? *Int J Mol Sci.* (2019) 20:4398. doi: 10.3390/ijms20184398
12. Trembley JH, Wang G, Unger G, Slaton J, Ahmed K. CK2: a key player in cancer biology. *Cell Mol Life Sci.* (2009) 66:1858–67. doi: 10.1007/s00018-009-9154-y
13. Borgo C, Ruzzene M. Role of protein kinase CK2 in antitumor drug resistance. *J Exp Clin Cancer Res.* (2019) 38:287. doi: 10.1186/s13046-019-1292-y
14. Pérez-Moreno P, Indo S, Niechi I, Huerta H, Cabello P, Jara L, et al. Endothelin-converting enzyme-1c promotes stem cell traits and aggressiveness in colorectal cancer cells. *Mol Oncol.* (2020) 14:347–62. doi: 10.1002/1878-0261.12609
15. Ortega CE, Seidner Y, Dominguez I. Mining CK2 in cancer. *PLoS ONE.* (2014) 9:e1155609. doi: 10.1371/journal.pone.0115609
16. Lee Y, Kim SY, Bae Y. Upregulation of miR-760 and miR-186 is associated with replicative senescence in human lung fibroblast cells. *Mol Cells.* (2014) 37:620–7. doi: 10.14348/molcells.2014.0157
17. Lee Y, Park J, Bae Y. Biochimie Regulation of protein kinase CK2 catalytic activity by protein kinase C and phospholipase D2. *Biochimie.* (2016) 121:131–9. doi: 10.1016/j.biochi.2015.12.005
18. Feliciano A, Castellvi J, Artero-castro A, Leal JA, Romagosa C, Peg V, et al. miR-125b acts as a tumor suppressor in breast tumorigenesis via its novel direct targets ENPEP, CK2-α, CCNJ, and MEGF9. *PLoS ONE.* (2013) 8:e76247. doi: 10.1371/journal.pone.0076247
19. Zhang H, Jiang S, Zhang X, Zhou Z. Protein kinase CK2 α catalytic subunit is overexpressed and serves as an unfavorable prognostic marker in primary hepatocellular carcinoma. *Oncotarget.* (2015) 6:3800–17. doi: 10.18632/oncotarget.5470
20. Giusiano S, Cochet C, Filhol O, Duchemin-pelletier E, Bonnier P, Carcopino X. Protein kinase CK2 a subunit over-expression correlates with metastatic risk in breast carcinomas : quantitative immunohistochemistry in tissue microarrays. *Eur J Cancer.* (2010) 7:792–801. doi: 10.1016/j.ejca.2010.11.028
21. Rabjerg M, Guerra B, Oliván-viguera A, Nedergaard ML, Köhler R, Issinger O, et al. Nuclear localization of the CK2α-subunit correlates with poor prognosis in clear cell renal cell carcinoma. *Oncotarget.* (2017) 8:1613–27. doi: 10.18632/oncotarget.13693
22. Laramas M, Pasquier D, Filhol O, Ringeisen F, Descotes JL, Cochet C, et al. Nuclear localization of protein kinase CK2 catalytic subunit (CK2α) is associated with poor prognostic factors in human prostate cancer. *Eur J Cancer.* (2007) 43:928–34. doi: 10.1016/j.ejca.2006.11.021
23. Lin KY, Tai C, Hsu JC, Li CF, Fang CL, Lai HC, et al. Overexpression of nuclear protein kinase CK2 alpha catalytic subunit (CK2alpha) as a poor prognosticator in human colorectal cancer. *PLoS ONE.* (2011) 6:e17193. doi: 10.1371/journal.pone.0017193
24. Lin KY, Fang CL, Chen Y, Li CF, Chen SH, Kuo CY, et al. overexpression of nuclear protein kinase CK2 β subunit and prognosis in human gastric Carcinoma. *Ann Surg Oncol.* (2010) 17:1695–702. doi: 10.1245/s10434-010-0911-9
25. Perea SE, Baladrón I, Valenzuela C, Perera Y. CIGB-300: a peptide-based drug that impairs the protein kinase CK2-mediated phosphorylation. *Semin Oncol.* (2018) 45:58–67. doi: 10.1053/j.seminoncol.2018.04.006
26. Buontempo F, Mccubrey JA, Orsini E, Ruzzene M, Cappellini A, Lonetti A, et al. Therapeutic targeting of CK2 in acute and chronic leukemias. *Leukemia.* (2017) 32:1–10. doi: 10.1038/leu.2017.301
27. Benavent F, Capobianco CS, Garona J, Cirigliano SM, Perera Y, Urtreger AJ, et al. CIGB-300, an anti-CK2 peptide, inhibits

angiogenesis, tumor cell invasion and metastasis in lung cancer models. *Lung Cancer*. (2016) 107:14–21. doi: 10.1016/j.lungcan.2016.05.026
28. Franchin C, Borgo C, Zaramella S, Cesaro L, Arrigoni G, Salvi M, et al. Exploring the CK2 paradox : restless, dangerous, dispensable. *Pharmaceutical*. (2017) 10:11. doi: 10.3390/ph10010011
29. Ruzzene M, Pinna LA. Addiction to protein kinase CK2: a common denominator of diverse cancer cells? *Biochim Biophys Acta Proteins Proteomics*. (2010) 1804:499–504. doi: 10.1016/j.bbapap.2009.07.018
30. Kim H, Choi K, Kang H, Lee S, Chi S, Lee M, et al. Identification of a novel function of CX-4945 as a splicing regulator. *PLoS ONE*. (2014) 9:e94978. doi: 10.1371/journal.pone.0094978
31. Jiang H, Dong J, Song K, Wang T, Huang W, Zhang J. A novel allosteric site in casein kinase 2α discovered using combining bioinformatics and biochemistry methods. *Acta Pharmacol Sin*. (2017) 38:1691–8. doi: 10.1038/aps.2017.55
32. Schwind L, Nalbach L, Zimmer AD, Katja B, Menegatti J, Grässer F, et al. Quinalizarin inhibits adipogenesis through down-regulation of transcription factors and microRNA modulation. *Biochim Biophys Acta Gen Subj*. (2017) 1861:3272–81. doi: 10.1016/j.bbagen.2017.09.018
33. Janani C, Kumari DRB. Diabetes & metabolic syndrome : clinical research & reviews PPAR gamma gene – a review. *Diabetes Metab Syndr Clin Res Rev*. (2015) 9:46–50. doi: 10.1016/j.dsx.2014.09.015
34. Li D, Chen L, Hu Z, Li H, Li J, Wei C, et al. Alterations of microRNAs are associated with impaired growth of MCF-7 breast cancer cells induced by inhibition of casein kinase 2. *Int J Clin Exp Pathol*. (2014) 7:4008–15.
35. Duchemin-pelletier E, Baulard M, Spreux E, Prioux M, Burute M, Mograbi B, et al. Stem cell-like properties of CK2β-down regulated mammary cells. *Cancers*. (2017) 9:1–14. doi: 10.3390/cancers9090114
36. Hanahan D, Weinberg RA. Hallmarks of cancer: the next generation. *Cell*. (2011) 144:646–74. doi: 10.1016/j.cell.2011.02.013
37. Corbet C, Feron O. Cancer cell metabolism and mitochondria: nutrient plasticity for TCA cycle fueling. *Biochim Biophys Acta Rev Cancer*. (2017) 1868:7–15. doi: 10.1016/j.bbcan.2017.01.002
38. Im DK, Cheong H, Lee JS, Oh MK, Yang KM. Protein kinase CK2-dependent aerobic glycolysis-induced lactate dehydrogenase A enhances the migration and invasion of cancer cells. *Sci Rep*. (2019) 9:5337. doi: 10.1038/s41598-019-41852-4
39. Yang KM, Kim K. Protein kinase CK2 modulation of pyruvate kinase M isoforms augments the Warburg effect in cancer cells. *J Cell Biochem*. (2018) 119:8501–10. doi: 10.1002/jcb.27078
40. Zhang X, Yang X, Yang C, Li P, Yuan W, Deng X, et al. Targeting protein kinase CK2 suppresses bladder cancer cell survival via the glucose metabolic pathway. *Oncotarget*. (2016) 7:87361–72. doi: 10.18632/oncotarget.13571
41. Qaiser F, Trembley JH, Kren BT, Wu JJ, Naveed AK, Ahmed K, et al. Cell. *Biochem*. (2014) 115:2103–15. doi: 10.1002/jcb.24887
42. Pate KT, Stringari C, Sprowl-Tanio S, Wang K, TeSlaa T, Hoverter NP, et al. Wnt signaling directs a metabolic program of glycolysis and angiogenesis in colon cancer. *EMBO J*. (2014) 33:1454–73. doi: 10.15252/embj.201488598
43. Sherwood V. WNT Signaling: an emerging mediator of cancer cell metabolism? *Mol Cell Biol*. (2015) 35:2–10. doi: 10.1128/MCB.00992-14
44. Ponce DP, Maturana JL, Cabello P, Yefi R, Niechi I, Silva E, et al. Phosphorylation of AKT/PKB by CK2 is necessary for the AKT-dependent up-regulation of beta-catenin transcriptional activity. *Cell Physiol*. (2011) 226:1953–9. doi: 10.1002/jcp.22527
45. Kim PJ, Plescia J, Clevers H, Fearon ER, Altieri DC. Survivin and molecular pathogenesis of colorectal cancer. *Lancet*. (2003) 362:205–9. doi: 10.1016/S0140-6736(03)13910-4
46. Tapia JC, Torres VA, Rodriguez DA, Leyton L, Quest AFG. Casein kinase 2 (CK2) increases survivin expression via enhanced β-catenin-T cell factor/lymphoid enhancer binding factor-dependent transcription. *Proc Natl Acad Sci USA*. (2006) 103:15079–84. doi: 10.1073/pnas.0606845103
47. Rivadeneira DB, Caino MC, Seo JH, Angelin A, Wallace DC, Languino LR, et al. Survivin promotes oxidative phosphorylation, subcellular mitochondrial repositioning, and tumor cell invasion. *Sci Signal*. (2015) 8:ra80. doi: 10.1126/scisignal.aab1624
48. El-Sahli S, Xie Y, Wang L, Liu S. Wnt signaling in cancer metabolism and immunity. *Cancers*. (2019) 11:904. doi: 10.3390/cancers11070904
49. Tapia JC, Bolanos-Garcia VM, Sayed M, Allende CC, Allende JE. Cell cycle regulatory protein p27KIP1 is a substrate interacts with the protein kinase CK2. *Cell Biochem*. (2004) 91:865–79. doi: 10.1002/jcb.20027
50. Matsumoto G, Wada K, Okuno M, Kurosawa M, Nukina N. Serine 403 phosphorylation of p62/SQSTM1 regulates selective autophagic clearance of ubiquitinated proteins. *Mol Cell*. (2011) 44:279–89. doi: 10.1016/j.molcel.2011.07.039
51. Silva-Pavez E, Villar P, Trigo C, Caamaño E, Niechi I, Pérez P, et al. CK2 inhibition with silmitasertib promotes methuosis-like cell death associated to catastrophic massive vacuolization of colorectal cancer cells. *Cell Death Dis*. (2019) 10:73. doi: 10.1038/s41419-019-1306-x
52. Wang C, Huang Z, Du Y, Cheng Y, Chen S, Guo F. ATF4 regulates lipid metabolism and thermogenesis. *Cell Res*. (2010) 20:174–84. doi: 10.1038/cr.2010.4
53. B'chir W, Maurin AC, Carraro V, Averous J, Jousse C, Muranishi Y, et al. The eIF2a/ATF4 pathway is essential for stress-induced autophagy gene expression. *Nucleic Acids Res*. (2013) 41:7683–99. doi: 10.1093/nar/gkt563
54. Schneider CC, Ampofo E, Montenarh M. CK2 regulates ATF4 and CHOP transcription within the cellular stress response signalling pathway. *Cell Signal*. (2012) 24:1797–802. doi: 10.1016/j.cellsig.2012.05.006
55. Intemann J, Saidu NEB, Schwind L, Montenarh M. ER stress signaling in ARPE-19 cells after inhibition of protein kinase CK2 by CX-4945. *Cell Signal*. (2014) 26:1567–75. doi: 10.1016/j.cellsig.2014.03.014
56. Ampofo E, Sokolowsky T, Götz C, Montenarh M. Functional interaction of protein kinase CK2 and activating transcription factor 4 (ATF4), a key player in the cellular stress response. *Biochim Biophys Acta*. (2013) 1833:439–51. doi: 10.1016/j.bbamcr.2012.10.025
57. Rozpedek W, Pytel D, Mucha B, Leszczynska H, Alan Diehl J, Majsterek I. The role of the PERK/eIF2α/ATF4/CHOP signaling pathway in tumor progression during endoplasmic reticulum stress. *Curr Mol Med*. (2016) 16:533–44. doi: 10.2174/1566524016666160523143937
58. Bliesath J, Huser N, Omori M, Bunag D, Proffitt C, Streiner N, et al. Combined inhibition of EGFR and CK2 augments the attenuation of PI3K-Akt-mTOR signaling and the killing of cancer cells. *Cancer Lett*. (2012) 322:113–8. doi: 10.1016/j.canlet.2012.02.032
59. So KS, Kim CH, Rho JK, Kim SY, Choi YJ, Song JS, et al. Autophagosome-mediated EGFR down-regulation induced by the CK2 inhibitor enhances the efficacy of EGFR-TKI on EGFR-mutant lung cancer cells with resistance by T790M. *PLoS ONE*. (2014) 9:e114000. doi: 10.1371/journal.pone.0114000
60. Mottet D, Ruys SPD, Demazy C, Raes M, Michiels C. Role for casein kinase 2 in the regulation of HIF-1 activity. *J Cancer*. (2005) 117:764–74. doi: 10.1002/ijc.21268
61. Pluemsampant S, Safronova OS, Nakahama KI, Morita I. Protein kinase CK2 is a key activator of histone deacetylase in hypoxia-associated tumors. *Int J Cancer*. (2008) 122:333–41. doi: 10.1002/ijc.23094
62. Guerra B, Rasmussen TDL, Schnitzler A, Jensen HH, Boldyreff BS, Miyata Y, et al. Protein kinase CK2 inhibition is associated with the destabilization of HIF-1α in human cancer cells, *Cancer Lett*. (2015) 356:751–61. doi: 10.1016/j.canlet.2014.10.026
63. Hubert A, Paris S, Piret JP, Ninane N, Raes M, Michiels C, et al. Casein kinase 2 inhibition decreases hypoxia-inducible factor-1 activity under hypoxia through elevated p53 protein level. *J Cell Sci*. (2006) 119:3351–62. doi: 10.1242/jcs.03069
64. Luo W, Semenza GL. Pyruvate kinase M2 regulates glucose metabolism by functioning as a coactivator for hypoxia-inducible factor 1 in cancer cells. *Oncotarget*. (2011) 2:551–6. doi: 10.18632/oncotarget.299
65. Torres J, Pulido R. The tumor suppressor PTEN is phosphorylated by the protein kinase CK2 at its C terminus. *J Biol Chem*. (2001) 276:993–8. doi: 10.1074/jbc.M009134200
66. Vazquez F, Grossman SR, Takahashi Y, Rokas VM, Nakamura N, Sellers WR. Phosphorylation of the PTEN Tail Acts as an Inhibitory Switch by Preventing Its Recruitment into a Protein Complex. *J Biol Chem*. (2001) 276:48627–31. doi: 10.1074/jbc.C100556200

67. Correia-Melo C, Passos JF. Mitochondria: are they causal players in cellular senescence? *Biochim Biophys Acta Bioenerg.* (2015) 1847:1373–9. doi: 10.1016/j.bbabio.2015.05.017
68. Liang H, He S, Yang J, Jia X, Wang P, Chen X, et al. PTENα, a PTEN isoform translated through alternative initiation, regulates mitochondrial function and energy metabolism. *Cell Metab.* (2014) 19:836–48. doi: 10.1016/j.cmet.2014.03.023
69. Gandin V, Masvidal L, Cargnello M, Gyenis L, McLaughlan S, Cai Y, et al. MTORC1 and CK2 coordinate ternary and eIF4F complex assembly. *Nat Commun.* (2016) 7:11127. doi: 10.1038/ncomms11127
70. Homma MK, Wada I, Suzuki T, Yamaki J, Krebs EG, Homma Y. CK2 phosphorylation of eukaryotic translation initiation factor 5 potentiates cell cycle progression. (2005) 102:2–7. doi: 10.1073/pnas.0506791102
71. Hoxhaj G, Manning BD. The PI3K–AKT network at the interface of oncogenic signalling and cancer metabolism. *Nat Rev Cancer.* (2020) 20:74–88. doi: 10.1038/s41568-019-0216-7
72. Engelman JA. Targeting PI3K signalling in cancer: opportunities, challenges and limitations. *Nat Rev Cancer.* (2009) 9:550–62. doi: 10.1038/nrc2664
73. Fang D, Hawke D, Zheng Y, Xia Y, Meisenhelder J, Nika H, et al. Protein phosphatase 2A in the regulation of Wnt signaling, stem cells, and cancer. *J Biol Chem.* (2007) 282:11221–9. doi: 10.1074/jbc.M611871200
74. MacDonald BT, Tamai K, He X. Wnt/beta-catenin signaling: components, mechanisms, and diseases. *Dev Cell.* (2009) 17:9–26. doi: 10.1016/j.devcel.2009.06.016
75. Liu C, Li Y, Semenov M, Han C, Baeg G, Tan Y, et al. Control of beta-catenin phosphorylation/degradation by a dual-kinase mechanism. *Cell.* (2002) 108:837–47. doi: 10.1016/S0092-8674(02)00685-2
76. Hurlstone A, Clevers H. New embro member's review T-cell factors : turn-ons and turn-offs. *EMBO J.* (2002) 21:2303–11. doi: 10.1093/emboj/21.10.2303
77. Araki Y, Okamura S, Hussain SP, Nagashima M, He P, Shiseki M, et al. Regulation of cyclooxygenase-2 expression by the WNT and ras pathways. *Cancer Res.* (2003) 63:728–34.
78. Cai CF, Ye GD, Shen DY, Zhang W, Chen ML, Chen XX, et al. Chibby suppresses aerobic glycolysis and proliferation of nasopharyngeal carcinoma via the Wnt/β-catenin-Lin28/let7-PDK1 cascade. *Exp Clin Cancer Res.* (2018) 37:104. doi: 10.1186/s13046-018-0769-4
79. Guerra B, Issinger OG. Protein kinase CK2 in human diseases. *Curr Med Chem.* (2008) 15:1870–86. doi: 10.2174/092986708785132933
80. Seldin DC, Landesman-Bollag E, Farago M, Currier N, Lou D, Dominguez I. CK2 as a positive regulator of Wnt signalling and tumourigenesis. *Mol Cell Biochem.* (2005) 274:63–67. doi: 10.1007/s11010-005-3078-0
81. Song DH, Dominguez I, Mizuno J, Kaut M, Mohr SC, Seldin DC, et al. CK2 phosphorylation of the armadillo repeat region of β-catenin potentiates Wnt signaling. *J Biol Chem.* (2003) 278:24018–25. doi: 10.1074/jbc.M212260200
82. Wu H, Symes K, Seldin DC, Dominguez I. Threonine 393 of β-catenin regulates interaction with axin. *J Cell Biochem.* (2009) 108:52–63. doi: 10.1002/jcb.22260
83. Yefi R, Ponce DP, Niechi I, Silva E, Cabello P, Rodriguez DA, et al. Protein kinase CK2 promotes cancer cell viability via up-regulation of cyclooxygenase-2 expression enhanced prostaglandin E2 production. *J Cell Biochem.* (2011) 112:3167–75. doi: 10.1002/jcb.23247
84. Hagenbuchner J, Kuznetsov AV, Obexer P, Ausserlechner MJ. BIRC5/Survivin enhances aerobic glycolysis and drug resistance by altered regulation of the mitochondrial fusion/fission machinery. *Oncogene.* (2013) 32:4748–57. doi: 10.1038/onc.2012.500
85. Vergara D, Stanca E, Guerra F, Priore P, Gaballo A, Franck J, et al. β-catenin knockdown affects mitochondrial biogenesis and lipid metabolism in breast cancer cells. *Front Physiol.* (2017) 8:544. doi: 10.3389/fphys.2017.00544
86. Yang W, Xia Y, Ji H, Zheng Y, Liang J, Huang W, et al. Nuclear PKM2 regulates β-catenin transactivation upon EGFR activation. *Nature.* (2011) 480:118–22. doi: 10.1038/nature10598
87. Guertin AD, Sabatini DM. Defining the role of mTOR in cancer. *Cancer Cell.* (2007) 12:9–22. doi: 10.1016/j.ccr.2007.05.008
88. Saxton RA, Sabatini DM. mTOR signaling in growth, metabolism, and disease. *Cell.* (2017) 168:960–76. doi: 10.1016/j.cell.2017.02.004
89. Morita M, Prudent J, Basu K, Goyon V, Katsumura S, Hulea L, et al. mTOR controls mitochondrial dynamics and cell survival via MTFP1. *Mol Cell.* (2017) 67:922–35.e5. doi: 10.1016/j.molcel.2017.08.013
90. Morita M, Gravel SP, Chenard V, Sikstrom K, Zheng L, Alain T, et al. mTORC1 controls mitochondrial activity and biogenesis through 4E-BP-dependent translational regulation. *Cell Metab.* (2013) 18:698–711. doi: 10.1016/j.cmet.2013.10.001
91. Santana-Codina N, Mancias JD, Kimmelman AC. The role of autophagy in cancer. *Annu Rev Cancer Biol.* (2017) 1:19–39. doi: 10.1146/annurev-cancerbio-041816-122338
92. Campos T, Ziehe J, Palma M, Escobar D, Tapia JC, Pincheira R, et al. Rheb promotes cancer cell survival through p27Kip1-dependent activation of autophagy. *Mol Carcinog.* (2016) 55:220–9. doi: 10.1002/mc.22272
93. Bjørkøy G, Lamark T, Pankiv S, Øvervatn A, Brech A, Johansen T. Chapter 12 monitoring autophagic degradation of p62/SQSTM1. *Methods Enzymol.* (2009) 451:181–97. doi: 10.1016/S0076-6879(08)03612-4
94. Ligresti G, Militello L, Steelman LS, Cavallaro A, Basile F, Nicoletti F, et al. PIK3CA mutations in human solid tumors: role in sensitivity to various therapeutic approaches. *Cell Cycle.* (2009) 8:1352–8. doi: 10.4161/cc.8.9.8255
95. Murugan AK, Liu R, Xing M. Identification and characterization of two novel oncogenic mTOR mutations. *Oncogene.* (2019) 38:5211–26. doi: 10.1038/s41388-019-0787-5
96. Chowdhury S. Restoration of PTEN activity decreases metastases in an orthotopic model of colon cancer. *Bone.* (2008) 23:755–60. doi: 10.1016/j.jss.2013.03.035
97. Roy HK. AKT proto-oncogene overexpression is an early event during sporadic colon carcinogenesis. *Carcinogenesis.* (2002) 23:201–5. doi: 10.1093/carcin/23.1.201
98. Gulhati P, Cai Q, Li J, Liu J, Rychahou PG, Qiu S, et al. Targeted inhibition of mammalian target of rapamycin signaling inhibits tumorigenesis of colorectal cancer. *Clin Cancer Res.* (2009) 15:7207–16. doi: 10.1158/1078-0432.CCR-09-1249
99. Di Maira G, Salvi M, Arrigoni G, Marin O, Sarno S, Brustolon F, et al. Protein kinase CK2 phosphorylates and upregulates Akt/PKB. *Cell Death Differ.* (2005) 12:668–77. doi: 10.1038/sj.cdd.4401604
100. Olsen BB, Svenstrup TH, Guerra B. Downregulation of protein kinase CK2 induces autophagic cell death through modulation of the mTOR MAPK signaling pathways in human glioblastoma cells. *Int J Oncol.* (2012) 41:1967–76. doi: 10.3892/ijo.2012.1635
101. Balsa E, Soustek MS, Thomas A, Gygi SP, Enriquez A. Article ER and nutrient stress promote assembly of respiratory chain supercomplexes through the PERK-eIF2 a Axis ER and nutrient stress promote assembly of respiratory chain supercomplexes through the PERK-eIF2α Axis. *Mol Cell.* (2019) 877–90. doi: 10.1016/j.molcel.2019.03.031
102. Lee SW, Song YS, Lee SY, Yoon YG, Lee SH, Park BS, et al. Downregulation of protein kinase CK2 activity facilitates tumor necrosis factor-α-mediated chondrocyte death through apoptosis and autophagy. *PLoS ONE.* (2011) 6:e19163. doi: 10.1371/journal.pone.0019163
103. Semenza GL. Targeting HIF-1 for cancer therapy. *Nat Rev Cancer.* (2003) 3:721–32. doi: 10.1038/nrc1187
104. Al Tameemi W, Dale TP, Al-Jumaily RMK, Forsyth NR. Hypoxia-modified cancer cell metabolism. *Front Cell Dev Biol.* (2019) 7:4. doi: 10.3389/fcell.2019.00004
105. Kaidi A, Williams AC, Paraskeva C. Interaction between β-catenin and HIF-1 promotes cellular adaptation to hypoxia. *Nat Cell Biol.* (2007) 9:210–7. doi: 10.1038/ncb1534
106. Masoud GN, Li W. HIF-1α pathway: role, regulation and intervention for cancer therapy. *Acta Pharm Sin B.* (2015) 5:378–89. doi: 10.1016/j.apsb.2015.05.007
107. Zhang J, Zhang Q. VHL and hypoxia signaling: beyond HIF in cancer. *Biomedicines.* (2018) 6:35. doi: 10.3390/biomedicines6010035

108. Chan DA, Sutphin PD, Nguyen P, Turcotte S, Lai EW, Banh A, et al. Targeting GLUT1 and the Warburg effect in renal cell carcinoma by chemical synthetic lethality. *Sci Transl Med.* (2011) 3:94ra70. doi: 10.1126/scitranslmed.3002394
109. Ampofo E, Kietzmann T, Zimmer A, Jakupovic M, Montenarh M, Götz C, et al. Phosphorylation of the von Hippel–Lindau protein (VHL) by protein kinase CK2 reduces its protein stability and affects p53 and HIF-1α mediated transcription Author links open overlay panel. *Int J Biochem Cell Biol*. (2010) 42:1729–35. doi: 10.1016/j.biocel.2010.07.008
110. Kaidi A, Qualtrough D, Williams AC, Paraskeva C. Direct transcriptional up-regulation of cyclooxygenase-2 by hypoxia-inducible factor (HIF)-1 promotes colorectal tumor cell survival and enhances HIF-1 transcriptional activity during hypoxia. *Cancer Res.* (2006) 66:6683–91. doi: 10.1158/0008-5472.CAN-06-0425

Conflict of Interest: The authors declare that the research was conducted in the absence of any commercial or financial relationships that could be construed as a potential conflict of interest.

frontiers in Oncology

REVIEW
published: 25 June 2020
doi: 10.3389/fonc.2020.01010

Metabolic Adaptations in Cancer Stem Cells

Umesh Prasad Yadav[1], Tashvinder Singh[1], Pramit Kumar[2], Praveen Sharma[1], Harsimrat Kaur[1,3], Sadhana Sharma[2], Sandeep Singh[1], Santosh Kumar[2]* and Kapil Mehta[4]*

[1] Laboratory of Molecular Medicine, Department of Human Genetics and Molecular Medicine, Central University of Punjab, Bathinda, India, [2] Department of Biochemistry, All India Institute of Medical Sciences, Patna, India, [3] Desh Bhagat Dental College, Mandi Gobindgarh, India, [4] Department of Experimental Therapeutics, MD Anderson Cancer Centre, The University of Texas, Houston, TX, United States

Cancer stem cells (CSCs) are a small and elusive subpopulation of self-renewing cancer cells with remarkable ability to initiate, propagate, and spread the malignant disease. In addition, they exhibit increased resistance to anticancer therapies, thereby contributing to disease relapse. CSCs are reported to be present in many tumor types such as melanoma, sarcoma, mammary tumors, colon cancer and other solid tumors. These cells from different tumors show unique energetic and metabolic pathways. For example, CSCs from one type of tumor may predominantly use aerobic glycolysis, while from another tumor type may utilize oxidative phosphorylation. Most commonly these cells use fatty acid oxidation and ketone bodies as the main source of energy production. CSCs have a remarkable ability to reprogram their metabolism in order to survive under adverse conditions such as hypoxia, acidosis, and starvation. There is increasing interest to identify molecular targets that can be utilized to kill CSCs and to control their growth. In this review, we discuss how an understanding of the unique metabolism of CSCs from different tumors can offer promising strategies for targeting CSCs and hence to prevent disease relapse and to treat the metastatic disease.

Keywords: cancer stem cell, self-renewal, metabolism, oxidative phosphorylation, anaerobic respiration

OPEN ACCESS

Edited by:
Rafael Moreno-Sánchez, Instituto Nacional de Cardiologia Ignacio Chavez, Mexico

Reviewed by:
Sara Rodriguez-Enriquez, Instituto Nacional de Cardiología, Mexico
Thomas N. Seyfried, Boston College, United States
Peter Bai, University of Debrecen, Hungary

****Correspondence:***
Sandeep Singh
sandeepsingh82@cup.edu.in
Santosh Kumar
santoshnccs@gmail.com

Specialty section:
This article was submitted to Cancer Metabolism, a section of the journal Frontiers in Oncology

Received: *14 January 2020*
Accepted: *21 May 2020*
Published: *25 June 2020*

Citation:
Yadav UP, Singh T, Kumar P, Sharma P, Kaur H, Sharma S, Singh S, Kumar S and Mehta K (2020) Metabolic Adaptations in Cancer Stem Cells. Front. Oncol. 10:1010. doi: 10.3389/fonc.2020.01010

INTRODUCTION

Cancer is the result of the accumulation of genetic and epigenetic changes that eventually lead to uncontrolled cell growth and the gain of invasive functions by cancer cells. Cancer cells from different tumors can exhibit different properties ranging from low to high metastatic potential, low to high cellular plasticity, and chemosensitivity to chemoresistance. Cancerous mass is itself extremely heterogeneous in terms of metabolism, proliferating ability, and morphology due to genetic and epigenetic variations in intra-tumor subpopulations (1). Cancer stem cells (CSCs) represent a small subpopulation of cancer cells within these heterogeneous tumors that are aggressive, undifferentiated, with self-renewal ability, sensitivity to ROS molecules, and are known for hyperactive metabolism. CSCs were first identified in AML in 1997 as a rare and phenotypically different subset of tumor cells. These cells are able to divide in immuno-compromised mice and to give rise to leukemic progenitor cells and then to differentiated tumor cells (2). It is now well-known that altered glucose (through aerobic glycolysis known as "Warburg effect") and lipid metabolism (β-oxidation) is a characteristic feature of CSCs, deciding the fate of their progression and self-renewal. This altered metabolism is now considered an important hallmark of CSCs and targeting cancer metabolism is emerging as a crucial therapy (3–5). Pioneer work by the German

physiologist, Otto Warburg, revealed that metabolic processes are exploited to meet increased energy demands for proliferation and survival. The highly proliferative cancerous state usually differs from normal metabolism by using high glucose uptake in the presence of oxygen (through glycolysis) producing biomass and lactate rather than relying on oxidative phosphorylation for energy (3). Cancer cells increase their glucose consumption with an equal rate of increased glucose supply, while glutamine utilization is also increased for macromolecule synthesis. Altered glucose metabolism by cancer cells is critical for their growth, and to respond to the environmental changes (6).

ONCOMETABOLISM

Metabolic rewiring is essential to meet the increased energy demands by cancer cells for their survival under stressful conditions and to generate metabolic intermediates to meet their rapid growth demands. These metabolic alterations could be the reason for higher proliferation, aggressive invasiveness, and chemo-resistant tumor cells (7–9). The importance of metabolic reprogramming was highlighted in a study showing that disallowing altered metabolic homeostasis using negative modulator of glucose metabolism, slowed the metabolic growth of triple-negative breast cancer (Negative for estrogen, progesterone, and epidermal growth factor 2 receptor) cells due to lowering of lactate production (9). Normal cells predominantly utilize glucose through glycolysis followed by subsequent metabolism of pyruvate via the tricarboxylic acid (TCA) cycle and oxidative phosphorylation (OxPhos) in mitochondria. But highly proliferative cancer cells need to adapt to cellular metabolism to provide regular support for the increased proliferation rate and rapidly generating higher amounts of ATP than non-proliferative cells. The normal proliferating cells such as regenerating hepatocyte or proliferative cells in culture media also utilize glucose anaerobically (10). The metabolic features of the proliferative cell either of normal or transformed differs from non-proliferative cells (11). The normal tissues cells switch their cellular metabolism for proliferation from OxPhos to aerobic glycolysis and once differentiated revert back to OxPhos. Cellular signaling helps in cell proliferation and in maintaining the undifferentiated state of cancer cells as well as in restructuring the metabolism during cancer cell proliferation. This high energy production metabolism is essential to fulfill the energy demands, maintain the increased demand for macromolecules, and tight regulation of the cellular redox status (12). Cancer cells meet their energy demand by metabolizing glucose to lactate via glycolysis in the presence of oxygen rather than mitochondrial OxPhos (13). The Warburg effect i.e., aerobic glycolysis is primarily found in malignant tumor cells for maintenance and survival for cancer cells due to impairment of mitochondrial function in the cancer cells. Studies show that in many cancers, mitochondria are functional and still the cells utilize aerobic glycolysis and show reverse Warburg effect when glycolysis is inhibited (14). The metabolic alterations of a cancer cell depend on various factors such as a change in oncogenes, tumor suppression genes, hypoxic microenvironment, mtDNA mutation, genetic factors, proliferation rate, and others (15). The reason for the decreased mitochondrial OxPhos could be deleted copies of mitochondrial pyruvate carrier (MPC) or its decreased expression. Indeed, forced expression of MPC-1 and MPC-2 increased the pyruvate oxidation (11, 16). Also, the glycolytic rate of ATP production is faster than OxPhos, but the energetic yield of glycolysis of 2 ATP is considerably lower in comparison to OxPhos, which produces 32 ATPs per molecule of glucose (17). For ATP generation, besides glycolysis, other important pathways involved are fatty acid oxidation and amino acid catabolism as shown in **Figure 1**.

Glycolysis, TCA, and OxPhos are an integral component of biosynthesis pathways that are needed to produce metabolic intermediates e.g., acetyl-CoA serves as a substrate for both catabolic and anabolic processes (18). Cells metabolism varies according to cell type i.e., adipocytes undergo increased lipolysis to provide simple lipid for β-oxidation in tumor cells. Adipocytes play a supportive role in tumor progression and metastasis by providing nutrients (lipids in this case) and adipokines that facilitate tumor growth by metabolizing adipocytes (19). Other studies suggest the polymorphism of mitochondria among benign, low malignant and malignant ovarian tumor. For example, platinum-resistant sublines such as SKOW3/CDPP, SKOW3/CBP, A2780/CDDP, and A2780/CBP have lower expression of electron transport chain proteins such as ATP- α, PRDX3, PHB, ETF and ALDH as compared to platinum-sensitive cells SKOW3 and A2780 (20, 21). Lactic acid generated during glycolysis elevates NF-kB mediated IL-8 expression and enhances the tumor progression and angiogenesis (22). Chemokine such as IL-8 mediates tumor progression, angiogenesis, and metastasis in both omental adipocytes and endothelial cells (19, 22). Acidic pH is another important factor regulating enzymatic microenvironment of tumor cells. It is observed that acidic pH results in a significant increase in metastasis of both weak and strong melanoma cell lines A375P and C8161, respectively (23). Lactic acid produced in the cell decreases the pH level activating the MMPs and Cathepsin B, and subsequently increased degradation of collagen IV, enhancing matrix degradation and tumor invasion thus supporting the acidification mediated invasion hypothesis both *in-vitro* and *in-vivo* (24). The Warburg effect i.e., aerobic glycolysis is primarily found in malignant tumor cells in the presence of oxygen while some cancerous cells acquire glycolytic metabolic phenotype only because of the hypoxic environment (25). Besides the overwhelming described role of lactate in tumor energy metabolism (hyperactive glycolysis mostly due to hypoxic environment), the role of oxidative phosphorylation is still important for fulfilling energy demands, macromolecule

Abbreviations: AML, Acute myeloid leukemia; CAM, cell adhesion molecule; CBC, Crypt base columnar; CD, Cluster of differentiation; CPT, Carnitine palmitoyl transferase; CSC, Cancer Stem Cell; CCSC, Circulating cancer stem cells; DCA, Dichloroacetic acid; EMT, Epithelial mesenchymal transition; ESCC, Esophageal squamous cell carcinoma; FAO, Fatty acid oxidation; FANS, Fatty acid synthase; HSC, Hematopoietic stem cells; MPC, Mitochondria pyruvate carrier; OxPhos, Oxidative phosphorylation; PDH, Pyruvate dehydrogenase; PK, Pyruvate kinase; PPP, Pentose phosphate pathway; FDG-PET, Fluorodeoxyglucose-Positron emission tomography; SCC, Squamous cell carcinoma; SCD1, Stearoyl-CoA-desaturase-1; SGLT, Sodium-glucose linked transporter.

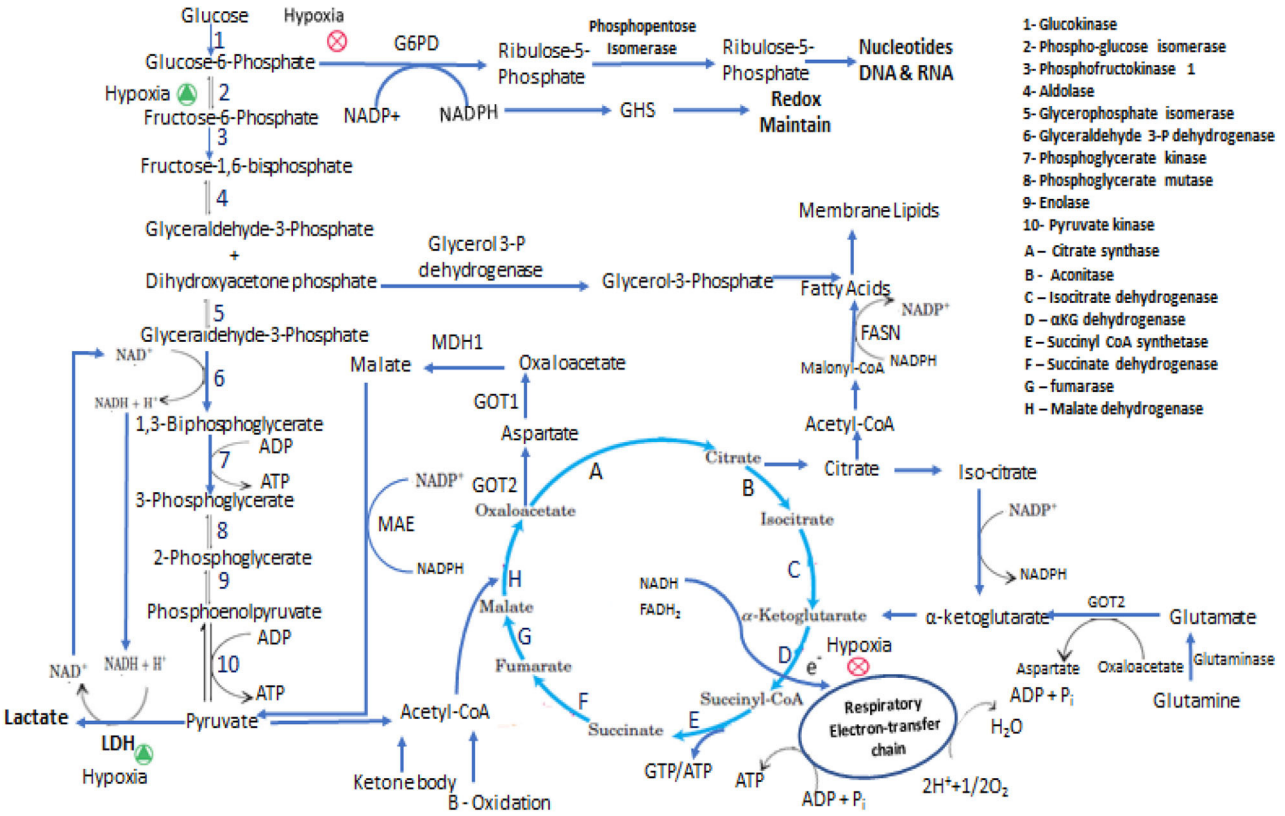

FIGURE 1 | Representation of some of the metabolic adaptation and reprogramming of cancer stem cells. In the interconnected metabolic pathways of glucose, the key junctions are glycolysis and pentose phosphate pathway and central molecules are Glucose-6-phosphate, Pyruvate and Acetyl-CoA. In proliferative state cells metabolized Glucose mainly through PPP and perform less glycolysis and ATP has been produced from TCA cycle via respiratory electron-transfer chain by Acetyl-CoA coming either from pyruvate, Fatty acids and Amino acids oxidation. In Hypoxic condition PPP is inhibited and glucose metabolized through anaerobic glycolytic pathway. In presence of low glucose intermediate metabolites and ATP are produced mainly by glutaminolysis and fatty acids oxidation. CSCs synthesize fatty acids for membrane formation and oxidized this for energy production the equilibrium between anabolism and catabolism of fatty acids is maintain by NADPH and ATP requirement.

biosynthesis in tumor cells (15, 26, 27). Now it is feasible to validate the inevitable role of different energy metabolic processes and their metabolic intermediates participating in macromolecule biosynthesis, cell survival, and supporting metastatic properties. Targeting CSC metabolism thus represents a promising approach to halt tumor growth and disease relapse by understanding their biology and designing novel therapeutic modalities (4, 28).

HETEROGENEITY OF CSCs

Cancer is not a single disease but a group of diseases in which cells share some common features of abnormal cellular processes with extremely heterogeneous metabolic features in each type of cancer. Even within the same tumor, constituent cells are heterogeneous and metabolic phenotypes vary from one cell to another.Despite predominant aerobic glycolytic metabolism and elevated glycolytic enzymes, proliferating cancer cells have poor prognosis in various types of cancer (29). Some studies have reported both inter- and intratumor metabolic heterogeneity within the same type of tumors (30, 31). According to somatic mutation theory, cancer arises from somatic mutations in cells that undergo clonal selection followed by expansion and ultimately becoming malignant. All somatic mutations are not cancer drivers as most but some are passive. One study reported that the prevalence of the somatic mutation in a kinase gene in different types of tumors (lung, breast, colorectal, gastric, ovarian) does not show the mutation in 73 cases out of 210 cases (32). Somatic mutation analysis of NOTCH1, NOTCH2, NOTCH3, TP53, CDKN2A, and other genes by biopsy in normal eyelid epidermis exposed to ultraviolet light of four donors indicated that these driving mutations help in a positive selection over normal tissue for development of colonies which are non-malignant and non- invasive. These genes are often expressed in squamous cell carcinoma (SCC) and are mutated in other skin cancers also. The clones are genetically heterogeneous and the driver mutations transform cells into malignant phenotype. Although the CDKN2A gene is not associated with positive selection over normal tissue but has a positive impact on progression to advanced-stage disease. Similarly, many somatic mutations found in normal esophageal epithelium tissue could yield heterogeneous colonies that could

lead to esophageal SCC in presence of driver mutation. The RNA sequencing of 29 normal tissues out of 6,700 tissue samples revealed multiple somatic variants (33). Studies conducted using deep genome sequencing, histopathological studies or molecular marker analyses revealed a surprising morphological, genetic and clinical heterogeneity of cancer cells that fluctuates within the tumor mass (34–36). There are two theories that explain the reason for heterogeneity; clonal variation and cancer stem cell theory; both vary with tumor subtypes. Clonal variations theory supports the role for genetic, epigenetic, and micro-environment changes that contribute to tumor heterogeneity where tumor cells differ in phenotypic and metabolic processes (37, 38). Whereas, the cancer stem cells theory supports the notion that transformed stem cells (sub populated part of the tumor mass) acquire the properties like high tumorigenic and malignant potential to generate differentiated tumor cell pools (39). The cancer therapeutics should be developed on the basis of tumor type and evaluating CSCs to identify the origin and reason for the problem that will help to find the solution (40). The tumor cells are phenotypically and functionally heterogeneous and this heterogeneity could be intra-tumor or inter-tumor. One such study conducted on 72 patients using FDG-PET analysis has quantified the intratumoral metabolic heterogeneity in primary cervix tumors indicating its relevance with tumor volume rather than tumor stage or histology (41). A similar study conducted on 93 patients with metabolic heterogeneity in cervical cancer using FDG-PET evaluated the significance of heterogeneity as a prognostic marker for predicting tumor relapse. Higher heterogeneity was seen in patients with poor survival and high disease relapse rates than in non-relapsed cancer patients (42). The CSCs contribute to this tumor heterogeneity within a single tumor mass and is responsible for reestablishing the same phenotypic heterogeneity (as in parent tumor) elsewhere upon serial passaging or transplanting *in-vivo* (43). Improved technology has uncovered additional features of heterogeneity of tumors including variations in cell surface markers, tumor growth, and response to therapy. There is strong evidence supporting that multiple tumor cell subpopulations exist within single cancer e.g., single subcutaneous tumor contained 6 clonal variations from slow-growing to fast-growing melanomas (44), karyotypic heterogeneity in fibrosarcoma (45), and genetic heterogeneity in mouse mammary tumor (46). Similarly, the tumor cell heterogeneity was reported in colon cancer (47) and other transplantable and inter-convertible solid tumors (48, 49). The heterogeneous tumors generally comprised of undifferentiated CSCs, supportive cells, differentiated tumor progenitors, and tumor-infiltrating cells (2, 50). In addition, revertible phenotypic heterogeneity in melanoma cells from the patient's sample without hierarchy (51) and cells contributing to variable tumorigenic frequency in SCID mice from single melanoma tumor has been observed (52). Furthermore, human glioma contains subpopulations of cells with morphological and karyotypic heterogeneity that further gets intensified upon clonal variation and microenvironment. These subpopulations of human glioma cells differed in morphological (fibrous, squamous, and astrocytes), chemosensitivity, and rate of tumor growth (53–55). While most of the studies point out the relationship between variations of phenotype and metabolic process, such is not always the case. Phenotypic heterogeneity of CSCs/clonal variation-derived differentiated tumorsare not necessarilyinvasive. These genes are often expressed in SCC and mutated in other skin cancersalso. The clones are genetically heterogenous and further driver mutation transform the cell into malignant. CDKN2A gene is not associated with positive selection over normal tissue but on advanced stage has positive selection impact. Similar observations found that mosaicism of somatic mutation found in physiological normal esophageal epithelium generating heterogenous colonies and driver mutations leading toesophageal SCC. Isolated tumor cells from metastatic colon cancer show self-renewal as well as tumor-initiating properties and maintain stemness up to several generations, resulting in homogeneity of tumor subpopulation (56). Within a tumor mass, microenvironmental stress-mediated cancer cell's response can result in heterogeneous gene expression; where some cells are more sensitive to these stresses than others. The malignant efficiency of heterogeneous tumor cells differs in terms of tumor initiation, invasiveness, metastasis, and chemo-resistance (57). The variable nature of cancer cells includes some highly active and self-renewal aggressive cells (referred to as CSCs) that are modulated by epigenetic factors such as DNA and histone modifications (DNA methylation, histone trimethylation, and mono acetylation), and chromatin modifiers (58, 59). CSCs represent a small and elusive subpopulation of cancer cells within a tumor mass with stem cell properties and are responsible for enhanced tumorigenesis, EMT-mediated metastasis, relapse, resistance to combinatorial treatment and variant epigenetic expression (60–63). CSCs divide to replenish the tumor cells pool in a symmetrical manner whereas asymmetrical cell division gives rise to non-CSCs that are less tumorigenic, less proliferative, poorly metastatic, and more differentiated. These differentiated non-CSCs tumor cells exhibit non-heterogeneous nature of the tumor where the majority of cells in the primary tumor do not show stemness properties. According to recent evidence, these CSCs and non-CSCs may exhibit inter-convertible plasticity (1, 64). The heterogeneity of CSCs and plasticity in differentiated tumor cells (non-CSCs) supports the inter-convertible feature of CSCs and heterogeneous tumor mass (64)On the basis of phenotypic and genetic heterogeneity, tumor cells are arranged in hierarchical order with the CSCs comes at the top while the most differentiated tumor cells at the bottom (65). Multiple CSCs have also been reported in many other cancers including prostate, lung, liver, pancreas, kidney, bladder, ovary, and brain etc. (66). Isolated pure normal human breast "stem cells" showed same marker expression as of breast tumors and more CSCs were isolated from undifferentiated grade 3 tumors than the differentiated grade 1 tumor. Taken together these observations suggest that CSCs give rise to more heterogeneous tumors than non-CSCs cancer cells (67). In ovarian cancer too, spheroid cells are known to have CSCs like properties with increased ALDH activity and show high tumorigenic and metastatic potential both *in-vitro* and *in-vivo* and are more resistant to cisplatin (68). Recent studies documented that most of the solid breast tumor cell lines expressing CD44 (basal-like cells), CD24 (luminal-like

cells), PROCR, and ESA are highly tumorigenic and show EMT markers on their surface and play role metastasis, instead of commonly thought CD44+ /CD24–/low and ALDH expression. The studies also advocated that not only CSC marker signature in breast cancer cells is heterogeneous but many subsets of CSC exist that vary from patient to patient and may be related to the individual genetic makeup of the tumor (69).

CSC MARKERS AND CIRCULATING CANCER STEM CELLS

CSCs from different cancer types can be isolated based on the presence of cell surface markers. CSCs express stemness markers such as CD133, CD34, CD24, CD44, CD166, and EpCAM, ESA, ALDH1on cell surfaces (66, 70). BCNU resistant subpopulation of Glioma cells exhibits stem cell-like properties, and express CD133, CD117, CD90, CD71, and CD45, also revealing tumorigenicity *in vivo* upon transfer to SCID mice (71). The markers expressed by these CSCs are required for their stemness, invasiveness, and tumorigenic properties and differ in different subtypes of cancers. For example, CD44+/CD24- in breast CSCs (72), ALDH1+ breast carcinoma (73); CD44 expression in prostate CSCs (74); CD133 (75), ALDH1(76), and CD44 (77) expression in lung CSCs; ALDH1expressing epithelial CSCs (78); while human glioblastoma expressing SSEA-1 (79), EGFR (80), CD44 and Id1 (81). These cancer stem cell markers are essential for their self -renewal, migratory ability, and tumorigenesis such as in the case of the role of CD133 and CXCR4 in pancreatic CSCs (82). The CXCR4 is inevitably responsible for tumor cell invasion to the site of metastasis and tumor cell mobility (pseudopodia formation and actin rearrangement) (83, 84). Brain tumor CSCs expressing CD133 antigen were able to develop tumors *in-vivo* in SCID mice while the CD133-negative brain tumor cells failed to establish tumors in these mice (85). All these findings suggest that CSCs exhibit particular kinds of stemness markers responsible for self-renewal and tumorigenicity. The therapeutic intervention targeting CSCs markers is still an undiscovered field of study. It not only could delay the cancer progression but may possibly kill CSCs having tumorigenic/stemness properties. There is a special circulating subset of CSCs known as circulating cancer stem cells (CCSCs). The CCSCs detected and analyzed by Raman imaging from four breast cancer subtypes, showed the expression of CD133 marker. Upon culture of CCSCs in breast cancer differential media these cells showed changes in the expression of cell surface markers such as Her2 and EGFR (beside CD133) suggesting their differentiation into Her2+ breast cancer. The CCSCs were endowed with self-renewal ability, tumorigenicity, differentiation, stemness, and metastatic property both *in-vitro* and *in-vivo* (86). Isolating CCSCs from a heterogeneous CSCs population from advanced-stage tumors may offer new insight into cancer metastasis and disease relapse. Poor prognosis and relapse with chemo-resistivity were reported in cervical cancer having chromosomal aberration and high genetic heterogeneity that generally developed during cancer progression (87). As in the case of cervical CSCs, traditional anticancer therapies do not work due to overexpression of drug efflux transporter i.e., ABCG2 in undifferentiated tumor subpopulation indicating its role in maintaining stemness (88). Liver metastatic colorectal cancer cells express high levels of various progenitor markers such as EpCAM, CD44, CD24, and CEA-CAM along with CDX1. Cells expressing these markers show a close correlation with stemness, disease progression, and susceptibility to chemotherapy however their continuous exposure to chemotherapy resulted in the development of drug resistance phenotype. These observations suggest that CSCs mediated heterogeneity of tumors is important for metastasis and chemoresistance and that failure to target these cells results in tumor relapse.

EMT AND CSCs

The epithelial-to-mesenchymal transition (EMT) defines the transition of some tumor cells from differentiated to an undifferentiated state, linking it with cancer progression and metastasis. EMT-related transcription factors such as Wnt, TGF-β, Notch ligands regulate EMT mediated cancer progression, tumor cell plasticity and increased tumorigenicity (89, 90). Thus, EMT is an important factor regulating heterogeneity, metastatic ability, and plasticity of the tumor cells. Plasticity in breast CSCs can be decoded with interchangeable expression of two marker profiles i.e., CD24-CD44+ (mesenchymal type) and slightly higher tumorigenic potent ALDH+ (epithelial type). Breast cancer cells undergoing EMT show the stemness and tumorigenic properties which are regulated by the tumor microenvironment (91). EMT pathway is multi-step process, which starts with loss of epithelial markers and acquiring the mesenchymal characteristicsenabling them to metastasizetodistantorgansvia activation of proteases, degradation of extracellular matrix and formation of new blood vessels (angiogenesis). EMT is a fundamental first step in successful invasion of cancer cells from primary tumor to distant organs in response to sensing the low nutrient supplies at primary tumor site. *In vitro* induction of EMT in human mammary epithelial cells is associated with loss of epithelial marker proteins, gain of mesenchymal marker proteins, ability to form spheroids, anchorage independent growth and acquisition of stem cell-like phenotype (92, 93). Similar*ex-vivo* results were reported in samples isolated from human breast carcinoma and normal mouse mammary stem cells with $CD44^{high}/CD24^{low}$ expression (94). Human mammary epithelial cells induced simultaneously by Ras-MAPK and EMT pathway activation exhibited both tumorigenic and stemness properties. Combined ectopic expression of $H\text{-}Ras^{v12}$ and TGF-β1 shortened the time taken to acquire mesenchymal phenotype in CD24+ cells (95). Activation of the Notch pathway resulted in increased NF-kB signaling and upregulated the expression of mesenchymal markers as observed in gemcitabine-resistant pancreatic cancer cells. Conversely, inhibition of the notch pathway or its downstream targets attenuated NF-kB activation, invasion, loss of epithelial markers and gain of mesenchymal markers in gemcitabine-resistant pancreatic cancer cells (96). Upregulated expression of EMT markers in hepatocellular carcinoma (HCC)

is considered to be essential for their malignant phenotype as well as for transformation of non-differentiated malignant cell (97). Various transcription activators/repressors and miRNAs either stabilize or antagonize the EMT-induced stem cell traits and undifferentiated state in cancer cells. These miRNAs silence the protein expression of mRNA transcripts by guiding them for degradation while transcriptional repressors and activators downregulate or upregulate the gene transcriptional activity, respectively. ZEB-1 a transcriptional repressor of epithelial marker genes (e.g., E-cadherin) is an inducer of EMT and inhibits the expression of miR-200c and miR-141, the negative regulators of an EMT pathway. Thus, ZEB1 and ZEB2 are responsible for upregulating and downregulating the mesenchymal and epithelial phenotypes, respectively, while miR-200 family has just the opposite effect (98–102). Expression of miR-200 family genes is inhibited when cancer cells acquire the stem cell traits and its expression inhibits mammosphere formation. However, the transient downregulation of miR-200b had no observable effect on CSCs formation. MiR-200b inhibits the Suz12 and its regulated E-cadherin repression (103). Micro RNAs that inhibit stemness (such as miR-200a, miR-200b, miR-200c, miR-141, miR-429, miR-205, miR-203 and miR-183) do so by inhibiting the stem cell regulators such as ZEB1, ZEB2, SIP1, Sox2, Klf4 and hence repress the stemness maintenance and EMT induced CSCs formation (104, 105). EMT regulation is not restricted to the miRNA repression/activation or to the action of activators/repressors such as ZEB1, TGF-β1 and Ras-MAPK pathway; rather it is controlled by many transcriptional factors. Wnt/β-catenin signaling is a key positive regulator of EMT and CSCs formation. Indeed, the high Wnt/β-catenin signaling correlates with the progression of EMT, increased malignant phenotype and acquiring of stem cell traits (106–111). Disrupted Wnt signaling regulates the expression of β-catenin in colorectal cancer cells and is another example of transcriptional activators of oncogenes. Overexpressed β-catenin in cells undergoing EMT at the invasive front was observed in colorectal cancer while such expression was absent in normal colon epithelial cells present far from the invasion site (106). High canonical Wnt/β-catenin signaling in breast cancer demonstrates the action of β-catenin-TCF complex-mediated Snail1 activity and thus regulating EMT in Axin2 dependent pathway (107). PGE2 mediated C-terminal phosphorylation of β-catenin stabilizes it and upregulates Wnt signaling which is the conserved path for hematopoietic stem cell (HSC) formation, self-renewal, and for their sustenance (110). In yet another study, the prevalence of β-catenin expression in T-cell malignancy and non-Hodgkin lymphomas were analyzed and the activated Wnt signaling and highly accumulated β-catenin levels were observed in the nucleus in almost one-third of the tumor samples with some having gained the functional mutation in the β-catenin gene (109). HSCs with β-catenin deletion have difficulty in maintaining the prolonged growth and stemness ability without having any effect on differentiation to their subsequent lineage. *In vivo* transplantation of cells with β-catenin deletion and expressing BCR-ABL transcripts imparted hind limb paralysis but could not induce leukemic phenotype in mice, while cells expressing wild type β-catenin could successfully induce CML in mice. The loss of β-catenin attenuated the progression of CML and self-renewal ability of CML stem cells, thus β-catenin could be one of the few hallmarks of CSCs survival and tumorigenicity (108). Take together, these observations suggest that Wnt/β-catenin signaling has an important role in the development of tumorigenicity and stemness features of CSCs. Thus, we can conclude that EMT is a necessarily parallel path by multi-grades tumor cells or CSCs for cancer progression, and thus to acquire metastatic and stem cell-like properties.

METABOLIC REWIRING OF CANCER STEM CELLS

Energy metabolism is an important physiological function to support the survival of cells and is critical for cancer progression. Hepatocellular CSCs expressing CD133+ stemness marker showed increased glucose metabolism than CD133- cells while inhibiting glycolytic enzymes in CD133+ CSCs by siRNA reduced the expression of Sox2, Oct4, and Nanog genes important for stemness. Providing extracellular glucose to CD133- cells, increased their stemness property (112). Pancreatic CSCs expressing stemness markers exhibit its dependency on the non-canonical pathway of glutamine metabolism and displayed increased apoptosis and ROS- generation in response to glutamine deprivation from the cell cultures. The pancreatic CSCs were readily sensitized to radiotherapy, accumulated ROS- in response to inhibition of glutamine metabolism both *in-vitro* and *in-vivo* (113). In another study, pancreatic CSCs showed increased expression of pluripotent stem cell markers (CD133, SSEA-1, CD44, and CXCR4) in response to activation of Nodal/Activin signaling or expression of its downstream mediators. The Nodal/Activin signaling pathway is important for stemness properties as their inhibition resulted in the sensitization of pancreatic CSCs to gemcitabine and abrogated theirs *in vivo* tumorigenic potential (114). CSCs exhibit unique metabolic adaptation to physiological and metabolic stresses such as decreased energy source, hypoxia, pH of the microenvironment, etc., thus CSCs differ in metabolic processes when compared to the non-CSC differentiated tumor. Evidence reports the similarity between CSCs and normal stem cells in their ability to differentiate into more mature cells and to self-renewal. CSCs metabolism is predominantly glycolytic but depending on the tumor type can partly be dependent on OxPhos too (115). The preference of glycolytic metabolism in CSCs over OxPhos will not be totally correct as growing evidence suggests that OxPhos has an enormous effect on CSCs survivability (116). In one such study, it was suggested that glioblastoma CSCs rely on Imp2 regulated OxPhos for their energy demand, survivability, *in vitro* clonogenicity and tumorigenic properties. Depletion of the Imp2 impaired the OxPhos and subsequently resulted in the loss of stem cell properties in glioblastoma CSCs (117). Leukemia CSCs expressing CD34+/CD38- in a dormant state are characterized by low ROS- production and lower glycolysis dependency while Bcl-2 regulated OxPhos is the main source of energy. Inhibition of the Bcl-2 impaired the OxPhos pathway and subsequently eradicated the quiescent leukemia CSCs (118). There is metabolic difference between CSCs and

normal stem cells and also between CSCs and differentiated tumor cells, so further studies are warranted to elucidate the role of preferred energy metabolic process over other metabolic processes in a particular type of CSCs (119). It has been reported in glioma cancer stem cell and progenitor cells that CSCs exhibit low glucose consumption, low lactate production, high ATP generation, and high mitochondrial oxidation for their energy demands than their differentiated glioma cell, suggesting OxPhos be the main source for metabolic and energy dependency. The factors that make the difference in metabolism include oxygen consumption rates, extracellular acidification rate, intracellular ATP level, glucose uptake, lactate production, pyruvate kinase M1 (PKM1) levels, and pyruvate kinase M2 (PKM2) expression, cell cycle duration (120). There are convincing reports demonstrating that pancreatic and lung CSCs too depends on OxPhos as the main source of energy production and cell survivability. High mitochondrial membrane potential, low mitochondrial DNA, low ATP and ROS-, lower oxygen consumption over glucose metabolism were reported in lung CSCs when compared to non-lung CSCs. Thus, mitochondrial metabolism is a significant measure of differentiating lung CSCs from non-lung CSCs and may be used to signify other CSCs types (121). Pancreatic CSCs with low metabolic plasticity are highly dependent on OxPhos and are sensitized to metformin drug when compared to primarily glycolytic insensitive non-CSCs (122). However, other investigators have reported that CSCs are more dependent on anaerobic glucose metabolism. The metabolism not only differs in differentiated and CSCs but also varies from their progeny. Breast CSCs predominantly use glycolytic metabolism with a high level of LDH-1 and PKM2 (anaerobic glycolytic enzymes) and low β-oxidation as its main metabolic feature; anaerobic glycolysis inhibitor, 2-deoxyglucose reduced the cell growth and survivability of breast CSCs (123). Human U87 glioblastoma CSCs isolated from xenograft modeled mice exhibited dependency on glycolytic metabolism along with low OxPhos and preference for hypoxia-mediated stemness and chemoresistance. *In vitro* inhibition of glycolysis induced cytotoxicity and retarded the tumor growth in mice (124). PKM2 plays an important role in anaerobic glycolysis, though is not essential for cancer cell survival or progression and is known to inhibit aerobic glycolysis (125, 126). However, in CSCs, which are more like non-dividing cancer cells, CSCs may require PKM2 for energy related functions as well as maintaining their status (126, 127).

Osteosarcoma CSCs are dependent on high glycolysis and low OxPhos for energy and survival when compared to non-CSCs MG63 cells. LDHA inhibition using sodium oxamate resulted in greater cytotoxicity against CSCs than the MG63 cells while low glucose induced increased fragmented mitochondrial morphology in contrast to network mitochondrial morphology in MG63 cells. These findings support the inability of CSCs mitochondria to become more active under glucose starvation (128). Breast CSCs showed expression of high glycolytic and low OxPhos related enzymes and fewer mitochondria when compared to non-tumorigenic cancer cells indicative of hyper glycolytic metabolism in these CSCs. DCA mediated increase in PDH enzyme (involved in OxPhos) expression in CSCs resulted in increased cytotoxicity *in vitro* and decreased tumor growth *in vivo* (129). Hypoxia-induced stemness and glycolytic dependency of breast CSCs is the main reason for chemoresistance in CSCs. However, glycolytic inhibitor along with combinatorial drugs under these conditions makes the CSCs more sensitive to conventional therapies. Leukemia CSCs exhibiting low FAO and high Myc expression with increased concentration of lactate, citrate, and succinate could be positively linked with CD133+ stemness marker as compared to non-cancer stem cells. High lactic acid production is correlated with hyperactive glycolysis in CD133+ cells, through the enzymatic activity of LDHA (112, 130). Radioresistant nasopharyngeal carcinoma CSCs and hypoxia resistant spheroid cells of ovarian cancer exhibiting stemness properties mainly follows the glycolytic pathway and use the byproduct amino acids in biosynthetic pathways rather than their complete oxidation and FA biosynthesis, respectively (68, 131). While the mitochondrial respiration was shut off in nasopharyngeal carcinoma CSCs, the mitochondrial activity and biogenesis were still active in expressing low-ROS and higher TFAM, POLG, and PGC-1a genes (131). The microenvironment of the cells gives clues about active metabolic programming. For example, Paneth cells with increased glycolytic metabolism that supports intestinal stem cells are known to be Lgr+ crypt base columnar cells (CBCs). Paneth cells are functional in the intestinal crypt and produce lactate which is converted into pyruvate to support mitochondrial OxPhos in CBCs having high mitochondrial activity and low redox burden (132). In general, stem cells such as hematopoietic stem cells and human mesenchymal stem cells mainly follow glycolytic metabolism to fulfill their energy demands and shift to other metabolic pathways upon their differentiation. Osteogenic induction of human mesenchymal stem cells is followed by increased mt-DNA copy number, OxPhos, and decrease in cytosolic ROS-, glycolytic metabolism, lactic acid formation while the accumulation of ROS- and increased OxPhos mitigates osteogenic differentiation of human mesenchymal stem cells (133). Glycolytic dependent and hypoxia-resistant HSCs showed low mitochondrial potential, low OxPhos, and high stemness properties and increased expression of HIF-1α both *in vitro* and *in vivo* (134). These findings suggest that CSCs can exhibit variable metabolic features depending on their origin and the microenvironment in which they metastasize. Metastatic competent 4T1 breast cancer cells expressed increased capacity for both glycolytic and oxidative metabolism compared to non-metastatic 67NR cells. For example, changes such as PDK-1 support glycolytic metabolism in liver cells but OxPhos metabolism in lung and bone cells (135). Hyperoxia mediated aerobic glycolysis downregulates ROS- in CSCs while in the absence of glucose and hypoxic conditions CSCs metabolism shifts to the mitochondrial respiration. These variations in glucose metabolisms may be influenced by the tumor microenvironment (136).

GLYCOLYSIS AND OXPHOS CORRELATION IN TUMORIGENICITY

Many metabolic processes e.g., Glycolysis and OxPhos (primary), fatty acid oxidation (secondary) that are regulated by the microenvironment may vary in ATP production in order to

fulfill the energy demands and to fuel the anabolic pathways for cancer cells growth (137). The glycolytic product pyruvate undergoes OxPhos under normal aerobic conditions but is converted to lactate by lactate dehydrogenase-A (LDH-A) under an anaerobic state and is transported to the extracellular fluid through MCT (subfamily of cell membrane transporters). These pathways are co-regulated to maintain energy balance. While glycolysis provides instant energy and is the main source for ATP under hypoxic environment, the energetic yield via ATP production is too low compared to ATP production via OxPhos pathway (15). Glycolysis is predominantly activated in tumor cells and aerobic glycolytic cells under hypoxic conditions but OxPhos too does not lose its ability to generate energy (ATP) required for tumor growth. OxPhos is rather suppressed by enhanced glycolysis. Suppression of one metabolic pathway in tumor cells is paved away by another metabolic process to be activated, and it is dependent on the tumor microenvironment. Tumor cells might have functional OxPhos (137–141) despite having multiple mtDNA mutations (142) due to large number of heterogenous genomic copies. The stroma adjacent to tumor cells exhibits high glycolysis which acts as a fuel for active OxPhos in epithelial tumor cells with functional mitochondria (143). Overall, factors such as nutrients, oxygen availability, tumor microenvironment, cell's energy demands, etc., determine the switch between different metabolic pathways.

METABOLISM OF GLUCOSE IN CSCs

As previously stated, glucose is one of the main sources of energy for both CSCs and differentiated tumor cells, providing instant energy but with a lower yield. Glycolysis serves two purposes, one it provides energy readily to the cell, and second, the glycolytic end-product (pyruvate) is involved in the biosynthesis of amino acids (through TCA cycle intermediates), and lipids (precursor for acetyl CoA). Thus, meeting the need of proliferating metastatic cancer cells, which require high energy and precursors for macromolecule biosynthesis in a very short time frame (3, 144). Increased glucose concentration and higher expression of glucose transporters such as GLUT and SGLT, increase glycolysis and is linked with increased viability of tumor cells and CSCs (145–147). There are two classes of glucose transporters which facilitate the transport of glucose by different mechanism.

The GLUT transporters facilitate glucose uptake along the gradient while sodium-dependent SGLT transporters does against the gradient by (148–150). GLUT1 is primarily responsible for glucose uptake in tumor cells e.g., relieving glucose depleted prostate tumor cells from oxidative stress (151, 152). There are also some reports supporting the role of GLUT3 in glucose uptake for cancer progression e.g., in non-small cell lung metastasis and colorectal cancer (153, 154). The dependency of CSCs for high glycolytic and low OxPhos metabolism increases glucose uptake induced by glucose's own concentration. Reduced glucose concentration, genetic knockdown or pharmacological inhibition of GLUT1 attenuated the stemness properties and spheroid formation in pancreatic, ovarian, and glioblastoma CSCs without compromising the cell viability (155). Similarly, the reduced tumorigenic potential was observed when pancreatic CSCs were treated with WZB117 prior to their administration in immuno-compromised mice (155). High glucose concentration resulted in increased GLUT1 and GLUT3 mRNA expression that was associated with increased HIF-1α expression (156). Pentose phosphate pathway (PPP) and glycolysis are inter-connected to each other through glucose-6P, pyruvate, and acetyl CoA. Glucose-6P is derived from glucose by the catalytic action of hexokinase, the enzyme that represents the starting link between glycolysis and PPP (157). Glucose metabolism through PPP pathway is necessary for HIF-1α stabilization in glucose-dependent hypoxic tumor cells and subsequently supports angiogenesis (156). Glioma CSCs undergoing hypoxia show up-regulated mRNA expression for both the glycolytic and PPP genes but protein expression was limited to only glycolytic enzymes such as LDH-A and hexokinase-2, while downregulation of PPP enzymes such as glucose-6-phosphate dehydrogenase, 6-phosphogluconate dehydrogenase and transketolase like protein was observed. Acute hypoxia although upregulated migration ability but slowed down proliferation activity, whereas acute oxygenation had just the opposite effect i.e., decreased migration. Under both the conditions increase in apoptotic cells was observed. Rapidly dividing cells have an up-regulated PPP pathway whereas under acute hypoxic conditions pathway shifted toward glycolysis (158). The glycolytic byproduct, lactate is a potent metabolite for inducing angiogenesis and invasiveness in macrophages and vascularisation of endothelial cells (159). The MCT1 mediated lactate uptake increases HIF-1α expression in endothelial cells while blocking MCT1 reduces the VEGFR2 and HIF-1α expression in both Genetic knockdown of glycolytic and PPP enzymes showed the same metabolic correlation both *in vitro* and *in vivo* (160). Glucose metabolism and lactate production were seen in at half of the contact inhibited mouse neural progenitor cells while low glucose/glutamine stimulated the proliferation in fibroblastic cells. Equal PPP metabolic activity among contact inhibited and proliferating cells led to the flux of ribose phosphate into glycolysis and nucleotide biosynthesis, respectively. Inhibition of PPP pathway, on the other hand, induced more apoptotic effect in contact inhibited cells than fibroblastic cells (161). Thus the profound activity of glycolysis in a hypoxic environment makes it an essential metabolic process for tumor cells residing in the center of the tumor mass with the lower blood supply of oxygen and nutrients.HUVEC and BAEC cells (162). Proliferating and migrating glioblastoma cells differ in their metabolic nature of consuming glucose and its downstream pathways as seen in *in vitro* and *in vivo* studies. Migratory cells showed increased and decreased expression of glycolytic enzymes and PPP enzymes, respectively. In contrast, proliferating cells had higher PPP enzymes expression but low glycolysis metabolic expression.

METABOLISM OF LIPIDS IN CSCs

Fatty acid synthase (FASN) is an intracellular enzyme that is involved in fatty acid synthesis by converting malonyl-CoA

and acetyl-CoA into palmitate in three steps using NADPH. Domain I of FASN catalyzes the formation of carbon-carbon bond between malonyl-CoA and acetyl-CoA and subsequent reduction of the elongated fatty acid chain by domain II followed by thioesterase activity of domain III (163). CSCs play an important role in cancer progression and are often reported to have increased activity of FASN (164). These elongated FA chains are structural components of membranes and their *de novo* synthesis is highly activated in tumor cells compared to normal tissues (165, 166). There are reports supporting increased FASN activity and expression in various human cancers such as breast cancer (167–169), thyroid cancer (170), ovarian cancer (171), prostate cancer (172, 173), oral cancer (174–176), colorectal cancer (177), endometrial metastatic cancer (178) and in mesothelioma (179), renal cancer (180), and retinoblastoma (181, 182). All these studies, inevitably describe FASN as an important metabolic target in cancer therapeutics. Increased FASN expression plays a fundamental role in maintaining the stemness, invasiveness and tumor-forming abilities of Glioma CSCs. Inhibition of FASN in these cells reduced their invasiveness and spheroid forming ability along with the reduced expression of stemness markers such as CD133, FABP7, while increased expression of differentiation marker GFAP (183). NANOG, a transcriptional factor is responsible for promoting the stemness properties and it is preferentially relevant to the mitochondrial metabolism. It reduces the expression of mitochondrial OxPhos genes and elevates the expression of mitochondrial fatty acid oxidation genes in tumor-initiating cells/CSCs of hepatocellular carcinoma.Inhibition of OxPhos gene COX6A2 or COX15 reduced ROS- production whereas activation of the fatty acid oxidation (FAO) gene inhibited glucose utilization via OxPhos and also altered the anaplerotic reactions that help in maintaining the stemness of cells. Induction of the Oxphos gene and inhibition of FAO reduced the spheroid formation ability of cells (184). Pancreatic CSCs showed increased expression of glycolytic and PPP enzymes and immensely induced FASN expression while decreased TCA metabolic enzymes in comparison to pancreatic non-CSCs. Pharmacological inhibition through cerulenin and atorvastatin reduced the cell-viability and dramatically distorted the mesenchymal appearance and spheroid forming ability of pancreatic CSCs (185). Lipid droplets store the excess fatty acids in the cell and act as a reservoir to maintain cholesterol levels, triglyceride levels for cell membranes synthesis, and conserving the energy. Lipid droplets are the key regulators of CSCs metabolism besides their role in the storage and synthesis of inflammatory factors (186, 187). FASN hyperactivation in colorectal cancer cells leads to lipid droplets accumulation, increased FAO and reliability on aerobic glycolysis, suggesting the dependence of tumor cells on stored lipid forms for energy homeostasis (188). All these studies, unequivocally suggest that FASN is an important metabolic target in cancer therapeutics. Stearoyl-CoA-desaturase-1(SCD1) is an enzyme involved in fatty acid synthesis by converting saturated fatty acids into mono-unsaturated FA which serves as a substrate for other lipids and has conserved activity in brain and pancreas (189). SCD1 expression is elevated in CSCs and serves as a marker for poor prognosis of lung adenocarcinoma along with other stemness markers. Pharmacological inhibition of SCD1 resulted in increased susceptibility of lung CSCs to cisplatin-induced apoptosis in (190). Besides aerobic glycolysis and TCA cycle, the role of FAO in satisfying energy demands, chemo- and immune-resistance, stemness, and cancer progression could be demonstrated by analyzing the lipolytic phenotype of CSCs that ispredominantly dictated by the tumor microenvironment (191). Gonadal adipose tissue enriched in pro-inflammatory leukemic CSCs undergoes lipolysis to serve as repository of lipids needed by the leukemic CSCs to maintain stemness and survival. Leukemic-CSCs with increased FAO and upregulated CD36 (FA transporter) expression exhibit chemoresistance while *in vivo* and *ex vivo* studies with CD36 knockout cells showed decreased tumor size when injected in mice. These findings suggest the importance of CD36 along with FAO for phenotypic and metabolic distinction in comparison to non-leukemic CSCs (192). FAO has been reported to be a crucial metabolic pathway for breast CSCs as pharmacological inhibition of FAO, reduced the cell viability, ATP levels, and tumor-forming ability in breast CSCs. While JAK-STAT is the key signal transduction pathway responsible for FAO-mediated chemoresistance and tumorigenicity as inhibition of STAT3 reduced the β-oxidation in these CSCs (193). CSCs display high levels of carnitine palmitoyltransferase (CPT) which facilitates the transport of fatty acid from the cytosol to mitochondria for their oxidation (194). In CSCs, CPT1 serves as an anti-apoptotic molecule by interacting with BH3 family of proteins and acts as a cell survival factor (194, 195). This is interesting how CSCs simultaneously complete synthesis and oxidation of fatty acids. During energy depleted state, NADPH generation by the PPP is impaired and this results in decreased FA synthesis. Under these conditions mitochondrial generation of NADPH is important. FAO provides acetyl-CoA which enters into the TCA cycle to form citrate and malate the substrates for NADPH producing enzymes isocitrate dehydrogenase and malic, respectively. AMPK mediated increased β-oxidation and decreased fatty acid synthesis during energy stress maintains the NADPH levels in tumor cells, thus supporting their survivability (196). Cancer cells optimize their requirements for growth and proliferation by regulating the lipid anabolic and catabolic switch. NADPH and ATP demand play an important role to equilibrate the fatty acid synthesis and oxidation in cancer cells.

MITOCHONDRIA AND STEMNESS IN CSCs

Mitochondrion is the cell organelle involved in the generation of ATP. In addition, they are also involved in many cellular processes such as maintaining the redox state, generation of ROS-, maintaining cytosolic Ca++ level, helping the biosynthesis, and inducing apoptotic death of the cell. Multiple reports have suggested that, despite enhanced glycolysis, cancer cells can produce a significant fraction of their ATP via mitochondrial respiration (197–199). Metabolic plasticity is a characteristic of cancer cells and anaerobic glycolysis performed by cancer cells is not only due to mitochondrial dysfunctions. Mitochondria are necessary for the development and progression of cancer

as removal of cancer cell mitochondria diminished cancer growth rate and tumorigenicity. When mtDNA is depleted from tumor cells (ρ° cells) they show reduced growth rate, poor colony-forming ability and considerably reduced tumor growth in mice (200–202). These observations suggest that functional mitochondria are required for the successful survival of cancer cells. Mitochondrial DNA mutations have been reported in many types of cancers such as renal adenocarcinoma, colon cancer cell, head, and neck cancer, breast cancer, prostate and bladder cancer, ovarian cancer, thyroid cancer and neuroblastoma (201, 203–207). MtDNA mutations are a risk factor in some cancer cell populations and are a positive selection in tumorigenesis. Mitochondrial mutations and reduced mtDNA cause stress in mitochondria and thus mitochondria reprogram itself. Studies in breast cancer cell line MCF-7 and normal mammary epithelial cells MCF-10A revealed that mtDNA mutation or reduced mtDNA induces the EMT and CSC phenotype resulting in increased migration and colonization at distant places. This contention was further supported by treatment of MCF-7 and MCF10A cells with ethidium bromide (50 ng/ml) up to 5 passages that resulted in an increased number and increased life span of mammospheres formed by reduced mtDNA.Moreover, flow cytometry analysis showed that cell surface stem cell markers (high $CD44^{+}$ and low $CD24^{-}$) are abundantly expressed in reduced mtDNA cells than normal and reverted cancer cells (201). Mutation or knockdown of mitochondrial transcription factor TFAM which is encoded by the nucleus and acts as the main transcription factor for mtDNA and also helps in mtDNA replication and packaging mitigated the tumorigenic potential of cancer cells (208). The mitochondrial morphology, its distribution, and mtDNA status in CSC vary when compared to the differentiated cancer cells or their normal counterparts. Other studies performed on lung CSCs A549 having high expression of CD34, CD133, c-kit, Twist1, Sox2, Oct4, NANOG, and Bmi show reduced mtDNA and higher $\Delta\psi m$ in comparison to non-lung CSC. CSCs have high $\Delta\psi m$ which suggest that the mitochondria play a role in cell differentiation, tumorigenesis and maintaining the stemness of cell (121). Mutations in oncogenes and mtDNA initiate the formation of cancer/CSC by altering the wave of transcription, which is overblown by the hypoxia and microenvironments, and the mitochondrial stress results in transcription to reprogram the cancer cell metabolism. Decreased mtDNA and mutation coordinates with a nucleus and reprograms the metabolism by sending mitochondrial retrograde signaling (208). Recent research supported that there might be a strong interplay between mitochondria and its role in stemness as mitochondria being an important player in providing energy for the maintenance of stemness. Overall it is necessary to explore the mitochondrial physiology in CSCs and its mechanism in promoting the therapy-resistance (209). While stemness induces suppression of mitochondrial biogenesis and maturity, it activates gene expression of glycolytic enzymes with increased substrate consumption and lactic acid production (210). It has been reported that CSCs from both ovarian adenocarcinoma and cervical SCC express stemness marker, low-ROS- levels, low lactate production, high amino acid intermediates of TCA when grown into spheroids (3D-culture) while opposite effects were seen in adherent tumor cells (2D-culture). These observations suggest that TCA and overall mitochondrial respiration guides and maintains the stemness properties of CSCs and their inhibition is activated upon differentiation, mediating the shifting of CSCs from OxPhos to glycolytic metabolism (211). Mitochondrial respiration and FAO are inter-linked where excess acetyl-CoA is used in TCA cycle. Ketones may too increase mitochondrial respiration and suppress ROS- production by its conversion into acetyl-CoA (212). The reduced ROS- level is favorable to CSCs survival under stress conditions and thus the utilization of ketone bodies may relieve CSCs from oxidative stress. While the ketone metabolism is active in the absence of nutrients, tumor cells and CSCs constitutively express it (213–217). Mitochondrial metabolic activity is also related to cell differentiation, as early passages of an adult primate stromal cell line have a higher OCR and a low ATP/mitochondrial DNA content compared with long-term cultured cells (218) but CD34+ hematopoietic stem cells have low mitochondrial OCR and mitochondrial mass (219). The HSC mitochondria play important roles in maintaining stemness and differentiation. However, whether the roles of CSC mitochondria are similar to HSC mitochondria or cancer cells, in general, is unknown. Two hypotheses on the origin of CSCs, both of which contribute to acute myeloid leukemia (220), have been proposed. One hypothesis supports that CSCs are derived from normal stem cells residing in various organs. Genetic mutations and epigenetic changes, which are crucial for the initiation and progression of tumor growth, accumulate in long-lived stem cells, and the transformation of stem cells into CSCs initiates the carcinogenesis. CSCs may also have a greater differentiation potential than normal stem cells. Another hypothesis assumes the existence of embryonic stem cell-like cells that transform into CSCs when they are exposed to damaging environmental factors. Additional differentiation and mutations of these cells may also contribute to the development of CSCs (221). As reported, ovarian CSCs show higher mitochondrial ROS- production and $\Delta\Psi m$ than non-CSCs. In addition, targeting mitochondrial biogenetics induced caspase-independent cell death in ovarian CSCs (222). In glioma CSCs, a higher mitochondrial reserve capacity was measured as compared to the differentiated cells (120). Glioblastoma CSCs also depend on OXPHOS for their energy production and survival (117). Besides, breast CSCs have higher ATP content compared to their differentiated progeny (223). Therefore, it is reasonable to believe that CSCs mitochondria show different roles and features depending on the cancer type and CSCs mitochondria differ from those of non-CSCs. Importantly, little information is available on the mitochondrial features related to energy metabolism and the ROS-/antioxidant enzyme system of CSCs in colon, stomach, liver, bone, and prostate cancer. Therefore, defining these features will be essential for developing a mitochondria-targeted therapeutic approach to facilitate the death of CSCs, and therefore, to reduce the risk of disease relapse and progression to refractory cancer.

Mitochondrial studies using whole-cell approaches make it difficult to distinguish mitochondria-specific effects from those contributed by the nucleus. This gap can be filled by using trans mitochondrial cybrid models in order to investigate the mitochondria-regulated energy and cancer pathways (224–226). Cybrid models using moderately metastatic triple-negative breast cancer cell line (SUM159) as a background control for nuclei and mitochondria and comparing them with the benign breast cells (MCF-10A or A1N4), and highly metastatic (MDA-MB-231) breast cancer cells can offer a good working model for this purpose. Indeed, these cybrids show the tumor-like properties both *in vitro* and *in vivo* according to their mitochondrial origin. Mitochondria obtained from benign cells almost completely abolished the tumorigenic properties of SUM159 cells when tested *in vitro* and *in vivo* (226). Proteomic and mass spectrometry analysis revealed several proteins related to mitochondrial. Fatty acid oxidation is also up regulated in cybrids with mitochondria derived from MDA 231 metastatic breast cancer cells. Knockdown of enzyme essential for fatty acid oxidation carnitine palmitoyltransferase-1(CPT1) or carnitine palmitoyltransferase-2 (CPT2) by shRNA significantly inhibited the migration potential and wound healing potential of these cells (226). Breast cancer patient dataset (n = 1,302) with long-term clinical follow-up showed that high CPT1A mRNA expression in tumors promotes distant metastasis (227). Altogether, these results show the role of mitochondrial energy reprogramming in fatty acid oxidation in CSCs and its significance in regulating the driving the protein of a major cancer pathway via its posttranslational modification.

METABOLISM OF GLUTAMINE IN CSCs

Glutamine is a non-essential amino acid that plays a key role in energy and metabolic homeostasis during CSCs proliferation. It mediates these effects by regulating the consumption and uptake of other amino acids, hence maintaining mitochondrial redox potential and NADPH levels. Besides maintaining energy homeostasis, glutamine is the precursor of TCA cycle intermediates, nucleotides, proteins, and biosynthesis of other amino acids. CSCs from small cell lung carcinoma utilize glutamine actively in anaplerotic reaction in order to produce ATP for substrate-level phosphorylation. Complete inhibition of OxPhos and glycolysis by oligomycin and 2-DG in CSCs and non-CSCs caused more substrate-level phosphorylation in uPAR+ CSCs. Under respiratory distress conditions, substrate-level phosphorylation provides the necessary GTP/ATP to CSCs and this is more efficient under hypoxic conditions (228, 229). *In vivo* and *ex vivo* studies in OxPhos defective mtDNA mutated cybrid A6MT cells and wild type cells that have no mtDNA mutations, showed that Glutamine accelerates the proliferation of A6MT cell and its uptake was higher in mtDNA mutated cells than in wild type cells. Glutamine undergoes oxidative or reductive pathways depending on the severity of OxPhos defect. Isotopic C13-labeled glutamine supplemented in culture media for tracking the glutamine-glucose-αKG flux and metabolic fate of glutamine in A6MT cells suggested that glutamine enters the TCA cycle in the form αKG in a clockwise direction and provides GTP/ATP for substrate-level phosphorylation following its conversion into succinate as mentioned in **Figure 1**. Succinate is then converted into aspartate that migrates into the cytosol and subsequently converted into alanine and lactate. Published work from other laboratories have revealed similar results and suggest that Glutamine enters the TCA cycle and actively participates in anaplerotic reaction; the amount of lactate formed is less compared to that formed by glucose (230–232). These events are critical in order to maintain the pace of TCA cycle and to re-oxidize glycolytic NADH to generate NADPH which is a critical cofactor needed in reductive pathways such as during lipid synthesis as notified in **Figure 1**. Thus, glutamine has an important role in metabolic rewiring in OxPhos impaired cells to provide energy and other synthetics intermediates (233). Many researchers are attempting to target the glutamine-dependent self-renewal ability of CSCs as a novel therapeutic approach (234–236). For example, attempts to inhibit glutamine transamination in glioblastoma, blocking the increased glutamine regulated signaling pathways (mTOR pathway), or by targeting c-myc regulated glutamine uptake were shown to induce significant cytotoxicity to tumor cells (237, 238). Deamidation product of glutamine, along with cysteine and glycine, is an important component of glutathione that is needed to maintain the redox balance and NADP+/NADPH ratio (239). The dependency of cancer cells on glutamine metabolism for nitrogen and redox balance is correlated with their tumorigenic potential and tumor survival (240). mTOR is an important signaling pathway for glutamine metabolism and is differentially regulated by glutamine concentration of tumor cells. Colorectal CSCs grown in glutamine lacking media were more sensitive to metformin drug (relevant to mTOR pathway) while being resistant when media contained glutamine. Combinatorial treatment with metformin and glutaminase inhibitor, induced higher cytotoxic effect against colorectal CSCs than treatment with each drug individually. The colorectal CSCs had higher expression of glutamine transporter protein (ASCT2) than the non-CSCs cancer cells. Accordingly, the ASCT2 knockdown dramatically reduced the number of CD133+/CD44+ CSCs (241). In pancreatic CSCs, glutamine deficiency significantly decreased the stemness, self-renewal, and increased the ROS- production resulting in increased the apoptotic death of these cells (242). The uptake of extracellular proteins in pancreatic adenocarcinoma and bladder carcinoma cells, expressing oncogenic Ras, this mediated through macro-pinocytosis and to make glutamine via lysosomal degradation of these proteins (243). The α-ketoglutarate, an intermediate of TCA cycle, when supplemented to cell cultures as an alternate to Glutamine, may alter the cellular requirements for glutamine metabolism in order to synthesize nucleotides. CD34+/CD38– hematopoietic stem cells expressing high ASCT2 levels and glutamine metabolism show commitment to erythroid niche whereas abrogating glutamine metabolism leads to myeloid differentiation *in-vitro*. On the other hand, *in-vivo* antagonistic metabolism of glutamine and glucose regulates the differentiation of HSC between myeloid and erythroid (244)Glutamine is an important

component in synthesis of glutathione (GSH), a tripeptide that serves as an intracellular antioxidant scavenger of ROS- and also is involved in DNA repair, activation of transcription factors, cell cycle regulation, and calcium homeostasis (245). Glutamine metabolizing enzymes such as glutamine synthetase and glutamate-oxaloacetate transaminase (GOT1 and GOT2) are highly expressed in CSCs (113). Glutamine metabolism varies with cancer types andgenerally proceeds through two pathways; acting as a mediator of anaplerotic flux through TCA cycle intermediates and a precursor for nucleotide synthesis (246). Incorporation of glucose carbon in glutamine and TCA cycle intermediates, non-dependency of tumor cells on glutamine was seen in non-small-cell lung carcinoma cells *in-vivo*. This phenomenon wasregulated by changes in the microenvironment and indicated glucose as a carbon source. These observations suggested glucose mediated glutamine synthesis and TCA cycle metabolite replenishment with the help of pyruvate carboxylase rather than dependency on glutamine anaplerosis (247). Glioblastoma expressing aerobic glycolysis and active TCA cycle predominantly depended on glucose-mediated lipogenesis and on anaplerotic glutamine metabolism to regenerate TCA cycle intermediates for NADPH production. Generally, low reliability of TCA mediated metabolites and high preference for glutamine is seen in proliferating cells than in contact inhibited fibroblasts. These findings support the contention that contact inhibition may induce mild anapleroticresponse in favor to glutamine metabolism and strong anapleroticresponse in favorto pyruvate-oxaloacetate flux (161). Myc mediated glutamine catabolism to α-ketoglutarate, replenishes the reduced TCA cycle metabolite pool in response to hypoxic stress and low pyruvate availabilityfor TCA cycle. Generated α-ketoglutarate undergoes reverse TCA cycle to form citrate, which is exported to the cytosol to form oxaloacetate and Acetyl-CoA for lipid synthesis and redox homeostasis of cell (248). Glutamine metabolism is undoubtedly a major metabolic pathway in CSCs and could be a promising therapeutic target toblock its functions and aidingthe replenishment of metabolites for energy and redox homeostasis.

CONCLUSION: CSCs ERADICATION BY TARGETING ITS METABOLISM

It is important to understand the exact nature of factors in heterogeneous tumor mass that fuel the tumorigenic growth, drug refractoriness, and metastasis of less differentiated tumor cells to distant organs. It is also clear that CSCs play a major role in replenishing the tumor pool and as a source of differentiated tumor cells. The immortal nature of CSCs might be the reason why the tumors relapse even after most of the tumor mass is removed or eradicated (249). Oxphos and glycolysis remains the primary energy generation mechanisms for CSCs while metabolism of ktone bodies and fatty acids also contributed significantly. This may vary for each CSC type depending on the primary tumor from which these CSCs have developed. Yuan et al. has shown that multiple mutations in mtDNA may render compromised OxPhos function (142) thus pushing the cell toward glycylysis. On the other hand, several studies have shown that glycolytic tumors can not metabolize fatty acid and ketone bodies (230, 250, 251) for energy production. Individual mitochodnria are genetically heterogenous due to large copy number of the genome, each copy may have different mutations. This may overall produce almost all mitochondrial functional proteins, albeit in very low levels, thus enabling OxPhos to a smaller extent, thus explaining the partial contribution of energy by multiple mechanisms.

Metastatic and self-renewal property of CSCs (while being more quiescent) is tightly regulated by the mitochondrial respiration and glycolysis, while the ATP generation and fulfilling energy demandsare secondary events. While Myc suppression induced the sensitivity of CSCs to metformin, overexpression of Myc has just opposite effects making cancer cells behave like chemo-resistant pancreatic adenocarcinoma CSCs. Drugs targeting the OxPhos could be the primary aspect of therapeutic intervention in pancreatic CSCs as some drugs exclusively target the CSCs metabolism while showing no effect on non-CSCs (122). A rationale reasoning for metabolic immuned CSCs is still unknown where CSCs evade the immune response and may confuse the immune cells to distinguish itself from normal stem cells. Genomic analyses, mRNA profiling and mutational analysis of breast cancer (252), ovarian cancer (253), lung cancer (254), glioblastoma cancer (255), prostate cancer (256), gastric cancer (257), B-cell lymphoma (258), acute lymphoid leukemia (259), metastatic cancers (260), and melanomas (261) has been performed using sophisticated techniques such as MSK-IMPACT, next-generation sequencing, and whole-genome sequencing. These studies have provided a detailed and perspective view of the diverse genetic and epigenetic nature of different mutated genes in different tumor types that may be involved in the regulation of metabolic processes and proliferating efficiency based on their origin and microenvironment in which they reside. Future efforts to elucidate the mechanisms responsible for genetic, epigenetic and micro environment-induced changes in CSCs that regulate tumor progression and chemoresistance might offer therapeutic opportunities for successful intervention to block the progression of cancer to untreatable disease. Alternative approaches should be taken, while focusing on similarities between different CSCs. For example, common metabolic features that dictate the tumorigenic potential and stemness of CSCs should be targeted. Targeting of metabolic wiring should be investigatedduring two transitional states; (a) from normal stem cells to cancer stem cells, and (b) from cancer stem cells todifferentiated tumor cells, rather than using chemo- and radiation therapiestokillthe whole tumor mass that results in major side effects. While we have no knowledge on the metabolic adaptations that take placeduring normal stem cell to CSCs transition, only a handful studies have been done to understand the transition of CSCs to differentiated tumor cells.

AUTHOR CONTRIBUTIONS

KM, SK, and SSi organized topics and contributed in writing the manuscript. UY, TS, PS, and PK collected the literature and contributing in write up. UY, TS, PS, SSh, and HK helped in

revising the manuscript. UY and PS designed the figure. All authors contributed to the article and approved the submitted version.

FUNDING

UY and TS received Senior and Junior Research Fellowship, respectively, from the CSIR. PS and SSi thank the financial support from DST SERB EMR (SR/SO/AS-31/2014). SK thanks the DST SERB for Ramanujan Fellowship Award and for funding the project (DST/SERB SB/S2/RJN-103/2015).

ACKNOWLEDGMENTS

The authors acknowledge Central University of Punjab and AIIMS Patna for providing all the facilities.

REFERENCES

1. Marjanovic ND, Weinberg RA, Chaffer CL. Cell plasticity and heterogeneity in cancer. *Clin Chem.* (2013) 59:168–79. doi: 10.1373/clinchem.2012.184655
2. Bonnet D, Dick JE. Human acute myeloid leukemia is organized as a hierarchy that originates from a primitive hematopoietic cell. *Nat Med.* (1997) 3:730–7. doi: 10.1038/nm0797-730
3. Vander Heiden MG, Cantley LC, Thompson CB. Understanding the warburg effect: the metabolic requirements of cell proliferation. *Science.* (2009) 324:1029–33. doi: 10.1126/science.1160809
4. Galluzzi L, Kepp O, Vander Heiden MG, Kroemer G. Metabolic targets for cancer therapy. *Nat. Rev. Drug Discov.* (2013) 12:829–46. doi: 10.1038/nrd4145
5. Mancini R, Noto A, Pisanu ME, De Vitis C, Maugeri-Sacca M, Ciliberto G. Metabolic features of cancer stem cells: the emerging role of lipid metabolism. *Oncogene.* (2018) 37:2367–78. doi: 10.1038/s41388-018-0141-3
6. Sauer LA, Stayman JW, Dauchy RT. Amino acid, glucose, and lactic acid utilization *in vivo* by rat tumors. *Cancer Res.* (1982) 42:4090–7.
7. Dumas JF, Brisson L, Chevalier S, Mahéo K, Fromont G, Moussata D, et al. Metabolic reprogramming in cancer cells, consequences on pH and tumour progression: integrated therapeutic perspectives with dietary lipids as adjuvant to anticancer treatment. In: *Seminars in Cancer Biology*. Elsevier (2017). p. 90–110. doi: 10.1016/j.semcancer.2017.03.004
8. Buono R, Longo VD. Starvation, stress resistance, and cancer. *Trends Endocrinol. Metab.* (2018) 29:271–80. doi: 10.1016/j.tem.2018.01.008
9. Kim H, Dong J, Xu J, Li D, Zheng Z, Ye N, et al. Abstract P1-02-08: reprogramming glucose metabolism and energy production in breast cancer Cells. In: *San Antonio Breast Cancer Symposium*. San Antonio, TX: AACR (2018). doi: 10.1158/1538-7445.SABCS17-P1-02-08
10. McKeehan WL. Glycolysis, glutaminolysis and cell proliferation. *Cell Biol. Int. Rep.* (1982) 6:635–50. doi: 10.1016/0309-1651(82)90125-4
11. Formentini L, Martínez-Reyes I, Cuezva JM. The mitochondrial bioenergetic capacity of carcinomas. *IUBMB Life.* (2010) 62:554–60. doi: 10.1002/iub.352
12. Martinez-Outschoorn UE, Peiris-Pagés M, Pestell RG, Sotgia F, Lisanti MP. Cancer metabolism: a therapeutic perspective. *Nat Rev Clin Oncol.* (2017) 14:11. doi: 10.1038/nrclinonc.2016.60
13. Hsu PP, Sabatini DM. Cancer cell metabolism: warburg and beyond. *Cell.* (2008) 134:703–7. doi: 10.1016/j.cell.2008.08.021
14. Bonuccelli G, Tsirigos A, Whitaker-Menezes D, Pavlides S, Pestell RG, Chiavarina B, et al. Ketones and lactate "fuel" tumor growth and metastasis: evidence that epithelial cancer cells use oxidative mitochondrial metabolism. *Cell Cycle.* (2010) 9:3506–14. doi: 10.4161/cc.9.17.12731
15. Zheng J. Energy metabolism of cancer: glycolysis versus oxidative phosphorylation. *Oncol Lett.* (2012) 4:1151–7. doi: 10.3892/ol.2012.928
16. Hu Y, Lu W, Chen G, Wang P, Chen Z, Zhou Y, et al. K-ras G12V transformation leads to mitochondrial dysfunction and a metabolic switch from oxidative phosphorylation to glycolysis. *Cell Res.* (2012) 22:399–412. doi: 10.1038/cr.2011.145
17. DeBerardinis RJ, Lum JJ, Hatzivassiliou G, Thompson CB. The biology of cancer: metabolic reprogramming fuels cell growth and proliferation. *Cell Metab.* (2008) 7:11–20. doi: 10.1016/j.cmet.2007.10.002
18. Pietrocola F, Galluzzi L, Bravo-San Pedro JM, Madeo F, Kroemer G. Acetyl coenzyme A: a central metabolite and second messenger. *Cell Metab.* (2015) 21:805–21. doi: 10.1016/j.cmet.2015.05.014
19. Nieman KM, Kenny HA, Penicka CV, Ladanyi A, Buell-Gutbrod R, Zillhardt MR, et al. Adipocytes promote ovarian cancer metastasis and provide energy for rapid tumor growth. *Nat Med.* (2011) 17:1498–1503. doi: 10.1038/nm.2492
20. Ishioka SI, Sagae S, Ito E, Kudo R. Ultrastructural study of benign, low-malignant potential (LMP), and malignant ovarian tumors. *Med Electron Microsc.* (2004) 37:37–44. doi: 10.1007/s00795-003-0189-0
21. Dai Z, Yin J, He H, Li W, Hou C, Qian X, et al. Mitochondrial comparative proteomics of human ovarian cancer cells and their platinum-resistant sublines. *Proteomics.* (2010) 10:3789–99. doi: 10.1002/pmic.200900685
22. Végran F, Boidot R, Michiels C, Sonveaux P, Feron O. Lactate influx through the endothelial cell monocarboxylate transporter MCT1 supports an NF-κB/IL-8 pathway that drives tumor angiogenesis. *Cancer Res.* (2011) 71:2550–60. doi: 10.1158/0008-5472.CAN-10-2828
23. Martínez-Zaguilán R, Seftor EA, Seftor RE, Chu Y-W, Gillies RJ, Hendrix MJ. Acidic pH enhances the invasive behavior of human melanoma cells. *Clin Exp Metastasis.* (1996) 14:176–86. doi: 10.1007/BF00121214
24. Rothberg JM, Bailey KM, Wojtkowiak JW, Ben-Nun Y, Bogyo M, Weber E, et al. Acid-mediated tumor proteolysis: contribution of cysteine cathepsins. *Neoplasia.* (2013) 15:1125–37. doi: 10.1593/neo.13946
25. Zu XL, Guppy M. Cancer metabolism: facts, fantasy, and fiction. *Biochem Biophys Res Commun.* (2004) 313:459–65. doi: 10.1016/j.bbrc.2003.11.136
26. Owen OE, Kalhan SC, Hanson RW. The key role of anaplerosis and cataplerosis for citric acid cycle function. *J Biol Chem.* (2002) 277:30409–12. doi: 10.1074/jbc.R200006200
27. Ahn CS, Metallo CM. Mitochondria as biosynthetic factories for cancer proliferation. *Cancer Metab.* (2015) 3:1. doi: 10.1186/s40170-015-0128-2
28. Zhao Y, Butler EB, Tan M. Targeting cellular metabolism to improve cancer therapeutics. *Cell Death Dis.* (2013) 4:e532. doi: 10.1038/cddis.2013.60
29. Yu M, Chen S, Hong W, Gu Y, Huang B, Lin Y, et al. Prognostic role of glycolysis for cancer outcome: evidence from 86 studies. *J Cancer Res Clin Oncol.* (2019) 145:967–99. doi: 10.1007/s00432-019-02847-w
30. Hensley CT, Faubert B, Yuan Q, Lev-Cohain N, Jin E, Kim J, et al. Metabolic heterogeneity in human lung tumors. *Cell.* (2016) 164:681–94. doi: 10.1016/j.cell.2015.12.034
31. Dai Z, Locasale JW. Metabolic pattern formation in the tumor microenvironment. *Mol Syst Biol.* (2017) 13:915. doi: 10.15252/msb.20167518
32. Greenman C, Stephens P, Smith R, Dalgliesh GL, Hunter C, Bignell G, et al. Patterns of somatic mutation in human cancer genomes. *Nature.* (2007) 446:153–8. doi: 10.1038/nature05610
33. Yizhak K, Agust F, Kim J, Hess JM, Kubler K, Grimsby J, et al. RNA sequence analysis reveals macroscopic somatic clonal expansion across normal tissues. *Science*. (2019) 364:eaaw0726. doi: 10.1126/science.aaw0726
34. Büttner J, Jöhrens K, Klauschen F, Hummel M, Lenze D, Saeger W, et al. Intratumoral morphological heterogeneity can be an indicator of genetic heterogeneity in colorectal cancer. *Exp Mol Pathol.* (2018) 104:76–81. doi: 10.1016/j.yexmp.2018.01.007
35. Lenz G, Onzi GR, Pereira LC, Breitenbach K, Leonardo BG, Dalsin E. Abstract IA09: The Dynamics of Cancer Cell Heterogeneity. In: *Translational Cancer Medicine*. São Paulo: AACR (2018). doi: 10.1158/1557-3265.TCM17-IA09
36. Sachs N, de Ligt J, Kopper O, Gogola E, Bounova G, Weeber F, et al. A living biobank of breast cancer organoids captures disease heterogeneity. *Cell*. (2018) 172:373–86 e310. doi: 10.1016/j.cell.2017.11.010

37. Nowell PC. The clonal evolution of tumor cell populations. *Science*. (1976) 194:23–8. doi: 10.1126/science.959840
38. Greaves M, Maley CC. Clonal evolution in cancer. *Nature*. (2012) 481:306–13. doi: 10.1038/nature10762
39. Reya T, Morrison SJ, Clarke MF, Weissman IL. Stem cells, cancer, and cancer stem cells. *Nature*. (2001) 414:105–11. doi: 10.1038/35102167
40. Shackleton M, Quintana E, Fearon ER, Morrison SJ. Heterogeneity in cancer: cancer stem cells versus clonal evolution. *Cell*. (2009) 138:822–9. doi: 10.1016/j.cell.2009.08.017
41. Kidd EA, Grigsby PW. Intratumoral metabolic heterogeneity of cervical cancer. *Clin Cancer Res*. (2008) 14:5236–41. doi: 10.1158/1078-0432.CCR-07-5252
42. Chong GO, Lee WK, Jeong SY, Park SH, Lee YH, Lee SW, et al. Prognostic value of intratumoral metabolic heterogeneity on F-18 fluorodeoxyglucose positron emission tomography/computed tomography in locally advanced cervical cancer patients treated with concurrent chemoradiotherapy. *Oncotarget*. (2017) 8:90402–12. doi: 10.18632/oncotarget.18769
43. Konrad CV, Murali R, Varghese BA, Nair RJC. The role of cancer stem cells in tumor heterogeneity and resistance to therapy. *Can J Physiol Pharmacol*. (2016) 95:1–15. doi: 10.1139/cjpp-2016-0079
44. Gray JM, Pierce GB Jr. Relationship between growth rate and differentiation of melanoma *in vivo*. *J Natl Cancer Inst*. (1964) 32:1201–11. doi: 10.1093/jnci/32.6.1201
45. Mitelman F, Mark J, Levan G, Levan AJS. Tumor etiology and chromosome pattern. *Science*. (1972) 176:1340–1. doi: 10.1126/science.176.4041.1340
46. Dexter DL, Kowalski HM, Blazar BA, Fligiel Z, Vogel R, Heppner GH, et al. Heterogeneity of tumor cells from a single mouse mammary tumor. *Cancer Res*. (1978) 38:3174–81.
47. Dexter DL, Spremulli EN, Fligiel Z, Barbosa JA, Vogel R, VanVoorhees A, et al. Heterogeneity of cancer cells from a single human colon carcinoma. *Am J Med*. (1981) 71:949–56. doi: 10.1016/0002-9343(81)90312-0
48. Klein G, Klein E. Conversion of solid neoplasms into ascites tumors. *Ann N Y Acad Sci*. (1956) 63:640–61. doi: 10.1111/j.1749-6632.1956.tb50883.x
49. Kreso A, Dick JE. Evolution of the cancer stem cell model. *Cell Stem Cell*. (2014) 14:275–91. doi: 10.1016/j.stem.2014.02.006
50. Meacham CE, Morrison SJJN. Tumour heterogeneity and cancer cell plasticity. *Nature*. (2013) 501:328–37. doi: 10.1038/nature12624
51. Quintana E, Shackleton M, Foster HR, Fullen DR, Sabel MS, Johnson TM, et al. Phenotypic heterogeneity among tumorigenic melanoma cells from patients that is reversible and not hierarchically organized. *Cancer Cell*. (2010) 18:510–23. doi: 10.1016/j.ccr.2010.10.012
52. Quintana E, Shackleton M, Sabel MS, Fullen DR, Johnson TM, Morrison SJJN. Efficient tumour formation by single human melanoma cells. *Nature*. (2008) 456:593–8. doi: 10.1038/nature07567
53. Shapiro JR, Yung W-KA, Shapiro WR. Isolation, karyotype, and clonal growth of heterogeneous subpopulations of human malignant gliomas. *Cancer Res*. (1981) 41:2349–59.
54. Yung W-KA, Shapiro JR, Shapiro WR. Heterogeneous chemosensitivities of subpopulations of human glioma cells in culture. *Cancer Res*. (1982) 42:992–8.
55. Prasetyanti PR, Medema JP. Intra-tumor heterogeneity from a cancer stem cell perspective. *Mol Cancer*. (2017) 16:41. doi: 10.1186/s12943-017-0600-4
56. Odoux C, Fohrer H, Hoppo T, Guzik L, Stolz DB, Lewis DW, et al. A stochastic model for cancer stem cell origin in metastatic colon cancer. *Cancer Res*. (2008) 68:6932–41. doi: 10.1158/0008-5472.CAN-07-5779
57. Cajal SRY, Castellvi J, Hümmer S, Peg V, Pelletier J, Sonenberg N. Beyond molecular tumor heterogeneity: protein synthesis takes control. *Oncogene*. (2018) 37:2490–501. doi: 10.1038/s41388-018-0152-0
58. Shen H, Laird PW. Interplay between the cancer genome and epigenome. *Cell*. (2013) 153:38–55. doi: 10.1016/j.cell.2013.03.008
59. Deshmukh A, Binju M, Arfuso F, Newsholme P, Dharmarajan A. Role of epigenetic modulation in cancer stem cell fate. *Int J Biochem Cell Biol*. (2017) 90:9–16. doi: 10.1016/j.biocel.2017.07.003
60. Clarke MF, Hass A, Medicine M. Cancer Stem Cells. In: *Reviews in Cell Biology and Molecular Medicine*, RA Meyers, editor. (2006). p. 221–41. doi: 10.1002/3527600906.mcb.200300130
61. Scheel C, Weinberg RA. Cancer stem cells and epithelial–mesenchymal transition: concepts and molecular links. *Semin Cancer Biol*. (2012) 22:396–403. doi: 10.1016/j.semcancer.2012.04.001
62. Gruber W, Scheidt T, Aberger F, Huber CG. Understanding cell signaling in cancer stem cells for targeted therapy–can phosphoproteomics help to reveal the secrets? *Cell Commun Signal*. (2017) 15:12. doi: 10.1186/s12964-017-0166-1
63. Azizi E, Granger J, Harouaka R, Luther TK, Wicha MS. Stem cells in breast development and cancer. In: *The Breast, 5th Edn*. Philadelphia, PA: Elsevier (2018). p. 308–14 e302. doi: 10.1016/B978-0-323-35955-9.00023-4
64. Tang DG. Understanding cancer stem cell heterogeneity and plasticity. *Cell Res*. (2012) 22:457–72. doi: 10.1038/cr.2012.13
65. Visvader JE, Lindeman GJ. Cancer stem cells in solid tumours: accumulating evidence and unresolved questions. *Nat Rev Cancer*. (2008) 8:755–68. doi: 10.1038/nrc2499
66. Kaur G, Sharma P, Dogra N, Singh S. Eradicating cancer stem cells: concepts, issues, and challenges. *Curr Treat Options Oncol*. (2018) 19:20. doi: 10.1007/s11864-018-0533-1
67. Pece S, Tosoni D, Confalonieri S, Mazzarol G, Vecchi M, Ronzoni S, et al. Biological and molecular heterogeneity of breast cancers correlates with their cancer stem cell content. *Cell*. (2010) 140:62–73. doi: 10.1016/j.cell.2009.12.007
68. Liao J, Qian F, Tchabo N, Mhawech-Fauceglia P, Beck A, Qian Z, et al. Ovarian cancer spheroid cells with stem cell-like properties contribute to tumor generation, metastasis and chemotherapy resistance through hypoxia-resistant metabolism. *PLoS ONE*. (2014) 9:e84941. doi: 10.1371/journal.pone.0084941
69. Hwang-Verslues WW, Kuo WH, Chang PH, Pan CC, Wang HH, Tsai ST, et al. Multiple lineages of human breast cancer stem/progenitor cells identified by profiling with stem cell markers. *PLoS ONE*. (2009) 4:e8377. doi: 10.1371/journal.pone.0008377
70. Yang M, Liu P, Huang PJTB. Cancer stem cells, metabolism, and therapeutic significance. *BMB Rep*. (2016) 37:5735–42. doi: 10.1007/s13277-016-4945-x
71. Kang M-K, Kang S-K. Tumorigenesis of chemotherapeutic drug-resistant cancer stem-like cells in brain glioma. *Stem Cells Dev*. (2007) 16:837–48. doi: 10.1089/scd.2007.0006
72. Al-Hajj M, Wicha MS, Benito-Hernandez A, Morrison SJ, Clarke MF. Prospective identification of tumorigenic breast cancer cells. *Proc Natl Acad Sci USA*. (2003) 100:3983–8. doi: 10.1073/pnas.0530291100
73. Ginestier C, Hur MH, Charafe-Jauffret E, Monville F, Dutcher J, Brown M, et al. ALDH1 is a marker of normal and malignant human mammary stem cells and a predictor of poor clinical outcome. *Cell Stem Cell*. (2007) 1:555–67. doi: 10.1016/j.stem.2007.08.014
74. Liu C, Kelnar K, Liu B, Chen X, Calhoun-Davis T, Li H, et al. The microRNA miR-34a inhibits prostate cancer stem cells and metastasis by directly repressing CD44. *Nat Med*. (2011) 17:211. doi: 10.1038/nm.2284
75. Eramo A, Lotti F, Sette G, Pilozzi E, Biffoni M, Di Virgilio A, et al. Identification and expansion of the tumorigenic lung cancer stem cell population. *Cell Death Differ*. (2008) 15:504–14. doi: 10.1038/sj.cdd.4402283
76. Sullivan JP, Spinola M, Dodge M, Raso MG, Behrens C, Gao B, et al. Aldehyde dehydrogenase activity selects for lung adenocarcinoma stem cells dependent on notch signaling. *Cancer Res*. (2010) 70:9937–48. doi: 10.1158/0008-5472.CAN-10-0881
77. Leung EL-H, Fiscus RR, Tung JW, Tin VP-C, Cheng LC, Sihoe AD-L, et al. Non-small cell lung cancer cells expressing CD44 are enriched for stem cell-like properties. *PLoS ONE*. (2010) 5:e14062. doi: 10.1371/journal.pone.0014062
78. Deng S, Yang X, Lassus H, Liang S, Kaur S, Ye Q, et al. Distinct expression levels and patterns of stem cell marker, aldehyde dehydrogenase isoform 1 (ALDH1), in human epithelial cancers. *PLoS ONE*. (2010) 5:e10277. doi: 10.1371/journal.pone.0010277
79. Son MJ, Woolard K, Nam D-H, Lee J, Fine HA. SSEA-1 is an enrichment marker for tumor-initiating cells in human glioblastoma. *Cell Stem Cell*. (2009) 4:440–52. doi: 10.1016/j.stem.2009.03.003
80. Mazzoleni S, Politi LS, Pala M, Cominelli M, Franzin A, Sergi LS, et al. Epidermal growth factor receptor expression identifies functionally and molecularly distinct tumor-initiating cells in human glioblastoma

multiforme and is required for gliomagenesis. *Cancer Res.* (2010) 70:7500–13. doi: 10.1158/0008-5472.CAN-10-2353
81. Anido J, Sáez-Borderías A, Gonzàlez-Juncà A, Rodón L, Folch G, Carmona MA, et al. TGF-β receptor inhibitors target the CD44high/Id1high glioma-initiating cell population in human glioblastoma. *Cancer Cell.* (2010) 18:655–68. doi: 10.1016/j.ccr.2010.10.023
82. Hermann PC, Huber SL, Herrler T, Aicher A, Ellwart JW, Guba M, et al. Distinct populations of cancer stem cells determine tumor growth and metastatic activity in human pancreatic cancer. *Cell Stem Cell.* (2007) 1:313–23. doi: 10.1016/j.stem.2007.06.002
83. Müller A, Homey B, Soto H, Ge N, Catron D, Buchanan ME, et al. Involvement of chemokine receptors in breast cancer metastasis. *Nature.* (2001) 410:50–6. doi: 10.1038/35065016
84. Balkwill F. The significance of cancer cell expression of the chemokine receptor CXCR4. *Semin Cancer Biol.* (2012) 14:171–9. doi: 10.1016/j.semcancer.2003.10.003
85. Singh SK, Hawkins C, Clarke ID, Squire JA, Bayani J, Hide T, et al. Identification of human brain tumour initiating cells. *Nature.* (2004) 432:396–401. doi: 10.1038/nature03128
86. Cho HY, Hossain MK, Lee JH, Han J, Lee HJ, Kim KJ, et al. Selective isolation and noninvasive analysis of circulating cancer stem cells through raman imaging. *Biosens Bioelectron.* (2018) 102:372–82. doi: 10.1016/j.bios.2017.11.049
87. Cooke S, Temple J, Macarthur S, Zahra M, Tan L, Crawford R, et al. Intra-tumour genetic heterogeneity and poor chemoradiotherapy response in cervical cancer. *Br J Cancer.* (2011) 104:361–8. doi: 10.1038/sj.bjc.6605971
88. Huang R, Rofstad EK. Cancer stem cells (CSCs), cervical CSCs and targeted therapies. *Oncotarget.* (2017) 8:35351–67. doi: 10.18632/oncotarget.10169
89. Chaffer CL, San Juan BP, Lim E, Weinberg RA. EMT, cell plasticity and metastasis. *Cancer Metastasis Rev.* (2016) 35:645–54. doi: 10.1007/s10555-016-9648-7
90. Brabletz T, Kalluri R, Nieto MA, Weinberg RA. EMT in cancer. *Nat Rev Cancer.* (2018) 18:128–34. doi: 10.1038/nrc.2017.118
91. Liu S, Cong Y, Wang D, Sun Y, Deng L, Liu Y, et al. Breast cancer stem cells transition between epithelial and mesenchymal states reflective of their normal counterparts. *Stem Cell Rep.* (2014) 2:78–91. doi: 10.1016/j.stemcr.2013.11.009
92. Kumar A, Xu J, Brady S, Gao H, Yu D, Reuben J, Mehta K. Tissue transdlutaminase prometes drug resistance and invasion by inducing mesenchymal transition in mammary epithelial cells. *PLoS ONE.* 5:e13390. doi: 10.1371/journal.pone.0013390
93. Kumar A, Xu J, Sung B, Kumar S, Yu D, Aggarwar B, et al. Evidance that GTP-binding domain but not catalytic domain of transglutaminase 2 is essential for epithelial-to-mesenchymal transtion in mammary epithelial cells. *Breast Cancer Res.* (2012) 14:R4. doi: 10.1186/bcr3085
94. Mani SA, Guo W, Liao M-J, Eaton EN, Ayyanan A, Zhou AY, et al. The epithelial-mesenchymal transition generates cells with properties of stem cells. *Cell.* (2008) 133:704–15. doi: 10.1016/j.cell.2008.03.027
95. Morel AP, Lièvre M, Thomas C, Hinkal G, Ansieau S, Puisieux AJP, et al. Generation of breast cancer stem cells through epithelial-mesenchymal transition. *PLoS ONE.* (2008) 3:e2888. doi: 10.1371/journal.pone.0002888
96. Wang Z, Li Y, Kong D, Banerjee S, Ahmad A, Azmi AS, et al. Acquisition of epithelial-mesenchymal transition phenotype of gemcitabine-resistant pancreatic cancer cells is linked with activation of the notch signaling pathway. *Cancer Res.* (2009) 69:2400–7. doi: 10.1158/0008-5472.CAN-08-4312
97. Niu R, Zhang L, Xi G, Wei X, Yang Y, Shi Y, et al. Up-regulation of twist induces angiogenesis and correlates with metastasis in hepatocellular carcinoma. *J Exp Clin Cancer Res.* (2007) 26:385–94.
98. Bracken CP, Gregory PA, Kolesnikoff N, Bert AG, Wang J, Shannon MF, et al. A double-negative feedback loop between ZEB1-SIP1 and the microRNA-200 family regulates epithelial-mesenchymal transition. *Cancer Res.* (2008) 68:7846–54. doi: 10.1158/0008-5472.CAN-08-1942
99. Burk U, Schubert J, Wellner U, Schmalhofer O, Vincan E, Spaderna S, et al. A reciprocal repression between ZEB1 and members of the miR-200 family promotes EMT and invasion in cancer cells. *EMBO Rep.* (2008) 9:582–9. doi: 10.1038/embor.2008.74
100. Korpal M, Lee ES, Hu G, Kang YJ. The miR-200 family inhibits epithelial-mesenchymal transition and cancer cell migration by direct targeting of E-cadherin transcriptional repressors ZEB1 and ZEB2. *J Biol Chem.* (2008) 283:14910–4. doi: 10.1074/jbc.C800074200
101. Park S-M, Gaur AB, Lengyel E, Peter ME. The miR-200 family determines the epithelial phenotype of cancer cells by targeting the E-cadherin repressors ZEB1 and ZEB2. *Genes Dev.* (2008) 22:894–907. doi: 10.1101/gad.1640608
102. Schmalhofer O, Brabletz S, Brabletz T. E-cadherin, β-catenin, and ZEB1 in malignant progression of cancer. *Cancer Metastasis Rev.* (2009) 28:151–66. doi: 10.1007/s10555-008-9179-y
103. Iliopoulos D, Lindahl-Allen M, Polytarchou C, Hirsch HA, Tsichlis PN, Struhl KJM, et al. (2010). Loss of miR-200 inhibition of Suz12 leads to polycomb-mediated repression required for the formation and maintenance of cancer stem cells. *Mol Cell.* 39:761–72. doi: 10.1016/j.molcel.2010.08.013
104. Gregory PA, Bert AG, Paterson EL, Barry SC, Tsykin A, Farshid G, et al. The miR-200 family and miR-205 regulate epithelial to mesenchymal transition by targeting ZEB1 and SIP1. *Nat Cell Biol.* (2008) 10:593–601. doi: 10.1038/ncb1722
105. Wellner U, Schubert J, Burk UC, Schmalhofer O, Zhu F, Sonntag A, et al. The EMT-activator ZEB1 promotes tumorigenicity by repressing stemness-inhibiting microRNAs. *Nat Cell Biol.* (2009) 11:1487–95. doi: 10.1038/ncb1998
106. Brabletz T, Jung A, Hermann K, Günther K, Hohenberger W, Kirchner T, et al. Nuclear overexpression of the oncoprotein β-catenin in colorectal cancer is localized predominantly at the invasion front. *Pathol Res Pract.* (1998) 194:701–4. doi: 10.1016/S0344-0338(98)80129-5
107. Yook JI, Li X-Y, Ota I, Hu C, Kim HS, Kim NH, et al. A Wnt–Axin2–GSK3β cascade regulates snail1 activity in breast cancer cells. *Nat Cell Biol.* (2006) 8:1398–406. doi: 10.1038/ncb1508
108. Zhao C, Blum J, Chen A, Kwon HY, Jung SH, Cook JM, et al. Loss of β-catenin impairs the renewal of normal and CML stem cells *in vivo*. *Cancer Cell.* (2007) 12:528–41. doi: 10.1016/j.ccr.2007.11.003
109. Groen RW, Oud ME, Schilder-Tol EJ, Overdijk MB, Ten Berge D, Nusse R, et al. Illegitimate WNT pathway activation by β-catenin mutation or autocrine stimulation in T-cell malignancies. *Cancer Res.* (2008) 68:6969–77. doi: 10.1158/0008-5472.CAN-08-1322
110. Goessling W, North TE, Loewer S, Lord AM, Lee S, Stoick-Cooper CL, et al. Genetic interaction of PGE2 and Wnt signaling regulates developmental specification of stem cells and regeneration. *Cell.* (2009) 136:1136–47. doi: 10.1016/j.cell.2009.01.015
111. Vermeulen L, Felipe De Sousa EM, Van Der Heijden M, Cameron K, De Jong JH, Borovski T, et al. Wnt activity defines colon cancer stem cells and is regulated by the microenvironment. *Nat Cell Biol.* (2010) 12:468–76. doi: 10.1038/ncb2048
112. Song K, Kwon H, Han C, Zhang J, Dash S, Lim K, et al. Active glycolytic metabolism in CD133 (+) hepatocellular cancer stem cells: regulation by MIR-122. *Oncotarget.* (2015) 6:40822–35. doi: 10.18632/oncotarget.5812
113. Li D, Fu Z, Chen R, Zhao X, Zhou Y, Zeng B, et al. Inhibition of glutamine metabolism counteracts pancreatic cancer stem cell features and sensitizes cells to radiotherapy. *Oncotarget.* (2015) 6:31151–63. doi: 10.18632/oncotarget.5150
114. Lonardo E, Hermann PC, Mueller M-T, Huber S, Balic A, Miranda-Lorenzo I, et al. Nodal/Activin signaling drives self-renewal and tumorigenicity of pancreatic cancer stem cells and provides a target for combined drug therapy. *Cell Stem Cell.* (2011) 9:433–46. doi: 10.1016/j.stem.2011.10.001
115. Sancho P, Barneda D, Heeschen C. Hallmarks of cancer stem cell metabolism. *Br J Cancer.* (2016) 114:1305–12. doi: 10.1038/bjc.2016.152
116. Snyder V, Reed-Newman TC, Arnold L, Thomas SM, Anant SJF. Cancer stem cell metabolism and potential therapeutic targets. *Front Oncol.* (2018) 8:203. doi: 10.3389/fonc.2018.00203
117. Janiszewska M, Suvà ML, Riggi N, Houtkooper RH, Auwerx J, Clément-Schatlo V, et al. Imp2 controls oxidative phosphorylation and is crucial for preserving glioblastoma cancer stem cells. *Genes Dev.* (2012) 26:1926–44. doi: 10.1101/gad.188292.112
118. Lagadinou ED, Sach A, Callahan K, Rossi RM, Neering SJ, Minhajuddin M, et al. BCL-2 inhibition targets oxidative phosphorylation and selectively

eradicates quiescent human leukemia stem cells. *Cell Stem Cell*. (2013) 12:329–41. doi: 10.1016/j.stem.2012.12.013
119. Peiris-Pagès M, Martinez-Outschoorn UE, Pestell RG, Sotgia F, Lisanti MP. Cancer stem cell metabolism. *Breast Cancer Res*. (2016) 18:55. doi: 10.1186/s13058-016-0712-6
120. Vlashi E, Lagadec C, Vergnes L, Matsutani T, Masui K, Poulou M, et al. Metabolic state of glioma stem cells and nontumorigenic Cells. *Proc Natl Acad Sci USA*. (2011) 108:16062–7. doi: 10.1073/pnas.1106704108
121. Ye XQ, Li Q, Wang GH, Sun FF, Huang GJ, Bian XW, et al. Mitochondrial and energy metabolism-related properties as novel indicators of lung cancer stem cells. *Int J Cancer*. (2011) 129:820–31. doi: 10.1002/ijc.25944
122. Sancho P, Burgos-Ramos E, Tavera A, Kheir TB, Jagust P, Schoenhals M, et al. MYC/PGC-1α balance determines the metabolic phenotype and plasticity of pancreatic cancer stem cells. *Cell Metab*. (2015) 22:590–605. doi: 10.1016/j.cmet.2015.08.015
123. Ciavardelli D, Rossi C, Barcaroli D, Volpe S, Consalvo A, Zucchelli M, et al. Breast cancer stem cells rely on fermentative glycolysis and are sensitive to 2-deoxyglucose treatment. *Cell Death Dis*. (2014) 5:e1336. doi: 10.1038/cddis.2014.285
124. Zhou Y, Zhou Y, Shingu T, Feng L, Chen Z, Ogasawara M, et al. Metabolic alterations in highly tumorigenic glioblastoma cells preference for hypoxia and high dependency on glycolysis. *J Biol Chem*. (2011) 286:32843–53. doi: 10.1074/jbc.M111.260935
125. Koppenol WH, Bound PL. The Warburg effect and metabolic efficiency: re-crunching the numbers. *Science*. (2009) 324:1029–33.
126. Israelsen WJ, Dayton TL, Davidson SM, Fiske BP, Hosios AM, Bellinger G, et al. PKM2 isoform-specific deletion reveals a differential requirement for pyruvate kinase in tumor cells. *Cell*. (2013) 155:397–409. doi: 10.1016/j.cell.2013.09.025
127. Guo CY, Yan C, Luo L, Goto S, Urata Y, Xu JJ, et al. Enhanced expression of PKM2 associates with the biological properties of cancer stem cells from A549 human lung cancer cells. *Oncol. Rep*. (2017) 37:2161–6. doi: 10.3892/or.2017.5438
128. Palorini R, Votta G, Balestrieri C, Monestiroli A, Olivieri S, Vento R, et al. Energy metabolism characterization of a novel cancer stem cell-l ike line 3 AB-OS. *J Cell Biochem*. (2014) 115:368–79. doi: 10.1002/jcb.24671
129. Feng W, Gentles A, Nair RV, Huang M, Lin Y, Lee CY, et al. Targeting unique metabolic properties of breast tumor initiating cells. *Stem Cells*. (2014) 32:1734–45. doi: 10.1002/stem.1662
130. Hur W, Ryu JY, Kim HU, Hong SW, Lee EB, Lee SY, et al. Systems approach to characterize the metabolism of liver cancer stem cells expressing CD133. *Sci Rep*. (2017) 7:45557. doi: 10.1038/srep45557
131. Shen YA, Wang CY, Hsieh YT, Chen YJ, Wei YH. Metabolic reprogramming orchestrates cancer stem cell properties in nasopharyngeal carcinoma. *Cell Cycle*. (2015) 14:86–98. doi: 10.4161/15384101.2014.974419
132. Rodríguez-Colman MJ, Schewe M, Meerlo M, Stigter E, Gerrits J, Pras-Raves M, et al. Interplay between metabolic identities in the intestinal crypt supports stem cell function. *Nature*. (2017) 543:424–7. doi: 10.1038/nature21673
133. Chen CT, Shih YRV, Kuo TK, Lee OK, Wei YH. (2008). Coordinated changes of mitochondrial biogenesis and antioxidant enzymes during osteogenic differentiation of human mesenchymal stem cells. *Stem Cells*. 26:960–68. doi: 10.1634/stemcells.2007-0509
134. Simsek T, Kocabas F, Zheng J, DeBerardinis RJ, Mahmoud AI, Olson EN, et al. The distinct metabolic profile of hematopoietic stem cells reflects their location in a hypoxic niche. *Cell Stem Cell*. (2010) 7:380–90. doi: 10.1016/j.stem.2010.07.011
135. Dupuy F, Tabariès S, Andrzejewski S, Dong Z, Blagih J, Annis MG, et al. PDK1-dependent metabolic reprogramming dictates metastatic potential in breast cancer. *Cell Metab*. (2015) 22:577–89. doi: 10.1016/j.cmet.2015.08.007
136. Luo M, Wicha MS. Metabolic plasticity of cancer stem cells. *Oncotarget*. (2015) 6:35141–2. doi: 10.18632/oncotarget.6177
137. De Francesco EM, Sotgia F, Lisanti MP. Cancer stem cells (CSCs): metabolic strategies for their identification and eradication. *Biochem. J*. (2018) 475:1611–34. doi: 10.1042/BCJ20170164
138. Moreno-Sánchez R, Rodríguez-Enríquez S, Marín-Hernández A, Saavedra E. Energy metabolism in tumor cells. *FEBS J*. (2007) 274:1393–418. doi: 10.1111/j.1742-4658.2007.05686.x
139. Koppenol WH, Bounds PL, Dang CV. Otto warburg's contributions to current concepts of cancer metabolism. *Nat Rev Cancer*. (2011) 11:325–37. doi: 10.1038/nrc3038
140. Ashton TM, McKenna WG, Kunz-Schughart LA, Higgins GS. Oxidative phosphorylation as an emerging target in cancer therapy. *Clin Cancer Res*. (2018) 24:2482–90. doi: 10.1158/1078-0432.CCR-17-3070
141. Pascual G, Domínguez D, Benitah SA. The contributions of cancer cell metabolism to metastasis. *Dis Models Mech*. (2018) 11:dmm032920. doi: 10.1242/dmm.032920
142. Yuan Y, Ju YS, Kim Y, Li J, Wang Y, Yoon CJ, et al. Comprehensive molecular characterization of mitochondrial genomes in human cancers. *Nat Genet*. (2020) 52:342–52. doi: 10.1038/s41588-019-0557-x
143. Whitaker-Menezes D, Martinez-Outschoorn UE, Flomenberg N, Birbe R, Witkiewicz AK, Howell A, et al. Hyperactivation of oxidative mitochondrial metabolism in epithelial cancer cells in situ: visualizing the therapeutic effects of metformin in tumor tissue. *Cell Cycle*. (2011) 10:4047–64. doi: 10.4161/cc.10.23.18151
144. Garber AJ, Karl I, Kipnis D. Alanine and glutamine synthesis and release from skeletal muscle. II the precursor role of amino acids in alanine and glutamine synthesis. *J. Biol. Chem*. (1976) 251:836–43.
145. Macheda ML, Rogers S, Best JD. Molecular and cellular regulation of glucose transporter (GLUT) proteins in cancer. *J Cell Physiol*. (2005) 202:654–62. doi: 10.1002/jcp.20166
146. Ganapathy V, Thangaraju M, Prasad PD. Nutrient transporters in cancer: relevance to warburg hypothesis and beyond. *Pharmacol Ther*. (2009) 121:29–40. doi: 10.1016/j.pharmthera.2008.09.005
147. Furuta E, Okuda H, Kobayashi A, Watabe K. Metabolic genes in cancer: their roles in tumor progression and clinical implications. *Biochim Biophys Acta*. (2010) 1805:141–52. doi: 10.1016/j.bbcan.2010.01.005
148. Crane RK. The restrictions on possible mechanisms of intestinal transport of sugars. In: *Membrane Transport and Metabolism. Proceedings of a Symposium held in Prague, August 22-27, 1960*. Prague: Czech Academy of Sciences (1961). p. 439–49.
149. Oka Y, Asano T, Shibasaki Y, Lin J-L, Tsukuda K, Katagiri H, et al. C-terminal truncated glucose transporter is locked into an inward-facing form without transport activity. *Nature*. (1990) 345:550. doi: 10.1038/345550a0
150. Hebert DN, Carruthers A. Glucose transporter oligomeric structure determines transporter function. Reversible redox-dependent interconversions of tetrameric and dimeric GLUT1. *J. Biol. Chem*. (1992) 267:23829–38.
151. Adekola K, Rosen ST, Shanmugam M. Glucose transporters in cancer metabolism. *Curr Opin Oncol*. (2012) 24:650. doi: 10.1097/CCO.0b013e328356da72
152. Gonzalez-Menendez P, Hevia D, Alonso-Arias R, Alvarez-Artime A, Rodriguez-Garcia A, Kinet S, et al. GLUT1 protects prostate cancer cells from glucose deprivation-induced oxidative stress. *Redox Biol*. (2018) 17:112–27. doi: 10.1016/j.redox.2018.03.017
153. Ha T-K, Her N-G, Lee M-G, Ryu B-K, Lee J-H, Han J, et al. Caveolin-1 increases aerobic glycolysis in colorectal cancers by stimulating HMGA1-mediated GLUT3 transcription. *Cancer Res*. (2012) 72:4097–109. doi: 10.1158/0008-5472.CAN-12-0448
154. Masin M, Vazquez J, Rossi S, Groeneveld S, Samson N, Schwalie PC, et al. GLUT3 is induced during epithelial-mesenchymal transition and promotes tumor cell proliferation in non-small cell lung cancer. *Cancer Metab*. (2014) 2:11. doi: 10.1186/2049-3002-2-11
155. Shibuya K, Okada M, Suzuki S, Seino M, Seino S, Takeda H, et al. Targeting the facilitative glucose transporter GLUT1 inhibits the self-renewal and tumor-initiating capacity of cancer stem cells. *Oncotarget*. (2015) 6:651–61. doi: 10.18632/oncotarget.2892
156. Osada-Oka M, Hashiba Y, Akiba S, Imaoka S, Sato T. Glucose is necessary for stabilization of hypoxia-inducible factor-1α under hypoxia: contribution of the pentose phosphate pathway to this stabilization. *FEBS Lett*. (2010) 584:3073–9. doi: 10.1016/j.febslet.2010.05.046

157. Cho ES, Cha YH, Kim HS, Kim NH, Yook JI. The pentose phosphate pathway as a potential target for cancer therapy. *Biomol Ther.* (2018) 26:29–38. doi: 10.4062/biomolther.2017.179
158. Kathagen A, Schulte A, Balcke G, Phillips HS, Martens T, Matschke J, et al. Hypoxia and oxygenation induce a metabolic switch between pentose phosphate pathway and glycolysis in glioma stem-like cells. *Acta Neuropathol.* (2013) 126:763–80. doi: 10.1007/s00401-013-1173-y
159. Hunt TK, Aslam RS, Beckert S, Wagner S, Ghani QP, Hussain MZ, et al. Aerobically derived lactate stimulates revascularization and tissue repair via redox mechanisms. *Antioxid Redox Signal.* (2007) 9:1115–24. doi: 10.1089/ars.2007.1674
160. Kathagen-Buhmann A, Schulte A, Weller J, Holz M, Herold-Mende C, Glass R, et al. Glycolysis and the pentose phosphate pathway are differentially associated with the dichotomous regulation of glioblastoma cell migration versus proliferation. *Neuro Oncol.* (2016) 18:1219–29. doi: 10.1093/neuonc/now024
161. Lemons JM, Feng X-J, Bennett BD, Legesse-Miller A, Johnson EL, Raitman I, et al. Quiescent fibroblasts exhibit high metabolic activity. *PLoS Biol.* (2010) 8:e1000514. doi: 10.1371/journal.pbio.1000514
162. Sonveaux P, Copetti T, De Saedeleer CJ, Végran F, Verrax J, Kennedy KM, et al. Targeting the lactate transporter MCT1 in endothelial cells inhibits lactate-induced HIF-1 activation and tumor angiogenesis. *PLoS ONE.* (2012) 7:e33418. doi: 10.1371/journal.pone.0033418
163. Wakil SJ. Fatty acid synthase, a proficient multifunctional enzyme. *Biochemistry.* (1989) 28:4523–30. doi: 10.1021/bi00437a001
164. Menendez JA, Lupu R. Fatty acid synthase and the lipogenic phenotype in cancer pathogenesis. *Nat Rev Cancer.* (2007) 7:763–77. doi: 10.1038/nrc2222
165. Kuhajda FP. Fatty-acid synthase and human cancer: new perspectives on its role in tumor biology. *Nutrition.* (2000) 16:202–8. doi: 10.1016/S0899-9007(99)00266-X
166. Mashima T, Seimiya H, Tsuruo T. *De novo* fatty-acid synthesis and related pathways as molecular targets for cancer therapy. *Br J Cancer.* (2009) 100:1369–72. doi: 10.1038/sj.bjc.6605007
167. Bobrow L, Happerfield L, Pasternack G, Smith P, Owens A. The expression of fatty acid synthase in primary breast cancer: is it an independent prognostic indicator. *Breast Cancer Res Treat.* (1993) 25:653–8.
168. Jensen V, Ladekarl M, Holm-Nielsen P, Melsen F, Sœrensen FB. The prognostic value of oncogenic antigen 519 (OA-519) expression and proliferative activity detected by antibody MIB-I in node-negative breast cancer. *J. Pathol.* (1995) 176:343–52. doi: 10.1002/path.1711760405
169. Alo PL, Visca P, Marci A, Mangoni A, Botti C, Di Tondo U. Expression of fatty acid synthase (FAS) as a predictor of recurrence in stage I breast carcinoma patients. *Cancer.* (1996) 77:474–82. doi: 10.1002/(SICI)1097-0142(19960201)77:3<474::AID-CNCR8>3.0.CO;2-K
170. Vlad L, Axiotis C, Merino M, Green W. Fatty acid synthase is highly expressed in aggressive thyroid tumors. In: *Laboratory Investigation.* Philadelphia, PA: Lippincott Williams & Wilkins. (1999). p. 70A
171. Gansler TS, Hardman WIII, Hunt DA, Schaffel S, Hennigar RA. Increased expression of fatty acid synthase (OA-519) in ovarian neoplasms predicts shorter survival. *Hum Pathol.* (1997) 28:686–92. doi: 10.1016/S0046-8177(97)90177-5
172. Epstein JI, Carmichael M, Partin AW. OA-519 (fatty acid synthase) as an independent predictor of pathologic stage in adenocarcinoma of the prostate. *Urology.* (1995) 45:81–6. doi: 10.1016/S0090-4295(95)96904-7
173. Shurbaji MS, Kalbfleisch JH, Thurmond TS. Immunohistochemical detection of a fatty acid synthase (OA-519) as a predictor of progression of prostate cancer. *Hum Pathol.* (1996) 27:917–21. doi: 10.1016/S0046-8177(96)90218-X
174. Krontiras H, Roye GD, Beenken SE, Myers RB, Mayo MS, Peters GE, et al. Fatty acid synthase expression is increased in neoplastic lesions of the oral tongue. *Head Neck.* (1999) 21:325–9. doi: 10.1002/(SICI)1097-0347(199907)21:4<325::AID-HED6>3.0.CO;2-P
175. Agostini M, Silva SD, Zecchin KG, Coletta RD, Jorge J, Loda M, et al. Fatty acid synthase is required for the proliferation of human oral squamous carcinoma cells. *Oral Oncol.* (2004) 40:728–35. doi: 10.1016/j.oraloncology.2004.01.011
176. Zhang Y, Guo C, Yu G. A pilot study of fatty acid metabolism in oral squamous cell carcinoma. *Int J Oral Maxillofac Surg.* (2005) 34:78–81. doi: 10.1016/j.ijom.2004.03.001
177. Rashid A, Pizer ES, Moga M, Milgraum LZ, Zahurak M, Pasternack GR, et al. Elevated expression of fatty acid synthase and fatty acid synthetic activity in colorectal neoplasia. *Am J Pathol.* (1997) 150:201.
178. Pizer ES, Lax SF, Kuhajda FP, Pasternack GR, Kurman RJ. Fatty acid synthase expression in endometrial carcinoma: correlation with cell proliferation and hormone receptors. *Cancer.* (1998) 83:528–37. doi: 10.1002/(SICI)1097-0142(19980801)83:3<528::AID-CNCR22>3.0.CO;2-X
179. Gabrielson EW, Pinn ML, Testa JR, Kuhajda FP. Increased fatty acid synthase is a therapeutic target in mesothelioma. *Clin. Cancer Res.* (2001) 7:153–7.
180. Horiguchi A, Asano T, Asano T, Ito K, Sumitomo M, Hayakawa M. Pharmacological inhibitor of fatty acid synthase suppresses growth and invasiveness of renal cancer cells. *J Urol.* (2008) 180:729–36. doi: 10.1016/j.juro.2008.03.186
181. Camassei FD, Cozza R, Acquaviva A, Jenkner A, Ravà, L, Gareri R, et al. Expression of the lipogenic enzyme fatty acid synthase (FAS) in retinoblastoma and its correlation with tumor aggressiveness. *Invest Ophthalmol Vis Sci.* (2003) 44:2399–403. doi: 10.1167/iovs.02-0934
182. Vandhana S, Deepa P, Jayanthi U, Biswas J, Krishnakumar S. Clinico-pathological correlations of fatty acid synthase expression in retinoblastoma: an Indian cohort study. *Exp. Mol. Pathol.* (2011) 90:29–37. doi: 10.1016/j.yexmp.2010.11.007
183. Yasumoto Y, Miyazaki H, Vaidyan LK, Kagawa Y, Ebrahimi M, Yamamoto Y, et al. Inhibition of fatty acid synthase decreases expression of stemness markers in glioma stem cells. *PLoS ONE.* (2016) 11:e0147717. doi: 10.1371/journal.pone.0147717
184. Chen C-L, Kumar DBU, Punj V, Xu J, Sher L, Tahara SM, et al. NANOG metabolically reprograms tumor-initiating stem-like cells through tumorigenic changes in oxidative phosphorylation and fatty acid metabolism. *Cell Metab.* (2016) 23:206–19. doi: 10.1016/j.cmet.2015.12.004
185. Brandi J, Dando I, Dalla Pozza E, Biondani G, Jenkins R, Elliott V, et al. Proteomic analysis of pancreatic cancer stem cells: functional role of fatty acid synthesis and mevalonate pathways. *J Proteomics.* (2017) 150:310–22. doi: 10.1016/j.jprot.2016.10.002
186. Tirinato L, Pagliari F, Limongi T, Marini M, Falqui A, Seco J, et al. An overview of lipid droplets in cancer and cancer stem cells. *Stem Cells Int.* (2017) 2017:1656053. doi: 10.1155/2017/1656053
187. Cruz AL, Barreto EDA, Fazolini NP, Viola JP, Bozza PT. Lipid droplets: platforms with multiple functions in cancer hallmarks. *Cell Death Dis.* (2020) 11:105. doi: 10.1038/s41419-020-2297-3
188. Zaytseva YY, Harris JW, Mitov MI, Kim JT, Butterfield DA, Lee EY, et al. Increased expression of fatty acid synthase provides a survival advantage to colorectal cancer cells via upregulation of cellular respiration. *Oncotarget.* (2015) 6:18891–904. doi: 10.18632/oncotarget.3783
189. Castro LFC, Wilson JM, Gonçalves O, Galante-Oliveira S, Rocha E, Cunha I. The evolutionary history of the stearoyl-CoA desaturase gene family in vertebrates. *BMC Evol Biol.* (2011) 11:132. doi: 10.1186/1471-2148-11-132
190. Pisanu ME, Noto A, De Vitis C, Morrone S, Scognamiglio G, Botti G, et al. Blockade of Stearoyl-CoA-desaturase 1 activity reverts resistance to cisplatin in lung cancer stem cells. *Cancer Lett.* (2017) 406:93–104. doi: 10.1016/j.canlet.2017.07.027
191. Ma Y, Temkin SM, Hawkridge AM, Guo C, Wang W, Wang X-Y, et al. Fatty acid oxidation: an emerging facet of metabolic transformation in cancer. *Cancer Lett.* (2018) 435:92–100. doi: 10.1016/j.canlet.2018.08.006
192. Ye H, Adane B, Khan N, Sullivan T, Minhajuddin M, Gasparetto M, et al. Leukemic stem cells evade chemotherapy by metabolic adaptation to an adipose tissue niche. *Cell Stem Cell.* (2016) 19:23–37. doi: 10.1016/j.stem.2016.06.001
193. Wang T, Fahrmann JF, Lee H, Li YJ, Tripathi SC, Yue C, et al. JAK/STAT3-regulated fatty acid β-oxidation is critical for breast cancer stem cell self-renewal and chemoresistance. *Cell Metab.* (2018) 27:136–50 e135. doi: 10.1016/j.cmet.2017.11.001
194. Paumen MB, Ishida Y, Han H, Muramatsu M, Eguchi Y, Tsujimoto Y, et al. Direct interaction of the mitochondrial membrane protein carnitine palmitoyltransferase I with Bcl-2. *Biochem Biophys Res Commun.* (1997) 231:523–5. doi: 10.1006/bbrc.1997.6089

195. Giordano A, Calvani M, Petillo O, Grippo P, Tuccillo F, Melone MAB, et al. tBid induces alterations of mitochondrial fatty acid oxidation flux by malonyl-CoA-independent inhibition of carnitine palmitoyltransferase-1. *Cell Death Differ.* (2005) 12:603–13. doi: 10.1038/sj.cdd.4401636
196. Jeon S-M, Chandel NS, Hay N. AMPK regulates NADPH homeostasis to promote tumour cell survival during energy stress. *Nature.* (2012) 485:661–5. doi: 10.1038/nature11066
197. LeBleu VS, O'Connell JT, Herrera KNG, Wikman H, Pantel K, Haigis MC, et al. PGC-1α mediates mitochondrial biogenesis and oxidative phosphorylation in cancer cells to promote metastasis. *Nat Cell Biol.* (2014) 16:992–1003. doi: 10.1038/ncb3039
198. Caino MC, Ghosh JC, Chae YC, Vaira V, Rivadeneira DB, Faversani A, et al. PI3K therapy reprograms mitochondrial trafficking to fuel tumor cell invasion. *Proc Natl Acad Sci. USA.* (2015) 112:8638–43. doi: 10.1073/pnas.1500722112
199. Lu J, Tan M, Cai Q. The warburg effect in tumor progression: mitochondrial oxidative metabolism as an anti-metastasis mechanism. *Cancer Lett.* (2015) 356:156–64. doi: 10.1016/j.canlet.2014.04.001
200. King MP, Attardi G. Injection of mitochondria into human cells leads to a rapid replacement of the endogenous mitochondrial DNA. *Cell.* (1988) 52:811–9. doi: 10.1016/0092-8674(88)90423-0
201. Copeland WC, Wachsman JT, Johnson F, Penta JS. Mitochondrial DNA alterations in cancer. *Cancer Invest.* (2002) 20:557–69. doi: 10.1081/CNV-120002155
202. Arya RK, Singh A, Yadav NK, Cheruvu SH, Hossain Z, Meena S, et al. Anti-breast tumor activity of eclipta extract *in-vitro* and *in-vivo*: novel evidence of endoplasmic reticulum specific localization of Hsp60 during apoptosis. *Sci Rep.* (2015) 5:18457. doi: 10.1038/srep18457
203. Chinnery PF, Samuels DC, Elson J, Turnbull DM. Accumulation of mitochondrial DNA mutations in ageing, cancer, and mitochondrial disease: is there a common mechanism? *Lancet.* (2002) 360:1323–5. doi: 10.1016/S0140-6736(02)11310-9
204. Brandon M, Baldi P, Wallace D. Mitochondrial mutations in cancer. *Oncogene.* (2006) 25:4647–62. doi: 10.1038/sj.onc.1209607
205. Gasparre G, Hervouet E, de Laplanche E, Demont J, Pennisi LF, Colombel M, et al. Clonal expansion of mutated mitochondrial DNA is associated with tumor formation and complex I deficiency in the benign renal oncocytoma. *Hum Mol Genet.* (2008) 17:986–95. doi: 10.1093/hmg/ddm371
206. Pereira L, Soares P, Máximo V, Samuels DC. Somatic mitochondrial DNA mutations in cancer escape purifying selection and high pathogenicity mutations lead to the oncocytic phenotype: pathogenicity analysis of reported somatic mtDNA mutations in tumors. *BMC Cancer.* (2012) 12:53. doi: 10.1186/1471-2407-12-53
207. Lleonart ME, Grodzicki R, Graifer DM, Lyakhovich A. Mitochondrial dysfunction and potential anticancer therapy. *Med Res Rev.* (2017) 37:1275–98. doi: 10.1002/med.21459
208. Guha M, Srinivasan S, Ruthel G, Kashina A, Carstens R, Mendoza A, et al. Mitochondrial retrograde signaling induces epithelial–mesenchymal transition and generates breast cancer stem cells. *Oncogene.* (2014) 33:5238–50. doi: 10.1038/onc.2013.467
209. Loureiro R, Mesquita KA, Magalhaes-Novais S, Oliveira PJ, Vega-Naredo I. Mitochondrial biology in cancer stem cells. In: *Seminars in Cancer Biology*. Elsevier (2017). p. 18–28. doi: 10.1016/j.semcancer.2017.06.012
210. Kim EJ, Jin X, Kim OR, Ham SW, Park S-H, Kim H. Glioma stem cells and their non-stem differentiated glioma cells exhibit differences in mitochondrial structure and function. *Oncol Rep.* (2018) 39:411–6. doi: 10.3892/or.2017.6075
211. Sato M, Kawana K, Adachi K, Fujimoto A, Yoshida M, Nakamura H, et al. Spheroid cancer stem cells display reprogrammed metabolism and obtain energy by actively running the tricarboxylic acid (TCA) cycle. *Oncotarget.* (2016) 7:33297–33305. doi: 10.18632/oncotarget.8947
212. Maalouf M, Sullivan PG, Davis L, Kim DY, Rho JM. Ketones inhibit mitochondrial production of reactive oxygen species production following glutamate excitotoxicity by increasing NADH oxidation. *Neuroscience.* (2007) 145:256–64. doi: 10.1016/j.neuroscience.2006.11.065
213. Sato K, Kashiwaya Y, Keon C, Tsuchiya N, King M, Radda G, et al. Insulin, ketone bodies, and mitochondrial energy transduction. *FASEB J.* (1995) 9:651–8. doi: 10.1096/fasebj.9.8.7768357
214. Veech RL, Chance B, Kashiwaya Y, Lardy HA, Cahill Jr GF. Ketone bodies, potential therapeutic uses. *IUBMB Life.* (2001) 51:241–7. doi: 10.1080/152165401753311780
215. Kim DY, Davis LM, Sullivan PG, Maalouf M, Simeone TA, Brederode J, et al. Ketone bodies are protective against oxidative stress in neocortical neurons. *J Neurochem.* (2007) 101:1316–26. doi: 10.1111/j.1471-4159.2007.04483.x
216. Abdelwahab MG, Lee SH, O'Neill D, Thompson RJ, Duff HJ, Sullivan PG, et al. Ketones prevent oxidative impairment of hippocampal synaptic integrity through KATP channels. *PLoS ONE.* (2015) 10:e0119316. doi: 10.1371/journal.pone.0119316
217. Ozsvari B, Sotgia F, Simmons K, Trowbridge R, Foster R, Lisanti MP. Mitoketoscins: novel mitochondrial inhibitors for targeting ketone metabolism in cancer stem cells (CSCs). *Oncotarget.* (2017) 8:78340–50. doi: 10.18632/oncotarget.21259
218. Lonergan T, Brenner C, Bavister B. Differentiation-related changes in mitochondrial properties as indicators of stem cell competence. *J Cell Physiol.* (2006) 208:149–53. doi: 10.1002/jcp.20641
219. Piccoli C, Ria R, Scrima R, Cela O, D'Aprile A, Boffoli D, et al. Characterization of mitochondrial and extra-mitochondrial oxygen consuming reactions in human hematopoietic stem cells novel evidence of the occurrence of NAD (P) H oxidase activity. *J Biol Chem.* (2005) 280:26467–76. doi: 10.1074/jbc.M500047200
220. Miyamoto T, Weissman IL, Akashi K. AML1/ETO-expressing nonleukemic stem cells in acute myelogenous leukemia with 8; 21 chromosomal translocation. *Proc Natl Acad Sci USA.* (2000) 97:7521–6. doi: 10.1073/pnas.97.13.7521
221. Kucia M, Ratajczak M. Stem cells as a two edged sword-from regeneration to tumor formation. *J Physiol. Pharmacol.* (2006) 57:5–16.
222. Alvero AB, Montagna MK, Holmberg JC. Targeting the mitochondria activates two independent cell death pathways in ovarian cancer stem cells. *Mol Cancer Ther.* (2011) 10:1385–93. doi: 10.1158/1535-7163.MCT-11-0023
223. Vlashi E, Lagadec C, Vergnes L, Reue K, Frohnen P, Chan M, et al. Metabolic differences in breast cancer stem cells and differentiated progeny. *Breast Cancer Res Treat.* (2014) 146:525–34. doi: 10.1007/s10549-014-3051-2
224. Ishikawa K, Takenaga K, Akimoto M, Koshikawa N, Yamaguchi A, Imanishi H, et al. ROS-generating mitochondrial DNA mutations can regulate tumor cell metastasis. *Science.* (2008) 320:661–4. doi: 10.1126/science.1156906
225. Kaipparettu BA, Ma Y, Wong LJC. Functional effects of cancer mitochondria on energy metabolism and tumorigenesis: utility of transmitochondrial cybrids. *Ann N Y Acad Sci.* (2010) 1201:137–46. doi: 10.1111/j.1749-6632.2010.05621.x
226. Park JH, Vithayathil S, Kumar S, Sung PL, Dobrolecki LE, Putluri V, et al. Fatty acid oxidation-driven Src links mitochondrial energy reprogramming and oncogenic properties in triple-negative breast cancer. *Cell Rep.* (2016) 14:2154–65. doi: 10.1016/j.celrep.2016.02.004
227. Kessler JD, Kahle KT, Sun T, Meerbrey KL, Schlabach MR, Schmitt EM, et al. A SUMOylation-dependent transcriptional subprogram is required for Myc-driven tumorigenesis. *Science.* (2012) 335:348–53. doi: 10.1126/science.1212728
228. Gao C, Shen Y, Jin F, Miao Y, Qiu X. Cancer stem cells in small cell lung cancer cell line H446: higher dependency on oxidative phosphorylation and mitochondrial substrate-level phosphorylation than non-stem cancer cells. *PLoS ONE.* (2016) 11:e0154576. doi: 10.1371/journal.pone.0154576
229. Flores RE, Brown AK, Taus L, Khoury J, Glover F, Kami K, et al. Mycoplasma infection and hypoxia initiate succinate accumulation and release in the VM-M3 cancer cells. *Biochim Biophys Acta.* (2018) 1859:975–83. doi: 10.1016/j.bbabio.2018.03.012
230. Ta NL, Seyfried TN. Influence of serum and hypoxia on incorporation of [14 C]-d-glucose or [14 C]-l-glutamine into lipids and lactate in murine glioblastoma cells. *Lipids.* (2015) 50:1167–84. doi: 10.1007/s11745-015-4075-z
231. Scott DA, Richardson AD, Filipp FV, Knutzen CA, Chaing GG, Zeev AR, et al. Comparative metabolic flux profiling of melanoma cell lines beyond the warburg effect. *J. Biol. Chem.* (2011) 286:42626–34. doi: 10.1074/jbc.M111.282046

232. Portairs JC, Voisin P, Merle M, Canioni P. Glucose and glutamine metabolism in C6 glioma cells studied by carbon 13 NMR. *Biochimie.* (1996) 78:155–64 doi: 10.1016/0300-9084(96)89500-9
233. Chen Q, Kirk K, Shurubor YI, Zhao D, Arreguin AJ, Shahi I, et al. Rewiring of glutamine metabolism is a bioenergetic adaptation of human cells with mitochondrial DNA mutations. *Cell Metab.* (2018) 27:1007–25 e1005. doi: 10.1016/j.cmet.2018.03.002
234. Zhang Y, Zhang SX, Trivedi J, Toll AD, Brahmer J, Hales R, et al. Pleural fluid secondary to pulmonary cryptococcal infection: a case report and review of the literature. *BMC Infect Dis.* (2019) 19:710. doi: 10.1186/s12879-019-4343-2
235. Reckzeh ES, Karageorgis G, Schwalfenberg M, Ceballos J, Stroet MC, Binici A, et al. Inhibition of glucose transporters and glutaminase synergistically impairs tumor cell growth. *Cell Chem Biol.* (2019) 26:1214–28. doi: 10.1016/j.chembiol.2019.06.005
236. Mukherjee P, Augur ZM, Li M, Hill C, Greenwood B, Domin MA, et al. Therapeutic benefit of combining calorie-restricted ketogenic diet and glutamine targeting in late-stage experimental glioblastoma. *Commun. Biol.* (2019) 2:200. doi: 10.1038/s42003-019-0455-x
237. DeBerardinis RJ, Cheng T. Q's next: the diverse functions of glutamine in metabolism, cell biology and cancer. *Oncogene.* (2010) 29:313. doi: 10.1038/onc.2009.358
238. Wise DR, Thompson CB. Glutamine addiction: a new therapeutic target in cancer. *Trends Biochem Sci.* (2010) 35:427–33. doi: 10.1016/j.tibs.2010.05.003
239. Locasale JW. Serine, glycine and one-carbon units: cancer metabolism in full circle. *Nat Rev Cancer.* (2013) 13:572–83. doi: 10.1038/nrc3557
240. Medina MA, Sánchez-Jiménez F, Márquez J, Quesada AR, de Castro Núñez I. Relevance of glutamine metabolism to tumor cell growth. *Mol Cell Biochem.* (1992) 113:1–15. doi: 10.1007/BF00230880
241. Kim JH, Lee KJ, Seo Y, Kwon J-H, Yoon JP, Kang JY, et al. Effects of metformin on colorectal cancer stem cells depend on alterations in glutamine metabolism. *Sci Rep.* (2018) 8:13111. doi: 10.1038/s41598-018-29895-5
242. Kamphorst JJ, Nofal M, Commisso C, Hackett SR, Lu W, Grabocka E, et al. Human pancreatic cancer tumors are nutrient poor and tumor cells actively scavenge extracellular protein. *Cancer Res.* (2015) 75:544–53. doi: 10.1158/0008-5472.CAN-14-2211
243. Commisso C, Davidson SM, Soydaner-Azeloglu RG, Parker SJ, Kamphorst JJ, Hackett S, et al. Macropinocytosis of protein is an amino acid supply route in Ras-transformed cells. *Nature.* (2013) 497:633–7. doi: 10.1038/nature12138
244. Oburoglu L, Tardito S, Fritz V, de Barros SC, Merida P, Craveiro M, et al. Glucose and glutamine metabolism regulate human hematopoietic stem cell lineage specification. *Cell Stem Cell.* (2014) 15:169–84. doi: 10.1016/j.stem.2014.06.002
245. Todorova VK, Harms SA, Kaufmann Y, Luo S, Luo KQ, Babb K, et al. Effect of dietary glutamine on tumor glutathione levels and apoptosis-related proteins in DMBA-induced breast cancer of rats. *Breast Cancer Res Treat.* (2004) 88:247–56. doi: 10.1007/s10549-004-0783-4
246. Cluntun AA, Lukey MJ, Cerione RA, Locasale JW. Glutamine metabolism in cancer: understanding the heterogeneity. *Trends Cancer.* (2017) 3:169–80. doi: 10.1016/j.trecan.2017.01.005
247. Davidson SM, Papagiannakopoulos T, Olenchock BA, Heyman JE, Keibler MA, Luengo A, et al. Environment impacts the metabolic dependencies of Ras-driven non-small cell lung cancer. *Cell Metab.* (2016) 23:517–28. doi: 10.1016/j.cmet.2016.01.007
248. Raimundo N, Baysal BE, Shadel GS. Revisiting the TCA cycle: signaling to tumor formation. *Trends Mol Med.* (2011) 17:641–9. doi: 10.1016/j.molmed.2011.06.001
249. Ayob AZ, Ramasamy TS. Cancer stem cells as key drivers of tumour progression. *J Biomed Sci.* (2018) 25:20. doi: 10.1186/s12929-018-0426-4
250. Bartmann C, Raman SJ, Floter J, Schulze A, Bahlke K, Willingstofer J, et al. Beta-hydroxybutyrate (3-OHB) can influence the energetic phenotype of breast cancer cells, but does not impact their proliferation and the response to chemotherapy or radiation. *Cancer Metab.* (2018) 6:8. doi: 10.1186/s40170-018-0180-9
251. Lin L, Ding Y, Wang Y, Wang Z, Yin XG, Shen H. Functional lipidomics: palmitic acid impairs hepatocellular carcinoma development by modulating membrane fluidity and glucose metabolism. *Hepatology.* (2017) 66:432–48. doi: 10.1002/hep.29033
252. Network CGA. Comprehensive molecular portraits of human breast tumours. *Nature.* (2012) 490:61–70. doi: 10.1038/nature11412
253. Network CGAR. Integrated genomic analyses of ovarian carcinoma. *Nature.* (2011) 474:609–15. doi: 10.1038/nature10166
254. Network CGAR. Comprehensive molecular profiling of lung adenocarcinoma. *Nature.* (2014) 511:543–50. doi: 10.1038/nature13385
255. Parsons DW, Jones S, Zhang X, Lin JC-H, Leary RJ, Angenendt P, et al. An integrated genomic analysis of human glioblastoma multiforme. *Science.* (2008) 321:1807–12. doi: 10.1126/science.1164382
256. Walter BA, Valera VA, Pinto PA, Merino MJ. Comprehensive microRNA profiling of prostate cancer. *J Cancer.* (2013) 4:350–7. doi: 10.7150/jca.6394
257. Wang K, Yuen ST, Xu J, Lee SP, Yan HH, Shi ST, et al. Whole-genome sequencing and comprehensive molecular profiling identify new driver mutations in gastric cancer. *Nat Genet.* (2014) 46:573–82. doi: 10.1038/ng.2983
258. Shipp MA, Ross KN, Tamayo P, Weng AP, Kutok JL, Aguiar RC, et al. Diffuse large B-cell lymphoma outcome prediction by gene-expression profiling and supervised machine learning. *Nat Med.* (2002) 8:68–74. doi: 10.1038/nm0102-68
259. Mancini M, Scappaticci D, Cimino G, Nanni M, Derme V, Elia L, et al. A comprehensive genetic classification of adult acute lymphoblastic leukemia (ALL): analysis of the GIMEMA 0496 protocol. *Blood.* (2005) 105:3434–41. doi: 10.1182/blood-2004-07-2922
260. Zehir A, Benayed R, Shah RH, Syed A, Middha S, Kim HR, et al. Mutational landscape of metastatic cancer revealed from prospective clinical sequencing of 10,000 patients. *Nat Med.* (2017) 23:703. doi: 10.1038/nm.4333
261. Smith AP, Hoek K, Becker D. Whole-genome expression profiling of the melanoma progression pathway reveals marked molecular differences between nevi/melanoma *in situ* and advanced-stage melanomas. *Cancer Biol Ther.* (2005) 4:1018–29. doi: 10.4161/cbt.4.9.2165

Conflict of Interest: The authors declare that the research was conducted in the absence of any commercial or financial relationships that could be construed as a potential conflict of interest.

frontiers in Oncology

ORIGINAL RESEARCH
published: 30 June 2020
doi: 10.3389/fonc.2020.01053

Metabolic and OXPHOS Activities Quantified by Temporal *ex vivo* Analysis Display Patient-Specific Metabolic Vulnerabilities in Human Breast Cancers

Andre Koit[1], Natalja Timohhina[1], Laura Truu[1], Vladimir Chekulayev[1], Shivakumar Gudlawar[1], Igor Shevchuk[1], Katrin Lepik[2], Lea Mallo[2], Riina Kutner[2], Vahur Valvere[2] and Tuuli Kaambre[1,3]*

[1] Chemical Biology Laboratory, National Institute of Chemical Physics and Biophysics, Tallinn, Estonia, [2] Oncology and Hematology Clinic at the North Estonia Medical Centre, Tallinn, Estonia, [3] School of Natural Sciences and Health, Tallinn University, Tallinn, Estonia

OPEN ACCESS

Edited by:
Federica Sotgia,
University of Salford, United Kingdom

Reviewed by:
Helene Lemieux,
University of Alberta, Canada
Cesar Cardenas,
Universidad Mayor, Chile

***Correspondence:**
Andre Koit
andre.koit@kbfi.ee

Specialty section:
This article was submitted to Cancer Metabolism, a section of the journal Frontiers in Oncology

Received: 29 February 2020
Accepted: 27 May 2020
Published: 30 June 2020

Citation:
Koit A, Timohhina N, Truu L, Chekulayev V, Gudlawar S, Shevchuk I, Lepik K, Mallo L, Kutner R, Valvere V and Kaambre T (2020) Metabolic and OXPHOS Activities Quantified by Temporal ex vivo Analysis Display Patient-Specific Metabolic Vulnerabilities in Human Breast Cancers. Front. Oncol. 10:1053. doi: 10.3389/fonc.2020.01053

Research on mitochondrial metabolism and respiration are rapidly developing areas, however, efficient and widely accepted methods for studying these in solid tumors are still missing. Here, we developed a new method without isotope tracing to quantitate time dependent mitochondrial citrate efflux in cell lines and human breast cancer samples. In addition, we studied ADP-activated respiration in both of the sample types using selective permeabilization and showed that metabolic activity and respiration are not equally linked. Three times lower amount of mitochondria in scarcely respiring MDA-MB-231 cells convert pyruvate and glutamate into citrate efflux at 20% higher rate than highly respiring MCF-7 mitochondria do. Surprisingly, analysis of 59 human breast cancers revealed the opposite in clinical samples as aggressive breast cancer subtypes, in comparison to less aggressive subtypes, presented with both higher mitochondrial citrate efflux and higher respiration rate. Additionally, comparison of substrate preference (pyruvate or glutamate) for both mitochondrial citrate efflux and respiration in triple negative breast cancers revealed probable causes for high glutamine dependence in this subtype and reasons why some of these tumors are able to overcome glutaminase inhibition. Our research concludes that the two widely used breast cancer cell lines fail to replicate mitochondrial function as seen in respective human samples. And finally, the easy method described here, where time dependent small molecule metabolism and ADP-activated respiration in solid human cancers are analyzed together, can increase success of translational research and ultimately benefit patients with cancer.

Keywords: mitochondrial flux, ADP-activated respiration, OXPHOS, citrate, glutaminolysis, metabolic dependencies, cancer metabolism, predictive biomarker

INTRODUCTION

Research in cancer metabolism is expanding despite seminal discoveries were made almost a century ago, when the Warburg effect was first described by three metabolic properties—elevated glucose uptake with increased lactate secretion despite the presence of oxygen (1). Decades of research has been conducted, but the nature of this metabolic phenotype is still poorly understood (2), however, it has become common knowledge, in contrast to Warburg's initial hypotheses, that mitochondria in cancer cells remain functional (3–5).

In malignancies, mitochondria have become metabolic hubs, that feed numerous cytosolic processes warranting cell growth and disease progression (6, 7) with two major extracellular sources for mitochondrial function being glucose and glutamine (6, 8). Despite cancers are able to direct glucose in the form of pyruvate into mitochondria and conduct oxidative phosphorylation (OXPHOS), part of the canonical tricarboxylic acid cycle (TCA) required for OXPHOS is truncated and citrate is directed out of the mitochondria (9). Mitochondrial citrate efflux can be further increased by reductive carboxylation of glutamate, which reverses the traditionally known direction of TCA (10) and emphasizes importance of metabolic flexibility in cancers. Citrate is cleaved in the cytosol by ATP citrate lyase, and the products are used for *de novo* lipid synthesis (9) or feed into downstream pathways necessary for synthesis of cholesterol, isoprenoids or protein acetylation (11). Among others, ATP citrate lyase and glutamine utilization have been considered as potential antineoplastic targets and even though these processes are active in most cancers, biomarkers for selecting suitable patients for respective treatments have remained unknown.

Isotope tracing has been widely used to trace nutrient faith in metabolic pathways and this method has led to numerous discoveries (10, 12). Isotope tracing is mainly used on cultured cells, but similar analysis has been optimized also for human cancer patients. In humans, this requires intravenous preoperative administration of labeled metabolite, rapid freezing of the target samples after resection and other non-standard interventions during surgery (4), which in turn can complicate wider use of this method. Despite the rapid nature of the metabolic experiments on human cancers, solute transporters and enzymes can have residual activity even at very low temperatures and can severely affect the results (13). Shortcomings in metabolomic studies have been noted by numerous groups and many of them have developed new methods to differentiate mitochondrial and cytosolic metabolite pools or metabolite fluxes within cells to answer critical questions in understanding cancer metabolism (14–17). Reliable, efficient and widely accepted methods for studying metabolism in solid tumors, however, are still missing.

Mitochondrial function is central in understanding metabolic activity of cancers cells, but interestingly OXPHOS, as a central aspect of mitochondrial functionality, has received only very limited attention by researchers. Functional studies on respiration using selective permeabilization of cells' outer membrane have long been conducted in cardiac and skeletal muscle samples (18, 19), but in solid human tumors, the research on OXPHOS is scarce and used by very limited number of groups (5, 20, 21). Selective permeabilization removes cholesterol from the outer membrane of cells and equalizes the cytosolic compartment with the reaction medium while mitochondria in the samples remain fully functional, maintain functional connections to cytoskeletal structures and can be directly manipulated with exogenous substances to expand knowledge on mitochondrial metabolism (19, 20, 22). However, OXPHOS studies on solid human cancer samples are preferably conducted by laboratories having experience in applying permeabilization method on healthy tissues (like muscles), but that in turn limits availability of this technique outside specialized centers.

In the present work, we study respiration in breast cancer cell lines and human breast cancer samples and simultaneously present and use newly developed metabolomic method. By combining these two approaches, we describe breast cancer mitochondrial function in time dependent manner and bring out dependencies not evident by using either approach alone. Importantly, human breast cancer samples are used in addition to cell lines as translational research needs better ways to understand subcellular metabolomic processes in order to help patients with this devastating disease.

Abbreviations: BTC, 1,2,3-benzene tricarboxylic acid; OXPHOS, oxidative phosphorylation; TNBC, triple negative breast cancer; MCE, mitochondrial citrate efflux; TCA, tricarboxylic acid cycle.

MATERIALS AND METHODS

Chemicals

All chemicals were purchased from Sigma-Aldrich Chemical Com. (USA) and were of the highest purity available (>98%).

Clinical Samples and Medical Data

The tissue samples were provided by the Oncology and Hematology Clinic at the North Estonian Medical Centre (Tallinn). All the samples were analyzed within 6 h after surgery. Only primary tumors were examined and information from respective pathology reports was provided by the North Estonian Medical Centre for all the analyzed samples. Informed consent was obtained from all the patients and coded identity protection was applied. All investigations were approved by the Tallinn Medical Research Ethics Committee and were in accordance with Helsinki Declaration and Convention of the Council of Europe on Human Rights and Biomedicine. The entire group consisted of 59 patients with breast cancer (57 females, 2 males).

Cell Cultures

MDA-MB-231 and MCF-7 cells were grown as adherent monolayers in low glucose (1.0 g/L) or high glucose (5 g/L) Dulbecco's Modified Eagle's Medium (DMEM) with stable L-glutamine (2 mM) and sodium pyruvate (from CAPRICORN scientific) supplemented with 10% heat-inactivated fetal bovine serum, 10 μg/mL human recombinant Zn-insulin, and antibiotics: penicillin (100 U/ml), streptomycin (100 μg/ml) and gentamicin at a final concentration of 50 μg/ml. Cells were

grown at 37°C in humidified incubator containing 5% CO_2 in air and were sub-cultured at 90% confluence.

Mitochondrial Respiration in Saponin-Permeabilized Tissue and Cell Culture Samples

Analysis was conducted as described previously (5). In brief—respiratory activity of tumor and control tissues *in situ* was captured using skinned sample technique (18, 20, 23, 24). This method allows analysis of the function of mitochondria in their natural environment and leaves links between cytoskeletal structures and mitochondrial outer membrane intact (22, 25–27). For cell lines, direct permeabilization in the oxygraphic chambers was used (21). Cytochrome c test was used to confirm integrity of the mitochondrial outer membrane (20, 23, 24, 28); mitochondrial inner membrane quality was checked using carboxyatractyloside test as the last procedure in every experiment (20, 23, 24, 28, 29). Rates of O_2 consumption were assayed at 25°C using Oxygraph-2k high-resolution respirometer (Oroboros Instruments, Innsbruck, Austria) loaded with pre-equilibrated respiration buffer—medium-B (20). All rates of respiration (V) are expressed in nmol O_2/min per mg wet tissue weight for solid tumors and in nmol O_2/min per million cells for cell cultures.

Mitochondrial Metabolite Efflux in Saponin-Permeabilized Samples

Experiment setup was equal to that described in paragraph 2.4. Oxygraph-2k respirometer chamber was loaded with pre-equilibrated respiration buffer and a single type of selectively permeabilized sample was divided into two oxygraphy chambers. Intended substrates (pyruvate or glutamate; both additionally supplemented with 2 mM malate) were injected and state 2 respiration was captured (30). In one of the parallel chambers, the sample was incubated without exogenous inhibitors, but in the other chamber mitochondrial citrate efflux was inhibited by addition of 1,2,3-benzene tricarboxylic acid (BTC) that selectively halts the function of mitochondrial citrate transporter (31). This parallel setup allows to differentiate citrate generated by mitochondria and citrate possibly generated by leftover cytosolic processes. Reaction was initiated by addition of 2 mM ADP.

Samples collected at different time points were immediately frozen in liquid nitrogen or cooled on ice-bath. Analysis of the samples was done using UV-VIS spectroscopy as described elsewhere (32) or GC-MS. Citrate content in BTC-supplemented parallel was termed to be extramitochondrial.

In the cytosol, ATP-citrate lyase can turn citrate into oxaloacetate and acetyl-CoA (11), and hence affect outcome of the analysis. To eliminate this reaction and allow uninterrupted accumulation of citrate produced by mitochondria, an inhibitor for ATP-citrate lyase was used in all experiments (BMS-303141). Suitability of the described method was further confirmed by running the analysis on cell lines without permeabilization, without addition of ADP or addition of ADP at 1 or 2 mM levels and concentration of BTC was titrated to best suit human breast cancer samples (data not shown).

Analysis of Metabolites

For GC-MS analysis on cell lines, the cells were allowed to grow to 90% confluence on d35 dishes. For collection, the dishes were placed on ice and growth medium aspirated. One milliliter of extraction solvent (80% methanol in water; stored at −80°C at least 1 h before use) was added and the dish was stored at −80°C for 15 min. The cell layer was thereafter scraped from the dish and the mixture was centrifuged at 20,000 g/4°C for 15 min. Supernatant was divided into two and the pellet was analyzed for protein content. In preparation of derivatization process, the supernatant was freeze-tried. For derivatization, 20 mL 20 mg/ml O-methoxylamine in pyridine solution was added and the mixture incubated in heater at 30°C for 90 min. Thereafter 80 mL of MSTFA/1%TMCS was added and the mixture was incubated in heater at 37°C for 30 min. Derivatized sample was centrifuged at 15,000 g for 15 min and supernatant transferred to 200 mL vial inserts placed in 2 mL vials for analysis on GC-MS.

The GC-MS analysis was performed on an Agilent GCMS MSD. Five microliters of each sample was injected with split less injection mode, with 120 s purge time at 9.4 psi and 3.1 ml/min helium purge flow, helium column carrier gas flow was maintained at 1 ml/min and flow rate of 20 ml/min for 3 min to purge the injector. Ion source temperature and quadrupole temperature were maintained at 230 and 150°C.

Chromatographic separation was performed using HP-5% phenylmethyl siloxane −30*250*0.25 μm. The front inlet temperature was maintained at 250°C and helium was used as carrier gas. Column temperature was maintained at 60°C for 1 min and then held for 1 more min, then increased to 325°C with 10° per minute and held for 10 min followed by post-runtime of 5 min at 60°C with a total runtime of 42.5 min. Solvent delay was set at 5.9 after making sure that pyridine, MSTFA peaks are non-detectable and pyruvate and lactate peaks are detectable.

Western Blot Analysis of the Level of Citrate Synthase Expression

Post-operative tissue samples (70–100 mg) were crushed in liquid nitrogen and homogenized in 20 volumes of RIPA lysis buffer [50 mM Tris-HCl pH 8.0, 150 mM NaCl, 2 mM EDTA, 0.5% sodium deoxycholate, 0.1% SDS, 0.1% Triton X-100, and complete protease inhibitor cocktail (Roche)] by Retsch Mixer Mill at 25 Hz for 2 min. After homogenization, samples were incubated for 30 min on ice and centrifuged at 12,000 rpm for 20 min at 4°C. The proteins in the supernatants were precipitated using acetone/TCA to remove non-protein contaminants. Briefly, supernatants were mixed with 8 volumes of ice-cold acetone and 1 volume of 100% TCA, kept at −20°C for 1 h and then pelleted at 11,500 rpm for 15 min at 4°C. The pellets were washed twice with acetone and resuspended in 1× Laemmli sample buffer. Proteins were separated by polyacrylamide gel electrophoresis, transferred to a polyvinylidene difluoride (PVDF) membrane and subjected to immunoblotting with anti-citrate synthase antibody (Abcam, ab96600). Then, the membranes were incubated with corresponding horseradish peroxidase-conjugated secondary antibody and visualized using an enhanced chemiluminescence system (ECL; Pierce,

Thermo Scientific). After chemoluminescence reaction, the PVDF membranes were stained with Coomassie brilliant blue R250 to measure the total protein amount. The signal intensities were calculated by ImageJ software and normalized to total protein intensities.

Citrate Synthase Activity

Citrate synthase activity was measured in whole-cell extracts at 412 nm using 5,5′-dithio-bis(2-nitrobenzoic acid) as described elsewhere (33).

Confocal Microscopy Imaging

Cells were seeded on glass coverslips in 12-well plates (Greiner bio-one) and allowed to adhere overnight, then passaged onto Matrigel coated glass coverslips and cultured in 12-well plates for 3 days. Then, the growth medium was removed, and cell samples treated *via* selective marking of mitochondrial outer membrane translocase Tom20 (Santa Cruz Biotechnology, sc17764). The Tom20 fluorescence intensity was normalized against whole β-tubulin (Abcam®, ab6046) fluorescence. After incubation, cells were washed with PBS and incubated with corresponding fluorescence-conjugated secondary antibodies. Finally, cells were incubated for 15 min with 4′,6-diamidino-2-phenylindole dihydrochloride (DAPI, Molecular Probes™) to visualize the cell nucleus. Cells were imaged by an Olympus FluoView FV10i-W inverted laser scanning confocal microscope.

Data Analysis

Data in the text, tables, and figures are presented as mean ± standard error (SEM). Results were analyzed using analysis of variance (ANOVA) and Student's *t*-test, *p*-values <0.05 were considered statistically significant.

RESULTS

Mitochondrial amount in MCF-7 and MDA-MB-231 was examined by confocal microscopy and calculated using ImageJ software. Analysis revealed that mitochondrial amount in MCF-7 cells is about three times higher than that in the MDA-MB-231 cells and the difference was significant (**Figure 1**). Mitochondrial content was additionally analyzed using citrate synthase activity and even though difference in the results was not found to be significant, results were similar to that found via confocal microscopy (**Figure 2**). Citrate synthase was also studied on expression level using Western blot analysis and the results were confirming that there is more citrate synthase in MCF-7 cells (**Figure 2**). These findings were in good agreement with our previous research results where we showed using permeabilization that ADP-initiated respiration rate in MCF-7 cells is about 2.5–3 times higher than that in MDA-MB-231 cells (5). As we were interested in understanding links between mitochondrial respiration and mitochondrial metabolism, we thereafter investigated the levels of citric acid cycle metabolites in the two cell lines. GC-MS analysis revealed that relative citrate content in MCF7 and MDA-MB-231 is similar (content of citrate is about 2 times higher in MCF7 cells), but in opposite to other results described above, levels of all other studied metabolites were found to be significantly higher in the MDA-MB-231 cells (**Figure 3**).

The results for mitochondrial amount, ADP-activated respiration, whole cell citrate content, citrate synthase activity and abundance of the same enzyme showed similar results. However, very low level of citrate in MDA-MB-231 cells, in relation to other TCA metabolites in the same lysates, could not be easily explained. Based on these findings we decided

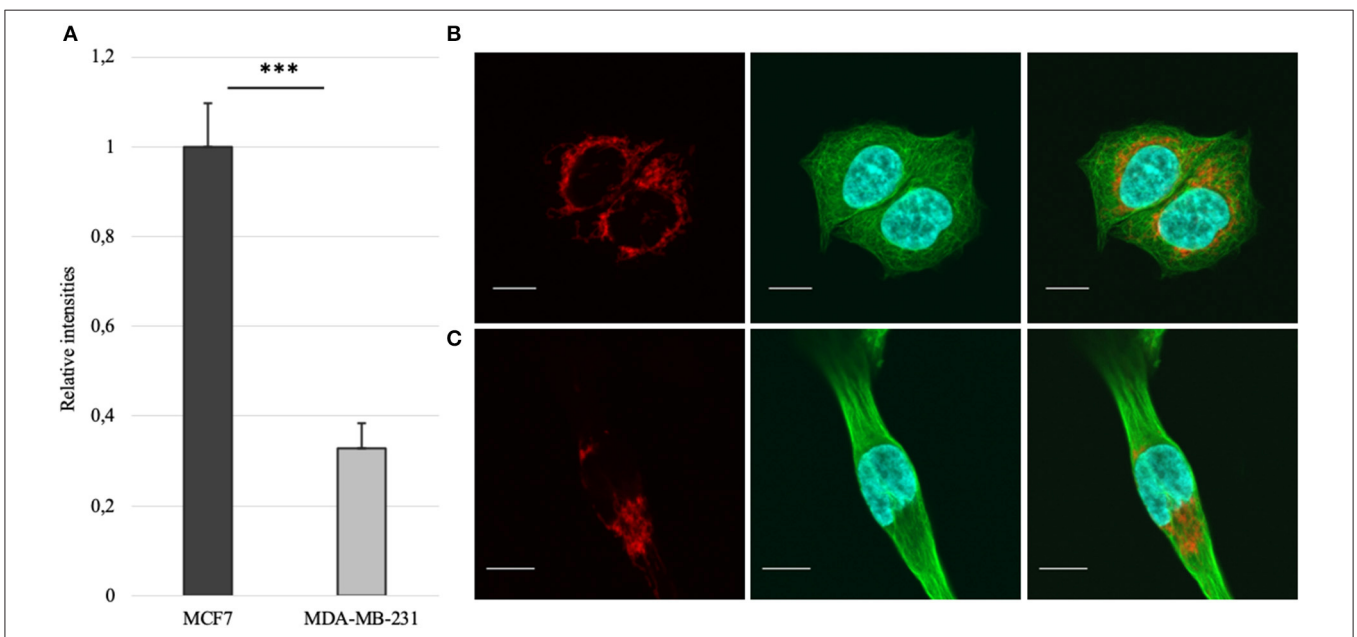

FIGURE 1 | (A) Mitochondrial amount in MCF-7 vs. MDA-MB-231 cells as assessed from confocal imaging [staining of mitochondria (red), whole β-tubulin (green) and nucleus (blue) on figures **(B)** for MCF-7 and **(C)** for MDA-MB-231; white bar 10 μm]. ***$p < 0.001$.

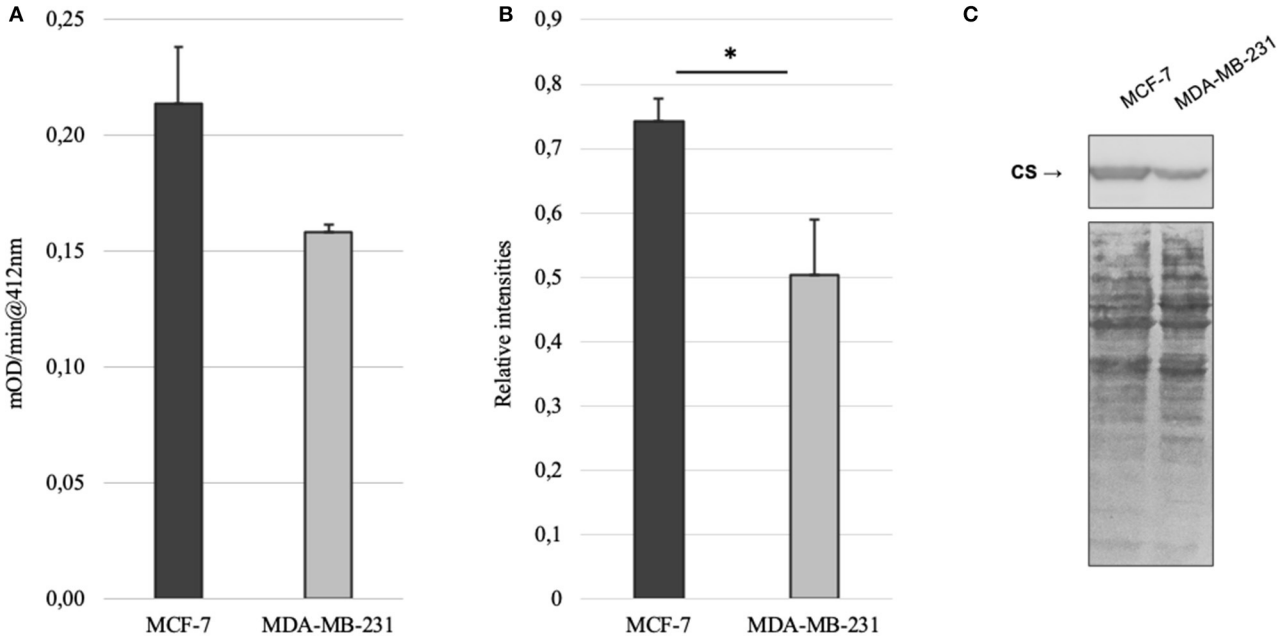

FIGURE 2 | (A) Citrate synthase (CS) activity in MCF-7 and MDA-MB-231 cell lines; **(B)** relative expression of citrate synthase based on western blot imaging in MCF-7 and MDA-MB-231 cell lines; **(C)** western blot images for citrate synthase and whole protein in MCF-7 and MDA-MB-231 cell lines. *$p < 0.05$.

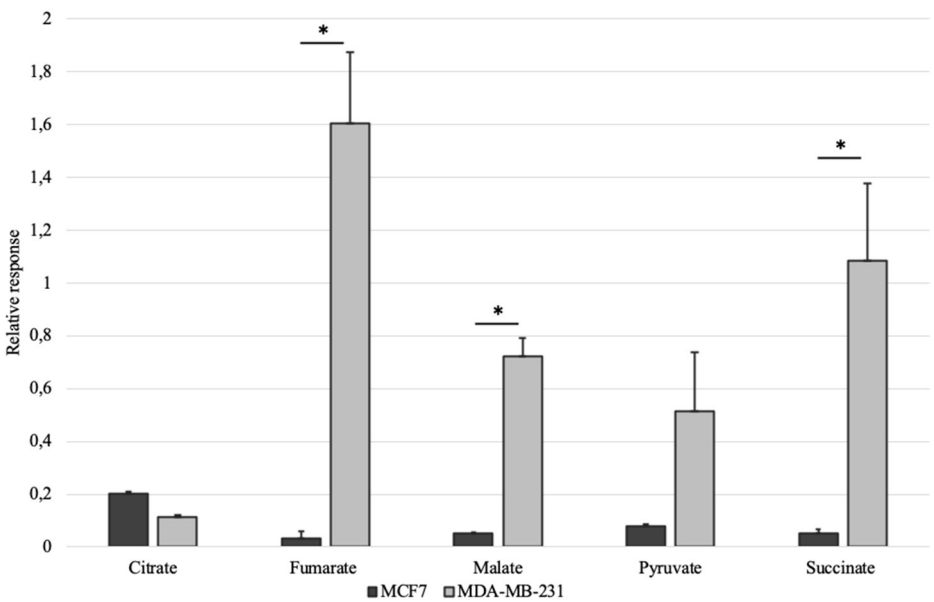

FIGURE 3 | Selected citric acid cycle metabolites in whole-cell lysates of MCF-7 vs. MDA-MB-231 cells normalized to internal standard and protein content. *$p < 0.05$.

to concentrate on citrate in the following study due to its numerous roles in maintaining cancer cell homeostasis and in connecting mitochondrial and cytosolic processes (11, 34, 35). We concluded that steady-state metabolite analysis as used above, is not sufficient in understanding the role of citrate and we need to measure TCA metabolic activity on functional level to see the process in time dependent manner. In order to achieve that, we designed a simple experiment to measure mitochondrial citrate efflux (MCE) in selectively permeabilized samples. Respirometry and metabolic methods were also incorporated into the new method as described in the Methods section.

Permeabilization and use of Oroboros respirometer allows to manipulate availability of mitochondrial substrates that the sample can use. Using that option, we tested each sample

separately with either pyruvate or glutamate as the main nutrient and both parallels were accompanied by additional sample supplemented with BTC (**Figure 4**). These two substrates were selected as mitochondrial citrate can mainly be synthesized through canonical TCA from pyruvate or through reductive carboxylation from glutamine derived glutamate (10) as depicted on **Figure 5**.

MCE was measured in MCF-7 and MDA-MB-231 cell lines as described above. Citrate accumulation into the reaction medium was stopped at 60 min post-addition of 2 mM ADP. Net MCE was calculated by subtracting result registered in the BTC supplemented parallel from that without added BTC (**Figure 6A**). Tests revealed that mitochondria in both of the cell lines generate similar amount of citrate if pyruvate is used as the main carbon source. However, significant differences appear if glutamate is used. Specifically, mitochondria of MDA-MB-231 cells efflux citrate in the presence of glutamate at 3 times higher rate than MCF7 cells. In addition, if MCE rates from both pyruvate and glutamate are summarized, then MDA-MB-231 cells, in comparison to MCF-7 cells, are able to direct 20% more external carbon into cytosolic processes through citrate. We thereafter decided to measure MCE for clinical samples to confirm if differences are present between the used model systems and real samples. Experiment was set up equally to that used for cell lines.

Altogether 59 human breast cancer samples were analyzed for both MCE and ADP-activated respiration in the presence of either pyruvate or glutamate as mitochondrial substrate. Quantity of tissue samples from five patients were not sufficient to apply the full testing algorithm (**Figure 4**). Every performed

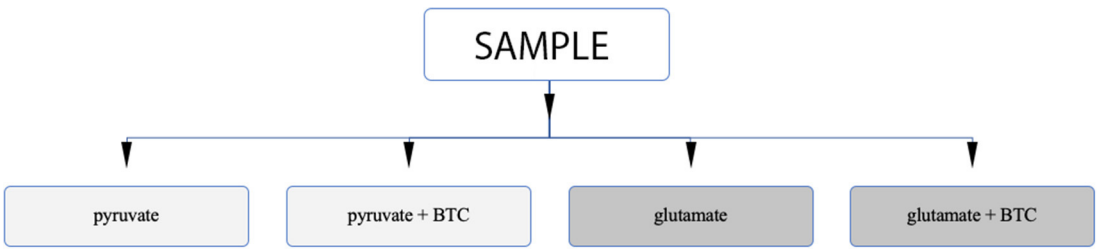

FIGURE 4 | Analysis algorithm to differentiate if citrate produced by mitochondria in permeabilized samples is originating from pyruvate or glutamate as the main carbon source. One type of sample is analyzed under four different settings.

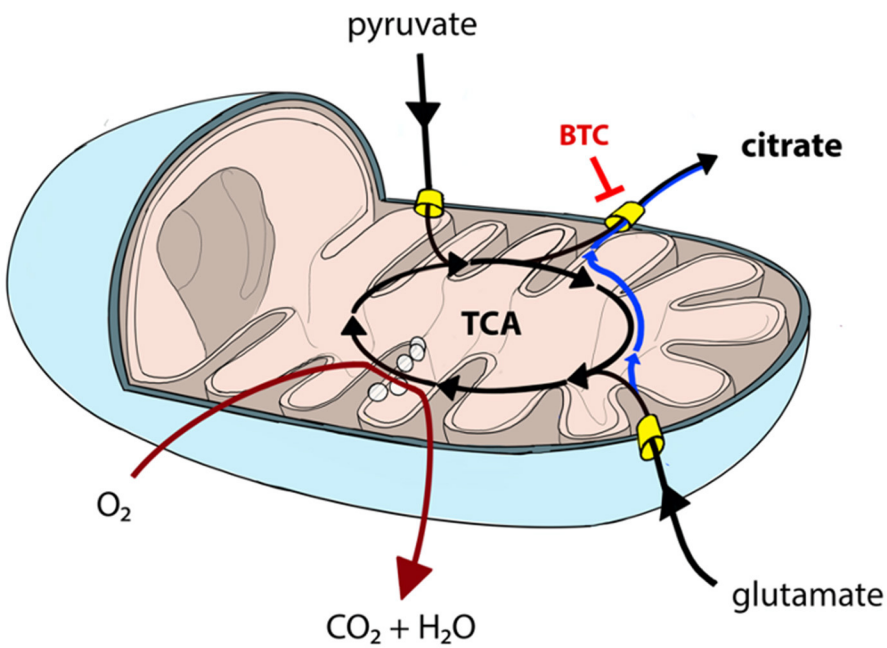

FIGURE 5 | Canonical TCA in mitochondria can be truncated resulting in pyruvate-derived carbon being transported back to cytosol as citrate (black lines). Similarly, glutamate can be converted into mitochondrial citrate efflux via reductive carboxylation (blue line) or used in canonical TCA (black lines). Mitochondrial citrate efflux from both sources can be inhibited by BTC. TCA and OXPHOS (dark red line) processes are partially overlapping and, hence, need to be analyzed together to comprehensively describe mitochondrial function.

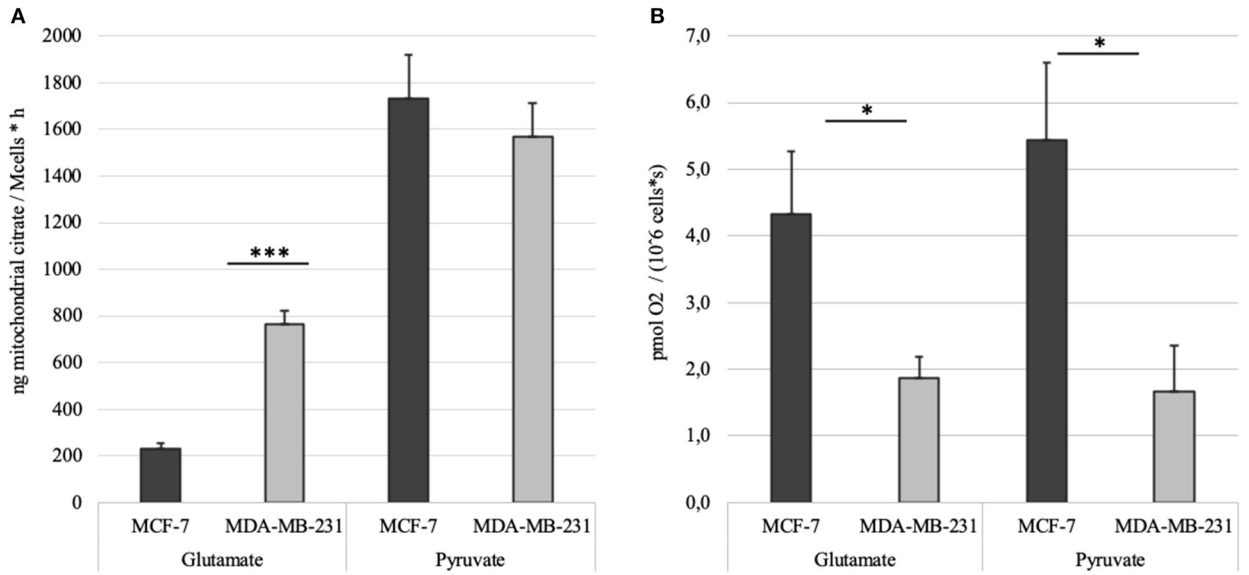

FIGURE 6 | (A) Time dependent mitochondrial citrate efflux (MCE) in MCF-7 and MDA-MB-231 cell lines with either pyruvate or glutamate as the main nutrient. Results are corrected with citrate accumulation rates registered for parallel BTC tests. **(B)** ADP-activated respiration rates in MCF-7 and MDA-MB-231 cells measured during MCE experiments. $^{*}p < 0.05$; $^{***}p < 0.001$.

TABLE 1 | Mitochondrial citrate efflux in five major human breast cancer subtypes grouped on pyruvate or glutamate as exogenous substrate. MCE values in ng citrate/mg wet tumor weight*h.

	Pyruvate	No of patients	Glutamate	No of patients
Luminal A	85.1 (±10.9)	19	46.5 (±5.8)	21
Luminal B	98.3 (±10.9)	17	48.1 (±9.8)	18
HER2	130.0 (±46.7)	4	69.7 (±12.1)	6
Triple negative	138.9 (±18.6)	8	80.0 (±15.1)	8
Luminal B/HER2+	146.6 (±62.2)	3	93.8 (±32.6)	3

experiment, however, always had BTC-supplemented parallel done to differentiate mitochondrial citrate efflux from residual cytosolic activity. The MCE rates for all samples were grouped based on breast cancer molecular subtypes (**Table 1**) and results for the least aggressive (Luminal A) and most aggressive (triple negative—TNBC) were plotted (**Figure 7**), respectively to present significant differences found for those two clinically opposing subtypes. Finally, for all human samples, MCE values from pyruvate were plotted against MCE values from glutamate to assess which systemic substrate mitochondria in these samples prefer (**Figure 8**). Similarly, ADP-activated state 3 respiration based on either pyruvate or glutamate were plotted to visualize respiratory substrate preferences in Luminal A and TNBC subgroups (**Figure 9**). healthy breast tissue collected from the same patients during the surgery, but notably, this tissue has very low activity for both of these properties and hence these numbers are not significant to this study and have not been included in the data.

DISCUSSION

Steady-State Markers and Citrate Levels in MCF-7 and MDA-MB-231 Cell Lines

We have shown previously, using permeabilization technique on human breast cancer samples, that ADP-activated respiration in TNBC tumors is significantly higher than that in Luminal A breast cancers. Surprisingly, the same study confirmed that in MDA-MB-231 (TNBC subtype) and MCF7 (Luminal A subtype) cell lines, exact opposite respiration ratio was evident (5). In continuation of this work, we wanted next to understand links between mitochondrial respiration and mitochondrial metabolism.

Mitochondrial content in the named cell lines was found to be well in line with the respiration data from our previous study (5). That is, both mitochondrial content and ADP-activated respiration (**Figure 6B**) in MCF-7 cells are 2.5–3 times higher than that in MDA-MB-231 cells. MDA-MB-231 cell line, however, is representing clinically most aggressive TNBC subtype and therefore we reasoned that the aggressive phenotype has to be expressed on metabolic level in the mitochondria as described before (6). We first looked at steady-state metabolite level in whole cell extracts using GC-MS. The results revealed that despite citrate levels in both cell lines are in line with mitochondrial content and citrate synthase activity, significant differences are present for other TCA metabolites in MDA-MB-231 cells (**Figure 3**). Surprisingly, the differences were showing that the metabolite levels in MDA-MB-231, besides that for citrate, were higher than in MCF-7 cells. In support of the low citrate levels in MDA-MB-231 cells, citrate synthase expression and citrate synthase activity were both measured to be lower in MDA-MB-231 cells

(**Figure 2**). In additional support for citrate level in MDA-MB-231 cell line, it has been previously shown that more aggressive tumors present with lower steady state levels of citrate (36, 37) and our findings confirm that understanding. We thereafter asked, that how can low citrate level justify central role of this metabolite in numerous cellular function that result in cancer cell homeostasis? For example, mitochondrial citrate, made available to cytosol via truncated TCA or reductive carboxylation from glutamate, feeds many cytosolic processes necessary for cell maintenance, survival and progression (11, 34, 35). Even more, high expression of citrate-malate antiporter that conducts MCE, has been associated with poor outcomes in both lung cancer and estrogen receptor negative breast cancers (38) and some authors have suggested this transporter as potential therapeutic target in cancers (39). Therefore, low steady-state citrate level in the more aggressive MDA-MB-231 cell line, despite expected by the literature, did not follow the importance of citrate in cancers. Possibly, the low citrate level is descriptive of high turnover of this metabolite pool, but steady-state methods are not sufficient in revealing this process.

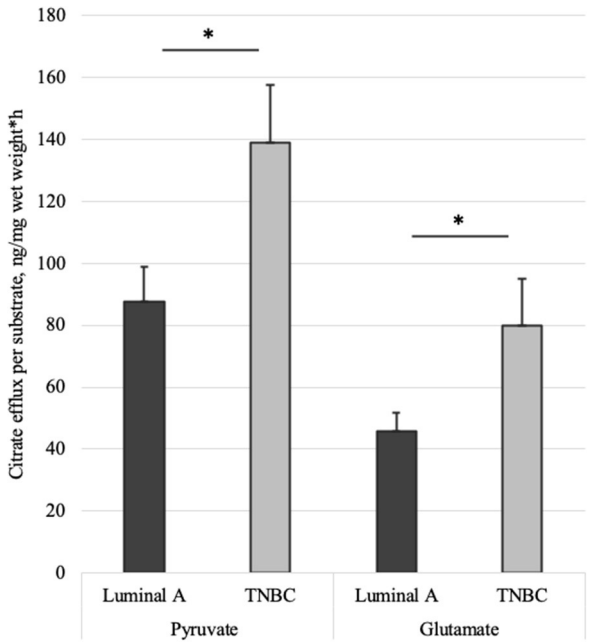

FIGURE 7 | Mitochondrial citrate efflux (MCE) measured for pyruvate or glutamate as the metabolic substrate in Luminal A and TNBC human breast cancer samples. MCE measured as ng citrate/mg wet tumor weight*h; Luminal A 11 patients, TNBC 7 patients. *$p < 0.05$.

MCE and Glutamine Dependence in MCF-7 and MDA-MB-231 Cell Lines

In attempt to understand MCE activity on mitochondrial outer membrane, we developed a simple method as described in the Results section. Studies on MCE dynamics have been done previously, but only on (cancer) cell lines or on isolated mitochondria from soft physiological tissues like the liver (31). In the framework of this study, we tried to isolate mitochondria from human breast cancer samples, but it proved not possible due to rubbery texture of cancers. Similarly, we did not succeed in isolating mitochondria from physiological breast tissue (data not shown). Other methods have been

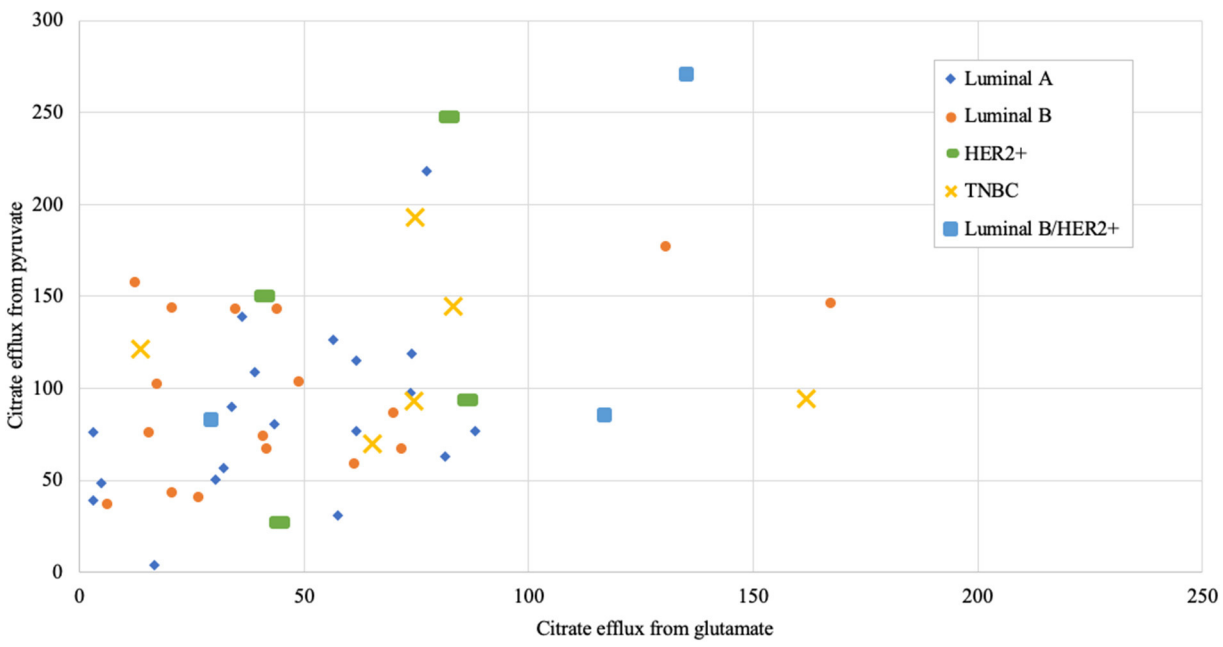

FIGURE 8 | Mitochondrial citrate efflux (MCE) values from pyruvate vs. from glutamate as main metabolic substrate measured in human breast cancer samples (MCE measured as ng citrate/mg wet tumor weight*h; Luminal A 19, Luminal B 17, HER2+ 4, TNBC 6, Luminal b/HER2+ 3 patients).

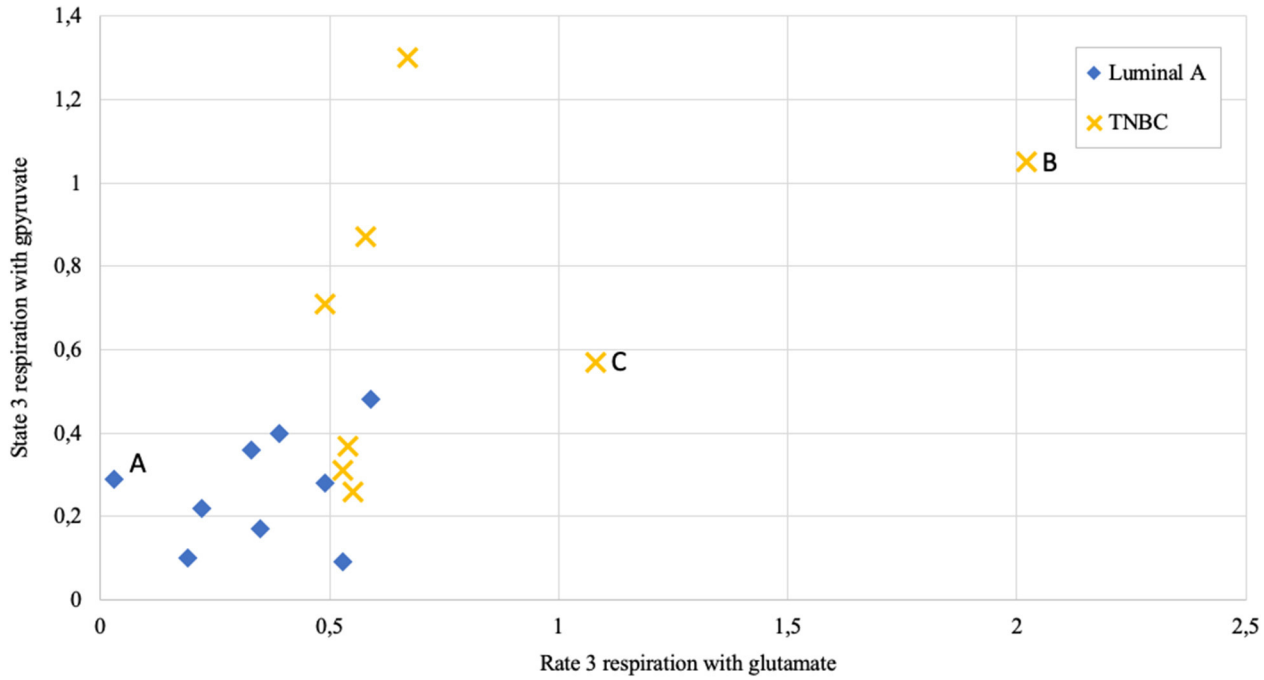

FIGURE 9 | State 3 respiration rate dependence on metabolic substrate (pyruvate vs. glutamate) in human breast cancer samples; measured as nmol O_2/min per mg wet; Luminal A 9 patients, triple negative breast cancer (TNBC) 8 patients. Letters A, B, and C as discussed in the text.

suggested possibly solving this target. For example (40) used selective permeabilization and isotope tracing on cell monolayer, which, unfortunately, is not applicable on solid tumors. Rapid fractionation combined with isotope tracing, computational deconvolution and network modeling have been applied, but its again only suitable on cell lines (14). Additionally, respiration has been studied using homogenization of muscle tissue (17), but this destroys mitochondrial structure, removes regulatory effect of the cytoskeleton (22) and does not allow measurement of flux across mitochondrial membrane. Similarly, using labeled isotopes on human patients (4) is difficult and reaching reasonable patient selection across all breast cancer molecular subtypes, is expensive, time consuming and, most importantly, it is not possible to differentiate mitochondrial or cytosolic citrate pools nor the activity between these two compartments.

We ran our newly developed method initially on MDA-MB-231 and MCF7 cell lines. To our surprise, despite ADP-activated respiration in MCF-7 cells is three times higher (**Figure 6B**), and MDA-MB-231 are expectedly more glycolytic cells, both cell lines conduct MCE in equal amounts if pyruvate is the main substrate. But strikingly, if pyruvate is switched to glutamate, then MCF-7 cells fail to use it in similar amounts for MCE as MDA-MB-231 cells do (**Figure 6A**). The results reveal that MDA-MB-231 cells are 3 times more efficient in incorporating glutamate into cellular processes. In our experiments glutamate was added directly to the permeabilized samples, but in cellular context glutamate is mainly derived from glutamine through activity of glutaminase (41). These results are supported by previous reports that MDA-MB-231 cells will not survive glutamine withdrawal while MCF7 cells are glutamine independent (42).

Our data shows that MCF7 cells require more pyruvate for mitochondrial processes than the MDA-MB-231 cells, as they use it for both high respiration and high mitochondrial citrate efflux (**Figures 6A,B**). Dual use of pyruvate in the MCF7 cells equally for both respiration (generation of ATP) and MCE, might causally explain the capacity of MCF7 cells to overcome glutamine withdrawal. However, if glutamine is removed from the MDA-MB-231 cells or glutaminase is inhibited, then MDA-MB-231 cells do not have sufficient capacity to maintain requirements for ATP only through glycolysis (as OXHOS as additional source is nearly missing) and maintain necessary level of MCE (as ∼32% of the MCE was derived from glutamate). Similarly, in SF188 glioblastoma cells 25% of fatty acyl carbons were derived from glutamine via MCE and the same for glucose was 60%, but complicated isotope based methods were applied to reach that conclusion (8).

Quantification of MCE in breast cancer cell lines confirmed that mitochondria are metabolic hubs for malignant cells and low/high respiration capacity does not lead to equally low/high metabolic activity. Importantly, mitochondrial amount or citrate synthase activity or citrate synthase expression do not predict metabolic activity in the given cell line. In conclusion, it can be predicted that TCA cycle and OXPHOS system are not directly coupled in all cell lines, however, both are necessary for cell survival and need to

be simultaneously measured in order to sufficiently describe mitochondrial function.

ADP-Activated Respiration and MCE in Human Breast Cancer Samples

Respiration in correctly permeabilized solid tumors can easily be jumpstarted with exogenous ADP if either pyruvate or glutamate are introduced to the test environment as substrates. From **Figure 9** it can be easily appreciated that not all breast cancers display similar respiration patterns even within the same molecular subgroup. Among Luminal A diseases, some cancers tend to respire predominantly on pyruvate and only minimally on glutamate (e.g., lower left Luminal A patient marked as "A," **Figure 9**), while some TNBC tumors conduct OXPHOS on both pyruvate or glutamate at very high level (TNBC patient marked with "B") or rely mainly on glutamate for respiration (TNBC patient marked "C"). While Luminal A tumors seem to form a cluster on **Figure 9**, TNBC cancers display wide distribution in results which is in line with high heterogeneity in this subgroup (43).

As we showed above for cell lines, then also in solid human tumors respiration alone is presumably not sufficient for describing mitochondrial activity. Based on this knowledge, MCE rates were measured for all breast cancer samples. In **Table 1**, MCE rates are grouped based on breast cancer molecular subtypes (44) and metabolic substrate. On average, breast cancers tend to use less glutamate for MCE than pyruvate (similarly to cell lines), however, conversion rates from both metabolic substrates rise along expected aggressiveness of the tumors. Luminal A cancers are considered to have the most favorable outcome and TNBC cancers tend to be the most difficult to treat, and as our results clearly show, differences in MCE between these two opposing subtypes are significant for both pyruvate and glutamate as substrates (**Figure 7**). Therefore, despite high heterogeneity between human breast cancers, in metabolic terms, the differences for these two subtypes are clearly present and fall in line with expected aggressiveness of either subtype. For three patients diagnosed as being both luminal B and HER2+ the MCE rates were the highest. Even though this scarcely studied subtype is considered clinically aggressive (45), the number of patients in this subgroup was too low for making conclusions. For wider view across all cancer subtypes in this study, MCE values from pyruvate vs. glutamate were plotted and the wide distribution of metabolic preferences become clearly evident (**Figure 8**).

Together with our previous finding on respiration in clinical samples (5), it can be concluded that in contrary to cell lines, human breast tumors sustain ability to conduct OXPHOS and simultaneously direct citrate from TCA to feed anabolic processes in the cytosol. Both of these processes are synchronously increasing together with rising aggressiveness of the tumors. Importantly, results found above for two widely used cell lines (MCF7 and MDA-MB-231) proved to be the opposite in clinical samples. This finding can contribute to explanation why preclinical research often fails to translate to clinical phase as preclinical models do not sufficiently represent the human disease biology, especially in metabolic terms.

Predictive Value of MCE and ADP-Activated Respiration in Clinical Samples

Given that inhibitors of glutaminolysis have reached clinical trials in TNBCs (46) and our results showed significant differences in glutamate use in cell lines, we asked if the combined data for MCE and state 3 respiration might be predictive for estimating treatment susceptibility in our clinical samples. **Table 2** presents data for 6 TNBC patients included to this study. It is apparent that TNBC #4 is using both pyruvate and glutamate equally low for MCE, while the tumor has high preference for glutamate in conducting OXPHOS. Therefore, it can be predicted that the given tumor might more likely respond to glutaminase inhibition as it does not have higher capacity to use pyruvate for MCE or OXPHOS to compensate lost availability of glutamine derived glutamate. The same can be predicted for TNBC #3. However, TNBC #1 and TNBC #2 present with phenotype that can easily compensate loss of glutamate via high usage of pyruvate for both MCE and respiration. The data in **Table 2** brings out ambiguity in some patients as evident with TNBC #5. TNBC#5 has high dependence on glutamate for conducting OXPHOS, however, the same tumor has only minimal use of glutamate for MCE. It can be predicted that loss of glutamine derived glutamate in the given tumor can easily be compensated by high use of pyruvate for MCE, but the tumors' ability to sustain OXPHOS and cell survival on pyruvate at sufficient level, is unknown. Similarly, TNBC #6 has by far the highest dependence on glutamate for MCE and also highest respiration rate on glutamate, however the role of high use of pyruvate for respiration in overcoming possible glutamate restriction, remains unknown. Although the present study can suggest possible causality for glutaminase inhibition success or failure in certain breast cancers, without further preclinical research or clinical trials, these suggestions remain hypothetical. However, the way we propose to analyse TNBC susceptibility for glutaminase inhibition is strongly supported by a very recent finding. The authors of the study describe a new compound for blocking glutamine availability in malignancies and conclude that glycolysis, OXPHOS and glutaminolysis in cancers are highly interdependent and lack noticeable plasticity (47). Therefore, if capacity for each three properties are separately known, then

TABLE 2 | Mitochondrial citrate efflux and state 3 respiration in human TNBC samples grouped on pyruvate or glutamate as exogenous substrates.

	Mitochondrial citrate efflux		State 3 respiration	
	Pyruvate	Glutamate	Pyruvate	Glutamate
TNBC #1	193.2	74.7	0.71	0.49
TNBC #2	144.6	83.3	1.30	0.67
TNBC #3	92.9	74.5	0.26	0.55
TNBC #4	69.6	65.1	0.57	1.08
TNBC #5	121.3	13.6	0.37	0.54
TNBC #6	94.5	161.7	1.05	2.02

*MCE measured as ng citrate/mg wet tumor weight*h; state 3 respiration measured as nmol O_2/min per mg wet tumor weight.*

predicting treatment susceptibility becomes possible. Here we have done those measurements on human breast cancers where MCE in cytosol-free samples acts as a quantified marker for capacity of using glucose or glutamine while OXPHOS on the same substrates is also measured. As mentioned above, further studies are needed to confirm this hypothesis.

Additionally, as OXPHOS and MCE must be separately analyzed for both pyruvate and glutamate, then it can be concluded that segregating patients for anti-glutaminase treatment using only glutamine-based positron emission tomography (48) is not sufficient. This approach describes affinity for only one major substrate, while misses to describe cancers ability to compensate glutamine withdrawal with pyruvate-based MCE and/or OXPHOS (as shown above for TNBC #3, #4, #5, #6; **Table 2**).

Limitations

This study includes a number of limitations. Firstly, it has not been detected if MCE from glutamate is coming through canonical TCA or reductively, nor were other mitochondrial metabolite effluxes included in the results besides citrate. Therefore, future studies with isotope tracing (including on solid tumors using the technique described here) are warranted. BTC can slightly affect respiration and it might affect the comparability of two parallels that we ran on all tumor samples and, additionally, it would be beneficial to design the analysis to work in a single chamber. Finally, it would have contributed to this study if a selection of patient samples would have been firstly analyzed for steady state metabolite levels (using rapid freezing of part the sample in the operating room) and later, for temporal MCE as described here.

CONCLUSIONS

We have shown that permeabilization-based approach is rapid for segregating metabolic and respiratory profiles in clear and quantified manner for both cell lines and solid human tumors. The method presented here offers time dependent view of intracellular metabolism and does not require changes in patient management before or during the surgery nor is it that time-critical as described before for isotope-based methods.

We showed that scarcely respiring MDA-MB-231 cells present with higher MCE than highly respiring MCF-7 cells do and, therefore, it can be concluded that OXPHOS and TCA are not directly coupled in all cell lines. Our data proved that in terms of MCE and OXPHOS, these two widely used cell lines (MCF7, MDA-MB-231) do not replicate the same properties in respective human breast cancer samples. Surprisingly, the findings for the two cell lines and clinical samples were directly opposing and that can explain difficulties in translational research. In contrast to cell lines, capacity for OXPHOS and MCE in human breast tumors are increasing together with increasing clinical aggressiveness of the tumors. Interestingly, when we analyzed our detailed data on the clinical samples of the most aggressive TNBC subtype, possible predictive value for glutaminase inhibitor treatment emerged that need to be confirmed by additional trials. Taken together, new and easier methods that quantify time dependent metabolism in solid human cancers can bring out shortcomings in our model systems and direct translational research in delivering new treatments to patients faster.

DATA AVAILABILITY STATEMENT

The raw data supporting the conclusions of this article will be made available by the authors, without undue reservation, to any qualified researcher.

ETHICS STATEMENT

The studies involving human participants were reviewed and approved by Tallinn Medical Research Ethics Committee. The patients/participants provided their written informed consent to participate in this study.

AUTHOR CONTRIBUTIONS

AK designed the study, developed temporal MCE quantification method, conducted most of the experiments, and wrote the manuscript. NT conducted the respiration studies together with quantification of citrate. LT and VC grew the cultured cells for experiments. SG developed the metabolite analysis method on GC-MS. IS, KL, LM, RK, and VV provided the fresh human samples for the experiments together with respective medical data. TK supervised the study and reviewed the manuscript. All authors contributed to the article and approved the submitted version.

FUNDING

The study was funded by a private company Mitogro OU active in developing predictive tools in cancer metabolism and by the European Regional Development Fund CoE programTK133 The Dark Side of the Universe. The funder (Mitogro OU) was not involved in the study design, collection, analysis, interpretation of data, the writing of this article or the decision to submit it for publication.

REFERENCES

1. Warburg O. On the origin of cancer cells. *Science.* (1956) 123:309–14. doi: 10.1126/science.123.3191.309
2. DeBerardinis RJ, Chandel NS. We need to talk about the Warburg effect. *Nat Metab.* (2020) 2:127–9. doi: 10.1038/s42255-020-0172-2
3. Dupuy F, Tabariès S, Andrzejewski S, Dong Z, Blagih J, Annis MG, et al. PDK1-dependent metabolic reprogramming dictates metastatic potential in breast cancer. *Cell Metab.* (2015) 22:577–89. doi: 10.1016/j.cmet.2015.08.007
4. Hensley CT, Faubert B, Yuan Q, Lev-Cohain N, Jin E, Kim J, et al. Metabolic heterogeneity in human lung tumors. *Cell.* (2016) 164:681–94. doi: 10.1016/j.cell.2015.12.034

5. Koit A, Shevchuk I, Ounpuu L, Klepinin A, Chekulayev V, Timohhina N, et al. Mitochondrial respiration in human colorectal and breast cancer clinical material is regulated differently. *Oxidat Med Cell Longev.* (2017) 2017:16. doi: 10.1155/2017/1372640
6. Pavlova NN, Thompson CB. The emerging hallmarks of cancer metabolism. *Cell Metab.* (2016) 23:27–47. doi: 10.1016/j.cmet.2015.12.006
7. Spinelli JB, Haigis MC. The multifaceted contributions of mitochondria to cellular metabolism. *Nat Cell Biol.* (2018) 20:745–54. doi: 10.1038/s41556-018-0124-1
8. DeBerardinis RJ, Mancuso A, Daikhin E, Nissim I, Yudkoff M, Wehrli S, et al. Beyond aerobic glycolysis: transformed cells can engage in glutamine metabolism that exceeds the requirement for protein and nucleotide synthesis. *Proc Natl Acad Sci USA.* (2007) 104:19345–50. doi: 10.1073/pnas.0709747104
9. Lunt SY, Vander Heiden MG. Aerobic glycolysis: meeting the metabolic requirements of cell proliferation. *Annu Rev Cell Dev Biol.* (2011) 27:441–64. doi: 10.1146/annurev-cellbio-092910-154237
10. Jiang L, Shestov AA, Swain P, Yang C, Parker SJ, Wang QA, et al. Reductive carboxylation supports redox homeostasis during anchorage-independent growth. *Nature.* (2016) 532:255–8. doi: 10.1038/nature17393
11. Hatzivassiliou G, Zhao F, Bauer DE, Andreadis C, Shaw AN, Dhanak D, et al. ATP citrate lyase inhibition can suppress tumor cell growth. *Cancer Cell.* (2005) 8:311–21. doi: 10.1016/j.ccr.2005.09.008
12. Intlekofer AM, Dematteo RG, Venneti S, Finley LW, Lu C, Judkins AR, et al. Hypoxia induces production of L-2-hydroxyglutarate. *Cell Metab.* (2015) 22:304–11. doi: 10.1016/j.cmet.2015.06.023
13. Chen WW, Freinkman E, Wang T, Birsoy K, Sabatini DM. Absolute quantification of matrix metabolites reveals the dynamics of mitochondrial metabolism. *Cell.* (2016) 166:1324–37.e1311. doi: 10.1016/j.cell.2016.07.040
14. Lee WD, Mukha D, Aizenshtein E, Shlomi T. Spatial-fluxomics provides a subcellular-compartmentalized view of reductive glutamine metabolism in cancer cells. *Nat Commun.* (2019) 10:1351. doi: 10.1038/s41467-019-09352-1
15. Liberti MV, Locasale JW. The Warburg effect: how does it benefit cancer cells? *Trends Biochem Sci.* (2016) 41:211–8. doi: 10.1016/j.tibs.2015.12.001
16. Metallo CM, Gameiro PA, Bell EL, Mattaini KR, Yang J, Hiller K, et al. Reductive glutamine metabolism by IDH1 mediates lipogenesis under hypoxia. *Nature.* (2011) 481:380–4. doi: 10.1038/nature10602
17. Vienne J-C, Cimetta C, Dubois M, Duburcq T, Favory R, Dessein A-F, et al. A fast method for high resolution oxymetry study of skeletal muscle mitochondrial respiratory chain complexes. *Anal Biochem.* (2017) 528:57–62. doi: 10.1016/j.ab.2017.04.015
18. Saks VA, Veksler VI, Kuznetsov AV, Kay L, Sikk P, Tiivel T, et al. Permeabilized cell and skinned fiber techniques in studies of mitochondrial function *in vivo*. *Mol Cell Biochem.* (1998) 184:81–100. doi: 10.1023/A:1006834912257
19. Veksler VI, Kuznetsov AV, Sharov VG, Kapelko VI, Saks VA. Mitochondrial respiratory parameters in cardiac tissue: a novel method of assessment by using saponin-skinned fibers. *Biochim Biophys Acta.* (1987) 892:191–6. doi: 10.1016/0005-2728(87)90174-5
20. Kaambre T, Chekulayev V, Shevchuk I, Karu-Varikmaa M, Timohhina N, Tepp K, et al. Metabolic control analysis of cellular respiration *in situ* in intraoperational samples of human breast cancer. *J Bioenerg Biomembr.* (2012) 44:539–58. doi: 10.1007/s10863-012-9457-9
21. Klepinin A, Chekulayev V, Timohhina N, Shevchuk I, Tepp K, Kaldma A, et al. Comparative analysis of some aspects of mitochondrial metabolism in differentiated and undifferentiated neuroblastoma cells. *J Bioenerg Biomembr.* (2014) 46:17–31. doi: 10.1007/s10863-013-9529-5
22. Appaix F, Kuznetsov AV, Usson Y, Kay L, Andrienko T, Olivares J, et al. Possible role of cytoskeleton in intracellular arrangement and regulation of mitochondria. *Exp Physiol.* (2003) 88:175–90. doi: 10.1113/eph8802511
23. Kaldma A, Klepinin A, Chekulayev V, Mado K, Shevchuk I, Timohhina N, et al. An *in situ* study of bioenergetic properties of human colorectal cancer: the regulation of mitochondrial respiration and distribution of flux control among the components of ATP synthasome. *Int J Biochem Cell Biol.* (2014) 55:171–86. doi: 10.1016/j.biocel.2014.09.004
24. Kuznetsov AV, Veksler V, Gellerich FN, Saks V, Margreiter R, Kunz WS. Analysis of mitochondrial function *in situ* in permeabilized muscle fibers, tissues and cells. *Nat Protoc.* (2008) 3:965–76. doi: 10.1038/nprot.2008.61
25. Kuznetsov AV, Tiivel T, Sikk P, Kaambre T, Kay L, Daneshrad Z, et al. Striking differences between the kinetics of regulation of respiration by ADP in slow-twitch and fast-twitch muscles *in vivo*. *Eur J Biochem.* (1996) 241:909–15. doi: 10.1111/j.1432-1033.1996.00909.x
26. Monge C, Beraud N, Tepp K, Pelloux S, Chahboun S, Kaambre T, et al. Comparative analysis of the bioenergetics of adult cardiomyocytes and nonbeating HL-1 cells: respiratory chain activities, glycolytic enzyme profiles, and metabolic fluxes. *Can J Physiol Pharmacol.* (2009) 87:318–26. doi: 10.1139/Y09-018
27. Saks VA, Kuznetsov AV, Khuchua ZA, Vasilyeva EV, Belikova JO, Kesvatera T, et al. Control of cellular respiration *in vivo* by mitochondrial outer membrane and by creatine kinase. A new speculative hypothesis: possible involvement of mitochondrial-cytoskeleton interactions. *J Mol Cell Cardiol.* (1995) 27:625–45. doi: 10.1016/S0022-2828(08)80056-9
28. Timohhina N, Guzun R, Tepp K, Monge C, Varikmaa M, Vija H, et al. Direct measurement of energy fluxes from mitochondria into cytoplasm in permeabilized cardiac cells *in situ*: some evidence for mitochondrial interactosome. *J Bioenerg Biomembr.* (2009) 41:259–75. doi: 10.1007/s10863-009-9224-8
29. Chekulayev V, Mado K, Shevchuk I, Koit A, Kaldma A, Klepinin A, et al. Metabolic remodeling in human colorectal cancer and surrounding tissues: alterations in regulation of mitochondrial respiration and metabolic fluxes. *Biochem Biophys Rep.* (2015) 4:111–25. doi: 10.1016/j.bbrep.2015.08.020
30. Chance B, Williams GR. The respiratory chain and oxidative phosphorylation. *Adv Enzymol Relat Subj Biochem.* (1956) 17:65–134. doi: 10.1002/9780470122624.ch2
31. Parlo RA, Coleman PS. Enhanced rate of citrate export from cholesterol-rich hepatoma mitochondria. The truncated Krebs cycle and other metabolic ramifications of mitochondrial membrane cholesterol. *J Biol Chem.* (1984) 259:9997–10003.
32. Petrarulo M, Facchini P, Cerelli E, Marangella M, Linari F. Citrate in urine determined with a new citrate lyase method. *Clin Chem.* (1995) 41:1518–21. doi: 10.1093/clinchem/41.10.1518
33. Srere PA. [1] Citrate synthase: [EC 4.1.3.7. Citrate oxaloacetate-lyase (CoA-acetylating)]. *Methods Enzymol.* (1969) 13:3–11. doi: 10.1016/0076-6879(69)13005-0
34. Daemen A, Liu B, Song K, Kwong M, Gao M, Hong R, et al. Pan-cancer metabolic signature predicts co-dependency on glutaminase and *de novo* glutathione synthesis linked to a high-mesenchymal cell state. *Cell Metab.* (2018) 28:383–99.29. doi: 10.1016/j.cmet.2018.06.003
35. Sousa CM, Biancur DE, Wang X, Halbrook CJ, Sherman MH, Zhang L, et al. Pancreatic stellate cells support tumour metabolism through autophagic alanine secretion. *Nature.* (2016) 536:479–83. doi: 10.1038/nature19084
36. Huang L, Wang C, Xu H, Peng G. Targeting citrate as a novel therapeutic strategy in cancer treatment. *Biochim Biophys Acta.* (2020) 1873:188332. doi: 10.1016/j.bbcan.2019.188332
37. Philippe I, Hubert L. The reduced concentration of citrate in cancer cells: an indicator of cancer aggressiveness and a possible therapeutic target. *Drug Resist Updates.* (2016) 29:47–53. doi: 10.1016/j.drup.2016.09.003
38. Kolukula VK, Sahu G, Wellstein A, Rodriguez OC, Preet A, Iacobazzi V, et al. SLC25A1, or CIC, is a novel transcriptional target of mutant p53 and a negative tumor prognostic marker. *Oncotarget.* (2014) 5:1212–25. doi: 10.18632/oncotarget.1831
39. Catalina-Rodriguez O, Kolukula VK, Tomita Y, Preet A, Palmieri F, Wellstein A, et al. The mitochondrial citrate transporter, CIC, is essential for mitochondrial homeostasis. *Oncotarget.* (2012) 3:1220–35. doi: 10.18632/oncotarget.714
40. Nonnenmacher Y, Palorini R, d'Herouël AF, Krämer L, Neumann-Schaal M, Chiaradonna F, et al.. Analysis of mitochondrial metabolism *in situ*: combining stable isotope labeling with selective permeabilization. *Metab Eng.* (2017) 43:147–55. doi: 10.1016/j.ymben.2016.12.005
41. Cluntun AA, Lukey MJ, Cerione RA, Locasale JW. Glutamine metabolism in cancer: understanding the heterogeneity. *Trends Cancer.* (2017) 3:169–80. doi: 10.1016/j.trecan.2017.01.005
42. Gross MI, Demo SD, Dennison JB, Chen L, Chernov-Rogan T, Goyal B, et al. Antitumor activity of the glutaminase inhibitor CB-839 in triple-negative breast cancer. *Mol Cancer Ther.* (2014) 13:890–901. doi: 10.1158/1535-7163.MCT-13-0870

43. Bianchini G, Balko JM, Mayer IA, Sanders ME, Gianni L. Triple-negative breast cancer: challenges and opportunities of a heterogeneous disease. *Nat Rev Clin Oncol.* (2016) 13:674–90. doi: 10.1038/nrclinonc.2016.66
44. Schnitt SJ. Classification and prognosis of invasive breast cancer: from morphology to molecular taxonomy. *Mod Pathol.* (2010) 23:S60–4. doi: 10.1038/modpathol.2010.33
45. Cheang MCU, Chia SK, Voduc D, Gao D, Leung S, Snider J, et al. Ki67 index, HER2 status, and prognosis of patients with luminal B breast cancer. *J Natl Cancer Inst.* (2009) 101:736–50. doi: 10.1093/jnci/djp082
46. Reis LM, Adamoski D, Ornitz Oliveira Souza R, Rodrigues Ascenção CF, Sousa de Oliveira KR, Corrêa-da-Silva F, et al. Dual inhibition of glutaminase and carnitine palmitoyltransferase decreases growth and migration of glutaminase inhibition–resistant triple-negative breast cancer cells. *J Biol Chem.* (2019) 294:9342–57. doi: 10.1074/jbc.RA119.008180
47. Leone RD, Zhao L, Englert JM, Sun I-M, Oh M-H, Sun I-H, et al. Glutamine blockade induces divergent metabolic programs to overcome tumor immune evasion. *Science.* (2019) 366:1013. doi: 10.1126/science.aav2588
48. Venneti S, Dunphy MP, Zhang H, Pitter KL, Zanzonico P, Campos C, et al. Glutamine-based PET imaging facilitates enhanced metabolic evaluation of gliomas *in vivo*. *Sci Transl Med.* (2015) 7:274ra217. doi: 10.1126/scitranslmed.aaa1009

Conflict of Interest: AK is scientific founder and holds equity in a start-up company, Mitogro, which is active in developing predictive tools for cancer metabolism. AK and TK are inventors for pending patent application No. US15/651,003 covering use of the described method in predictive setting in oncology.

The remaining authors declare that the research was conducted in the absence of any commercial or financial relationships that could be construed as a potential conflict of interest.

frontiers in Oncology

ORIGINAL RESEARCH
published: 19 August 2020
doi: 10.3389/fonc.2020.01333

The Warburg Effect in Yeast: Repression of Mitochondrial Metabolism Is Not a Prerequisite to Promote Cell Proliferation

Cyrielle L. Bouchez[1,2†], *Noureddine Hammad*[1,2†], *Sylvain Cuvellier*[1,2], *Stéphane Ransac*[1,2], *Michel Rigoulet*[1,2] *and Anne Devin*[1,2*]

[1] CNRS, Institut de Biochimie et Génétique Cellulaires, UMR 5095, Bordeaux, France, [2] Univ. de Bordeaux, Institut de Biochimie et Génétique Cellulaires, UMR 5095, Bordeaux, France

OPEN ACCESS

Edited by:
Sara Rodriguez-Enriquez, Instituto Nacional de Cardiología, Mexico

Reviewed by:
Alvaro Marín Hernández, Instituto Nacional de Cardiología, Mexico
Mariafrancesca Scalise, University of Calabria, Italy
Salvador Uribe-Carvajal, National Autonomous University of Mexico, Mexico

***Correspondence:**
Anne Devin
anne.devin@ibgc.cnrs.fr

[†] These authors share first authorship

Specialty section:
This article was submitted to Cancer Metabolism, a section of the journal Frontiers in Oncology

Received: 18 February 2020
Accepted: 25 June 2020
Published: 19 August 2020

Citation:
Bouchez CL, Hammad N, Cuvellier S, Ransac S, Rigoulet M and Devin A (2020) The Warburg Effect in Yeast: Repression of Mitochondrial Metabolism Is Not a Prerequisite to Promote Cell Proliferation. Front. Oncol. 10:1333. doi: 10.3389/fonc.2020.01333

O. Warburg conducted one of the first studies on tumor energy metabolism. His early discoveries pointed out that cancer cells display a decreased respiration and an increased glycolysis proportional to the increase in their growth rate, suggesting that they mainly depend on fermentative metabolism for ATP generation. Warburg's results and hypothesis generated controversies that are persistent to this day. It is thus of great importance to understand the mechanisms by which cancer cells can reversibly regulate the two pathways of their energy metabolism as well as the functioning of this metabolism in cell proliferation. Here, we made use of yeast as a model to study the Warburg effect and its eventual function in allowing an increased ATP synthesis to support cell proliferation. The role of oxidative phosphorylation repression in this effect was investigated. We show that yeast is a good model to study the Warburg effect, where all parameters and their modulation in the presence of glucose can be reconstituted. Moreover, we show that in this model, mitochondria are not dysfunctional, but that there are fewer mitochondria respiratory chain units per cell. Identification of the molecular mechanisms involved in this process allowed us to dissociate the parameters involved in the Warburg effect and show that oxidative phosphorylation repression is not mandatory to promote cell growth. Last but not least, we were able to show that neither cellular ATP synthesis flux nor glucose consumption flux controls cellular growth rate.

Keywords: Warburg effect, mitochondria, oxidative phosphorylation, mitochondrial biogenesis, Hap4p, yeast

INTRODUCTION

Cell proliferation requires anabolic pathways that require energy for their accomplishment. ATP is the central molecule in energy conversion processes that can be synthesized through two kinds of reaction: substrate-level phosphorylation (glycolysis and Krebs cycle) and mitochondrial oxidative phosphorylation. Mitochondria has long been proposed to play a central role in ATP turn-over since they synthesize most of the cellular ATP. It is well-known that the energetic yield of both pathways is very different since when one glucose is being oxidized, glycolysis will generate 2 ATP, whereas mitochondria can generate over ten times more but requires oxygen, the final electron acceptor of the respiratory chain.

O. Warburg conducted one of the first studies on tumor energy metabolism. His early discoveries showed that cancer cells display a decreased respiration and an increased glycolysis proportional to the increase in their growth rate, suggesting that they mainly depend on fermentative metabolism for ATP generation (1). Because the repression of oxidative metabolism occurs even if oxygen is plentiful, this metabolic phenomenon was named "aerobic glycolysis." Warburg later proposed that dysfunctional mitochondria are the root of aerobic glycolysis (2) and further hypothesized that this event is the primary cause of cancer. It should be stressed here that the Warburg effect, as defined by O. Warburg, requires the concomitant and correlated variations of the three parameters mentioned above: respiratory rate, glycolysis and growth rate. If one of these parameters does not evolve as expected, one can no longer consider the observed phenomenon to be a Warburg effect. Warburg's results and hypothesis generated controversies that are persistent to this day. Moreover, this effect is very different from the Crabtree effect, which is defined as the inhibition of cellular oxygen consumption upon glucose addition to cells and fall under a kinetic regulation of mitochondrial oxidative phosphorylation (3).

It has been shown that oxidative phosphorylation activity can be increased in cultured cancer cells (4), which implies that the decrease in mitochondrial activity in these cells is not irreversible. In the same line of thought, it has been shown that some cancer cells, when cultured in petri dishes, can reversibly switch between fermentation and oxidative metabolism, depending on the absence or the presence of glucose and the environmental conditions (4–6). Another hypothesis was that the down regulation of oxidative phosphorylation was used by cancer cells to proliferate in hypoxic environments. Nonetheless, a considerable body of evidence challenges the paradigm of the purely "glycolytic" cancer cell (7). Some glioma, hepatoma and breast cancer cell lines possess functional mitochondria and they obtain their ATP mainly from oxidative phosphorylation (8–11). Moreover, a model proposed that "glycolytic" cells could establish a metabolic symbiosis with the "oxidative" ones through lactate shuttling (12). This points out that the metabolic plasticity observed *in vitro* may have an impact on tumor physiology *in vivo*.

Therefore, it is crucial to understand the mechanisms by which cancer cells can reversibly regulate the two pathways of their energy metabolism as well as the functioning of this metabolism in cell proliferation. Both pathways are thermodynamically controlled by two forces: the phosphate potential (ΔGp) and the redox potential (ΔG_{redox}), which implies that they are inherently linked. Further, they are kinetically regulated by metabolites that can arise from one another (13, 14). These pathways being so intertwined raises the question whether the downregulation of mitochondrial metabolism is a mandatory step to increase the flux through glycolysis.

A more finalist way of analyzing the Warburg effect is to investigate its added value to promote cell growth. A review of the literature shows that the possible benefits of this energy metabolism rewiring for cancer cell growth are not clear. Indeed, it is well-known that aerobic glycolysis is inefficient in terms of ATP synthesis yield when compared with mitochondrial respiration (15–17). However, in mammals, the rate of glucose metabolism through aerobic glycolysis is 10–100 higher than complete oxidation of glucose by mitochondrial oxidative phosphorylation. One could thus hypothesize that one of the functions of the Warburg effect would be to allow the rapid production of ATP that can be rapidly tuned to answer the demand for ATP synthesis. It has also been proposed that intense aerobic glycolysis was necessary to ensure the supply of glycolytic intermediates as building blocks to biosynthetic pathways. To this day, and despite numerous studies, the possible advantages of this metabolic rewiring are still under investigation.

There is a number of limitations to the use of cancer cells in culture in order to study their energy metabolism. First and foremost, in these cells, the metabolic deviation is already in place, not allowing a study of the molecular mechanisms giving rise to that deviation. Second, most of the studies conducted in these cells are conducted under hyperglycemic (22.5 mM glucose) and hyperoxic (21% O_2) conditions. These are two crucial parameters when one considers cell energy metabolism, glucose feeding glycolysis and oxygen being the electrons acceptor in the respiratory chain. From a metabolic point of view, the fermenting yeast Saccharomyces cerevisiae and tumor cells share several features (18, 19). In both cell types, there are mechanisms that enhance glycolytic flux concomitantly with the repression of oxidative phosphorylation in the presence of glucose, and fermentation is preferred even in the presence of oxygen. Here, we made use of yeast as a model to study the Warburg effect and its eventual function in supporting an increased ATP demand to support cell proliferation. The role of oxidative phosphorylation repression in this effect was investigated. We show that yeast is a good model to study the Warburg effect, where all parameters can be reconstituted. Moreover, contrary to what was proposed by Warburg and in accordance with a number of reports from the literature, we show that in this model mitochondria are not dysfunctional: there are fewer mitochondria respiratory chain units per cell. Identification of the molecular mechanisms involved in this process allowed us to dissociate the parameters involved in the Warburg effect and show that oxidative phosphorylation repression is not mandatory to favor cell growth. Last but not least, we were able to show that cellular ATP synthesis flux does not control cellular growth rate.

Abbreviations: ATP, Adenosine triphosphate; ΔGp, phosphate potential; ΔG_{redox}, redox potential; O_2, dioxygen; HAP, heme activator protein; Hxk, Hexokinase; CCCP, carbonyl cyanide m-chlorophenylhydrazone; KOH, Potassium hydroxide; NAD^+, Nicotinamide adenine dinucleotide; PCA, Perchloric acid; NaOH, Sodium hydroxide; SDS, Sodium dodecyl sulfate; OD, Optical density; PGK1, phosphoglycerate kinase 1; HCl, hydrochloric acid; PiK, Potassium phosphate; EtOH, Ethanol; WT, Wild Type; w/, with; w/o, without.

EXPERIMENTAL PROCEDURES

Yeast Strains, Plasmids, and Culture Medium

The following yeast strains were used in this study: BY4742 (MATα; his3Δ1; leu2Δ0; lys2Δ0; ura3Δ0); BY4742 Δ*hap4*

(MATα; his3Δ1; leu2Δ0; lys2Δ0; ura3Δ0; hap4:: kanMX4); BY4742 Δ*hxk2* (MATα; his3Δ1; leu2Δ0; lys2Δ0; ura3Δ0; Hxk2:: kan MX4); *Candida utilis* (CBS621) and *Saccharomyces cerevisiae* (yeast foam). Strains Δhxk2-Hap4p↑ and Δhap4-Hap4p↑ are BY4742 strains previously described (14).

Cells were grown aerobically at 28°C in the following medium: 0.175% yeast nitrogen base (Difco), 0.2% casein hydrolysate (Merck), 0.5% $(NH_4)_2SO_4$, 0.1% KH_2PO_4, 2% lactate (w/v) (Prolabo), pH 5.5, 20 mg.L^{-1} L-tryptophan (Sigma), 40 mg.L^{-1} adenine hydrochloride (Sigma) and 20 mg.L^{-1} uracil (Sigma). When cells carried a plasmid, uracil was omitted in the growth medium [pTET-HAP4 (20, 21)]. Where indicated, glucose (60 mM) was added to the medium. Growth was measured at 600 nm in a Safas spectrophotometer (Monaco) in a 1 mL cuvette. Dry weight determinations were performed on samples of cells harvested throughout the growth period, washed twice in distilled water and weighed after extensive drying.

Oxygen Consumption Assays

Oxygen consumption was measured polarographically at 28°C using a Clark oxygen electrode in a 1 mL thermostatically controlled chamber. 1 mL of culture was transferred to the chamber and respiratory rates (JO_2) were determined from the slope of a plot of O_2 concentration vs. time. The measured activities are normalized per mg dry weight. Respiration assays of growing cells were performed in the growth medium. In the case of uncoupled respiratory rate (10 μM CCCP), 100 mM Ethanol was added to the culture medium (22).

Glucose Measurement

Cells were grown in 2% lactate synthetic complete medium. Each hour, 1 mL of the culture was harvested and centrifuged. Culture supernatant was heated at 80°C for 5 min. Glucose was quantified in the supernatant with the Megazyme "D-Glucose HK assay Kit."

Ethanol Measurement

Cells were grown in 2% lactate synthetic complete medium. Each hour, 1 mL of the culture was harvested and centrifuged. Culture supernatant was mixed with 25% of PCA. Then, KOMO (KOH 2M, MOPS 0.3M) was added to adjust the pH to 7. Samples were diluted in potassium phosphate buffer (50 mM) pH9 containing NAD^+ (2 mM), Aldehyde dehydrogenase (0.3 U/mL) and alcohol dehydrogenase (70 U/mL). Ethanol was quantified by NAD^+ reduction at 340 nm and 28°C.

Cytochrome Content Determination

The cellular content of mitochondrial cytochromes $c+c_1$, b and $a+a_3$ was calculated as described in Dejean et al. (23) considering the respective molar extinction coefficient values and the reduced-minus-oxidized spectra recorded using a dual beam spectrophotometer (Varian, cary 4000).

Enzymatic Activities Determination

Cells were washed and then broken by vigorous shaking with an equal volume of glass beads in a buffer containing 50 mM Tris-HCl pH 7.4 and a mixture of protease inhibitors (Complete EDTA-freeTM, Roche). Centrifugations (700 g, 2 min) allowed the elimination of pelleted unbroken cells and glass beads. Cellular proteins were quantified by the Lowry method. Citrate synthase (2.3.3.1) activity was determined by monitoring at 412 nm the oxidation of coenzyme A (produced by citrate synthase activity) by 5,5'-dithiobis-2-nitrobenzoic acid (DTNB) as a function of time, in a Safas spectrophotometer. The enzyme activity was calculated using an extinction coefficient of 13 600 $M^{-1}.cm^{-1}$ at 412 nm. One citrate synthase unit was equal to 1 μmole of DTNB reduced per minute per mg dry weight. Cytochrome c oxidase activity (1 mM potassium cyanide–sensitive) was determined by monitoring spectrophotometrically (550 nm) the rate of disappearance of reduced cytochrome c in the following buffer: 50 mM PiK, 100 μM reduced cytochrome c. The enzyme activity was determined using an extinction coefficient of 18,500 $M^{-1}.cm^{-1}$ at 550 nm for reduced cytochrome c (all from Sigma). Hexokinase activity was determined by monitoring the rate of NAD^+ reduction spectrophotometrically (340 nm) (2 mM) in the presence of 0.5 U/mL glucose-6-phosphate dehydrogenase (G6PDH), 10 mM glucose, 1 mM ATP, 1 mM $MgCl_2$.

Protein Extraction, Electrophoresis, and Western-Blot

Cells were lysed using a mixture of 7.5% β-mercaptoethanol in 1.85M NaOH. After 10 min incubation on ice, proteins were precipitated by the addition of an equal volume of 3M trichloroacetic acid for 10 min on ice. After a rapid centrifugation at 4°C, the protein pellet was suspended in a mixture of 10% SDS and sample buffer (0.06M Tris, 2% SDS, 2% ß-mercaptoethanol, 5% glycerol, 0.02% bromophenol blue). Protein amounts corresponding to 0.5 OD units of cells were separated by 10% SDS-PAGE performed according to the method of Laemmli (24). After electro-transfer onto nitrocellulose membranes (Amersham Biosciences), proteins were probed with the desired primary antibodies: α-Hap4p (see below) and α-PGK1 (monoclonal antibody, Invitrogen) and detected using peroxidase-conjugated secondary antibodies (Jackson ImmunoResearch) ECL Prime reagent (Amersham Biosciences), according to the manufacturer instructions. Signal quantifications were done using the ImageJ software.

Antibodies

Polyclonal anti-Hap4p antibodies were generated by Eurogentec using the Hap4p fragment 330–554 as an antigen. Phosphoglycerate kinase antibody was a commercial antibody (PGK1; Invitrogen).

Statistical Analysis

Results are expressed as mean ± SD. Statistical analysis was carried out using ANOVA test for all results. Prism software (GraphPad, San Diego, CA) was used for all tests. A $p < 0.05$ was considered significant. A $p < 0.05$ was considered significant and $^*p < 0.05$; $^{**}p < 0.01$; $^{***}p < 0.001$; $^{****}p < 0.0001$.

RESULTS AND DISCUSSION

Yeast as a Model to Study the Warburg Effect

As stated above, in his seminal paper, Warburg showed a tight link between cell proliferation, cell respiration repression and aerobic glycolysis stimulation. Thus, what is now referred to as the Warburg effect must rely on these three parameters and their relationship(s). In order to define whether yeast would be a good model to study the induction of the Warburg effect, these three parameters were assessed in the presence or in the absence of glucose during yeast growth on non-fermentable medium. **Figure 1** shows that whereas in the absence of glucose both growth and respiration are constant, upon glucose addition, cellular growth is significantly increased (A). This is associated with a decrease in cellular respiratory rate (B) and an increase in glucose fermentation (C). Altogether, these parameters evolution upon glucose addition shows that yeast is a suitable model for a kinetic study of the Warburg effect induction.

As shown in **Figure 1**, during the 8-h kinetic measurement up to 30 mM in glucose are consumed. 60 mM glucose was thus the lowest concentration used to ensure that glucose would not run low under our experimental conditions. To assess an eventual role of glucose concentration on the induction of the Warburg effect cellular growths, respiratory rates and glucose consumptions were assessed upon addition of three distinct glucose concentrations. **Figure 2** shows that upon glucose addition, cellular growth is increased in a comparable extent whichever the glucose concentration (A). This is associated with a decrease in cellular respiratory rate to a comparable extent whichever the glucose concentration (B) and glucose fermentation to a comparable extent whichever the glucose concentration, after 8 h about 30 mM of glucose were consumed whichever the initial glucose concentration (C).

Mitochondria Are Not Dysfunctional, There Are Fewer Mitochondria

A decrease in cellular respiratory rate can originate in a number of distinct processes such as an alteration of mitochondria [i.e., dysfunctional mitochondria as proposed by Warburg (2, 25)], a modulation of the respiratory state (such as a decrease in phosphorylating processes), or a decrease in cellular mitochondrial content (herein assimilated to the content in respiratory chain units). In order to pinpoint the origin of the glucose-induced decrease in respiratory rate, a number of mitochondrial parameters were assessed. **Figure 3A** shows that whereas in the absence of glucose the uncoupled cellular respiratory rate is stable throughout exponential growth of the

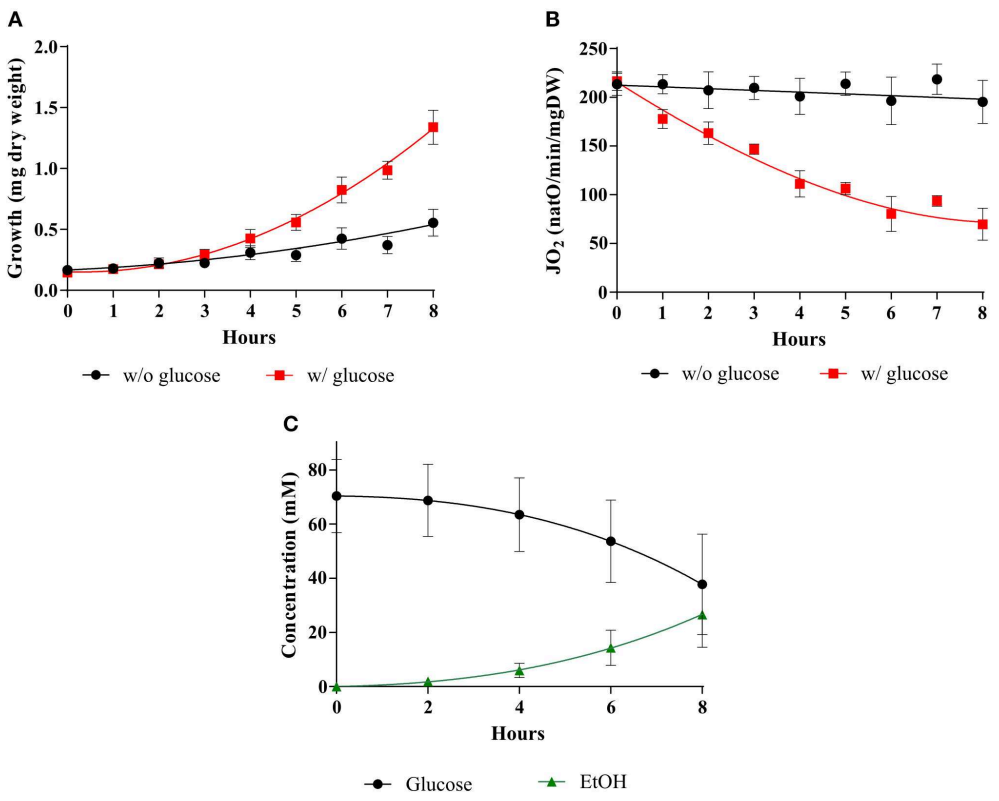

FIGURE 1 | Induction of the Warburg effect in *S. cerevisiae*. The growth medium of *S. cerevisiae* was supplemented with (w/) 60 mM of glucose at T0 (■) or without (w/o) (•). **(A)** For each condition, growth was followed for 8 h. Results shown are means of at least 10 separate experiments ± SD. **(B)** For each condition, the respiratory rate was followed for 8 h. Results shown represent means of at least 10 separate experiments ± SD. **(C)** Glucose consumption (•) and ethanol (EtOH) production (▲) were quantified. Results shown represent means of at least seven separate experiments ± SD.

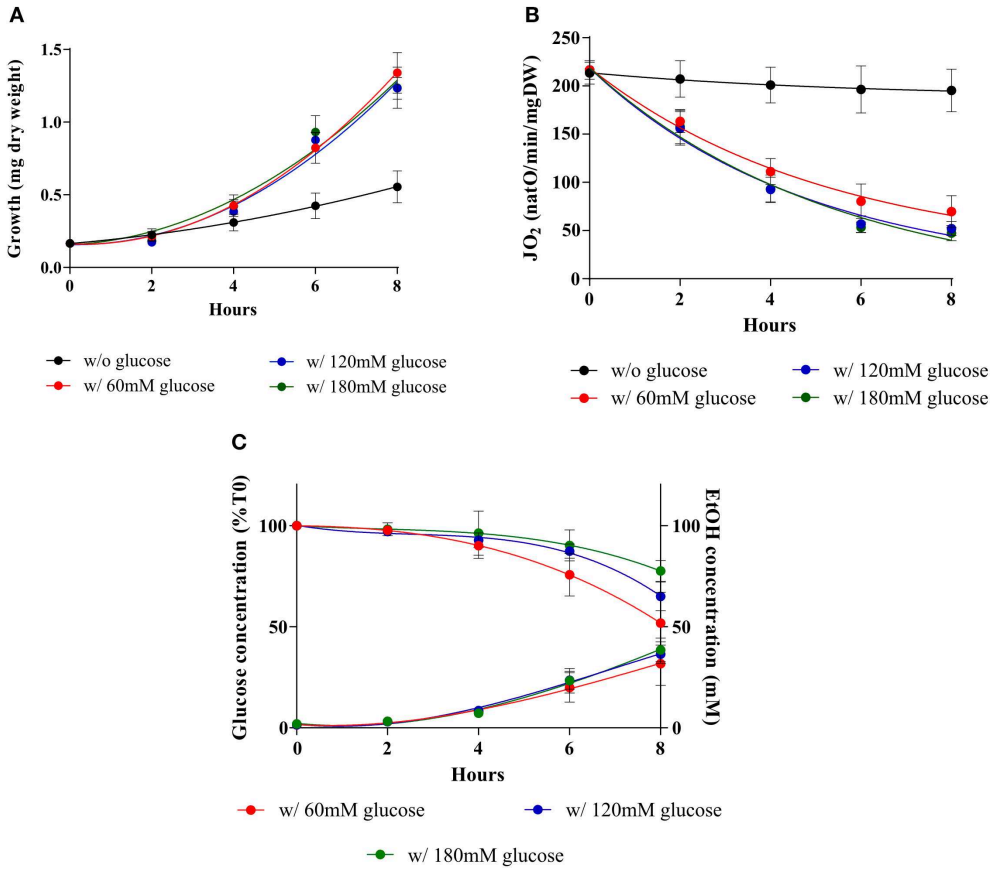

FIGURE 2 | Induction of the Warburg effect in *S. cerevisiae* at various external glucose concentrations. *S. cerevisiae* growth medium was supplemented with 60 mM (•), 120 mM (•), 180 mM (•) of glucose or not (•) at T0. **(A)** For each condition, growth was followed for 8 h. Results shown represent means of at least seven separate experiments ± SD. **(B)** The respiratory rate was followed for 8 h. Results shown represent means of at least seven separate experiments ± SD. **(C)** After addition of the different glucose concentrations in the medium culture, glucose consumption and ethanol production were quantified. Results shown represent means of at least four separate experiments ± SD.

cells, glucose addition induces a decrease of this rate, i.e., a decrease in respiratory chain activity. Because this decrease in respiratory chain activity can be due to either a kinetic regulation of the respiratory chain or a quantitative decrease in respiratory chain complexes, we quantified mitochondrial cytochromes within the cells. In the absence of glucose, the cytochromes are stable throughout exponential growth of the cells (**Figure 3B**). When the Warburg effect was induced (glucose addition) a continuous decrease of all types of cytochromes was assessed (**Figure 3C**). Moreover, the decrease in respiratory rate is directly proportional to the decrease in mitochondrial cytochromes (inset), showing that this oxygen consumption decrease is actually due to a decrease in mitochondrial respiratory chain units within the cells. This decrease in mitochondrial content was further confirmed by measuring mitochondrial enzymatic activities i.e., citrate synthase and cytochrome c oxidase. Both were decreased upon glucose addition to cells (**Table 1**). However, it should be stressed here that citrate synthase activity modulation should be interpreted with caution in yeast where a peroxisomal citrate synthase exists and is downregulated by glucose (26–28).

The Decrease in Mitochondrial Amount Originates in a Decrease in Mitochondrial Biogenesis

The amount of mitochondria within a cell is controlled by its turnover *i.e.,* the respective rates of mitochondrial biogenesis and mitochondrial degradation. The HAP complex has been shown to be involved in the specific induction of genes involved in gluconeogenesis, metabolism of alternate carbon sources, respiration, and mitochondrial development. Indeed, the disruption of any subunit of this complex renders the cells unable to grow on non-fermentable carbon sources (29–32). Moreover, many genes involved in energy metabolism have been shown to be regulated by this complex (33–35). In order to determine whether the biogenesis of the mitochondrial compartment was affected upon glucose addition to the cells, we assessed the cellular amount of the master regulator of the activity of this multicomplex, the subunit Hap4p. **Figure 4A** shows that Hap4p amount was decreased upon glucose addition, independently of glucose concentration. This protein tends to increase after 4 h in the presence of glucose and goes back to low levels for the 6

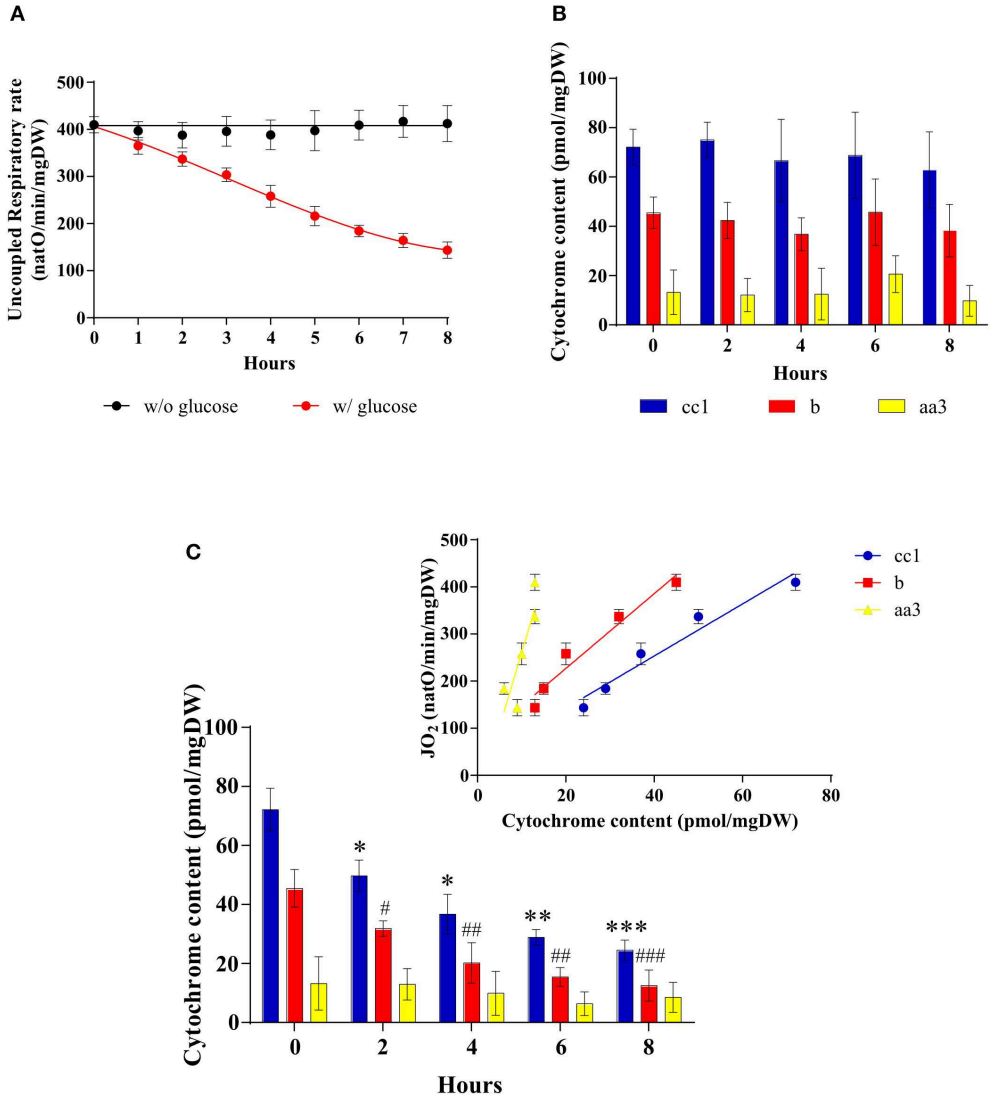

FIGURE 3 | Mitochondrial amount after induction of the Warburg effect in *S. cerevisiae*. The growth medium of *S. cerevisiae* was supplemented with 60 mM of glucose at T0 (•) or not (•). **(A)** The uncoupled respiratory rate was followed for 8 h. Results shown represent means of at least five separate experiments ± SD. **(B)** Cytochrome content was quantified every 2 h in cells in absence of glucose in the medium. Results shown represent means of at least three separate experiments ± SD. **(C)** Cytochrome content was quantified every 2 h in cells after glucose addition in the medium. Inset: A linear regression between respiratory rate and cytochrome content is presented for each cytochrome. Results shown represent means of at least four separate experiments ± SD. For each condition values are compared to the corresponding T0 and the *p*-value is represented as * for cc1; # for b.

and 8 h' time points. Quantitation of the western blots for this protein shows that is it almost undetectable after induction of the Warburg effect (**Figure 4B**). Further, porin, a mitochondrial outer membrane protein is shown to decrease, albeit to a lower level than the mitochondrial cytochromes, upon glucose addition to cells, independently of the glucose concentration used (**Figures 4C,D**). PGK1, a cytosolic enzyme was used as a loading control. This confirms the decrease in cellular mitochondrial content within the cells upon glucose addition. Further experiments showed no degradation (mitophagy) of the mitochondrial compartment upon glucose addition to cells (data not shown).

Repression of Mitochondrial Metabolism Is Not a Prerequisite to Promote Cell Proliferation

To further investigate the role of the decrease in mitochondrial respiratory rate on the Warburg effect we explored means to prevent mitochondrial biogenesis decrease upon glucose addition. First, we envisioned limiting the glycolytic flux. Hexokinase is the first enzyme of the glycolysis pathway. Among the three isoenzymes in both yeast and mammalian cells, hexokinase2 (Hxk2p) is the predominant hexokinase during growth on glucose. It is the yeast homologous of glucokinase

TABLE 1 | Citrate synthase and cytochrome c oxidase activities in wild type and mutant cells.

		T0	T2		T4		T6		T8	
		–	–	+	–	+	–	+	–	+
S. c – WT	CS	0.37 (± 0.2)	0.34 (± 0.19)	0.19 (± 0.1)**	0.30 (± 0.16)	0.08 (± 0.04)**	0.33 (± 0.17)	0.04 (± 0.01)**	0.33 (± 0.17)	0.04 (± 0.02)**
	COX	0.07 (± 0.02)	0.06 (± 0.02)	0.04 (± 0.01)	0.06 (± 0.02)	0.03 (± 0.01)**	0.05 (± 0.01)	0.02 (± 0.01)**	0.05 (± 0.02)	0.03 (± 0.01)*
S. c – Δ*hxk2*	CS	0.39 (± 0.12)	0.48 (± 0.05)	0.28 (± 0.09)**	0.4 (± 0.14)	0.15 (± 0.05)***	0.44 (± 0.1)	0.1 (± 0.03)***	0.56 (± 0.13)	0.08 (± 0.03)***
	COX	0.09 (± 0.03)	0.09 (± 0.03)	0.06 (± 0.02)	0.08 (± 0.02)	0.05 (± 0.01)*	0.09 (± 0.03)	0.05 (± 0.02)*	0.1 (± 0.03)	0.05 (± 0.02)*
S. c – Δ*hap4*↑	CS	0.28 (± 0.03)	0.35 (± 0.03)	0.23 (± 0.03)*	0.32 (± 0.07)	0.23 (± 0.02)	0.32 (± 0.04)	0.23 (± 0.05)*	0.35 (± 0.01)	0.22 (± 0.06)*
	COX	0.14 (± 0.04)	0.16 (± 0.04)	0.14 (± 0.03)	0.19 (± 0.04)	0.15 (± 0.02)	0.18 (± 0.02)	0.18 (± 0.05)	0.18 (± 0.02)*	0.14 (± 0.05)
S. c – Δ*hxk2hap4*↑	CS	0.55 (± 0.06)	0.58 (± 0.09)	0.55 (± 0.06)*	0.51 (± 0.05)	0.38 (± 0.05)*	0.53 (± 0.05)	0.35 (± 0.08)**	0.57 (± 0.02)*	0.31 (± 0.05)*
	COX	0.1 (± 0.03)	0.1 (± 0.03)	0.1 (± 0.03)	0.11 (± 0.03)	0.1 (± 0.04)	0.13 (± 0.03)	0.11 (± 0.04)	0.13 (± 0.02)	0.12 (± 0.03)
C. u	CS	0.09 (± 0.04)	0.1 (± 0.04)	0.08 (± 0.03)	0.11 (± 0.05)	0.08 (± 0.04)	0.1 (± 0.03)	0.09 (± 0.02)	0.13 (± 0.04)	0.1 (± 0.02)
	COX	0.11 (± 0.03)	0.09 (± 0.03)	0.08 (± 0.03)	0.11 (± 0.03)	0.08 (± 0.01)	0.1 (± 0.04)	0.1 (± 0.03)	0.12 (± 0.04)	0.09 (± 0.04)

CS, citrate synthase; COX, cytochrome oxidase. Enzymatic activities were measured as stipulated in the Materials and Methods section and is expressed in μmol/min/mg protein. (–) indicates in the absence of glucose. (+) indicates in the presence of glucose. T0-2-4-6-8 are the hours of incubation w/ or w/o glucose. Results shown are means of at least three separate experiments ± SD.

(overexpressed in tumor cells) and has a dual function being both a catalyst in the cytosol and an important regulator of the glucose repression signal in the nucleus (36–39). The consequences of deleting this enzyme on the induction of the Warburg effect was thus investigated. No significant effect was observed on growth or glucose consumption (**Supplementary Figures 1A,C**), indicating that Hxk2p isoenzymes' carry out the glucose phosphorylating function. This was further confirmed by measuring Hxk activity in our cells (**Table 2**). Of note, Hxk activity was much more increased after glucose addition in Δhxk2 and Δ*hap4*↑ cells, indicating a stronger activation of Hxk2p isoenzymes by glucose in the absence of Hxk2p. The deletion of Hxk2p associated with Hap4p overexpression (see below) restores this activity to a wild-type level suggesting a repression of these enzymes by Hap4p. Deletion of Hxk2p allowed a decrease in mitochondrial oxygen consumption and in mitochondrial enzymatic activities (**Table 1**) upon glucose addition, this decrease was smaller than in the wild type cells (**Supplementary Figure 1B**). However, this deleted strain was not sufficient to prevent the induction of the Warburg effect. Since Hap4p was shown to be strongly decreased upon glucose addition to cells (see **Figure 4A**), we ectopically overexpressed this protein, hoping to maintain mitochondrial biogenesis in the presence of glucose. No significant effect was observed on growth or glucose consumption/fermentation (**Supplementary Figures 2A,C**). However, although a decrease in mitochondrial oxygen consumption and in mitochondrial enzymatic activities (**Table 1**) upon glucose addition was observed with the overexpression of Hap4p (Δ*hap4*↑), this decrease was smaller than in the wild type cells, with a delay observed in its induction (**Supplementary Figure 2B**). Next, this protein was overexpressed in the Δ*hxk2* strain (Δ*hxk2hap4p*↑, **Figure 5**). Considering the function of both Hxk2p and Hap4p, such a strain should exhibit an increased mitochondrial content and a strong orientation of energetic metabolism toward respiratory metabolism, altering the relationship between glycolysis and respiratory rate. In the absence of glucose, this strain exhibits a slight increase in growth (**Figure 5A**, data not shown) and an increase in cellular respiratory rate of about 25% (**Figure 5B**). Glucose addition to this strain led to an increase in proliferation comparable to the one in the wild type strain (**Figure 5A**). However, regarding the respiratory rate of this strain in the presence of glucose, only a slight decrease was assessed after 4 h delay and, more importantly, after 8 h, its respiratory rate was comparable to the one in the wild type strain in the absence of glucose (**Figure 5B**), indicating a strong maintenance of mitochondrial function even in the presence of glucose. Despite this high respiratory rate, the Δ*hxk2hap4p*↑ strain exhibits a significant -and comparable to the wild type- glucose consumption and ethanol production upon glucose addition, in accordance with the hxk activity exhibited in this strain (**Figure 5C** & **Table 2**). The ectopically overexpressed Hap4p was shown to be stable over time both in the presence and absence of glucose (**Figure 5D**). The origin of the maintenance of the respiratory chain activity in the presence of glucose was investigated by means of quantifying the mitochondrial cytochromes within the cells. **Figure 5E** shows that in this strain and in the presence of glucose, mitochondrial cytochromes are stable throughout the cell's growth. Of note, the cytochrome content in this strain in the absence of glucose is higher than in the wild type strain, in agreement with the increase in cellular respiration in absence of glucose. Mitochondrial content was further shown not to decrease by measuring cytochrome oxidase activity (**Table 1**). A slight decrease of citrate synthase activity was assessed after 6-h incubation in the presence of glucose (**Table 1**). Altogether, these results show that repression of mitochondrial metabolism is not a prerequisite to promote cell proliferation.

A Crabtree Negative Strain Exhibits an Increase in Growth Rate Without Any Mitochondrial Repression

The unexpected above-mentioned results were obtained in a *Saccharomyces cerevisiae* mutant strain. We then sought to confirm these results (increase in growth rate in the presence of glucose with little/no decrease in mitochondrial respiration)

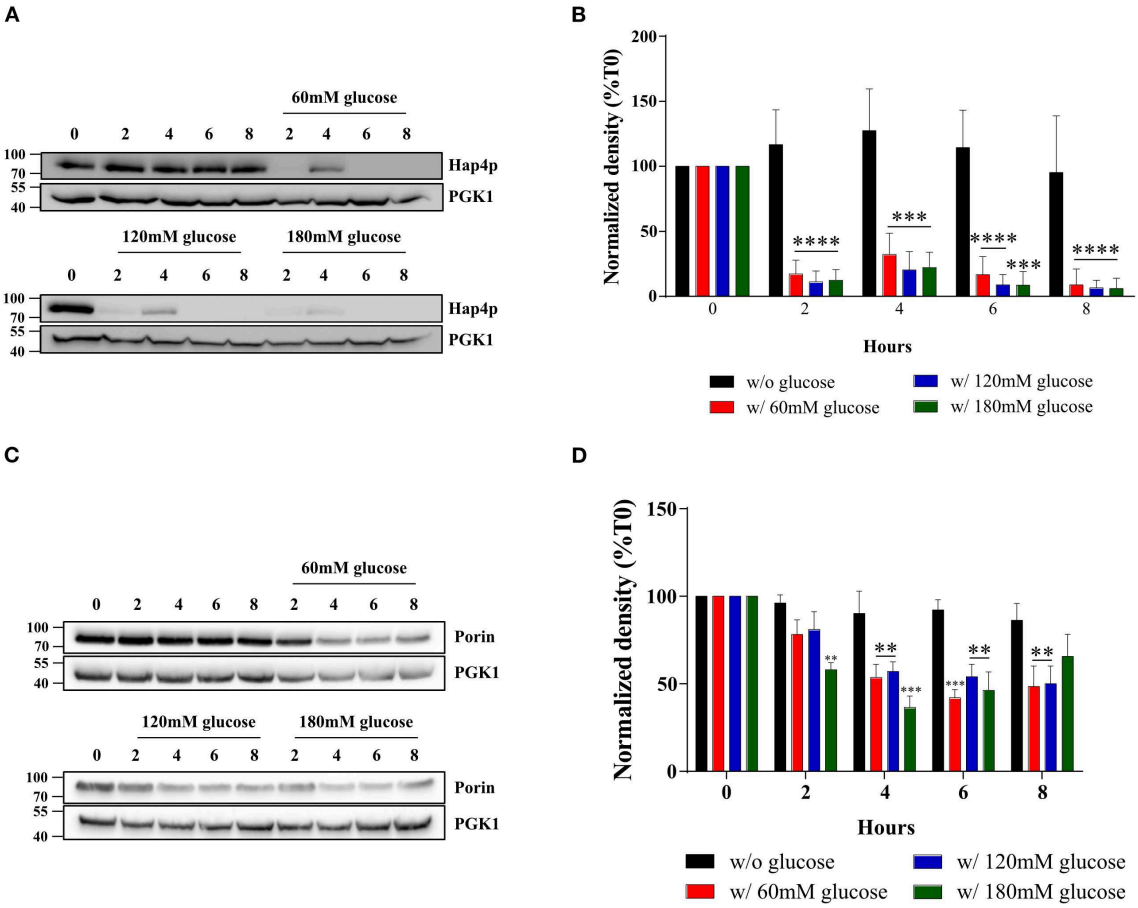

FIGURE 4 | Hap4p and porin amount after induction of the Warburg effect in *S. cerevisiae*. The growth medium of *S. cerevisiae* was supplemented with 60, 120, and 180 mM of glucose or not at T0. **(A)** The relative levels of the co-activator Hap4p were assessed every 2 h. Total protein extracts were analyzed by SDS-PAGE and western blot using antibodies directed against Hap4p and phospho-glycerate kinase (PGK1) as a loading control. **(B)** Results representative of at least four experiments are shown. Hap4p signal was quantified, signal intensity was normalized to PGK1 and expressed in percentage of T0 for each experiment. The bar-graph shows mean % of T0 ± SD for all experiments. **(C)** The relative levels of a mitochondrial protein, Porin, were assessed every 2 h. Total protein extracts were analyzed by SDS-PAGE and western blot using antibodies directed against porin and phospho-glycerate kinase (PGK1) as a loading control. **(D)** Results representative of at least four experiments are shown. Porin signal was quantified, signal intensity was normalized to PGK1 signal and expressed in percentage of T0 for each experiment. The bar-graph shows mean % of T0 ± SD for all experiments.

TABLE 2 | Hexokinase activity in wild type and mutant cells.

	T0	T2		T4		T6		T8	
	–	–	+	–	+	–	+	–	+
S. c – WT	UD	0.01 (± 0.02)	0.03 (± 0.03)	0.02 (± 0.03)	0.07 (± 0.05)	0.01 (± 0.02)	0.16 (± 0.04)*	0.01 (± 0.01)	0.21 (± 0.01)**
S. c – Δ*hxk2*	UD	0.01 (± 0.01)	0.09 (± 0.09)	0.01 (± 0.03)	0.36 (± 0.14)**	0.01 (± 0.02)	0.4 (± 0.16)**	UD	0.53 (± 0.30)**
S. c – Δ*hap4*↑	0.17 (± 0.07)	0.18 (± 0.09)*	0.18 (± 0.08)	0.29 (± 0.14)	0.44 (± 0.27)	0.3 (± 0.14)	0.45 (± 0.23)	0.32 (± 0.14)	0.38 (± 0.22)
S. c – Δ*hxk2hap4*↑	0.01 (± 0.01)	UD	0.08 (± 0.06)	UD	0.09 (± 0.04)	UD	0.13 (± 0.08)	UD	0.12 (± 0.05)

Enzymatic activity was measured as stipulated in the Materials and Methods section and is expressed in μmol/min/mg protein. (–) indicates in absence of glucose. (+) indicates in the presence of glucose. T0-2-4-6-8 are the hours of incubation w/ or w/o glucose. Results shown are means of at least three separate experiments ± SD.
UD, Undetectable.

with an alternate model. In the yeast community, yeast strains have long been characterized depending on their mitochondrial oxidative phosphorylation response to the presence of glucose. Crabtree-negative strains, also known as respiratory-obligatory strains are well-known as requiring an active mitochondrial metabolism for growth in the presence of glucose. Consequently, we made use of a yeast strain known not to exhibit glucose-induced repression of oxidative phosphorylation metabolism.

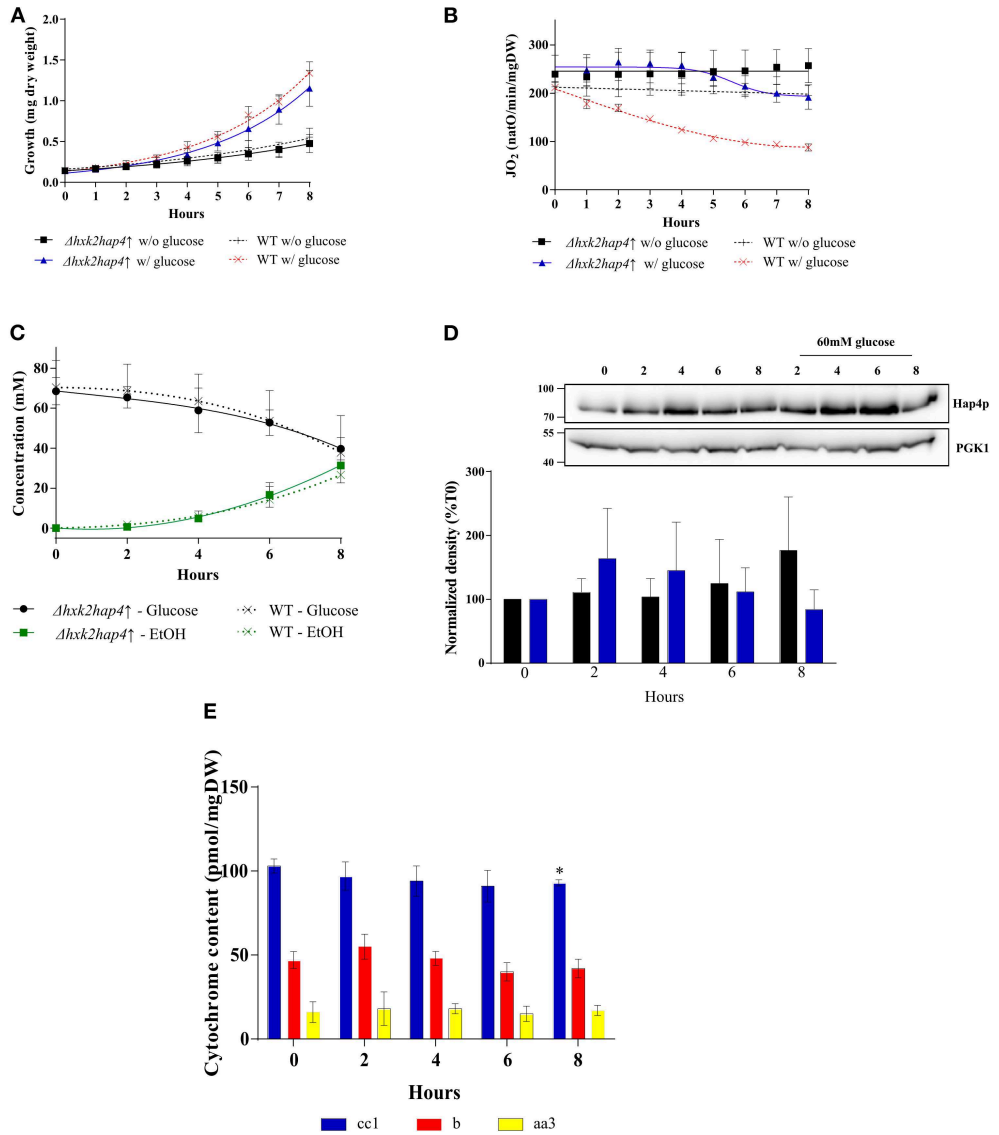

FIGURE 5 | Induction of the Warburg effect in *S. cerevisiae* Δ*hxk2hap4*↑. A *S. cerevisiae* strain deleted for *hxk2* (Δ*hxk2*) was transformed with pCM189-Hap4p (Δ*hxk2hap4*↑). The growth medium was supplemented with 60 mM of glucose at T0 (▲ Δ*hxk2hap4*↑) and (x WT) or not (■Δ*hxk2hap4*↑) and (+ WT). **(A)** Growth was followed for 8 h. Results shown represent means of at least 10 separate experiments ± SD. **(B)** The respiratory rate was followed for 8 h. Results shown represent means of at least 10 separate experiments ± SD. **(C)** Glucose consumption (• Δ*hxk2hap4*↑) and (x WT) and ethanol production (• Δ*hxk2hap4*↑) and (x WT) were quantified. Results shown represent means of at least five separate experiments ± SD. **(D)** The relative levels of the co-activator Hap4p were determined every 2 h. Total protein extracts were analyzed by SDS-PAGE and western blot using antibodies directed against Hap4p and phospho-glycerate kinase (PGK1) as a loading control. Inset: Results representative of at least four experiments are shown. Hap4p signal was quantified, signal intensity was normalized to PGK1 signal and expressed as percentage of T0 for each experiment. The bar-graph shows mean % of T0 ± SD for all experiments. **(E)** Cytochrome content was quantified every 2 h. Results shown represent means of at least four separate experiments ± SD.

In this *Candida utilis* strain, as previously shown with a *Saccharomyces cerevisiae* strain, glucose induces an increase in cell growth (**Figure 6A**). Mitochondrial respiratory rate is not significantly modified upon glucose addition although a slight decrease is observed in absence of glucose (**Figure 6B**). The increase in growth rate is associated with glucose consumption, albeit to a lower level than in the *Saccharomyces cerevisiae* strain (**Figure 6C**). EtOH production was minimal in this strain upon glucose addition in agreement with the maintenance of oxidative phosphorylation (**Figure 6C**). Further, no significant changes in mitochondrial cytochromes and mitochondrial enzymatic activities were observed upon glucose addition in this strain (**Figure 6D** and **Table 1**). Since *Candida utilis* exhibits a proton pumping complex I -which *Saccharomyces cerevisiae* does not exhibit-, similar experiments were done in the presence of Piericidin A, a complex I inhibitor (40–42), to ensure that glucose

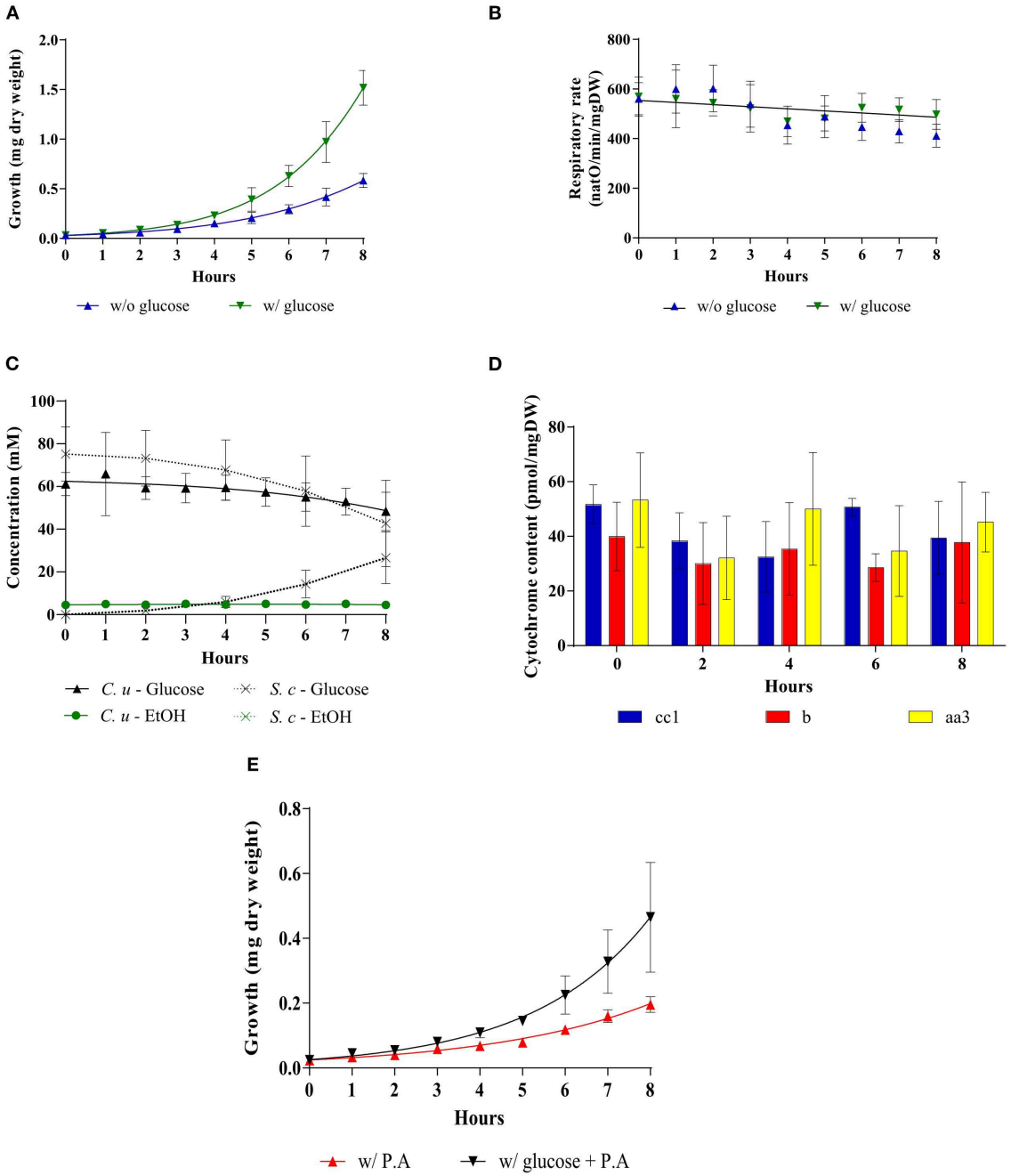

FIGURE 6 | Addition of glucose to a Crabtree-negative strain, *Candida utilis*. The growth medium was supplemented with 60 mM of glucose at T0 (▼) or not (▲). **(A)** Growth was followed for 8 hours. Results shown represent means of at least 15 separate experiments ± SD. **(B)** The respiratory rate was followed for 8 h. Results shown represent means of at least 15 separate experiments ± SD. **(C)** Glucose consumption (• *C. utilis*) or (x *S. cerevisiae*) and ethanol production (• *C. utilis*) or (x *S. cerevisiae*) were quantified. Results shown are means of at least four separate experiments ± SD. **(D)** Cytochrome content was quantified every 2 h after glucose addition to the medium. Results shown represent means of at least five separate experiments ± SD. **(E)** For each condition, growth was followed for 8 h in the presence or absence of Piericidin A (200 μM). Results shown represent means of at least three separate experiments ± SD.

addition did not change the proton pumping stoichiometry of the respiratory chain which could lead to an increase in oxidative phosphorylation efficiency. Indeed, glycolysis will generate NADH that is reoxidized at the level of complex I. Since ATP/O is higher from complex I (2.5) than for all other dehydrogenases (1.5), one could imagine that glucose addition to these cells will increase oxidative phosphorylation efficiency (43–46). **Figure 6E** shows that the increase in growth rate assessed

upon glucose addition occurs in the absence of a functional complex I, eluding an eventual role of oxidative phosphorylation efficiency change in the growth rate increase.

There Is No Direct Link Between Oxidative Phosphorylation Repression and Cellular Growth Rate

Here, we developed a number of *S. cerevisiae* cellular models that allowed us to study the induction of the Warburg effect. As described above, these models exhibit various respiratory rate repression levels and various growth rates in the presence or absence of glucose. We calculated growth rates for every strain for the 4- to 8-h incubation time points since most changes in terms of growth and respiratory metabolism occur in the first 4 h. These growth rates were then plotted against the average respiratory rates for the same incubation time. This showed that there is not direct/simple link between oxidative phosphorylation repression and an increase in cell growth rate (data not shown but see results from **Figures 1**, **3**, SD1 & SD2). Further, this occurs at a comparable coupling level between oxidation and phosphorylation at the level of the oxidative phosphorylation as shown by the constant ratio between spontaneous respiratory rate and non-phosphorylating respiratory rate (**Table 3**).

ATP Synthesis Flux Does Not Control Cellular Growth Rate

The behavior of the Δ*hxk2hap4*↑ strain that is not typical of a Warburg effect raises a number of questions. Indeed, one of the proposed functions of the Warburg effect is an increased ATP synthesis flux through glycolysis allowing for an increased growth. We thus calculated glycolytic flux in both the wild type and Δ*hxk2hap4*↑ strain (data from **Figures 1C**, **5C**). In the yeast *Saccharomyces cerevisiae*, the end product of "aerobic glycolysis" as defined by Warburg -that is fermentation- is EtOH (lactate in mammalian cells). Glucose consumption flux and EtOH production rate in the wild type (WT) and Δ*hxk2hap4*↑ strains are presented in **Figures 7A,B**, respectively. Glucose consumption flux reached a stationary state after about 4 h for both strains and this flux in the Δ*hxk2hap4*↑ strain is lower than that of the wild type strain (**Figure 7A**). EtOH production flux reached a stationary state after about 4 h for both strains and this flux in the Δ*hxk2hap4*↑ strain is lower than in the wild type strain (**Figure 7B**).

Upon fermentation, one mole of glucose allows for the production of two moles of EtOH. Since both glucose consumption flux and EtOH production flux are comparable in each strain after 4 h, only half the glucose is being fermented. Consequently, since 2 ATP are produced per fully metabolized glucose, under our conditions the glycolysis-linked ATP synthesis flux could be assimilated to EtOH production flux. The yeast Saccharomyces cerevisiae mitochondria lack a proton pumping complex I (47, 48). Thus, electron transfer through that respiratory chain always involves two proton pumping sites, the efficiency of the oxidative phosphorylation is assumed to be constant and about 1.5 ATP produced per oxygen (1/2 O_2) consumed. Since we measured the respiratory rates of our strains throughout growth, we can estimate the ATP synthesis flux linked to mitochondrial oxidative phosphorylation. Mitochondria and glycolysis-derived ATP synthesis fluxes for the wild type and the mutant strains are presented in **Figures 8A,B**, respectively. In the wild type strain, upon glucose addition, a consequent decrease in mitochondria-linked ATP synthesis was associated with a concomitant increase in glycolysis-linked ATP synthesis (**Figure 8A**). In the Δ*hxk2hap4*↑ strain, glucose addition only slightly decreases mitochondria-derived ATP synthesis and glycolysis-linked ATP synthesis only accounts for about 30% of the total flux (**Figure 8B**). More importantly, there is no clear link between growth rate and ATP synthesis, whichever the origin of the ATP (**Figure 8C**). Further, if one plots cell growth vs. the glucose consumption flux, again, there is no clear link between these two parameters (**Figure 8D**).

TABLE 3 | Spontaneous and non-phosphorylating respiratory rates in wild type and mutant cells.

Strains	JO_2	$JO_{2\text{-non phosphorylating}}$	Ratio
S. c – WT	70 (± 4.5)	27 (± 0.8)****	2.59 (± 0.2)
S. c – Δ*hxk2*	91 (± 2.4)	36 (± 1.9)****	2.57 (± 0.4)
S. c – Δ*hap4*↑	122 (± 5.3)	50 (± 0.4)****	2.52 (± 0.2)
S. c – Δ*hxk2hap4*↑	192 (± 6.5)	73 (± 4.2)****	2.61 (± 0.2)
C. u	498 (± 14.6)	ND	ND

Respiratory rates were assessed after 8-h incubation in the presence of glucose. Non-phosphorylating respiratory rate was determined in the presence of 0.1 mM Triethyltin, an inhibitor of mitochondrial ATPsynthase.
ND, not determined.

CONCLUSION

Throughout its history, the possible added value of the Warburg Effect has remained controversial and the potential function(s) of this energy metabolism rewiring remain(s) unclear. In this paper, we investigated the role of this rewiring in promoting cell growth and division. We made use of yeast to study the induction of the Warburg effect and its kinetics. Further, the use of mutants allowed us to further study the relationship between growth rate and the two pathways that support ATP synthesis namely glycolysis and oxidative phosphorylation. We show that yeast is a good model to study the Warburg effect, since all three parameters and their modulation by glucose can be reconstituted upon glucose addition to cells. Otto Warburg proposed that the decrease in oxidative phosphorylation activity was due to dysfunctional mitochondria. Here, we show that in our model upon induction of the Warburg effect, the decrease of mitochondrial oxidative phosphorylation is not due to dysfunctional mitochondria but to a decrease in mitochondrial biogenesis. Upon growth and while mitochondrial biogenesis is strongly decreased, mitochondria are diluted in the daughter cells. This result is in good agreement with a number of studies showing that mitochondrial are not dysfunctional in a number of cancer cells since their oxidative phosphorylation activity can be increased (4). However, this does not preclude that in

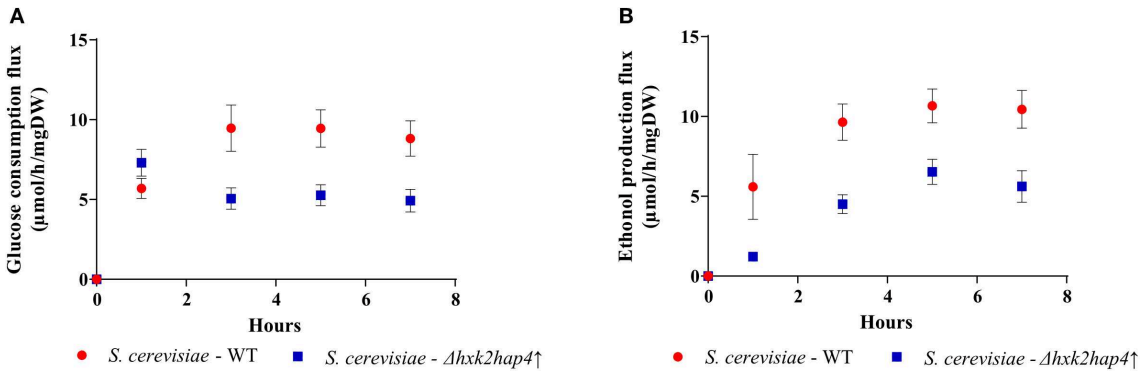

FIGURE 7 | Glucose consumption and ethanol production fluxes. **(A)** The glucose consumption flux was calculated from glucose concentration in the culture medium and the amount of cells for each time point. Results shown represent means of at least four separate experiments ± SD. **(B)** The ethanol production flux was calculated from ethanol concentration in the culture medium and the amount of cells for each time point. Results shown represent means of at least four separate experiments ± SD.

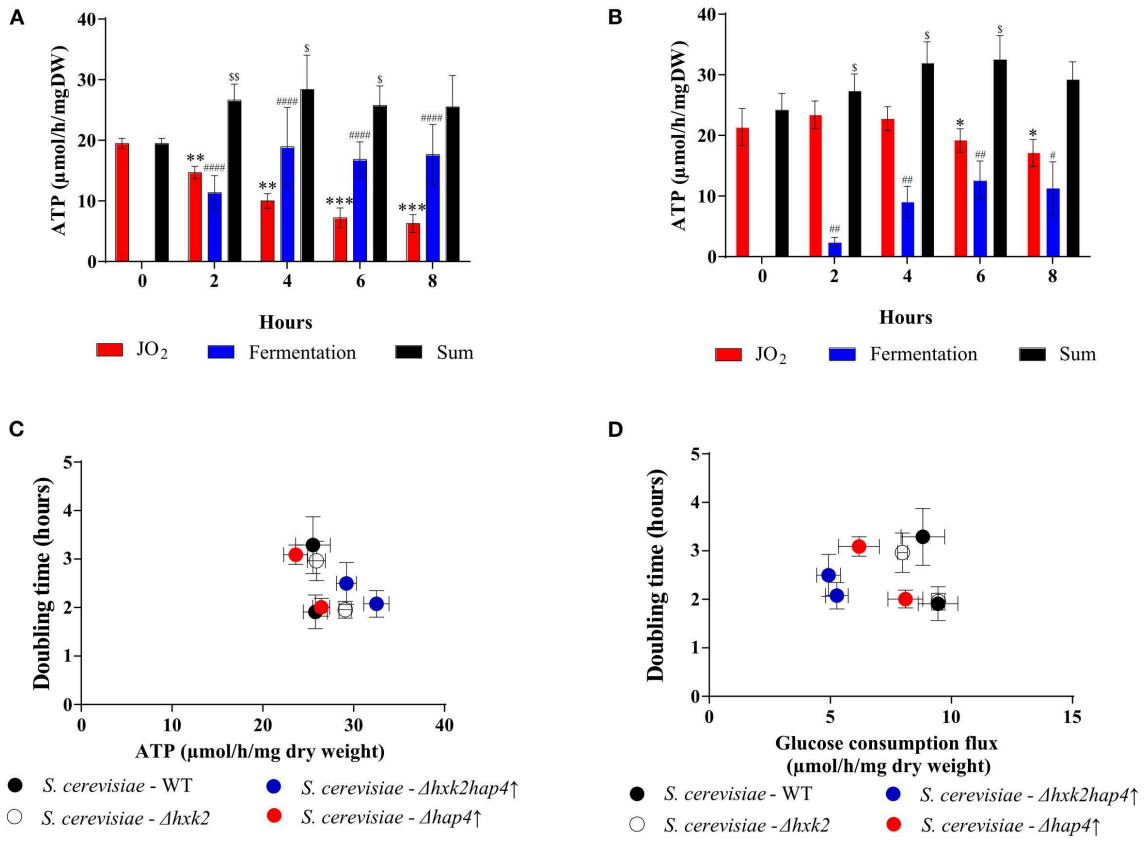

FIGURE 8 | Effect of glucose on ATP synthesis flux in the different strains. ATP synthesis flux was calculated from the respiratory rate and the ethanol production flux according to the oxidation balance-sheet: ½ O_2 = 1,5 ATP for respiratory rate; 1 EtOH = 2 ATP for fermentation to **(A)** *S. cerevisiae* - WT and **(B)** *S. cerevisiae* - Δ*hxk2hap4*↑. **(C)** Growth as a function of ATP synthesis flux at T6 and T8. **(D)** Growth as a function of glucose consumption flux at T6 and T8. For each strain, in the presence of glucose, doubling times were calculated between 4 and 6 h and then between 6 and 8 h after glucose addition in the medium. (•) *S. cerevisiae* WT, (•) Δ*hap4*↑, (○) Δ*hxk2*, (•) Δ*hxk2hap4*↑. For each condition values are compared to the corresponding T0 and the *p*-value is represented as * for JO2; # for Fermentation; $ for Sum.

some cases mitochondria cannot be dysfunctional since it has been shown that in some cancer cell line, succino-dehydrogenase was mutated and mostly inactive (49–52). The point here is that there is no need for mitochondria to be dysfunctional to evidence a Warburg effect. We next investigated the link between oxidative phosphorylation repression and the increase

in growth rate. We were able to uncouple growth rate and oxidative phosphorylation repression by deleting Hxk2p and overexpressing Hap4p, indicating that both the maintenance of mitochondrial biogenesis and the loss of *Hxk2* function are necessary for this uncoupling. Since glycolysis is maintained in Δ*hxk2* cells, it is tempting to speculate that the transcription factor function of *hxk2* is involved here. The use of mutant cells as well as Crabtree negative cells allowed us to show that there is no direct link between the decrease in oxidative phosphorylation activity and the increase in growth rate. Indeed, when oxidative phosphorylation activity is maintained upon glucose addition to cells there is a clear increase in growth rate, indicating no correlation between both parameters. This indicates that growth rate is not controlled by the modulation of energetic metabolism but rather depends on the presence of glucose. Whether glucose here acts as a signaling molecule or as a substrate of biosynthetic pathways remains to be determined. However, this is no easy task since it seems that in terms of fluxes, the flux through biosynthetic pathways is minor compared to the flux through glycolysis. Last, ATP synthesis fluxes in the presence of absence of a Warburg effect were calculated in our cellular models from fermentation and oxidative phosphorylation fluxes. We were able to show that ATP synthesis fluxes do not control cell growth. This experimental result is in accordance with previous calculations that suggest that the amount of ATP required for cell growth and division may be far lower than that required for basal cellular maintenance (53). Consequently, one can conclude that the growth-promoting role of the Warburg effect does not go through an increase in ATP synthesis fluxes.

In recent studies tumor energy metabolism has been assessed under more physiological concentrations of glucose and hypoxic conditions. It has been shown that lower mitochondrial biogenesis, deficient HIF-1α/mutant p53 interaction, and development of a pseudohypoxic state under normoxia were the apparent biochemical mechanisms underlying glycolysis activation and OxPhos downregulation in HeLa-M cells (54). Further, decreasing glucose concentration down to 2.5 mM restrains the Warburg phenotype, in hypoxic HeLa cell cultures and microspheroids (55). This clearly indicates that both parameters are crucial for the study of the Warburg effect in mammalian cells and should be considered more often.

In this paper, we show that the cell energy metabolism reorganization observed upon de Warburg effect is not mandatory for an increase in cell growth. Further, maintenance of oxidative phosphorylation activity does not affect the glucose growth promoting effect that occurs at various glycolysis rate. Last, cell ATP synthesis flux is shown not to control the growth rate. A number of reports in human cancer cells have pointed out a quite variable mitochondrial content in these cells. Indeed, while some studies demonstrate a reduction of oxidative phosphorylation capacity in different types of cancer cells, other investigations revealed contradictory modifications with the upregulation of oxidative phosphorylation components and a larger dependency of cancer cells on oxidative energy substrates for anabolism and energy production (56). Studying these cells in terms of cell growth and ATP synthesis flux in normoxia and normoglycemia would be of great interest to unravel the added value of the Warburg effect in cell proliferation.

DATA AVAILABILITY STATEMENT

All datasets generated for this study are included in the article/**Supplementary Material**.

AUTHOR CONTRIBUTIONS

CB, NH, and SC designed and performed the experiments. CB, NH, SC, MR, SR, and AD analyzed the corresponding results. CB and NH wrote the paper with SR, MR, and AD. All authors contributed to the article and approved the submitted version.

FUNDING

This work was supported by the CNRS (Conseil National de la Recherche Scientifique), the Comité de Dordogne & Gironde de la Ligue Nationale Contre le Cancer, The Fondation ARC pour la recherche sur le Cancer, the Plan cancer 2014-2019 No BIO 2014 06, The ANR. This project has been funded with support of the European Commission. This publication reflects the view only of the authors, and the Commission cannot be held responsible for any use which may be made of the information contained therein.

ACKNOWLEDGMENTS

The authors are grateful to all members of the Cell Energetic Metabolism team for discussions and proofreading of this manuscript.

SUPPLEMENTARY MATERIAL

The Supplementary Material for this article can be found online at: https://www.frontiersin.org/articles/10.3389/fonc.2020.01333/full#supplementary-material

Supplementary Figure 1 | Induction of the Warburg effect in *S. cerevisiae* Δ*hxk2*. The growth medium of *S. cerevisiae* was supplemented with 60 mM of glucose at T0 (■ Δ*hxk2*) and (**x** WT) or not (• Δ*hxk2*) and (+ WT). **(A)** Growth was followed for 8 h. Results shown are means of at least five separate experiments ± SD. **(B)** The respiratory rate was followed for 8 h. Results shown represent means of at least five separate experiments ± SD. **(C)** Glucose consumption (• Δ*hxk2*) or (**x** WT) and ethanol production (▲ Δ*hxk2*) or (**x** WT) were quantified. Results shown represent means of at least seven separate experiments ± SD.

Supplementary Figure 2 | Induction of the Warburg effect in *S. cerevisiae* Δ*hap4*↑. The growth medium of *S. cerevisiae* was supplemented with 60 mM of glucose at T0 (■ Δ*hap4*↑) and (**x** WT) or not (• Δ*hap4*↑) and (+ WT). **(A)** Growth was followed for 8 h. Results shown are means of at least five separate experiments ± SD. **(B)** The respiratory rate was followed for 8 h. Results shown represent means of at least five separate experiments ± SD. **(C)** Glucose consumption (• Δ*hap4*↑) or (**x** WT) and ethanol production (▲ Δ*hap4*↑) or (**x** WT) were quantified. Results shown represent means of at least seven separate experiments ± SD.

REFERENCES

1. Warburg O. The metabolism of carcinoma cells. *Cancer Res.* (1925) 9:148–63. doi: 10.1158/jcr.1925.148
2. Warburg O. On the origin of cancer cells. *Science.* (1956) 123:309–14. doi: 10.1126/science.123.3191.309
3. Crabtree HG. Observations on the carbohydrate metabolism of tumours. *Biochem J.* (1929) 23:536–45. doi: 10.1042/bj0230536
4. Rossignol R, Gilkerson R, Aggeler R, Yamagata K, Remington SJ, Capaldi RA. Energy substrate modulates mitochondrial structure and oxidative capacity in cancer cells. *Cancer Res.* (2004) 64:985–93. doi: 10.1158/0008-5472.CAN-03-1101
5. Rodriguez-Enriquez S, Gallardo-Perez JC, Marin-Hernandez A, Carreno-Fuentes L, Maldonado-Lagunas V, Moreno-Sanchez R. Energy metabolism transition in multi-cellular human tumor spheroids. *J Cell Physiol.* (2008) 216:189–97. doi: 10.1002/jcp.21392
6. Smolková K, Bellance N, Scandurra F, Génot E, Gnaiger E, Plecita-Hlavata L, et al. Mitochondrial bioenergetic adaptations of breast cancer cells to aglycemia and hypoxia. *J bioenerg Biomembr.* (2010) 42:55–67. doi: 10.1007/s10863-009-9267-x
7. Moreno-Sanchez R, Rodriguez-Enriquez S, Marin-Hernandez A, Saavedra E. Energy metabolism in tumor cells. *FEBS J.* (2007) 274:1393–418. doi: 10.1111/j.1742-4658.2007.05686.x
8. Martin M, Beauvoit B, Voisin PJ, Canioni P, Guerin B, Rigoulet M. Energetic and morphological plasticity of C6 glioma cells grown on 3-D support; effect of transient glutamine. *J Bioenerg Biomembr.* (1998) 30:565–78. doi: 10.1023/A:1020584517588
9. Guppy M, Leedman P, Zu X, Russell V. Contribution by different fuels and metabolic pathways to the total ATP turnover of proliferating MCF-7 breast cancer cells. *Biochem J.* (2002) 364:309–15. doi: 10.1042/bj3640309
10. Pasdois P, Deveaud C, Voisin P, Bouchaud V, Rigoulet M, Beauvoit B. Contribution of the phosphorylable complex i in the growth phase-dependent respiration of C6 glioma cells *in vitro*. *J Bioenerg Biomembr.* (2003) 35:439–50. doi: 10.1023/A:1027391831382
11. Rodríguez-Enríquez S, Vital-González PA, Flores-Rodríguez FL, Marín-Hernández A, Ruiz-Azuara L, Moreno-Sánchez R. Control of cellular proliferation by modulation of oxidative phosphorylation in human and rodent fast-growing tumor cells. *Toxicol Appl Pharmacol.* (2006) 215:208–17. doi: 10.1016/j.taap.2006.02.005
12. Sonveaux P, Végran F, Schroeder T, Wergin MC, Verrax J, Rabbani ZN, et al. Targeting lactate-fueled respiration selectively kills hypoxic tumor cells in mice. *J Clin Investig.* (2008) 118:3930–42. doi: 10.1172/JCI36843
13. Díaz-Ruiz R, Avéret N, Araiza D, Pinson B, Uribe-Carvajal S, Devin A, et al. Mitochondrial oxidative phosphorylation is regulated by fructose 1,6-bisphosphate: a possible role in crabtree effect induction? *J Biol Chem.* (2008) 283:26948–55. doi: 10.1074/jbc.M800408200
14. Lemus MR, Roussarie E, Hammad N, Mougeolle A, Ransac S, Issa R, et al. The role of glycolysis-derived hexose phosphates in the induction of the crabtree effect. *J Biol Chem.* (2018) 293:12843–54. doi: 10.1074/jbc.RA118.003672
15. Locasale JW, Cantley LC. Review metabolic flux and the regulation of mammalian cell growth. *Cell Metab.* (2011) 14:443–51. doi: 10.1016/j.cmet.2011.07.014
16. Lunt SY, Vander Heiden MG. Aerobic glycolysis: meeting the metabolic requirements of cell proliferation. *Annu Rev Cell Dev Biol.* (2011) 27:441–64. doi: 10.1146/annurev-cellbio-092910-154237
17. Wu W, Zhao S. Metabolic changes in cancer: beyond the warburg effect. *Acta Biochim Biophys Sin.* (2013) 45:18–26. doi: 10.1093/abbs/gms104
18. Diaz-ruiz R, Uribe-carvajal S, Devin A, Rigoulet M. Tumor cell energy metabolism and its common features with yeast metabolism. *BBA - Rev Cancer.* (2009) 1796:252–65. doi: 10.1016/j.bbcan.2009.07.003
19. Diaz-Ruiz R, Rigoulet M, Devin A. The warburg and crabtree effects: On the origin of cancer cell energy metabolism and of yeast glucose repression. *Biochim Biophys Acta - Bioenerg.* (2011) 1807:568–76. doi: 10.1016/j.bbabio.2010.08.010
20. Gari E, Piedrafita L, Aldea M, Herrero E. A set of vectors with a tetracycline-regulatable promoter system for modulated gene expression in *Saccharomyces cerevisiae*. *Yeast.* (1997) 13:837–48. doi: 10.1002/(SICI)1097-0061(199707)13:9<837::AID-YEA145>3.0.CO;2-T
21. Chevtzoff C, Yoboue ED, Galinier A, Casteilla L, Daignan-Fornier B, Rigoulet M, et al. Reactive oxygen species-mediated regulation of mitochondrial biogenesis in the yeast saccharomyces cerevisiae. *J Biol Chem.* (2010) 285:1733–42. doi: 10.1074/jbc.M109.019570
22. Beauvoit B, Rigoulet M, Bunoust O, Raffard G, Canioni P, Guérin B. Interactions between glucose metabolism and oxidative phosphorylations on respiratory-competent *Saccharomyces cerevisiae* cells. *Eur J Biochem.* (1993) 214:163–72. doi: 10.1111/j.1432-1033.1993.tb17909.x
23. Dejean L, Beauvoit B, Guérin B, Rigoulet M. Growth of the yeast *Saccharomyces cerevisiae* on a non-fermentable substrate: Control of energetic yield by the amount of mitochondria. *Biochim Biophys Acta - Bioenerg.* (2000) 1457:45–56. doi: 10.1016/S0005-2728(00)00053-0
24. Laemmli UK. Cleavage of structural proteins during the assembly of the head of bacteriophage T4. *Nature.* (1970) 227:680–5. doi: 10.1038/227680a0
25. Warburg O. On respiratory impairment in cancer cells. *Science.* (1956) 124:269–70.
26. Rickey TM, Lewin AS. Extramitochondrial citrate synthase activity in bakers' yeast. *Mol Cell Biol.* (1986) 6:488–93. doi: 10.1128/MCB.6.2.488
27. Lewin AS, Hines V, Small GM. Citrate synthase encoded by the CIT2 gene of *Saccharomyces cerevisiae* is peroxisomal. *Mol Cell Biol.* (1990) 10:1399–405. doi: 10.1128/MCB.10.4.1399
28. Van Rossum HM, Kozak BU, Niemeijer MS, Duine HJ, Luttik MAH, Boer VM, et al. Alternative reactions at the interface of glycolysis and citric acid cycle in *Saccharomyces cerevisiae*. *FEMS Yeast Res.* (2016) 16:1–13. doi: 10.1093/femsyr/fow017
29. Olesen J, Hahn S, Guarente L. Yeast HAP2 and HAP3 activators both bind to the CYC1 upstream activation site, UAS2, in an interdependent manner. *Cell.* (1987) 51:953–61. doi: 10.1016/0092-8674(87)90582-4
30. Forsburg SL, Guarente L. Mutational analysis of upstream activation sequence 2 of the CYC1 gene of *Saccharomyces cerevisiae*: a HAP2-HAP3-responsive site. *Mol Cell Biol.* (1988) 8:647–54. doi: 10.1128/MCB.8.2.647
31. Hahn S, Pinkham J, Wei R, Miller R, Guarente L. The HAP3 regulatory locus of *Saccharomyces cerevisiae* encodes divergent overlapping transcripts. *Mol Cell Biol.* (1988) 8:655–63. doi: 10.1128/MCB.8.2.655
32. Lascaris R, Bussemaker HJ, Boorsma A, Piper M, van der Spek H, Grivell L, et al. Hap4p overexpression in glucose-grown *Saccharomyces cerevisiae* induces cells to enter a novel metabolic state. *Genome Biol.* (2003) 4:R3. doi: 10.1186/gb-2002-4-1-r3
33. Dang V-D, Valens M, Bolotin-Fukuhara M, Daignan-Fornier B. A Genetic screen to isolate genes regulated by the yeast CCAAT-box binding protein Hap2p. *Yeast.* (1994) 10:1273–83. doi: 10.1002/yea.320101004
34. Fondrat C, Kalogeropoulos A. Approaching the function of new genes by detection of their potential upstream activation sequences in *Saccharomyces cerevisiae*: application to chromosome III. *Curr Genet.* (1994) 25:396–406. doi: 10.1007/BF00351777
35. Buschlen S, Amillet JM, Guiard B, Fournier A, Marcireau C, Bolotin-Fukuhara M. The *S. cerevisiae* HAP complex, a key regulator of mitochondrial function, coordinates nuclear and mitochondrial gene expression. *Comp Funct Genomics.* (2003) 4:37–46. doi: 10.1002/cfg.254
36. Randez-gil F, Sanz P, Entian K, Prieto JA. Carbon source-dependent phosphorylation of hexokinase PII and its role in the glucose-signaling response in yeast. *Mol Cell Biol.* (1998) 18:2940–8. doi: 10.1128/MCB.18.5.2940
37. Rodriguez A, de la Cera T, Herrero P, Moreno F. HXK2 genes of *Saccharomyces cerevisiae*. *Biochem J.* (2001) 355:625–31. doi: 10.1042/bj3550625
38. Ahuatzi D, Herrero P, Cera T, Moreno F. The glucose-regulated nuclear localization of hexokinase 2 in *Saccharomyces cerevisiae* is mig1-dependent. *J Biol Chem.* (2004) 279:14440–6. doi: 10.1074/jbc.M313431200
39. Ahuatzi D, Riera A, Pela R, Herrero P, Moreno F. Hxk2 regulates the phosphorylation state of Mig1 and therefore its nucleocytoplasmic distribution. *J Biol Chem.* (2007) 282:4485–93. doi: 10.1074/jbc.M606854200
40. Ohnishi T. Factors controlling the occurrence of site i phosphorylation in *C. Utilis* mitochondria. *FEBS Lett.* (1972) 24:305–9. doi: 10.1016/0014-5793(72)80378-8

41. Coles CJ, Gutman M, Singer TP. On the reaction of piericidin A with the reduced nicotinamide adenine dinucleotide dehydrogenase of *Candida utilis*. *J Biol Chem.* (1974) 249:3814–8.
42. Avéret N, Jobin ML, Devin A, Rigoulet M. Proton pumping complex I increases growth yield in *Candida utilis*. *Biochim Biophys Acta - Bioenerg.* (2015) 1847:1320–6. doi: 10.1016/j.bbabio.2015.07.001
43. Duszynski J, Bogucka K, Letko G, Kuster U, Kunz W, Wojtczak L. Relationship between the energy cost of Atp transport and Atp synthesis in mitochondria. *BBA - Bioenerg.* (1981) 637:217–23. doi: 10.1016/0005-2728(81)90160-2
44. Stoner CD. Determination of the P/2e- stoichiometries at the individual coupling sites in mitochondrial oxidative phosphorylation. *J Biol Chem.* (1987) 262:10445–53.
45. Fitton V, Rigoulet M, Ouhabi R, Guérin B. Mechanistic stoichiometry of yeast mitochondrial oxidative phosphorylation. *Biochemistry.* (1994) 33:9692–8. doi: 10.1021/bi00198a039
46. Ouhabi R, Boue-Grabot M, Mazat J-P. Mitochondrial ATP synthesis in permeabilized cells : assessment of the ATP/O values *in Situ*. *Anal Biochem.* (1998) 263:169–75. doi: 10.1006/abio.1998.2776
47. Nosek J, Fukuhara H. NADH dehydrogenase subunit genes in the mitochondrial DNA of yeasts. *J Bacteriol.* (1994) 176:5622–30. doi: 10.1128/JB.176.18.5622-5630.1994
48. Friedrich T, Steinmtiller K, Weiss H. The proton-pumping respiratory complex I of bacteria and mitochondria and its homologue in chloroplasts. *FEBS Lett.* (1995) 367:107–11. doi: 10.1016/0014-5793(95)00548-N
49. Italiano A, Chen C, Sung Y, Singer S, DeMatteo RP, LaQuaglia MP, et al. SDHA loss of function mutations in a subset of young adult wild-type gastrointestinal stromal tumors. *BMC Cancer.* (2012) 12:1–7. doi: 10.1186/1471-2407-12-408
50. Comono-Méndez I, de Cubas AA, Bernal C, Alvarez-Escola C, Sanchez-Malo C, Ramirez-Tortosa CL, et al. Tumoral EPAS1 (HIF2A) mutations explain sporadic pheochromocytoma and paraganglioma in the absence of erythrocytosis. *Hum Mol Genet.* (2013) 22:2169–76. doi: 10.1093/hmg/ddt069
51. Clark GR, Sciacovelli M, Gaude E, Walsh DM, Kirby G, Simpson MA, et al. Mutations presenting with pheochromocytoma. *JCEM.* (2014) 99:2046–50. doi: 10.1210/jc.2014-1659
52. Tsai T-H, Lee W-Y. Succinate dehydrogenase – deficient renal cell. *Arch Pathol Lab Med.* (2019) 143:643–7. doi: 10.5858/arpa.2018-0024-RS
53. Kilburn DG, Lilly MD, Webb FC. The energetics of mammalian cell growth. *J Cell Sci.* (1969) 4:645–54.
54. Hernández-Reséndiz I, Gallardo-Pérez JC, Lopez-Macay A, Robledo-Cadena DX, Garcia-Villa E, Gariglio P, et al. Mutant p53 R248Q downregulates oxidative phosphorylation and upregulates glycolysis under normoxia and hypoxia in human cervix cancer cells. *J Cell Physiol.* (2019) 234:5524–36. doi: 10.1002/jcp.27354
55. Marin-Hernandez A, Gallardo-Pérez JC, Hernández-Reséndiz I, Del Mazo-Monsalvo I, Robledo-Cadena DX, Moreno-Sanchez R, et al. Hypoglycemia enhances epithelial-mesenchymal transition and invasiveness, and restrains the warburg phenotype, in hypoxic HeLa cell cultures and microspheroids. *J Cell Physiol.* (2017) 232:1346–59. doi: 10.1002/jcp.25617
56. Jose C, Bellance N, Rossignol R. Choosing between glycolysis and oxidative phosphorylation : A tumor' s dilemma? *BBA - Bioenerg.* (2011) 1807:552–61. doi: 10.1016/j.bbabio.2010.10.012

Conflict of Interest: The authors declare that the research was conducted in the absence of any commercial or financial relationships that could be construed as a potential conflict of interest.

frontiers in Oncology

ORIGINAL RESEARCH
published: 19 August 2020
doi: 10.3389/fonc.2020.01277

In situ Metabolic Profiling of Ovarian Cancer Tumor Xenografts: A Digital Pathology Approach

Ilaria Piga[1,2†], *Martina Verza*[1†], *Francesca Montenegro*[2], *Giorgia Nardo*[1], *Elisabetta Zulato*[1], *Tiziana Zanin*[3], *Paola Del Bianco*[4], *Giovanni Esposito*[1†] and *Stefano Indraccolo*[1*†]

[1] Immunology and Molecular Oncology Unit, Istituto Oncologico Veneto, IOV—IRCCS, Padua, Italy, [2] Department of Surgery, Oncology and Gastroenterology, University of Padua, Padua, Italy, [3] Pathology Unit, Istituto Oncologico Veneto, IOV—IRCCS, Padua, Italy, [4] Clinical Research Unit, Istituto Oncologico Veneto, IOV—IRCCS, Padua, Italy

Metabolic profiling of cancer is a rising interest in the field of biomarker development. One bottleneck of its clinical exploitation, however, is the lack of simple and quantitative techniques that enable to capture the key metabolic traits of tumor from archival samples. In fact, liquid chromatography associated with mass spectrometry is the gold-standard technique for the study of tumor metabolism because it has high levels of accuracy and precision. However, it requires freshly frozen samples, which are difficult to collect in large multi-centric clinical studies. For this reason, we propose here to investigate a set of established metabolism-associated protein markers by exploiting immunohistochemistry coupled with digital pathology. As case study, we quantified expression of MCT1, MCT4, GLS, PHGDH, FAS, and ACC in 17 patient-derived ovarian cancer xenografts and correlated it with survival. Among these markers, the glycolysis-associated marker MCT4 was negatively associated with survival of mice. The algorithm enabling a quantitative analysis of these metabolism-associated markers is an innovative research tool that can be exported to large sets of clinical samples and can remove the variability of individual interpretation of immunohistochemistry results.

Keywords: ovarian cancer, metabolism, IHC, digital pathology, MCT4

OPEN ACCESS

Edited by:
Sara Rodriguez-Enriquez, Instituto Nacional de Cardiología, Mexico

Reviewed by:
Domenica Scumaci, Magna Graecia University of Catanzaro, Italy
Angela Ostuni, University of Basilicata, Italy

***Correspondence:**
Stefano Indraccolo
stefano.indraccolo@unipd.it

†These authors have contributed equally to this work

Specialty section:
This article was submitted to Cancer Metabolism, a section of the journal Frontiers in Oncology

Received: *24 February 2020*
Accepted: *19 June 2020*
Published: *19 August 2020*

Citation:
Piga I, Verza M, Montenegro F, Nardo G, Zulato E, Zanin T, Del Bianco P, Esposito G and Indraccolo S (2020) In situ Metabolic Profiling of Ovarian Cancer Tumor Xenografts: A Digital Pathology Approach. Front. Oncol. 10:1277. doi: 10.3389/fonc.2020.01277

INTRODUCTION

Metabolic alterations are recognized hallmarks of cancer (1) and have been described in thousands of publications. Key metabolic alterations described in tumors involve glycolysis, glutamine and lipid metabolism, and they contribute to generate ATP that is required for cell proliferation and simultaneously represents a source for macromolecule synthesis and for the replenishment of reactive oxygen species scavenging systems (2). From a general perspective in the context of solid tumors, we can distinguish metabolic alterations of cancer cells from those of the stroma, including endothelial cells (3), fibroblasts (4), and adipocytes (5), as well as those of mobile cells, such as lymphocytes, macrophages, and specialized subpopulations of myeloid cells (6). These two components interact with each other and with the extracellular matrix, and these interactions can take the form of either metabolic competition or metabolic symbiosis. An additional feature of tumor metabolism is represented by its heterogeneity, which can be accounted for by (1) cancer

cell autonomous factors, (2) local microenvironment factors such as hypoxia and acidosis, and (3) external factors, including diet, the microbiome, and certain drugs that can generate signals which modulate metabolism in the tumor microenvironment (7).

Advanced technologies, including metabolomics (8) and metabolic flux analysis (9), are key to decode the heterogeneous metabolic preferences and dependencies of tumors *in vivo,* but they can only be performed in a very limited number of patients given the high costs of the equipment and the level of specialization of personnel involved in this type of analysis. Moreover, these techniques do not enable to study intra-tumor metabolic heterogeneity as they assess levels of metabolites in whole tumor lysates or track the incorporation of a labeled substrate into downstream metabolites.

Parallel to these high-tech approaches, which remain fundamental for basic research studies, it is important to evaluate *in situ* biomarkers of dysregulated cancer metabolic pathways which could be analyzed in standard laboratories on archival samples. One possibility is represented by certain transporters or enzymes which, according to many studies, are key for the activity of the underlying metabolic pathway, such as monocarboxylate transporter 4 (MCT4) for glycolysis (10, 11), glutaminase (GLS) for glutamine metabolism (12), and a few others. The protein expression levels of these markers can be easily assessed by immunohistochemistry (IHC), the signal being digitalized and quantified by digital pathology techniques at a reasonable cost per sample (13). The integration of signal quantification into appropriate mathematical models can then be used to define cutoff values in order to stratify samples into biomarker positive or negative and eventually investigate their prognostic or predictive value.

In this study, we tested this hypothesis by staining, for a panel of representative metabolism-associated markers, a set of patient-derived ovarian cancer xenografts (PDXs) and correlated the quantitative expression of these markers with the survival of mice bearing these tumors. Ovarian cancer has a dismal prognosis in most patients because it is often diagnosed at a late stage and cancer cells often become resistant to platinum-based chemotherapy (14). The metabolic traits of ovarian cancer have been reported in several studies which, however, focused on one single aspect of metabolism (15–17). Moreover, there are studies showing that resistance to chemotherapy can be accounted for by certain metabolic features of ovarian cancer cells (18, 19). Stimulated by these considerations, we present here an *in situ* metabolic profiling of ovarian cancer xenografts. The results obtained in this pilot study are hypothesis generating and will be further investigated in patients' samples.

MATERIALS AND METHODS

Patient Data

The studies involving human participants were reviewed and approved by the IOV Institutional Review Board and Ethics Committee (EM 23/2017) and were performed in accordance with the Declaration of Helsinki. The patients/participants provided their written informed consent to participate in this study. Patient-derived xenografts were derived from cancer cells contained in ascitic effusions and obtained from patients bearing epithelial ovarian cancer (EOC). The clinical samples were obtained from either newly diagnosed patients or relapsing patients with EOC at different stages and grades (**Table 1**).

TABLE 1 | Clinical features of the patient-derived xenograft (PDX) utilized in this study.

Sample ID	Histotype	Stage	Grade	Diagnosis/relapse
PDOVCA 14	Endometrioid	3C	G1	Diagnosis
PDOVCA 15	Serous-papillary	4	G3	Relapse
PDOVCA 17	Serous-papillary	3C	G3	Diagnosis
PDOVCA 24	Serous-papillary	3A	G3	Relapse
PDOVCA 36	Serous	4	G3	Relapse
PDOVCA 39	Serous-papillary	3B	G2	Relapse
PDOVCA 44	Serous-papillary	3C	G3	Diagnosis
PDOVCA 49	Serous-papillary	3A	G1	Relapse
PDOVCA 52	Serous-papillary	3C	G3	Diagnosis
PDOVCA 53	Endometrioid	3C	G3	Relapse
PDOVCA 54	Serous-papillary	4	G1	Relapse
PDOVCA 57	Serous-papillary	3C	G3	Relapse
PDOVCA 58	Serous-papillary	3A	G3	Relapse
PDOVCA 62	Serous-papillary	3C	G3	Relapse
PDOVCA 69	Serous-papillary	3C	G3	Relapse
PDOVCA 70	Serous-papillary	3C	G3	Relapse
PDOVCA 82	Serous-papillary	3C	G3	Relapse

Histotype, stage, and grade refer to the patient samples from whom PDXs were derived. Diagnosis/relapse indicates that PDXs were established from ascitic fluid samples obtained at diagnosis or relapse, respectively.

Generation of Ovarian Xenografts

Tumor cells from the ascitic fluid were isolated as previously described (20). PDXs were obtained and propagated by injecting 1×10^6 tumor cells intraperitoneally into 8-week-old female NOD/SCID mice purchased from Charles River Laboratories (Wilmington, MA, USA) and housed in our specific pathogen-free animal facility. The animals developed solid tumors with a substantial ascitic component at different time points, depending on tumor engraftment and growth. At sacrifice, tumors were harvested by dissection, fixed in formalin, and embedded in paraffin for histology and immunohistochemistry analyses. All procedures involving animals and their care conformed to institutional guidelines that comply with national and international laws and policies (EEC Council Directive 86/609, OJ L 358, 12 December 1987). The animal study was reviewed and approved by the Italian Ministry of Health (n. 217/2013-B).

Histology and Immunohistochemistry

Three-micron-thick formalin-fixed, paraffin-embedded tumor samples were either stained with hematoxylin and eosin or processed for IHC. In this case, IHC was performed by using an automatic stainer BOND III (Leica Microsystems, Wetzlar, Germany) and by using the following antibodies according to the manufacturer's instructions: anti-ACC rabbit mAb (clone C83B10, dilution 1:100), anti-FAS rabbit mAb

(clone C20G5, dilution 1:100), anti-phospho-histone H3 (pHH3) rabbit polyclonal Ab (dilution 1:100), all from Cell Signaling Technology Danvers, Massachusetts, USA; anti-GLS rabbit mAb (clone EP7212, dilution 1:200), anti-PHGDH mouse mAb (clone Ab57030, dilution 1:100) both from Abcam, Cambridge, UK, anti-MCT1 rabbit polyclonal Ab (dilution 1:50; Millipore, Burlington, MA, USA), anti-MCT4 rabbit polyclonal Ab (dilution 1:300; Santa Cruz Biotechnology, Dallas, TX, USA), and anti-mouse CD31 rat mAb (clone SZ31, dilution 1:20; DIANOVA GmbH-Hamburg, Germany).

Image Acquisition and Analysis

Tumor representation and quality of staining were initially evaluated by one experienced pathologist (GE). The slides were digitally acquired at ×20 magnification by the Aperio CS2 (Leica Biosystems, Wetzlar, Germany), and the evaluation of the IHC score was assessed through the Scanscope Image Analysis software (ImageScope v12.4.0.708). On the basis on their localization, the different markers were analyzed by using the Aperio membrane algorithm v9 (MCT1, MCT4), the Aperio cytoplasmic algorithm v2 (GLS, FAS, PHGDH, and ACC), the Aperio nuclear algorithm (pHH3), and the microvessel analysis v1 (CD31). The Aperio Genie Classifier was trained to recognize tumor tissue, stroma, and background (glass) and then combined with Aperio Membrane v9 and Aperio Cytoplasmic v9. The results provided the percentage of cells with different expressions of proteins classified as 3+ (highly positive), 2+ (intermediate positive), 1+ (low positive), and 0 (negative). In the case of GLS in view of the granular pattern of cytoplasmic staining obtained a two-tier classification system was used: 0 (negative) and 1 (positive). The sum of the percentage of marker-positive cells for these tiers equals 100%. The digital quantification performed by the software was confirmed by the pathologist.

Immunoblotting Assay

Whole-cell lysates (1×10^6 cells) were prepared in RIPA lysis buffer (Cell Signaling Technology) containing a protease and a phosphatase inhibitor cocktail (Sigma Aldrich, St. Louis, MO, USA). Proteins were quantified using Quantum Protein Assay (EuroClone, Milan, Italy), and about 30 μg were denatured and loaded in a midi polyacrylamide gel 4–12% (Life Technologies). Separated proteins were transferred for 2.5 h at 400 mA on a nitrocellulose membrane (GE Health Care, Glattbrugg, Switzerland). Membranes were saturated overnight at 4°C with Tris-buffered saline−0.1% Tween−5% milk and then incubated with primary antibody, according to the manufacturer's instructions. Immunoprobing was performed using the same antibody described for the IHC assay, and it was followed by hybridization with a horseradish peroxidase-conjugated anti-rabbit or anti-mouse Ab (Perkin Elmer, Waltham, MA, USA). The antigens were identified by luminescent visualization using Western Lightning Plus ECL reagents (Perkin Elmer, Waltham, MA, USA), and signal intensity was detected using UVITEC Alliance Software (Cambridge, UK). Protein expression was assessed and normalized to actin (Sigma Aldrich) as the housekeeping gene.

Statistical Analysis

Data were analyzed with RStudio (RStudio: Integrated Development for R. RStudio Inc., Boston, MA, US). The quantitative variables were summarized as median and interquartile range. A descriptive analysis of the strength of the relationship between the levels of all the considered markers was performed using Spearman's rank correlation coefficient. The survival times were estimated with the Kaplan–Meier method and compared among groups of markers with the log-rank test. The *P*-values were adjusted for multiple comparisons using the Benjamini–Hochberg method.

RESULTS

Selection of Metabolism-Associated Markers and Panel Setup

We selected the following markers to be included in our IHC panel: MCT1, MCT4, GLS, phosphoglycerate dehydrogenase (PHGDH), FAS, and ACC. These markers identify key transporters or enzymes involved in glycolysis (MCT1, MCT4) and in glutamine (GLS), glycine (PHGDH), and fatty acid metabolism (FAS and ACC). For all markers analyzed but GLS, the algorithm first identifies tumor cells and then quantifies the expression levels according to a four-tier classification system (0, 1+, 2+, and 3+) as described in the "MATERIALS AND METHODS" section. In the case of GLS, a two-tier classification system is used. Representative pictures showing the IHC score of two PDX samples stained with anti-MCT4 antibody are shown in **Figure 1**. For statistical analysis, for each sample we grouped the percentage of cells with 0/1+ and 2+/3+ values. The median value of the percentage of positive cells of all analyzed PDX samples was used to stratify them into two groups based on the expression of a given marker: samples whose quantitative value were above the median value were classified as "high" and those below as "low." The detailed results of marker expression in the 17 PDXs analyzed are presented in **Supplementary Tables 1**, **2**. Representative pictures of PDX samples stained for the six metabolism-associated markers are shown in **Figure 2**.

Association Between Markers

As the markers selected identify key metabolic processes, profiling PDX samples enabled us to investigate possible associations between the markers. This analysis disclosed that MCT4 was negatively associated with FAS ($r = -0.55$). In contrast, MCT1 and GLS1 were positively associated ($r = 0.41$), as well as FAS and GLS1 ($r = 0.31$) and FAS and ACC ($r = 0.32$). No other association was found between the other markers analyzed.

Association With Survival

Next, we investigated whether the expression of any of these markers was associated with survival in tumor-bearing mice. The survival of mice is defined by an ethical end-point, i.e., the time when mice have to be euthanized because they develop ascites or show signs of sufferance. In our set of samples, this parameter ranged from 33 to 222 days, depending on the PDX. No anti-tumor drug was administered to the mice in these experiments,

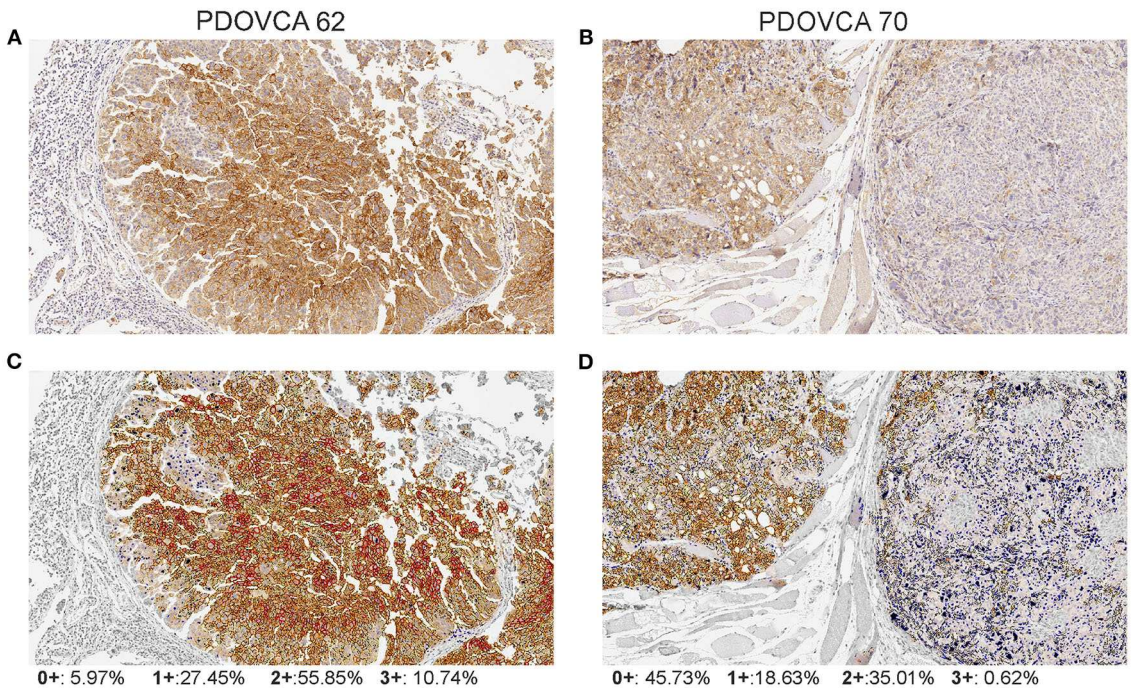

FIGURE 1 | Visualization of the Aperio membrane algorithm to quantify MCT4 expression in tumor. **(A,B)** Two representative samples of patient-derived xenograft with different levels of MCT4 expression (hematoxylin counterstain; original magnification ×20). **(C,D)** The same samples showing final a mark-up of the analyzed tissue. The algorithm utilized automatically detects and classifies cell membrane positivity as strong (3+/red), moderate (2+/orange), or weak (1+/yellow). Negative/0+ cells show only nuclear staining (blue). The gray areas were excluded from the analysis.

and survival time was calculated by averaging the survival of $n = 3$ mice per PDX. The results show that only high levels of MCT4 expression were associated with worse survival in this cohort. None of the other markers analyzed correlated with survival (**Figure 3**). We asked whether the reduced survival of mice bearing MCT4-positive tumors could be due to increased proliferation, as it is known that a link exists between this metabolic process and proliferation (21). We assessed mitotic cells and found that the expression of the pHH3 marker had a positive association with MCT4 ($r = 0.72$). Since lactate, which is exported by MCT4 from tumor cells, can modulate tumor angiogenesis (22), we stained PDX sections with the endothelial cell marker CD31 and calculated MVD. The results show a positive association between MCT4 and MVD ($r = 0.56$).

Validation of IHC Results

Finally, we sought to validate the IHC results by an orthogonal technique. To this end, we generated lysates from PDX cells freshly obtained from mice and performed Western blot analysis for the expression of MCT4, the only marker associated with survival in this study. In these experiments, we focused on four PDX samples bearing a high or a low expression of the marker considered, based on quantitative IHC analysis. In the case of the remaining PDXs, Western blot analysis could not be performed due to the lack of tumor lysates available for this assay. Albeit limited by the small number of PDXs analyzed, the results confirmed that the expression levels of the target protein assessed by the IHC-based marker quantification system substantially correlated with those detected in the corresponding tumor lysates by Western blot analysis (**Figure 4**).

DISCUSSION

Cancer cells often have increased glycolytic activity compared with normal tissues. In fact, normal cells convert glucose to pyruvate that enters the TCA cycle, whereas cancer cells reduce pyruvate to lactate in order to recycle NADH back to NAD+ to maintain the metabolic flux via glycolysis even in the presence of sufficient levels of oxygen, the so-called Warburg effect (23). This metabolic aberration is considered as a metabolic hallmark of many malignant tumors and, although energetically unfavorable, supports anabolic growth during nutrient limitation (24). This excess of lactate must be expelled from the tumor to the microenvironment in order to prevent cell death via intracellular acidosis. The principal transporter involved in this lactate efflux is MCT4, a member of the H+/monocarboxylate transporter family found to be overexpressed in many types of human cancers, including

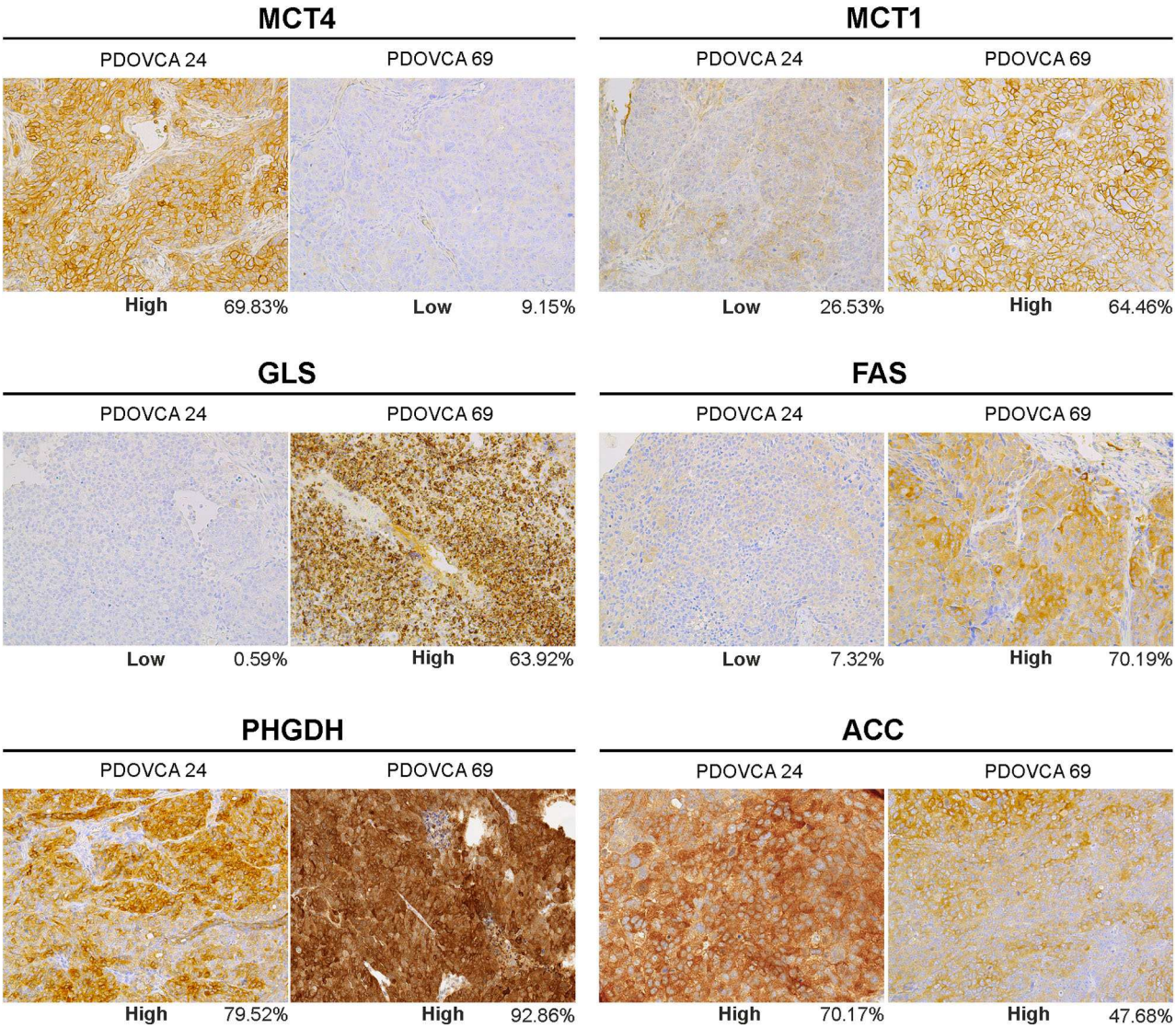

FIGURE 2 | Representative pictures of two patient-derived xenograft samples (PDOVCA 24 and PDOVCA 69) stained for the various metabolism-associated markers: MCT4, MCT1, GLS, FAS, PHGDH, and ACC (original magnification, ×20). The percentage below each panel indicates the sum of 2+ and 3+ values of the marker according to digital pathology analysis.

ovarian cancer (15). Notably, elevated MCT4 expression is associated with decreased overall survival in many cancer types (25).

It is interesting to note that, among the six metabolism-associated markers analyzed, only MCT4 expression was negatively associated with the survival of mice. Highly glycolytic tumors grew faster than poorly glycolytic tumors in these intraperitoneal PDX models, a result which is in line with our previous observations with subcutaneous xenografts of ovarian cancer cell lines (26). MCT4 expression in tumor sections also matched the MCT4 expression levels in cell lysates from PDX cells, confirming the specificity of the antibody used. Previous studies by our group also demonstrated the high correlation between MCT4 expression as evaluated by using this antibody and the glycolytic phenotype of tumor cells both *in vitro* and in mouse models (10). Cancer cells with high MCT4 expression proliferated faster than MCT4-negative cancer cells, according to the results of pHH3 expression in tumor sections. Moreover, the accelerated growth of high MCT4 PDX could also be accounted for by the effects of lactate on the tumor microenvironment, including the promotion of angiogenesis (27), as supported by the strong association between MVD and MCT4 markers. Understanding metabolic reprogramming of tumor cells is fundamental for understanding tumor drug resistance and developing anticancer therapy. We recently reported that glucose-addicted ovarian cancer samples yield better response to platinum-based chemotherapy compared with non-glucose-addicted tumors (19), thus marking the possible

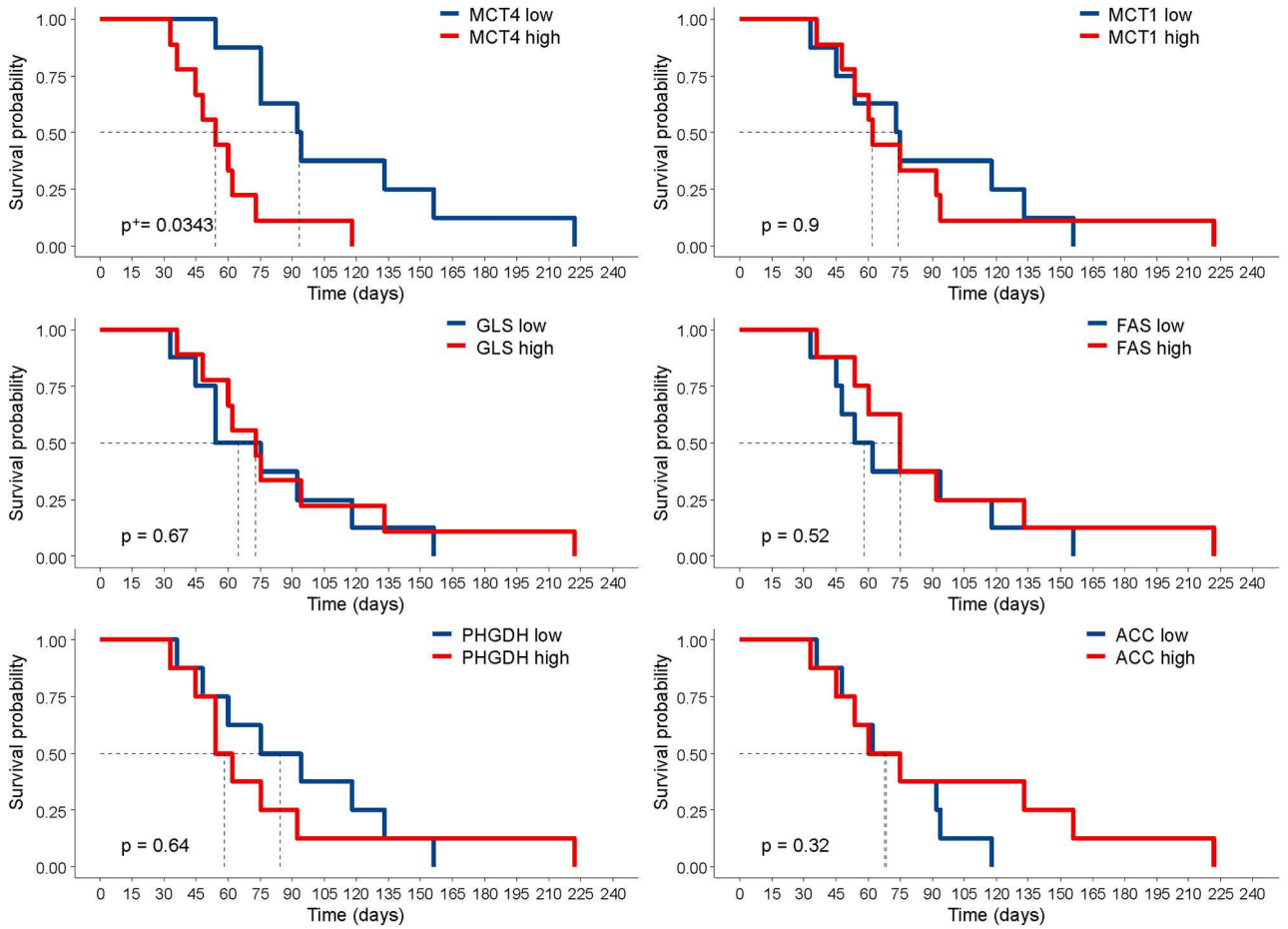

FIGURE 3 | Correlation of marker expression with survival. Kaplan–Meier curves according to the levels of marker expression, dichotomized according to their median value. Statistical significance was calculated with the log-rank test. ^{+}P-value was adjusted for multiple comparisons using the Benjamini–Hochberg method.

clinical implications of the metabolic traits of tumors on drug response.

Cancer cells do not only present alterations in glycolytic phenotype but also of other metabolic pathways interrogated by our panel, including lipid and amino acid metabolism. FAS is the enzyme accounting for the *de novo* synthesis of fatty acids, and it is highly expressed in many human cancers, including ovarian cancer (28). A high expression of FAS provides proliferative and metastatic potential; moreover, the high expression of FAS in EOC is associated with poor prognosis (29).

Another important metabolic pathway altered in cancer cells is glutamine. By using isotype tracer and bio-energetic analysis, Yang et al. found a correlation between glutamine dependence and cancer invasiveness. Therefore, in their studies, high-invasive ovarian cancer cells are markedly glutamine dependent, whereas low-invasive OVCA cells are glutamine independent (30). Furthermore, GLS overexpression is associated with poor survival and it is associated with platinum resistance in ovarian cancer (31). GLS is not the only marker associated with glutamine metabolism; the glutamine transporter ASCT2 (SLC1A5) is actively investigated as a possible therapeutic target to block cancer cell growth and development (32). In order to support tumor expansion and the *de novo* production of amino acids, lipids and nucleic acid tumor cells present an increased request of glycine. The *de novo* serine synthesis pathway initiated by phosphoglycerate dehydrogenase has been considered as a hallmark of metabolic adaption in carcinogenesis (33). In any case, despite the strong evidence of the link between these metabolic dysregulations and cancer, none of these markers was associated with the survival of mice in our pilot study. However, we observed a negative correlation between the expression of MCT4 and that of FAS in PDX samples, suggesting that these two markers could underscore the prevailing glycolytic and oxidative metabolism, respectively.

To investigate the metabolic profile of cancer, very complex, and high-resolution techniques can be used, including liquid chromatography–mass spectrometry. Liquid chromatography allows the physical separation of the metabolites that are than analyzed with the high sensitivity of mass spectrometry. These tandem techniques can be used with biological samples like plasma or tumor cell lysates, allowing the tracking of disease progression (34). However, there are also some drawbacks of

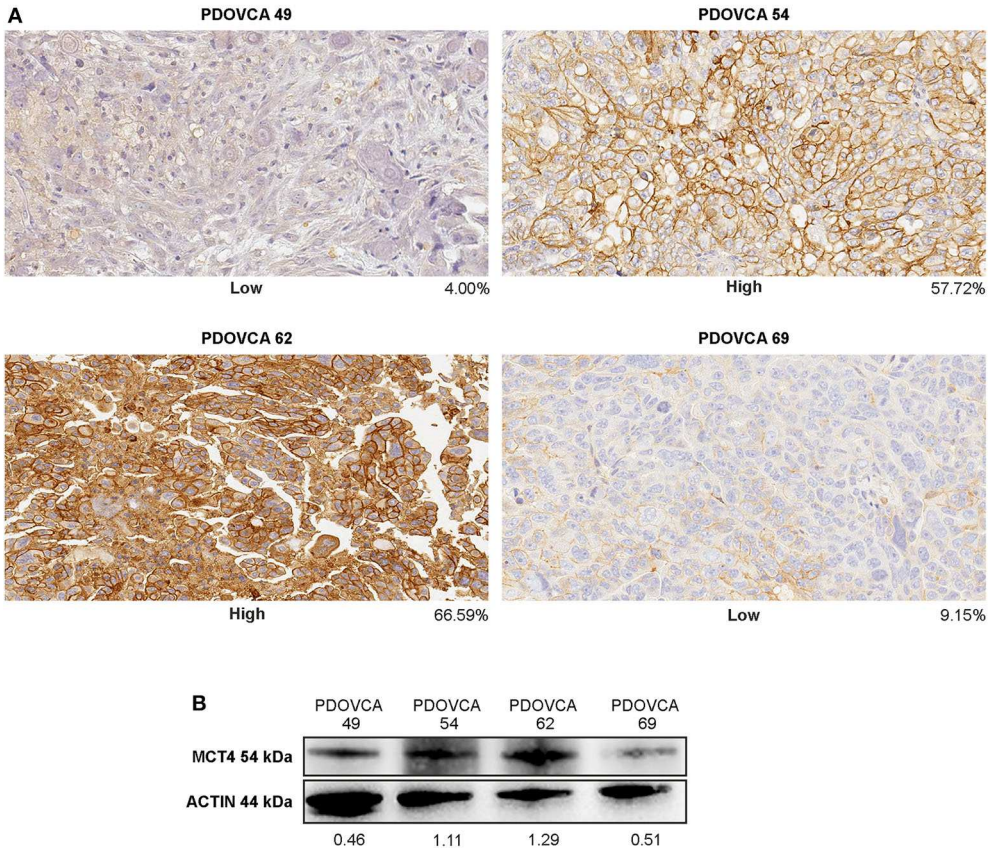

FIGURE 4 | (A) Immunohistochemistry staining of MCT4 in representative patient-derived xenograft (PDX) samples showing different protein intensities as assessed by image analysis software on digitalized slides (original magnification, ×20). **(B)** Cell lysates of the same PDX were analyzed in western blot for MCT4 marker. Protein quantification was determined by densitometric analysis, and the values reported in the figure were normalized to actin as loading control.

these techniques, including (1) the high cost, (2) the relatively low number of samples which can be simultaneously analyzed (thus incrementing the variability of the experiments), (3) the complex sample preparation and analysis, and (4) the requirement of freshly frozen tumor samples.

In contrast, IHC is an established technique available in all pathology units. Some *in situ* biomarkers, such as ER/PG receptors and HER2/neu in the case of breast cancer, have been used for decades for therapy stratification purposes (35), underlying the clinical value of IHC assessment of predictive biomarkers. The digital evolution of the analysis of IHC data offers an opportunity to overcome traditional limitations of this technique and enables the quantification of candidate metabolism-associated biomarkers to improve the prediction of disease aggressiveness and patient outcome (36). One limitation of our study is that we did not validate MCT4 as a prognostic biomarker in patients. Translational research demands a large cohort of patients to have enough power to draw solid conclusions. Along this line, we started the evaluation of the prognostic value of MCT4 expression in human ovarian cancer samples from the MITO2 clinical trial. MITO2 is a randomized, multicenter phase 3 trial conducted with 820 advanced ovarian cancer patients assigned with carboplatin/paclitaxel or carboplatin/PLD-pegylated liposomal doxorubicin as first-line treatment. Sixteen biomarkers were already studied in 229 patients in a tissue microarray (37), and additional biomarkers such as MCT4 can easily be analyzed. We foresee that the *in situ* metabolic panel presented in this pilot study will be useful to profile clinical samples in future studies.

DATA AVAILABILITY STATEMENT

The raw data supporting the conclusions of this article will be made available by the authors, without undue reservation, to any qualified researcher.

ETHICS STATEMENT

The studies involving human participants were reviewed and approved by IOV Institutional Review Board and Ethics Committee (EM 23/2017), and were performed in accordance

with the declaration of Helsinki. The patients/participants provided their written informed consent to participate in this study. This animal study was reviewed and approved by the Italian Ministry of Health (n. 217/2013-B).

AUTHOR CONTRIBUTIONS

IP contributed to the design of the study, performed the analysis, and wrote sections of the manuscript. MV collected the samples and performed the experiments. FM performed the experiments, analyzed the data, and wrote sections of the manuscript. GN, EZ, and TZ performed the experiments. PD performed the statistical analysis. GE analyzed the data and reviewed the manuscript. SI contributed conception and design of the study, wrote the first draft of the manuscript revising it critically for important intellectual content, and provide approval for publication of the content. All authors contributed to manuscript revision, read, and approved the submitted version. All authors contributed to the article and approved the submitted version.

FUNDING

This study was supported by AIRC (Grant IG18803 to SI).

SUPPLEMENTARY MATERIAL

The Supplementary Material for this article can be found online at: https://www.frontiersin.org/articles/10.3389/fonc.2020.01277/full#supplementary-material

REFERENCES

1. Hanahan D, Weinberg RA. Hallmarks of cancer: the next generation. *Cell.* (2011) 144, 646–74. doi: 10.1016/j.cell.2011.02.013
2. Pavlova NN, Thompson CB. The emerging hallmarks of cancer metabolism. *Cell Metab.* (2016) 23, 27–47. doi: 10.1016/j.cmet.2015.12.006
3. Draoui N, de Zeeuw P, Carmeliet P. Angiogenesis revisited from a metabolic perspective: role and therapeutic implications of endothelial cell metabolism. *Open Biol.* (2017) 7:170219. doi: 10.1098/rsob.170219
4. Wu D, Zhuo L, Wang X. Metabolic reprogramming of carcinoma-associated fibroblasts and its impact on metabolic heterogeneity of tumors. *Semin Cell Dev Biol.* (2017) 64:125–31. doi: 10.1016/j.semcdb.2016.11.003
5. Wu Q, Li B, Li Z, Li J, Sun S. Cancer-associated adipocytes: key players in breast cancer progression. *J Hematol Oncol.* (2019) 12:95. doi: 10.1186/s13045-019-0778-6
6. Singer K, Cheng WC, Kreutz M, Ho PC, Siska PJ. Immunometabolism in cancer at a glance. *Dis Model Mech.* (2018) 11:dmm034272. doi: 10.1242/dmm.034272
7. Lehuede C, Dupuy F, Rabinovitch R, Jones RG, Siegel PM. Metabolic plasticity as a determinant of tumor growth and metastasis. *Cancer Res.* (2016) 76:5201–8. doi: 10.1158/0008-5472.CAN-16-0266
8. Kumar A, Misra BB. Challenges and opportunities in cancer metabolomics. *Proteomics.* (2019) 19:e1900042. doi: 10.1002/pmic.201900042
9. Antoniewicz MR. A guide to (13)C metabolic flux analysis for the cancer biologist. *Exp Mol Med.* (2018) 50:19. doi: 10.1038/s12276-018-0060-y
10. Fabian C, Koetz L, Favaro E, Indraccolo S, Mueller-Klieser W, Sattler UG. Protein profiles in human ovarian cancer cell lines correspond to their metabolic activity and to metabolic profiles of respective tumor xenografts. *FEBS J.* (2012) 278:882–91. doi: 10.1111/j.1742-4658.2012.08479.x
11. Payen VL, Mina E, Van Hee VF, Porporato PE, Sonveaux P. Monocarboxylate transporters in cancer. *Mol Metab.* (2019) 33:48–66. doi: 10.1016/j.molmet.2019.07.006
12. Mates JM, Campos-Sandoval JA, Marquez J. Glutaminase isoenzymes in the metabolic therapy of cancer. *Biochim Biophys Acta Rev Cancer.* (2018) 1870:158–64. doi: 10.1016/j.bbcan.2018.07.007
13. Maiques O, Georgouli M, Sanz-Moreno V. Recent advances in tissue imaging for cancer research. *F1000Res.* (2019) 8. doi: 10.12688/f1000research.19037.1
14. Ozols RF, Bookman MA, Connolly DC, Daly MB, Godwin AK, Schilder RJ, et al. Focus on epithelial ovarian cancer. *Cancer Cell.* (2004) 5:19–24. doi: 10.1016/s1535-6108(04)00002-9
15. Chen H, Wang L, Beretov J, Hao J, Xiao W, Li Y. Co-expression of CD147/EMMPRIN with monocarboxylate transporters and multiple drug resistance proteins is associated with epithelial ovarian cancer progression. *Clin Exp Metastasis.* (2010) 27:557–69. doi: 10.1007/s10585-010-9345-9
16. Yuan L, Sheng X, Willson AK, Roque DR, Stine JE, Guo H, et al. Glutamine promotes ovarian cancer cell proliferation through the mTOR/S6 pathway. *Endocr Relat Cancer.* (2015) 22:577–91. doi: 10.1530/ERC-15-0192
17. Zhao G, Cardenas H, Matei D. Ovarian cancer-why lipids matter. *Cancers.* (2019) 11:1870. doi: 10.3390/cancers11121870
18. Giacomini I, Ragazzi E, Pasut G, Montopoli M. The pentose phosphate pathway and its involvement in cisplatin resistance. *Int J Mol Sci.* (2020) 21:937. doi: 10.3390/ijms21030937
19. Pasto A, Pagotto A, Pilotto G, De Paoli A, De Salvo GL, Baldoni A, et al. Resistance to glucose starvation as metabolic trait of platinum-resistant human epithelial ovarian cancer cells. *Oncotarget.* (2017) 8:6433–45. doi: 10.18632/oncotarget.14118
20. Indraccolo S, Tisato V, Agata S, Moserle L, Ferrari S, Callegaro M, et al. Establishment and characterization of xenografts and cancer cell cultures derived from BRCA1$^{-/-}$ epithelial ovarian cancers. *Eur J Cancer.* (2006) 42:1475–83. doi: 10.1016/j.ejca.2006.01.057
21. Vander Heiden MG, Cantley LC, Thompson CB. Understanding the Warburg effect: the metabolic requirements of cell proliferation. *Science.* (2009) 324:1029–33. doi: 10.1126/science.1160809
22. Ferguson BS, Rogatzki MJ, Goodwin ML, Kane DA, Rightmire Z, Gladden LB. Lactate metabolism: historical context, prior misinterpretations, and current understanding. *Eur J Appl Physiol.* (2018) 118, 691–728. doi: 10.1007/s00421-017-3795-6
23. Mathupala SP, Colen CB, Parajuli P, Sloan AE. Lactate and malignant tumors: a therapeutic target at the end stage of glycolysis. *J Bioenerg Biomembr.* (2007) 39:73–7. doi: 10.1007/s10863-006-9062-x
24. DeBerardinis RJ, Chandel NS. Fundamentals of cancer metabolism. *Sci Adv.* (2016) 2:e1600200. doi: 10.1126/sciadv.1600200
25. Bovenzi CD, Hamilton J, Tassone P, Johnson J, Cognetti DM, Luginbuhl A, et al. Prognostic indications of elevated MCT4 and CD147 across cancer types: a meta-analysis. *Biomed Res Int.* (2015) 2015:242437. doi: 10.1155/2015/242437
26. Nardo G, Favaro E, Curtarello M, Moserle L, Zulato E, Persano L, et al. Glycolytic phenotype and AMP kinase modify the pathologic response of tumor xenografts to VEGF neutralization. *Cancer Res.* (2011) 71:4214–25. doi: 10.1158/0008-5472.CAN-11-0242
27. Sonveaux P, Copetti T, De Saedeleer CJ, Vegran F, Verrax J, Kennedy KM, et al. Targeting the lactate transporter MCT1 in endothelial cells inhibits lactate-induced HIF-1 activation and tumor angiogenesis. *PLoS ONE.* (2012) 7:e33418. doi: 10.1371/journal.pone.0033418
28. Zhou W, Han WF, Landree LE, Thupari JN, Pinn ML, Bililign T, et al. Fatty acid synthase inhibition activates AMP-activated protein kinase in SKOV3 human ovarian cancer cells. *Cancer Res.* (2007) 67:2964–71. doi: 10.1158/0008-5472.CAN-06-3439
29. Rizzo A, Napoli A, Roggiani F, Tomassetti A, Bagnoli M, Mezzanzanica D. One-carbon metabolism: biological players in epithelial ovarian cancer. *Int J Mol Sci.* (2018) 19:2092. doi: 10.3390/ijms19072092

30. Yang L, Moss T, Mangala LS, Marini J, Zhao H, Wahlig S, et al. Metabolic shifts toward glutamine regulate tumor growth, invasion and bioenergetics in ovarian cancer. *Mol Syst Biol.* (2014) 10:728. doi: 10.1002/msb.20134892
31. Hudson CD, Savadelis A, Nagaraj AB, Joseph P, Avril S, DiFeo A, Avril N. Altered glutamine metabolism in platinum resistant ovarian cancer. *Oncotarget.* (2016) 7:41637–49. doi: 10.18632/oncotarget.9317
32. Broer A, Fairweather S, Broer S. Disruption of amino acid homeostasis by novel ASCT2 inhibitors involves multiple targets. *Front Pharmacol.* (2018) 9:785. doi: 10.3389/fphar.2018.00785
33. Zhu J, Ma J, Wang X, Ma T, Zhang S, Wang W, et al. High expression of PHGDH predicts poor prognosis in non-small cell lung cancer. *Transl Oncol.* (2016) 9:592–9. doi: 10.1016/j.tranon.2016.08.003
34. Ke C, Li A, Hou Y, Sun M, Yang K, Cheng J, et al. Metabolic phenotyping for monitoring ovarian cancer patients. *Sci Rep.* (2016) 6:23334. doi: 10.1038/srep23334
35. Nicolini A, Ferrari P, Duffy MJ. Prognostic and predictive biomarkers in breast cancer: past, present and future. *Semin Cancer Biol.* (2018) 52(Pt 1):56–73. doi: 10.1016/j.semcancer.2017.08.010
36. Madabhushi A, Lee G. Image analysis and machine learning in digital pathology: challenges and opportunities. *Med Image Anal.* (2016) 33:170–5. doi: 10.1016/j.media.2016.06.037
37. Perrone F, Baldassarre G, Indraccolo S, Signoriello S, Chiappetta G, Esposito F, et al. Biomarker analysis of the MITO2 phase III trial of first-line treatment in ovarian cancer: predictive value of DNA-PK and phosphorylated ACC. *Oncotarget.* (2016) 7:72654–61. doi: 10.18632/oncotarget.12056

Conflict of Interest: The authors declare that the research was conducted in the absence of any commercial or financial relationships that could be construed as a potential conflict of interest.

frontiers in Oncology

ORIGINAL RESEARCH
published: 02 November 2020
doi: 10.3389/fonc.2020.01703

Total Cellular ATP Production Changes With Primary Substrate in MCF7 Breast Cancer Cells

*Maggie C. Louie[1], Justin Ton[2], Maurice L. Brady[1], Diem T. Le[2], Jordon N. Mar[2], Chad A. Lerner[3], Akos A. Gerencser[3] and Shona A. Mookerjee[2,3]**

[1] Department of Natural Sciences and Mathematics, Dominican University of California, San Rafael, California, CA, United States, [2] Department of Biological and Pharmaceutical Sciences, Touro University California College of Pharmacy, Vallejo, CA, United States, [3] Buck Institute for Research on Aging, Novato, CA, United States

Cancer growth is predicted to require substantial rates of substrate catabolism and ATP turnover to drive unrestricted biosynthesis and cell growth. While substrate limitation can dramatically alter cell behavior, the effects of substrate limitation on total cellular ATP production rate is poorly understood. Here, we show that MCF7 breast cancer cells, given different combinations of the common cell culture substrates glucose, glutamine, and pyruvate, display ATP production rates 1.6-fold higher than when cells are limited to each individual substrate. This increase occurred mainly through faster oxidative ATP production, with little to no increase in glycolytic ATP production. In comparison, non-transformed C2C12 myoblast cells show no change in ATP production rate when substrates are limited. In MCF7 cells, glutamine allows unexpected access to oxidative capacity that pyruvate, also a strictly oxidized substrate, does not. Pyruvate, when added with other exogenous substrates, increases substrate-driven oxidative ATP production, by increasing both ATP supply and demand. Overall, we find that MCF7 cells are highly flexible with respect to maintaining total cellular ATP production under different substrate-limited conditions, over an acute (within minutes) timeframe that is unlikely to result from more protracted (hours or more) transcription-driven changes to metabolic enzyme expression. The near-identical ATP production rates maintained by MCF7 and C2C12 cells given single substrates reveal a potential difficulty in using substrate limitation to selectively starve cancer cells of ATP. In contrast, the higher ATP production rate conferred by mixed substrates in MCF7 cells remains a potentially exploitable difference.

Keywords: glycolysis, oxidative phosphorylation, Crabtree, ATP supply flexibility, bioenergetic capacity

OPEN ACCESS

Edited by:
Rafael Moreno-Sánchez, Instituto Nacional de Cardiologia Ignacio Chavez, Mexico

Reviewed by:
Alvaro Marín Hernández, Instituto Nacional de Cardiología, Mexico
Petr Ježek, Institute of Physiology (ASCR), Czechia

***Correspondence:**
Shona A. Mookerjee
shona.mookerjee@tu.edu

Specialty section:
This article was submitted to Cancer Metabolism, a section of the journal Frontiers in Oncology

Received: *15 January 2020*
Accepted: *30 July 2020*
Published: *02 November 2020*

Citation:
Louie MC, Ton J, Brady ML, Le DT, Mar JN, Lerner CA, Gerencser AA and Mookerjee SA (2020) Total Cellular ATP Production Changes With Primary Substrate in MCF7 Breast Cancer Cells. Front. Oncol. 10:1703. doi: 10.3389/fonc.2020.01703

INTRODUCTION

The ability of cancer cells to respond and adapt to available substrate conditions is widely studied (1–3), with the primary goals of using cancer cell metabolism to develop diagnostic and therapeutic strategies. Like any cell, cancer cells must respond to acute fluctuations in substrate availability to meet the demands for energy and intermediates required to survive and proliferate (4–6). Over longer time frames, cancer cells adapt to longer-term effects of the microenvironment with extensive transcriptional and architectural remodeling that enables unrestricted growth in different tissues and under wide ranges of conditions. A better understanding of both the acute metabolic responses and longer-term metabolic remodeling is critical to identifying and selectively targeting metabolism in cancer cells (7, 8).

Though targeting the metabolic alteration that occurs in cancer is a long-pursued goal [recently reviewed in (9, 10)], a successful therapeutic strategy based on metabolic disruption remains unrealized. Though many observations suggest that "cancer cell metabolism" is sufficiently different from normal cellular metabolism to be selectively targetable, the wide metabolic variation among cancers in different tissues, and even cells within a tumor, makes it difficult to test this hypothesis (11–14). Differences that are described as characteristic of cancer are difficult to interpret. The Warburg effect, for example, characterized by high rates of glycolysis and/or glucose uptake (15), has persisted for almost a century (16) despite its ambiguous definition and non-testable construction with respect to cellular bioenergetic behavior (17). Proposed mechanisms for the Warburg effect include altered expression of proteins, including levels or isoforms of glycolytic enzymes (18), the mitochondrial pyruvate carrier (19) as a wide variety of specific transcriptional alterations (20). Taken together, no cohesive model emerges. Moreover, the hallmark Warburg effect characteristic of high rates of glucose flux is ambiguous: while faster glycolysis could represent a consistent shift toward glycolysis, it could also represent higher ATP demand with no alteration of catabolic machinery.

An additional problem is the highly responsive nature of metabolic networks. Unlike earlier models of cancer metabolism that proposed an irreversible "switch," most recent models recognize the high degree of metabolic flexibility that allows a cancer cell to meet energy and biosynthesis demands even under rapidly changing conditions (21, 22). Whether this is more true in cancer cells than other cells is not clear, but limiting such flexibility should be an advantage if it can be made selective to cancer. Here, the homeostatic control over steady-state metabolic flux is a necessary consideration.

Metabolic rates (e.g., rate of glucose catabolism) are controlled by the concentrations of common intermediates in linked reactions (e.g., glycolysis) and activities of reactions linking these intermediates, which are influenced (23) but cannot be predicted (24) solely by the isoforms and abundance of the enzymes that carry out those reactions (e.g., hexokinase), as both concentrations and activities influence these rates. Analysis of proteomic and transcriptomic data provide a good understanding of the changes in metabolic machinery that occur in cancer cells (25), but not of the kinetic behavior of the metabolic system (26). Distinguishing between the plastic remodeling of metabolic networks via protein expression changes and the kinetic function of the network would greatly strengthen the hypothesis-testing ability of both conceptual and mathematical metabolic models.

The energy needs of cancer cells are a specific topic of interest within the larger field of cancer metabolism, where ATP turnover is presumably increased to meet increased the energy demand of rapidly growing and dividing cells. Although faster ATP turnover has been inferred from high rates of glycolysis in many cancer models [e.g., (27)], clear demonstration of this is currently lacking. One reason is that many assessments of energy supply and demand in whole cells end at the raw rates of associated fluxes, such as oxygen consumption and extracellular acidification. Because these rates are differently geared to ATP, and because the units (e.g., pH to moles O_2) are not directly comparable, no combination of these raw rates can yield useful information about total cellular ATP production when both pathways are operating. In addition, each of these rates is confounded by non-ATP-generating portions which must be empirically determined and subtracted. However, when each raw rate is properly converted, powerful conclusions can be reached, including what the rate of total cellular ATP production is, and how ATP production rate is divided between glycolysis and oxidative phosphorylation (28).

Existing measurements of ATP production demonstrate their value in understanding cancer cell energetics. Using the MCF7 epithelial, ER^+ breast cancer cell line, Guppy et al. demonstrated that in contrast to prevailing models of high "aerobic glycolysis" by these cells, as commonly extrapolated from the Warburg effect and later applied to the "addiction" of cancer cells to glutamine and glucose, these cells were primarily oxidative and derived less than half of their ATP from either glucose or from glutamine under the conditions assayed (29).

Recent instrumentation advances have greatly simplified the measurements of ATP production-associated rates in a way that makes further elucidation of cancer cell bioenergetics, specifically ATP production and consumption, much more straightforward. The Agilent XF Analyzer, which measures simultaneous O_2 and H^+ fluxes, is one example. However, as mentioned above, these extracelular flux rates cannot be used to draw conclusions about total cellular ATP production without correction and conversion to ATP flux (J_{ATP}).

We have developed a method for performing the correction and conversion needed to calculate rates of glycolytic ATP production ($J_{ATPglyc}$) and oxidative ATP production ($J_{ATPglyc}$) rate from all intracellular sources, allowing their summation to total cellular ATP production ($J_{ATPproduction}$) as well as determination of the proportional contributions of each ATP-generating pathway as summarized in the Materials and Methods and in Mookerjee et al. (28). Here, we apply this method to re-examine the bioenergetic behavior of MCF7 cells in culture. We investigate their ability to use different common extracellular substrates to meet energy demand, and to determine how flexibly these cells can meet that demand specifically by shifting between glycolysis and oxidative phosphorylation. In addition to flexibility of ATP supply, we also demonstrate that MCF7 cells display flexibility in the substrate-driven and maximum rates of ATP production supported by different substrate conditions. Finally, we demonstrate that increased ATP supply through recruitment of substrate oxidation is the likely driver of bioenergetic variation in MCF7 cells.

MATERIALS AND METHODS

Reagents

Chemicals (substrates, drugs, assay medium components) were from Sigma-Aldrich (St. Louis, MO) unless otherwise noted. Cell culture reagents were from Corning (Bedford, MA). Seahorse XF consumables (cartridges, cell culture plates) were from Agilent (Santa Clara, CA). The bicinchoninic (BCA) assay for

protein, tetramethylrhodamine methyl ester (TMRM) and other fluorescence probes were from Life Technologies (Carlsbad, CA). The FLIPR Membrane Potential Assay Explorer Kit was from Molecular Devices (Sunnyvale, CA; #R8126 red version). Zosuquidar was from Cayman Chemical (Ann Arbor, MI).

Cell Culture

MCF7 cells (ATCC) and mouse C2C12 myoblasts (ATCC) were cultured in Dulbecco's modified Eagle's medium (Corning #10-013) with added 10% (v/v) fetal bovine serum (FBS), 100 units/ml penicillin, and 100 μg/ml streptomycin. Cells were analyzed within 1 year of purchase from ATCC.

Seahorse XFe96 Assay and Analysis

Twenty four to forty eight hours before the assay, adherent cells were plated in 100 μl culture medium at 10,000–12,000 cells/well in the inner 60 wells of a 96-well polystyrene Seahorse V3-PS Flux plate with no additional coating. Culture medium was added to the remaining outer wells. Twenty five minutes before the assay start, all wells were washed three times and then incubated in 180 μl of Krebs-Ringer phosphate HEPES (KRPH) medium [2 mM HEPES, 136 mM NaCl, 2 mM NaH_2PO_4, 3.7 mM KCl, 1 mM $MgCl_2$, 1.5 mM $CaCl_2$, 0.1% (w/v) fatty-acid-free bovine serum albumin, pH 7.4 at 37°C]. This starvation protocol is consistent with our prior work and similar to others (30) and within the measurement error, measured rates are consistent with the assumption of exclusive catabolism of added substrates (28). At the start of the assay, medium was replaced with 180 μl fresh KRPH at 37°C. All assays were carried out at 37°C at a starting pH of 7.4. Cell respiratory control (31) and glycolytic capacity (32) were assayed by measuring oxygen consumption and extracellular acidification rates in a Seahorse XFe96 extracellular flux analyzer as previously described (28). Cell respiratory control was assessed by the addition via ports A–D of either 10 mM glucose, 10 mM pyruvate, 2 mM glutamine, or a mix of all three in A, followed in all cases by 2 μg/ml oligomycin in B, 0.5–1 μM FCCP [carbonyl cyanide 4-(trifluoromethoxy)phenylhydrazone] in C, and 1 μM rotenone plus 1 μM myxothiazol in D. To minimize FCCP toxicity dampening maximum respiration rate, FCCP was carefully titrated in both cell lines prior to performing experiments. 0.5 μM was used for MCF7 cells while 1 μM was used for C2C12 cells. To minimize the potential for energetic collapse dampening maximum respiration rate after oligomycin addition, we conducted separate experiments where oligomycin and FCCP were added simultaneously. The highest rate of maximum respiration achieved in the presence of oligomycin and FCCP, whether sequential or simultaneous, was used to calculate maximum J_{ATPox}. Substrate concentrations were close to common concentrations in cell culture and consistent with our previous analyses (32, 33).

Glycolytic capacity was assessed with the same substrate additions as for cell respiratory control in port A, 1 μM rotenone plus 1 μM myxothiazol in B, and 100 μM monensin in C. All measurement cycles consisted of a 1 min mix, 1 min wait, and 3 min rate measurement. Three measurement cycles were performed prior to any addition, 6 cycles after the port A substrate addition, and 3 cycles after all subsequent additions. Assay duration was ∼75 min. Following the assay, the cell-containing plate wells were washed three times with 100 μl PBS (137 mM NaCl, 2.7 mM KCl, 10 mM Na_2HPO_4, 1.8 mM KH_2PO_4, pH 7.4 @ 22°C). 10 μl 5.0 % (w/v) sodium deoxycholate was added to each well and plates were agitated on a plate shaker at 800 rpm for 5 min to lyse cells. Thirty μL water was then added, and 10 μL of the resulting sample from each well was analyzed by BCA assay for total protein content calibrated to a BSA standard. Protein values (μg/well) were used to normalize the rates of oxygen consumption and extracellular acidification in each well.

The Wave software native to the XF Analyzer was used to extract rates of oxygen consumption and extracellular acidification.

Calculation of ATP Production Rate ($J_{ATPproduction}$)

We have previously described a method for calculation of total cellular ATP production rate from extracellular acidification and oxygen consumption rates (28). This calculation fully accounts for net ATP production in the cell, including net ATP production in glycolysis (at phosphoglycerate kinase and pyruvate kinase, minus consumption at hexokinase and phosphofructokinase), the TCA cycle (at succinyl CoA synthetase), and by the mitochondrial ATP synthase. A brief description of the calculation and its underlying assumptions is presented here.

To calculate $J_{ATPglyc}$, the extracellular acidification rate was first converted to total proton production rate. The contribution of respiratory CO_2 to total proton production rate was subtracted to yield glycolytic rate of glucose catabolism terminating in lactate. This rate was multiplied by the ratio of ATP produced in glycolysis terminating in lactate per extracellular H^+ (the P/H^+ ratio). Additional glycolytic flux generating the pyruvate that is later fully oxidized in the mitochondria generates additional ATP, and is represented in the mitochondrial respiration rate (see below). Therefore, mitochondrial respiration rate was multiplied by the ratio of ATP produced in glycolysis terminating in pyruvate per O_2 consumed for each substrate ($P/O_{glycolysis}$). Glycolytic ATP production ($J_{ATPglyc}$) was calculated as the sum of these two rates.

To calculate J_{ATPox}, mitochondrial respiration rate was isolated by subtracting from the total oxygen consumption rate any additional oxygen consumption in the presence of mitochondrial poisons rotenone and myxothiazol. Mitochondrial respiration rate was further divided into ATP-coupled and uncoupled respiration rates using the mitochondrial ATP synthase inhibitor oligomycin. The ATP-coupled respiration rate was multiplied by the portion of the P/O ratio attributable to the mitochondrial ATP synthase (P/O_{oxphos}). To account for oxidative substrate-level phosphorylation in the TCA cycle, the mitochondrial respiration rate was multiplied by the P/O ratio attributable to succinyl CoA synthetase (P/O_{TCA}). Oxidative ATP production (J_{ATPox}) was calculated as the sum of these two rates.

Finally, $J_{ATPglyc}$ and J_{ATPox} were summed to yield the total cellular ATP production rate, $J_{ATPproduction}$. Note that

when FCCP (or another mitochondrial uncoupler) is present and respiration is fully uncoupled, J_{ATPox} is theoretical, as actual oxidative phosphorylation does not occur under these conditions. Though the biological meaning of the maximum respiration rate achievable in a cell with the addition of an uncoupler is not clear, it is generally interpreted as the theoretical capacity of oxidative phosphorylation (31).

The biological assumptions of the ATP calculation model include exclusive use of exogenous substrates, proportional use of single substrates when substrate combinations are given, complete oxidation of these substrates (for glutamine, partial oxidation to lactate), transport of reducing equivalents into the mitochondrial matrix primarily by the malate-aspartate shuttle, and negligible cell growth under the conditions and timeframe assayed. Technical assumptions and calibration of the XF Analyzer measurements have been described previously (34, 35).

Mitochondrial Membrane Potential Measurement and Analysis

Absolute mitochondrial membrane potential ($\Delta\psi M$) was measured by fluorescence microscopy as previously described (36, 37). Briefly, MCF7 cells were plated in 100 µl culture medium in Matrigel-coated glass-bottom 96-well culture plates at 10,000 cells/well 48 h prior to the experiment. Three hours before recording, cells were washed twice with a modified culture medium containing TMRM (non-fluorescent DMEM with 10% FBS, 4.5 mg/L glucose, 1 mM $NaHCO_3$, 20 mM TES, 1 mM pyruvate, 4 mM glutamine, 10 nM TMRM) in an air incubator at 37°C in order to equilibrate the probe. Next, the recording was set up (2 positions/well and 18 wells per plate), and then cultures were washed 3× with a Potentiometric Medium (PM) closely resembling the assay medium used for $J_{ATPglyc}$ and J_{ATPox} determinations (KRPH; 10 nM TMRM, 1:100 FLIPR, 1 µM tetraphenylborate, 1 µM zosuquidar) with no substrates. In order to keep constant probe concentration during the assay, all media and substrates added to the cultures were prepared by 1:1 mixing of a common 2×PM (with 32 mM NaCl) with 240 mM NaCl (resulting PM), or aqueous stocks of substrates. Subsequently, after 10 min wait, a baseline recording of 30 min was started, followed by 30-min segments of substrate additions. Imaging was performed on a Nikon Eclipse Ti Perfect Focus System fully motorized wide-field fluorescence microscope and equipped with a custom Lambda 821 LED light source (Sutter Instruments, Novato, CA) with Lambda 10-3 emission filter wheel an Andor iXon Life 888 EMCCD camera (Oxford Instruments, UK) and a Nikon motorized stage with Elements 5.20 (Nikon, Melville, NY) using an S-Fluor 20× air lens. TMRM and FLIPR signals were collected at 100 s intervals, using the following filter sets, given as LED nm, excitation—emission in nm/bandwidth, for TMRM: 561, 586/20–641/75 (30 ms exposure time, 14% power) and for FLIPR: 506, 509/22–542/27, using a 459/526/596 beamsplitter (30 ms, 7%; all from Semrock, Rochester, NY). Recordings were analyzed in Image Analyst MKII (Image Analyst Software, Novato, CA) using the "Mitochondrial membrane potential assay (TMRM/PMPI) with masking dead cells" standard pipeline. $\Delta\psi P$ and $\Delta\psi M$ were calibrated using the "Complete Iterative" and "Complete (known k)" paradigms, respectively, with $k_T = 0.01\ s^{-1}$. To this end, two calibrants were used; first $\Delta\psi M$ was completely depolarized using 1 µM oligomycin, 1 µM FCCP, 4 µM antimycin A, 4 µM myxothiazol and 1 µM valinomycin (a K^+-ionophore) in PM and the decay in TMRM fluorescence was recorded immediately for 30 min. This was followed by complete depolarization of the $\Delta\psi P$ by adding PM containing 2% paraformaldehyde, 120 mM KCl, and 5 µg/mL gramicidin (a Na^+ ionophore). The upstroke of the FLIPR fluorescence intensity upon this calibration step was used as "Part complete $\Delta\psi P$ depolarization," and each cell in each viewfield was independently calibrated. Changes in $\Delta\psi M$ after exogenous substrate addition were calculated and analyzed using GraphPad Prism and Microsoft Excel.

Statistical Analysis

Statistical analysis was performed in GraphPad Prism. Welch's *t*-test (no assumption of equal standard deviation) was performed for all pairwise comparisons as described in the figure captions. For multiple comparisons, ordinary one-way ANOVA followed by Tukey's *post-hoc* multiple comparisons test was performed as described in figure captions. Technical replicate error (of 3–6 wells/plate) was discarded. Error bars for all values represent the standard error of the mean of 4–6 independent experiments except where noted.

RESULTS

Mixed Substrates Drive Higher Rates of Total Cellular ATP Production ($J_{ATPproduction}$) in MCF7 Cells

To determine how $J_{ATPproduction}$ in MCF7 cells changes with substrate provided, MCF7 cells cultured under standard conditions were briefly starved (25 min) to deplete endogenous substrates (30) and then assayed for extracellular flux of H^+ and O_2 in the minimal salts buffer KRPH. The extracellular substrates glucose, glutamine, and pyruvate, either singly or as a combination of all three, were added during the experiment. **Figure 1A** shows the significant variation in $J_{ATPproduction}$ that results under the conditions assayed.

Glucose, glutamine, and pyruvate yielded similar $J_{ATPproduction}$, of 63.4 ± 2.2, 56.7 ± 3.0, and 57.6 ± 1.8 pmol ATP/min/µg protein, respectively, with no statistically significant differences. When all three substrates were combined, $J_{ATPproduction}$ increased significantly ($p \leq 0.001$) to 91.6 ± 3.7 pmol ATP/min/µg protein. The highest substrate-driven rate achieved under the conditions tested (91.6 pmol ATP/min/µg protein, mixed substrates) was 1.6-fold higher than the lowest recorded substrate-driven $J_{ATPproduction}$ of 56.7 pmol ATP/min/µg protein for pyruvate. The single substrates were likely being used by cells, as they supported respiration after the addition of FCCP in the cell respiratory control assays, while rates in cells receiving no exogenous substrate fell to zero, presumably through energetic collapse (not shown). The glycolytic index (GI) values for these substrate conditions

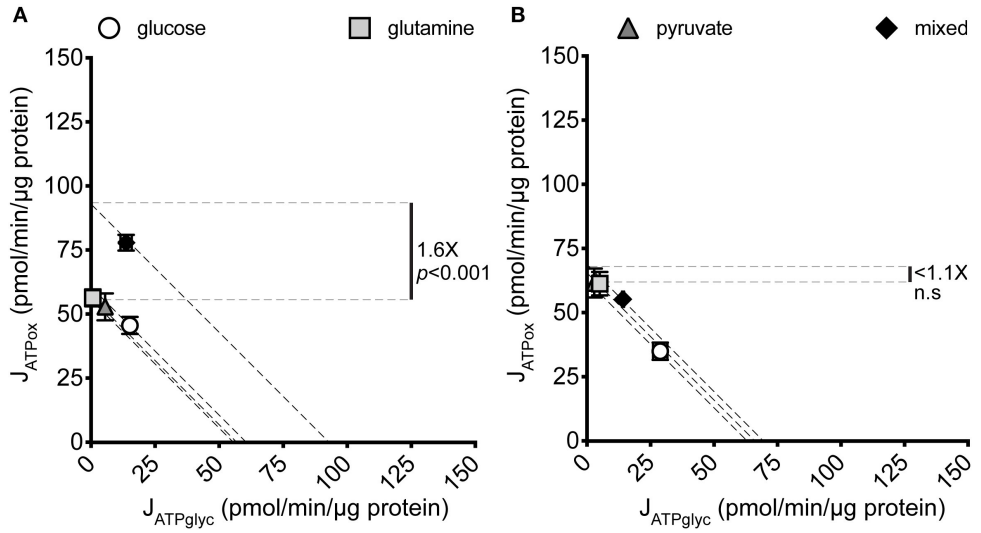

FIGURE 1 | $J_{ATPproduction}$ of MCF7 and C2C12 cells under different substrate conditions. Glycolytic ATP production rate ($J_{ATPglyc}$) and oxidative ATP production rate (J_{ATPox}) are plotted on the *x* and *y* axes, respectively. Each data point represents the mean of 4–6 independent experimental replicates ± SEM. Independent replicates are the average of 3–6 technical replicates per plate. Statistical comparisons were made using ordinary one-way ANOVA with Tukey's multiple comparisons test. Dashed diagonal lines represent all possible distributions of $J_{ATPglyc}$ and J_{ATPox} for the substrate-driven $J_{ATPproduction}$ shown. **(A)** MCF7 cells. **(B)** C2C12 mouse myoblast cells.

TABLE 1 | Quantification of MCF7 bioenergetic phenotypes under different substrate conditions.

MCF7 Bioenergetic Indices by Substrate in KRPH Assay Medium				
	Glucose	**Glutamine**	**Pyruvate**	**Mixed**
GI (%)	23.6 ± 1.0	−0.1 ± 0.5	9.6 ± 0.3	15.0 ± 0.7
CI (%)	20.2 ± 0.9	–	–	12.2 ± 0.6
SFI (%)	100	30	33	100

The Glycolytic Index (GI) describes the percent of total cellular energy production that is produced by glycolysis; GI = 100 $J_{ATPglyc}/J_{ATPproduction}$. The Crabtree Index (CI) describes the degree to which cells will shift from oxidative to glycolytic ATP production when a glycolyzable substrate is introduced (or increased); CI = $GI_{condition2} - GI_{condition1}$, where condition 1 is prior to substrate addition (here in the absence of exogenous substrates) and condition 2 is after this addition. Dashes denote conditions not applicable to CI measurement. The Substrate Flexibility Index (SFI) describes the range over which a cell can shift between $J_{ATPglyc}$ and J_{ATPox} to maintain a particular $J_{ATPproduction}$, limited by the maximum rates of glycolysis and respiration achievable under the conditions given. Each data point represents the mean of 4–6 independent experimental replicates ± SEM. Independent replicates are the average of 3–6 technical replicates per plate.*

demonstrate that substantial rates of $J_{ATPglyc}$ only occurred when glucose was present (**Table 1**).

Access to Mixed Substrates Does Not Consistently Increase $J_{ATPproduction}$ in Cultured Cells

To ask whether the increased $J_{ATPproduction}$ in MCF7 cells given multiple substrates occurs as a function of cell culturing, and is not intrinsic to these cells, we analyzed another cultured cell line under the same substrate conditions as the MCF7 cells. **Figure 1B** shows that the non-transformed C2C12 mouse myoblast line displayed no significant variation across the same single- and mixed-substrate conditions; for glucose, 60.1 ± 9.8; glutamine, 64.1 ± 6.5; pyruvate, 64.52 ± 6.4; mixed substrates, 68.9 ± 9.3. There were additionally no consistent trends in the C2C12 rates between individual experiments, suggesting no potential for small but meaningful differences between the substrate conditions as measured. The C2C12 measurements under glucose-only conditions were consistent with our previously published values for this cell line under the same conditions (28).

Mixed Substrates Increase $J_{ATPproduction}$ by Increasing J_{ATPox} in MCF7 Cells

To understand how changes in $J_{ATPproduction}$ occur in the MCF7 cells under different substrate conditions, we examined the constituent rates of $J_{ATPglyc}$ and J_{ATPox} in the same dataset shown in **Figure 1A**. **Figures 2A,B** show the composition of $J_{ATPproduction}$ in absolute units, while **Figures 2C,D** show the proportional contributions of each pathway in the MCF7 and C2C12 lines, respectively. Glycolytic ATP production in the absence of exogenous substrates was 1.6 ± 0.3 pmol ATP/min/µg protein (not shown), and changes negligibly with the addition of glutamine or pyruvate, as expected for these non-glycolyzable substrates. While pyruvate could be reduced to lactate, the charge of each molecule is the same and therefore no net acidification would occur. No significant changes occur in J_{ATPox} after the addition of glutamine or pyruvate individually. $J_{ATPproduction}$ and proportional distribution between $J_{ATPglyc}$ and J_{ATPox} were comparable between these cell lines.

In contrast to the single substrates glutamine and pyruvate, glucose, either alone or combined with glutamine and pyruvate,

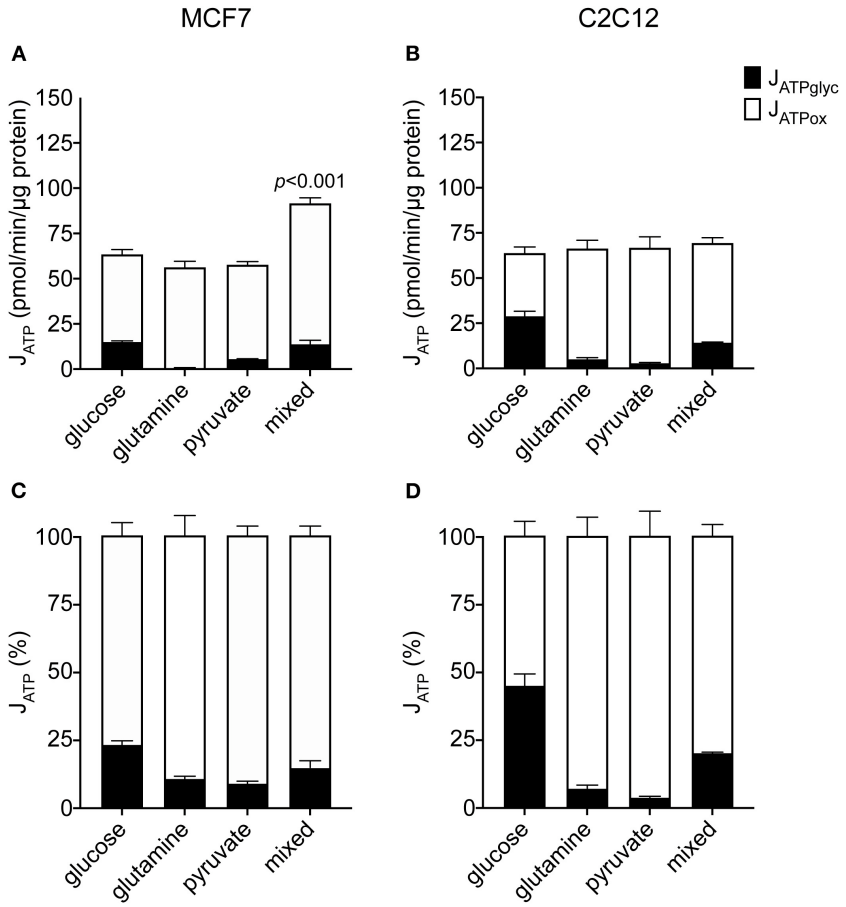

FIGURE 2 | Absolute and proportional $J_{ATPglyc}$ and J_{ATPox} in MCF7 and C2C12 cells. Absolute rates (pmol ATP/min/µg protein) from **Figure 1** are displayed as stacked columns **(A,C)** and as percent of total $J_{ATPproduction}$ **(B,D)**. Each column represents the mean of 4–6 independent experimental replicates ± SEM. Independent replicates are the average of 3–6 technical replicates per plate. Statistical comparisons of total $J_{ATPproduction}$ were made using ordinary one-way ANOVA with Tukey's multiple comparisons test.

recruits glycolysis and drives $J_{ATPglyc}$ (**Figures 2A,B**). The percentage $J_{ATPglyc}$ is the cell's glycolytic index (GI) value (**Figures 2C,D**, **Table 1**) under the stated conditions. Since glycolysis requires a glycolysis substrate, $J_{ATPglyc}$ would be expected only from a sugar, e.g., glucose, and the GI index value should be zero. For glutamine, this is true within the error of the calculation. For pyruvate, there was a small non-zero rate, which may represent a source of acidification not accounted for in the calculation model or an overestimate of the total proton production rate.

Glucose addition and subsequent $J_{ATPglyc}$ was accompanied by a roughly equal decrease in J_{ATPox}, resulting in no net change to $J_{ATPproduction}$. The illustrates the Crabtree effect (17), and is quantified in **Table 1** as the Crabtree index. When glucose was the sole substrate, the decrease in J_{ATPox} was balanced by a roughly equal increase in $J_{ATPglyc}$, so that $J_{ATPproduction}$ did not change, and was not significantly different from the rates conferred by the other single substrates. However, combination of all three substrates allowed recruitment of $J_{ATPglyc}$ similar to glucose alone, as well as a substantial increase in J_{ATPox}, to yield an overall increase in $J_{ATPproduction}$ in the MCF7 cells.

Glutamine, but Not Pyruvate, Confers Additional Oxidative Capacity in MCF7 Cells

The results above are consistent with an expectation that glutamine and pyruvate will support similar bioenergetic rates, as both are respiratory substrates. However, while the $J_{ATPproduction}$ resulting from their individual use was similar, a few notable differences emerged when cells were driven to their oxidative capacities under each condition (**Table 2**, **Figure 3**). The addition of the mitochondrial uncoupler FCCP to provoke maximum respiration did not increase pyruvate-driven respiration past its substrate-driven rate, suggesting that pyruvate was being used at its capacity under the conditions measured. In the presence of glutamine, however, MCF7 cells were able to increase theoretical J_{ATPox} (as a function of respiration) 1.75-fold above its initial rate (**Figure 3A**).

C2C12 cells did not appear to utilize glutamine to access higher rates of J_{ATPox} (**Figure 3B**). Glutamine-driven J_{ATPox} in C2C12 cells did not significantly change with FCCP addition to drive maximum respiration under the experimental conditions tested. Pyruvate-driven J_{ATPox} was also unable to increase when

TABLE 2 | Maximum rates and bioenergetic capacities in MCF7 under different substrate conditions.

Maximum rates of $J_{ATPproduction}$ in MCF7 cells in KRPH assay medium (pmol ATP/min/μg protein)				
	Glucose	**Glutamine**	**Pyruvate**	**Mixed**
$J_{ATPglycmax}$	149.8 ± 13.8	23.0 ± 4.3	27.0 ± 3.8	154.5 ± 7.8
$J_{ATPoxmax}$	83.4 ± 6.8	98.5 ± 5.7	52.1 ± 1.8	120.2 ± 8.6
Bioenergetic capacity	233.2 ± 15.4	121.5 ± 7.1	79.1 ± 4.1	274.7 ± 11.5

*Maximum rates of $J_{ATPglyc}$ and J_{ATPox} were determined as described in Methods and shown in **Figure 5**. The theoretical bioenergetic capacity is the sum of these values. Each data point represents the mean of 4–6 independent experimental replicates ± SEM. Independent replicates represent the average of 3–6 technical replicates per plate.*

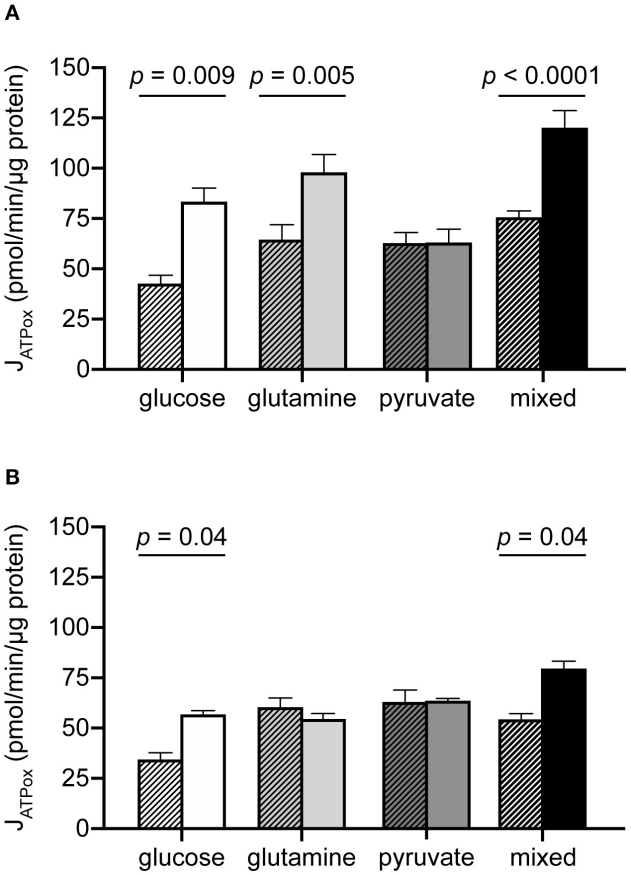

FIGURE 3 | Additional oxidative capacity conferred by glutamine but not pyruvate in MCF7 cells. J_{ATPox} for MCF7 **(A)** and C2C12 **(B)** under substrate-driven (hatched bars) and maximum respiration-eliciting conditions for all substrate conditions assayed. Each column represents the mean of 4–6 independent experimental replicates ± SEM. Independent replicates are the average of 3–6 technical replicates per plate. Statistical comparisons were made using ordinary one-way ANOVA with Tukey's multiple comparisons test.

driven to its theoretical capacity by FCCP. For glucose and mixed substrates, oxidative capacity was significantly higher than substrate-driven rates.

Pyruvate, but Not Glutamine, Stimulates Increased Substrate-Driven $J_{ATPproduction}$ by Increasing J_{ATPox}

To resolve how the mixed-substrate condition confers higher $J_{ATPproduction}$ in MCF7, we carried out a pairwise analysis of all added substrates. We found that pyruvate, in any combination, was associated with increased $J_{ATPproduction}$ similar to the mixed-substrate condition (**Figures 4A,C**). Curiously, pyruvate alone did not confer this effect, supporting the same $J_{ATPproduction}$ as each substrate alone (**Figure 1A**). Cells using glucose plus glutamine displayed substrate-driven $J_{ATPproduction}$ no different from either substrate alone (**Figure 4B**). Similar to **Figure 1**, the same analysis of paired substrates in C2C12 cells revealed no significant differences in $J_{ATPproduction}$ between any substrate pair and each single substrate (**Figures 4D–F**). Notably, while glucose alone induced the highest $J_{ATPglyc}$ (almost 50% of $J_{ATPproduction}$), substrate pairs containing glucose shifted to intermediate positions along the "iso-J_{ATP}" line denoting the same $J_{ATPproduction}$ along different proportional contributions of $J_{ATPglyc}$ and J_{ATPox}, further supporting the assumption of exogenous substrate catabolism by the cells. $J_{ATPproduction}$ for each substrate pair is plotted in **Figure 4G**, together with the mixed-substrate $J_{ATPproduction}$. The last column shows that $J_{ATPproduction}$ was sensitive to decreased ATP demand caused by inhibiting protein synthesis using cycloheximide.

Glutamine Allows Access to Additional Oxidative Capacity in MCF7 Cells by Increasing ATP Supply Through Substrate Oxidation

To test possible mechanisms of the increase in J_{ATPox} conferred by substrate combinations containing pyruvate, we measured mitochondrial membrane potential in MCF7 cells under the conditions used for extracellular flux analysis. An increase in cellular J_{ATPox} requires an increase in total activities of substrate oxidation, e.g., by recruitment of additional substrates to feed ATP supply, or an increase in ATP consumption by additional ATP demand. These supply and demand reactions are linked by the $\Delta\psi M$ as a common intermediate (31), which will increase (hyperpolarize) if increased J_{ATPox} results from faster substrate oxidation. Conversely, $\Delta\psi M$ will decrease (depolarize) if increased J_{ATPox} results from increased ATP demand. Glutamine hyperpolarized $\Delta\psi M$ when it was added to MCF7 cells in the presence of the other two substrates (**Figure 4H**). This indicates an increased activity of substrate oxidation pathways when glutamine oxidation is recruited, and this may explain the observed increase in oxidative capacity in the presence of glutamine (**Figure 3A**).

Pyruvate Increases J_{ATPox} by Increasing Both Supply and Cellular ATP Demand

In contrast to glutamine, pyruvate added to the other two substrates did not change $\Delta\psi M$ (**Figure 4H**). In light of the increased $J_{ATPproduction}$ with pyruvate (**Figures 4A–C**), pyruvate

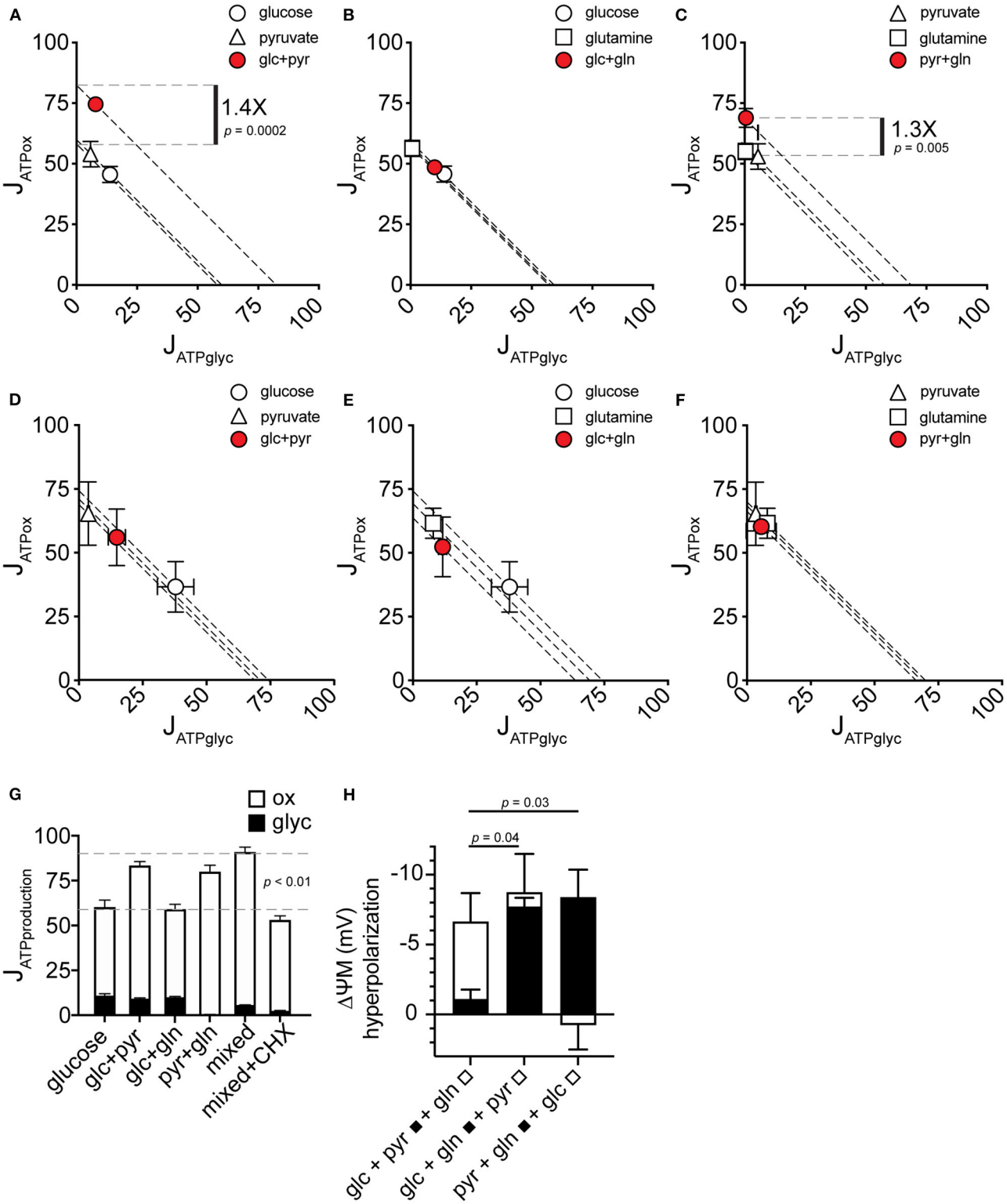

FIGURE 4 | $J_{ATPproduction}$ in pairwise substrate combinations. **(A–F)** Glycolytic ATP production rate ($J_{ATPglyc}$) and oxidative ATP production rate (J_{ATPox}) are plotted on the *x* and *y* axes, respectively, for MCF7 **(A–C)** and C2C12 **(D–F)** cells catabolizing the substrates indicated. Open symbols indicate single substrates; filled symbols indicate substrate pairs. Each data point represents the mean of 4–6 independent experimental replicates ± SEM. Independent replicates are the average of 3–6 technical replicates per plate. Statistical comparisons were made using ordinary one-way ANOVA with Tukey's multiple comparisons test. Dashed diagonal lines

(Continued)

FIGURE 4 | represent all possible distributions of $J_{ATPglyc}$ and J_{ATPox} for the substrate-driven $J_{ATPproduction}$ shown. **(G)** MCF7 $J_{ATPproduction}$ from substrate pairs with comparison to mixed substrates and to mixed substrates plus 10 μM cycloheximide (CHX). glc, glucose; pyr, pyruvate; gln, glutamine. **(H)** Change in $\Delta\psi M$ after addition of the indicated substrates. A pair of substrates (black bars) was followed by the addition of the third substrate (white bars). Data are mean ± SEM of $n = 3$ independent experimental replicates.

likely independently increased the activities of both supply and demand. Direct stimulation of ATP demand by pyruvate is further supported by the finding that the $\Delta\psi M$ hyperpolarization with glutamine did not increase ATP turnover, suggesting that a change in supply activities is not sufficient to alter ATP demand, and further that control of overall energy metabolism was largely by ATP demand.

MCF7 Supply Flexibility and Bioenergetic Capacity Changes With Substrate Availability

We previously described how substrate-driven $J_{ATPproduction}$ could be analyzed within the context of cellular bioenergetic capacity [**Figure 5**, (28)] to assess the theoretical flexibility of cellular $J_{ATPproduction}$ to increase, decrease, and shift between $J_{ATPglyc}$ and J_{ATPox}. We apply that analysis to the MCF7 cells examined here. **Figures 5A–D** show the substrate-driven $J_{ATPproduction}$ for a different substrate condition; the single substrates glucose (A), glutamine (B), and pyruvate (C), and the mixed-substrate condition containing all three (D). Each panel shows a shaded area representing the theoretical bioenergetic activity in the cells under each condition. The theoretical maximum J_{ATPox}, as calculated from the respiratory rate after mitochondrial uncoupling with FCCP in the presence of oligomycin, forms the horizontal boundary intersecting the *y*-axis. Maximum $J_{ATPglyc}$, determined by adding the Na^+-ionophore monensin in the presence of rotenone and myxothiazol (but not oligomycin, which will inhibit ATP hydrolysis by the mitochondrial ATP synthase), forms the vertical boundary intersecting the *x*-axis. Using this convention, we assessed the ATP supply flexibility of the cell, that is, how flexibly the cell can meet a given ATP demand by drawing on $J_{ATPglyc}$ and J_{ATPox} before it reaches the capacity of either production pathway.

ATP supply flexibility was quantified using the Supply Flexibility Index [SFI (28), **Table 1**]. As shown in **Figure 5** and **Table 1**, MCF7 cells catabolizing glucose displayed a $J_{ATPproduction}$ of 63.4 ± 2.2 pmol/min/μg protein, with 23.6% of the total $J_{ATPproduction}$ derived from glycolysis. $J_{ATPglyc}$ and J_{ATPox} were both below their individual maxima (149.8 ± 13.8 and 83.4 ± 6.8, respectively), and the $J_{ATPproduction}$ itself was about half of the theoretical bioenergetic capacity (sum of the two maxima) of 233.2 ± 15.4 pmol ATP/min/μg protein. To maintain substrate-driven $J_{ATPproduction}$, the cell therefore had access to a wide range of its apparent bioenergetic capacity. ATP supply flexibility was quantified from the angle formed by lines extending from the origin to the intersection of the iso-J_{ATP} line with the ATP production capacity under the specified conditions. In cells catabolizing glucose (**Figure 5A**), the iso-J_{ATP} line extends to each axis without intersecting either capacity, so that the angle measured at the axis is 90°. The substrate flexibility of the MCF7 cells under these conditions was therefore 100*90/90 = 100%. In other words, MCF7 cells using glucose had access to 100% of the possible distribution between $J_{ATPglyc}$ and J_{ATPox} to meet ATP demand. In contrast, glutamine should confer no glycolytic capacity and therefore an SFI of zero. The small calculated $J_{ATPglyc}$ that does appear might represent extracellular acidification in the presence of monensin that is not accounted for in the calculation model. The calculated SFI of 100*26.7/90 = 30% is therefore likely an overestimate of ATP supply flexibility under these conditions. Similarly, the calculated SFI of 100*30/90° = 33% for cells oxidizing pyruvate is also likely to be an overestimate of ATP supply flexibility. Finally, under the mixed substrate condition, because it contains glucose, maintenance of substrate-driven $J_{ATPproduction}$ was possible with any combination of $J_{ATPglyc}$ and J_{ATPox}, yielding an SFI of 100%.

DISCUSSION

We report here that MCF7 cells display considerable bioenergetic flexibility, demonstrated by their ability to support the same substrate-driven $J_{ATPproduction}$ with different individual substrates (**Figure 1**), each with a different catabolic entry point, and in their ability to support substrate-driven $J_{ATPproduction}$ with any proportional distribution of $J_{ATPglyc}$ and J_{ATPox} (**Figure 5**). We find that this flexibility was not unique to malignant cells, as non-malignant C2C12 myoblasts, which behave similarly with respect to $J_{ATPproduction}$, displayed similar flexibilities. However, MCF7 used its given substrates differently than C2C12 cells, particularly at high $J_{ATPproduction}$. The higher $J_{ATPproduction}$ associated with mixed substrates (**Figure 1**) appeared to be driven by pyruvate under substrate-driven conditions (**Figure 4**), and by glutamine when maximum respiration was elicited (**Figure 5**).

Interestingly, the comparison between these two cell lines shows that when provided a glycolysis substrate, MCF7 cells derived only a small proportion of its total cellular ATP from glycolysis (about 20%) even when glucose was the sole exogenous substrate, while the non-malignant C2C12 line was more glycolytically active both as a proportion of the total rate (about 50%) and in absolute glycolytic rate, despite similar $J_{ATPproduction}$ to MCF7. The proportional assignment of $J_{ATPglyc}$ and J_{ATPox} in MCF7 exactly matched prior determinations of these ratios made by measuring partial pressures of O_2 and CO_2 in closed glass culture chambers (29). This recapitulation supports the validity of applying our ATP calculation model to MCF7 cells (28).

These data also demonstrate the error of assuming that glycolysis produces all or most ATP in cancer cells, a common extrapolation of the Warburg effect. The Warburg effect is a useful observation as applied to e.g., tumor detection *in vivo*

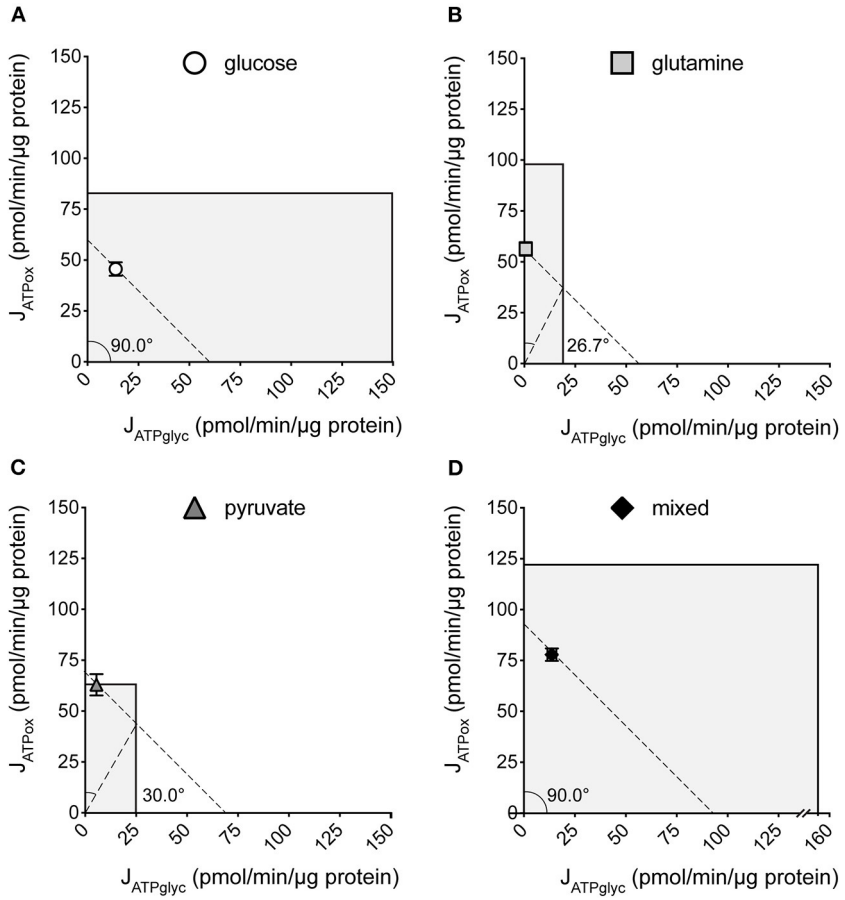

FIGURE 5 | Bioenergetic capacities and substrate flexibilities in MCF7 cells. Maximum J_{ATPox} and $J_{ATPglyc}$ determined as described (Methods) for cells catabolizing exogenous glucose **(A)**, glutamine **(B)**, pyruvate **(C)**, or a mix of all three **(D)**. Boundaries of the shaded boxes represent theoretical (J_{ATPox}) or actual ($J_{ATPglyc}$) capacities, with their x,y intersection the theoretical "bioenergetic capacity" afforded under each tested condition. Shaded area within each box is the theoretical "bioenergetic space," or all possible values of $J_{ATPglyc}$ and J_{ATPox} that the cell could achieve under experimental conditions. Angular notation illustrates supply flexibility for the substrate-driven $J_{ATPproduction}$ shown. Dashed diagonal lines represent all possible distributions of $J_{ATPglyc}$ and J_{ATPox} for the substrate-driven $J_{ATPproduction}$ shown, within the bioenergetic capacities represented by the *x*- and *y*- boundaries of the shaded box. Each point and capacity represents the mean of 4–6 independent experimental replicates ± SEM. Independent replicates are the average of 3–6 technical replicates per plate.

using positron tomography, but cannot be similarly applied to characterizing cancer cells *in vivo* or in cell culture, or to understanding their bioenergetic behavior.

The 1.6-fold, or 60% increase between the highest and lowest $J_{ATPproduction}$ by MCF7 represents a substantial range of substrate-driven flux. The main driver of this increase appeared to be pyruvate oxidation, in combination with either glucose or glutamine but not alone. Pyruvate-driven increases in J_{ATPox} appeared to be due to roughly equal increases in ATP supply and ATP demand, as $\Delta\psi M$ hyperpolarization was relatively small (∼1 mV, **Figure 4H**). In contrast, the presence of glutamine in any combination triggered a much more substantial hyperpolarization (∼7 mV) indicating faster ATP supply. Glutamine-driven $\Delta\psi M$ hyperpolarization did not consistently correspond to faster J_{ATPox} (**Figure 4B**). Because glutamine did not increase $J_{ATPproduction}$ (**Figure 4B**), despite the $\Delta\psi M$ hyperpolarization, it is possible that $\Delta\psi M$ has a weak control over ATP demand, i.e., higher ATP/ADP in the presence of more negative $\Delta\psi M$ does not drive demand reactions faster, so J_{ATPox} does not show a net increase.

Additionally, while the substrate-driven rates in both cell types supported by glutamine alone or by pyruvate alone were all similar, their oxidative capacities diverged considerably, with glutamine conferring substantially higher rates than pyruvate. One possible explanation for pyruvate's lack of ability to support additional capacity across both cell lines is artifactual; FCCP-mediated $\Delta\psi M$ collapse to drive maximum respiration rate could selectively slow H^+/pyruvate symport into the mitochondrial matrix. If so, pyruvate-mediated J_{ATPox} might be higher with intact membrane potential but not detectable under our experimental conditions.

For glutamine, the different responses of C2C12 and MCF7 could represent differences in the architecture of glutamine

oxidation between the two cell types. This observation may explain at least in part why a cancer cell might appear to be "glutamine-addicted," if glutamine withdrawal deprives cells of access to a portion of its capacity that cannot be accessed by pyruvate or other substrates. Prior work on the iBMK cell line supports a substantial contribution of glutamine oxidation to ATP production (38), though this may vary by cell type (29). Further, as uncoupled respiration is controlled primarily by substrate oxidation, changes in the protein levels of substrate oxidation machinery, includine glutamine transporters (39) or catabolic enzymes (40), may underlie differences in capacity that are not detectable in the substrate-driven rates, in which control by ATP demand is much greater.

The maximum $J_{ATPglyc}$ ($J_{ATPglyc|max}$) calculated for glutamine and pyruvate (**Figure 5**) were surprising, since glycolytic capacity from exclusive catabolism of non-glycolytic substrates was expected to be zero. These calculated rates likely result either from an overestimate of acidification rate, or from a true acidification rate not accounted for by respiratory CO_2, In either case, these rates probably do not represent true $J_{ATPglyc}$. Overestimated $_{JATPglyc|max}$ would also cause overestimation of SFI values and bioenergetic capacities, which are both determined using $J_{ATPglyc|max}$. Since our major findings of (1) full ATP supply flexibility at substrate-driven $J_{ATPproduction}$ for both MCF7 and C2C12 cells, (2) $J_{ATPproduction}$ responsive to substrate composition in MCF7, and (3) the ability of MCF7 to access additional oxidative capacity using glutamine, are not reliant on $J_{ATPglycmax}$, potential error in the calculation of $J_{ATPglycmax}$ do not change our major conclusions.

However, these discrepancies do highlight some of the limitations of the ATP calculation model. The assumptions underlying the conversion of extracellular H^+ and O_2 flux to $J_{ATPglyc}$ and J_{ATPox}, allowing determination of $J_{ATPproduction}$, are fully validated for glucose, but not for glutamine or pyruvate, in an intact-cell system. We find negligible contributions attributable to fluxes other than through glycolysis and oxidative phosphorylation under the conditions assayed (with the exception of $J_{ATPglycmax}$), suggesting that deviations from the model are small. However, this calculation is currently reliable only for non-growing cells, as growth would change the H^+/O_2 and P/O ratios on which the calculation relies. This represents a potential limitation on applying these findings to rapidly growing cells. In addition, this approach would fail to detect the potentially significant operation of pathways whose sum of errors happens to be small.

In conclusion, we demonstrate here that despite the common constraints of cell culturing in the same medium, MCF7 cancer cells display notable differences from a non-cancer cell type that are consistent with, and further refine, existing models of metabolic flexibility in cancer, including a potential bioenergetic basis for the hypothesis that glutamine oxidation provides access to bioenergetic capacity not afforded by other oxidized substrates. In contrast to many prevailing models of cancer cell metabolism, these differences do not always include substrate-driven ATP supply flexibility, greater ATP demand, or a greater reliance on glycolysis to meet ATP demand.

DATA AVAILABILITY STATEMENT

The datasets generated for this study are available on request to the corresponding author.

AUTHOR CONTRIBUTIONS

ML co-wrote the manuscript. JT, MB, JM, AG, CL, and DL collected and analyzed data presented and edited the manuscript. SM conceived the project, designed the experiments, and wrote the manuscript. All authors contributed to the article and approved the submitted version.

FUNDING

ML and SM received support from 1 R15 ES025917-01A1. JT and DL were supported by funds from the Touro University MSMHS-PS program. JM and MB were supported by federal work-study funding.

ACKNOWLEDGMENTS

We thank Martin D. Brand for lab support and for critical comments on the manuscript.

REFERENCES

1. DeBerardinis RJ, Lum JJ, Hatzivassiliou G, Thompson CB. The biology of cancer: metabolic reprogramming fuels cell growth and proliferation. *Cell Metab.* (2008) 7:11–20. doi: 10.1016/j.cmet.2007.10.002
2. Cascante M, Benito A, Zanuy M, Vizan P, Marin S, de Atauri P. Metabolic network adaptations in cancer as targets for novel therapies. *Biochem Soc Trans.* (2010) 38:1302–6. doi: 10.1042/BST0381302
3. Avagliano A, Ruocco MR, Aliotta F, Belviso I, Accurso A, Masone S, et al. Mitochondrial flexibility of breast cancers: a growth advantage and a therapeutic opportunity. *Cells.* (2019) 8:401. doi: 10.3390/cells8050401
4. Chekulayev V, Mado K, Shevchuk I, Koit A, Kaldma A, Klepinin A, et al. Metabolic remodeling in human colorectal cancer and surrounding tissues: alterations in regulation of mitochondrial respiration and metabolic fluxes. *Biochem Biophys Rep.* (2015) 4:111–25. doi: 10.1016/j.bbrep.2015.08.020
5. Koit A, Shevchuk I, Ounpuu L, Klepinin A, Chekulayev V, Timohhina N, et al. Mitochondrial respiration in human colorectal and breast cancer clinical material is regulated differently. *Oxid Med Cell Longev.* (2017) 2017:1372640. doi: 10.1155/2017/1372640
6. Tanner LB, Goglia AG, Wei MH, Sehgal T, Parsons LR, Park JO, et al. Four key steps control glycolytic flux in mammalian cells. *Cell Syst.* (2018) 7:49–62 e48. doi: 10.1016/j.cels.2018.06.003
7. Diers AR, Vayalil PK, Oliva CR, Griguer CE, Darley-Usmar V, Hurst DR, et al. Mitochondrial bioenergetics of metastatic breast cancer cells in response to dynamic changes in oxygen tension: effects of HIF-1alpha. *PLoS ONE.* (2013) 8:e68348. doi: 10.1371/journal.pone.0068348
8. Zdralevic M, Marchiq I, de Padua MMC, Parks SK, Pouyssegur J. Metabolic plasiticy in cancers-distinct role of glycolytic enzymes GPI, LDHs or membrane transporters MCTs. *Front Oncol.* (2017) 7:313. doi: 10.3389/fonc.2017.00313

9. Amoedo ND, Obre E, Rossignol R. Drug discovery strategies in the field of tumor energy metabolism: limitations by metabolic flexibility and metabolic resistance to chemotherapy. *Biochim Biophys Acta.* (2017) 1858:674–85. doi: 10.1016/j.bbabio.2017.02.005
10. Luengo A, Gui DY, Vander Heiden MG. Targeting metabolism for cancer therapy. *Cell Chem Biol.* (2017) 24:1161–80. doi: 10.1016/j.chembiol.2017.08.028
11. Gentric G, Mieulet V, Mechta-Grigoriou F. Heterogeneity in cancer metabolism: new concepts in an old field. *Antioxid Redox Signal.* (2017) 26:462–85. doi: 10.1089/ars.2016.6750
12. Grzywa TM, Paskal W, Wlodarski PK. Intratumor and intertumor heterogeneity in melanoma. *Transl Oncol.* (2017) 10:956–75. doi: 10.1016/j.tranon.2017.09.007
13. Reznik E, Luna A, Aksoy BA, Liu EM, La K, Ostrovnaya I, et al. A landscape of metabolic variation across tumor types. *Cell Syst.* (2018) 6:301–13 e303. doi: 10.1016/j.cels.2017.12.014
14. Xiao Z, Dai Z, Locasale JW. Metabolic landscape of the tumor microenvironment at single cell resolution. *Nat Commun.* (2019) 10:3763. doi: 10.1038/s41467-019-11738-0
15. Epstein T, Gatenby RA, Brown JS. The Warburg effect as an adaptation of cancer cells to rapid fluctuations in energy demand. *PLoS ONE.* (2017) 12:e0185085. doi: 10.1371/journal.pone.0185085
16. Koppenol WH, Bounds PL, Dang CV. Otto Warburg's contributions to current concepts of cancer metabolism. *Nat Rev Cancer.* (2011) 11:325–37. doi: 10.1038/nrc3038
17. Handel M, Brand MD, Mookerjee SA. The whys and hows of calculating total cellular ATP production rate. *Trends Endoc Metab.* (2019) 10:956–75. doi: 10.1016/j.tem.2019.04.007
18. Diaz-Ruiz R, Rigoulet M, Devin A. The Warburg and Crabtree effects: on the origin of cancer cell energy metabolism and of yeast glucose repression. *Biochim Biophys Acta.* (2011) 1807:568–76. doi: 10.1016/j.bbabio.2010.08.010
19. Schell JC, Olson KA, Jiang L, Hawkins AJ, Van Vranken JG, Xie J, et al. A role for the mitochondrial pyruvate carrier as a repressor of the Warburg effect and colon cancer cell growth. *Mol Cell.* (2014) 56:400–13. doi: 10.1016/j.molcel.2014.09.026
20. Cairns RA, Harris I, McCracken S, Mak TW. Cancer cell metabolism. *Cold Spring Harb Symp Quant Biol.* (2011) 76:299–311. doi: 10.1101/sqb.2011.76.012856
21. Andrzejewski S, Klimcakova E, Johnson RM, Tabaries S, Annis MG, McGuirk S, et al. PGC-1alpha promotes breast cancer metastasis and confers bioenergetic flexibility against metabolic drugs. *Cell Metab.* (2017) 26:778–87. doi: 10.1016/j.cmet.2017.09.006
22. Hsu BE, Tabaries S, Johnson RM, Andrzejewski S, Senecal J, Lehuede C, et al. Immature low-density neutrophils exhibit metabolic flexibility that facilitates breast cancer liver metastasis. *Cell Rep.* (2019) 27:3902–15 e3906. doi: 10.1016/j.celrep.2019.05.091
23. Moreno-Sanchez R, Rodriguez-Enriquez S, Marin-Hernandez A, Saavedra E. Energy metabolism in tumor cells. *FEBS J.* (2007) 274:1393–418. doi: 10.1111/j.1742-4658.2007.05686.x
24. Fell D. *Understanding the Control of Metabolism*. London: Portland Press (1997).
25. Rodriguez-Enriquez S, Marin-Hernandez A, Gallardo-Perez JC, Pacheco-Velazquez SC, Belmont-Diaz JA, Robledo-Cadena DX, et al. Transcriptional regulation of energy metabolism in cancer cells. *Cells.* (2019) 8:1225. doi: 10.3390/cells8101225
26. Moreno-Sanchez R, Saavedra E, Gallardo-Perez JC, Rumjanek FD, Rodriguez-Enriquez S. Understanding the cancer cell phenotype beyond the limitations of current omics analyses. *FEBS J.* (2016) 283:54–73. doi: 10.1111/febs.13535
27. Vander Heiden MG, Cantley LC, Thompson CB. Understanding the Warburg effect: the metabolic requirements of cell proliferation. *Science.* (2009) 324:1029–33 e775. doi: 10.1126/science.1160809
28. Mookerjee SA, Gerencser AA, Nicholls DG, Brand MD. Quantifying intracellular rates of glycolytic and oxidative ATP production and consumption using extracellular flux measurements. *J Biol Chem.* (2017) 292:7189–207. doi: 10.1074/jbc.M116.774471
29. Guppy M, Leedman P, Zu X, Russell V. Contribution by different fuels and metabolic pathways to the total ATP turnover of proliferating MCF-7 breast cancer cells. *Biochem J.* (2002) 364:309–15. doi: 10.1042/bj3640309
30. Zeidler JD, Fernandes-Siqueira LO, Carvalho AS, Cararo-Lopes E, Dias MH, Ketzer LA, et al. Short-term starvation is a strategy to unravel the cellular capacity of oxidizing specific exogenous/endogenous substrates in mitochondria. *J Biol Chem.* (2017) 292:14176–87. doi: 10.1074/jbc.M117.786582
31. Brand MD, Nicholls DG. Assessing mitochondrial dysfunction in cells. *Biochem J.* (2011) 435:297–312. doi: 10.1042/BJ20110162
32. Mookerjee SA, Nicholls DG, Brand MD. Determining maximum glycolytic capacity using extracellular flux measurements. *PLoS ONE.* (2016) 11:e0152016. doi: 10.1371/journal.pone.0152016
33. Mookerjee SA, Goncalves RLS, Gerencser AG, Nicholls DG, Brand MD. The contributions of respiration and glycolysis to extracellular acid production. *Biochim Biophys Acta.* (2015) 1847:171–81. doi: 10.1016/j.bbabio.2014.10.005
34. Gerencser AA, Neilson A, Choi SW, Edman U, Yadava N, Oh RJ, et al. Quantitative microplate-based respirometry with correction for oxygen diffusion. *Anal Chem.* (2009) 81:6868–78. doi: 10.1021/ac900881z
35. Mookerjee SA, Brand MD. Measurement and analysis of extracellular acid production to determine glycolytic rate. *J Vis Exp.* (2015) 106:e53464. doi: 10.3791/53464
36. Gerencser AA, Chinopoulos C, Birket MJ, Jastroch M, Vitelli C, Nicholls DG, et al. Quantitative measurement of mitochondrial membrane potential in cultured cells: calcium-induced de- and hyperpolarization of neuronal mitochondria. *J Physiol.* (2012) 590:2845–71. doi: 10.1113/jphysiol.2012.228387
37. Gerencser AA, Mookerjee SA, Jastroch M, Brand MD. Measurement of the absolute magnitude and time courses of mitochondrial membrane potential in primary and clonal pancreatic beta-cells. *PLoS ONE.* (2016) 11:e0159199. doi: 10.1371/journal.pone.0159199
38. Fan J, Kamphorst JJ, Mathew R, Chung MK, White E, Shlomi T, et al. Glutamine-driven oxidative phosphorylation is a major ATP source in transformed mammalian cells in both normoxia and hypoxia. *Mol Syst Biol.* (2013) 9:712. doi: 10.1038/msb.2013.65
39. Yoo HC, Park SJ, Nam M, Kang J, Kim K, Yeo JH, et al. A variant of SLC1A5 is a mitochondrial glutamine transporter for metabolic reprogramming in cancer cells. *Cell Metab.* (2019) 7:306. doi: 10.1016/j.cmet.2019.11.020
40. Dorai T, Dorai B, Pinto JT, Grasso M, Cooper AJL. High levels of glutaminase II pathway enzymes in normal and cancerous prostate suggest a role in "glutamine addiction". *Biomolecules.* (2019) 10:2. doi: 10.3390/biom10010002

Conflict of Interest: AG declares financial interest in Image Analyst Software.

The remaining authors declare that the research was conducted in the absence of any commercial or financial relationships that could be construed as a potential conflict of interest.

Advantages of publishing in Frontiers

OPEN ACCESS
Articles are free to read for greatest visibility and readership

FAST PUBLICATION
Around 90 days from submission to decision

HIGH QUALITY PEER-REVIEW
Rigorous, collaborative, and constructive peer-review

TRANSPARENT PEER-REVIEW
Editors and reviewers acknowledged by name on published articles

Frontiers
Avenue du Tribunal-Fédéral 34
1005 Lausanne | Switzerland

Visit us: www.frontiersin.org
Contact us: info@frontiersin.org | +41 21 510 17 00

REPRODUCIBILITY OF RESEARCH
Support open data and methods to enhance research reproducibility

DIGITAL PUBLISHING
Articles designed for optimal readership across devices

FOLLOW US
@frontiersin

IMPACT METRICS
Advanced article metrics track visibility across digital media

EXTENSIVE PROMOTION
Marketing and promotion of impactful research

LOOP RESEARCH NETWORK
Our network increases your article's readership